The Dissertation Committee for Manal Abdelsalam Salem Certifies that this is the approved version of the following dissertation:

Stiffness of Unsaturated Compacted Clays at Small Strains

Committee:

Stephen G. Wright, Supervisor

Kenneth H. Stokoe II

Ellen M. Rathje

John L. Tassoulas

Clark R. Wilson

Stiffness of Unsaturated Compacted Clays at Small Strains

by

Manal Abdelsalam Salem, B.Sc.; M.Sc.

Dissertation

Presented to the Faculty of the Graduate School of

The University of Texas at Austin

in Partial Fulfillment

of the Requirements

for the Degree of

Doctor of Philosophy

The University of Texas at Austin

December, 2006

Dedication

To the most loving and caring parents,

Abdelsalam Salem and Laila El-Alfy

To my beloved husband,

Rami El-Sherbiny

Acknowledgements

I would like to express my sincere gratitude to Professor Stephen G. Wright for his valuable guidance, continuing encouragement, and substantial support throughout my doctoral study. I would also like to express my deep appreciation to Professor Kenneth H. Stokoe II for his continuing support, valuable discussions, and comments throughout the course of my study. Sincere thanks and appreciations are also expressed to Professor Ellen M. Rathje for her support, valuable contribution, and guidance during this project. Deep appreciation to Professors Clark R. Wilson and John L. Tassoulas for their interest in this project, their willingness to serve on my dissertation committee, and their valuable discussions and comments.

I am indebted to the Texas Department of Transportation (TxDOT) for providing financial support during this study. Thanks are also due to the Department of Civil Engineering in the University of Texas at Austin and to the Brunswick Abernathy Professorship for providing financial support during the last year of this study.

I would like to thank my colleagues Celestino Valle-Molina and Min Jae Jung for their assistance and valuable contributions throughout the first stages of this research. Sincere gratitude is also expressed to the administrative staff at the University, in particular, Teresa Tice-Boggs, Chris Trevino, and Norma J. Gonzales from the Geotechnical Engineering Center. Thanks and appreciations are also due to the staff of the Learning Recourse Center (LRC), namely Daniel Quiroz, Timothy J. Plover, Wesley T. Maxwell, and William J. Wise for their continuous help with computer resources. I would like also to thank Frank J. Wise for his technical assistance and advice with the instrumentation.

Thanks are also due to Gonzalo Zapata, Maximo R. Trevino, and Johnie Williams for their help and for providing technical assistance. Thanks are also expressed to William T. Crooks and Wayne E. Fontenot for their great work in machining various parts throughout the manufacturing of the test setup.

Finally, I would like to express my deep and sincere gratitude to my parents Abdelsalam M. Salem and Laila A. El-Alfy, and my husband Rami M. El-Sherbiny for their patience, encouragement, and their continuous love and support throughout the course of this work.

Manal A. Salem

The University of Texas at Austin
December, 2006

Stiffness of Unsaturated Compacted Clays at Small Strains

Publication No._____

Manal Abdelsalam Salem, PhD

The University of Texas at Austin, 2006

Supervisor: Stephen G. Wright

The objective of the research presented in this dissertation is to investigate the effects of compaction conditions and the state of stress on the small-strain stiffness of unsaturated specimens of a low plasticity clay. An experimental study was conducted to address this objective. A pressure plate apparatus was developed to study the effects of compaction water content, dry unit weight, and degree of saturation on soil matric suction. Matric suction decreases as the compaction water content increases regardless of the dry unit weight and degree of saturation.

A triaxial cell equipped with piezoelectric transducers was developed to investigate the effects of compaction water content, dry unit weight, and degree of saturation on soil stiffness under undrained test conditions. Shear and compression wave

velocities generally decrease as the compaction water content increases. The variation of shear and compression wave velocities with dry unit weight depends on the compaction water content. For specimens compacted at similar water contents, the initial dry unit weight does not seem to have a significant effect on shear and compression wave velocities. Accordingly, soil stiffness was judged to be inapplicable to determine dry unit weights for compaction control purposes.

Results from pressure plate tests were used to estimate the initial matric suction for specimens tested in the undrained triaxial cell, which was then used to investigate the effects of matric suction ($u_a - u_w$) on soil stiffness. For specimens compacted at similar dry unit weights or compactive efforts, soil stiffness increased as the matric suction increased and tended towards a nearly constant value beyond which the stiffness did not appear to increase further for the range of matric suctions being investigated. For similar degrees of saturation, soil stiffness increased as matric suction increased for the range of matric suctions being investigated. Relationships between soil stiffness and matric suction are not unique and depend on factors such as compaction dry unit weight and degree of saturation, which essentially relate to the soil fabric, and overconsolidation ratio. For specimens compacted at similar dry unit weights, the relationship between soil stiffness and matric suction was investigated to determine the applicability of using stiffness and matric suction to infer dry unit weight for compaction control purposes. The variation observed in this relationship seems to be beyond what can be used to determine dry unit weights for compaction control purposes.

A suction-controlled triaxial cell equipped with piezoelectric transducers was developed to investigate the effects of matric suction ($u_a - u_w$) and net stress ($\sigma_c - u_a$) on soil stiffness. Constant water content tests were performed on specimens compacted at

similar degrees of saturation and compactive efforts. Three-dimensional diagrams were plotted to illustrate the variation of soil stiffness with matric suction and net stress. Generally, soil stiffness increases as matric suction increases, but at a decreasing rate. Stiffness also increases as net stress increases. Relationships between stiffness, matric suction, and net stress are not unique and depend on factors such as compaction degree of saturation and compactive effort, which essentially relate to the soil fabric, and overconsolidation ratio. Several empirical equations reported in the literature were evaluated with respect to their validity for modeling the variation of shear modulus with stress for the soil tested in this study.

Table of Contents

List of Tables

List of Figures

CHAPTER 1: INTRODUCTION

1.1 Background

Compacted soils represent a significant portion of the soils encountered in engineering practice. Quality control of compaction of such fills for embankments and mechanically stabilized earth (MSE) walls is of great importance to avoid costly failures. Currently, dry unit weight and water content are the main parameters used for compaction control purposes. Dry unit weight and water content are measured in the field using either direct sampling methods or the nuclear gage device. Sampling methods are time consuming and cannot be used for instantaneous assessment of compactness of soils. On the other hand, there are significant safety concerns regarding the radioactive material in the nuclear gage. Accordingly, studies have been undertaken to examine alternatives to direct sampling methods and the nuclear gage device with a safer and time efficient technology.

One approach is to use the soil stiffness at small strains as a measure of the compactness of fills. However, compacted fills are unsaturated materials possessing negative pore-water pressures and pore-air pressures that, in addition to density, significantly affect the state of stress and thus the shear strength and stiffness of the soil. Understanding the effects of compaction conditions and state of stress on soil stiffness at small strains is an important prerequisite to using soil stiffness to assess compactness of fills. Other potential applications for measuring soil stiffness at small strains are monitoring the construction and operation of earth dams, designing and evaluating the

performance of base, subbase, and subgrade layers in pavements, and designing and evaluating the dynamic response of foundations.

Currently, experimental data concerning the effects of compaction conditions on stiffness of unsaturated soils at small strains are contradicting and, thus, need further investigation. Few researchers have investigated the effect of state of stress of unsaturated soil on its stiffness at small strains. Lack of experimental evidence on this aspect is probably due to difficulties encountered in working with devices that measure and/or control the state of stress of unsaturated soils.

1.2 Research scope

This study is part of a research project sponsored by The Texas Department of Transportation (TxDOT) to evaluate alternative methods for determining soil compactness. The objective of the research presented in this dissertation is to investigate the effects of compaction conditions and the state of stress on the small-strain stiffness of compacted clays. Pressure plate tests were performed to study the effects of compaction conditions on the soil matric suction. An undrained triaxial apparatus equipped with piezoelectric transducers was used to investigate the effects of compaction conditions on the soil stiffness. Most of the equipment and test procedures reported in the literature to investigate the effect of state of stress on stiffness of unsaturated soils at small strains have been developed for testing coarser silts and sands. Very few tests have been conducted on clays due to the long testing periods necessitated by the low hydraulic conductivity of clays. In this study, a new triaxial cell has been developed to measure the stiffness of unsaturated soils under controlled states of stress. A testing procedure has

been developed that allows for testing compacted clays in time periods comparable to those reported for compacted silts and sands.

This dissertation consists of fourteen chapters. An introduction including the scope of this study is presented in this chapter. A literature review of measurements of soil stiffness at small strains using piezoelectric transducers is presented in Chapter 2. A background of the history of development of stress state variables for unsaturated soils, measuring soil suction, testing unsaturated soils under controlled state of stress is presented in Chapter 3. Prior work done to investigate the effects of compaction conditions on matric suction, the effects of compaction conditions on stiffness at small strains, and the effect of state of stress on stiffness at small strains is presented in Chapter 4. The physical properties of the soil tested and the procedures used to prepare test specimens are presented in Chapter 5. The experimental equipment and testing procedure used to perform pressure plate tests are described in Chapter 6. Measurements of matric suction using pressure plate apparatus are presented and discussed in Chapter 7. The experimental equipment and testing procedure used to measure the soil stiffness at small strains in triaxial apparatus under undrained conditions are presented in Chapter 8. Details on the interpretation of shear and compression waveforms recorded in tests are presented in Chapter 9. Measurements of soil stiffness in undrained tests are presented and discussed in Chapter 10. The experimental equipment and testing procedure used to measure the soil stiffness at small strains in suction–controlled triaxial apparatus are presented in Chapter 11. Measurements of soil stiffness in suction-controlled triaxial tests are presented and discussed in Chapter 12. Fitting stiffness measurements performed in this study into existing empirical equations relating small-strain stiffness to state of stress is presented and discussed in Chapter 13. Finally, a summary of the research and main conclusions are presented in Chapter 14.

CHAPTER 2: BACKGROUND ON CHARACTERIZATION AND MEASUREMENTS OF THE STATE OF STRESS IN UNSATURATED SOILS

2.1 Introduction

Unsaturated soils are involved in many engineering applications such as embankments, earth dams, and mechanically stabilized earth (MSE) walls. The mechanical behavior of the soil depends on the state of stress in the soil. A summary of studies that addressed variables required to describe the state of stress for unsaturated soils is presented in this chapter. An overview of equipment and testing procedures developed to measure and/or control the state of stress of unsaturated soils is presented as well.

2.2 State of stress of unsaturated soils

An unsaturated soil has commonly been referred to as a three-phase system: solid, air, and water (Lambe and Whitman, 1969). Recently, the importance of the air-water interface (i.e., the contractile skin) has been realized and therefore the contractile skin has been considered as a fourth phase (Fredlund and Morgenstern, 1977). The thickness of the contractile skin is of the order of a few molecular layers, therefore, the contractile skin is included as part of the water phase when establishing volume-mass relationships. An element of unsaturated soil with the four phases is idealized in Figure 2.1. The air phase might be continuous or occluded depending on the degree of saturation of the soil. Corey (1957) showed that the value of the air permeability dropped to zero when the degree of saturation of the soil approached 85%. Ladd (1960), Olson (1963), and Langfelder et al. (1968) showed that the value of the air permeability dropped to zero

around the optimum water content of the soil, which corresponded to a degree of saturation of about 85%.

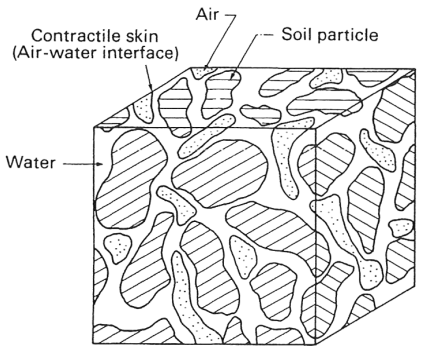

Figure 2.1. An idealized element of unsaturated soil (from Fredlund and Morgenstern, 1977).

The mechanical behavior of the soil depends on the state of stress of the soil. Several stress state variables have been proposed to express the state of stress of unsaturated soils. An overview of the history of development of stress state variables for unsaturated soils and of the stress state variables used in this study is presented in the following sections.

2.2.1 HISTORY OF DEVELOPMENT OF SINGLE STRESS VARIABLE FOR UNSATURATED SOILS

The state of stress in soil should be expressed in terms of stress state variables that are independent of the physical properties of the soil (Fung, 1977). For saturated soils, one stress state variable, known as the effective stress, is required to describe the mechanical behavior of the soil (Terzagi, 1936). The effective stress is expressed as:

$$\sigma' = \sigma - u_w \quad \text{(2.1)}$$

where σ' is the effective normal stress, σ is the total normal stress, and u_w is the pore-water pressure.

For unsaturated soils, various "effective stress" equations have been proposed that use only one stress state variable to express the state of stress of the soil. For example, Croney et al. (1958) proposed the following effective stress equation:

$$\sigma' = \sigma - \beta' u_w \quad (2.2)$$

where β' is a holding or bonding factor which was a measure of the number of bonds of water under tension contributing to the shear strength of the soil.

Bishop (1959) suggested the following effective stress equation that has been widely used:

$$\sigma' = (\sigma - u_a) + \chi(u_a - u_w) \quad (2.3)$$

where u_a is the pore-air pressure, and χ is a parameter related to the degree of saturation of the soil, with a value of unity for saturated soils and zero for dry soils.

Aitchison (1961) examined the relationships of matric suction and effective stress components based on a capillary model. He proposed the following effective stress equation:

$$\sigma' = \sigma + \psi p'' \quad (2.4)$$

where p" is the pressure deficiency (i.e., matric suction), and ψ is a parameter related to the degree of saturation of the soil with values, ranging from zero to one.

Jennings (1961) suggested a modified effective stress law that was a function of the soil moisture suction and a parameter β. He proposed the following effective stress equation:

$$\sigma' = \sigma + \beta p'' \quad \text{(2.5)}$$

where p" is the negative pore-water pressure taken as a positive value and β is a statistical factor (measured experimentally) of the same type as the contact area.

Richards (1967) incorporated a solute suction (i.e., osmotic suction) component into the effective stress equation, which he expressed as:

$$\sigma' = \sigma - u_a + \chi_m (h_m + u_a) + \chi_s (h_s + u_a) \quad \text{(2.6)}$$

where χ_m is an effective stress parameter for matric suction, h_m is the matric suction, χ_s is an effective stress parameter for solute suction, and h_s is the solute suction.

Aitchison (1965, 1973) proposed an effective stress equation slightly modified from that of Richards (1967):

$$\sigma' = \sigma + \chi_m p''_m + \chi_s p''_s \quad \text{(2.7)}$$

where p''_m is the matric suction, p''_s is the solute suction, and χ_m and χ_s are soil parameters, which were within the range of zero to one and were dependent upon stress paths.

All of the proposed effective stress equations based on a single-valued effective stress have incorporated a soil parameter. This soil parameter has different magnitudes for different problems (volume change versus shear strength), different stress paths, and different types of soil (Coleman, 1962; Jennings and Burland, 1962; Bishop and Blight, 1963; Burland, 1964; Burland, 1965; Blight, 1965; and Matyas and Radhakrishna, 1968).

Reexamination of the proposed effective stress equations has led researchers to suggest using instead two independent stress state variables to describe the mechanical behavior of unsaturated soils (Bishop and Blight, 1963; Matyas and Radhakrishna, 1968; Fredlund and Morgenstern, 1977; and Vinale et al., 1999).

2.2.2 STRESS STATE VARIABLES FOR UNSATURATED SOILS

Matyas and Radhakrishna (1968) mentioned that the principle of effective stress was inadequate to explain the volumetric behavior of partially saturated soils. The use of the effective stress equation proposed by Bishop (1959) for both compression and wetting processes resulted in anomalous values of the parameter χ (negative values). Bishop and Blight (1963) and Matyas and Radhakrishna (1968) suggested expressing the soil behavior in terms of two independent stress components rather than in terms of a single effective stress. The two stress state variables defined by these authors were: $(\sigma - u_a)$ and $(u_a - u_w)$.

Fredlund and Morgenstern (1977) presented a theoretical stress analysis for unsaturated soils based on multi-phase continuum mechanics. The unsaturated soil was considered as a four-phase system. The soil particles were assumed incompressible and the soil was considered chemically inert. The analysis concluded that any two of three possible variables $(\sigma - u_a)$, $(u_a - u_w)$, and $(\sigma - u_w)$ could be used to describe the state of normal stress in unsaturated soils. Three possible combinations of the proposed variables could be used to express the state of stress of unsaturated soils:

1. $(\sigma - u_a)$ and $(u_a - u_w)$,
2. $(\sigma - u_w)$ and $(u_a - u_w)$, and
3. $(\sigma - u_a)$ and $(\sigma - u_w)$.

Any two of these stress state variables can be used to describe the shear strength and volume change behavior of unsaturated soils. The components of these variables are physically measurable quantities. The first combination of stress state variables, $(\sigma - u_a)$ and $(u_a - u_w)$, has been the most widely used because the effect of a change in the total normal stress can be separated from the effect caused by a change in the pore-water pressure. In addition, the pore-air pressure is considered to be atmospheric (i.e., zero gauge pressure) for most practical engineering problems (Fredlund et al., 1978; and Fredlund and Rahardjo, 1993). The stress state variables $(\sigma - u_a)$ and $(u_a - u_w)$ are used throughout this text to express the state of stress for unsaturated soils. The term $(\sigma - u_a)$ is referred to as the "net normal stress", and the term $(u_a - u_w)$ is referred to as the "matric suction".

Fredlund and Morgenstern (1977) verified that the proposed stress state variables were valid experimentally by running "null" tests. In these tests, the components of the stress state variables (σ, u_a, and u_w) were varied equally in order to maintain constant values for the stress state variables ($(\sigma - u_a)$, $(u_a - u_w)$, and $(\sigma - u_w)$) while the volume changes were monitored. If the proposed stress state variables were valid, there should be no change in the volume of the soil specimen or the degree of saturation throughout the test. No volume change and little water flow were observed during these null tests. The stress state variables were therefore considered to be valid for describing the mechanical properties of unsaturated soils.

2.3 Measurement of soil suction

Measuring the soil suction is essential to understand the mechanical behavior of unsaturated soils. Suction represents one of the stress state variables required to express

the state of stress for unsaturated soils. A brief background on soil suction and techniques for measurement are presented in the following sections.

2.3.1 COMPONENTS OF SOIL SUCTION

Croney and Coleman (1948) first introduced the importance of soil suction in explaining the mechanical behavior of unsaturated soils. Aitchison (1965) later provided quantitative definitions of soil suction and its components. Soil suction is commonly called "total suction" which refers to the free energy of the soil water. Total suction has two components, namely, matric and osmotic (solute) suctions. The matric suction component is mainly associated with the capillary phenomenon resulting from the surface tension of the pore water. Surface tension is the result of the intermolecular forces acting on the water molecules at the air-water interface, often referred to as the contractile skin. The difference between air and water pressures across the contractile skin ($u_a - u_w$) is defined as the matric suction. The radius of the contractile skin is inversely proportional to the matric suction. The osmotic suction component results from the concentration of the dissolved salts in the pore water. Generally, the compaction water content of compacted soils appears to have a direct relation with the developed matric suction, while the osmotic suction does not seem to be sensitive to the compaction water content (Fredlund and Rahardjo, 1993).

2.3.2 PRESSURE PLATE TEST

Several techniques have been developed to measure soil suction among which pressure plate apparatus, tensiometers, psychrometers, filter paper, and electric conductivity sensors. The pressure plate apparatus has been used in this study to measure

the matric suction. The pressure plate apparatus and the testing procedure are presented in the following sections.

2.3.2.1 Apparatus

The pressure plate apparatus has been widely used to measure the matric suction of unsaturated soils (Croney et al., 1952; Aitchison and Richards, 1965; Olson and Langfelder, 1965; Widger, 1976; Filson, 1980; Yong, 1980; Mou and Chu, 1981; Tsai and Petry, 1995; Oloo and Fredlund, 1996; Toyota et al., 2001; Walker et al., 2005; Agus and Schanz, 2006; and Leong et al., 2006). A schematic diagram of the pressure plate apparatus is shown in Figure 2.2. The pressure plate apparatus consists of a platen equipped with a high air-entry porous stone mounted on top of the base plate of a pressure chamber.

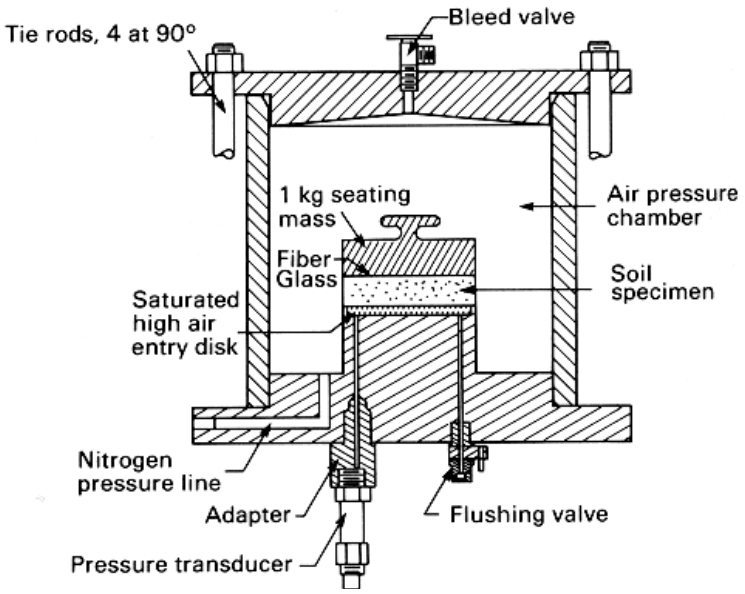

Figure 2.2. Schematic diagram of a pressure plate apparatus (from Olson and Langfelder, 1965).

A high air-entry porous stone is a porous stone with very small pores. Once the porous stone is saturated with water, it can resist entry of air into the pores due to the surface tension, T_s, developed by the air-water interface or the contractile skin. The contractile skin acts like an elastic membrane in tension joining the small pores of radius, R_s, on the surface of the porous stone and separates the pore air in the soil and the water in the measuring system as illustrated in Figure 2.3. The difference between the air pressure above the contractile skin and the water pressure below the contractile skin is the matric suction ($u_a - u_w$). The maximum matric suction that can be held across the porous stone is called the air-entry value, $(u_a - u_w)_d$. The air-entry value of a given porous stone can be expressed using Kelvin's equation:

$$(u_a - u_w)_d = \frac{2T_s}{R_s} \quad \text{.....} \quad (2.8)$$

where $(u_a - u_w)_d$ is the air-entry value of the high air-entry porous stone, T_s is the surface tension of the contractile skin, and R_s is the radius of curvature of the contractile skin or the radius of the largest pore size.

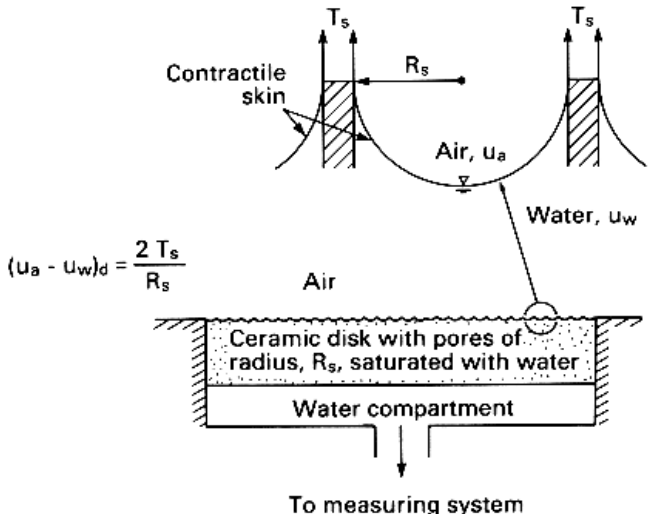

Figure 2.3. Operating principle of a high air-entry porous stone as described by Kelvin's capillary model (from Fredlund and Rahardjo, 1993).

The surface tension, T_s, is nearly constant for a given fluid (changes slightly with temperature). Therefore, the radius, R_s, of the largest pore in the porous stone mainly controls the air-entry value. The smaller the porous stone pores, the higher the air-entry value of the porous stone. The ability of a high air-entry porous stone to withstand a difference between air and water pressures makes the porous stone suitable to measure the negative pore-water pressures directly in unsaturated soils. The water in the porous stone is the link between the pore water in the soil and the water in the measuring system. The matric suction of the soil should not exceed the air entry value of the porous stone so that air cannot penetrate the porous stone into the measuring system.

The high air-entry porous stone is placed over a cavity filled with water and provided with an inlet and an outlet to flush out air that diffuses through the high air-entry porous stone during a test. Air diffusion occurs in response to a concentration gradient of air between two regions. Air movement takes place from the region with higher air concentration to the region with lower air concentration (Fredlund and Rahardjo, 1993). In a pressure plate test, the air present in the unsaturated soil specimen diffuses through the de-aired water present in the high air-entry porous stone and appears in the water cavity beneath the high air-entry porous stone.

The pressure plate apparatus is equipped with two pressure transducers. The first transducer is connected to the inlet of the water cavity and used to measure the pore-water pressure developed within the specimen. The second transducer is connected to the pressure line controlling the air pressure inside the pressure chamber.

2.3.2.2 Test procedure

One of the difficulties in the measurement of negative pore-water pressures in unsaturated soils is caused by water cavitating at a pressure approximately of –1 atmosphere. Hilf (1956) developed the "axis translation technique" that has helped to overcome the problem of cavitation. In this technique, the ambient air pressure is increased by a certain amount, and the pore-water pressure increases by an equal amount, preserving constant matric suction. This is true because the radius of curvature of the air-water menisci does not change significantly. Olson and Langfelder (1965) stated that the axis translation technique could be theoretically justified. An increase in air pressure in a soil specimen tends to compress the soil particles and the pore water isotropically.

However, since both are considered incompressible, the increase in the air pressure cannot significantly change the curvature of the air-water menisci.

In a pressure plate test, the soil specimen is placed on top of the saturated high air-entry porous stone in the pressure chamber as shown in Figure 2.2. Good contact between the specimen and the high air-entry porous stone is required for rapid response of the equipment (Aitchison and Richards, 1965; Olson and Langfelder, 1965; and Juca, 1993). The specimen tends to draw water up through the porous stone immediately after it is placed on top of the porous stone, and the pore-water pressure transducer starts registering a negative value. If the negative pore-water pressure is small such that the system is not subjected to cavitation, the pressure transducer registers the negative pore-water pressure directly. Otherwise, if it is expected for the specimen to have high negative pore-water pressure, then the air pressure inside the pressure chamber is increased in increments (axis translation technique) until there is no further tendency for the water to move through the porous stone. Equilibrium is inferred when the readings of the pore-water pressure transducer stabilizes. At equilibrium, the matric suction is the difference between the readings of the pore-air and pore-water pressure transducers. The pressure plate apparatus can be used to measure soil-suctions up to 1500 kPa (Fredlund and Rahardjo, 1993).

Typical response time curves for the measurement of matric suction using the pressure plate apparatus is shown in Figure 2.4 (Widger, 1976). Fredlund and Morgenstern (1977) reported that any flexibility in the pressure measuring system could greatly affect the response time. The matric suction response versus time is a function of the hydraulic conductivity of the high air-entry porous stone and the soil (Fredlund and Rahardjo, 1993). Bocking and Fredlund (1980) observed that for relatively compressible

soils and with short adjustment intervals, an overshooting response curve might be obtained.

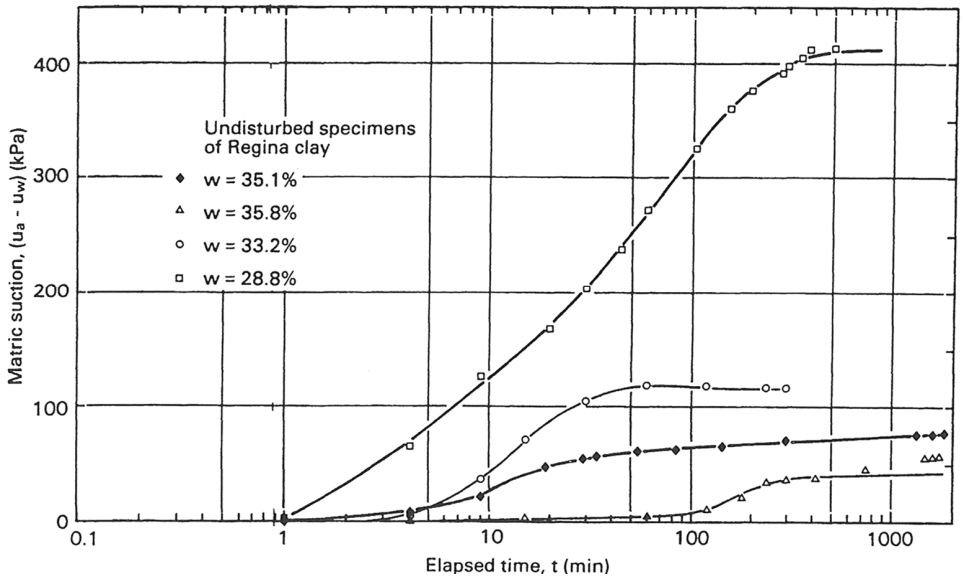

Figure 2.4. Time-response curve for matric suction measurements on Regina clay using the axis-translation technique (from Widger, 1976).

The volume changes of a specimen are not measured in the pressure plate test. Bocking and Fredlund (1980) noted that during a pressure plate test, a small but finite amount of water must flow out of the soil specimen for the water pressure transducer to register pressure changes. Therefore, they concluded that a soil specimen must undergo some volume changes during the test.

In order for the axis translation technique to be applicable for measuring matric suction in a pressure plate test, the ambient air pressure in the pressure chamber should be equal to the pore-air pressure within the specimen. This requires that the air phase within the specimen be continuous (Olson and Langfelder, 1965). Corey (1957), Ladd (1960), Olson (1963), and Langfelder et al. (1968) showed that occlusion occurred around the

optimum water content, which corresponds to a degree of saturation of about 85%. Bocking and Fredlund (1980) mentioned that applying the axis translation technique for soils with occluded air bubbles might result in an overestimation of the measured matric suction by up to 100 percent or more. For the current research, the validity of the matric suction measurements using the axis translation technique for specimens compacted on the wet side of the line optimums is investigated.

Bocking and Fredlund (1980) developed a theoretical mathematical model for the axis translation technique and discussed the effect of air diffusing through a high air-entry porous stone on the matric suctions calculated using the theoretical model. For soils with occluded air bubbles, the effect of diffusion of air was insignificant. For soils with continuous air phase, the effect of air diffusion depended on the value of the diffusivity and the test duration. When the effect of air diffusion was significant, diffusion caused a gradual increase in the water pressure (u_w) beneath the high air-entry porous stone until; ultimately, it approached the applied chamber pressure (u_a). Therefore, the measured suction peaked and then dropped off, as shown in Figure 2.5, and the actual suction was underestimated. Accordingly, flushing out air that diffuses through the high air-entry porous stone during a pressure plate test is essential to measure the true value of the matric suction.

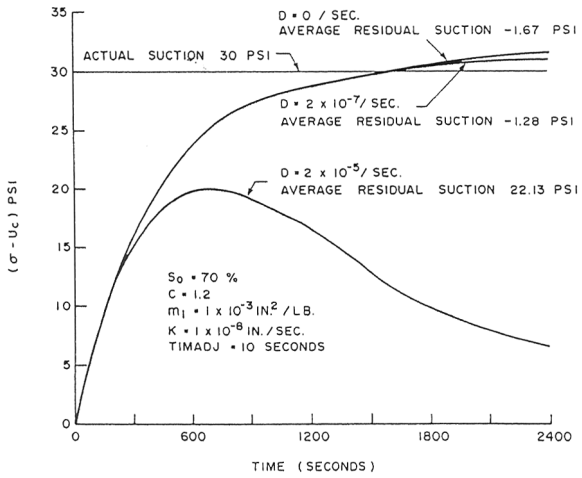

Figure 2.5. Typical effect of air diffusion on the time-response curve of a continuous air phase soil (from Bocking and Fredlund, 1980).

2.4 Testing unsaturated soil under controlled state of stress

A few laboratory devices have been modified to test unsaturated soils under a controlled state of stress among which triaxial apparatus, oedometers, and resonant column apparatus. For the current research, a triaxial apparatus has been developed to test unsaturated soils under controlled state of stress. A brief review of triaxial cells that have been developed to test unsaturated soils under controlled states of stress and the testing procedures that have been followed is presented in the following sections.

2.4.1 TRIAXIAL APPARATUS

Attempts to test unsaturated soils in triaxial cells under controlled states of stress have been based on modifying the standard triaxial apparatus developed for testing saturated soils. Bishop et al. (1960), Bishop and Donald (1961), Matyas and Radhakrishna (1968), Josa et al. (1987), Fredlund and Rahardjo (1993), Sivakumar (1993), Romero et al. (1997), Cabarkapa et al. (1999), Rampino et al. (1999, 2000),

Sivakumar and Wheeler (2000), Taha et al. (2000), Vassallo and Mancuso (2000), Hoyos and Macari (2001), Ng and Chiu (2001), Toyota et al. (2001), Aversa and Nicotera (2002), Sun et al. (2003, 2004, 2006), Lauer and Engel (2004, 2005), Gallage and Uchimura (2006), Mun et al. (2006), Padilla et al. (2006), and Schwarz et al. (2006) modified the standard triaxial apparatus to accommodate independent measurement and/or control of the pore-air and pore-water pressures. In these studies, pore-water pressure was measured and/or controlled using a saturated high air-entry porous stone with suitable air-entry value depending on the anticipated matric suction to occur during the test. The high air-entry porous stone was mounted over a water compartment filled with de-aired water. Pore-air pressure was measured and/or controlled using a coarse porous stone. A schematic diagram of a modified triaxial cell to test unsaturated soils is shown in Figure 2.6. The cell pressure, pore-water, and pore-air pressures were controlled independently. The changes in water content of the specimen were determined by monitoring the water going in or out of the specimen through the high air-entry porous stone(s).

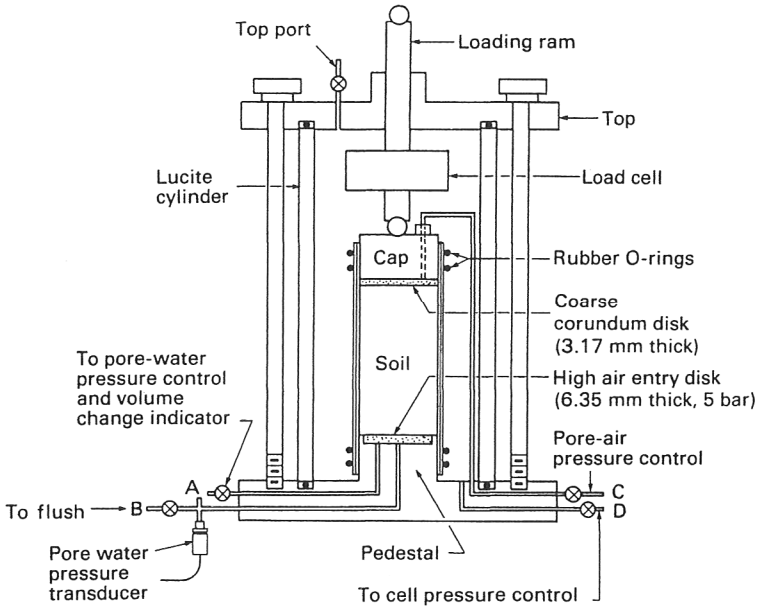

Figure 2.6. Modified triaxial cell for testing unsaturated soils (from Fredlund and Rahardjo, 1993).

Bishop and Donald (1961), Matyas and Radhakrishna (1968), Fredlund and Rahardjo (1993), Sivakumar (1993), Romero et al. (1997), Rampino et al. (1999, 2000), Taha et al. (2000), Hoyos and Macari (2001), Macari and Hoyos (2001), Aversa and Nicotera (2002), Mancuso et al. (2002), Lauer and Engel (2004, 2005), and Padilla et al. (2006) noted that air diffused through the high air-entry porous stone and air bubbles appeared beneath the porous stone in the water compartment. The authors emphasized that the diffused air should be flushed out from the water compartment continuously. Bishop and Donald (1961), Fredlund and Rahardjo (1993), Romero et al. (1997), Lawrence et al. (2005), and Padilla et al. (2006) mentioned that the volume of the diffused air bubbles should be measured to track changes in the water content of the specimen caused by air diffusion.

Bishop et al. (1960), Bishop and Donald (1961), Josa et al. (1987), Fredlund and Rahardjo (1993), Sivakumar (1993), Cabarkapa et al. (1999), Rampino et al. (1999, 2000), Sivakumar and Wheeler (2000), Taha et al. (2000), Vassallo and Mancuso (2000), Hoyos and Macari (2001), Ng and Chiu (2001), Toyota et al. (2001), Aversa and Nicotera (2002), Sun et al. (2003, 2004, and 2006), Lauer and Engel (2004, 2005), Gallage and Uchimura (2006), Mun et al. (2006), Padilla et al. (2006), and Schwarz et al. (2006) mounted the high air-entry porous stone in the bottom platen and the coarse porous stone in the top platen of the triaxial cell. Matyas and Radhakrishna (1968) and Romero et al. (1997) designed triaxial platens in which both air and water pressures were applied independently and simultaneously to both ends of the specimen. This ensured a significantly shorter equalization durations which was an important advantage when testing low permeability unsaturated soils.

Three alternatives were proposed in previous studies to monitor the overall volume changes of the specimen. Josa et al. (1987), Fredlund and Rahardjo (1993), Romero et al. (1997), Geiser et al. (2000), Chiu (2001), Ng and Chiu (2001), Sun et al. (2003, 2004, 2006), and Chavez et al. (2005) determined the overall volume changes based on local strain measurements by measuring the vertical deflection and radial deformation of the specimen. Bishop and Donald (1961), Matyas and Radhakrishna (1968), Josa et al. (1987), Cui and Delage (1996), Aversa and Nicotera (2002), and Gallage and Uchimura (2006) measured the overall volume changes of the specimen by monitoring the fluid level in the triaxial chamber. Wheeler and Sivakumar (1992), Sivakumar (1993), Rampino et al. (1999), Sivakumar and Wheeler (2000), Toyota et al. (2001), Ng et al. (2002), Lauer and Engel (2004, 2005), Chavez et al. (2005), Mun et al. (2006), Padilla et al. (2006), and Schwarz et al. (2006) determined the overall volume

changes of the specimen by measuring the volume of the fluid flowing into or out of the triaxial chamber.

Measuring the overall volume changes of the specimen by monitoring the level of the fluid in the triaxial chamber or by monitoring the volume of the fluid flowing into or out of the triaxial chamber is encountered with problems such as expansion and contraction of the cell wall and cell fluid because of pressure and temperature variations, creep and hysteresis of the cell wall, and possible leakage of cell fluid (Geiser et al., 2000; Leong et al., 2004; and Padilla et al., 2006). Bishop and Donald (1961), Matyas and Radhakrishna (1968), Josa et al. (1987), Wheeler and Sivakumar (1992), Sivakumar (1993), Cui and Delage (1996), Rampino et al. (1999), Sivakumar and Wheeler (2000), Toyota et al. (2001), Aversa and Nicotera (2002), Ng et al. (2002), Lauer and Engel (2004, 2005), Chavez et al. (2005), Gallage and Uchimura (2006), Padilla et al. (2006), and Schwarz et al. (2006) used double-walled triaxial cells to minimize the effects of expansion and contraction of the cell and cell fluid. Accordingly, it is preferable to use double-walled triaxial cells if the overall volume changes of the specimen are to be measured based on the volume of the water flowing into or out of the triaxial cell.

Air diffuses from the soil specimen to the surrounding cell fluid through rubber membranes during testing unsaturated soils in triaxial cells. The effect of the air diffusion on the measurements of the overall volume changes is significant when tests last for long periods. Bishop and Donald (1961), Josa et al. (1987), and Egeli (1992) suggested using mercury as a cell fluid to minimize the volume of diffused air. Though mercury reduces air diffusion significantly due to its high density, mercury is considered to be a hazardous material and it is not recommended to be used as a cell fluid. Wu et al. (1984), Qian et al. (1991), Cabarkapa et al. (1999), and Taha et al. (2000) surrounded the specimen with

double membranes with vacuum grease in between to reduce the volume of the diffused air. Bishop et al. (1960) noted that using a layer of aluminum foil underneath the rubber membrane surrounding the specimen reduced the air diffusion through the rubber membrane. Ng et al. (2002) recommended using double membranes with vacuum grease and a layer of aluminum foil in between. Accordingly, it is recommended to use double membranes with a layer of aluminum foil in between to minimize the volume of air diffusing from the soil specimen to the surrounding cell fluid.

2.4.2 TEST PROCEDURES

The drainage of the pore fluid permitted upon the application of confining pressure distinguishes among three types of tests: drained, constant water content, and undrained tests. In *drained* tests, both pore air and pore water are allowed to drain upon the application of the confining pressure, while maintaining constant pore-air and pore-water pressures. In *constant water content* tests, the pore air is allowed to drain while pore water is kept from flowing into or out of the specimen upon the application of the confining pressure. In *undrained* tests, pore air and pore water are not allowed to flow into or out of the specimen upon the application of the confining pressure. Bishop et al. (1960) and Fredlund and Rahardjo (1993) mentioned that undrained tests were usually avoided because it was hard to measure the pore-air pressure over a long period because of the ability of air to diffuse through rubber membranes, water, tubing, fittings, and other materials. In the three types of tests, researchers implemented the axis translation technique when testing specimens with matric suctions higher than one atmosphere to avoid cavitation in the water compartment below the high air-entry porous stone. In the current research, a single drained test and a series of constant water content tests were performed.

The drained test performed in this study was conducted based on the procedure outlined by Sivakumar (1993). Sivakumar (1993) divided the drained test procedure into two stages: equalization and compression. The goal of the equalization stage was to bring the specimen to the target values of matric suction ($u_a - u_w$) and net stress ($\sigma - u_a$) selected to start the compression stage. The author assumed equalization was reached when the flow of water into the specimen reduced to 0.1 ml/day, which is equivalent to 0.04% change in water content per day. The equalization stage extended for 7 days. In the compression stage, the specimen was compressed isotropically by increasing the cell pressure at a rate of 0.6 kPa/h. The authors allowed for a period of 24 hours after the target cell pressure was reached to ensure complete dissipation of any excess pore-water pressure. Other studies were performed to test unsaturated soils under drained conditions following the procedure outlined by Sivakumar (1993). The test procedures reported in the literature to test unsaturated soils under drained conditions are summarized in Table 2.1.

The adequate rate of loading unsaturated specimens was investigated experimentally by Macari and Hoyos (2001). The authors found that an inappropriate rate would cause the menisci to break apart, and the effect of the matric suction to be lost. For compacted silty sand specimens, the authors concluded that a maximum loading rate of 16 kPa/h should be used. The authors used a loading rate of 10 kPa/h. Accordingly, it is preferable to perform preliminary tests to check the adequate rate of loading before testing unsaturated specimens.

T**able 2.1.** Test procedures reported in literature to perform drained tests on unsaturated soils under controlled states of stress.

Reference	Soil type	Criterion for equilibrium in equalization stage	Time for equilibrium in equalization stage	Rate of isotropically compressing specimen in compression stage	Criterion for equilibrium in compression stage
Sivakumar (1993)	Kaolin	Rate of change of water content = 0.04%/day	≈ 7 days	0.6 kPa/h	Dissipation of excess pore-water pressure
Rampino et al. (1999, 2000) Vinale et al. (1999) Mancuso et al. (2002)	Silty sand	Rate of change of water content = 0.04%/day	≈ 7 days	4 kPa/h	Dissipation of excess pore-water pressure + stabilization of water content
Vassalo et al. (2006)	Clayey-slightly sandy silt	Stabilization of volume and weight	NA	4 kPa/h	Stabilization of volume and weight
Cabarkapa et al. (1999)	Quartz silt	Stabilization of volumetric water content	3 weeks	NA	NA
Sivakumar and Wheeler (2000)	Kaolin	Rate of change of specific water volume* < 0.001/day	6 to 10 days	0.6 kPa/h	Dissipation of excess pore-water pressure
Macari and Hoyos (2001)	Silty sand	Stabilization of volumetric water content	NA	10 kPa/h	NA
Silva et al. (2002)	Silt	NA	NA	10 kPa/h	Dissipation of excess pore-water pressure

* Specific water volume is the volume of water and solids divided by the volume of solids.

CHAPTER 3: BACKGROUND ON SMALL-STRAIN STIFFNESS MEASUREMENTS USING PIEZOELECTRIC TRANSDUCERS

3.1 Introduction

Several laboratory techniques have been developed to measure the shear modulus at small strains. Techniques for measuring shear moduli include torsional resonant column, cyclic torsional shear, and piezoelectric transducers. The constrained modulus has also been measured at small strains using piezoelectric transducers. For the current research, piezoelectric transducers were used to measure shear and compression moduli at small strains. An overview of previous work done with piezoelectric transducers, including a description of piezoelectric transducers, measurement procedures, experimental set-up, and interpretation of recorded waveforms is presented in the following sections.

3.2 Piezoelectric transducers

Piezoelectricity is the ability of certain crystalline minerals to convert between mechanical energy and electrical energy. Piezoelectricity can be found in nature in crystals of quartz and tourmaline (a complex crystalline silicate containing aluminum, boron, and other elements). Piezoelectricity is often obtained artificially with certain ceramics such as lead zirconate titanate, barium titanate, and lead titanate (Lawrence, 1963; Manke and Gallaway, 1966; Stephenson, 1978; Hamdi and Taylor-Smith, 1981; Brignoli et al., 1996; Lee and Santamarina, 2005; and Leong et al., 2005). Piezoelectric ceramics can be trimmed to desired shapes such as discs, rods, plates, etc., and then electrodes are applied to the appropriate surfaces. The polarization of the piezoelectric

ceramics is achieved by applying a high D-C voltage between a pair of electrode faces. After polarization, the piezoelectric element (transducer) can be used to both generate and receive shear and/or compression waves.

Piezoelectric transducers were first introduced to generate and receive compression waves by Lawrence (1963). For the generation of compression (P) waves, the piezoelectric element, usually referred to as piezoelectric disk, consists of one piezoceramic plate that is polarized across the least dimension of the plate. The electrodes are placed externally on the element faces perpendicular to the direction of polarization. When the voltage is applied to the electrodes, the piezoelectric disk shrinks and expands in the direction of wave propagation causing the generation of compression waves (Strassburger, 1982 and Brignoli et al., 1996). A schematic diagram for the piezoelectric disk is shown in Figure 3.1(a). Vaghela and Stokoe (1995) have shown that mounting the compression wave sources and receivers at the center of each end of the test specimens results in measuring constrained compression wave velocities.

Lawrence (1965) and Shirly and Anderson (1975) introduced piezoelectric transducers to generate shear waves. The piezoelectric element required for the generation of shear (S) waves, usually referred to as bender element, consists of two piezoceramic plates that are rigidly bonded to a central metallic plate. Two thin conductive layers (electrodes) are applied externally to the bender element. When applying the voltage, one plate elongates and the other shortens so that the element bends and shear waves are generated at the free end of the bender element (Schultheiss, 1981; Strassburger, 1982; Dyvik and Madshus, 1985; Bates, 1989; Thomann and Hryciw, 1990; Agarwal and Ishibashi, 1991; de Alba and Baldwin, 1991; Gohl and Finn, 1991; Viggiani and Atkinson, 1995a&b; Brignoli et al., 1996; Jovicic et al., 1996; Brocanelli and

Rinaldi, 1998; Blewett et al., 2000; Silva et al., 2002; Mohsin and Airey, 2003; Theron et al., 2003; Kung et al., 2004; Lee and Santamarina, 2005; and Leong et al., 2005). A schematic diagram for the bender element is shown in Figure 3.1(b).

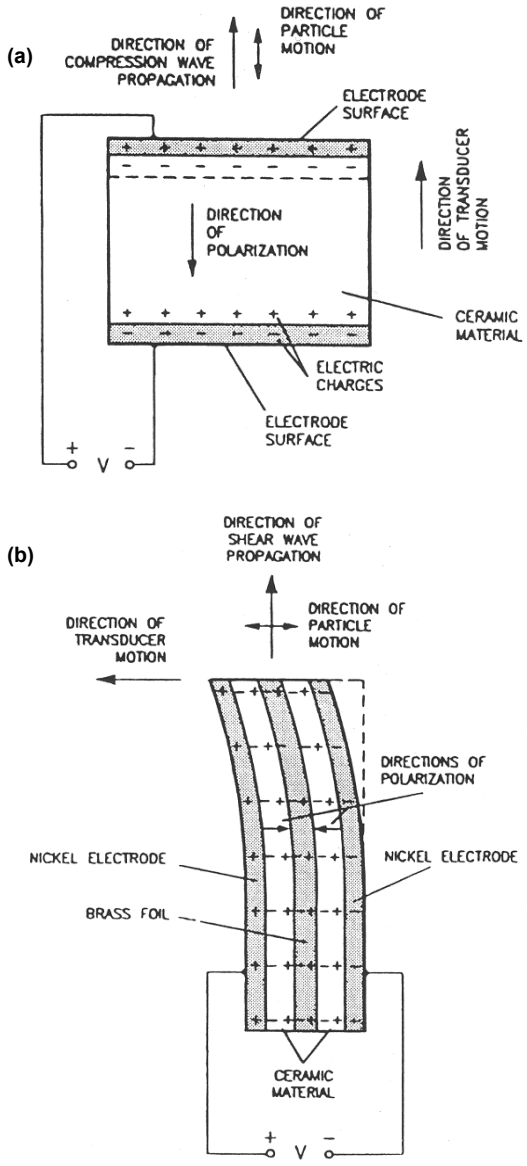

Figure 3.1. Schematic diagram for: (a) the piezoelectric disk and (b) the piezoelectric bender element (from Strassburger, 1982).

3.3 Experimental set-up

Measurement of soil stiffness using piezoelectric transducers has been implemented in many laboratory equipment such as: oedometers, torsional resonant column apparatus, and triaxial cells (Hamdi and Taylor-Smith, 1981; Schultheiss, 1981; Bennell et al., 1984; Dyvik, 1984; Dyvik and Madshus, 1985; Dyvik and Olsen, 1989; Ladd and Dutko, 1985; Bates, 1989; Thomann and Hryciw, 1990; Agarwal and Ishibashi, 1991; de Alba and Baldwin, 1991; Fam and Santamarina, 1995; Jamiolkowski et al., 1995; Viggiani and Atkinson, 1995a&b; Brignoli et al., 1996; Nakagawa et al., 1996; Gajo et al., 1997; Rampello et al., 1997; Shibuya et al., 1997; Arulnathan et al., 1998; Brocanelli and Rinaldi, 1998; Jovicic and Coop, 1997b; Jovicic and Coop, 1998; Kuwano and Jardine, 1998; Cabarkapa et al., 1999; Lohani et al., 1999; Blewett et al., 2000; Cho and Santamarina, 2001; Diaz-Rodriguez et al., 2001; Pennington et al., 2001; Callisto and Rampello, 2002; Silva et al., 2002; Mohsin and Airey, 2003; Theron et al., 2003; Kung et al., 2004; Leong et al., 2005, 2006; and Valle, 2006).

Piezoelectric transducers should be coated with a waterproofing material to provide protection against moisture. The coating should be a good insulating electrical material and ductile enough to allow the transducers to move freely (Schultheiss, 1981; Dyvik and Madshus, 1985; Bates, 1989; de Alba and Baldwin, 1991; Gohl and Finn, 1991; Fam and Santamarina, 1995; Brignoli et al., 1996; Gajo et al., 1997; Viggiani and Atkinson, 1997; Arulnathan et al., 1998; Brocanelli and Rinaldi, 1998; Cabarkapa et al., 1999; Cho and Santamarina, 2001; Santamarina et al., 2001; Zeng et al., 2004; Lee and Santamarina, 2005; and Leong et al., 2005).

de Alba and Baldwin (1991) mentioned the disadvantages of using the bender elements with dense specimens as their insertion into the specimen can damage the

waterproofing and may crack the bender. Marinho et al. (1995) and Jovicic and Coop (1998) tested stiff clays with bender elements. They cut small slots into the top and bottom of the specimens to avoid damaging the bender elements upon insertion. In order to obtain good coupling between the soil and the bender elements, Marinho et al. (1995) placed soft remolded soil in the slot before inserting the bender elements. The slot was lined with 'cling film' to prevent local softening of the test specimen. Mendoza et al. (2005) and Mendoza and Colmenares (2006) tested compacted kaolin with bender elements. In order to have good coupling between the soil and the bender elements, small slots with dimensions a little smaller than the bender elements were made at the top and the bottom of the specimens. The bender element was then lubricated with silicon grease before insertion in the slots to avoid any damage during the insertion.

After waterproofing the piezoelectric transducers, a conductive paint should be applied which creates an electric shield that is later grounded to avoid electromagnetic coupling and cross-talk between the source and the receiver (Gohl and Finn, 1991; Brocanelli and Rinaldi, 1998; Pennington et al., 2001; Santamarina et al., 2001; Theron et al., 2003; and Lee and Santamarina, 2005). Dyvik and Madshus (1985) and Brignoli et al. (1996) highlighted the importance of protecting the cables connecting the transducers with the external devices from the water inside the triaxial cell, either by coating them with a waterproofing material or by putting them in plastic tubes inside the triaxial cell.

The instrumentation required for any experimental setup supporting piezoelectric transducers includes the following: a function generator to produce the excitation signal, an amplifier to amplify the signal before sending it to the transducers, and an oscilloscope to display the excitation and received signals. To enhance the recorded signals (reduce the noise), averaging (stacking) can be employed through a digital oscilloscope. The

more the number of averaged signals the lesser the effect of noise. A computer coupled with the measuring system assists in the storage and analysis of the waves recorded by the oscilloscope (Agarwal and Ishibashi, 1991; de Alba and Baldwin, 1991; Fam and Santamarina, 1995; Brignoli et al., 1996; Nakagawa et al., 1996; Gajo et al., 1997; Brocanelli and Rinaldi, 1998; Viggiani and Atkinson, 1995b; Cho and Santamarina, 2001; Pennington et al., 2001; Mohsin and Airey, 2003; Kung et al., 2004; Leong et al., 2005; Mendoza et al., 2005; and Puppala et al., 2006). A schematic diagram of piezoelectric transducers and the associated electronics required during testing is shown in Figure 3.2.

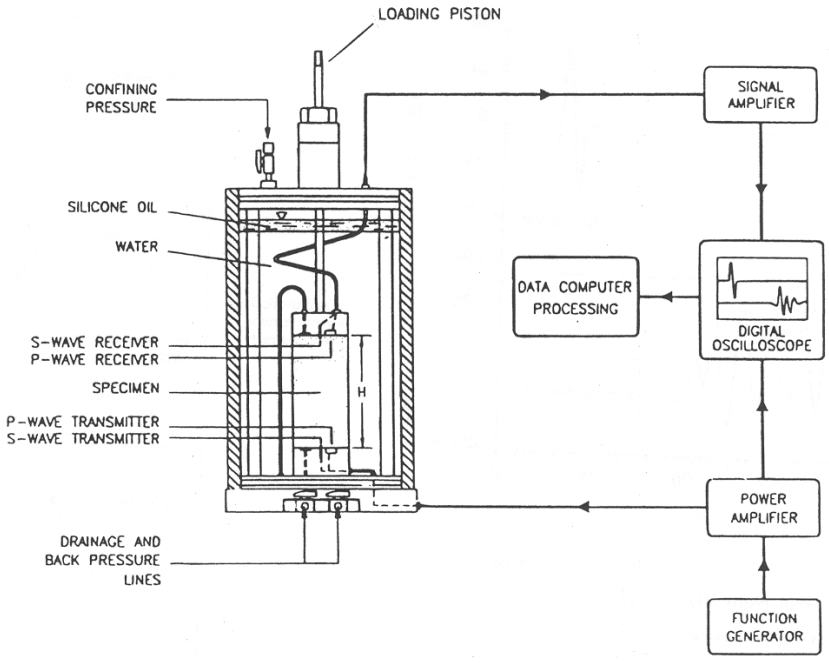

Figure 3.2. Schematic diagram for piezoelectric transducers and associated electronics used during testing (from Brignoli et al., 1996).

3.4 Measurement procedure

An overview of studies that have discussed the procedures followed to measure shear and compression wave velocities using piezoelectric transducers is presented in this section.

Alignment of piezoelectric transducers

Great care must be taken in the alignment of the piezoelectric source and receiver (Cherry, 1962; Ladd and Dutko, 1985; Bates, 1989; Gohl and Finn, 1991; and Brignoli et al., 1996). Cherry (1962) showed that if the bender element receiver is located directly under the source and in the same vertical plane, shear waves dominate the transmitted waves. However, if the receiver is offset perpendicular to the vertical plane of the source, compression waves strike the bender elements.

Waveforms

Different waveforms have been used to excite piezoelectric transducers such as square waves and sinusoidal waves. Schultheiss (1981), Bennell et al. (1984), Dyvik and Madshus (1985), Bates (1989), Dyvik and Olsen (1989), Thomann and Hryciw (1990), Gohl and Finn (1991), Fam and Santamarina (1995), Marinho et al. (1995), Viggiani and Atkinson (1995a&b), Jovicic et al. (1996), Rampello et al. (1997), Shibuya et al. (1997), Lohani et al. (1999), Cho and Santamarina (2001), Callisto and Rampello (2002), Theron et al. (2003), and Leong et al. (2005) used square waves to excite bender elements. The problem with using square waves is the fact that a square wave is composed of a spectrum of different frequencies, which makes it hard to define the arrival of the received wave as shown in Figure 3.3 (Jovicic et al., 1996; Lohani et al., 1999; and Blewett et al., 2000). Leong et al. (2005) referred the uncertainty in the determination of

the travel time when exciting with square waves to: (1) the received signal does not resemble the transmitted signal; (2) the received signal has more distortion near the arrival.

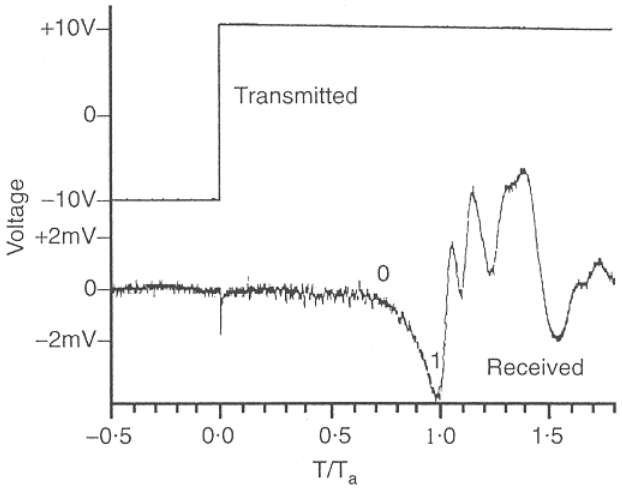

Figure 3.3. Bender element response to a square input signal (from Jovicic et al., 1996).

Sinusoidal waves have been widely used to excite piezoelectric transducers (Dyvik and Madshus, 1985; Agarwal and Ishibashi, 1991; de Alba and Baldwin, 1991; Viggiani and Atkinson, 1995a; Brignoli et al., 1996; Jovicic et al. 1996; Gajo et al., 1997; Jovicic and Coop, 1997b; Arulnathan et al., 1998; Cabarkapa et al., 1999; Lohani et al. 1999; Blewett et al., 2000; Callisto and Rampello, 2002; Mohsin and Airey, 2003; Theron et al., 2003; Kung et al., 2004; Leong et al. 2005; and Puppala et al., 2006). Using sinusoidal waves reduces the subjectivity in interpreting the received wave because the sinusoidal pulse is composed of only one frequency. This results in an output signal that is of a similar shape to the input signal, which makes the determination of the arrival of the received wave easier as shown in Figure 3.4. Accordingly, it is preferable to excite piezoelectric transducers using sinusoidal waves.

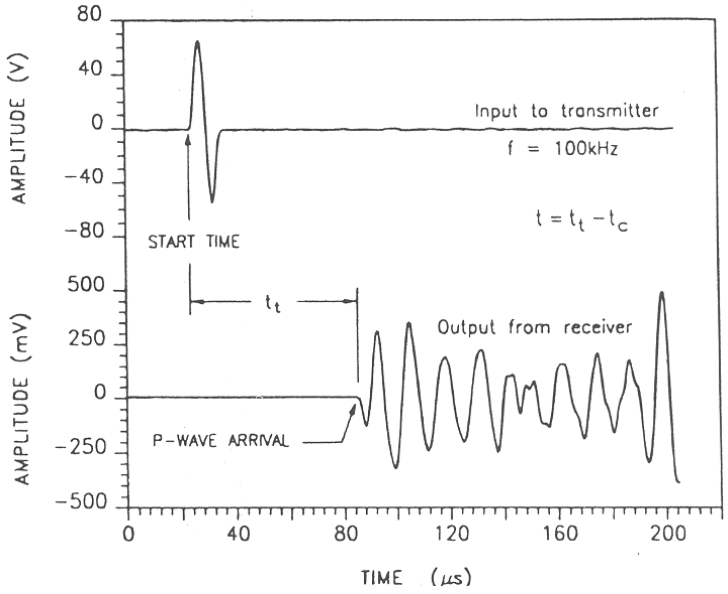

Figure 3.4. Piezoelectric disk response to a sinusoidal input signal (from Brignoli et al., 1996).

Excitation voltage

The magnitude of the excitation voltage does not affect the shape of the received signal but affect the signal to noise ratio (SNR). Higher excitation voltage increases the SNR, which results in received waves with clearer arrivals (Leong et al., 2005). The excitation voltage is limited to a value that would not cause depolarization of piezoelectric transducers, which depends primarily on the thickness of the transducer (Brignoli et al., 1996 and Leong et al., 2005). Bennell et al. (1984), Dyvik and Madshus (1985), de Alba and Baldwin (1991), Brignoli et al. (1996), Rampello et al. (1997), Brocanelli and Rinaldi (1998), Viggiani and Atkinson, (1995a&b), Pennington et al. (2001), and Callisto and Rampello (2002) used an input wave of an amplitude of 10 volts to excite their bender elements. Piezoelectric disks are generally thicker than bender elements and can withstand higher voltages. Typical excitation voltages that have been

used to excite piezoelectric disks are 65 volts by Brignoli et al. (1996) and 240 volts by Bennell et al. (1984).

Excitation frequency

The magnitude of the excitation frequency affects the shape of the received signal, and thus the clarity of the wave arrival. For sinusoidal inputs, the transducer response is improved when the frequency of the input wave approaches the resonant frequency of the transducer-soil system (Agarwal and Ishibashi, 1991; Jovicic et al., 1996; Kawaguchi et al., 2001; and Lee and Santamarina, 2005). The determination of the optimum excitation frequency (the resonant frequency) depends on many factors such as the soil stiffness, the stiffness of the transducer, and the cantilever length in case of the bender elements (Lee and Santamarina, 2005). In addition, the state of stress in the soil being tested affects the resonant frequency of the transducer-soil system (Santamarina and Fam, 1997).

For shear wave velocity measurements, Brignoli et al. (1996) and Arulnathan et al. (1998) recommended examining the received signal for several excitation frequencies during each velocity measurement. This approach is particularly helpful for shear wave measurements because shear and compression waves are strongly coupled but travel at different frequencies. Accordingly, the shear wave velocity measurement should be performed at the frequency that results in the most clear wave arrival. Excitation frequencies ranging from 1 to 15 kHz have been widely used by researchers (Dyvik and Madshus, 1985; Agarwal and Ishibashi, 1991; de Alba and Baldwin, 1991; Viggiani and Atkinson, 1995a; Brignoli et al., 1996; Gajo et al., 1997; Cabarkapa et al., 1999; Pennington et al., 2001; Callisto and Rampello, 2002; and Theron et al., 2003). Kung et al. (2004) recommended using an input wave frequency that is larger than the resonant

frequency of the transducer-soil system (ranging from 10 to 15 kHz). For compression wave velocity measurements, Brignoli et al., (1996) recommended exciting the piezoelectric disk with the highest possible frequency, which would still result in a clear wave arrival, to develop constrained compression waves.

Calibration of piezoelectric transducers

Piezoelectric transducers should be calibrated to account for the delay time introduced in the measurements by the electronics, the transducers, and the coating materials that are used to ground and water proof the transducers. The calibration is conducted by placing the source and the receiver in direct contact and measuring the time between the initiation of the electric impulse sent to the source and the initial arrival of the received signal (Manke and Gallaway, 1966; de Alba and Baldwin, 1991; Brignoli et al., 1996; Gajo et al., 1997; Pennington et al., 2001; Santamarina et al., 2001; and Theron et al., 2003). The initial polarities of the received signals depend on the alignment and polarization directions of the transducers. The initial polarization of signals should be defined during calibration. In the calibration process, the absence of wave transmission paths other than through the soil specimen should be checked. This is conducted by setting up the equipment without a specimen and generating shear and compression waves by the source. If the equipment (oedometer or triaxial cell) is empty, no wave arrivals should be recorded by the receiver; while if the equipment is filled with water, the observed arrivals should correspond to the arrival of compressive waves in water (Brignoli et al., 1996 and Viggiani and Atkinson, 1997).

3.5 Interpretation of recorded waveforms

For the current study, sinusoidal waves were used to excite the piezoelectric transducers. The distance between the source and the receiver, L, and the time required for the wave to travel this distance, t, were measured and the wave velocity, V, was calculated as follows:

$$V = \frac{L}{t} \quad \text{(3.1)}$$

Moduli at small strains were calculated using the measured wave velocities. The shear modulus, G, was calculated based on the shear wave velocity, V_s, as follows:

$$G = \rho V_s^2 \quad \text{(3.2)}$$

where ρ is the mass density of the soil. The constrained modulus at small strains, M, was calculated based on the measured constrained compression wave velocity, V_p, as follows:

$$M = \rho V_p^2 \quad \text{(3.3)}$$

3.5.1 DETERMINATION OF TRAVEL TIME

The travel time for compression waves is easily determined in both saturated and unsaturated soils. This is because compression waves are the fastest propagating waves and the first ones to reach a receiver. Shear wave measurements require more care in analyzing the signal because compression waves might arrive before and during the arrival of shear waves. Therefore, the first deflection of the received signal may not correspond to the arrival of the shear wave but to the arrival of the compression wave or the near-field component of the shear wave explained in the next paragraph (Sanchez-

Salinero et al., 1986; Gohl and Finn, 1991; Viggiani and Atkinson, 1995a; Brignoli et al., 1996; Jovicic et al., 1996; Gajo et al., 1997; and Lohani et al., 1999).

3.5.1.1 Near-field effect

The near-field component of the shear wave is a transverse motion that has the following characteristics: propagates with the constrained compression wave velocity, has initial polarity opposite to the propagating shear wave (far-field component), and decays rapidly with increasing the number of wavelengths between the source and the receiver. These characteristics help in identifying the near-field component preceding the shear wave and thus identify the arrival of the shear wave as accurate as possible (Sanchez-Salinero at al., 1986 and Brignoli et al., 1996).

Numerous researchers have investigated the conditions required to minimize the effect of the near-field component on the determination of the shear wave arrival. Most of the studies concluded that the near-field effect is related to the number of wavelengths between the source and the receiver. The recommendations reported in these studies are summarized in Table 3.1.

Table 3.1. Recommendations for number of wavelengths between source and receiver to minimize near-field effect.

Reference	Recommendations
Sanchez-Salinero at al. (1986) de Alba and Baldwin (1991) Brignoli et al. (1996) Arulnathan et al. (1998) Puppala et al. (2006)	# wavelengths > 2
Modoni et al. (2000)	# wavelengths > 4
Jovicic et al. (1996) Jovicic and Coop (1997b) Blewett et al. (2000) Mohsin and Airey (2003) Leong et al. (2005)	Near-field effect decreases as the number of wavelengths increases
Gajo et al. (1997)	# wavelengths = (6 to 9)
Cabarkapa et al. (1999)	# wavelengths = (4.5 to 6.5)
Pennington et al. (2001)	# wavelengths ≈ 2
Theron et al. (2003)	# wavelengths > 1
Leong et al. (2005)	# wavelengths > 3

Other factors affecting the near-field component include the soil type, waveform, and the state of stress in the soil. Jovicic et al. (1996) mentioned that near-field effects would be worse in stiffer materials (higher velocities) as well as when using square waves (carried a whole spectrum of frequencies). Kawaguchiet al. (2001) found that the near-field effects were more pronounced at low pressures. Kung et al. (2004) recommended using input wave frequencies higher than the resonant frequency of the transducer-soil system to minimize near-field effects. Accordingly, it is preferable to excite the transducers with sinusoidal waves to minimize the near-field effects. In addition, for each test set up and soil type, the optimum number of wavelengths between

the source and the receiver should be determined to minimize the near-field effects during shear wave velocity measurements.

3.5.1.2 Approaches to determine total travel time

For the current research, three approaches were investigated to determine the total travel time of the transmitted waves using: (1) the first arrival of the received signal; (2) characteristic points (first peaks, first troughs, and zero-crossings) in input and output signals; (3) and cross-correlation between input and output signals.

Total travel time determined using the first arrival of the received wave has been defined as the time between the initiation of the electric impulse sent to the source and the first significant excursion in the received signal that has the proper polarity (Brignoli et al., 1996). An example of the travel time determined using the first arrival of the received signal is illustrated in Figure 3.5. This approach has been widely used to determine the travel time of transmitted waves (Manke and Gallaway, 1966; Sanchez-Salinero at al., 1986; Thomann and Hryciw, 1990; Brignoli et al., 1996; Gajo et al., 1997; Jovicic and Coop, 1997a; Cabarkapa et al., 1999; Pennington et al., 2001; Jung, 2005; Leong et al., 2005; Puppala et al., 2006; and Valle, 2006).

The total travel time determined using the characteristic points has been defined as the time between the first peaks, first troughs, or zero-crossings of the input and output signals. An example of the travel times determined using the characteristic points is illustrated in Figure 3.5. This approach has been widely used to determine the travel time of transmitted waves (Sanchez-Salinero at al., 1986; Marinho et al., 1995; Shibuya et al., 1997; Lohani et al., 1999; Callisto and Rampello, 2002; and Theron et al., 2003).

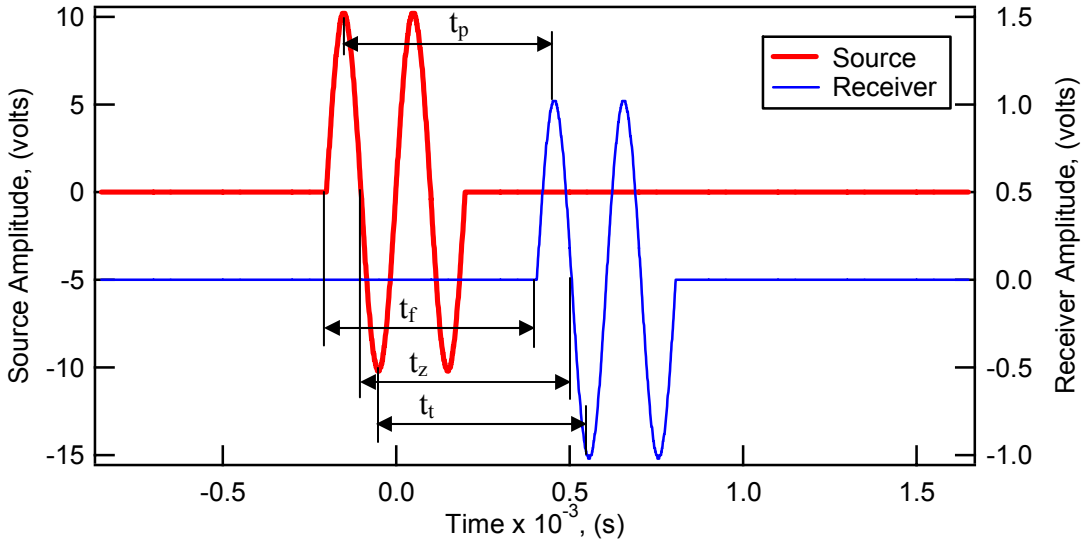

Figure 3.5. Travel times using first arrival (t_f) and characteristic points: first peaks (t_p), first troughs (t_t), and zero crossings (t_z).

Generally, the cross-correlation technique is applied to transmitted and received signals that are digitized and sampled at the same times. The transmitted signal is multiplied by the received signal, point by point, and the products are summed over the whole time record. The calculated sum represents one point in the cross-correlation sequence. Then, the received signal is shifted relative to the transmitted signal by a fixed Δt and the operation of multiplying and summing the two signals is repeated. If each of the transmitted and received signals consists of M data points, the cross-correlation sequence will consist of (2M-1) data points. Zero lag of the output correlation is in the middle of the sequence (at element M). The time interval between the peak and the middle of the cross-correlation sequence corresponds to the total time delay between both signals. An example of transmitted and received waveforms and the cross-correlation sequence is illustrated in Figure 3.6. Woods (1978), Sanchez-Salinero at al. (1986), Viggiani and Atkinson (1995a), Gajo et al. (1997), Jovicic and Coop (1997a), Santamarina and Fam (1997), Mohsin and Airey (2003), Lee and Santamarina (2005),

and Leong et al. (2005) investigated using this approach to determine the travel time of transmitted waves.

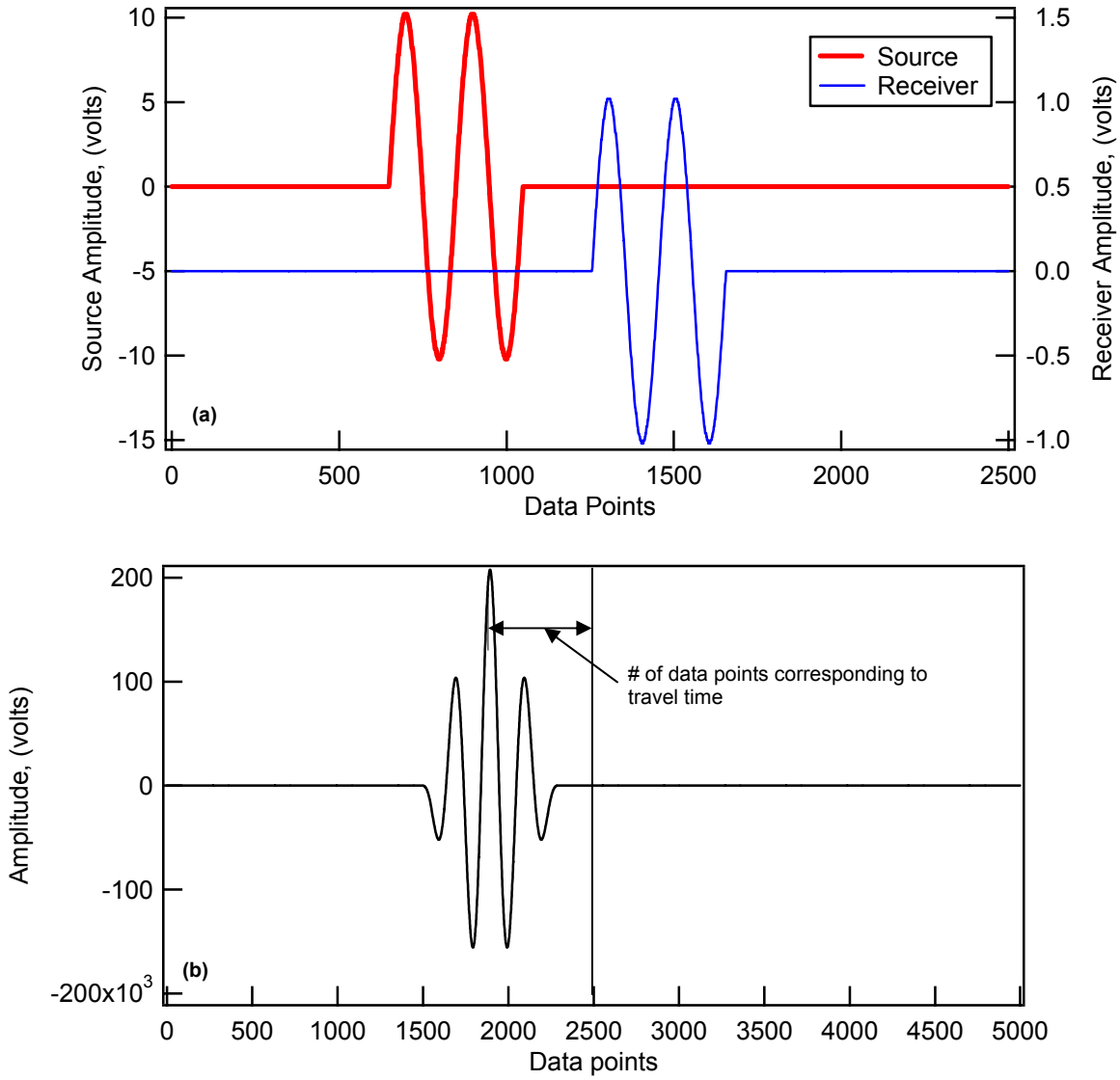

Figure 3.6. (a) Transmitted and received waveforms and (b) cross-correlation sequence.

An overview on the studies performed to investigate the three approaches to determine the travel time of transmitted waves is presented in this section. Brignoli et al. (1996) divided the forms of the recorded waves into three main waveforms shown in

Figure 3.7. Based on experimental studies, the authors concluded that the first arrival should be used to define the arrival of the shear wave and that the "X" arrival (Figure 3.7) preceding the shear wave arrival represented the near-field component. Leong et al. (2005) conducted experimental study to investigate the reliability of using the first arrival, characteristic points, and the cross-correlation technique to determine the travel times of transmitted waves. The authors concluded that the first arrival should be used to determine the travel times. They also concluded that travel times based on characteristic points and the cross-correlation method were unreliable.

Sanchez-Salinero at al. (1986) recommended using the characteristic points to avoid possible small personal errors in defining the arrival time based on the first arrival. Lohani et al. (1999) recommended using the characteristic points because the travel time remained relatively constant irrespective of the excitation frequency and near field effects. Kawaguchi et al. (2001) recommended using the first zero crossing point of the output signal as the arrival time. Kung et al. (2004) recommended using characteristic points to define the travel time on the condition that the excitation frequency is higher than the resonant frequency of the transducer-soil system.

Jovicic and Coop (1997a) discussed the validity of using the characteristic points to determine the travel time. The authors observed that the transmitted wave experienced gentle spreading as it traveled through the specimen. Therefore, the travel time based on the first arrival should be considered the closest to the correct travel time and the travel time based on characteristic points could be used only if it agreed with the travel time based on the first arrival.

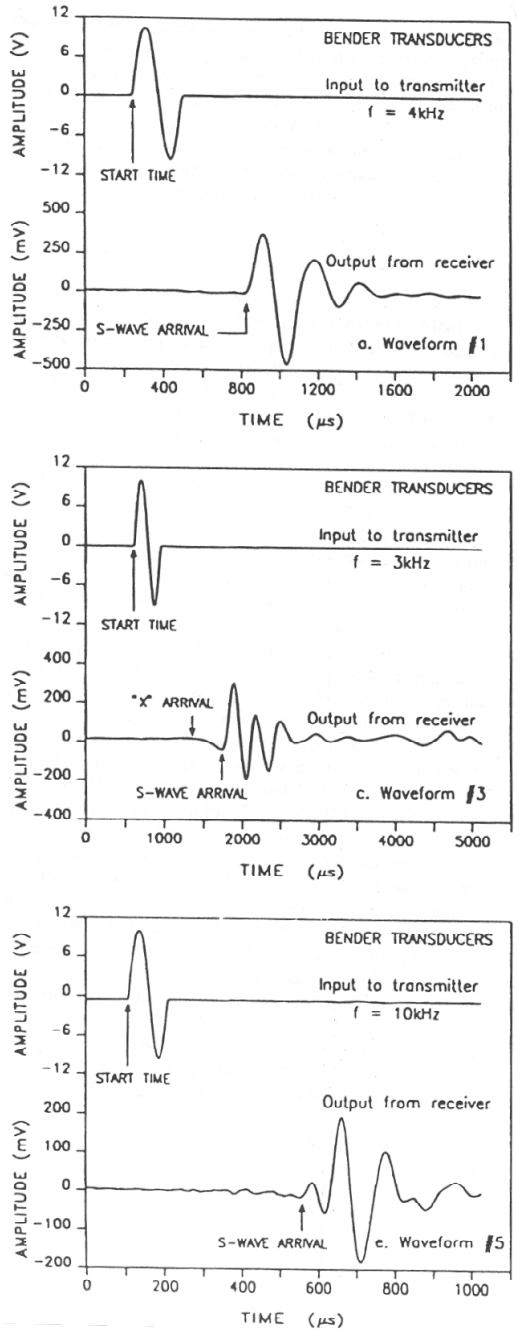

Figure 3.7. Typical examples of shear wave arrivals recorded in saturated soils (from Brignoli et al., 1996).

Viggiani and Atkinson (1995a) mentioned that: (1) the travel time could not be accurately determined from the first arrival due to near field effects; (2) the most accurate travel time was determined using the cross-correlation technique; (3) the use of the characteristic points to define the travel time was a simple alternative provided that it was proven first to be consistent with the travel time determined from the cross-correlation technique. Gajo et al. (1997) found that travel times were underestimated when the cross-correlation technique was used.

Sanchez-Salinero at al. (1986) mentioned that for successful use of the cross-correlation technique, transmitted and received waves should consist of only one predominant wave type. Santamarina and Fam (1997) pointed out that the cross-correlation method would produce correct travel times only if both waves were of the "same nature". Therefore, cross-correlation might not be the best idea to determine travel times when one of the received signals was the result of multiple travel paths and diffraction effects. Jovicic and Coop (1997a) mentioned that the cross-correlation technique could only be applied to determine the travel time if the shape of the transmitted and received wave were the same, therefore, the waves must be of predominantly one type, either compression or shear waves.

Mohsin and Airey (2003) found that using the cross-correlation technique provided a robust technique to automate the measurement of shear wave velocity. The authors emphasized that the travel time would correspond to the maximum peak in the cross-correlation sequence if transmitted and received waveforms were similar. However, if transmitted and received waveforms were not similar due to wave reflection and dispersion, one of the peaks in the cross-correlation sequence, but not necessarily the maximum peak, should correspond to the correct travel time. A visual check would be

required to select the peak that would coincide with the first arrival of the received wave. Arulnathan et al. (1998) mentioned that travel times obtained from characteristic points or cross-correlation between input and output signals were theoretically incorrect because of the effects of wave interference at the boundaries, phase lag or signal distortion, multi-dimensional wave travel, and near-field effects. The authors mentioned that the determination of the travel times using the first arrival was affected by errors due to multi-dimensional wave travel and near-field effects as well.

The conclusions drawn in previous studies regarding the approach to be used to determine the travel time of transmitted waves are somewhat contradicting. For the current research, the three approaches: first arrival, characteristic points, and cross-correlation technique are investigated.

3.5.2 DETERMINATION OF TRAVEL DISTANCE

In order to calculate the wave velocity through the specimen, the wave travel distance must be accurately defined. Piezoelectric disks might slightly protrude into the soil specimen while the bender elements protrude into the soil specimen by about one third of their total length. The distance used to calculate the wave velocity should be defined as the least distance between the crystals (from tip to tip). This distance is calculated by subtracting the length of each crystal that extended into the specimen from the specimen height (Dyvik and Madshus, 1985; Dyvik and Olsen, 1989; Thomann and Hryciw, 1990; Gohl and Finn, 1991; Marinho et al., 1995; Viggiani and Atkinson, 1995(a&b); Brignoli et al., 1996; Jovicic and Coop, 1997b; Shibuya et al., 1997; Arulnathan et al., 1998; Cabarkapa et al., 1999; Lohani et al.,1999; Kawaguchi et al., 2001; Pennington et al., 2001; Callisto and Rampello, 2002; Mohsin and Airey, 2003;

Kung et al., 2004; Zeng et al., 2004; Lee and Santamarina, 2005; and Puppala et al., 2006).

CHAPTER 4: BACKGROUND ON EFFECTS OF COMPACTION CONDITIONS ON THE STATE OF STRESS AND STIFFNESS OF UNSATURATED SOIL AT SMALL STRAINS

4.1 Introduction

Understanding the effects of compaction conditions and state of stress on soil stiffness at small strains is an important prerequisite to using soil stiffness to assess compactness of embankments and MSE walls. An overview of studies that have investigated the effect of compaction conditions on matric suction and the effect of compaction conditions and state of stress on the small strain stiffness of unsaturated soils are presented in this chapter.

4.2 Effects of compaction conditions on matric suction

The effects of water content, dry unit weight, degree of saturation, compaction energy, and compaction technique on the matric suction ($u_a - u_w$) of compacted soils have been investigated in several studies. Data reported in previous studies regarding the effect of compaction conditions on the matric suction was somewhat in agreement with few exceptions. All studies reported in this section agreed on the fact that the matric suction decreases as the water content increases. Mou and Chu (1981) showed that for water contents dry of optimum, a slight decrease in the water content resulted in a substantial increase in the matric suction.

The majority of previous studies performed to study the effect of compaction conditions on the matric suction agreed that the matric suction was primarily dependent on the compaction water content. Croney and Coleman, (1954) noted that the relationship

between the matric suction and the water content appeared to be unique regardless of the soil structure. Olson and Langfelder (1965), Krahn and Fredlund, (1972), Fredlund and Rahardjo (1993), Tsai and Petry (1995), Wan et al. (1995), Bernier et al. (1997), Sivakumar and Wheeler (2000), and Agus and Schanz (2006) showed that for compacted soils, the matric (or total) suction was primarily dependent on the compaction water content and almost independent of the dry unit weight as shown in Figure 4.1.

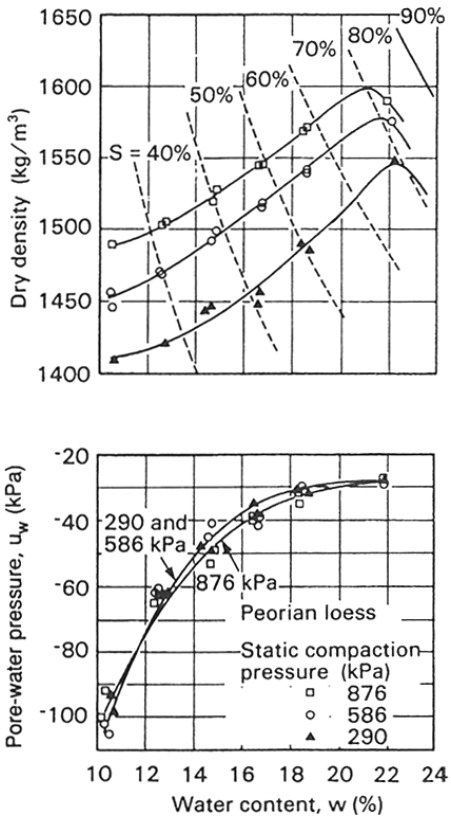

Figure 4.1. Effect of compaction water content and dry unit weight on matric suction for compacted Goose Lake clay (from Olson and Langfelder, 1965).

Agus and Schanz (2006) suggested vertical suction isolines on the Proctor compaction curves indicating that the suction was mainly function of the compaction water content as shown in Figure 4.2. The Proctor compaction curve and matric suction

measurements reported by Gonzalez and Colmenares (2006) are presented in Figure 4.3. The authors plotted contours of constant suction. The suction contours were nearly vertical at low dry unit weights and tended to curve to the left at high dry unit weights. Above the optimum water content of the standard energy, the contour curves became asymptotic to the 100% degree of saturation line. The authors concluded that the matric suction depended mainly on the water content with some influence of the dry unit weight and the compaction technique (static or dynamic) in less extent.

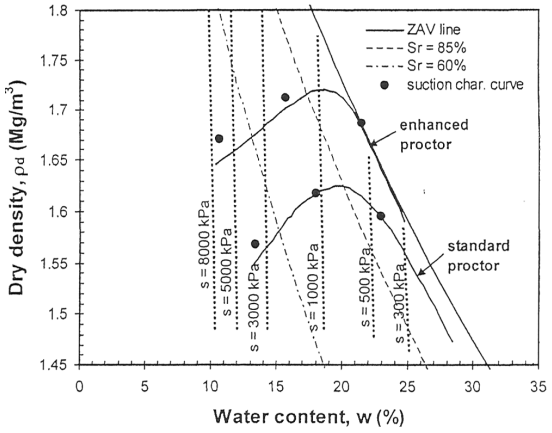

Figure 4.2. Proctor compaction curves, initial compaction water content and dry unit weight of tested specimens, and suction isolines (from Agus and Schanz, 2006).

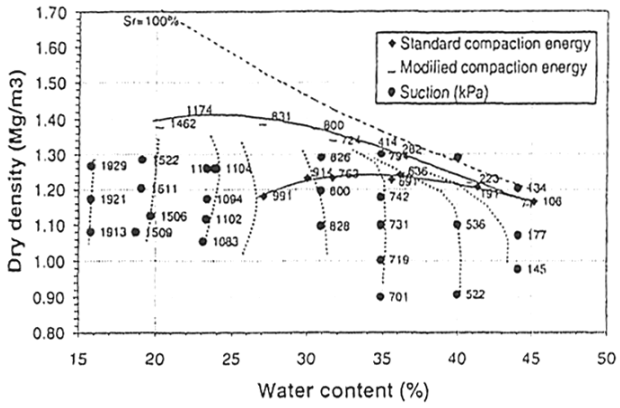

Figure 4.3. Proctor compaction curves, initial compaction water content and dry unit weight of tested specimens, and suction contours (from Gonzalez and Colmenares, 2006).

On the other side, Shackel (1973) mentioned that the matric suction depended primarily on the degree of saturation and was slightly influenced by the dry unit weight. Yong (1980) observed that for a given soil, there was a single soil-water potential surface (i.e., total suction), which shows the relationship between the water content, dry unit weight, and soil-water potential.

Data reported in previous studies concerning the effect of the compaction dry unit weight on the matric suction at constant water content was contradicting. Mou and Chu (1981) mentioned that for specimens compacted at the same water content, the matric suction increased slightly for specimens compacted at higher unit weights. Sudhakar and Revanasiddappa (2003) mentioned that at a constant water content, the matric suction decreased as the compaction dry unit weight increased.

The effect of the compaction dry unit weight and degree of saturation on the matric suction was investigated by Sudhakar and Revanasiddappa (2000) and Gonzalez and Colmenares (2006). In both studies, the authors agreed that at a constant dry unit weight, the matric suction decreased with increasing the compaction degree of saturation;

and at a constant degree of saturation, the matric suction increased as the compaction dry unit weight increased as shown in Figure 4.4.

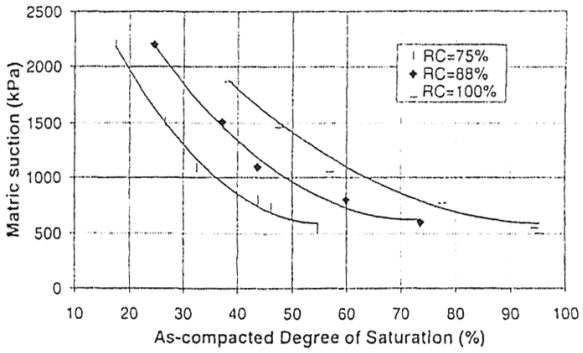

Figure 4.4. Effect of compaction degree of saturation and dry unit weight on the matric suction (from Gonzalez and Colmenares, 2006).

4.3 Effects of compaction conditions on stiffness at small strains

The effects of water content, dry unit weight, degree of saturation, compaction energy, and compaction technique on the behavior of compacted soils at small strains have been investigated in several studies. Stiffness at small strains has been studied in terms of shear wave velocity (V_s) (or shear modulus, G_{max}) and compression wave velocity (V_p) (or constrained modulus, M_{max}).

4.3.1 SHEAR WAVE VELOCITIES

Data reported in previous studies regarding the effect of the compaction water content on the shear wave velocity (or shear modulus) was contradicting. Ooi and Pu (2002, 2003) mentioned that the shear modulus reached maximum value at water contents dry of optimum for specimens compacted at the same compactive effort. Inci et al. (2003) and D'Onforio and Penna (2003) showed that for specimens compacted at the same compactive effort, the shear wave velocity was observed to peak at the optimum

water content. On the other side, Sawangsuriya et al. (2006) showed that the shear modulus at small strains increased as the compaction water content decreased for specimens compacted at water contents ranging between ± 4% of optimum water content using the standard Proctor effort as shown in Figure 4.5.

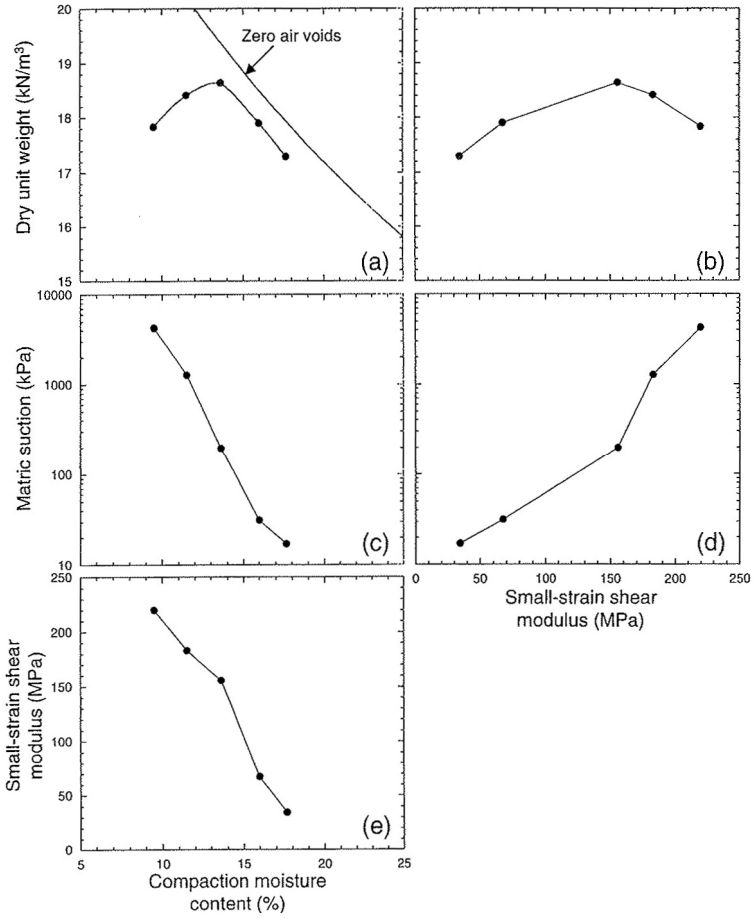

Figure 4.5. Results of stiffness testing on compacted clayey sand: (a) compaction curve, (b) dry unit weight versus stiffness, (c) matric suction versus compaction water content, (d) stiffness versus matric suction, and (e) stiffness versus compaction water content (from Sawangsuriya et al., 2006).

Data reported in previous studies regarding the effect of the compaction dry unit weight on the shear modulus was contradicting. Stephenson (1978) reported that for a given degree of saturation, the shear modulus decreased with increasing the void ratio as shown in Figure 4.6. Ooi and Pu (2002, 2003) mentioned that the stiffness increased as the dry unit weight increased until the peak stiffness associated with a particular compactive effort was attained, then a rapid drop in the stiffness was observed for further increase in the dry unit weight. This reduction was associated with water contents wet of peak stiffness as shown in Figures 4.7 and 4.8. Sawangsuriya et al. (2006) reported that no particular trend was observed for the variation of the shear modulus with the dry unit weight as shown in Figure 4.5.

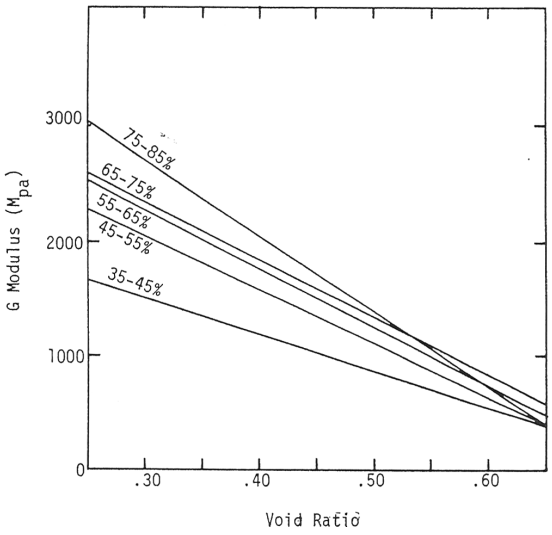

Figure 4.6. Effect of void ratio and degree of saturation on shear modulus at small strains (from Stephenson, 1978).

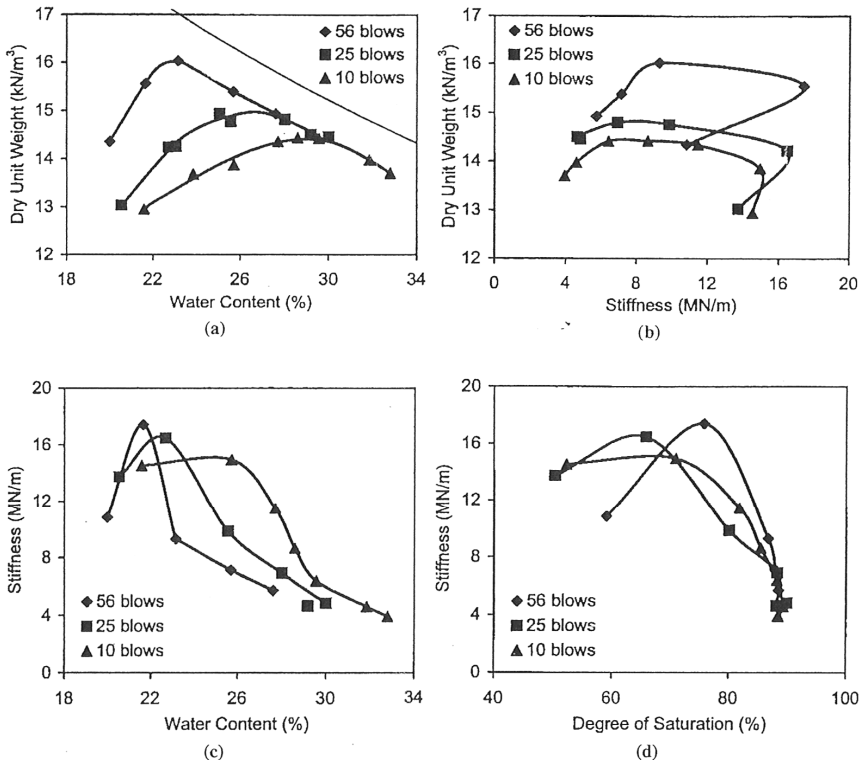

Figure 4.7. Results of stiffness testing on compacted silt: (a) compaction curves, (b) dry unit weight versus stiffness, (c) stiffness versus water content, and (d) stiffness versus degree of saturation (from Ooi and Pu, 2003).

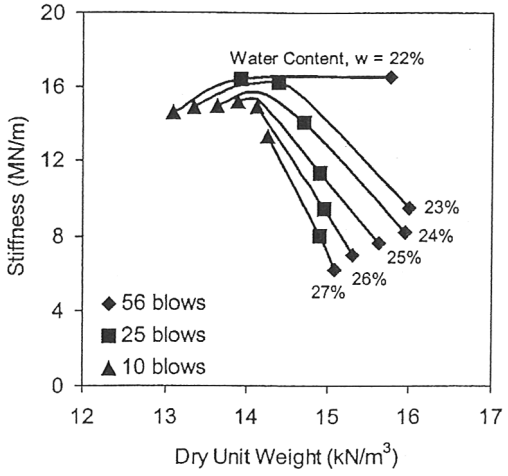

Figure 4.8. Variation of stiffness with dry unit weight at constant water content (from Ooi and Pu, 2003).

Data reported in previous studies regarding the effect of the compaction degree of saturation on the shear wave velocity (or shear modulus) was contradicting. Stephenson (1978) showed that at a constant void ratio, the shear modulus increased with increasing the degree of saturation as shown in Figure 4.6. Wu et al. (1984) and Qian et al. (1991) mentioned that at a constant void ratio, maximum values for shear moduli were observed at degrees of saturation ranging from 5 to 20% as shown in Figures 4.9 and 4.10. Ooi and Pu (2002, 2003) showed that stiffness values peaked within degrees of saturation ranging from 66 to 76% as shown in Figure 4.7.

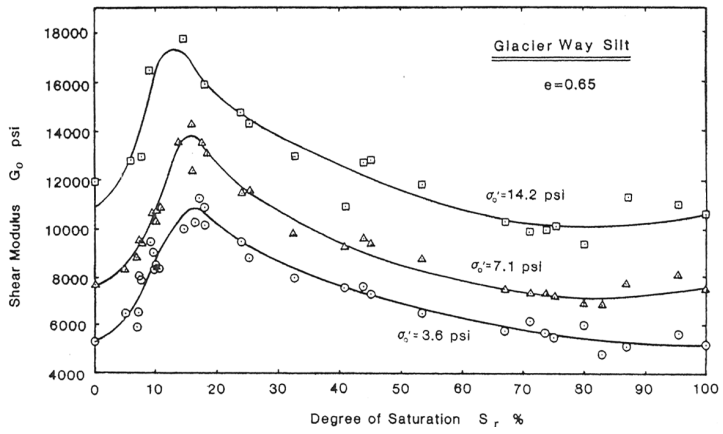

Figure 4.9. Effect of degree of saturation on shear modulus at small strains (from Wu et al., 1984).

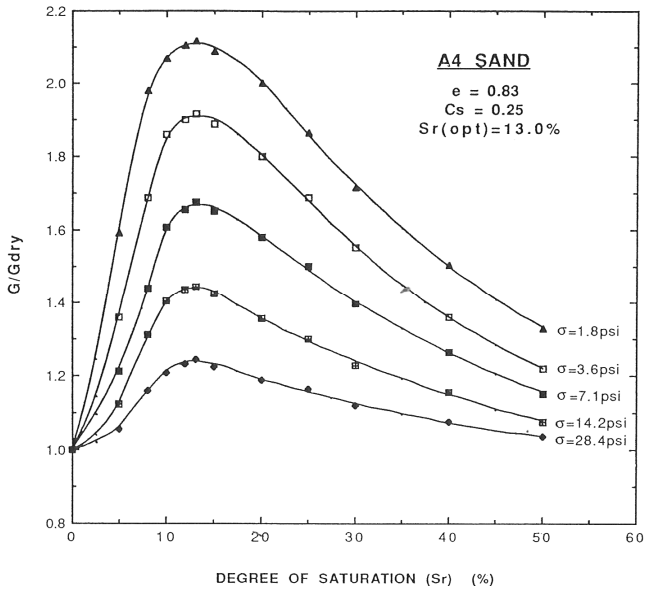

Figure 4.10. Effect of degree of saturation and confining pressure on shear modulus ratio, G_{max}/G_{dry}, (from Qian et al., 1991).

Data presented in literature concerning the effects of compaction conditions on the shear wave velocity at small strains are contradicting. In the current research, the effects of the compaction conditions on the shear wave velocity are further investigated.

4.3.2 COMPRESSION WAVE VELOCITIES

Data reported in previous studies regarding the effect of the compaction water content on the compression wave velocity agreed to some extent. Leslie (1950), Sheeran et al. (1967), Yesiller et al. (2000), and Inci et al. (2003) reported that for specimens compacted at the same compactive effort, the maximum compression wave velocity occurred at the optimum water content as shown in Figures 4.11 and 4.12. Manke and Gallaway (1966) mentioned that maximum compression wave velocity occurred at water contents within 1 to 1.5% dry of optimum for specimens compacted at the same compactive effort as shown in Figure 4.13.

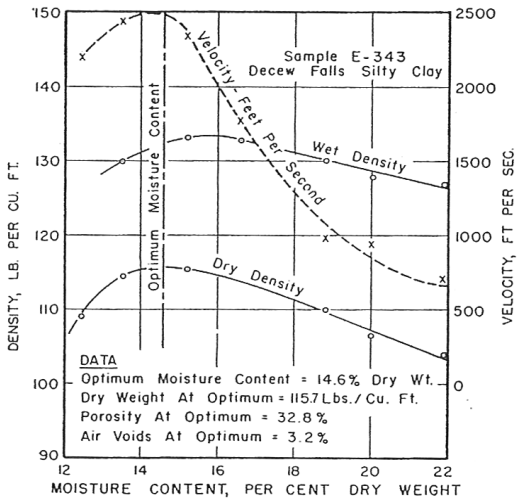

Figure 4.11. Effect of compaction water content and dry unit weight on compression wave velocity (from Leslie, 1950).

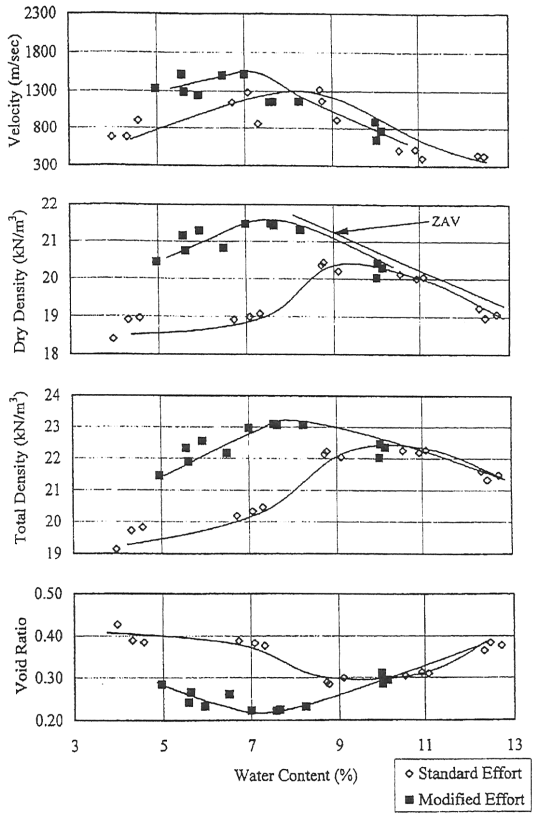

Figure 4.12. Variation of compression wave velocity and dry unit weight with water content (from Yesiller et al., 2000).

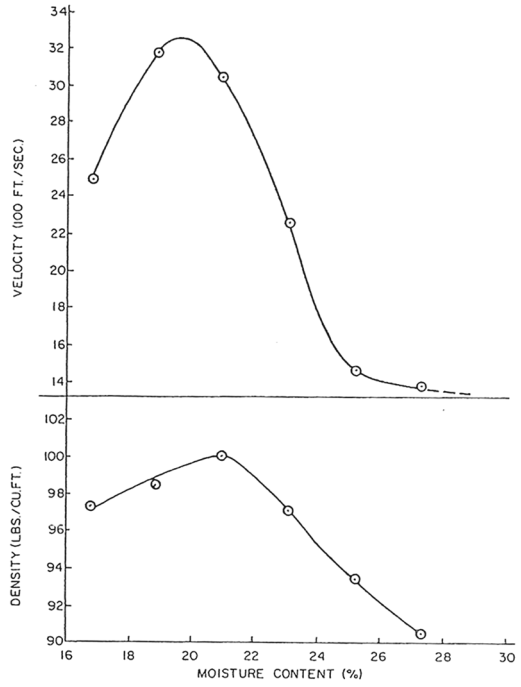

Figure 4.13. Effect of compaction water content and dry unit weight on compression wave velocity (from Manke and Gallaway, 1966).

Data reported in previous studies regarding the effect of the compaction dry unit weight on the compression wave velocity was contradicting. Leslie (1950) mentioned that at optimum water content, the compression wave velocity increased as the dry unit weight increased. Stephenson (1978) noted that for a given degree of saturation, compression wave velocity decreased with increasing the void ratio as shown in Figure 4.14. Yesiller et al. (2000) reported that the compression wave velocity increased with increasing the dry unit weight as shown in Figure 4.15. On the other side, Sheeran et al. (1967) showed that for constant water contents, the compression wave velocity increased as the dry unit weight increased until the optimum water content associated with a particular compactive effort was reached, then a rapid drop in the compression wave velocity was observed for further increase in the dry unit weight as shown in Figure 4.16.

In addition, Sheeran et al. (1967) observed that for specimens compacted dry of optimum, the product of the compaction water content and the compression wave velocity increased linearly as the dry unit weight increased as shown in Figure 4.17.

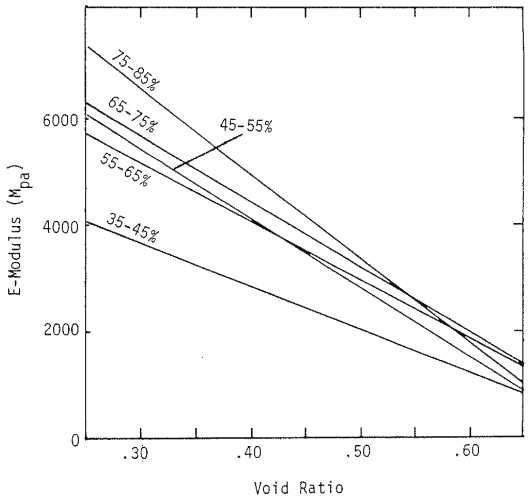

Figure 4.14. Effects of void ratio and degree of saturation on small strain unconstrained modulus (from Stephenson, 1978).

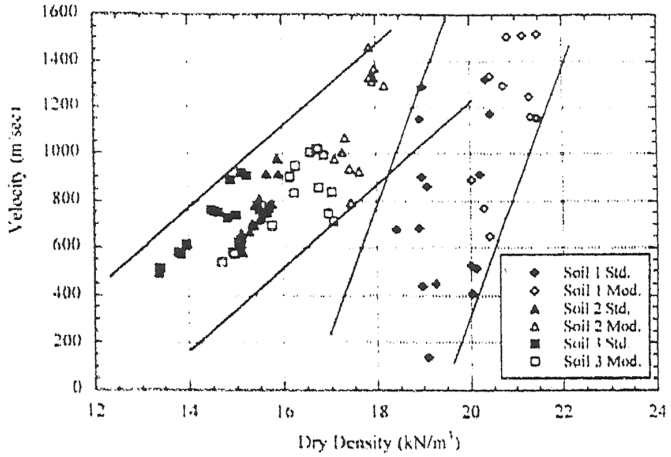

Figure 4.15. Effect of dry unit weight on compression wave velocity (from Yesiller et al., 2000).

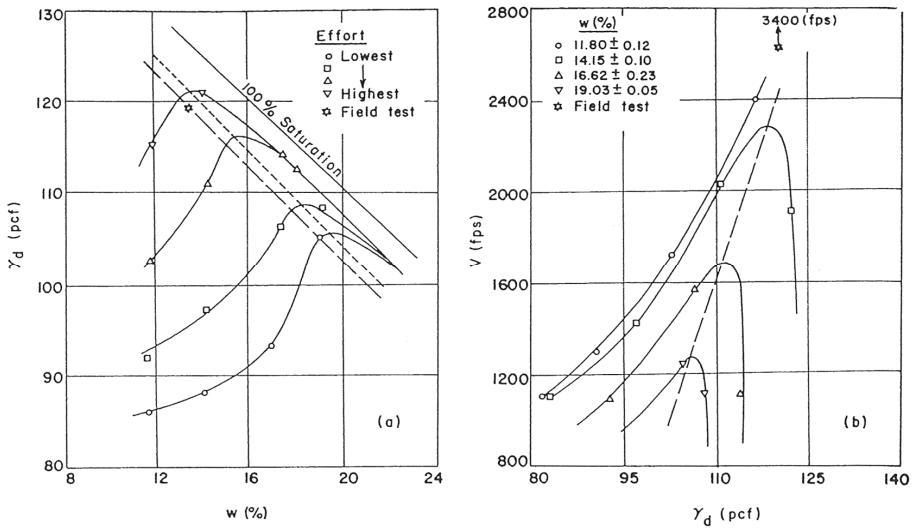

Figure 4.16. Effect of compaction water content, dry unit weight, and compactive effort on compression wave velocity (from Sheeran et al., 1967).

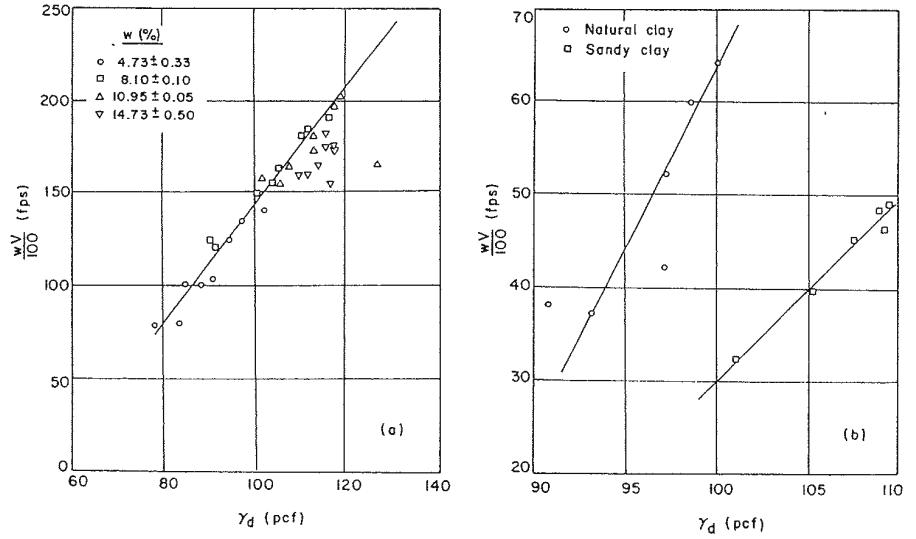

Figure 4.17. Effect of dry unit weight on the product of the compression wave velocity and the compaction water content (from Sheeran et al., 1967).

The effect of the compaction degree of saturation on the compression wave velocity was studied by Stephenson (1978). The author mentioned that at a constant void ratio, the compression wave velocity increased with increasing the degree of saturation as shown in Figure 4.14.

Data presented in literature concerning the effects of compaction conditions on the compression wave velocity at small strains are contradicting. In the current research, the effects of the compaction conditions on the compression wave velocity are further investigated.

4.4 Effect of state of stress on stiffness at small strains

The effect of the state of stress on the stiffness of compacted soils at small strains has been investigated in several studies. Stiffness at small strains has been studied in terms of shear wave velocity (V_s) (or shear modulus (G_{max})). The state of stress for unsaturated soil has been generally expressed in terms of two stress state variables: net normal stress ($\sigma - u_a$) and matric suction ($u_a - u_w$).

The data reported in previous studies regarding the effect of the matric suction on the shear wave velocity (or shear modulus (G_{max})) at constant net stress is contradicting. Picornell and Nazarian (1998), Vinale et al. (1999), Vassalo and Mancuso (2000), and Mancuso et al. (2002) showed that for specimens compacted at the same compaction conditions, the shear modulus increased as suction increased up to a certain suction value beyond which the soil stiffness stopped increasing as shown in Figure 4.18 and 4.19. On the other side, Cabarkapa et al. (1999), Leong et al. (2006), and Sawangsuriya et al. (2006) reported continuous increase in the soil stiffness with increasing the matric suction as shown in Figures 4.20 and 4.21. Sawangsuriya et al. (2006) noted that for the same

matric suction and net stress, the shear modulus at small strains increased as the compaction water content decreased.

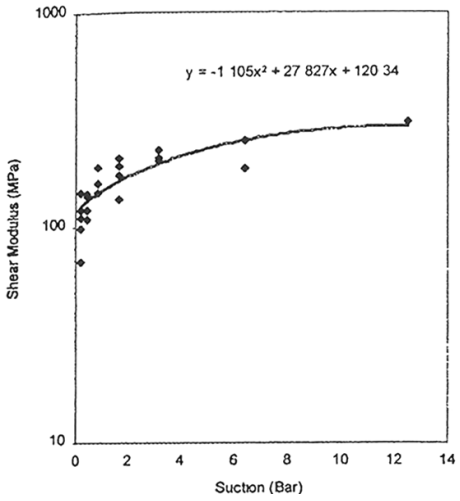

Figure 4.18. Variation of shear modulus at small strains with matric suction (from Picornell and Nazarian, 1998).

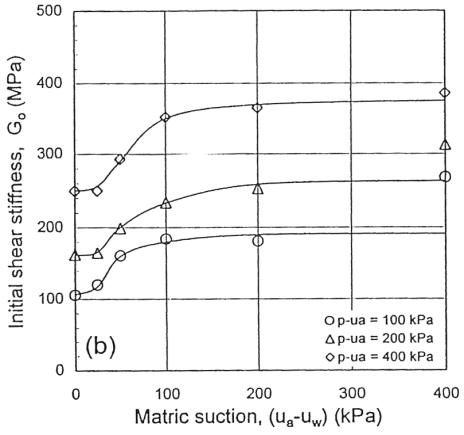

Figure 4.19. Variation of shear modulus at small strains with matric suction at constant mean net stress (from Vinale et al., 1999).

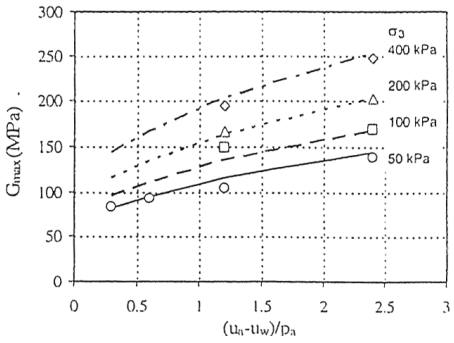

Figure 4.20. Variation of shear modulus at small strains with matric suction (from Leong et al., 2006).

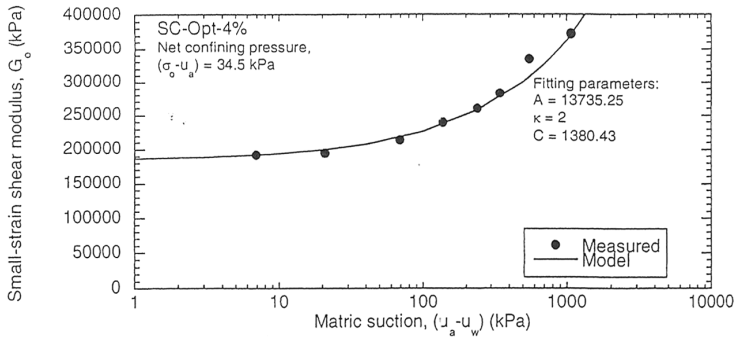

Figure 4.21. Variation of shear modulus at small strains with matric suction at constant net stress (from Sawangsuriya et al., 2006).

The variation of the soil stiffness with the variation of matric suction upon drying of specimens was investigated in several studies. Marinho et al. (1995) mentioned that soil stiffness increased with increasing the matric suction up to a certain suction value, beyond which soil stiffness either decreased or stopped increasing as shown in Figure 4.22. However, Cho and Santamarina (2001), Mendoza et al. (2005), and Mendoza and Colmenares (2006) observed continuous increase in the soil stiffness upon drying. Cho and Santamarina (2001), Mendoza et al. (2005), and Mendoza and Colmenares (2006) attributed the increase of the soil stiffness at low degrees of saturation to the capillary stresses.

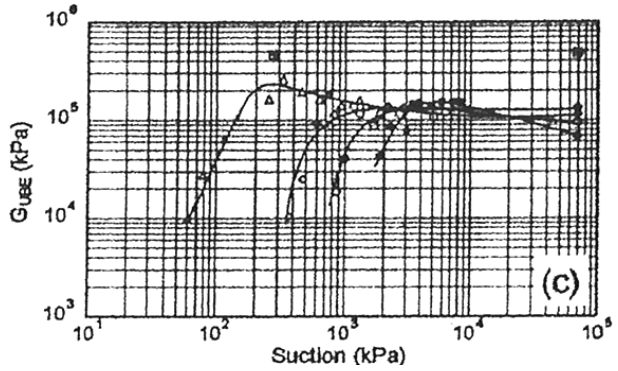

Figure 4.22. Variation of shear modulus at small strains with matric suction (from Marinho et al., 1995).

The data reported in previous studies regarding the effect of the net stress on the shear modulus (G_{max}) at constant matric suction is in agreement. Cabarkapa et al. (1999), Vinale et al. (1999), Vassalo and Mancuso (2000), Mancuso et al. (2002), and Vassalo et al. (2006) reported that at constant matric suction, the shear modulus at small strains increased with increasing the mean net stress as shown in Figures 4.23 and 4.24.

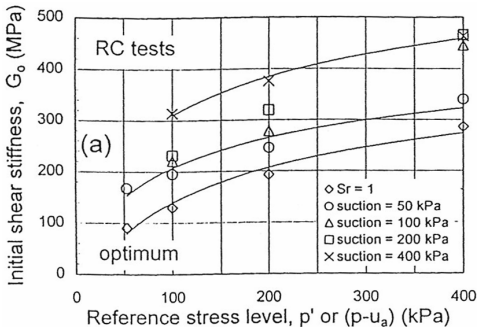

Figure 4.23. Variation of shear modulus at small strains with mean net stress at constant matric suction (from Vinale et al., 1999).

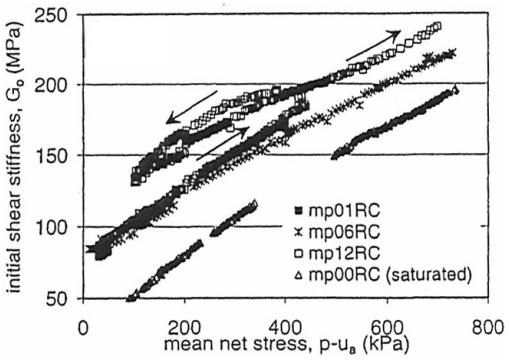

Figure 4.24. Variation of shear modulus at small strains with net stress at constant matric suction (from Vassalo et al., 2006).

Mancuso et al. (2002) investigated the effect of matric suction (at constant net stress) and the effect of the net stress (at constant matric suction) on the shear modulus. The authors plotted the shear modulus versus the net stress and the matric suction on a 3-D plot shown in Figure 4.25.

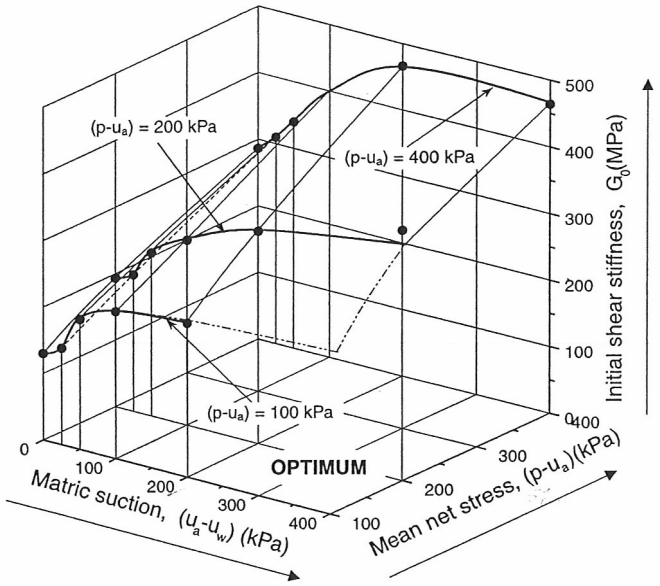

Figure 4.25. Variation of shear modulus at small strains with matric suction and mean net stress (from Mancuso et al., 2002).

Data reported in the literature concerning the effect of the matric suction on the shear wave velocity (or shear modulus) at constant net stress is somehow inconsistent. In the current research, the effect of the matric suction on shear and compression wave velocities at constant net stress is further investigated. In the literature, the effect of increasing the net stress on the shear wave velocity (or shear modulus) at constant matric suction was investigated for coarser silts and sands. No data has been reported for clays due to the long testing periods necessitated by the low hydraulic conductivity of clays. In the research presented in this dissertation, the effect of the net stress on shear and compression wave velocities is investigated for compacted clays.

CHAPTER 5: PHYSICAL PROPERTIES OF TEST SOIL AND SPECIMEN PREPARATION

5.1 Introduction

The soil selected for testing represented a typical clay fill material used by The Texas Department of Transportation (TxDOT) for construction of embankments. The soil was obtained from an active TxDOT construction site (Austin, Texas) in June 2004. The physical properties of the test soil along with the procedure followed for specimen preparation are presented in this chapter.

5.2 Physical properties of test soil

The grain size distribution, Atterberg limits, specific gravity, and compaction moisture-density relationships for the test soil are presented in the following sections.

5.2.1 GRAIN SIZE DISTRIBUTION

Large lumps of clay and oversized particles were observed in the clay fill material upon visual inspection. The large lumps of clay were manually broken into smaller pieces and then sieved through a No. 4 (4.75 mm) sieve. The soil retained on the No. 4 sieve was discarded. The soil that passed through the No. 4 sieve consisted of lumps of clay lumps and coarse-grained particles. This soil was then ground using a pulverizer (Bico Inc., model UD). The pulverized soil consisted of clay particles and crushed coarse-grained particles. A sample of the test soil was washed through sieve No. 200 (75 μm) to determine the percentage of fines (particles with diameters smaller than 75 μm) according to the procedure outlined in ASTM C 117. The percentage of fines in the test soil was about 61%. The grain size distribution of the processed soil retained on the No.

200 sieve after washing was determined in accordance with ASTM D 422. A hydrometer test was performed on the processed soil according to the procedure outlined in ASTM D 422. The clay fraction in the test soil was about 23%. The grain size distribution of the test soil is shown in Figure 5.1.

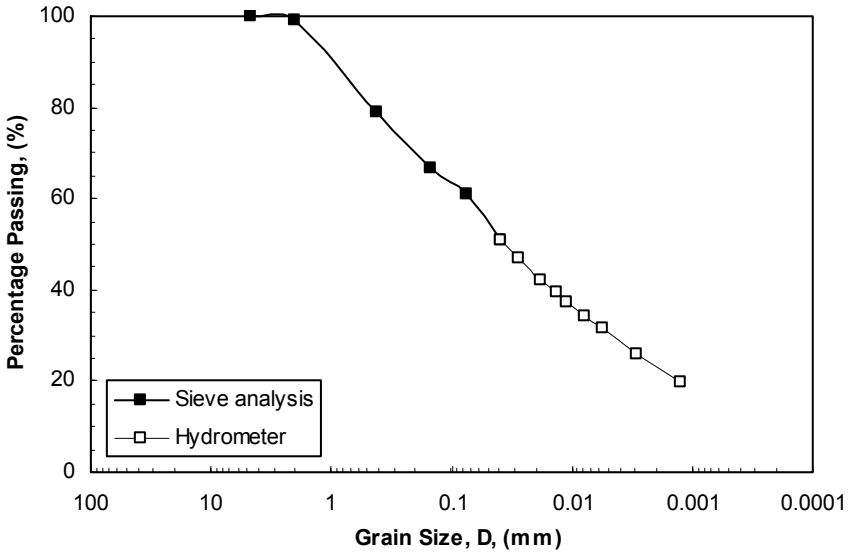

Figure 5.1. Grain size distribution of the test soil.

5.2.2 ATTERBERG LIMITS

Atterberg limits of the test soil were determined according to the procedure outlined in ASTM D 4318. The soil had a liquid limit of 37.5% and a plasticity index of 17%. The liquid limit was also determined for a sample of soil that was dried overnight in an oven at 110 degrees Celsius. The liquid limit of the oven-dried soil was 36%, which is less than the liquid limit before oven drying by about 4%. The results of the liquid limit tests performed on the test soil before and after oven drying is shown in Figure 5.2. According to the Unified Soil Classification System (USCS) (ASTM D 2487), clay is to be considered organic if the liquid limit decreases by more than 25% when oven-dried.

Thus, the soil does not appear to be organic. The soil was classified as low plasticity clay (CL) according to the Unified Soil Classification System (USCS) (ASTM D 2487).

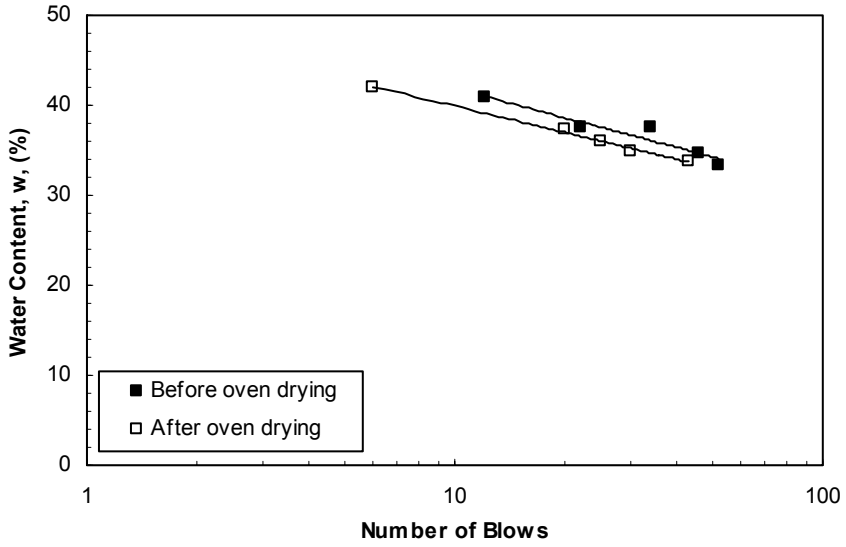

Figure 5.2. Liquid limit test results of test soil before and after oven drying.

5.2.3 SPECIFIC GRAVITY

Two specific gravity measurements were performed in accordance with ASTM D 854. The specific gravity values from the two measurements were 2.69 and 2.71 with an average value of 2.70.

5.2.4 MOISTURE-DENSITY RELATIONSHIP

Standard and modified Proctor compaction tests were performed according to the procedures outlined in ASTM D 698 and ASTM D 1557, respectively, to determine the compaction moisture-density relationships for the soil. The standard Proctor optimum water content was approximately 19% with a corresponding maximum dry unit weight of 106 pcf. The modified Proctor optimum water content was approximately 13% with a

corresponding maximum dry unit weight of 116 pcf. The standard and modified Proctor compaction curves are shown with the zero air voids curve in Figure 5.3.

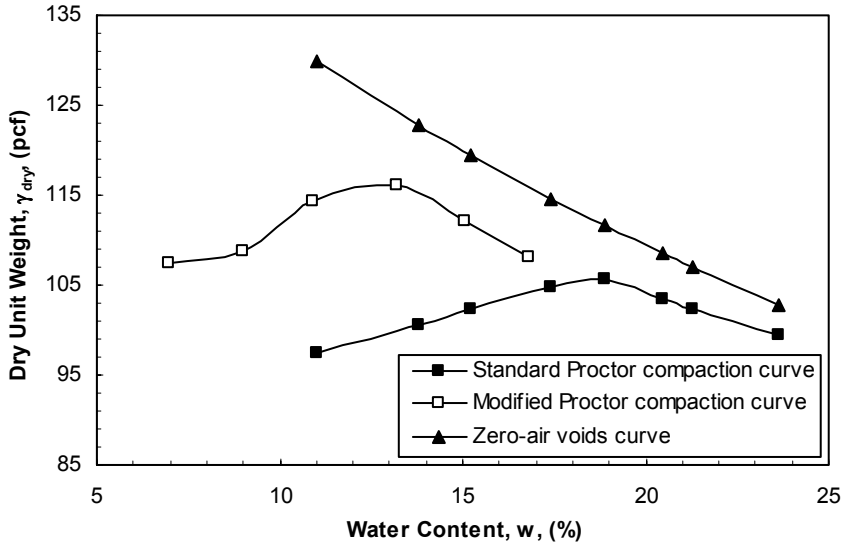

Figure 5.3. Standard and modified Proctor compaction curves of the test soil.

5.3 Specimen preparation

Specimens to be tested in the undrained triaxial apparatus or in the suction-controlled triaxial apparatus were prepared by kneading compaction. The compacted specimens were 2 inches in diameter and 4.6 inches tall. For the pressure plate tests, the specimens were trimmed from the 4.6 inches tall specimens to a final height of 0.6 inch. The soil was mixed with water to moisture contents ranging from approximately 10 to 25%. Once mixed, the soil was sealed in plastic bags, and the water content was allowed to equilibrate in the soil for at least 16 hours in a sealed contained prior to compaction as specified by ASTM D 698, ASTM D 1557, and ASTM D 2850. The compaction mold and the procedure followed to compact the specimens are described in the following sections.

5.3.1 COMPACTION MOLD

The soil was compacted in an aluminum split mold that was designed and fabricated at The University of Texas at Austin. The mold consisted of four quadrants, a base, and a collar as shown in Figure 5.4. The split mold was disassembled after compaction and the specimen was removed. The base of the mold had extrusions equal in size to the bender elements and disks that extruded from the end platens of the triaxial cells. This was done to facilitate insertion of the bender elements and disks into the specimens. Further details of the design of the split mold are presented in Appendix A.

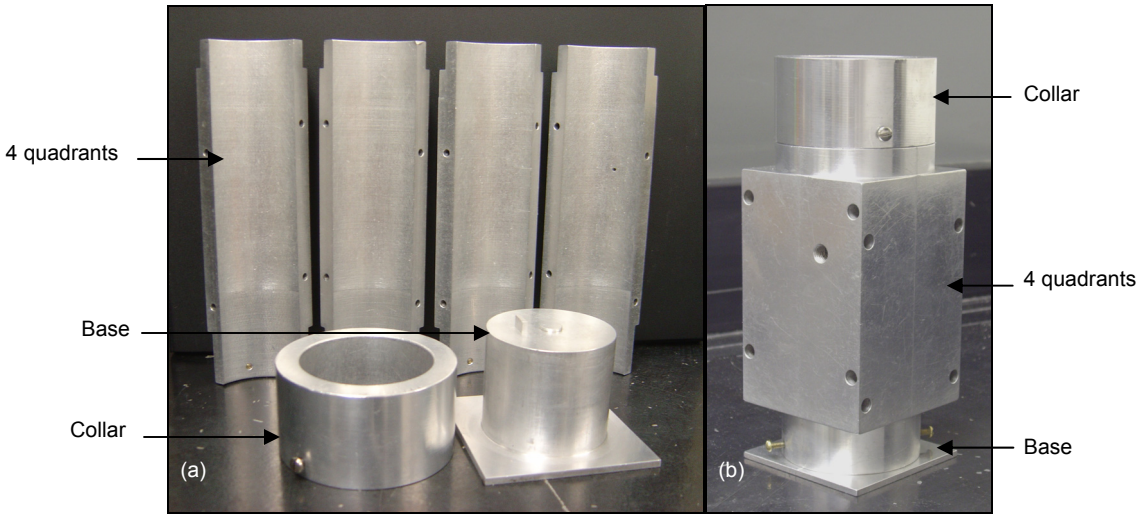

Figure 5.4. Compaction split mold: (a) disassembled and (b) assembled.

5.3.2 COMPACTION PROCEDURE

Test specimens were compacted using a Marsh-Bellofram, model 980-077-000 air piston with an attached ½-inch diameter tamping rod as shown in Figure 5.5. The air piston consists of a polyester fabric reinforced Nitrile diaphragm separating between an aluminum shell and an aluminum end cap. Prior compaction, air pressure was applied on one side of the air piston to push the attached aluminum tamping rod outwards by a

maximum distance of 1.75 inches. The kneading action was performed by pushing the aluminum rod manually downwards into the soil against the applied air pressure until the tamping rod started to move in the opposite direction.

Figure 5.5. Kneading compaction set-up.

Specimens were compacted in six lifts as specified by ASTM D 2850. A series of trial compaction tests was performed to determine the combination of number of blows per lift and kneading pressure required to reach the desired unit weights. Twenty-five blows per lift were eventually selected. The pressure applied to the air piston ranged from 10 to 40 psi to prepare specimens at different dry unit weights ranging from 90 to 115 pcf. Once the specimen was compacted, the top of the specimen was trimmed flush with the top of the mold. The base of the mold was then disassembled and pushed into the top of the specimen to form bender element and disk intrusions into the top of the specimen. A vertical groove marked on the side and on the bottom of the base of the mold was used to align the top and bottom intrusions. Once the top of the specimen was finished, the

mold was disassembled and the specimen was removed and wrapped in saran. Specimens were allowed to sit for at least one day in a sealed container prior testing.

CHAPTER 6: PRESSURE PLATE TEST APPARATUS AND PROCEDURE

6.1 Introduction

Two pressure plate apparatus were designed and fabricated for this study to measure soil matric suction. Details of the apparatus and the testing procedures followed to perform pressure plate tests are described in this chapter.

6.2 Apparatus

A schematic diagram of the apparatus used to perform the pressure plate tests is shown in Figure 6.1.

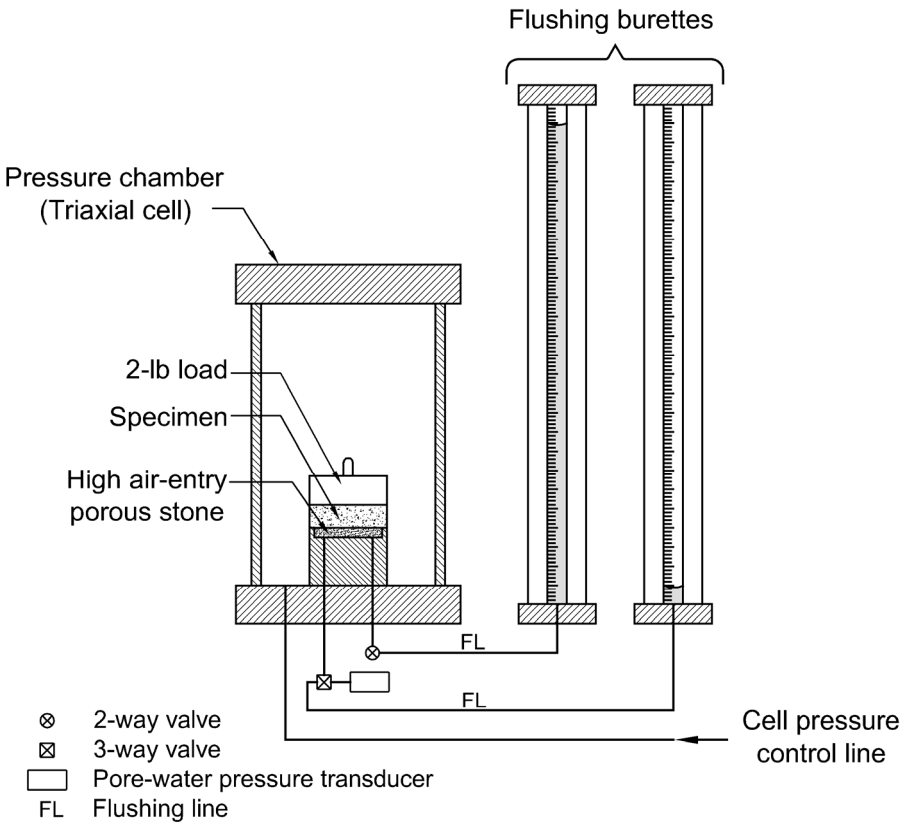

Figure 6.1. Schematic diagram of apparatus used to perform pressure plate tests.

The apparatus consists of an acrylic platen equipped with a high air-entry porous stone mounted in a standard triaxial cell. Two acrylic platens with diameters of 2 inches were designed and fabricated at The University of Texas at Austin. Each platen has a cavity where the high air-entry porous stone was placed and sealed on the sides using a Soilmoisture Equipment Corp., model 0980V004 two-component epoxy resin. One platen is equipped with a Soilmoisture Equipment Corp., model 0604D01.5-B05M1 5-bar high air-entry porous stone; and the other platen is equipped with a Soilmoisture Equipment Corp., model 0604D01.5-B15M1 15-bar high air-entry porous stone. The epoxy is a special epoxy that had an air-entry value of over 15 bars. The diameter of the cavity is larger than the diameter of the high air-entry porous stone by 0.155 inch, which is

necessary to enable placing the epoxy all around the high air-entry porous stone to provide the required seal. A 0.125-inch wide by 0.05-inch deep groove was machined along the diameter of the platen to allow for flushing out any air that diffuses through the high air-entry porous stone during the test. The groove beneath the high air-entry porous stone connects between two 1/8-inch vertical holes that were drilled through the platen and the base plate. The platen was fastened to the base plate with a single 1/4-20x1-1/4" socket head cap screw. A photograph and a schematic diagram of the pressure plate platen are shown in Figures 6.2 and 6.3, respectively.

The inlet to the flushing groove was connected to a 3-way valve and the outlet was connected to a 2-way valve. A Validyne Engineering Corp., model DP15-40 pressure transducer was connected to one of the outlets of the 3-way valve to measure the pore-water pressure in the specimen. The transducer had an operational pressure range of $\pm$ 12.5 psi. The other outlet of the 3-way valve and the 2-way valve were connected to two double-walled burettes to flush de-aired water through the groove.

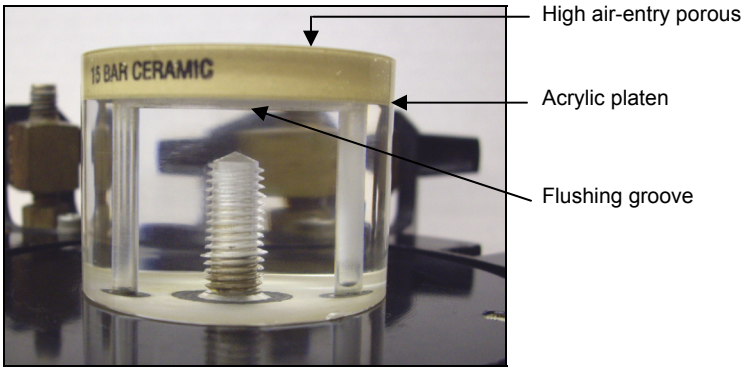

Figure 6.2. Pressure plate platen.

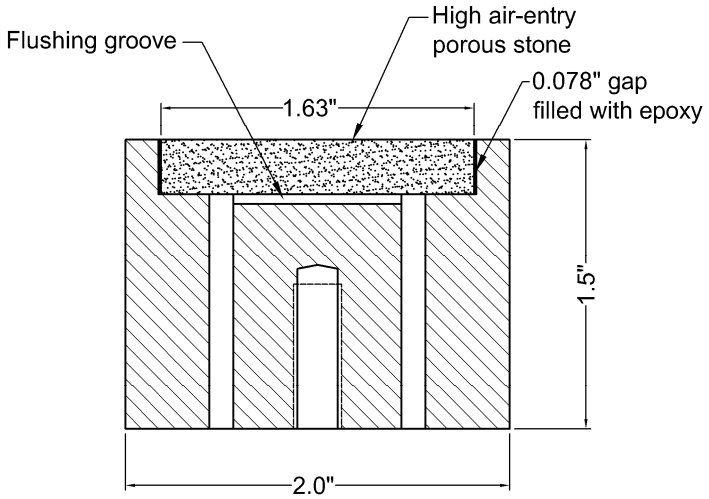

Figure 6.3. Schematic diagram of the pressure plate platen.

The base plate is equipped with a valve to apply air pressure inside the pressure chamber. The pressure chamber is made of acrylic with an inner diameter of 4.5 inches, wall thickness of 0.25 inch, and a design pressure of 175 psi. A pressure transducer was connected to the cell pressure line to measure the air pressure inside the pressure chamber. For the 5-bar pressure plate apparatus, a Validyne Engineering Corp., model DP15-46 pressure transducer with an operational pressure range of $\pm$ 50 psi was used to measure the cell pressure. While for the 15-bar pressure plate apparatus, a Validyne Engineering Corp., model DP15-50 pressure transducer with an operational pressure range of $\pm$ 125 psi was used to measure the cell pressure. The cell pressure was applied using a Geotac Co. pressure panel with a capacity of 160 psi. Details of the design of the platen of the pressure plate apparatus are presented in Appendix B. Details of the data acquisition and control system involved in the pressure plate tests are presented in Appendix C.

6.3 Test procedure

The test procedure for the pressure plate test consisted of two stages: (1) saturation of the system for measuring pore-water pressures and (2) matric suction measurements.

6.3.1 SATURATION OF WATER PRESSURE MEASURING SYSTEM

Saturation of the system for measuring water pressure involved saturating the high air-entry porous stone, the water cavity beneath the porous stone, and the pressure transducer used to measure the water pressure. The apparatus was assembled and the pressure chamber was filled with de-aired water. A confining pressure of 90 psi was applied inside the pressure chamber. Air was flushed out of the water cavity beneath the porous stone by switching the 3-way valve to connect the flushing line to the water cavity, opening the 2-way valve, and flushing de-aired water through the flushing lines and water cavity under a pressure of 60 psi. To saturate the pressure transducer, the 3-way valve was switched to the pressure transducer, the 2-way valve was opened, and de-aired water was flushed through the flushing line connected to the 2-way valve and the transducer under a pressure of 10 psi.

After saturating the pressure transducer, with the 3-way valve still switched to the pressure transducer, the 2-way valve was opened, and the high air-entry porous stone was saturated by allowing de-aired water to flow from the pressure chamber through the porous stone into the flushing line connected to the 2-way valve. De-aired water was flushed periodically through the water cavity to remove air bubbles accumulating beneath the porous stone by switching the 3-way valve to connect the flushing line to the water

cavity, opening the 2-way valve, and flushing de-aired water through the flushing lines and water cavity under a pressure of 60 psi.

The porous stone was usually saturated after water flowed through the porous stone for about 16 hours. If air bubbles were still observed to appear in the water cavity, the 3-way valve was switched to connect the flushing line to the water cavity, the 2-way valve was closed, and a backpressure of 60 psi was applied through the flushing line connected to the 3-way valve for about two hours to dissolve any air bubbles into the water. Then, the 2-way valve was opened and de-aired water was flushed through the flushing lines and water cavity under a pressure of 60 psi. The saturation of the high air-entry porous stone was checked by measuring its hydraulic conductivity, which was expected to equal the saturated hydraulic conductivity specified by the manufacturer.

6.3.2 MATRIC SUCTION MEASUREMENT

Two-inch diameter specimens were trimmed from 4.6 inches tall compacted specimens to a final height of 0.6 inch. The initial water content of the specimen was determined from the cuttings while trimming the specimen. The water in the pressure chamber was removed (after saturating the system for measuring the water pressure). Excess water in the chamber and on the porous stone was removed. The 3-way valve was switched to the pressure transducer, and the 2-way valve was opened. The specimen was placed on top of the saturated high air-entry porous stone. A 2-lb weight was placed on top of the specimen to ensure good contact between the specimen and the porous stone. The pressure chamber was assembled and the 2-way valve was closed. The volume of water absorbed by the specimen through the porous stone after mounting the specimen and before closing the 2-way valve was insignificant.

Once the 2-way valve was closed, the specimen immediately tended to draw water up through the porous stone, causing the transducer to start registering a negative water pressure. The air pressure inside the pressure chamber was increased (axis translation technique) manually until the readings of the pressure transducer stabilized (no further tendency for the water to move through the porous stone). The difference between the air pressure in the chamber and the measured pore-water pressure at equilibrium was equivalent to the matric suction of the specimen. At the end of the test, the pressure chamber was disassembled and the final water content of the specimen was determined.

During the suction measurement, air diffused through the high air-entry porous stone into the water cavity beneath the porous stone. Any air that diffused through the porous stone was flushed out of the water compartment periodically following the procedure outlined in Section 6.3.1. After flushing the air out, the 2-way valve was closed and the 3-way valve was switched to the pressure transducer to resume the test.

CHAPTER 7: MEASUREMENTS OF MATRIC SUCTION IN PRESSURE PLATE TESTS

7.1 Introduction

A series of pressure plate tests was performed to determine the effects of the compaction water content, dry unit weight, and degree of saturation on the soil matric suction. The results of the pressure plate tests and the effects of the compaction conditions on the soil matric suction are discussed in this chapter. The validity of the matric suction measurements using the axis translation technique for specimens compacted on the wet side of the line of optimums is discussed at the end of this chapter.

7.2 Test results

Matric suctions were measured for 48 specimens prepared at initial water contents ranging from 10 to 25%, and initial dry unit weights ranging from 90 to 115 pcf. Typical suction-time response curves for the measurements of matric suction and the effect of air diffusion on measurements are discussed below.

7.2.1 TYPICAL SUCTION-TIME RESPONSE CURVES AND TEST RESULTS

In the pressure plate test, the specimen was placed on top of the high air-entry porous stone and the air pressure inside the pressure chamber was adjusted manually (axis translation technique) until there was no further tendency for the specimen to absorb or expel water through the high air-entry porous stone. A typical suction-time response curve for a test is shown in Figure 7.1. The matric suction increased with time at a decreasing rate until it reached an asymptotic value (equilibrium condition), which was interpreted as the matric suction of the specimen. In this test, the air pressure inside the

pressure chamber was increased to maintain the pore-water pressure within the specimen either at zero or slightly negative. In a few tests, the air pressure inside the pressure chamber was increased by an amount that exceeded the amount required to maintain the pore-water pressure within the specimen at zero. In these tests, pore-water pressures within the specimen gradually increased to positive values and thus the matric suction gradually decreased until equilibrium was reached. Accordingly, the matric suction in the suction-time response curve increased to a peak value and then dropped off before it reached equilibrium as shown in Figure 7.2.

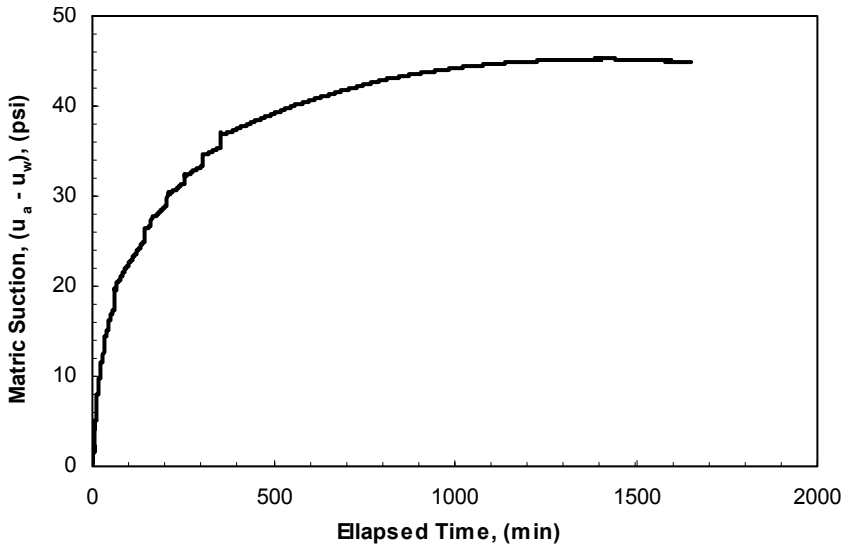

Figure 7.1. Typical suction-time response curve for the measurement of matric suction in pressure plate test.

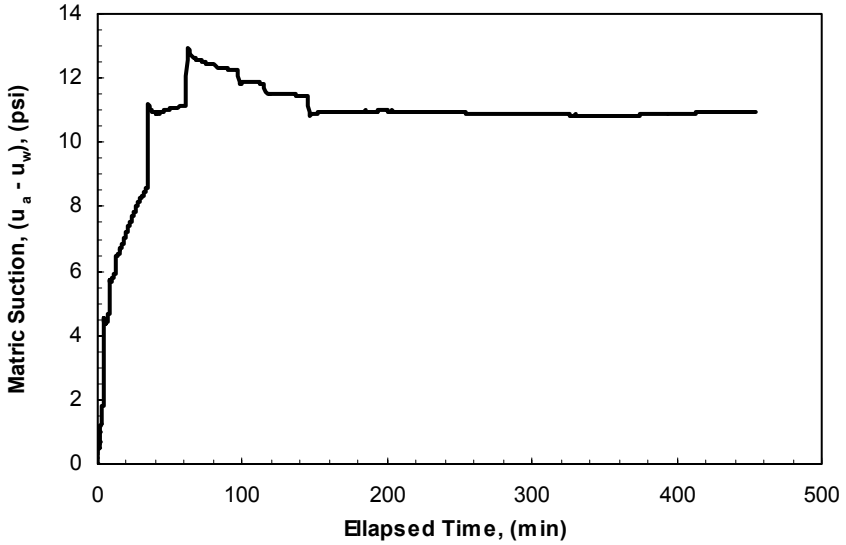

Figure 7.2. Suction-time response curve in pressure plate test in which matric suction peaked before reaching equilibrium.

The suction-time response curves for all pressure plate tests are presented in Appendix D. In addition, a summary table including the matric suction measurements and the compaction conditions for all specimens followed by the response time curves is presented in this appendix. The standard Proctor (ASTM D 698) compaction moisture-density curve and the measured matric suctions for all specimens are presented in Figure 7.3. The time required to reach equilibrium varied from 1 to 54 hours depending on the matric suction within the specimen and the air-entry value of the porous stone. Long equalization periods were generally required for specimens with high matric suctions tested using the 15 bar high air-entry porous stone. However, relatively short equalization periods were required for few specimens with high matric suctions tested using the 15 bar high air-entry porous stone for unknown reasons.

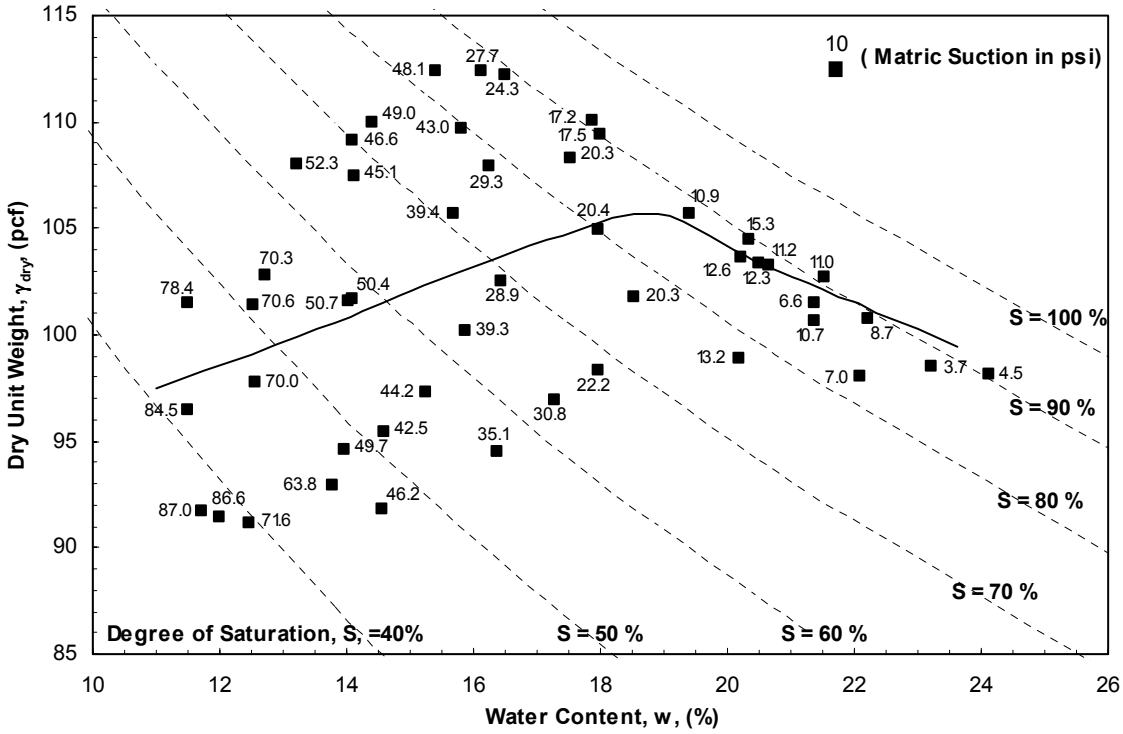

Figure 7.3. Standard Proctor compaction curve and matric suction measurements for all specimens compacted at different water contents and dry unit weights.

The water content of the specimens changed slightly during the test. The initial water content was estimated while trimming the 0.6-inch thick specimen from the 4.6-inch tall compacted specimen. The final water content was determined at the end of the test by drying the test specimen. Because the specimen is not sealed with a rubber membrane; therefore, evaporation of water from the specimen cannot be avoided. Water evaporation during the test decreased the water content of the specimen. On the other side, air diffusing from the specimen into the measuring system of water pressure displaced a volume of water equal to the volume of the diffused air into the specimen, which increased the water content of the specimen. Generally, the final water content of the specimen was within $\pm$ 2.5% of the estimated initial water content.

7.2.2 EFFECT OF AIR DIFFUSION ON MATRIC SUCTION MEASUREMENTS

During pressure plate tests, air diffused through the high air-entry porous stone into the system used to measure the pore-water pressure. This caused the pore-water pressure to increase gradually for a given air pressure. Accordingly, the matric suction was observed to decrease when air diffused into the measuring system. De-aired water was periodically flushed through the water cavity beneath the high air-entry porous stone to remove the diffused air. Periodical flushing of the diffused air caused some small irregularities in the suction-time response curve as shown in Figure 7.4. The amount of air diffusion increased in the specimens compacted at lower water contents and as the test duration increased. For specimens compacted at water contents higher than the optimum water content, air diffusion was not observed to occur.

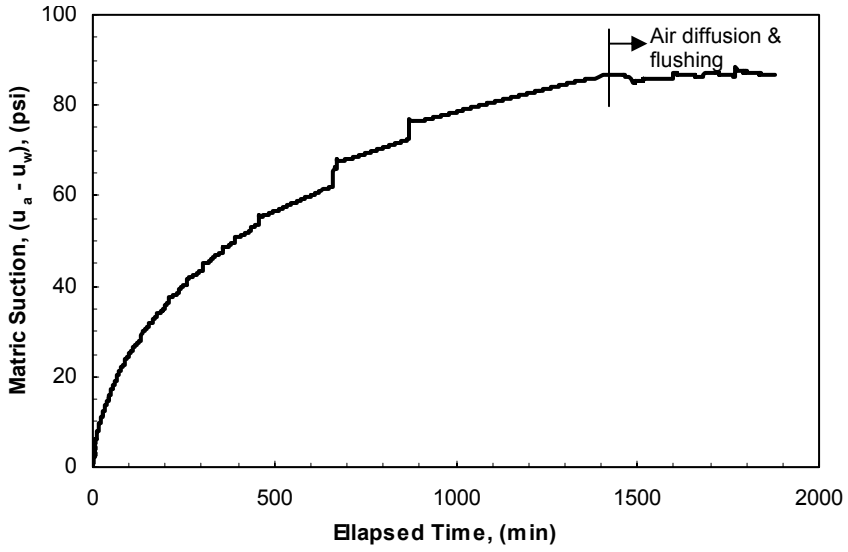

Figure 7.4. Effect of air diffusion followed by water flushing on the suction-time response curve for the measurement of matric suction.

Similar observations were reported by Bocking and Fredlund (1980) regarding the effect of air diffusion on the matric suction measurements. Bocking and Fredlund (1980)

mentioned that the effect of air diffusion could or could not be significant depending on the value of the diffusivity constant (for the flow of air through water) and the test duration. The authors noted that air diffusion caused a gradual increase in the water pressure (u_w) beneath the high air-entry porous stone until; ultimately, the water pressure would approach the applied air pressure (u_a). Therefore, the measured suction peaked and then dropped off, and the actual suction was underestimated.

7.2.3 THIXOTROPY EFFECTS ON MATRIC SUCTION MEASUREMENTS

Thixotropy is defined as an isothermal, reversible, time-dependent process that occurs under conditions of constant composition and water content, and where a material stiffens while at rest and softens upon remolding (Mitchell, 1976). Day (1955) reported a continual increase in pore-water tension (decrease in pore-water pressure) with time after compaction or remolding. For the current research, specimens compacted for testing in the pressure plate apparatus were stored for various lengths of time after compaction and before they were tested. Accordingly, thixotropy could have affected the measured matric suctions. This was investigated by comparing the measured matric suctions for specimens that were stored after compaction and before testing for different durations. The results are illustrated in Figure 7.5. For the same compaction water content, higher matric suctions were measured for specimens that were stored for longer durations after compaction and before testing. In addition, thixotropic effects on matric suction increased as the compaction water content increased. Thixotropic effects on the measured matric suctions were considered insignificant, and thus were ignored.

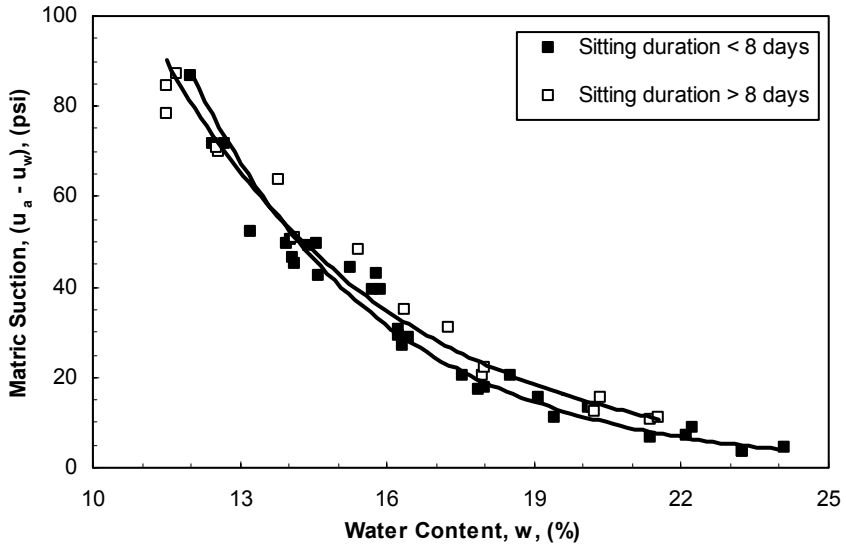

Figure 7.5. Thixotropy effects on matric suction measurements.

7.3 Effects of compaction conditions on matric suction measurements

The effects of the compaction water content, dry unit weight, and degree of saturation on measured matric suctions were investigated. The results from the current research are compared with data reported in previous studies below.

The matric suction decreased as the compaction water content increased irrespective of the compaction dry unit weight as shown in Figure 7.6(a). Similar observations were presented by Croney and Coleman (1954), Olson and Langfelder (1965), Krahn and Fredlund (1972), Fredlund and Rahardjo (1993), Tsai and Petry (1995), Wan et al. (1995), Bernier et al. (1997), and Sivakumar and Wheeler (2000). The matric suction decreased as the initial water content increased irrespective of the compaction degrees of saturation as shown in Figure 7.6(b).

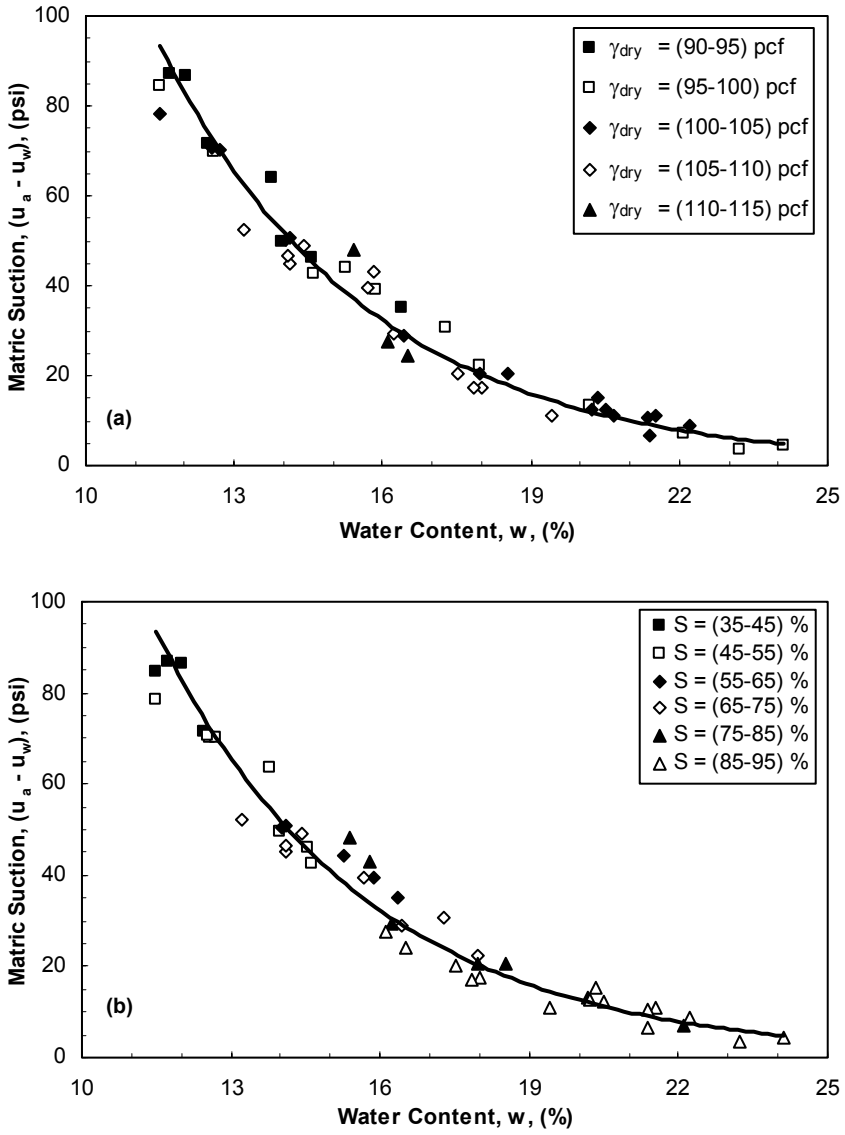

Figure 7.6. Effect of compaction water content on matric suction for specimens compacted at similar: (a) dry unit wieghts and (b) degrees of saturation.

For specimens compacted at similar water contents, the matric suction remained almost constant with increasing the initial dry unit weight as shown in Figure 7.7(a). However, Sudhakar and Revanasiddappa (2003) showed that at constant water content, the matric suction decreased as the dry unit weight increased. While Mou and Chu (1981)

observed that for specimens compacted at the same water content, the matric suction slightly increased for specimens compacted at higher unit weights. For similar initial degrees of saturation, the matric suction increased, with appreciable scatter, as the initial dry unit weight increased as shown in Figure 7.7(b). Similar observations were reported by Sudhakar and Revanasiddappa (2000) and Gonzalez and Colmenares (2006).

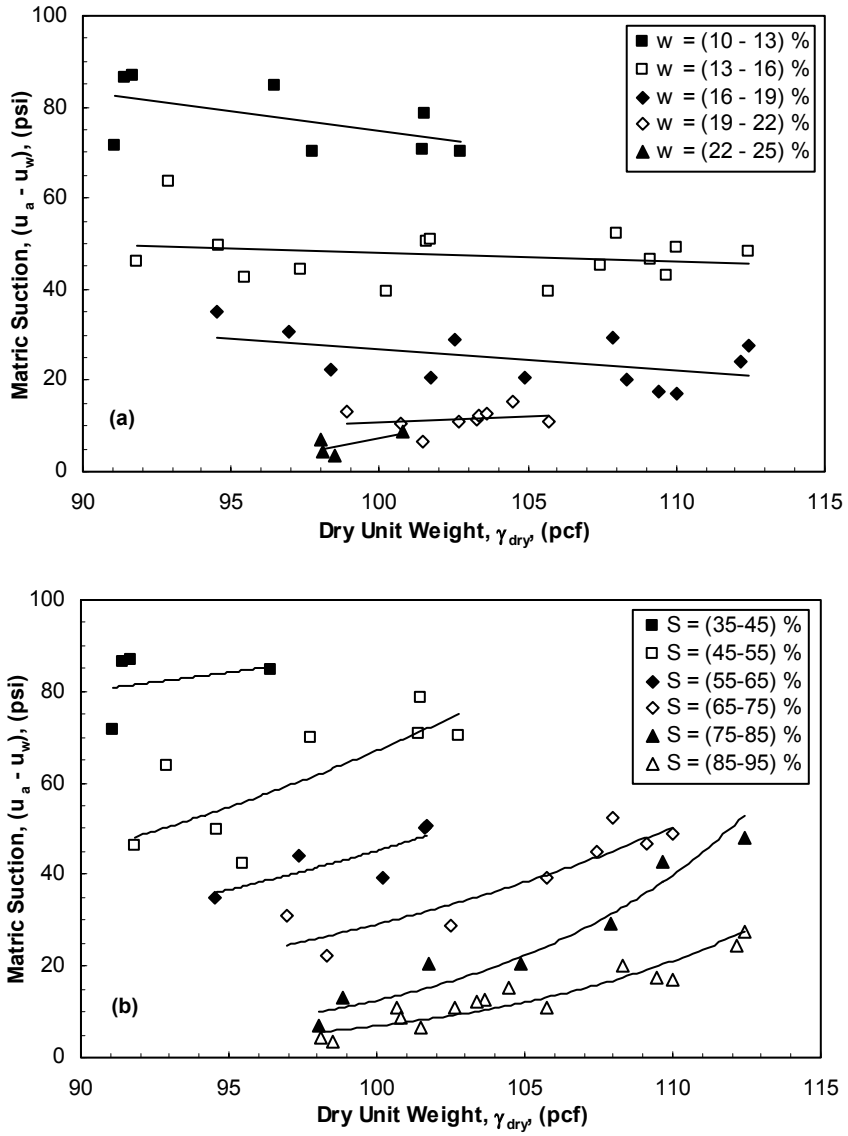

Figure 7.7. Effect of compaction dry unit weight on matric suction for specimens compacted at similar: (a) water contents and (b) degrees of saturation.

For specimens compacted at similar water contents, the matric suction remained almost constant with increasing the initial degree of saturation as shown in Figure 7.8(a). For similar initial dry unit weights, the matric suction decreased as the initial degree of

saturation increased as shown in Figure 7.8(b). Similar observations were reported by Sudhakar and Revanasiddappa (2000) and Gonzalez and Colmenares (2006).

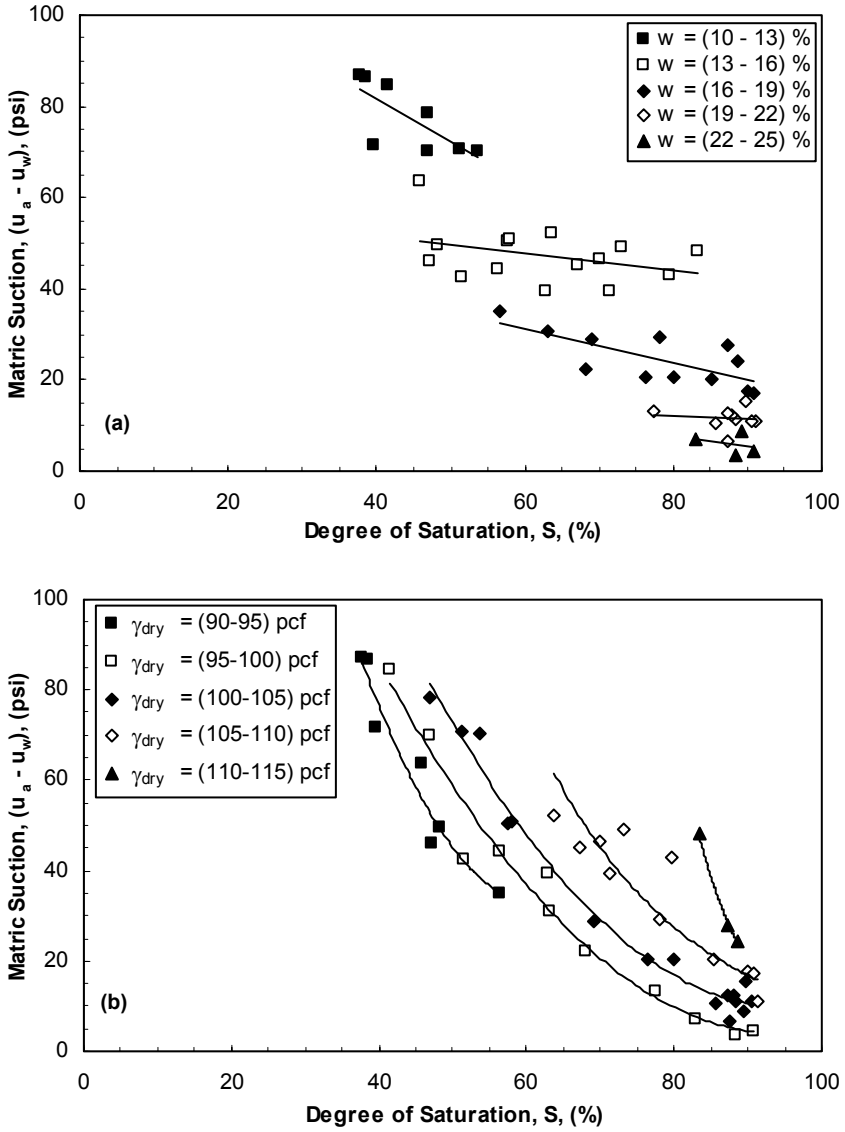

Figure 7.8. Effect of compaction degree of saturation on the matric suction for specimens compacted at similar: (a) water contents and (b) dry unit weights.

Based on Figures 7.6, 7.7(a), and 7.8(a), it was concluded that the matric suction was primarily dependent on the compaction water content and vertical suction contours

were plotted on the standard Proctor compaction curve, as shown in Figure 7.9. Similar trends were reported by Agus and Schanz (2006) and Gonzalez and Colmenares (2006). On the other side, Shackel (1973) mentioned that the matric suction depended primarily on the degree of saturation.

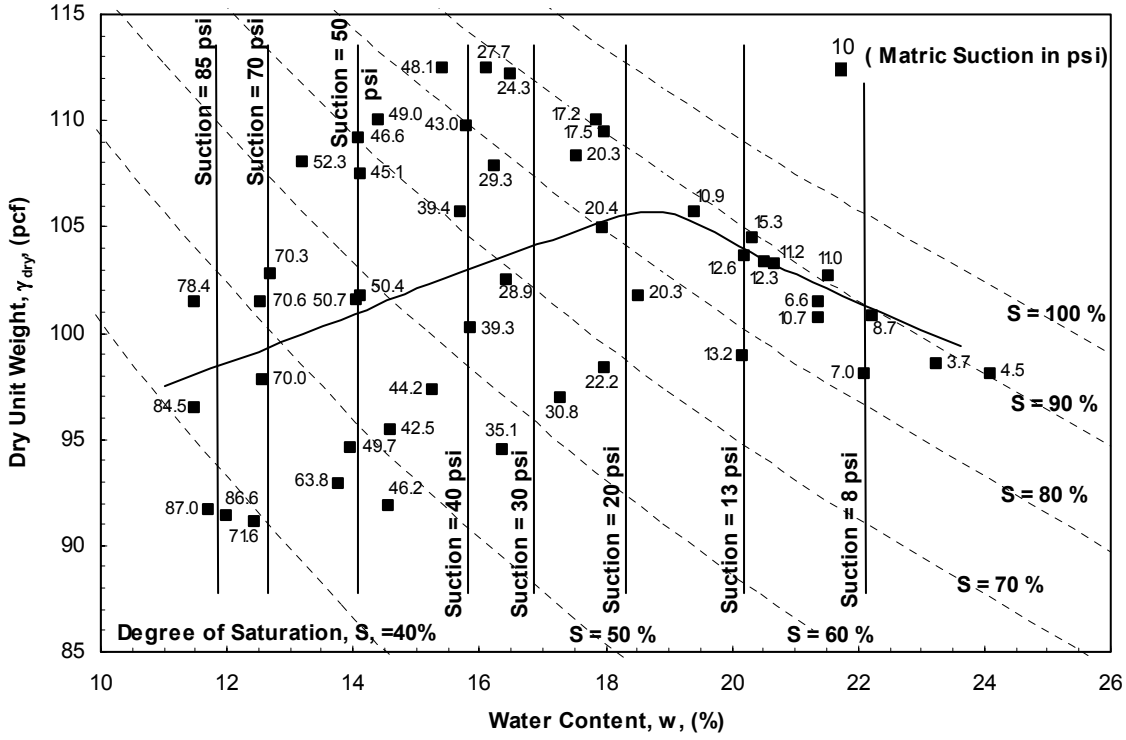

Figure 7.9. Standard Proctor compaction curve, matric suction measurements for specimens compacted at different water contents and dry unit weights, and suction contours.

7.4 The validity of matric suction measurements for specimens compacted on the wet side of the line of optimums

In order for the axis translation technique to be applicable for measuring matric suction in a pressure plate test, the ambient air pressure in the pressure chamber should be equal to the pore-air pressure within the specimen. This requires that the air phase within

the specimen be continuous. Bocking and Fredlund (1980) mentioned that applying the axis translation technique for soils with occluded air bubbles might result in an overestimation of the measured matric suction by up to 100 percent or more.

Data reported in the literature regarding the condition at which the air phase in the soil was considered occluded is contradicting. Corey (1957) showed that the value of the air permeability dropped to zero when the degree of saturation of the soil approached 85%. Ladd (1960), Olson (1963), and Langfelder et al. (1968) showed that the value of the air permeability dropped to zero around the optimum water content of the soil, which corresponded to a degree of saturation (S) of about 85%. On the other side, Barden and Pavlakis (1971) mentioned that matric suction approached zero when the air phase was occluded. Barden and Pavlakis (1971) showed that zero matric suction condition was reached near the optimum water content for soils with low clay content (10%). However, for soils with high clay content (60%), the suction was appreciable at optimum water content. Matyas (1967) showed that the air phase for specimens compacted at the optimum water content was continuous and that the air permeability decreased as the degree of saturation increased, but the air phase remained continuous as long as the matric suction was not zero. Accordingly, the condition at which the air phase in the soil was considered occluded, and thus the axis translation technique would not be applicable for measuring matric suction in a pressure plate test, is controversial.

For the current research, the optimum water content on the standard Proctor (ASTM D 698) compaction moisture-density curve corresponded to a degree of saturation of 86%. The moisture content – dry unit weight relationship corresponding to a degree of saturation of 86% was assumed to coincide with the line of optimums for the tested soil. To explore the validity of the matric suction measurements for the specimens

compacted wet of optimum, three additional pressure plate tests were performed on specimens compacted on the wet side of the line of optimums to directly measure the negative pore-water pressure with the ambient air pressure equal atmospheric. The measured negative pore-water pressure is numerically equal to the matric suction when pore-air pressure is atmospheric. The results were compared with the corresponding tests performed using the axis translation technique.

In the latter three tests, the specimens were placed on top of the high air-entry porous stone and the pressure transducer, connected to the water cavity beneath the porous stone, was used to record the negative pore-water pressure within the specimens (with atmospheric pressure in the surrounding pressure chamber). The three tests were performed on specimens compacted at water contents ranging from 17 to 23% and dry unit weights ranging from 101 to 111 pcf. The three specimens had degrees of saturation ranging from 89 to 93%. The suction-time response curves for the matric suction measurements in the three tests are shown in Figure 7.10.

For the specimen compacted at water content of 17%, the measured matric suction was about 13 psi as shown in Figure 7.10(a). A matric suction value of 13 psi was unreasonably low for a specimen compacted at water content of 17% for this soil, which was attributed to water cavitation that happened around a negative pore-water pressure of 13 psi. The matric suctions of the two specimens compacted at water contents 19.5 and 23% matched well with the matric suctions measured using the axis translation technique as shown in Figure 7.11. Therefore, it was concluded that the matric suctions measured using the axis translation technique for the specimens compacted on the wet side of the line of optimums was reasonably close to the true matric suctions measured directly.

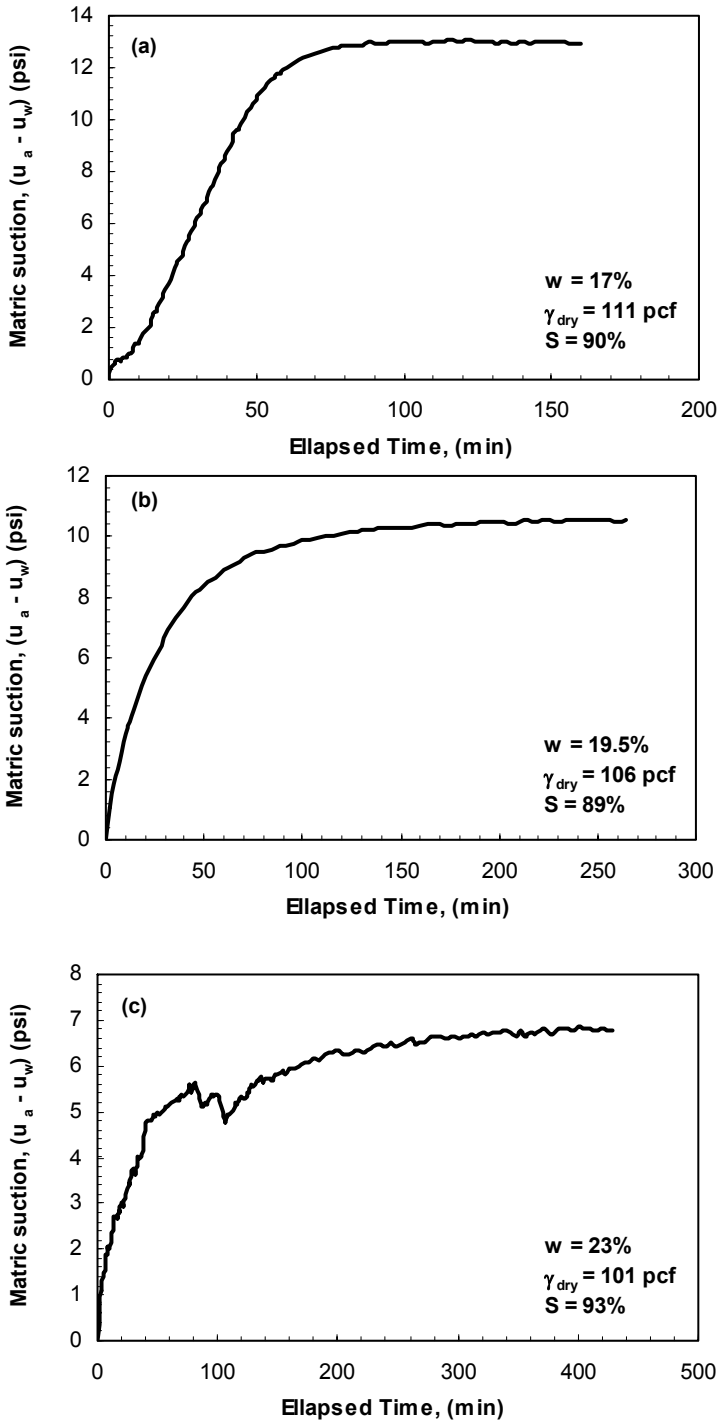

Figure 7.10. Suction-time response curves for the measurement of matric suction in pressure plate tests without implementing the axis translation technique.

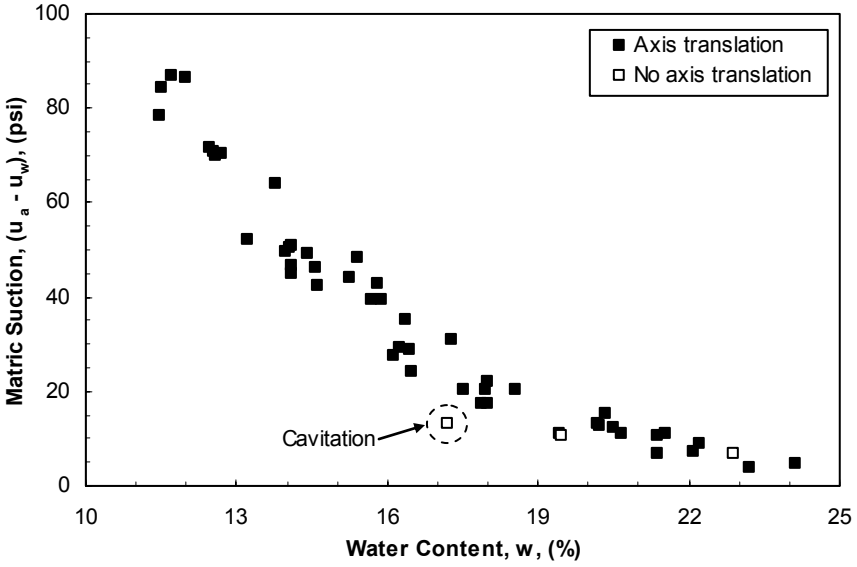

Figure 7.11. Compaction water content - matric suction relationship.

7.5 Summary

A series of pressure plate tests was performed to determine the effects of compaction water content, dry unit weight, and degree of saturation on the soil matric suction. The time required to reach equilibrium in the pressure plate test depended on the value of the matric suction in the specimen and the air-entry value of the porous stone. Long equalization periods were experienced for specimens with high matric suctions tested on the 15 bar high air-entry porous stone. Air diffusion increased in the specimens compacted at lower water contents and as the test duration increased. The effect of air diffusion on matric suction measurements was minimized by periodically flushing de-aired water through the water cavity beneath the high air-entry porous stone. For specimens compacted at water contents higher than the optimum water content, air diffusion was not observed to occur.

The matric suction decreased as the compaction water content increased irrespective of the compaction dry unit weight or degree of saturation. For specimens compacted at similar degrees of saturation, the matric suction increased as the initial dry unit weight increased. For specimens compacted at similar dry unit weights, the matric suction decreased as the initial degree of saturation increased.

For specimens compacted on the wet side of the line of optimums, where matric suctions were lower than one atmosphere, matric suctions measured directly and using the axis translation technique matched well. Based on this, it was concluded that matric suctions measured using the axis translation technique for specimens compacted on the wet side of the line of optimums were reasonably close to the matric suctions measured directly.

CHAPTER 8: TRIAXIAL APPARATUS AND PROCEDURE FOR MEASUREMENT OF STIFFNESS UNDER UNDRAINED CONDITIONS

8.1 Introduction

A triaxial cell equipped with piezoelectric transducers was designed and fabricated for this study to measure soil stiffness under undrained conditions. Details of the apparatus and the testing procedures followed to measure the soil stiffness under undrained conditions are described in this chapter.

8.2 Apparatus

A standard triaxial cell was modified to measure the soil stiffness under undrained conditions. A schematic diagram of the apparatus is shown in Figure 8.1.

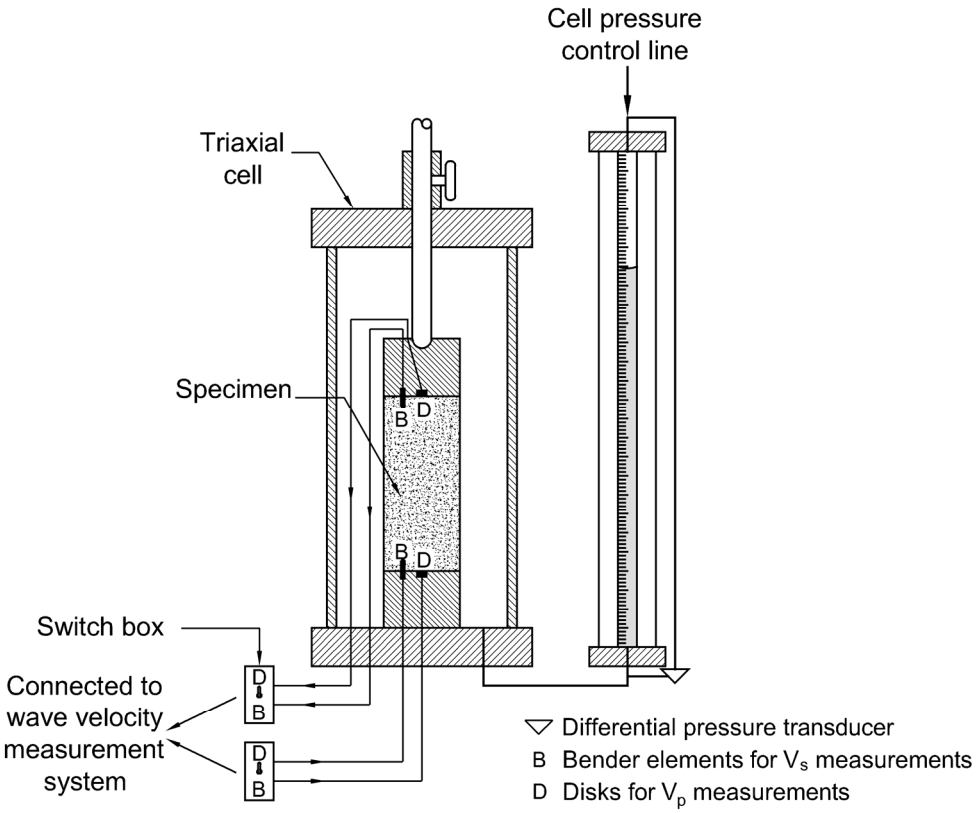

Figure 8.1. Schematic diagram of apparatus used to measure soil stiffness in triaxial cell under undrained conditions.

8.2.1 END PLATENS

Top and bottom triaxial acrylic platens equipped with piezoelectric transducers were designed and fabricated at The University of Texas at Austin. The platens were mounted in a standard triaxial cell. The end platens are 2 inches in diameter. Shear wave velocity was measured using Morgan Electro Ceramics Corp., model PZT-5H bender elements; and compression wave velocity was measured using Morgan Electro Ceramics Corp., model PZT-5A disks. Further details on the physical properties of the piezoelectric transducers used in this study and the required stages of preparation of the transducers

prior to assembly in the apparatus and use are presented in Appendix E. A photograph and a schematic diagram of the platens are shown in Figures 8.2 and 8.3, respectively.

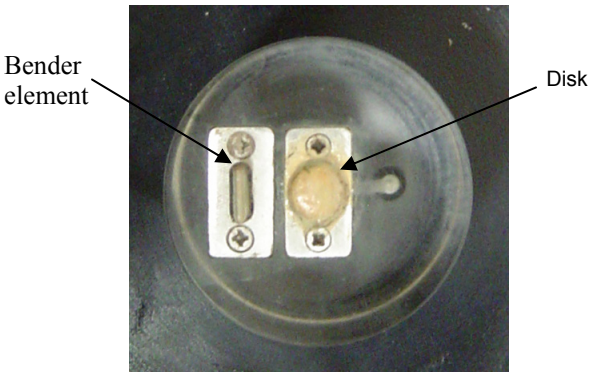

Figure 8.2. Triaxial platen designed to test specimens under undrained conditions.

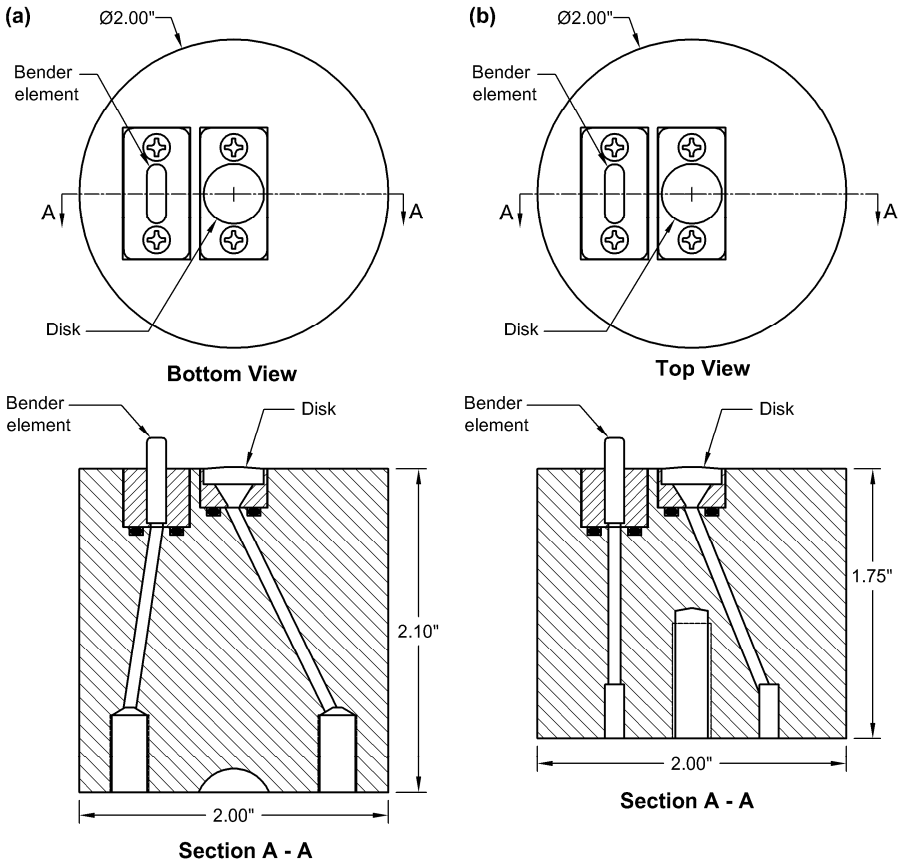

Figure 8.3. Schematic diagram of triaxial platens designed to test specimens under undrained conditions: (a) top platen and (b) bottom platen.

The disks were mounted in the center of the platens to produce *constrained* compression waves. A special technique was implemented to incorporate the bender elements and disks in the end platens. Each piezoelectric transducer was mounted in a separate stainless steel block, which was fastened into the triaxial platen using #2-56x1/2" flat head machine screws. If one of the transducers was damaged, the block and the transducer could be exchanged without damaging the other transducer mounted in the same platen. The stainless steel blocks were sealed at the bottom using o-rings. Details of the design of the triaxial platens and the stainless steel blocks are presented in Appendices F and G, respectively.

8.2.2 PRESSURE CHAMBER

The triaxial cell has an inner diameter of 4.5 inches, wall thickness of 0.25 inch, and a design pressure of 175 psi. The base plate is equipped with a valve to apply the cell pressure. The diameter of the loading piston is 0.5 inch. The bottom platen was fastened to the base plate with a single 1/4-20x1-1/4" socket head cap screw. The base plate has four 1/8-inch diameter holes. The wires connected to each piezoelectric transducer exited the triaxial cell through one hole. For the piezoelectric transducers mounted in the top platen, the wires were protected against moisture (from the cell fluid) in 1/8-inch polyethylene tubing. The cell pressure was measured using a Validyne Engineering Corp., model DP15-50 pressure transducer with an operational pressure range of $\pm$ 125 psi. The cell pressure was applied using a Geotac Co. pressure panel with a capacity of 160 psi.

Volume changes of the specimen were monitored by measuring the volume of the cell fluid going into or out of the triaxial cell. Accordingly, corrections for expansion of the cell and penetration of the axial load piston into the triaxial cell were required. The cell was calibrated for its expansion under confining pressures ranging from 0 to 100 psi. The overall volume changes of the specimen were measured using a Validyne Engineering Corp., model DP15-32 differential pressure transducer (DPT) connected from one side to the top and from the other side to the bottom of a 25-ml double-walled burette mounted on the pressure panel. The DPT had an operational pressure range of $\pm$ 2 psi, which provided a resolution of approximately 0.05 ml in volume change. The idea of using a differential pressure transducer to measure volume changes is based on the fact that water head (pressure) in a burette is proportional to the height of the water column; and the height of the water column is proportional to the volume of the water in the

burette. Therefore, a DPT can be calibrated to convert the changes in water head in the burette to volume changes.

A Wykeham Farrance Limited Co., model 10021 load press with a capacity of 2000 lb was used to shear the specimens. The axial load was measured using one of two load cells depending on the anticipated load to be measured. One load cell had a capacity of 300 lb (Lebow Products Inc., model 3167); and the other load cell had a capacity of 1000 lb (Lebow Products Inc., model 3143-1K). Axial deformation of the specimen was measured using a Trans-Tek Inc., model 0243-0000 linear variable differential transformer (LVDT) with a range of 0.75 inch. Details of the data acquisition and control system involved in the triaxial tests performed to measure the soil stiffness under undrained conditions are presented in Appendix C.

8.2.3 PIEZOELECTRIC TRANSDUCERS TEST SET-UP

A photograph and a schematic diagram for the apparatus used to perform shear and compression wave velocity measurements using piezoelectric transducers mounted in platens of a triaxial cell are shown in Figures 8.4 and 8.5, respectively.

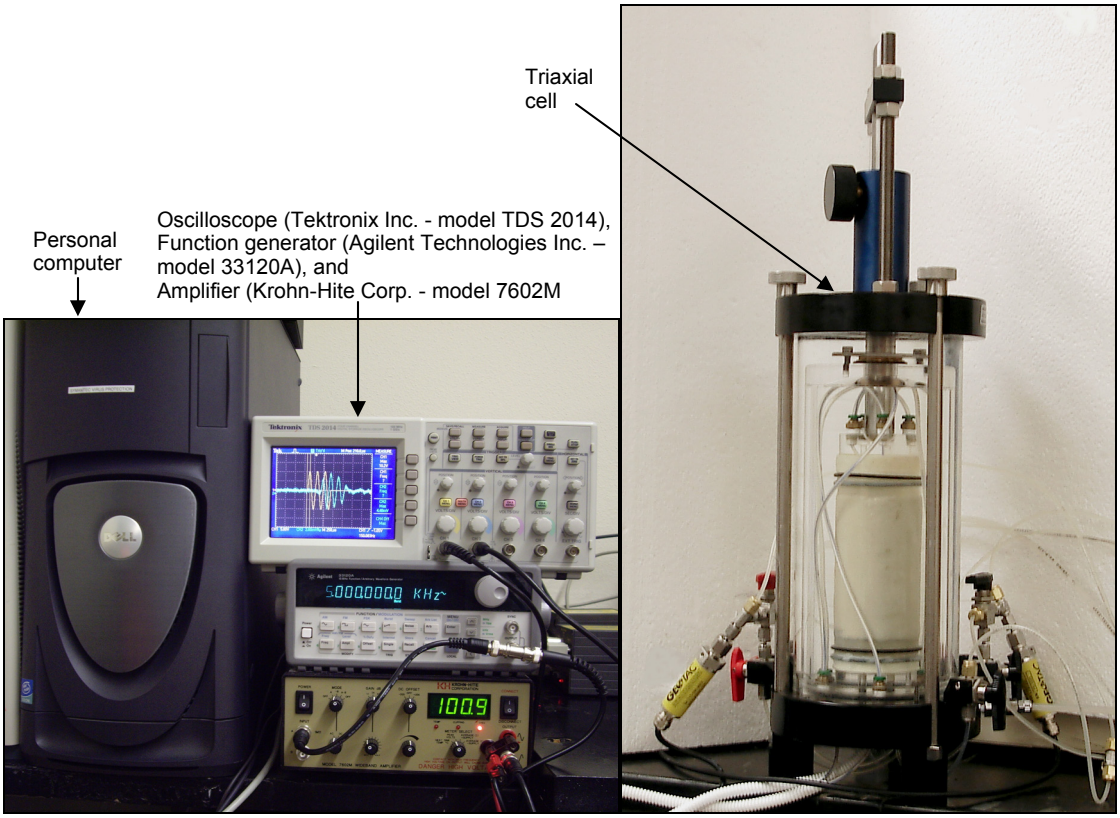

Figure 8.4. Apparatus used for shear and compression wave velocity measurements using piezoelectric transducers mounted in triaxial cell.

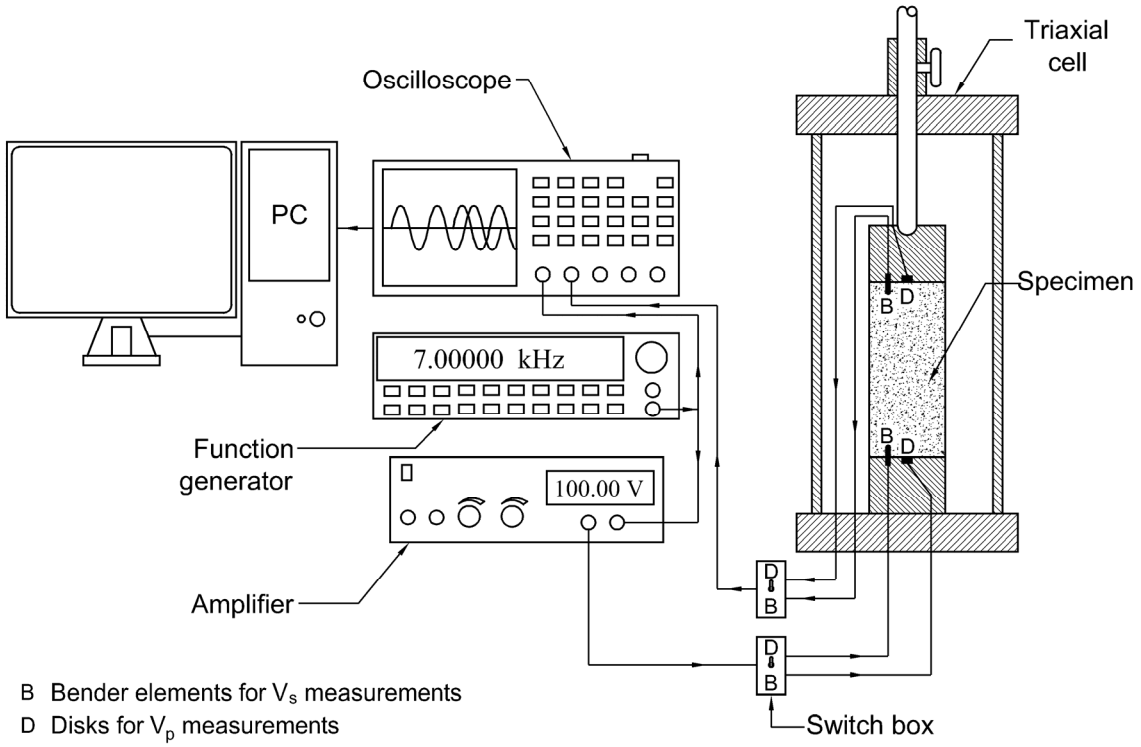

Figure 8.5. Schematic diagram of apparatus used for shear and compression wave velocity measurements using piezoelectric transducers mounted in a triaxial cell.

An Agilent Technologies Inc., model 33120A function generator with a maximum output voltage of 10 volts was used to generate the excitation signal sent to the transducers mounted at the bottom end of the specimen. A Krohn-Hite Corp., model 7602M amplifier was used to amplify the excitation signal by a factor of 10 and 20 for the bender elements and disks, respectively. The amplified signal was transmitted to a switch box, which was used to divert the signal to either the bender element or the disk. Another switch box was connected to the receiving transducers to transmit the received signal from either the bender element or the disk to a Tektronix Inc., model TDS 2014 digital oscilloscope. The oscilloscope was used to digitize and display the transmitted and received analog signals. The oscilloscope was connected to a personal computer through

a National Instruments Corp., model NI-488.2 GPIB-USB-B to record the digitized signals for further analyses.

8.3 Test procedure

Shear and compression wave velocity measurements were made under undrained conditions using the triaxial cell equipped with bender elements and disks but with no provisions for controlling or measuring either pore-water or pore-air pressures. Details on the preparation of the apparatus prior to setting up specimen, specimen set-up, compression stage, shearing stage, and shear and compression wave velocity measurements are discussed in the following sections.

8.3.1 PREPARATION PRIOR TO SETTING UP SPECIMEN

The capacitance and the resistance of piezoelectric transducers were checked before each test to make sure that the transducers were functioning properly. An additional layer of the polyurethane coating was applied on the transducers and was allowed to cure for 24 hours at room temperature before proceeding. The differential pressure transducer mounted on the double-walled burette used to measure volume changes in the specimen and the pressure transducer used to measure the cell pressure were saturated by flushing de-aired water through the transducers.

8.3.2 SPECIMEN SET-UP

The specimen was mounted between the platens of the triaxial cell such that the top and bottom piezoelectric transducers fit in the assigned intrusions that were carved in the ends of the specimen during compaction. The bender element source and receiver were aligned in the same vertical plane (using the intrusions at the specimen ends). This

was done to minimize compression waves from striking the receiver, and thus allow shear waves to dominate. A thin coating of silicon grease was applied on the vertical sides of the top and bottom platens. A rubber membrane was then placed around the specimen. Two o-rings were used to seal the membranes to the top and bottom platens. Finally, the triaxial cell was filled with tap water.

8.3.3 COMPRESSION STAGE

Before applying the confining pressure, shear and compression wave velocity measurements were recorded following the procedure outlined in Section 8.3.5. The majority of the specimens were compressed to a final isotropic confining pressure of 15 psi. Few tests were performed at increasing isotropic confining pressures ranging from 0.2 to 90 psi. For each confining pressure, shear and compression wave velocities were recorded after compressing the specimen for 30 minutes.

8.3.4 SHEARING STAGE

For the few tests in which the specimens were compressed to a final isotropic confining pressure of 90 psi, the specimens were sheared at the end of the isotropic compression stage. Axial displacement was applied to produce axial strain at a rate of approximately 1%/min (ASTM D 2850). Shear and compression wave velocities were measured throughout the shearing stage. Eight stiffness measurements on average could be made for both shear and compression waves during shear of the specimen to a peak strain of approximately 20%. The stiffness measurements were made at approximately equal strain increments of 2.5%. At the end of the test, the apparatus was disassembled and the water content of the specimen was determined.

8.3.5 SHEAR AND COMPRESSION WAVE VELOCITY MEASUREMENTS

The shear and compression wave velocities were measured using the piezoelectric transducers mounted in the end platens. In order to calculate the velocity of the transmitted wave, the wave travel time and distance between the source and the receiver were measured. Further details on the determination and interpretation of travel times are discussed in Chapter 9. The travel distance for waves was taken as the least distance between the crystals (from tip to tip) by subtracting the length of the portion of each crystal that extended into the specimen from the total specimen height.

8.3.5.1 Waveform

A sinusoidal wave, with a peak amplitude of 10 volts, was generated using the function generator to excite the piezoelectric transducers. Sinusoidal waves reduced the subjectivity in interpreting the received wave because the output signal was of a similar shape to the input signal (Chapter 2, Section 2.4).

8.3.5.2 Excitation voltage

The excitation signal was amplified using the amplifier to produce detectable shear and compression waves at the receivers. High excitation voltages increased the signal to noise ratio (SNR), which resulted in received waves with clearer arrivals. For shear waves, the excitation voltage was limited to a value that would not cause depolarization of the bender elements. The maximum voltage that could be applied was defined from the manufacturer's specifications to be 125 volts. An excitation voltage of 100 volts was used to excite the bender elements. For compression waves, the excitation voltage was limited by the amplifier because the voltage that would depolarize the disk

(500 volts) is higher than the voltage capacity of the amplifier (200 volts). An excitation voltage of 200 volts was used to excite the disks.

8.3.5.3 Excitation frequency

For shear waves, waves with frequencies ranging from 3 to 8 kHz were used to excite the bender elements. For compression waves, waves with frequencies ranging from 5 to 55 kHz were used to excite the disks. Further details of the determination of the optimum excitation frequencies for bender elements and disks are discussed in Chapter 9.

8.3.5.4 Calibration of piezoelectric transducers

Piezoelectric transducers were calibrated (to account for the delay time introduced in the measurements by the electronics, the transducers, and the coating materials) by placing the source and the receiver in direct contact and measuring the time between the initiation of the electric impulse sent to the source and the initial arrival of the received signal. Each pair of piezoelectric transducers was calibrated at the range of frequencies to be used in the wave velocity measurements. In addition, the initial polarization of the received signals was determined during calibration.

CHAPTER 9: INTERPRETATION OF SHEAR AND COMPRESSION WAVEFORMS

9.1 Introduction

Shear and compression wave velocities were measured using piezoelectric transducers. Details of the procedures used for signal processing and determination of the travel times of transmitted shear and compression waves are presented in the following sections. Results of preliminary tests performed to investigate the effect of the excitation frequency and the effect of exciting the piezoelectric transducers with different numbers of cycles of a sinusoidal pulse on the measured travel times are presented in this chapter.

9.2 Signal-processing procedures

High-frequency noise was observed in the signals received by the piezoelectric transducers. To enhance the quality of the received signal, signal-processing procedures of stacking and filtering were applied to increase the signal to noise ratio (SNR). Stacking was conducted by averaging 128 signals using a digital oscilloscope prior to storing them in the computer. Comparison of transmitted and received shear waves before and after stacking is shown in Figure 9.1. The magnitude of the high-frequency noise was significantly reduced after stacking and a shear waveform was clearly identifiable. However, the clarity of the waveform could be further improved by filtering as discussed below.

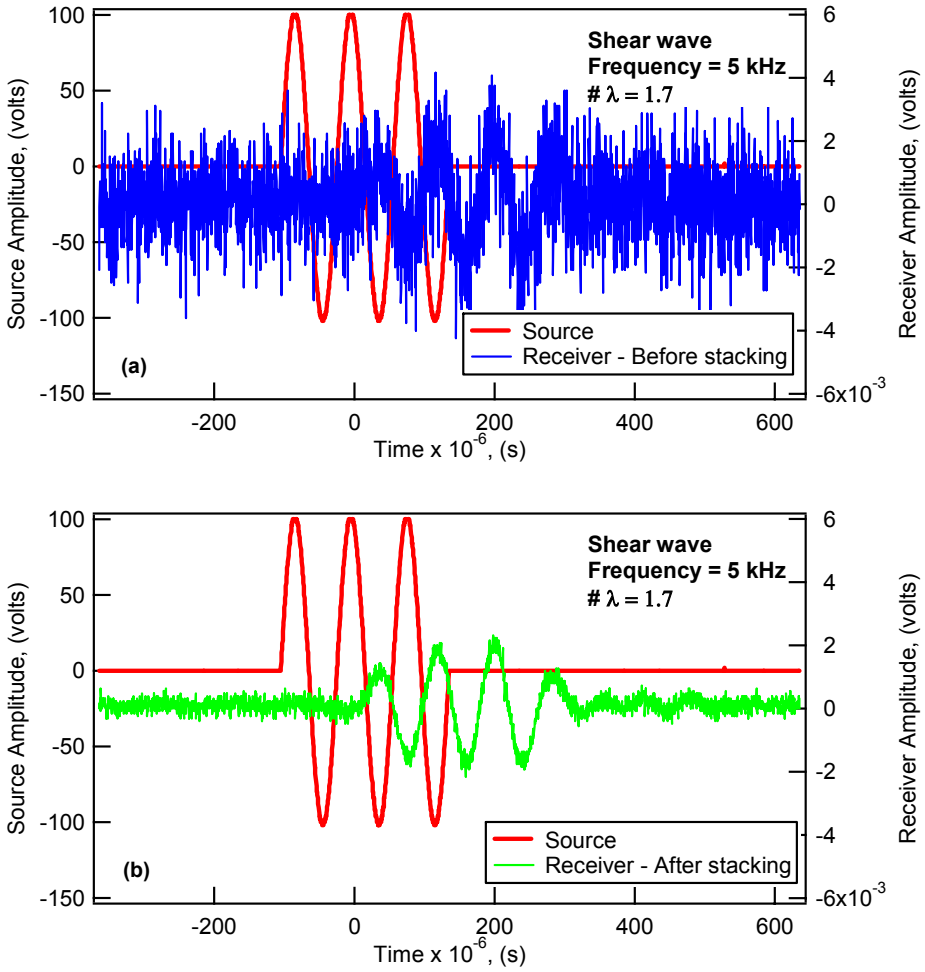

Figure 9.1. Comparison of transmitted and received shear waves: (a) before and (b) after stacking.

A moving average (MA) digital filter was designed to reduce the amplitude of the high-frequency noise that remained in the recorded wave after stacking. The filter equation had the form:

$$y_k = \frac{1}{n} \sum_{i=k-n+1}^{i=k} x_i \quad \text{..... (9.1)}$$

where y_k is an individual value of the output time series at data point k, x_i is an individual value of the input time series at data point i, and n is the number of averaged data points.

The output of the moving average filter, y_k, represented the average of *n* adjacent values of the input, x_i. A value of 10 was chosen for the variable *n* in the filter equation. The filter was implemented using MATLAB. The MATLAB function (m-file) written to compute and implement the filter is presented in Appendix H. Comparison of transmitted and received shear waveforms before and after applying the moving average (MA) filter is shown in Figure 9.2. The received shear wave before filtering is the received shear wave after stacking shown in Figure 9.1.

The high-frequency noise was greatly reduced by using the moving average (MA) filter. No phase shift between the received signals before and after filtering was observed as shown in Figure 9.2(c). The function FILTFILT in MATLAB was implemented to apply the filter without introducing a phase shift. In FILTFILT, the filter is applied on the input data in the forward direction and then in the reverse direction. The phase shift introduced by the filter in the forward direction is reversed when the filter is applied in the reverse direction, resulting in zero phase shift.

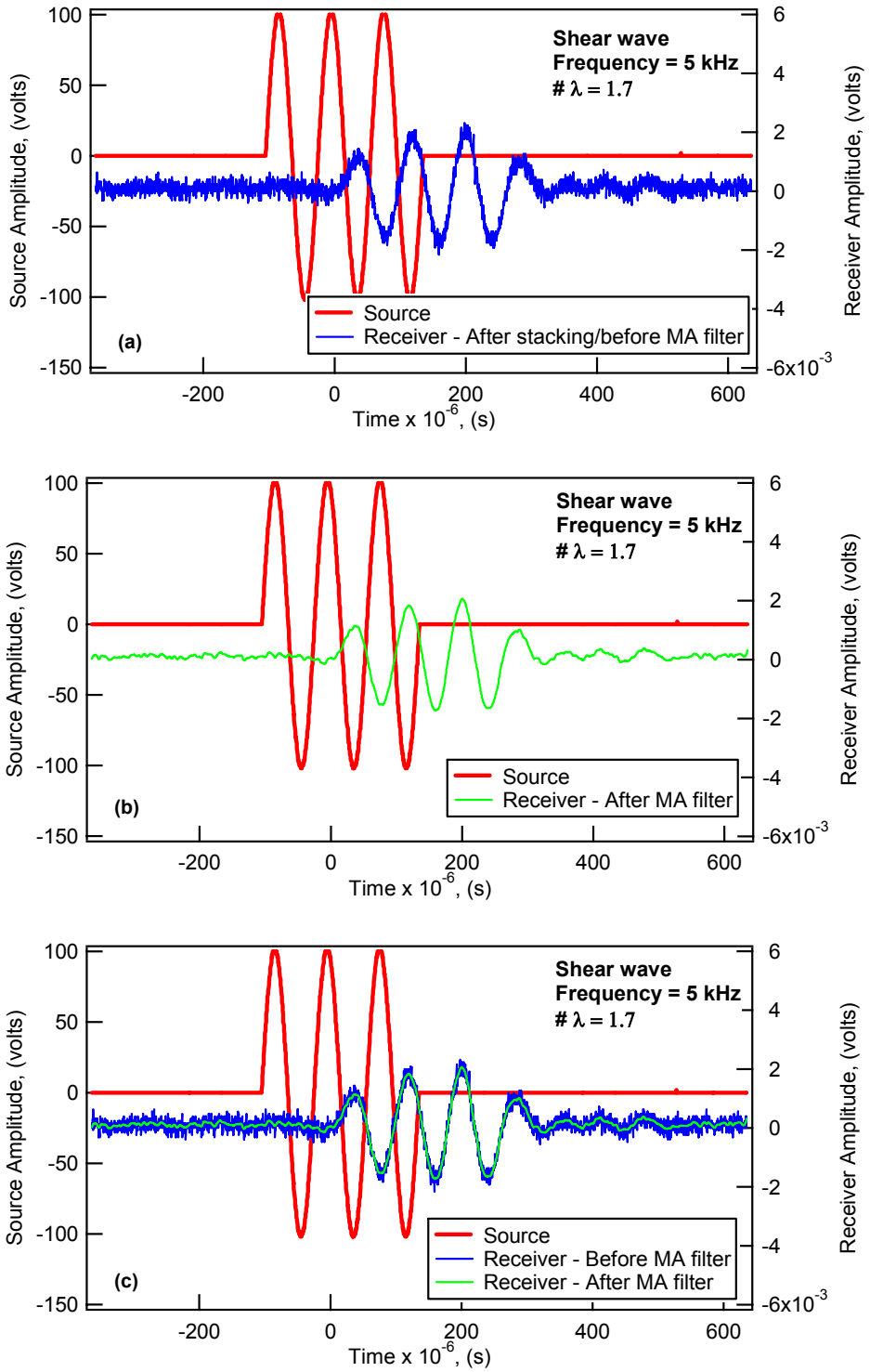

Figure 9.2. Comparison of transmitted and received shear waves: (a) before, (b) after, and (c) before and after applying the moving average (MA) filter.

9.3 Determination of wave travel time

Several approaches were investigated to determine the total travel time of transmitted shear and compression waves. The total travel time is defined as the time required for the electric impulse sent to the source transducer to travel through the specimen and the instrumentation involved in the measuring system. The measured total travel time was corrected for the time delay introduced by the electronics, the transducers, and the coating materials used to ground and waterproof the transducers, which was measured during calibration of the transducers as discussed in Section 9.3.2.

9.3.1 APPROACHES TO DETERMINE TOTAL TRAVEL TIME

Three approaches were investigated to determine the total travel time of transmitted shear and compression waves. Total travel times were determined using: (1) the first arrival of the received signal; (2) characteristic points corresponding to the first peaks, first troughs, and zero-crossings in the input and output signals; and (3) the computed cross-correlation between the input and output signals. Total travel time determined using the first arrival of the received signal is the time between the initiation of the electric impulse sent to the source and the first significant excursion in the received signal that has the proper polarity. Total travel time determined using the characteristic points is the time between the first peaks, first troughs, or zero-crossings of the input and output signals.

For this research, the cross-correlation between the input and output signals was computed using a MATLAB function (m-file) presented in Appendix H. All signals were sampled at time intervals of 10^{-6} sec. Each transmitted and received signal consisted of 2500 data points. Therefore, the cross-correlation sequence consisted of 4999 (2x2500-1)

data points. Generally, zero lag of any cross-correlation sequence is in the middle of the sequence (at element 2500 for this study). The time interval corresponding to the number of data points enclosed between the maximum peak and the middle of the cross-correlation sequence corresponds to the time delay between transmitted and received signals.

Typical shear and compression waveforms recorded in this study were used to compare the total travel times determined using the three approaches: (1) first arrival of the received signal; (2) the characteristic points corresponding to first peaks, first troughs, and zero-crossings in the input and output signals; and (3) the cross-correlation between the input and output signals. In this comparison, the piezoelectric transducers were excited with 3 cycles of a sinusoidal pulse. The effect of number of cycles on the measured travel times are discussed in Section 9.5.

9.3.1.1 Shear wave velocities

Transmitted and received shear waveforms and the cross-correlation sequence are shown in Figure 9.3. Total travel times determined using: (1) the first arrival of the received signal; (2) characteristic points corresponding to first peaks, first troughs, and zero-crossings in the input and output signals; and (3) cross-correlation technique are shown in this figure and are summarized in Table 9.1.

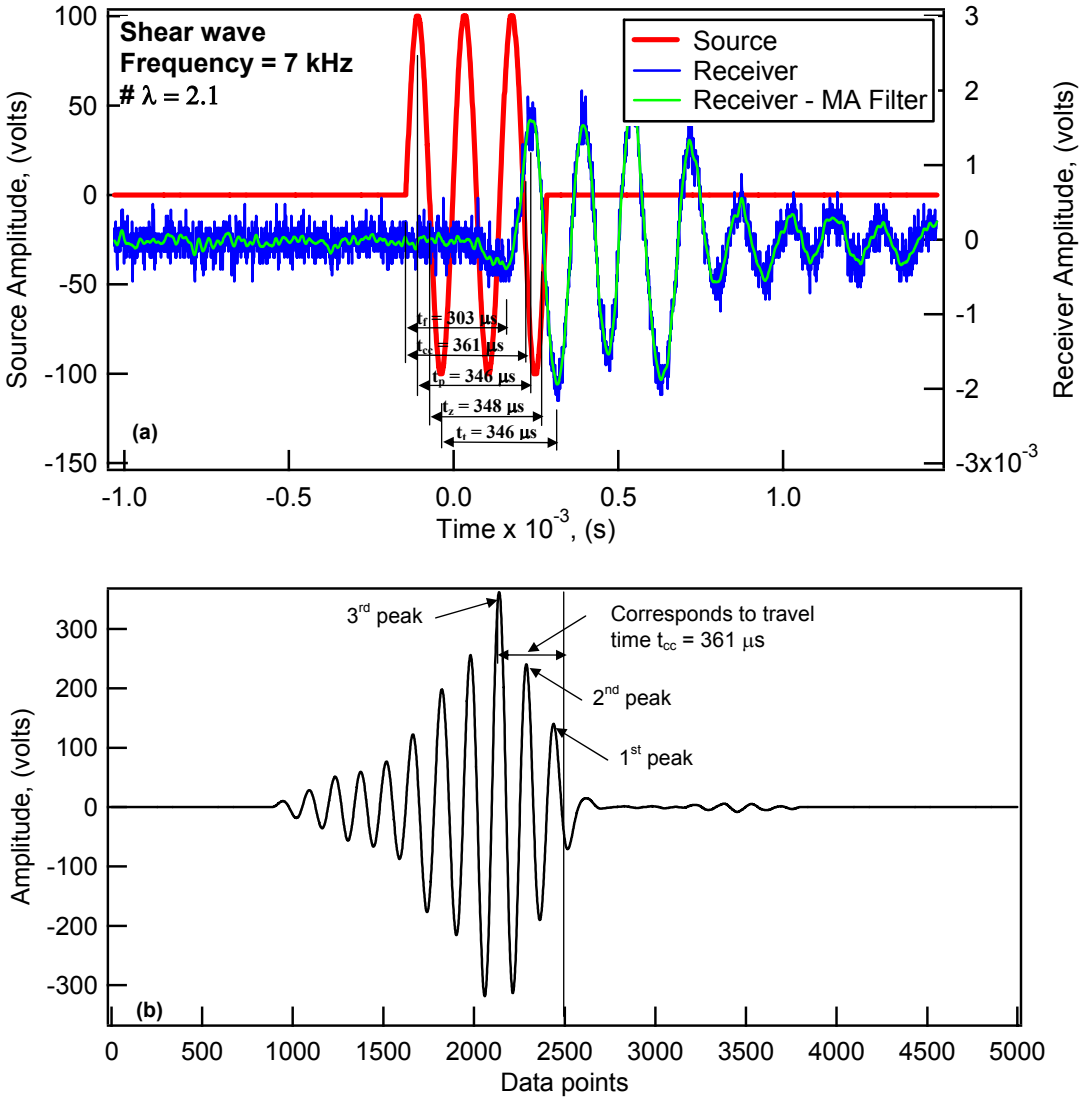

Figure 9.3. Shear waves: (a) transmitted and received waveforms and (b) cross-correlation sequence.

Table 9.1. Travel times for shear waves using different approaches.

Approach	Shear wave travel time, (μs)
First arrival	$t_f = 303$
Cross-correlation (3rd peak)	$t_{cc} = 361$
Characteristic points, first peaks	$t_p = 346$
Characteristic points, zero-crossings	$t_z = 348$
Characteristic points, first troughs	$t_t = 353$

The total travel time determined using the first arrival of the received signal was less than that determined using the characteristic points and the cross-correlation technique. The total travel time determined using the first peaks was less than that determined using the first troughs, which indicates that the transmitted wave experienced some spreading as it traveled through the specimen. This phenomenon is known as dispersion. Similar observations were reported by Hoar and Stokoe (1978) and Jovicic and Coop (1997a). The travel times determined using the three approaches were different because the shapes of the transmitted and received waveforms were not identical due to several reasons among which are wave dispersion, wave reflections, and near-field effects (Jovicic and Coop, 1997a and Santamarina and Fam, 1997).

For the current research, total travel times based on the first arrival of the received signal were judged to correspond to the correct and most reliable travel times because the first arrival is less affected by wave dispersion and wave reflections. Near-field effects were minimized by selecting the proper excitation frequency as discussed in Section 9.4. In addition, the first arrival of the received signal represents the phase velocity, which is related to the soil stiffness (Sanchez-Salinero et al., 1986).

Mohsin and Airey (2003) mentioned that the cross-correlation technique could be used to determine the travel time even if transmitted and received waveforms were not identical. The authors noted that if transmitted and received waveforms were not identical due to wave reflections and/or dispersion, one of the peaks in the cross-correlation sequence, but not necessarily the maximum peak, would correspond to the correct travel time. In this case, a visual check would be required to select the peak that would coincide with the first arrival of the received wave. In this study, the travel times corresponding to all peaks in the cross-correlation sequence shown in Figure 9.3(b) were investigated to

check if any of the peaks (other than the maximum peak) would result in a travel time that was more relevant compared to that determined using the maximum peak. The maximum peak corresponded to the most relevant travel time, compared to the other peaks, yet did not coincide with the first arrival of the received signal because the shapes of the transmitted and received waveforms were not identical.

9.3.1.2 Compression wave velocities

Transmitted and received compression waveforms and the cross-correlation sequence are shown in Figure 9.4. Total travel times determined using: (1) the first arrival of the received signal; (2) characteristic points corresponding to first peaks, first troughs, and zero-crossings in the input and output signals; and (3) cross-correlation technique are shown in this figure and are summarized in Table 9.2.

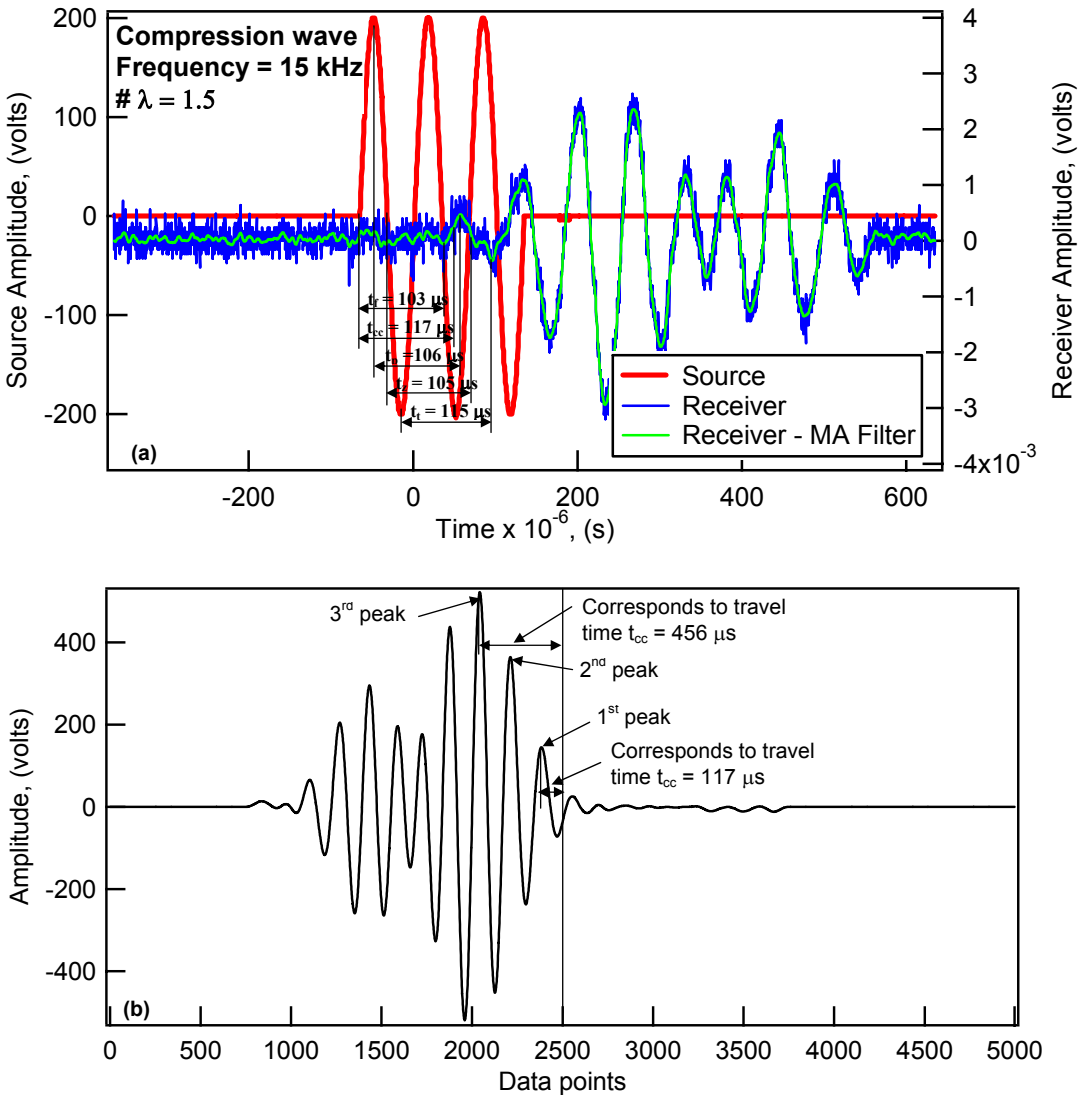

Figure 9.4. Compression waves: (a) transmitted and received waveforms and (b) cross-correlation sequence.

Table 9.2. Travel times for compression waves using different approaches.

Approach	Compression wave travel time, (μs)
First arrival	$t_f = 103$
Cross-correlation	$t_{cc} = 117$
Characteristic points, first peaks	$t_p = 106$
Characteristic points, zero-crossings	$t_z = 105$
Characteristic points, first troughs	$t_t = 115$

The total travel time determined using the maximum peak (3rd peak) in the cross-correlation sequence was significantly larger (and obviously incorrect) than the travel time determined using the first arrival of the received signal (456 μs versus 103 μs based on the first arrival of the received signal). Accordingly, the travel times corresponding to all peaks in the cross-correlation sequence were investigated to check if any of the peaks (other than the maximum peak) would result in a travel time that was more relevant compared to that determined using the maximum peak (Mohsin and Airey, 2003). The first peak in Figure 9.4(b) corresponded to the most relevant travel time (117 μs), compared to the other peaks.

The total travel time determined using the first arrival of the received signal was less than that determined using the characteristic points and the cross-correlation technique. The travel times determined using the three approaches were different because the shapes of the transmitted and received waveforms were not identical due to several reasons among which are wave dispersion and wave reflections. The effects of wave dispersion and reflections were less pronounced for the compression waves compared to shear waves (Section 9.3.1.1). For the current research, total travel times based on the first arrival of the received signal were judged to correspond to the correct and most reliable travel times because the first arrival is less affected by wave dispersion and wave reflections.

9.3.2 CALIBRATION OF PIEZOELECTRIC TRANSDUCERS

Piezoelectric transducers were calibrated to account for the delay time introduced in the measurements by the electronics, piezoelectric transducers, and coating materials. The calibration was performed by placing the source and the receiver in direct contact and measuring the time required for the electric impulse sent to the source transducer to

travel through the instrumentation involved in the measuring system. Each pair of piezoelectric transducers was calibrated for the range of frequencies used in the wave velocity measurements. Sample results of transmitted and received signals during calibration of bender elements and disks are shown in Figure 9.5.

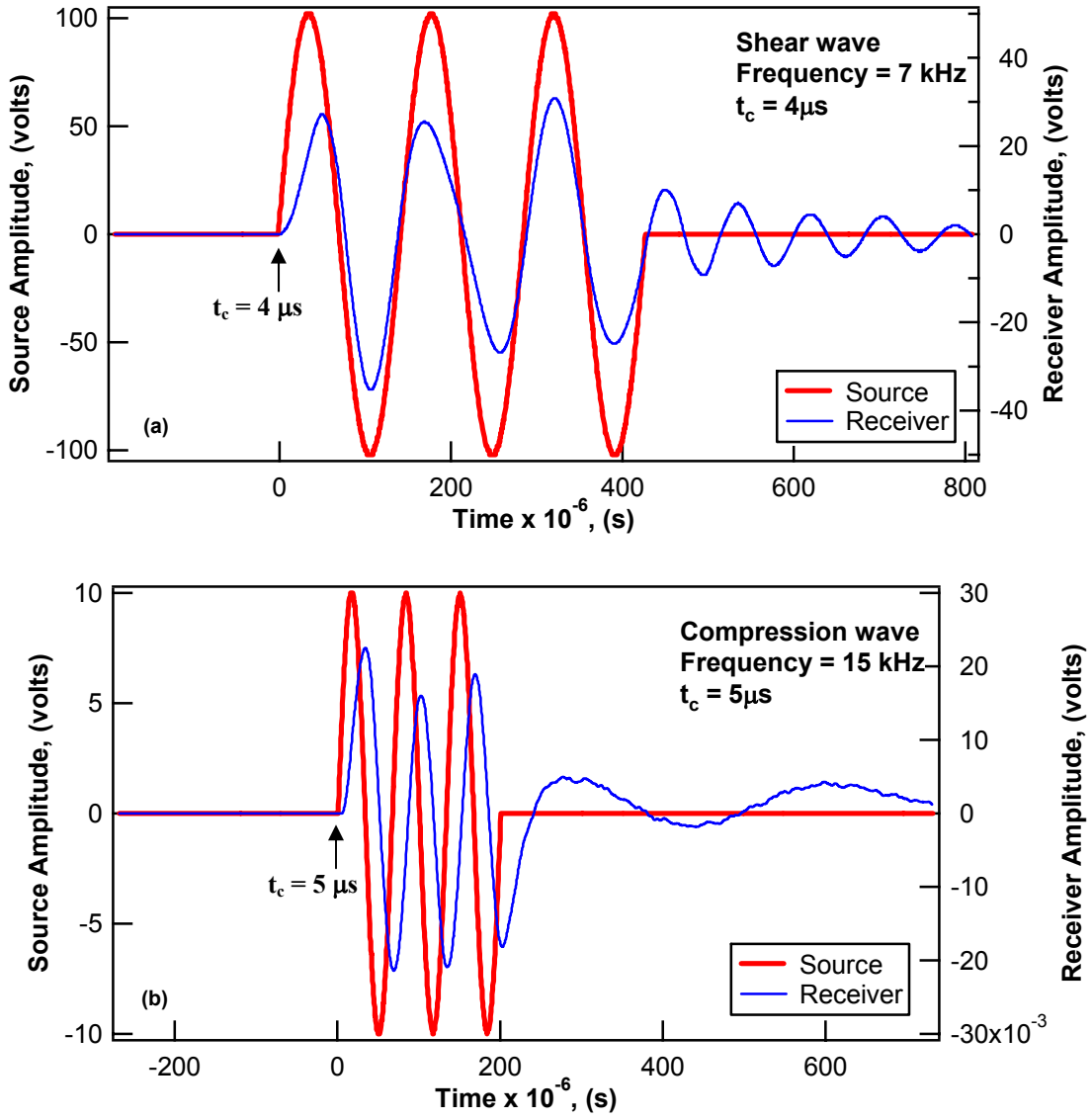

Figure 9.5. Sample result of transmitted and received signals during calibration of: (a) bender elements and (b) disks.

The calibration travel time, t_c, used to correct the total travel time measurements determined based on first arrivals is defined as the travel time between the initiation of the electric impulse sent to the source and the first arrival of the received signal. Calibration travel times that would be used to correct the total travel times determined

using the first peaks, zero crossings, first troughs or the cross correlation technique are likely different from the calibration time determined using the first arrival because the shapes of the transmitted and received waveforms were not identical.

The effect of the excitation frequency on the calibration travel time is illustrated for two pairs of bender elements and disks in Figure 9.6. The calibration travel time, t_c, decreased as the frequency increased. For a given frequency, the calibration travel time, t_c, varied for each pair of transducers depending on the length of the co-axial cables and the thickness of the coating materials used to ground and waterproof the transducers. The initial polarization of the piezoelectric transducers was defined during calibration. For the signals shown in Figure 9.5, the source and the receiver had the same polarity for the bender elements and the disks.

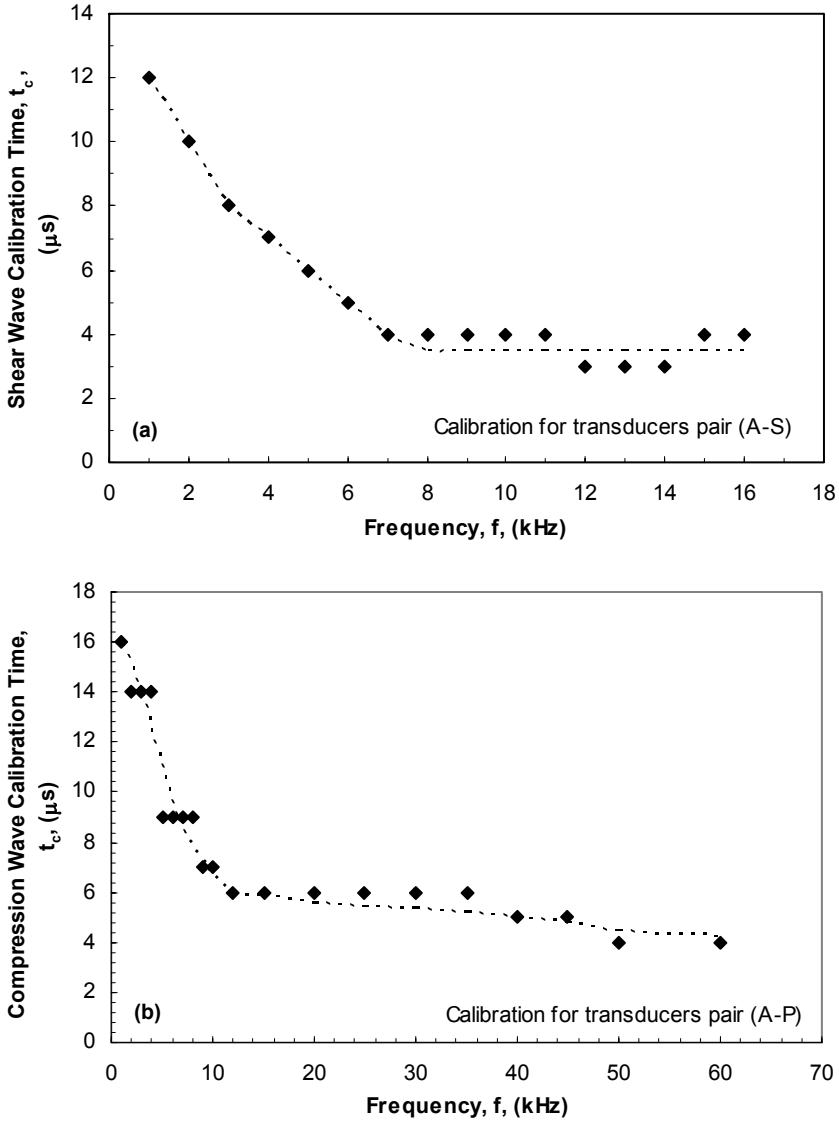

Figure 9.6. Calibration travel times, t_c, measured at various frequencies during the calibration of: (a) bender elements and (b) disks.

9.4 Effect of excitation frequency on measured travel times

A preliminary undrained triaxial test was performed to investigate the effect of the excitation frequency on shear moduli computed from measured shear wave velocities. The bender elements were excited with 3 cycles of a sinusoidal pulse. The effect of

number of cycles on the measured travel times is discussed in the next section. The specimen was tested under confining pressures ranging from 1 to 60 psi. Travel times, based on the first arrival of the received signal, were determined for excitation frequencies ranging from 1 to 10 kHz. The effect of the excitation frequency on the shear modulus is shown in Figure 9.7.

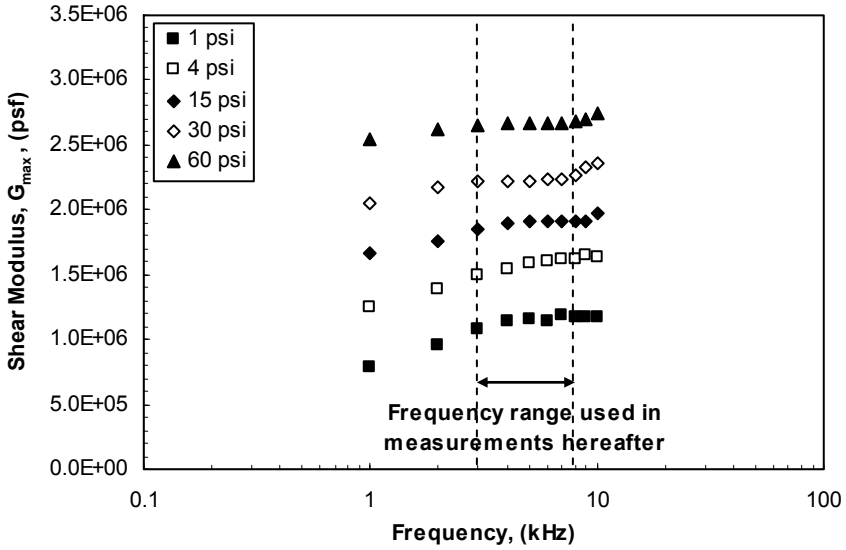

Figure 9.7. Effect of excitation frequency on shear modulus, G_{max}.

The clearest wave arrivals occurred at frequencies ranging from 1 to 8 kHz. The shear modulus increased with frequency as the frequency increased from 1 to 2 kHz, especially at the lower confining pressures. At frequencies of 1 and 2 kHz, there was less than one complete wavelength within the length of the specimen (specimen height/wavelength). This might explain why the shear modulus was affected by the excitation frequency; as the near-field effect adversely affected the measurements. Shear moduli were relatively independent of the excitation frequency for frequencies ranging from 3 to 8 kHz. For this frequency range, the number of waves traveling within the length of the specimen ranged from 2.0 to 5.2 at a confining pressure of 1 psi and from

1.3 to 3.4 at a confining pressure of 60 psi. In addition, for this frequency range, the amplitude of the received wave was relatively large (high signal to noise ratio) and the excursion in the received signal was sharp, which helped in defining the arrival of the received wave more accurately. Therefore, all further measurements of the shear wave velocity were done for frequencies ranging from 3 to 8 kHz. Five transmitted and received shear waveforms recorded at frequencies of 1, 3, 5, 8, and 9 kHz and one confining pressure (15 psi) are compared in Figure 9.8.

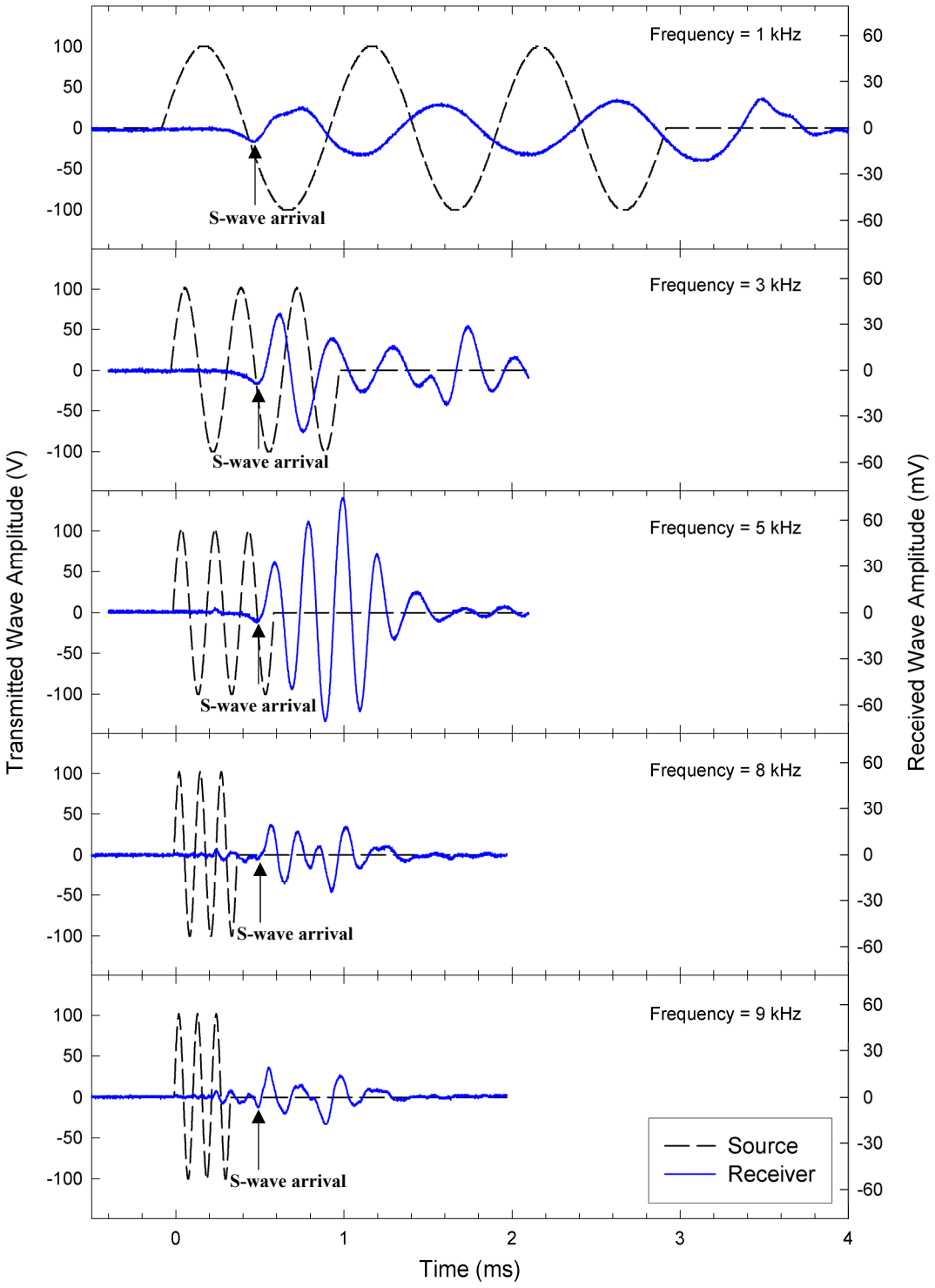

Figure 9.8. Effect of excitation frequency on the shape and amplitude of the received shear waveform.

Measurements of compression wave velocity could not be made in this test due to problems encountered with the grounding of the disks that lead to a low signal to noise ratio. Accordingly, a second undrained triaxial test was performed to investigate the effect of excitation frequency on the constrained moduli computed from measured compression wave velocities. The disks were excited with 3 cycles of a sinusoidal pulse. The effect of number of cycles on the measured travel times is discussed in the next section. The specimen was tested under confining pressures ranging from 1 to 60 psi. Travel times, based on the first arrival of the received signal, were determined for excitation frequencies ranging from 1 to 20 kHz. No measurements were taken for frequencies higher than 20 kHz because the arrival of the received signal was not clear. The effect of the excitation frequency on the constrained modulus is shown in Figure 9.9.

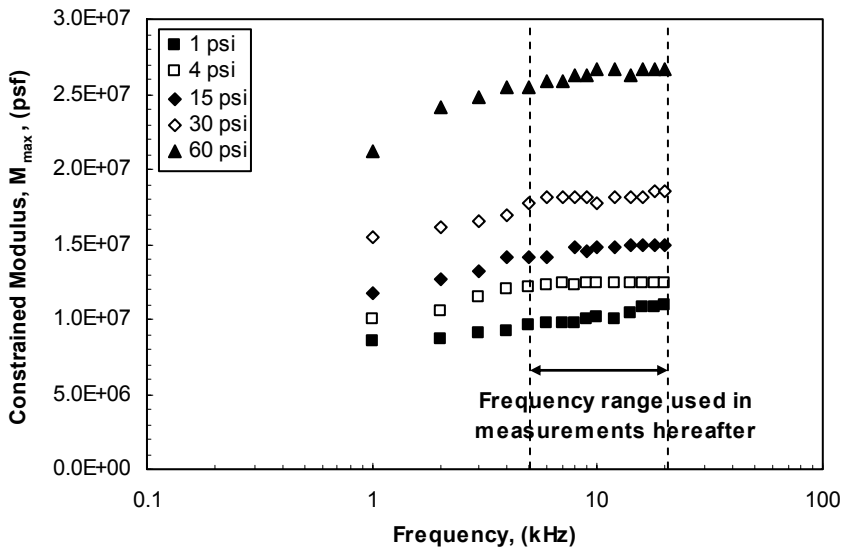

Figure 9.9. Effect of excitation frequency on the constrained modulus, M_{max}.

The constrained modulus increased with frequency as the frequency increased from 1 to 4 kHz. For this frequency range, there was less than one complete wavelength within the length of the specimen, which is not recommended for the generation of

constrained compression waves. Constrained moduli were relatively independent of excitation frequency for frequencies ranging from 5 to 20 kHz. For this frequency range, the number of waves traveling within the length of the specimen ranged between 1.1 and 4.2 at a confining pressure of 1 psi and ranged between 0.7 and 2.8 at a confining pressure of 60 psi. In addition, for this frequency range, the amplitude of the received wave was relatively large (high signal to noise ratio) and the excursion in the received signal was sharp, which helped in defining the arrival of the received wave more accurately. In later tests, it was observed that the clearest arrival of compression waves sometimes occurred at frequencies higher than 20 kHz (up to 55 kHz). Therefore, the optimum excitation frequency that would result in the clearest arrival was checked for all further measurements of the compression wave velocity. High frequencies are generally recommended to generate short wavelengths and therefore generate constrained compression waves. Five transmitted and received compression waveforms that were recorded at frequencies of 1, 3, 6, 10, and 16 kHz and one confining pressure (15 psi) are compared in Figure 9.10.

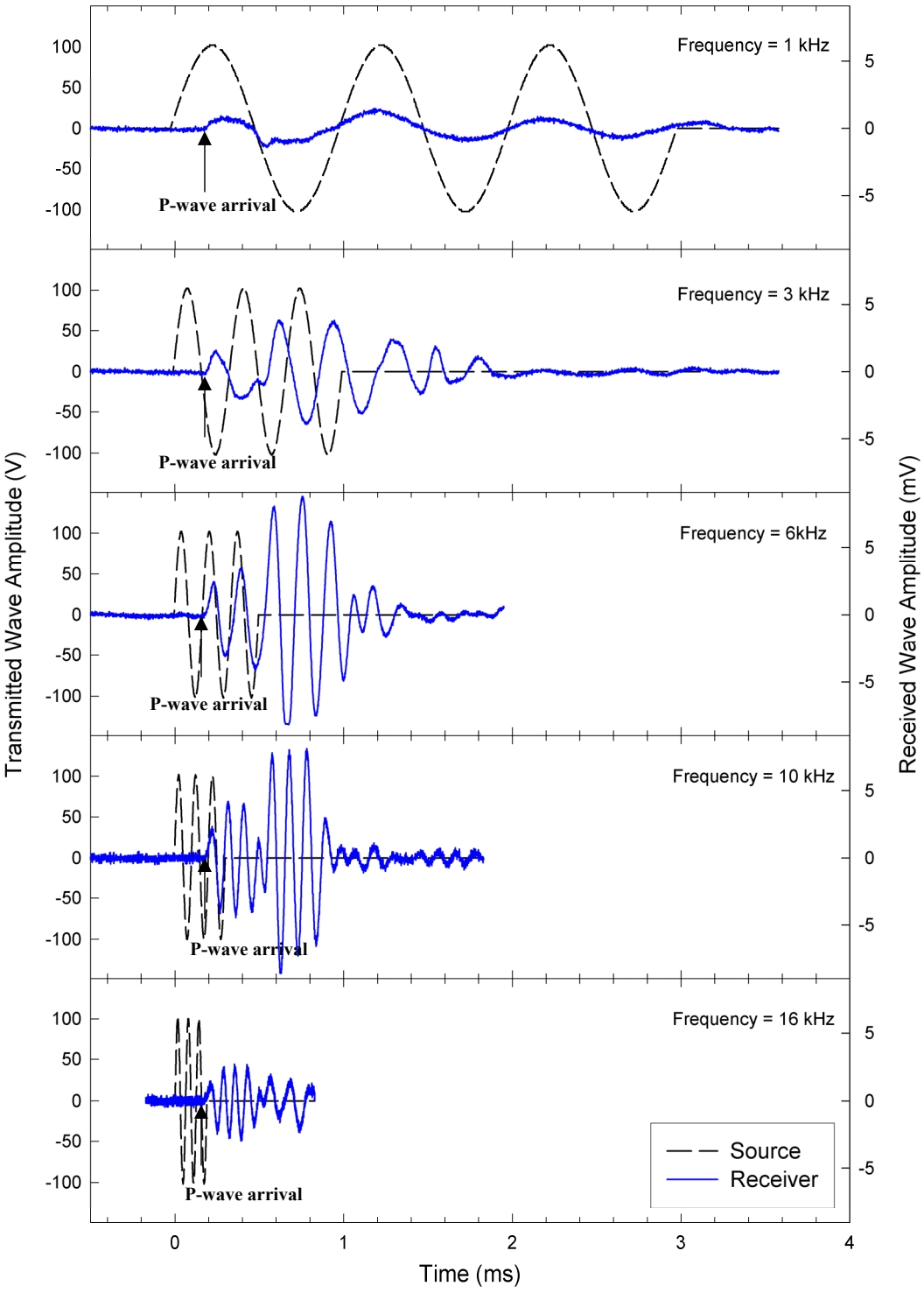

Figure 9.10. Effect of excitation frequency on the shape and amplitude of the received compression waveform.

9.5 Effect of number of cycles of sinusoidal pulse on measured travel times

A preliminary undrained triaxial test was performed to investigate the effect of exciting the piezoelectric transducers with different numbers of cycles of a sinusoidal pulse on the measured travel times. The piezoelectric transducers were excited with 1 and 3 cycles of a sinusoidal pulse. Transmitted and received shear waves using pulses of 1 and 3 cycles are shown in Figure 9.11. Similar waveforms for compression waves using pulses of 1 and 3 cycles are shown in Figure 9.12. The travel times determined using the first arrival of the received signal for shear and compression waves are summarized in Table 9.3. The number of cycles of the sinusoidal pulse did not have any significant effect on the measured travel times for shear and compression waves. Therefore, a consistent number of 3 cycles of the sinusoidal pulse was used to excite the piezoelectric transducers throughout this study.

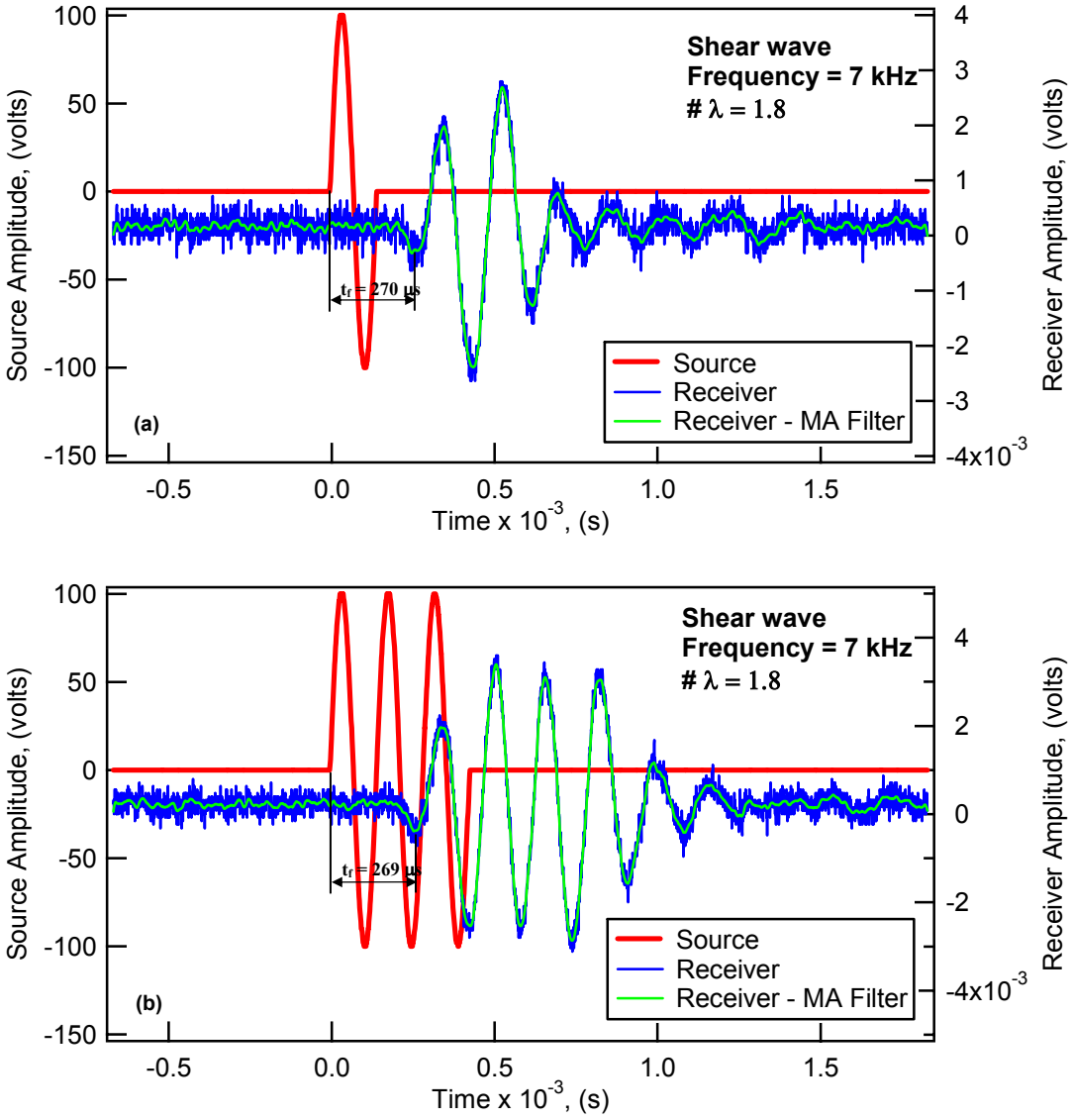

Figure 9.11. Transmitted and received shear waves excited with different number of cycles of the sinusoidal pulse: (a) 1 cycle and (b) 3 cycles.

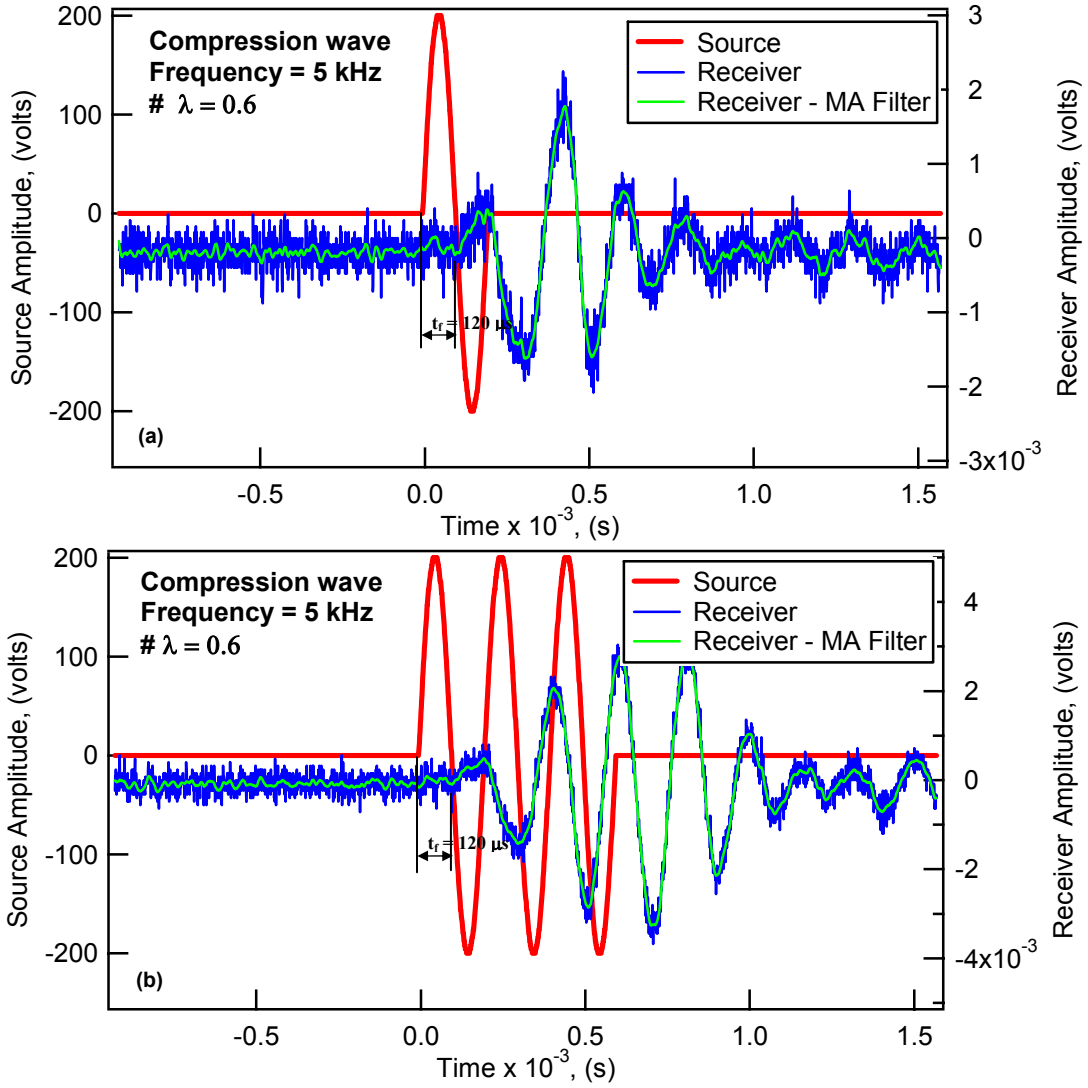

Figure 9.12. Transmitted and received compression waves excited with different number of cycles of the sinusoidal pulse: (a) 1 cycle and (b) 3 cycles.

Table 9.3. Travel times of shear and compression waves using different number of cycles of the excitation sinusoidal pulse.

Number of cycles	Shear wave travel time, (μs)	Compression wave travel time, (μs)
1	270	120
3	269	120

9.6 Summary

For the current research, shear and compression wave velocities were measured using piezoelectric transducers. High-frequency noise was observed in the received signals. Signal-processing procedures of stacking (128 signals) and filtering (moving average filter) were applied to the received signals to increase the signal to noise ratio. The high-frequency noise was significantly reduced after stacking and filtering. No phase shift was observed between the received signals before and after filtering because the filter was applied on the input data in the forward direction and then in the reverse direction. The phase shift introduced by the filter in the forward direction was reversed when the filter was applied in the reverse direction, resulting in zero phase shift.

Three approaches were investigated to determine the total travel time of transmitted shear and compression waves. Total travel times were determined using: (1) the first arrival of the received signal; (2) characteristic points corresponding to the first peaks, first troughs, and zero-crossings in input and output signals; and (3) the computed cross-correlation between input and output signals. The travel times determined using the three approaches were different because the shapes of the transmitted and received waveforms were not identical due to several reasons among which are wave dispersion, wave reflections, and near-field effects (for shear waveforms). For the current research, total travel times based on the first arrival of the received signal were judged to correspond to the correct and most reliable travel times because the first arrival is less affected by wave dispersion and wave reflections. For shear wave velocities, near-field effects were minimized by exciting the transducers with excitation frequencies ranging from 3 to 8 kHz. The measured travel time was corrected for the time delay introduced by

the electronics, piezoelectric transducers, and coating materials used to ground and waterproof the transducers, which was measured during the calibration of the transducers.

Preliminary undrained triaxial tests were performed to investigate the effect of the excitation frequency on shear and constrained moduli computed from measured shear and compression wave velocities, respectively. Shear moduli were relatively independent of the excitation frequency for frequencies ranging from 3 to 8 kHz. Constrained moduli were relatively independent of the excitation frequency for frequencies higher than 5 kHz. For these frequency ranges, there was more than about one complete wavelength within the length of the specimen. In addition, the amplitude of the received wave was relatively large (high signal to noise ratio) and the first excursion in the received signal was sharp, which helped in defining the arrival of the received wave accurately. Therefore, all further measurements were done at frequencies ranging from 3 to 8 kHz for shear wave velocities and frequencies larger than 5 kHz for compression wave velocities. For compression wave velocities, high frequencies are generally recommended to generate short wavelengths and therefore generate constrained compression waves.

A preliminary undrained triaxial test was performed to investigate the effect of exciting the piezoelectric transducers with different numbers of cycles of a sinusoidal pulse on the measured travel times. The number of cycles of the sinusoidal pulse did not have any significant effect on the measured travel times for shear and compression waves.

CHAPTER 10: MEASUREMENTS OF SOIL STIFFNESS UNDER UNDRAINED CONDITIONS

10.1 Introduction

Soil stiffness was measured in a triaxial apparatus under undrained conditions using top and bottom platens equipped with piezoelectric transducers. Tests were performed to investigate the effects of compaction water content, dry unit weight, and degree of saturation on soil stiffness. In addition, the effects of increasing the confining pressure under undrained conditions on soil stiffness and the variation of soil stiffness during shearing under undrained conditions were studied. Finally, the results from stiffness measurements were combined with the results from pressure plate tests reported in Chapter 7 to investigate the effect of matric suction on soil stiffness. Factors other than compaction conditions and matric suction that likely affect shear and compression wave velocities include soil fabric and overconsolidation ratio. The effects of soil fabric and overconsolidation ratio on soil stiffness have not been investigated in this study.

10.2 Effects of compaction conditions on wave velocity measurements

Shear and compression wave velocities were measured under undrained conditions for 26 specimens compacted at water contents ranging from 12 to 25% and dry unit weights ranging from 92 to 112 pcf. Shear and compression wave velocities were measured under confining pressures of 0.2 and 15 psi for all specimens. Velocities measured under confining pressure of 0.2 psi represented the as-compacted values for shear and compression wave velocities. The effects of compaction conditions on shear and compression wave velocities are discussed for velocities measured under a confining

pressure of 0.2 psi, and compared with data reported in previous studies. The effects of increasing the confining pressure to 15 psi, under undrained conditions, on measured shear and compression wave velocities in relation to compaction conditions are also discussed. The velocities measured along with the compaction water content, dry unit weight, and degree of saturation for each specimen are tabulated in Appendix I.

10.2.1 SHEAR WAVE VELOCITIES

Effects of compaction conditions on shear wave velocities measured under confining pressures of 0.2 and 15 psi are presented separately below. The effects of compaction conditions on shear wave velocities were investigated for specimens compacted at similar water contents, dry unit weights, degrees of saturation, and for specimens compacted to coincide with the standard Proctor compaction curve, i.e. presumably at similar compactive efforts. None of the specimens compacted at water contents lower than the optimum water content (19%) coincided with the standard Proctor compaction curve. Accordingly, interpolation was implemented to estimate shear wave velocities for specimens compacted dry of optimum that would coincide with the standard Proctor compaction curve.

10.2.1.1 Measurements under confining pressure of 0.2 psi

The standard Proctor compaction curve and measured shear wave velocities, for all 26 specimens, tested under confining pressure of 0.2 psi are presented in Figure 10.1. Effects of compaction water content, dry unit weight, and degree of saturation on shear wave velocity are discussed below.

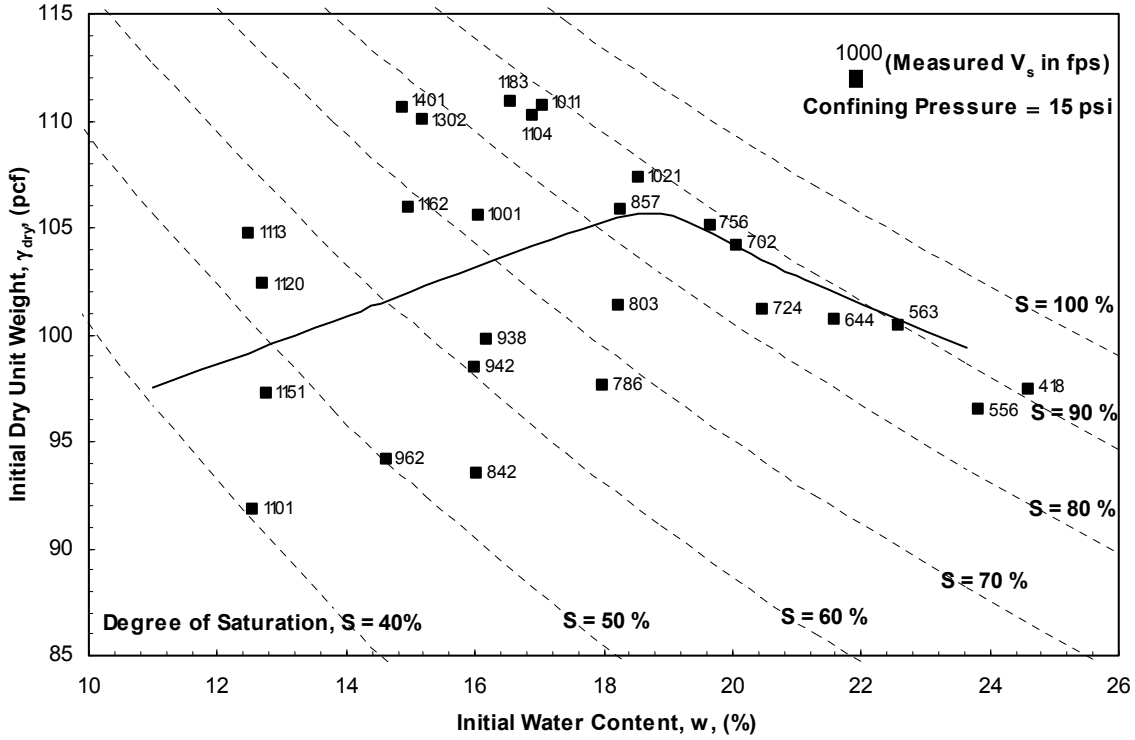

Figure 10.1. Standard Proctor compaction curve and shear wave velocities measured under a confining pressure of 0.2 psi.

Effects of compaction water content on shear wave velocity are illustrated in Figure 10.2 for specimens compacted at similar dry unit weights, degrees of saturation, and compactive efforts. For similar initial dry unit weights ranging from 90 to 100 pcf, the effect of the initial water content on shear wave velocity was insignificant for water contents ranging from 13 to 16% (w_{opt} = 19%) as illustrated in Figure 10.2(a). For water contents higher than 16%, the shear wave velocity decreased as the initial water content increased. For higher initial dry unit weights, ranging from 100 to 115 pcf, the shear wave velocity decreased as the initial water content increased. With the compaction procedure being used, specimens could not be compacted at water contents lower than approximately 15% with dry unit weights ranging from 105 to 115 pcf. Accordingly, the

relationship between shear wave velocity and initial water content could not be investigated at water contents lower than 15% for specimens compacted at dry unit weights ranging from 105 to 115 pcf. The decrease in shear wave velocity associated with increase in water content is partially due to decrease in matric suction as discussed in Section 10.5.

For similar initial degrees of saturation, the shear wave velocity decreased as the initial water content increased as illustrated in Figure 10.2(b). However, the relationship between shear wave velocity and compaction water content at constant degree of saturation could not be studied over a wide range of water contents because specimens could not be compacted at either very high or very low dry unit weights with the compaction procedure being used. For specimens compacted at similar degrees of saturation, the dry unit weights and matric suctions essentially increase as the water content decreases. Accordingly, changes in shear wave velocity with water content could be partially attributed to changes in dry unit weight and matric suction as discussed in following sections.

For specimens compacted at similar compactive efforts, the effect of the initial water content on shear wave velocity was insignificant for water contents ranging from 13 to 16% (w_{opt} = 19%) as illustrated in Figure 10.2(c). For water contents higher than 16%, the shear wave velocity decreased as the initial water content increased. The decrease in shear wave velocity associated with increase in water content is partially due to decrease in matric suction. Sawangsuriya et al. (2006) reported that the shear wave velocity decreased as the compaction water content increased for specimens compacted at the same compactive effort. The rate of decrease in shear wave velocity as the water content increased did not appear to decrease for water contents dry of optimum, which

disagreed with the data reported in this study. For specimens compacted at the same compactive effort, Inci et al. (2003) and D'Onforio and Penna (2003) reported that the shear wave velocity tended to peak at the optimum water content, which also disagreed with the data reported in this study. For specimens compacted at the same compactive effort, Ooi and Pu (2002, 2003) showed that the shear wave velocity peaked at water contents dry of optimum. The data presented in Figure 10.2(c) suggested that higher shear wave velocities occurred at water contents dry of optimum, but did not confirm a distinct peak for the range of water contents being tested.

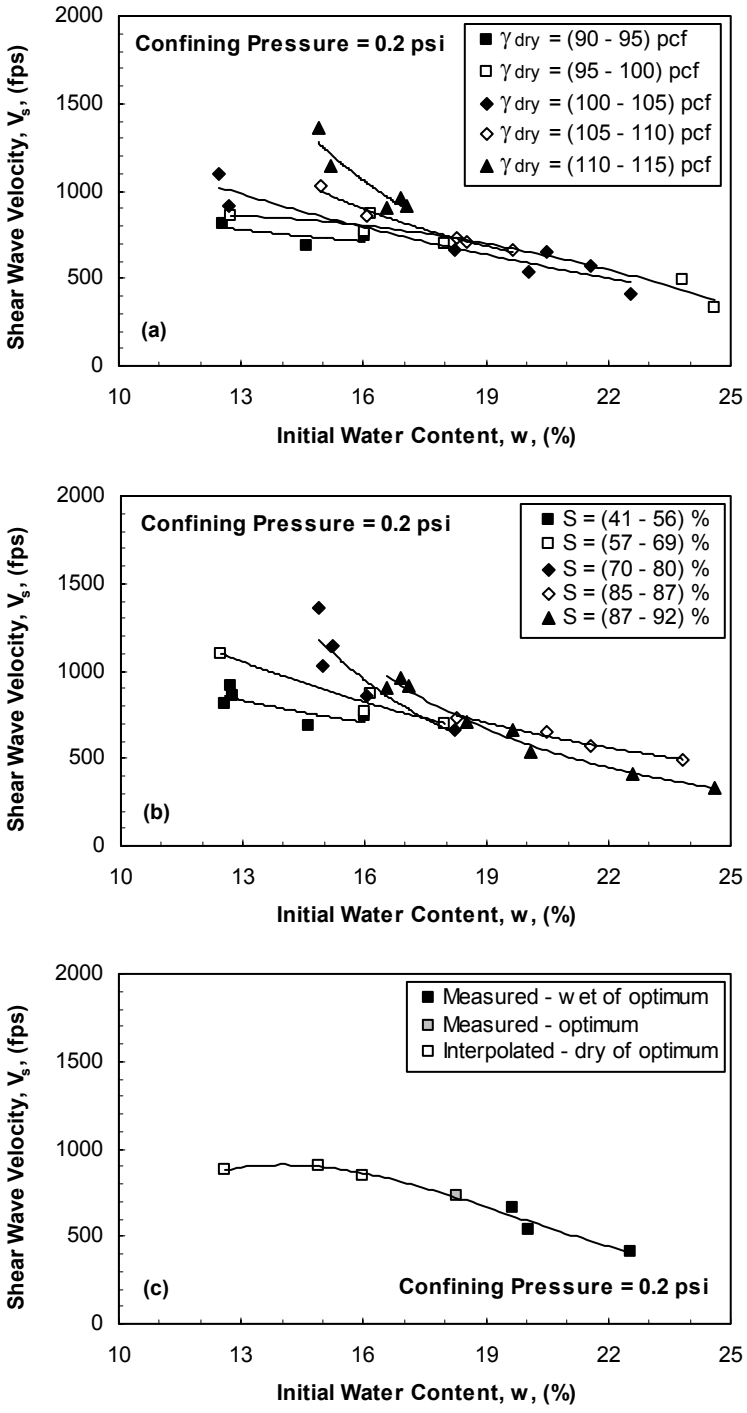

Figure 10.2. Effects of compaction water content on shear wave velocity for specimens compacted at similar: (a) dry unit weights, (b) degrees of saturation, and (c) compactive efforts.

Effects of compaction dry unit weight on shear wave velocity are illustrated in Figure 10.3 for specimens compacted at similar degrees of saturation, water contents, and compactive efforts. For similar initial degrees of saturation, the shear wave velocity increased as the initial dry unit weight increased as illustrated in Figure 10.3(a). Similar observations were reported by Stephenson (1978). For specimens compacted at similar degrees of saturation, the water content essentially decreases as the initial dry unit weight increases, and thus the initial matric suction increases. The observed increase in shear wave velocity is partially due to increase in matric suction and dry unit weight.

Specimens compacted at similar water contents essentially have similar initial matric suctions as discussed in Chapter 7. Accordingly, for specimens compacted at similar water contents, the effect of the initial matric suction on the relationship between shear wave velocity and initial dry unit weight is likely eliminated. For similar initial water contents lower than 17% (w_{opt} = 19%), the shear wave velocity increased as the initial dry unit weight increased as illustrated in Figure 10.3(b). The rate of increase in shear wave velocity with increase in dry unit weight is lower than that observed for specimens compacted at similar degrees of saturation shown in Figure 10.3(a). This lower rate is probably because the effect of matric suction on shear wave velocity is likely eliminated for specimens compacted at similar water contents. For specimens compacted at similar water contents higher than 17%, the effect of the initial dry unit weight on shear wave velocity was not pronounced. The difference between the trends observed for specimens compacted at water contents lower and higher than 17% might be related to unexamined effects of soil fabric and overconsolidation ratio. For similar compaction water contents, Ooi and Pu (2002, 2003) showed that the stiffness increased as the dry unit weight increased up to a point, then dropped for further increase in the dry unit weight. The dry unit weight where the peak stiffness occurred varied with the compactive

effort as shown in Figures 10.4 and 10.5. The data reported by Ooi and Pu (2002, 2003) disagreed with the data presented in this study for the range of dry unit weights and water contents being tested.

The effect of the initial dry unit weight on shear wave velocity for specimens compacted at similar compactive efforts is illustrated in Figure 10.3(c). For specimens compacted wet of optimum, the shear wave velocity increased as the dry unit weight increased, while for specimens compacted dry of optimum, the shear wave velocity decreased as the dry unit weight increased. Changes in shear wave velocity along the standard Proctor compaction curve could be partially attributed to changes in matric suctions associated with changes in water contents and also due to changes in dry unit weight.

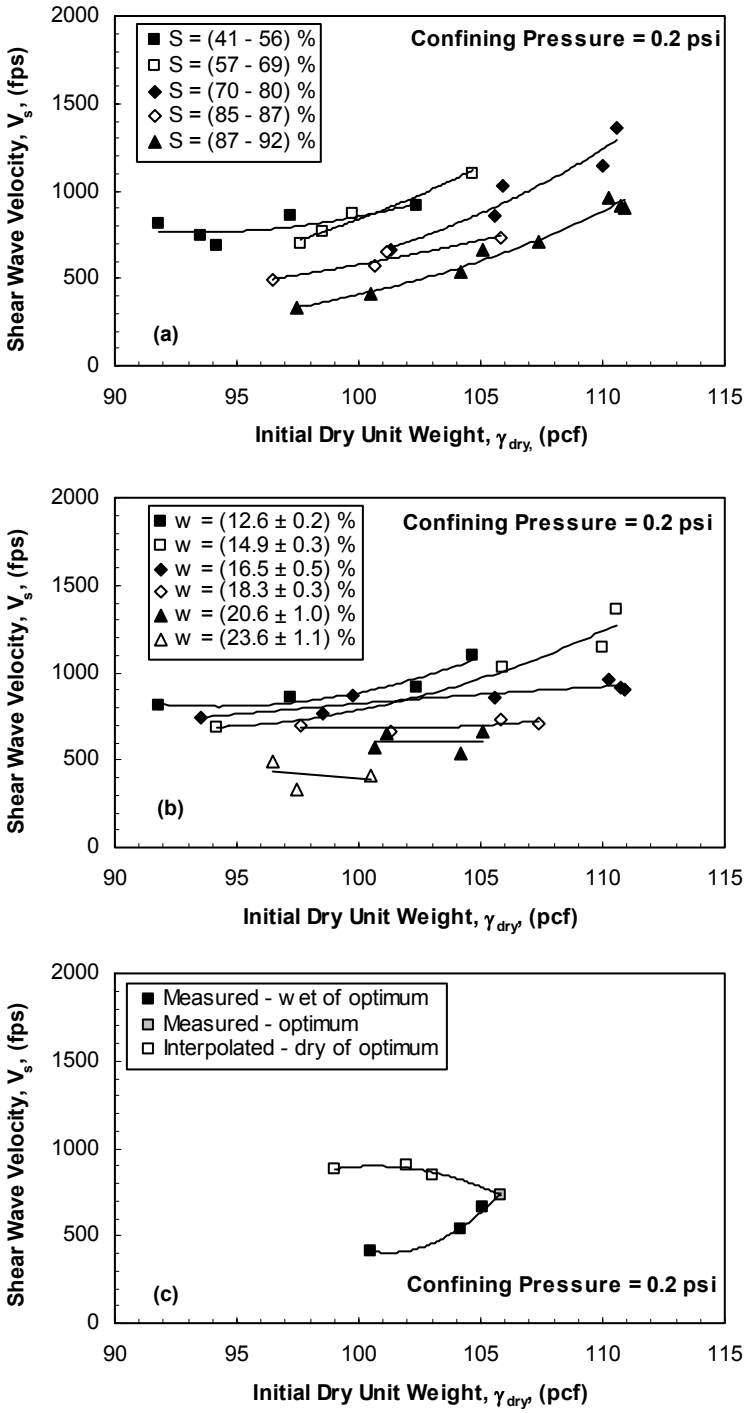

Figure 10.3. Effects of compaction dry unit weight on shear wave velocity for specimens compacted at similar: (a) degrees of saturation, (b) water contents, and (c) compactive efforts.

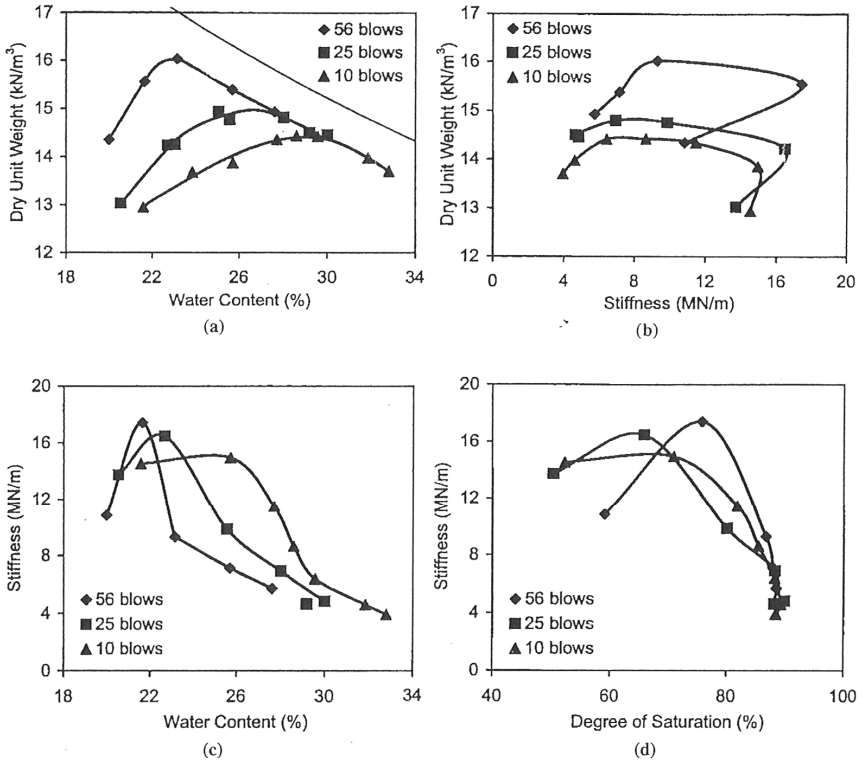

Figure 10.4. Results of stiffness measurements on compacted silt: (a) compaction curves, (b) dry unit weight versus stiffness, (c) stiffness versus water content, and (d) stiffness versus degree of saturation (from Ooi and Pu, 2003).

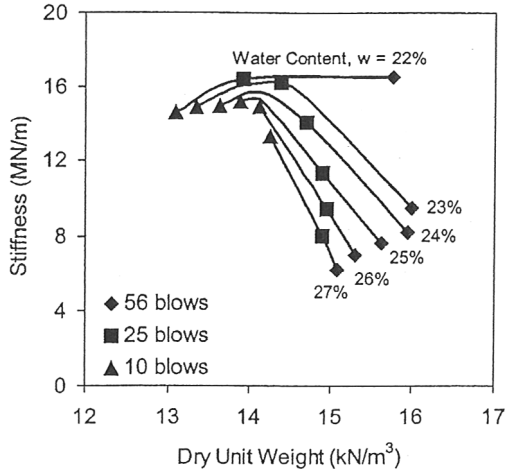

Figure 10.5. Variation of stiffness with dry unit weight at constant water content (from Ooi and Pu, 2003).

For specimens compacted at degrees of saturation dry of optimum, Sheeran et al. (1967) showed linear relationship between the compaction dry unit weight and the product of the compaction water content and *compression* wave velocity. To investigate if this trend is valid for shear wave velocity, the variation of the product of the compaction water content (in decimal form, not in percent) and shear wave velocity with the initial dry unit weight was studied and illustrated in Figure 10.6. Trends similar to those shown by Sheeran et al. (1967) were observed for specimens compacted at degrees of saturation dry or wet of optimum (S_{opt} = 86%). For specimens compacted at degrees of saturation wet of optimum, the rate of increase of the product of the compaction water content and shear wave velocity with the initial dry unit weight was slightly higher than that observed for specimens compacted at degrees of saturation dry of optimum.

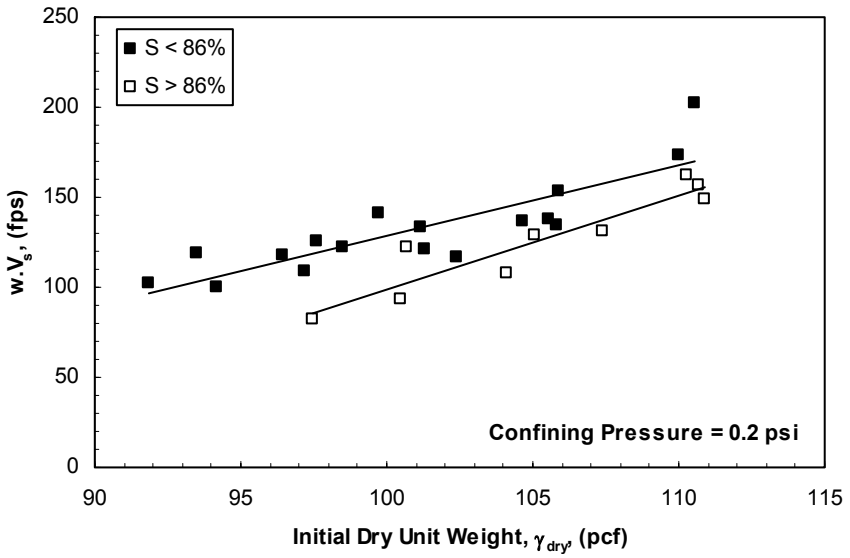

Figure 10.6. Effect of compaction dry unit weight on the product of compaction water content and shear wave velocity.

Effects of compaction degree of saturation on shear wave velocity are illustrated in Figure 10.7 for specimens compacted at similar dry unit weights, water contents, and

compactive efforts. For specimens compacted at dry unit weights ranging from 90 to 100 pcf, the effect of the degree of saturation on shear wave velocity was insignificant for degrees of saturation ranging from 41 to 69% (S_{opt} = 86%) as illustrated in Figure 10.7(a). For degrees of saturation higher than 69%, the shear wave velocity decreased as the degree of saturation increased. For initial dry unit weights ranging from 100 to 115 pcf, the shear wave velocity decreased as the initial degree of saturation increased. With the compaction procedure being used, specimens could not be compacted at degrees of saturation lower than approximately 72% with dry unit weights ranging from 105 to 115 pcf. Therefore, the relationship between shear wave velocity and initial degree of saturation could not be investigated at degrees of saturation lower than 72% for specimens compacted at dry unit weights ranging from 105 to 115 pcf. The decrease in shear wave velocity associated with increase in degree of saturation is partially due to decrease in matric suction. At constant dry unit weights (constant void ratios), Stephenson (1978) showed that the shear modulus increased as the degree of saturation increased from 35 to 85%, which disagreed with the data presented in this study.

For specimens compacted at similar water contents lower than 17% (w_{opt} = 19%), the shear wave velocity increased as the initial degree of saturation increased as illustrated in Figure 10.7(b). The rate of increase of the shear wave velocity with increase in initial degree of saturation decreased as the initial water content increased. Similar observation was noted for the relationship between shear wave velocity and dry unit weight shown in Figure 10.3(b). For specimens compacted at initial water contents ranging from 18 to 21%, the effect of the initial degree of saturation on shear wave velocity was not pronounced. At an initial water content of approximately 24%, the shear wave velocity decreased as the initial degree of saturation increased. The difference

between the trends observed for specimens compacted at different water contents might be related to unexamined effects of soil fabric and overconsolidation ratio.

For specimens compacted at similar compactive efforts, the effect of degree of saturation on shear wave velocity was insignificant for degrees of saturation ranging from 46 to 69% (S_{opt} = 86%). For degrees of saturation higher than 69%, the shear wave velocity decreased as the degree of saturation increased as illustrated in Figure 10.7(c). The decrease in shear wave velocity associated with increase in degree of saturation is partially due to decrease in matric suction. For specimens compacted at the same compactive effort, Ooi and Pu (2002, 2003) indicated that the shear wave velocity peaked within degrees of saturation ranging from 66 to 76% as shown in Figure 10.4. The data presented in Figure 10.7(c) suggested that higher shear wave velocities occurred at lower degrees of saturation, but did not confirm a distinct peak for the range of degrees of saturations being tested.

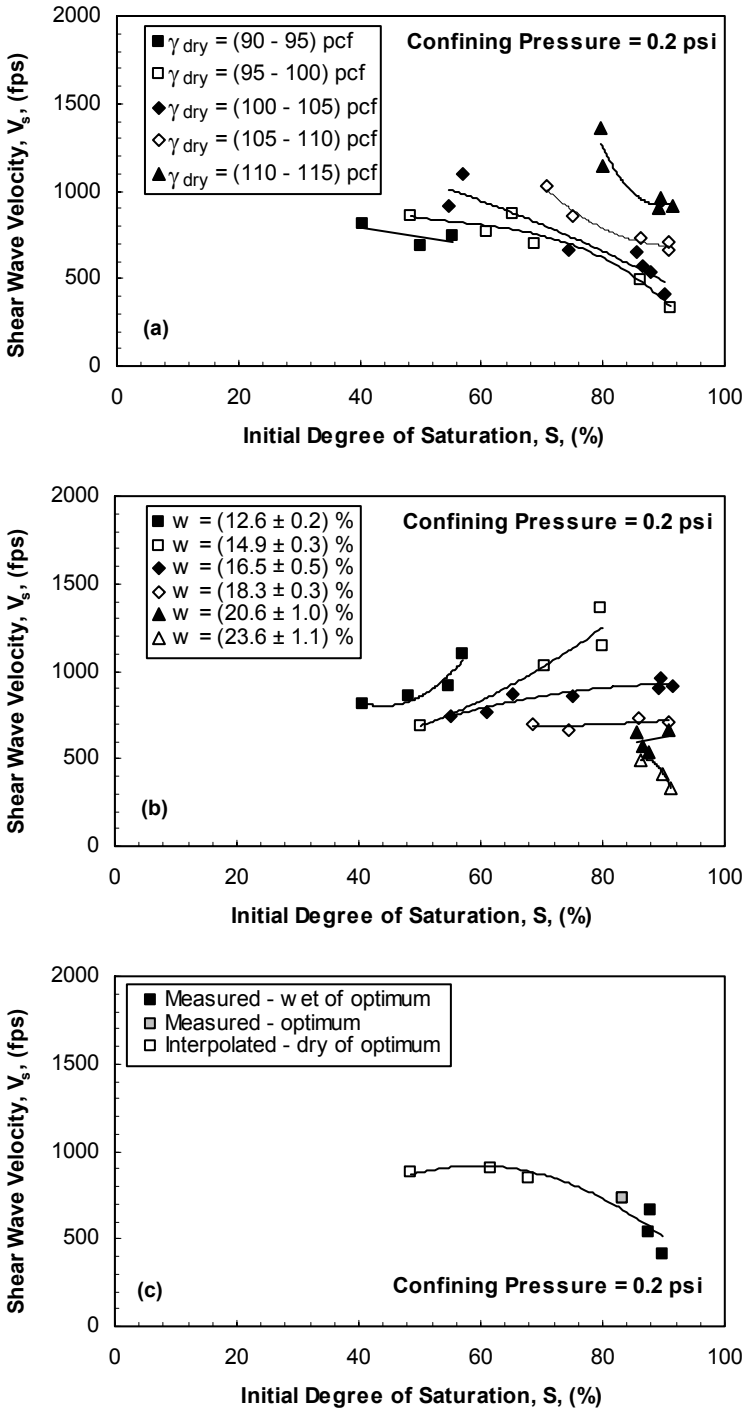

Figure 10.7. Effects of compaction degree of saturation on shear wave velocity for specimens compacted at similar: (a) dry unit weights, (b) water contents, and (c) compactive efforts.

10.2.1.2Measurements under a confining pressure of 15 psi

The standard Proctor compaction curve and measured shear wave velocities, for all 26 specimens, after increasing the confining pressure from 0.2 to 15 psi are presented in Figure 10.8. Effects of compaction water content, dry unit weight, and degree of saturation on shear wave velocities measured under confining pressures of 0.2 and 15 psi are compared below.

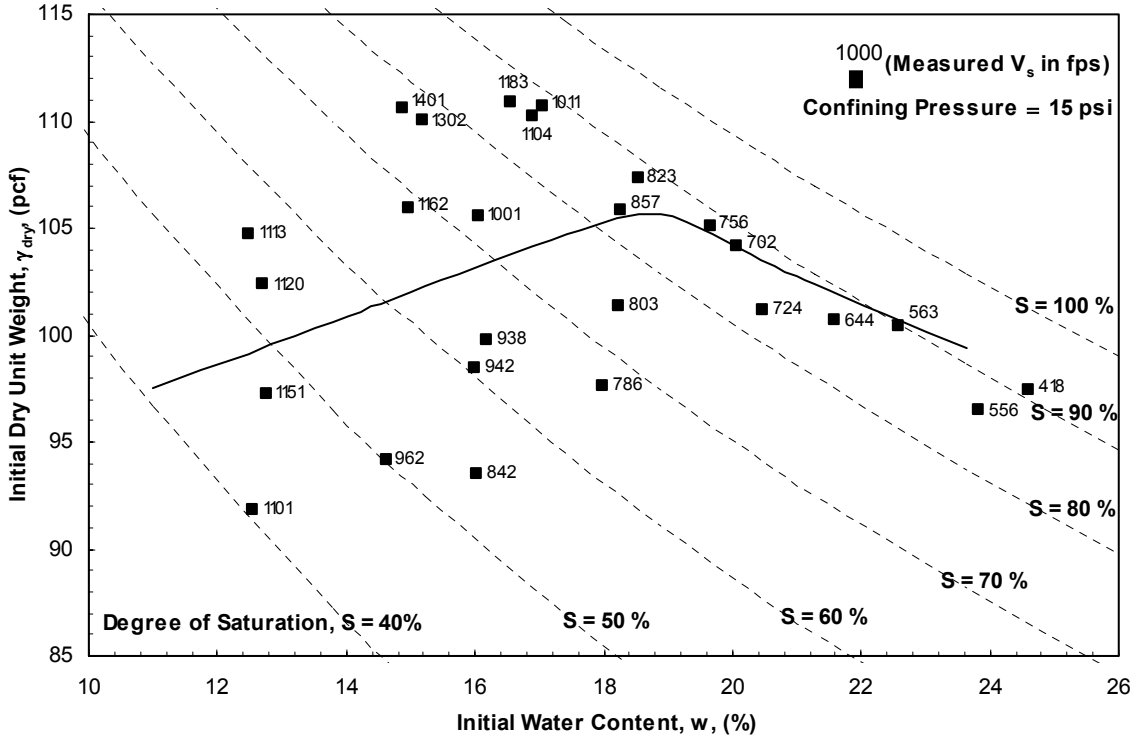

Figure 10.8. Standard Proctor compaction curve and shear wave velocities measured under confining pressure of 15 psi.

Effects of compaction water content on shear wave velocity are illustrated in Figure 10.9 for specimens compacted at similar dry unit weights, degrees of saturation, and compactive efforts. For similar initial dry unit weights, the effect of the compaction water content on shear wave velocity shown in Figure 10.9(a) was slightly different from

that observed under confining pressure of 0.2 psi shown earlier in Figure 10.2(a). Under a confining pressure of 15 psi, for initial dry unit weights ranging from 90 to 100 pcf, the shear wave velocity decreased as the water content increased for water contents ranging from 13 to 16%. Under a confining pressure of 0.2 psi, the effect of the initial water content on shear wave velocity was insignificant for the same ranges of water contents and dry unit weights. For similar initial degrees of saturation, the effect of the initial water content on shear wave velocity shown in Figure 10.9(b) was generally similar to that observed under confining pressure of 0.2 psi shown earlier in Figure 10.2(b). For specimens compacted at similar compactive efforts, the effect of the compaction water content on shear wave velocity shown in Figure 10.9(c) was slightly different from that observed under confining pressure of 0.2 psi shown earlier in Figure 10.2(c). Under a confining pressure of 15 psi, the shear wave velocity slightly increased as the initial water content decreased for water contents ranging from 13 to 16%. Under a confining pressure of 0.2 psi, the effect of the initial water content on shear wave velocity was insignificant for the same range of water contents.

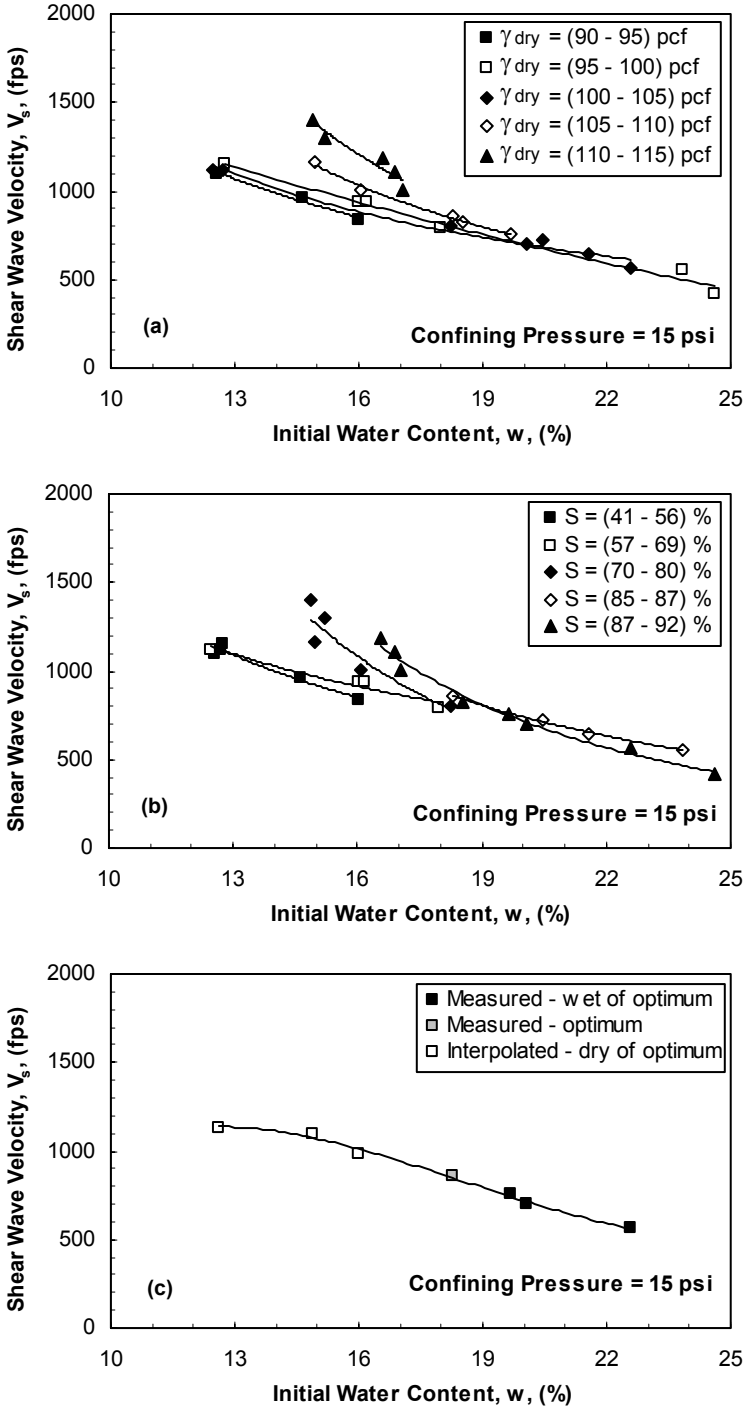

Figure 10.9. Effects of compaction water content on shear wave velocity for specimens compacted at similar: (a) dry unit weights, (b) degrees of saturation, and (c) compactive efforts.

Effects of compaction dry unit weight on shear wave velocity are illustrated in Figure 10.10 for specimens compacted at similar degrees of saturation, water contents, and compactive efforts. For similar initial degrees of saturation, the effect of the initial dry unit weight on shear wave velocity shown in Figure 10.10(a) was generally similar to that observed under confining pressure of 0.2 psi shown earlier in Figure 10.3(a). For similar initial water contents, the effect of the initial dry unit weight on shear wave velocity shown in Figure 10.10(b) was slightly different from that observed under confining pressure of 0.2 psi shown earlier in Figure 10.3(b). Under a confining pressure of 15 psi, at an initial water content of approximately 13%, the effect of the initial dry unit weight on shear wave velocity was not pronounced. Under a confining pressure of 0.2 psi, the shear wave velocity increased as the initial dry unit weight increased at the same water content. For specimens compacted at similar compactive efforts, the effect of increasing the initial dry unit weight on shear wave velocity shown in Figure 10.10(c) was similar to that observed under confining pressure of 0.2 psi shown earlier in Figure 10.3(c).

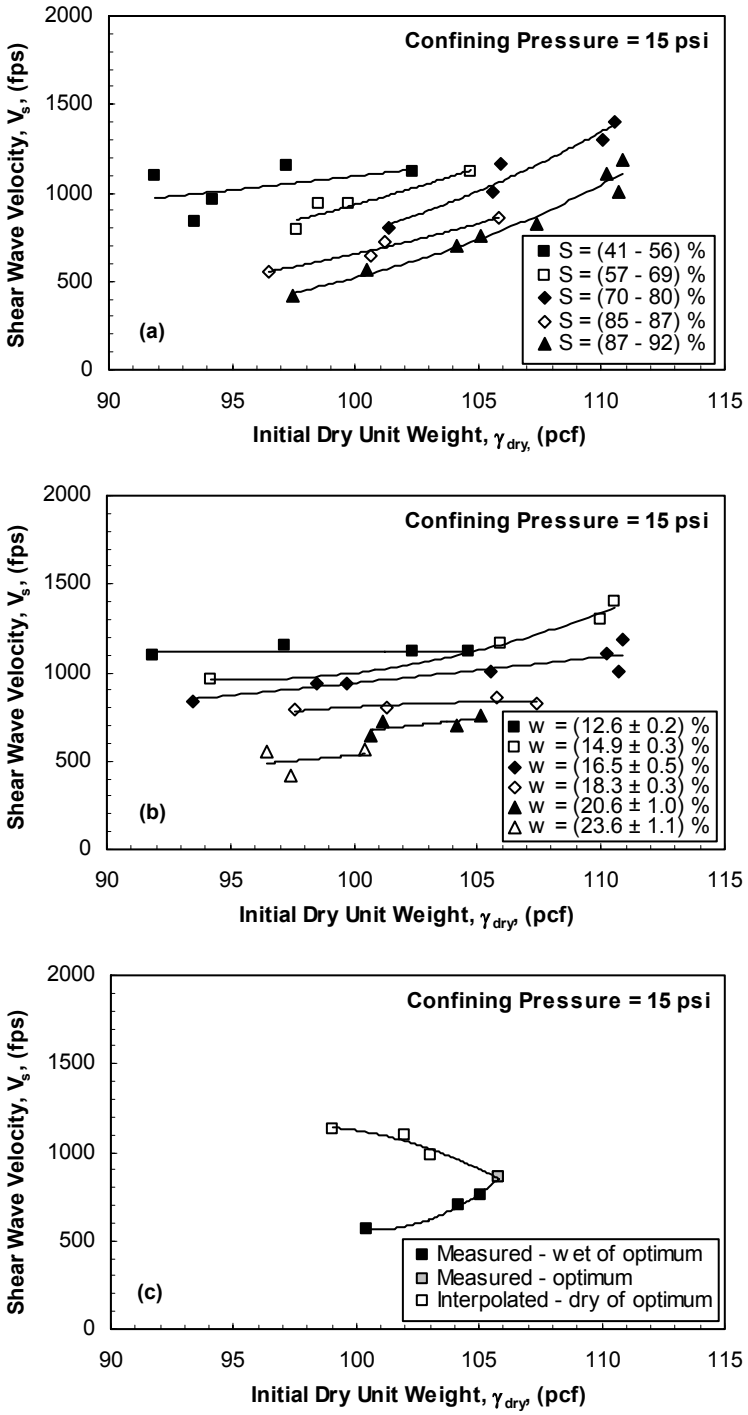

Figure 10.10. Effects of compaction dry unit weight on shear wave velocity for specimens compacted at similar: (a) degrees of saturation, (b) water contents, and (c) compactive efforts.

The effect of the compaction dry unit weight on the product of the compaction water content and shear wave velocity is illustrated in Figure 10.11. The general trend for the variation of the product of the compaction water content (in decimal form, not in percent) and shear wave velocity with the initial dry unit weight was similar to that observed under confining pressure of 0.2 psi shown earlier in Figure 10.6. For specimens compacted at degrees of saturation wet of optimum, the rate of increase of the product of the compaction water content and shear wave velocity with the increase in initial dry unit weight was significantly higher than that observed for specimens compacted at degrees of saturation dry of optimum, which was not observed under confining pressure of 0.2 psi. Under confining pressure of 0.2 psi, for specimens compacted at degrees of saturation wet of optimum, the rate of increase of the product of the compaction water content and shear wave velocity with the increase in initial dry unit weight was slightly higher than that observed for specimens compacted at degrees of saturation dry of optimum.

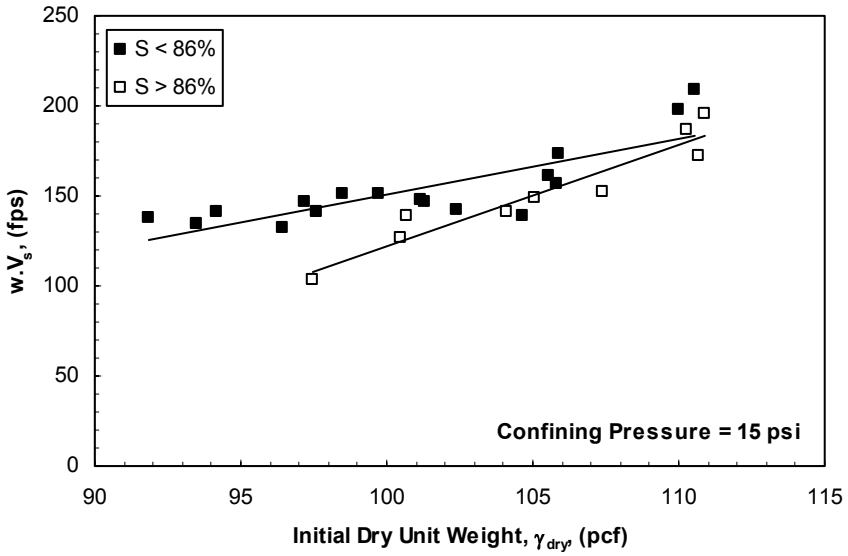

Figure 10.11. Effect of compaction dry unit weight on the product of the shear wave velocity and the compaction water content.

Effects of compaction degree of saturation on shear wave velocity are illustrated in Figure 10.12 for specimens compacted at similar dry unit weights, water contents, and compactive efforts. For similar initial dry unit weights, the effect of the degree of saturation on shear wave velocity shown in Figure 10.12(a) was slightly different from that observed under confining pressure of 0.2 psi shown earlier in Figure 10.7(a). Under a confining pressure of 15 psi, for initial dry unit weights ranging from 90 to 100 pcf, the shear wave velocity decreased as the initial degree of saturation increased for degrees of saturation ranging from 41 to 69%. Under a confining pressure of 0.2 psi, the effect of the initial degree of saturation on shear wave velocity was insignificant for the same ranges of degrees of saturation and dry unit weights. For specimens compacted at similar water contents, the effect of the initial degree of saturation on shear wave velocity shown in Figure 10.12(b) was slightly different from that observed under confining pressure of 0.2 psi shown earlier in Figure 10.7(b). Under a confining pressure of 15 psi, at an initial

water content of approximately 13%, the effect of the initial dry unit weight on shear wave velocity was not pronounced. Under confining pressure of 0.2 psi, the shear wave velocity increased as the initial degree of saturation increased for the same water content. For specimens compacted at similar compactive efforts, the effect of increasing the initial degree of saturation on shear wave velocity shown in Figure 10.12(c) was similar to that observed under confining pressure of 0.2 psi shown earlier in Figure 10.7(c).

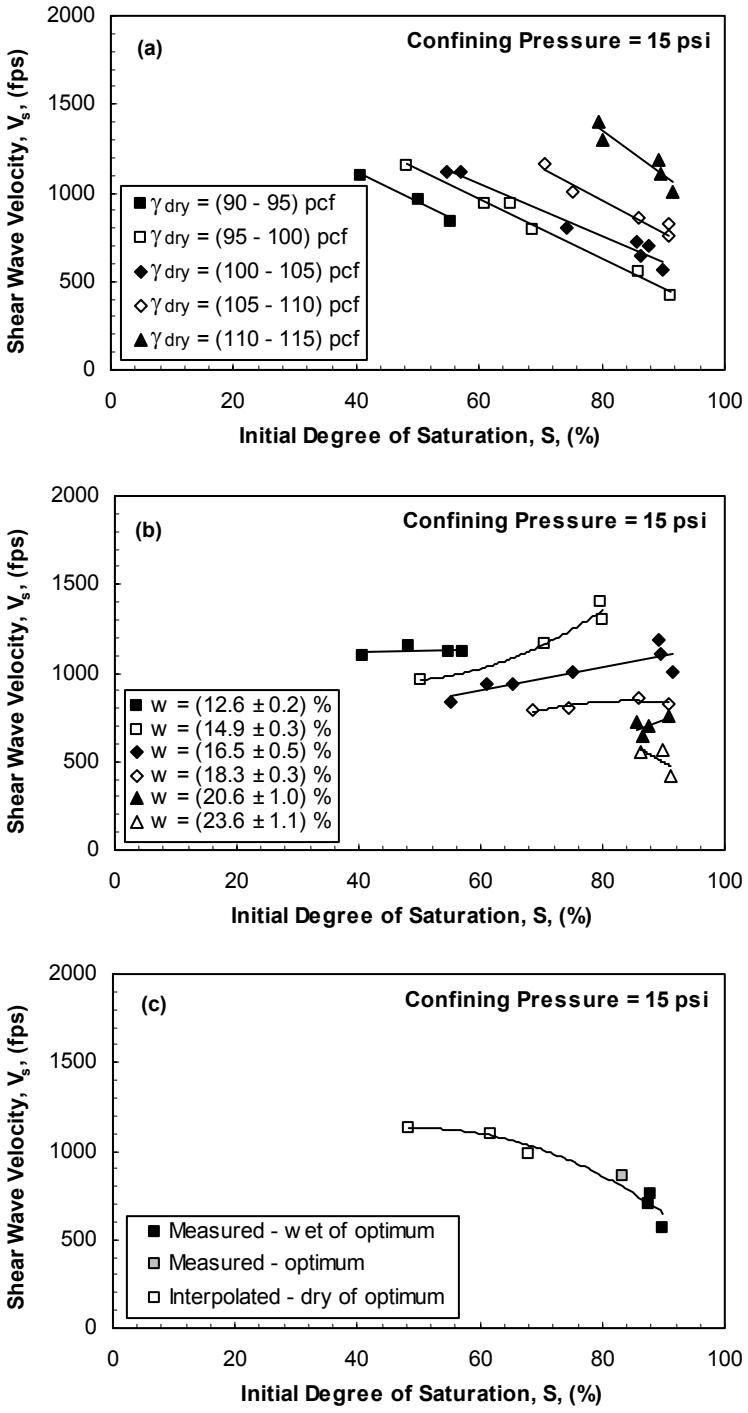

Figure 10.12. Effects of compaction degree of saturation on shear wave velocity for specimens compacted at similar: (a) dry unit weights, (b) water contents, and (c) compactive efforts.

In summary, increasing the confining pressure from 0.2 to 15 psi, under undrained conditions, slightly affected the effects of compaction conditions on shear wave velocity. Possible reasons for the different trends observed at confining pressures of 0.2 and 15 psi are discussed in Section 10.2.3.

10.2.2 COMPRESSION WAVE VELOCITIES

The effects of compaction conditions on compression wave velocities measured under confining pressures of 0.2 and 15 psi are presented separately below. The effects of compaction conditions on compression wave velocities were investigated for specimens compacted at similar water contents, dry unit weights, degrees of saturation, and compactive efforts. Interpolation was implemented to estimate compression wave velocities for specimens compacted dry of optimum that would coincide with the standard Proctor compaction curve.

10.2.2.1 Measurements under a confining pressure of 0.2 psi

The results of 16 out of 26 tests conducted at the confining pressure of 0.2 psi are presented in this section. The remaining 10 tests were excluded because there was no good contact between the piezoelectric disks and both ends of the specimen. This poor contact was probably due to the difficulty in making precise indentations in the specimen need to fit the piezoelectric disks. Good contact between the piezoelectric transducers and the specimen is required to receive detectable waves. The standard Proctor compaction curve and measured compression wave velocities for the 16 specimens, for which the measurements are believed to be valid, are presented in Figure 10.13.

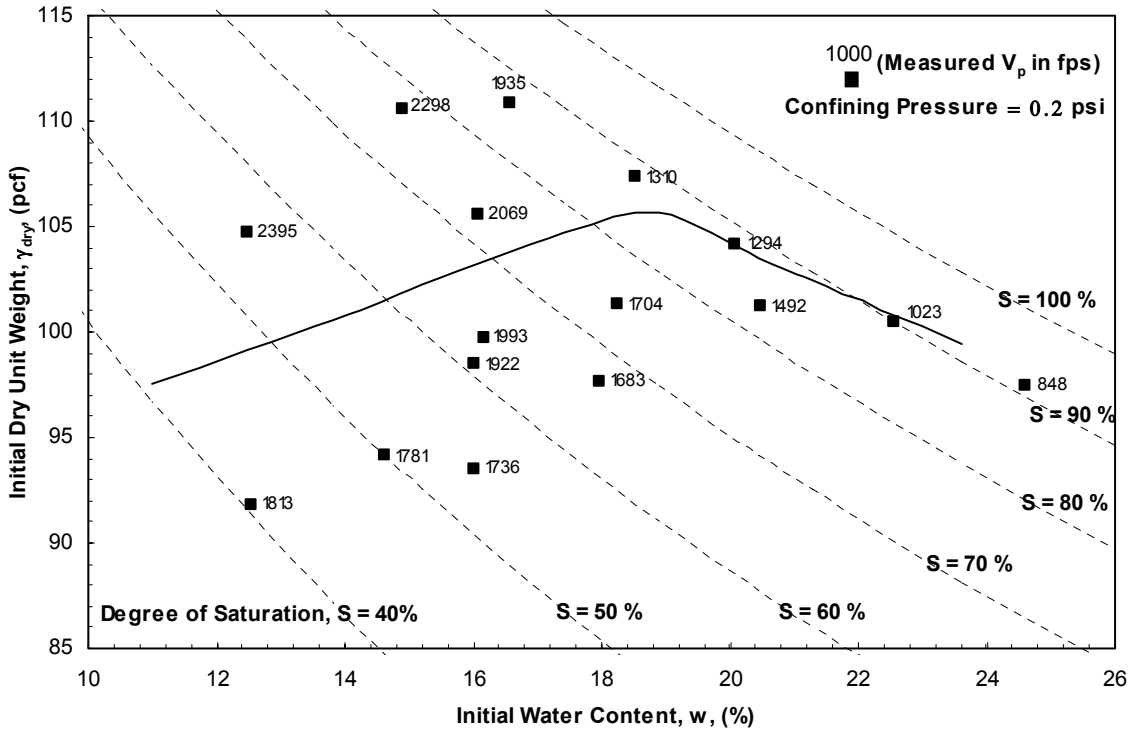

Figure 10.13. Standard Proctor compaction curve and compression wave velocities measured under confining pressure of 0.2 psi.

Effects of compaction water content on compression wave velocity are illustrated in Figure 10.14 for specimens compacted at similar dry unit weights, degrees of saturation, and compactive efforts. For initial dry unit weights ranging from 90 to 95 pcf, the effect of the initial water content on compression wave velocities was insignificant for water contents ranging from 13 to 16% (w_{opt} = 19) as illustrated in Figure 10.14(a). For higher initial dry unit weights, ranging from 95 to 115 pcf, the compression wave velocity decreased as the initial water content increased. However, the relationship between the compression wave velocity and compaction water content could not be studied at water contents lower than approximately 15% with dry unit weights ranging from 105 to 115 pcf as discussed in Section 10.2.1.1. The decrease in compression wave

velocity associated with increase in water content is partially due to decrease in matric suction as discussed in Section 10.5.

For initial degrees of saturation ranging from 41 to 56%, the initial water content did not have a significant effect on the compression wave velocity as illustrated in Figure 10.14(b). For similar initial degrees of saturation higher than 56%, the compression wave velocity decreased as the initial water content increased. However, the relationship between the compression wave velocity and compaction water content at a constant degree of saturation could not be studied over a wide range of water contents for the reasons discussed earlier in Section 10.2.2.1. For specimens compacted at similar degrees of saturation, the dry unit weights and matric suctions essentially increase as the water content decreases. Accordingly, changes in compression wave velocity with water content could be partially attributed to changes in dry unit weight and matric suction as discussed in following sections.

For specimens compacted at similar compactive efforts, the effect of the initial water content on compression wave velocity was insignificant for water contents ranging from 13 to 16% (w_{opt} = 19%) as illustrated in Figure 10.14(c). For water contents higher than 16%, the compression wave velocity decreased as the initial water content increased. The decrease in compression wave velocity associated with increase in water content is partially due to decrease in matric suction.

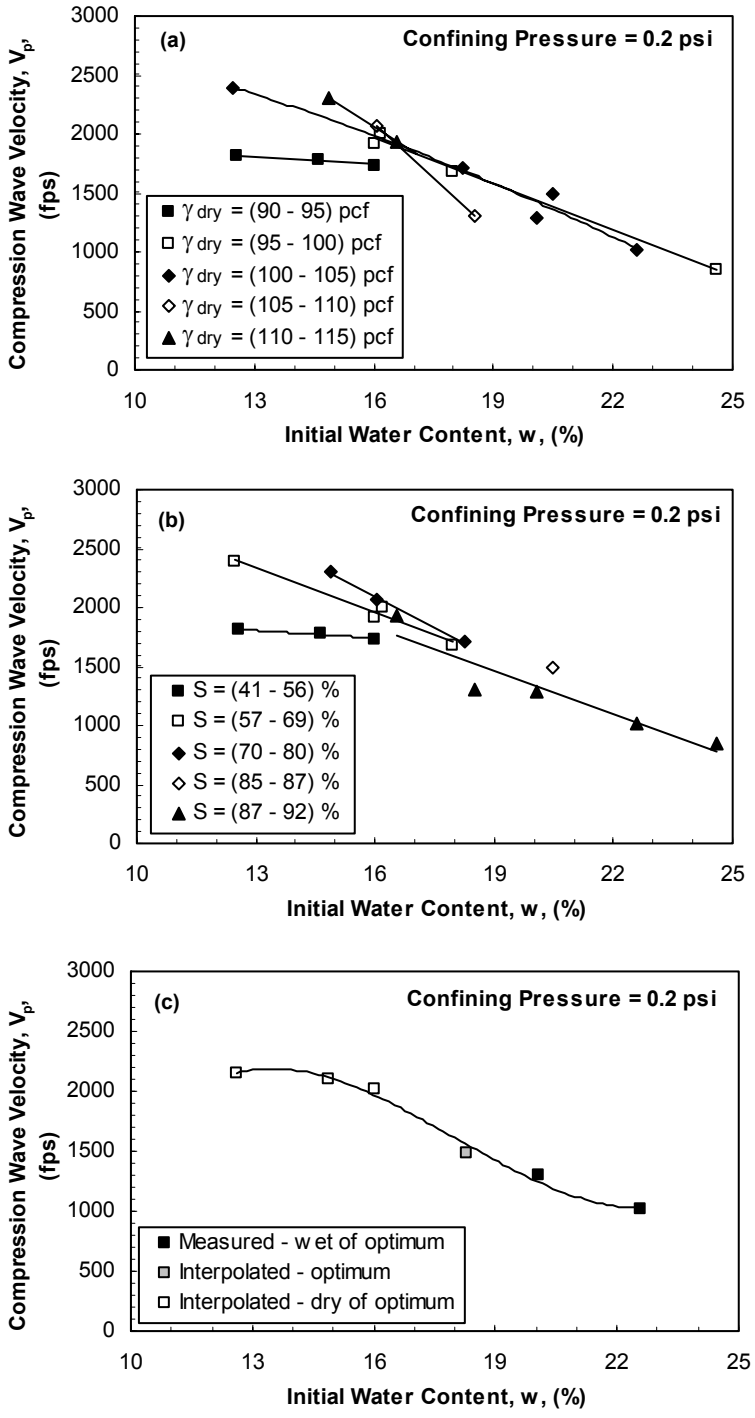

Figure 10.14. Effects of compaction water content on compression wave velocity for specimens compacted at similar: (a) dry unit weights, (b) degrees of saturation, and (c) compactive efforts.

Effects of compaction dry unit weight on compression wave velocity are illustrated in Figure 10.15 for specimens compacted at similar degrees of saturation, water contents, and compactive efforts. For similar initial degrees of saturation ranging from 41 to 56%, no clear trend could be defined for the effect of initial dry unit weight on the compression wave velocity because the specimens were not compacted over a wide range of dry unit weights. For similar initial degrees of saturation higher than 56%, the compression wave velocity increased as the initial dry unit weight increased as illustrated in Figure 10.15(a). Similar observations were reported by Stephenson (1978). The observed increase in compression wave velocity is partially due to increase in dry unit weight and matric suction as discussed in Section 10.2.1.1.

For similar initial water contents, the effect of the initial matric suction on the relationship between compression wave velocity and initial dry unit weight is likely eliminated. For specimens compacted at similar water contents lower than approximately 16% (w_{opt} = 19%), the compression wave velocity increased as the initial dry unit weight increased as illustrated in Figure 10.15(b). For similar initial water contents ranging from 16 to 19%, the compression wave velocity increased as the initial dry unit weight increased and then decreased for further increase in dry unit weight. Similar observations were reported by Sheeran et al. (1967). For similar initial water contents higher than 19%, no clear trend could be defined for the effect of the initial dry unit weight on compression wave velocity because the specimens were not compacted over a wide range of dry unit weights. The difference between the trends observed for specimens compacted at different water contents might be related to unexamined effects of soil fabric and overconsolidation ratio. Leslie (1950) reported that at the optimum water content, the compression wave velocity increased as the dry unit weight increased, which disagrees with the data reported in this study.

The effect of the initial dry unit weight on compression wave velocity for specimens compacted at similar compactive efforts is illustrated in Figure 10.15(c). For specimens compacted wet of optimum, the compression wave velocity increased as the dry unit weight increased; while for specimens compacted dry of optimum, the compression wave velocity decreased as the dry unit weight increased. Changes in compression wave velocity along the standard Proctor compaction curve could be partially attributed to changes in matric suction and dry unit weight as discussed in Section 10.2.1.1.

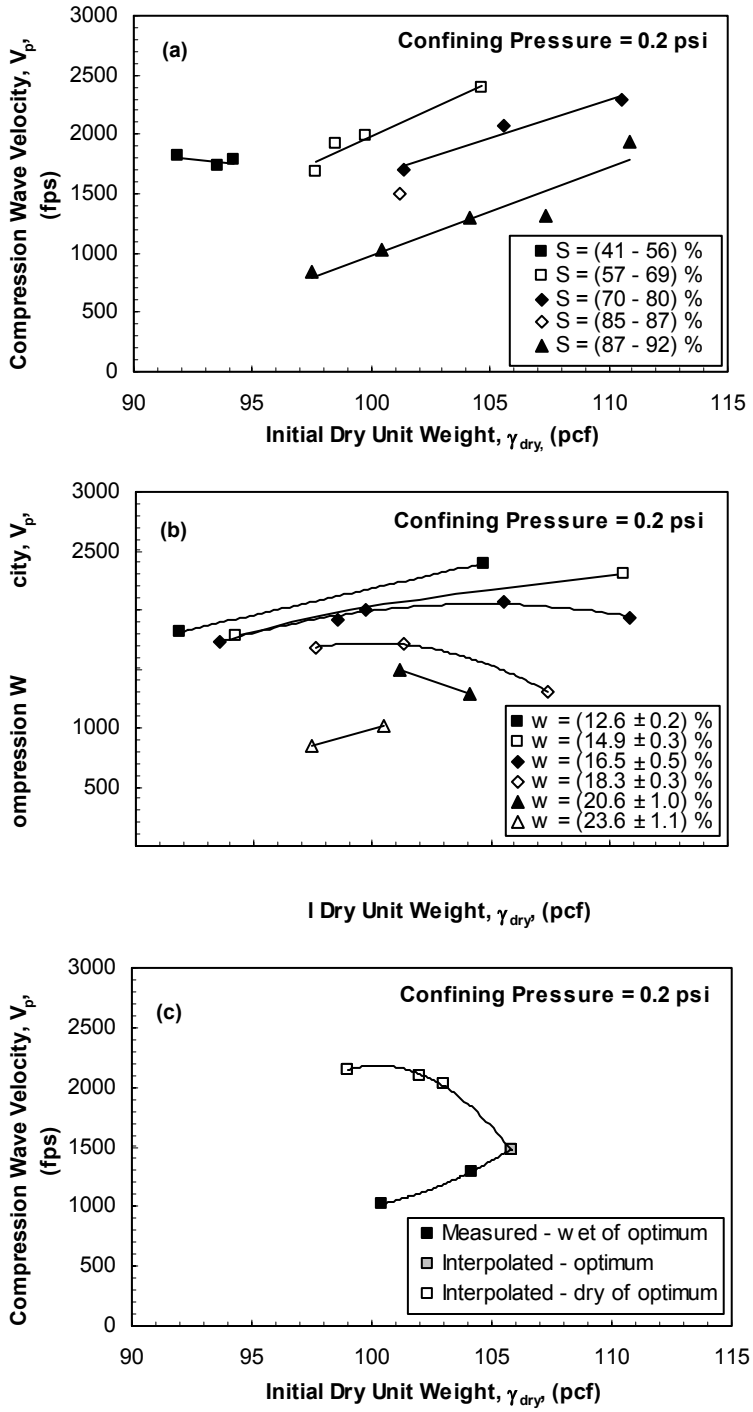

Figure 10.15. Effects of compaction dry unit weight on compression wave velocity for specimens compacted at similar: (a) degrees of saturation, (b) water contents, and (c) compactive efforts.

For specimens compacted at degrees of saturation dry of optimum, Sheeran et al. (1967) showed linear relationship between the compaction dry unit weight and the product of the compaction water content and compression wave velocity as shown in Figure 10.16. To investigate if this trend is valid for the data presented in this study, the variation of the product of the compaction water content (in decimal form, not in percent) and compression wave velocity with the initial dry unit weight was studied and illustrated in Figure 10.17. Trends similar to those shown by Sheeran et al. (1967) were observed for specimens compacted at degrees of saturation dry or wet of optimum (S_{opt} = 86%). For specimens compacted at degrees of saturation wet of optimum, the rate of increase of the product of compaction water content and compression wave velocity with increase in initial dry unit weight was slightly higher than that observed for specimens compacted at degrees of saturation dry of optimum.

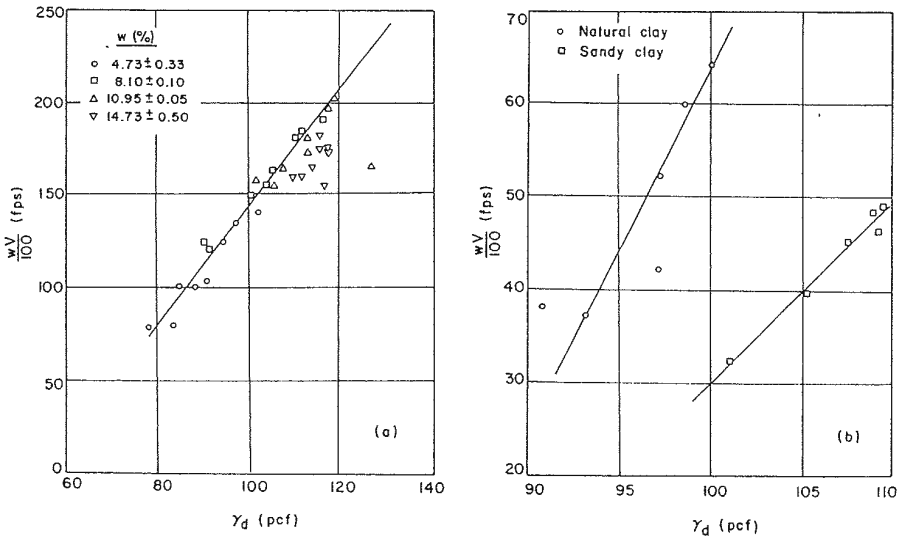

Figure 10.16. Effect of dry unit weight on the product of the compression wave velocity and the compaction water content (from Sheeran et al., 1967).

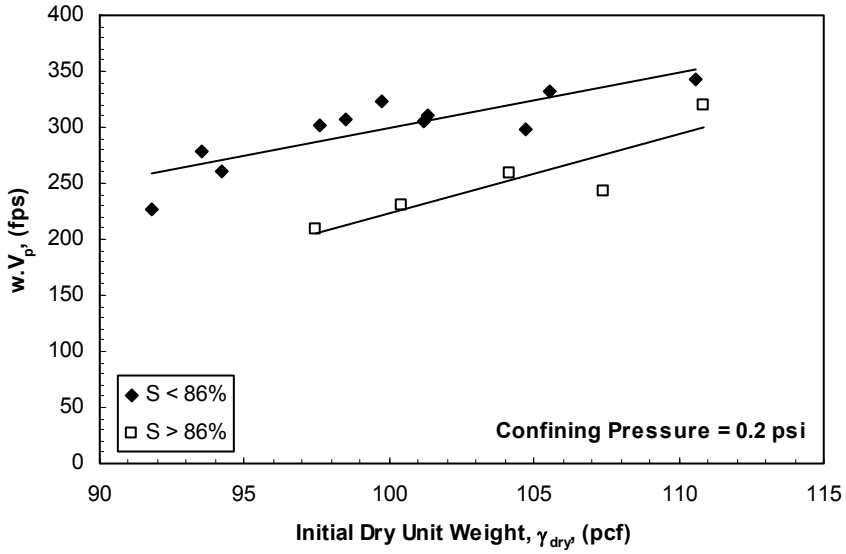

Figure 10.17. Effect of compaction dry unit weight on the product of the compression wave velocity and the compaction water content.

Effects of compaction degree of saturation on compression wave velocity are illustrated in Figure 10.18 for specimens compacted at similar dry unit weights, water

contents, and compactive efforts. For specimens compacted at dry unit weights ranging from 90 to 95 pcf, the initial degree of saturation did not have a significant effect on the compression wave velocity as illustrated in Figure 10.18(a). For higher initial dry unit weights, ranging from 95 to 115 pcf, the compression wave velocity decreased as the initial degree of saturation increased. The decrease in compression wave velocity associated with increase in degree of saturation is partially due to decrease in matric suction. At constant dry unit weights (constant void ratios), Stephenson (1978) showed that the constrained modulus increased as the degree of saturation increased from 35 to 85%, which disagreed with the data presented in this study.

For specimens compacted at similar water contents, the effect of the initial matric suction on the relationship between compression wave velocity and initial degree of saturation is likely eliminated. For similar water contents lower than 16% (w_{opt} = 19%), the compression wave velocity increased as the initial degree of saturation increased as illustrated in Figure 10.18(b). For similar water contents ranging from 16 to 19%, the compression wave velocity increased as the degree of saturation increased and then decreased for further increase in degree of saturation. For similar water contents higher than 19%, the compression wave velocity decreased as the initial degree of saturation increased. Similar trends were observed for the relationship between compression wave velocity and dry unit weight shown in Figure 10.15(b). The difference between the trends observed for specimens compacted at different water contents might be related to unexamined effects of soil fabric and overconsolidation ratio.

For specimens compacted at similar compactive efforts, the effect of degree of saturation on compression wave velocity was insignificant for degrees of saturation ranging from 46 to 68% (S_{opt} = 86%). For degrees of saturation higher than 68%, the

compression wave velocity decreased as the degree of saturation increased as illustrated in Figure 10.18(c). The decrease in compression wave velocity associated with increase in degree of saturation is partially due to decrease in matric suction.

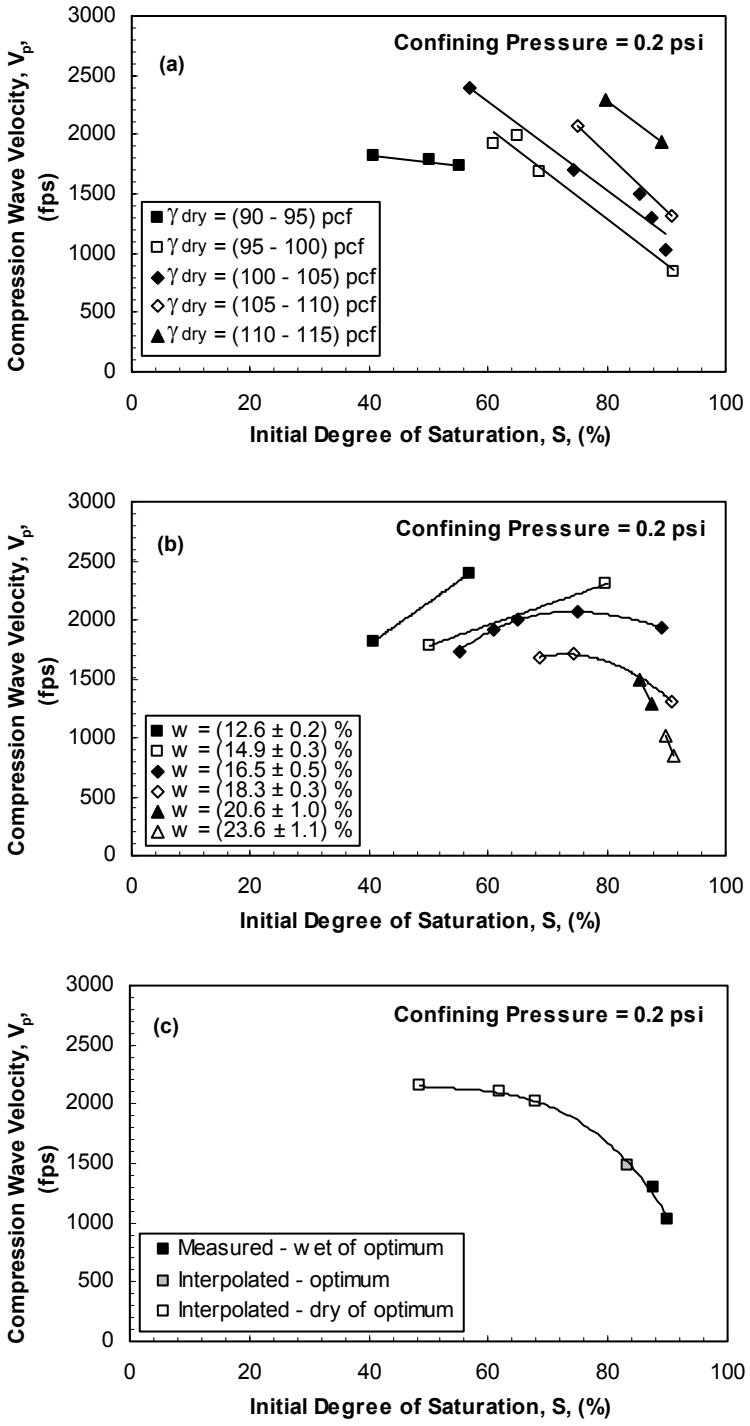

Figure 10.18. Effects of compaction degree of saturation on compression wave velocity for specimens compacted at similar: (a) dry unit weights, (b) water contents, and (c) compactive efforts.

10.2.2.2Measurements under a confining pressure of 15 psi

The results of 24 out of 26 tests conducted at the confining pressure of 15 psi are presented in this section. The remaining two tests were excluded because there was no good contact between the piezoelectric disks and both ends of the specimen. The standard Proctor compaction curve and measured compression wave velocities for the 24 specimens, for which the measurements are believed to be valid, are presented in Figure 10.19.

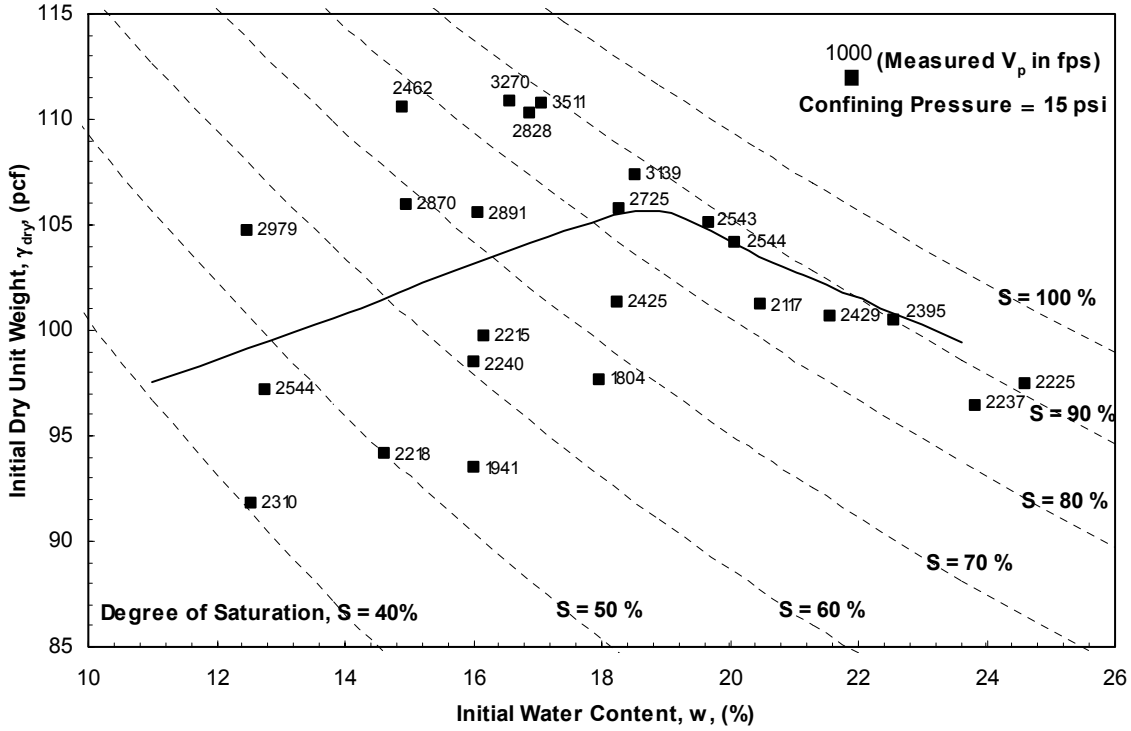

Figure 10.19. Standard Proctor compaction curve and compression wave velocities measured under confining pressure of 15 psi.

Effects of compaction water content on compression wave velocity are illustrated in Figure 10.20 for specimens compacted at similar dry unit weights, degrees of saturation, and compactive efforts. For similar initial dry unit weights, the effect of

compaction water content on compression wave velocity shown in Figure 10.20(a) was different from that observed under confining pressure of 0.2 psi shown earlier in Figure 10.14(a). Under a confining pressure of 15 psi, no clear trend could be defined for the effect of the initial water content on compression wave velocity. Under confining pressure of 0.2 psi, for initial dry unit weights ranging from 90 to 95 pcf, the effect of the initial water content on compression wave velocities was insignificant for water contents ranging from 13 to 16% (w_{opt} = 19). For higher initial dry unit weights, ranging from 95 to 115 pcf, the compression wave velocity decreased as the water content increased.

For similar initial degrees of saturation, the effect of the initial water content on compression wave velocity shown in Figure 10.20(b) was slightly different from that observed under confining pressure of 0.2 psi shown earlier in Figure 10.14(b). Under a confining pressure of 15 psi, for initial degrees of saturation ranging from 41 to 56%, the compression wave velocity decreased as the water content increased for water contents ranging from 13 to 16%. Under a confining pressure of 0.2 psi, the effect of the initial water content on compression wave velocity was insignificant for the same ranges of degree of saturation and water content.

For specimens compacted at similar compactive efforts, the effect of the compaction water content on compression wave velocity shown in Figure 10.20(c) was different from that observed under confining pressure of 0.2 psi shown earlier in Figure 10.14(c). Under a confining pressure of 15 psi, the effect of the compaction water content on compression wave velocity was insignificant. Under confining pressure of 0.2 psi, the effect of the initial water content on compression wave velocity was insignificant for water contents ranging from 13 to 16% (w_{opt} = 19%). For water contents higher than 16%, the compression wave velocity decreased as the initial water content increased.

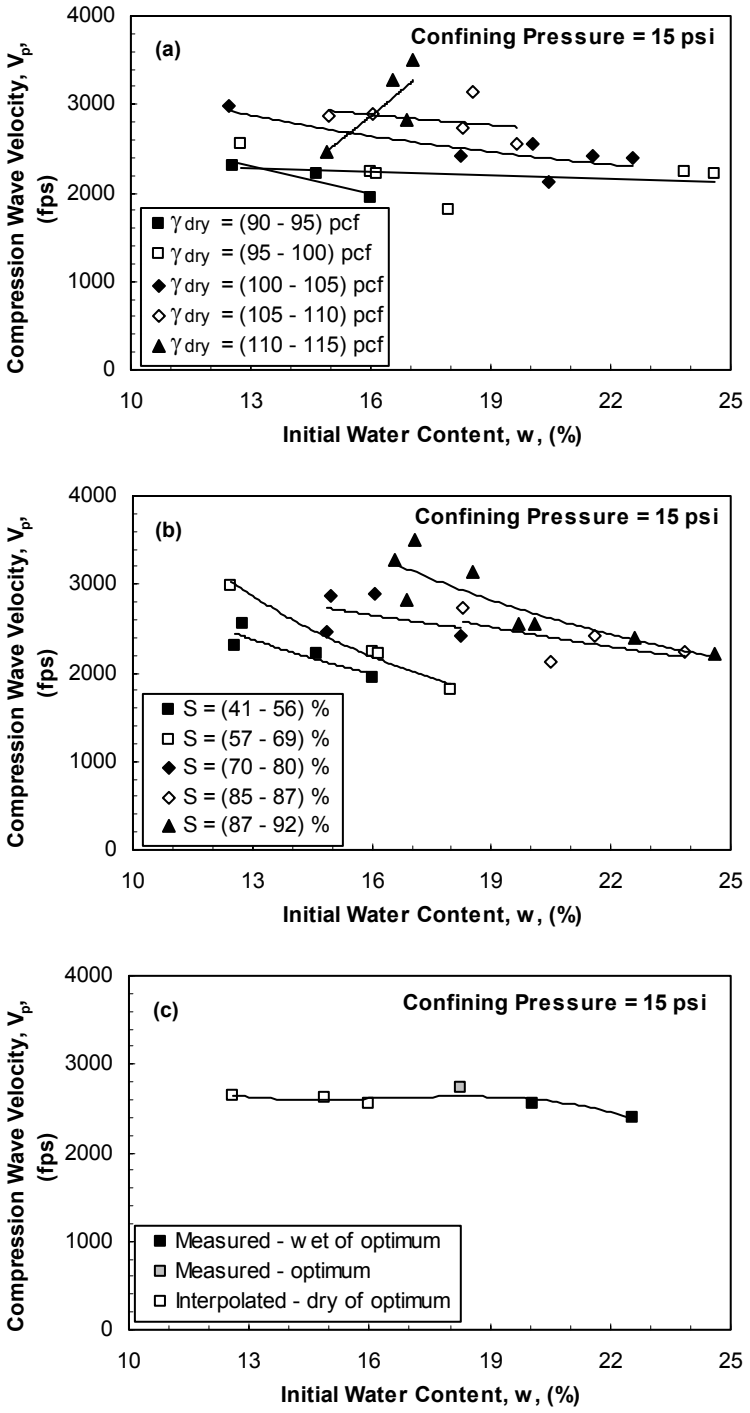

Figure 10.20. Effects of compaction water content on compression wave velocity for specimens compacted at similar: (a) dry unit weights, (b) degrees of saturation, and (c) compactive efforts.

Effects of compaction dry unit weight on compression wave velocity are illustrated in Figure 10.21 for specimens compacted at similar degrees of saturation, water contents, and compactive efforts. For similar initial degrees of saturation, the effect of the initial dry unit weight on compression wave velocity shown in Figure 10.21(a) was generally similar to that observed under confining pressure of 0.2 psi shown earlier in Figure 10.15(a). The scatter observed in the velocities measured at confining pressure of 15 psi was more pronounced than that measured at confining pressure of 0.2 psi.

For similar initial water contents, the effect of the initial dry unit weight on compression wave velocity shown in Figure 10.21(b) was different from that observed under confining pressure of 0.2 psi shown earlier in Figure 10.15(b). Under confining pressure of 15 psi, the compression wave velocity increased as the initial dry unit weight increased, with appreciable scatter. Under confining pressure of 0.2 psi, for specimens compacted at similar water contents lower than approximately 16% (w_{opt} = 19%), the compression wave velocity increased as the initial dry unit weight increased. For similar initial water contents ranging from 16 to 19%, the compression wave velocity increased as the initial dry unit weight increased and then decreased for further increase in dry unit weight. For similar initial water contents higher than 19%, no clear trend could be defined for the effect of the initial dry unit weight on compression wave velocity.

For specimens compacted at similar compactive efforts, the effect of compaction dry unit weight on compression wave velocity shown in Figure 10.21(c) was different from that observed under confining pressure of 0.2 psi shown earlier in Figure 10.15(c). Under a confining pressure of 15 psi, the effect of compaction dry unit weight on compression wave velocity was insignificant. Under confining pressure of 0.2 psi, for specimens compacted wet of optimum, the compression wave velocity increased as the

dry unit weight increased; while for specimens compacted dry of optimum, the compression wave velocity decreased as the dry unit weight increased.

The effect of the compaction dry unit weight on the product of the compaction water content (in decimal form, not in percent) and compression wave velocity is illustrated in Figure 10.22. For specimens compacted at degrees of saturation dry of optimum, the effect of increasing the initial dry unit weight on the product of the compaction water content and compression wave velocity was similar to that observed under confining pressure of 0.2 psi shown earlier in Figure 10.17. For specimens compacted at degrees of saturation wet of optimum, the rate of increase of the product of the compaction water content and compression wave velocity with the initial dry unit weight was significantly lower than that observed for specimens compacted at degrees of saturation dry of optimum, which was different from that observed under confining pressure of 0.2 psi. Under confining pressure of 0.2 psi, for specimens compacted at degrees of saturation wet of optimum, the rate of increase of the product of the compaction water content and compression wave velocity with the initial dry unit weight was slightly higher than that observed for specimens compacted at degrees of saturation dry of optimum.

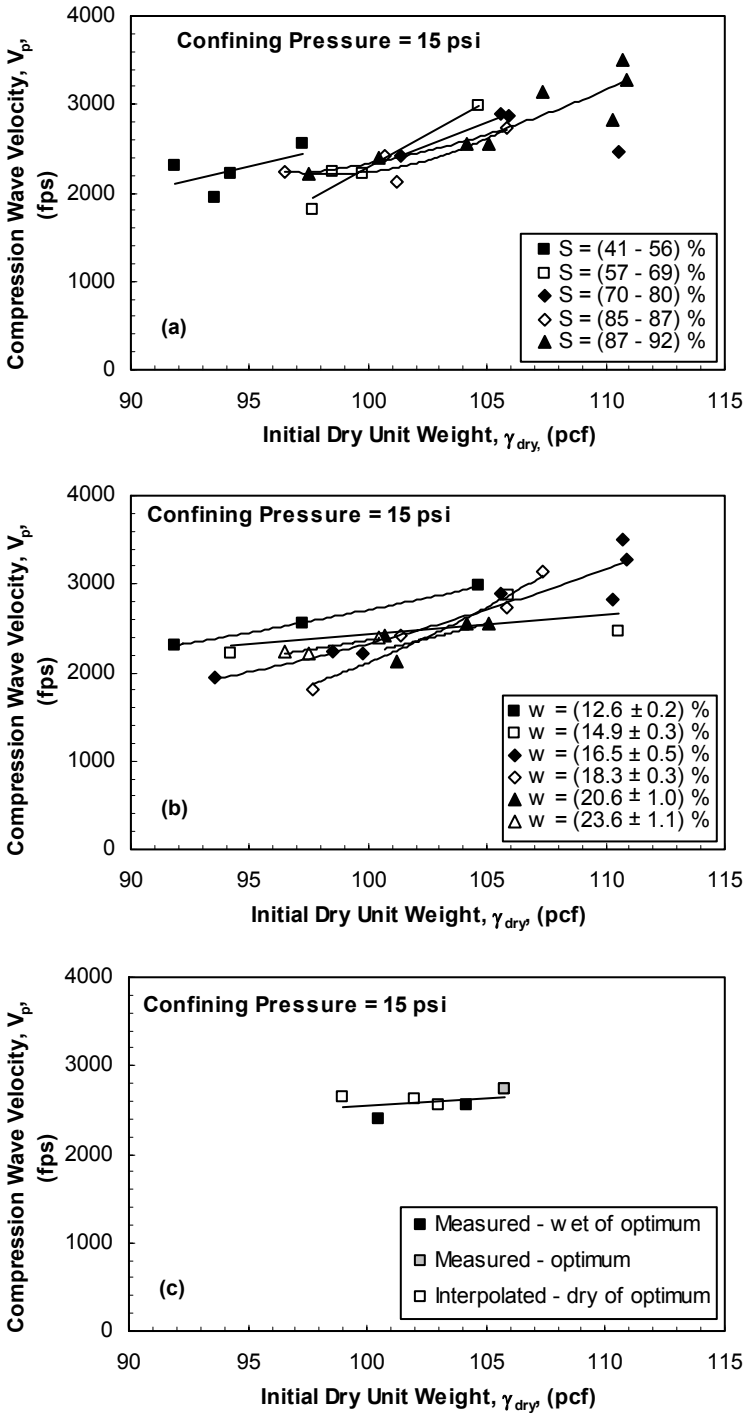

Figure 10.21. Effects of compaction dry unit weight on compression wave velocity for specimens compacted at similar: (a) degrees of saturation, (b) water contents, and (c) compactive efforts.

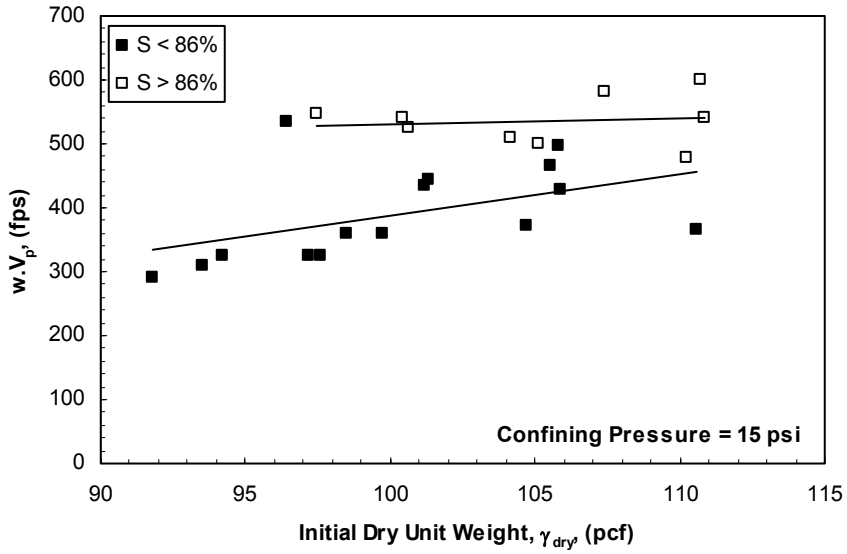

Figure 10.22. Effect of compaction dry unit weight on the product of the compression wave velocity and the compaction water content.

Effects of compaction degree of saturation on compression wave velocity are illustrated in Figure 10.23 for specimens compacted at similar dry unit weights, water contents, and compactive efforts. For similar initial dry unit weights, the effect of the initial degree of saturation on compression wave velocity shown in Figure 10.23(a) was different from that observed under confining pressure of 0.2 psi shown earlier in Figure 10.18(a). Under confining pressure of 15 psi, no clear trend could be defined for the effect of the initial degree of saturation on compression wave velocity. Under confining pressure of 0.2 psi, for specimens compacted at dry unit weights ranging from 90 to 95 pcf, the initial degree of saturation did not have a significant effect on the compression wave velocity. For higher initial dry unit weights, ranging from 95 to 115 pcf, the compression wave velocity decreased as the initial degree of saturation increased.

For similar initial water contents, the effect of the initial degree of saturation on compression wave velocity shown in Figure 10.23(b) was different from that observed

under confining pressure of 0.2 psi shown earlier in Figure 10.18(b). Under confining pressure of 15 psi, the compression wave velocity generally increased as the initial degree of saturation increased, with appreciable scatter. Under confining pressure of 0.2 psi, for similar water contents lower than 16% (w_{opt} = 19%), the compression wave velocity increased as the initial degree of saturation increased. For similar water contents ranging from 16 to 19%, the compression wave velocity increased as the degree of saturation increased and then decreased for further increase in degree of saturation. For similar water contents higher than 19%, the compression wave velocity decreased as the initial degree of saturation increased.

For specimens compacted at similar compactive efforts, the effect of the compaction degree of saturation on compression wave velocity shown in Figure 10.23(c) was different from that observed under confining pressure of 0.2 psi shown earlier in Figure 10.18(c). Under a confining pressure of 15 psi, the effect of the compaction degree of saturation on compression wave velocity was insignificant. Under confining pressure of 0.2 psi, the effect of degree of saturation on compression wave velocity was insignificant for degrees of saturation ranging from 46 to 68% (S_{opt} = 86%); while for degrees of saturation higher than 68%, the compression wave velocity decreased as the degree of saturation increased.

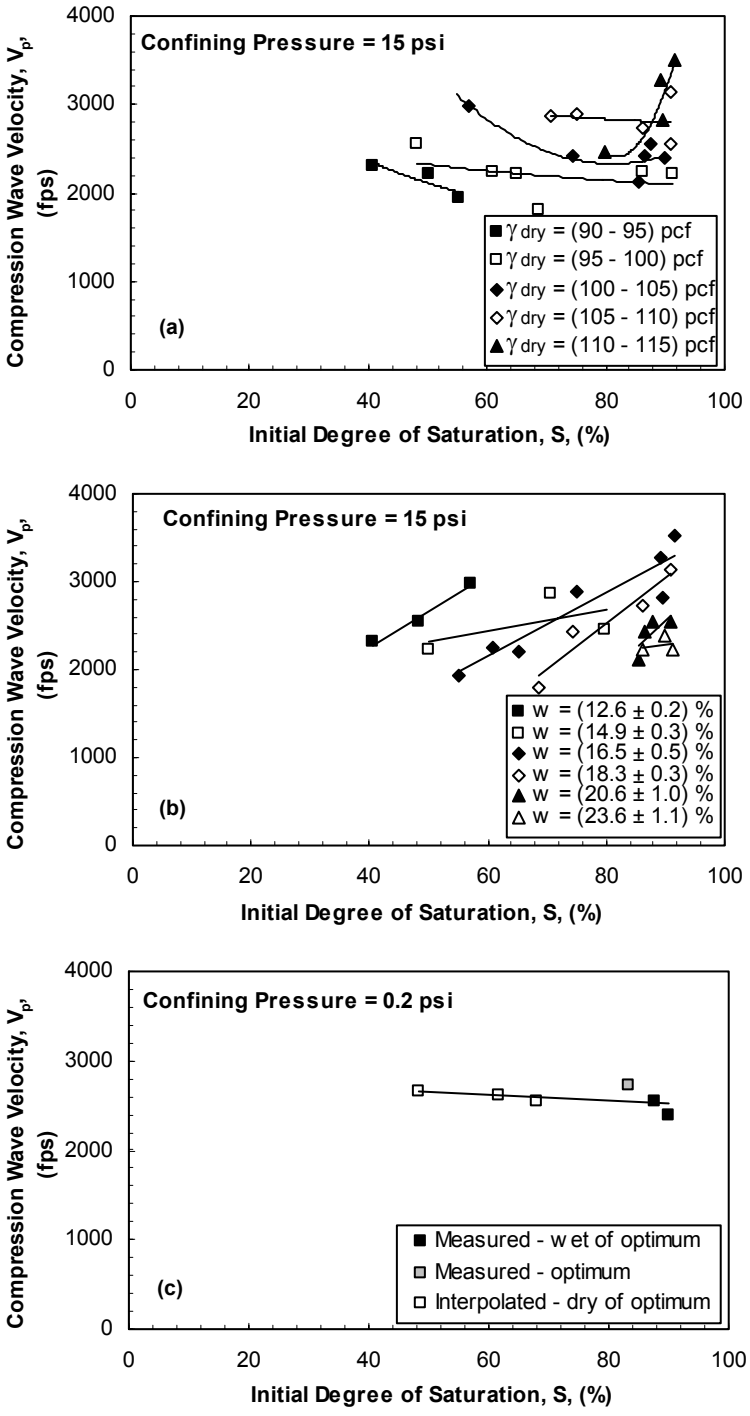

Figure 10.23. Effects of compaction degree of saturation on compression wave velocity for specimens compacted at similar: (a) water contents, (b) dry unit weights, and (c) compactive efforts.

In summary, increasing the confining pressure from 0.2 to 15 psi, under undrained conditions, significantly affected the effects of compaction conditions on compression wave velocity. Possible reasons for the different trends observed at confining pressures of 0.2 and 15 psi are discussed in the following sections.

10.2.3 DISCUSSION

The effects of compaction water content, dry unit weight, and degree of saturation on shear and compression wave velocities are generally similar. This similarity is expected because both velocities represent the velocity of waves through the material skeleton for the range of degrees of saturation being tested (S < 99%). For degrees of saturation higher than 99%, the pore water starts to affect the compression wave velocity, until ultimately the compression wave velocity represents the velocity through the pore water at full saturation. The effect of degree of saturation on compression wave velocity is discussed further in Section 10.3.1.

The velocities measured under confining pressure of 0.2 psi represented the as-compacted values for shear and compression wave velocities. The relationship between shear wave velocity and compaction dry unit weight shown in Figure 10.3(b) was investigated to determine the applicability of using shear wave velocity to infer dry unit weight for compaction control purposes. The relationship between shear wave velocity and compaction dry unit weight depended on compaction water content. For specimens compacted at similar water contents, the initial dry unit weight did not seem to have a significant effect on the shear wave velocity. Similar trends were observed for compression wave velocities. Accordingly, shear and compression wave velocities were judged to be inapplicable to determine dry unit weights for compaction control purposes.

At confining pressure of 0.2 psi, the net stress ($\sigma_c - u_a$) and matric suction ($u_a - u_w$) were known for each specimen at this confining pressure. The confining pressures and pore-air pressures were essentially zero, and thus, the net stress ($\sigma_c - u_a$) was essentially zero. The matric suction ($u_a - u_w$) depended primarily on the compaction water content as discussed in Chapter 7. After increasing the confining pressure to 15 psi, under undrained conditions, the state of stress of the soil changed due to the increase in pore-air and pore-water pressures associated with the increase in the confining pressure. This difference in stress state might explain why some of the trends observed for the effects of compaction conditions on shear and compression wave velocities were not similar for measurements taken under confining pressures of 0.2 and 15 psi. Effects of state of stress on soil stiffness are further studied in Chapter 12.

10.3 Effect of confining pressure on wave velocity measurements

Seven specimens compacted at water contents ranging from 12 to 25% and dry unit weights ranging from 92 to 104 pcf were compressed under undrained conditions at confining pressures ranging from 0.2 to 90 psi. Three specimens were compacted at water contents wet of optimum (w_{opt} = 19%) and four specimens were compacted at water contents dry of optimum. The variation of shear and compression wave velocities with confining pressure was investigated.

The effects of confining pressure on measured shear and compression wave velocities are shown in Figures 10.24(a) and 10.24(b), respectively. The effects of confining pressure on the ratio between compression and shear wave velocities are shown in Figure 10.24(c). The specimens compacted at water content wet of optimum were given solid symbols, and the specimens compacted at water contents dry of optimum

were given open symbols. The variation of shear and compression wave velocities with confining pressure for specimens compacted wet and dry of optimum is presented separately below.

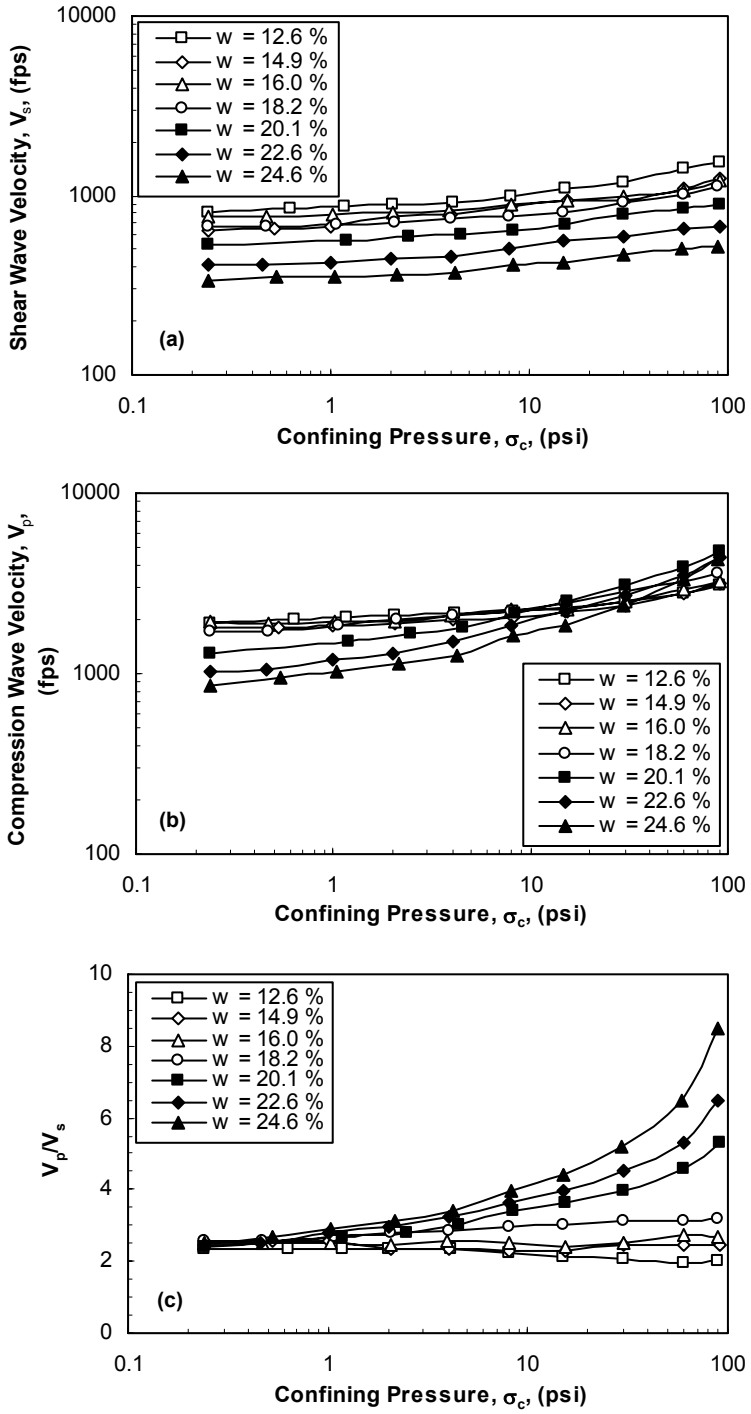

Figure 10.24. Effect of confining pressure applied under undrained conditions on: (a) shear wave velocity, (b) compression wave velocity, and (c) ratio of compression to shear wave velocities.

10.3.1 SPECIMENS COMPACTED WET OF OPTIMUM

The effects of confining pressure on shear and compression wave velocities for specimen compacted wet of optimum are illustrated in Figure 10.25. Sometimes it is convenient to view these trends using normalized wave velocities. The effect of increasing the confining pressure on normalized compression wave velocity ($V_p/V_{p,1psi}$) is illustrated in Figure 10.26. The compression wave velocities increased from approximately 1000 to 4500 fps upon increasing the confining pressure from 0.2 to 90 psi. Allen et al. (1980) and Valle (2006) reported that the compression wave velocity increased to a value of about 5000 fps at full saturation as shown in Figure 10.27. The authors indicated that for degrees of saturation less than about 99%, the compression wave velocity represented the velocity through the material skeleton; and at full saturation, the compression wave velocity represented the compression wave velocity through the pore water. For the current research, the fact that the compression wave velocities approached 5000 fps suggested that the specimens were becoming saturated.

The degrees of saturation of the specimens at each confining pressure were calculated based on the measured volume changes of the specimens. At confining pressure of 90 psi, the degrees of saturation for the specimens were higher than 100%, which is essentially impossible. The volume changes measurements were not accurate enough to track the changes in degrees of saturation precisely; however, it supported the fact that the specimens were becoming saturated.

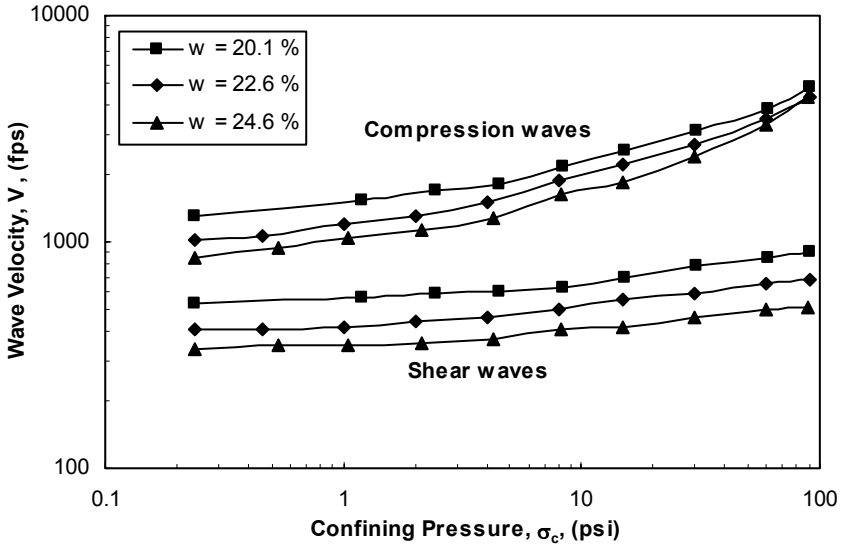

Figure 10.25. Effect of confining pressure on shear and compression wave velocities for specimens compacted wet of optimum.

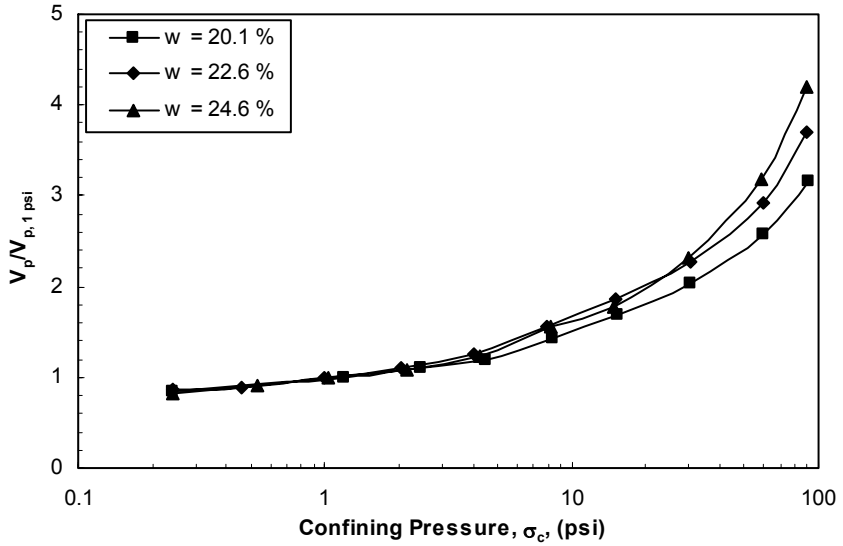

Figure 10.26. Effect of confining pressure on normalized compression wave velocity for specimens compacted wet of optimum.

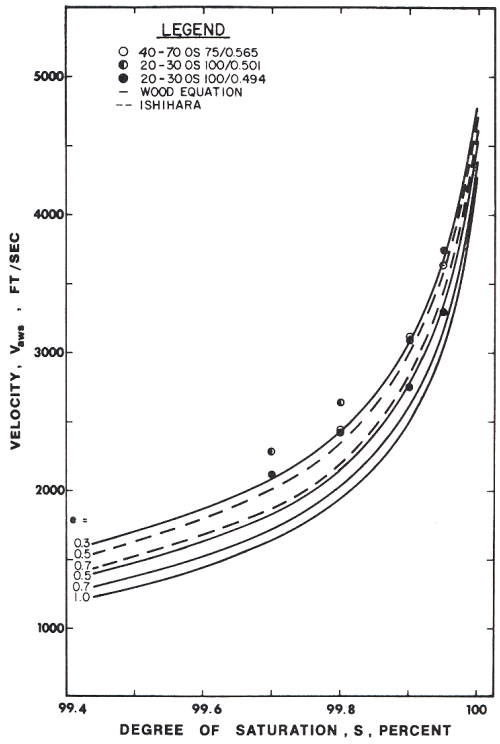

Figure 10.27. Effect of degree of saturation on compression wave velocity for Ottawa sand (from Allen et al., 1980).

The shear wave velocities shown in Figure 10.25 remained almost constant with increasing confining pressure in the range of 0.2 to 1 psi. This lack of effect of the confining pressure can be attributed to the fact that specimens had relatively high initial matric suctions such that the effect of increasing the confining pressure from 0.2 to 1 psi did not significantly change the matric suction. As the confining pressure was further increased from 1 to 60 psi, the shear wave velocity increased. For confining pressures higher than 60 psi, the effect of increasing the confining pressure seemed to diminish slightly. This reduction in the rate of increase of shear wave velocity with the increase in confining pressure was expected, as the specimens were becoming pressure saturated, which lead to the development of increasing positive pore-water pressures with

increasing confining pressure. The effect of increasing the confining pressure on normalized shear wave velocity ($V_s/V_{s,1psi}$) is illustrated in Figure 10.28.

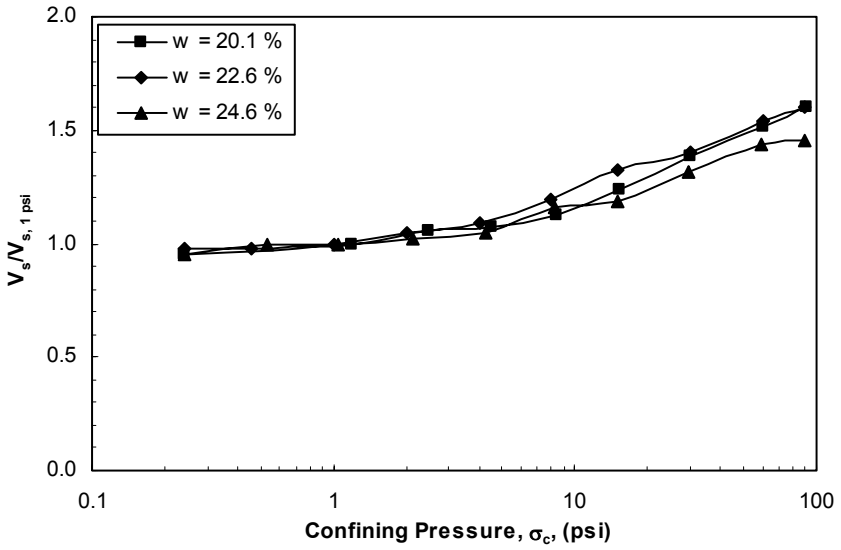

Figure 10.28. Effect of confining pressure on normalized shear wave velocity for specimens compacted wet of optimum.

Values of Poisson's ratio were calculated from measured shear and compression wave velocities using the following relationship:

$$\upsilon = \frac{(V_p^2 - 2V_s^2)}{2(V_p^2 - V_s^2)} \quad \text{..... (10.1)}$$

where υ is Poisson's ratio. The variation of Poisson's ratio with confining pressure is shown in Figure 10.29. Generally, Poisson's ratio for saturated soils is around 0.5. Poisson's ratio increased with increasing the confining pressure from about 0.41 to about 0.49. The variation of Poisson's ratio with confining pressure supported the conclusion that specimens were becoming pressure saturated as the confining pressure was increased to 90 psi. An alternative way to express the relationship between shear and compression wave velocities, other than Poisson's ratio, is the ratio between compression and shear

wave velocities (V_p/V_s). The variation of the ratio between compression and shear wave velocities with confining pressure is shown in Figure 10.30. The ratio between compression and shear wave velocities increased with increasing the confining pressure from about 2.5 to about 8.5.

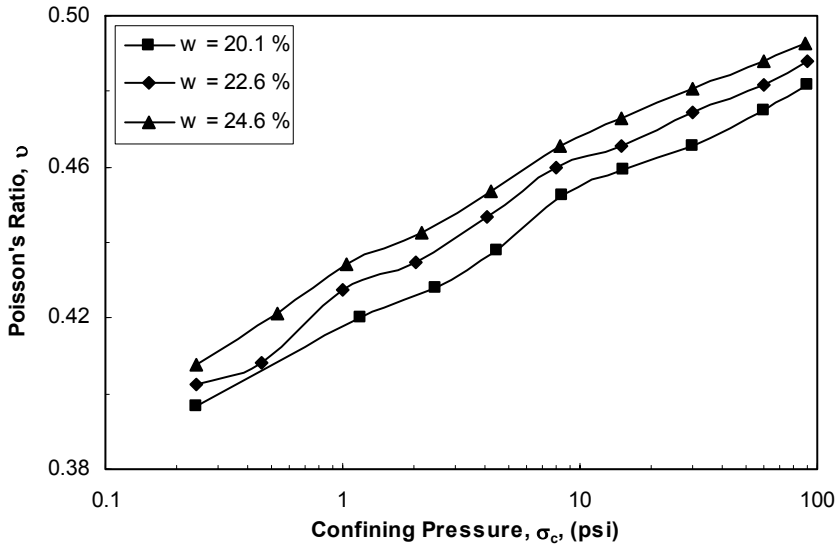

Figure 10.29. Effect of confining pressure on Poisson's ratio for specimens compacted wet of optimum.

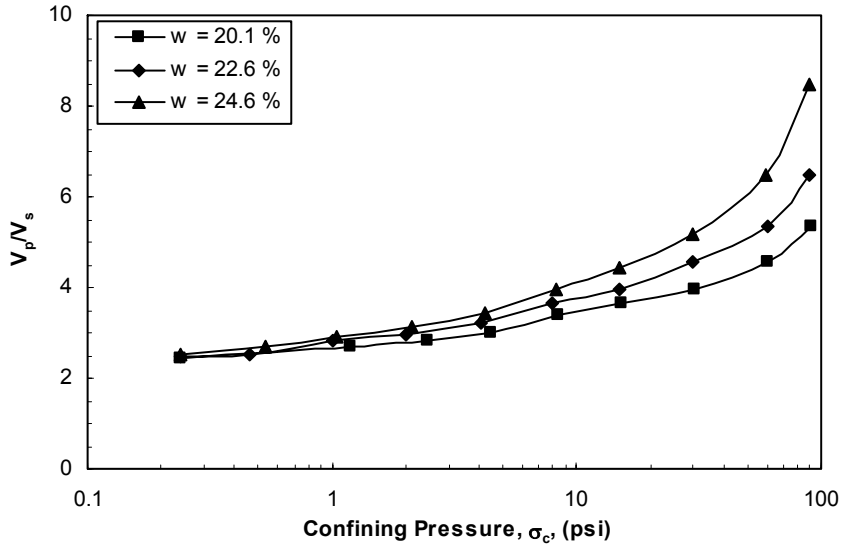

Figure 10.30. Effect of confining pressure on ratio between compression and shear wave velocities for specimens compacted wet of optimum.

10.3.2 SPECIMENS COMPACTED DRY OF OPTIMUM

For specimens compacted dry of optimum, the variation of compression and shear wave velocities with confining pressure were similar as illustrated in Figure 10.31. This similarity suggested that the compression wave velocity represented the velocity of waves through the material skeleton over the complete range of confining pressures (0.2 to 90 psi). The effects of increasing the confining pressure on normalized compression and shear wave velocities are illustrated in Figures 10.32 and 10.33, respectively.

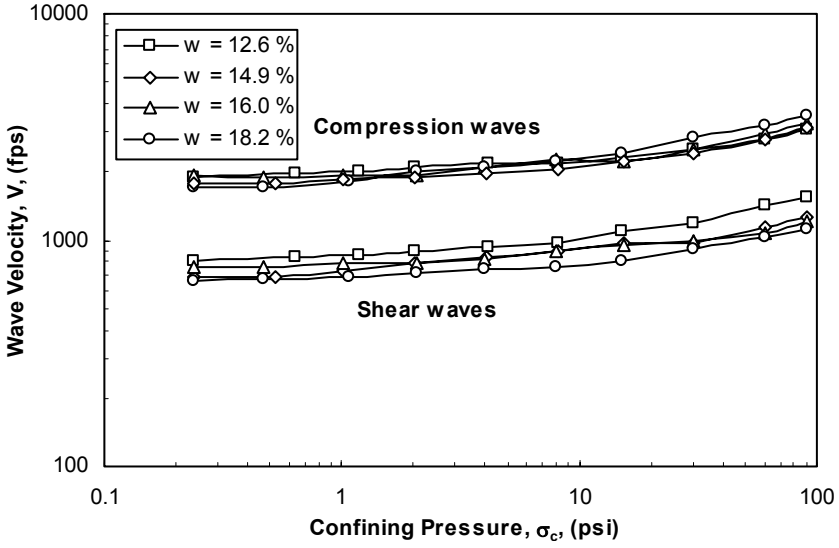

Figure 10.31. Effect of confining pressure on shear and compression wave velocities for specimens compacted dry of optimum.

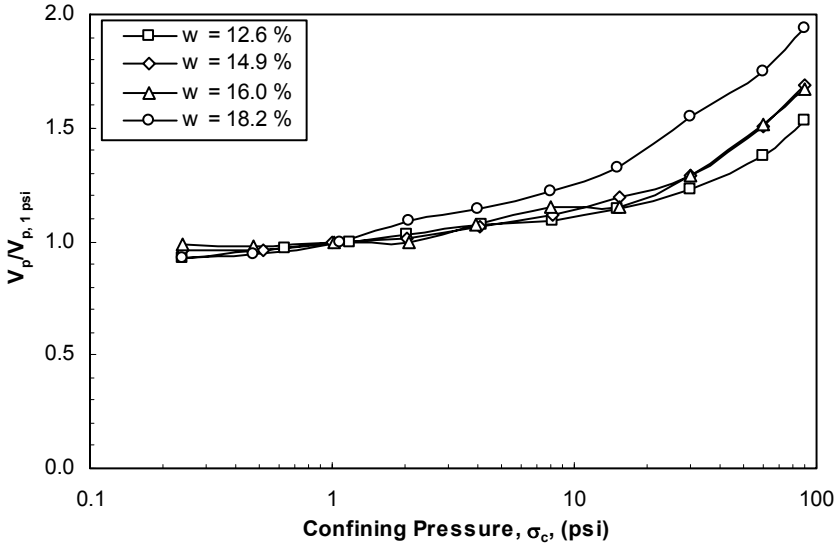

Figure 10.32. Effect of confining pressure on normalized compression wave velocity for specimens compacted dry of optimum.

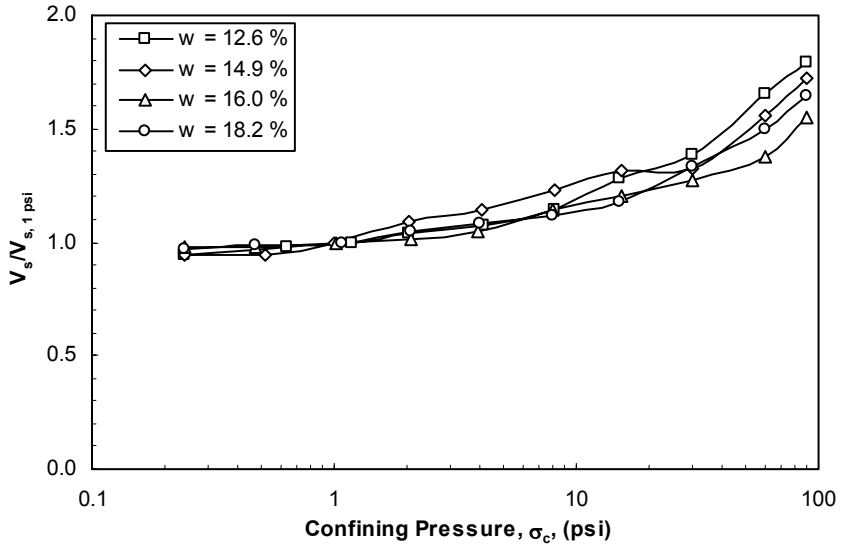

Figure 10.33. Effect of confining pressure on normalized shear wave velocity for specimens compacted dry of optimum.

The variation of shear wave velocity with confining pressure was similar to that observed for specimens compacted wet of optimum up to a confining pressure of approximately 60 psi. However, for higher confining pressures, the shear wave velocity continued to increase with increasing confining pressure at a rate similar to that observed at lower confining pressures. A decrease in the rate at higher confining pressures like that shown for specimens compacted wet of optimum did not occur. This response was likely caused by the specimens having low initial degrees of saturation such that they did not approach saturation even at confining pressures of 90 psi.

The variation of Poisson's ratio with confining pressure is illustrated in Figure 10.34. For the specimen compacted at a water content of approximately 18% (w_{opt} = 19%), Poisson's ratio increased from approximately 0.41 to 0.45 as the confining pressure increased from 0.2 to 90 psi. For the two specimens compacted at water contents of approximately 15 and 16%, the confining pressure did not have a significant effect on

Poisson's ratio, which had an average value of about 0.4 over the complete range of confining pressures (0.2 to 90 psi). For the specimen compacted at a water content of approximately 13%, Poisson's ratio decreased from approximately 0.39 to 0.34 as the confining pressure increased from 0.2 to 90 psi. Similar trends were observed for the effects of confining pressure on the ratio between compression and shear wave velocities shown in Figure 10.35.

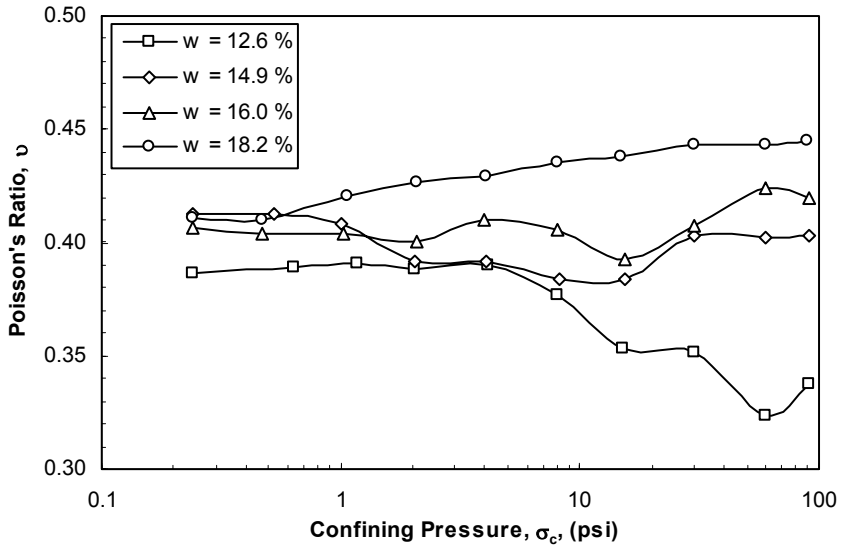

Figure 10.34. Effect of confining pressure on Poisson's ratio for specimens compacted dry of optimum.

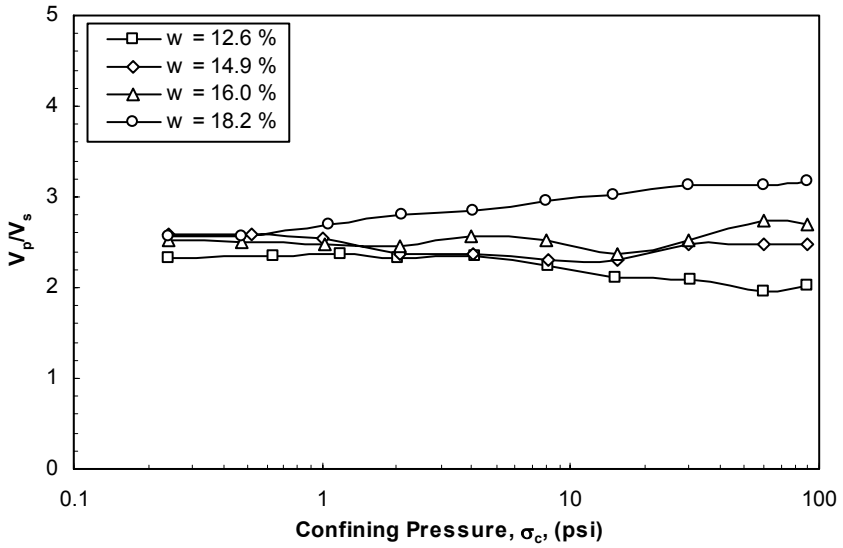

Figure 10.35. Effect of confining pressure on ratio between compression and shear wave velocities for specimens compacted dry of optimum.

10.4 Variation of shear and compression wave velocities during shearing under undrained conditions

The seven specimens tested in Section 10.3 were sheared to failure statically under undrained conditions at confining pressure of 90 psi up to an axial strain of approximately 20%. An average of eight measurements of shear and compression wave velocities were performed during shearing. The variations of normalized void ratio and shear and compression wave velocities with axial strain are illustrated in Figure 10.36 and discussed below.

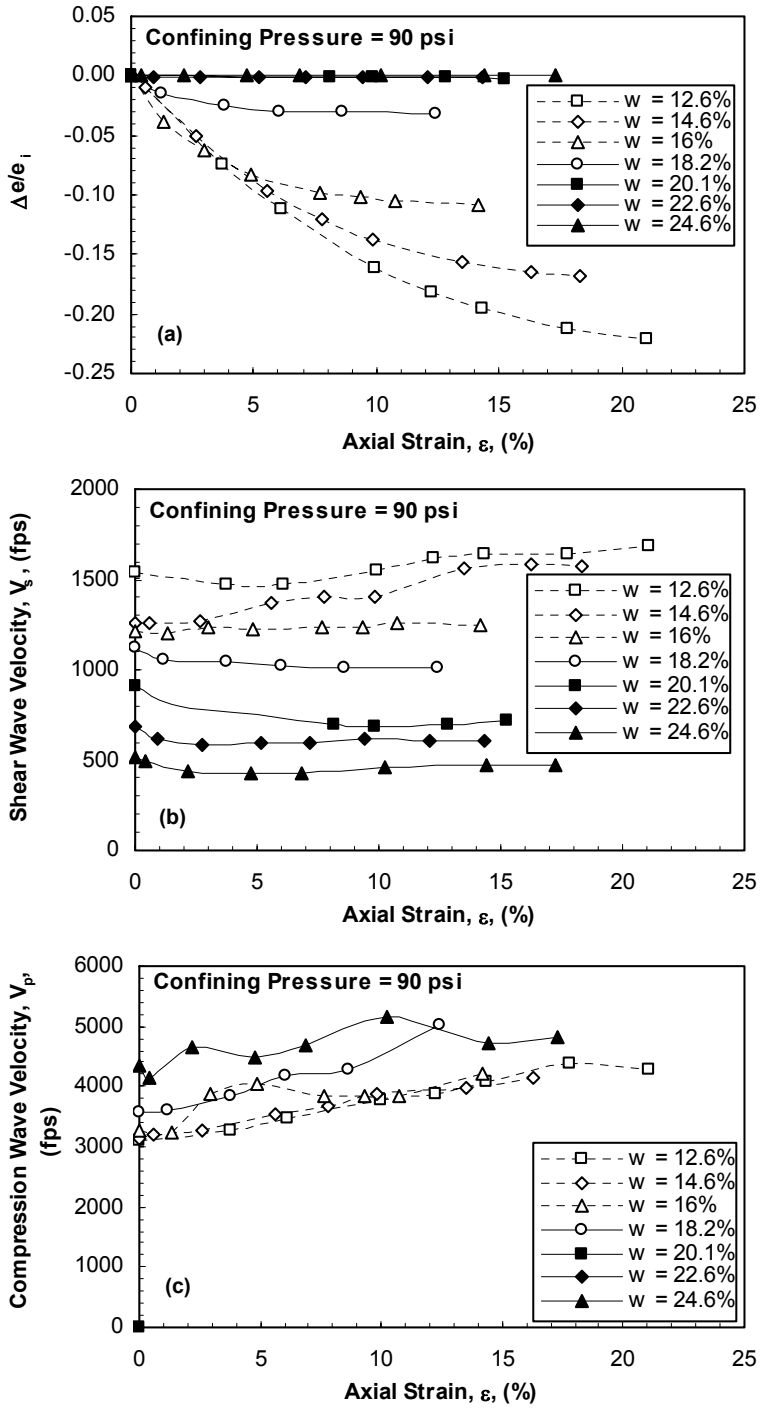

Figure 10.36. Variation of: (a) shear wave velocity, (b) compression wave velocity, and (c) normalized void ratio during shearing with axial strain.

The changes in void ratio during shearing were normalized to the initial void ratio before the specimen was sheared. The variation of the normalized void ratios with the axial strain is presented in Figure 10.36(a). For specimens compacted wet of optimum (w_{opt} = 19%), the normalized void ratios decreased by less than 0.3% during shearing, which was considered insignificant. For specimens compacted dry of optimum, the normalized void ratios decreased by up to 22% during shearing.

The variation of shear wave velocity with axial strain is presented in Figure 10.36(b). For specimens compacted wet of optimum, shear wave velocity decreased with increasing the axial strain. At confining pressure of 90 psi, the specimens were nearly saturated as discussed in Section 10.3.1. The decrease in the shear wave velocity was probably due to a decrease in the mean effective normal stress caused by increase in pore-water pressures during shear and due to non-linearity of soil stiffness at large strains. For specimens compacted dry of optimum, shear wave velocity increased with increasing the axial strain. The increase in shear wave velocity might be attributed to combined effects of decrease in void ratio and increase in mean normal stress. These two effects dominated the effect of non-linearity of soil stiffness at large strains.

The variation of compression wave velocity with axial strain is presented in Figure 10.36(c). For specimens compacted wet of optimum, compression wave velocity remained relatively constant or only slightly increased with increasing the axial strain. At confining pressure of 90 psi, the specimens were nearly saturated and the compression wave velocity represented the compression wave velocity through the pore water. For specimens compacted dry of optimum, compression wave velocity increased with increasing the axial strain. The increase in compression wave velocity might be attributed to combined effects of decrease in void ratio and increase in vertical normal stress. The

compression wave velocity of the specimen compacted at a water content of 18.2% (slightly dry of optimum) increased to about 5000 fps at an axial strain of 13%, which indicated that the specimen was becoming saturated by the end of the shearing stage.

The specimens compacted wet of optimum were nearly saturated at confining pressure of 90 psi as discussed in Section 10.3.1. Thus, the behavior of those specimens can be compared with the behavior of saturated specimens reported by other researchers. Nakagawa et al. (1996) used piezoelectric transducers to measure compression and shear wave velocities during shear of *saturated* normally consolidated kaolinite under undrained conditions. Typical compression and shear waveforms for various axial strains are shown in Figure 10.37. During shearing, the distance between the piezoelectric transducers is decreasing. The calculated velocities are reported on the right axis of each plot shown in Figure 10.37. The compression wave velocities shown in Figure 10.37(a) remained almost constant (approximately 1522 $\pm$ 4 m/sec), regardless of the axial strain. The shear wave velocity shown in Figure 10.37(b) decreased from 130 to 101 m/sec as the axial strain increased from 0 to 10%. The authors attributed the decrease in shear wave velocity with increase in axial strain to reduction in the effective stress due to the contractive tendency of the specimens upon shearing.

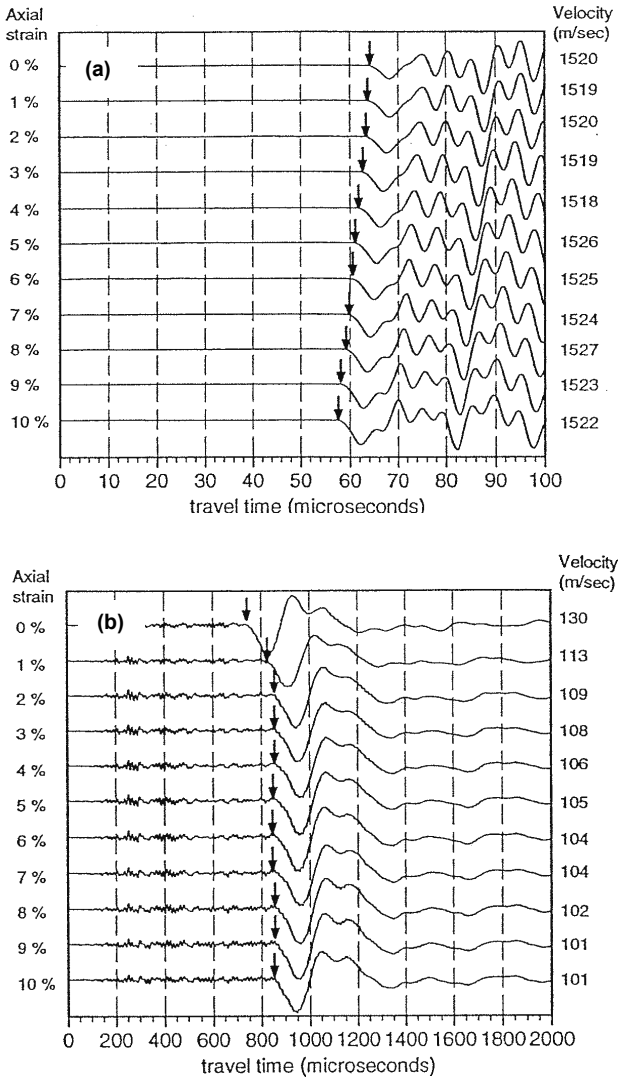

Figure 10.37.(a) Compression waveforms and (b) shear waveforms recorded during shear of saturated kaolinite clay under undrained conditions (from Nakagawa et al., 1996).

10.5 Stiffness – suction relationship

For the 26 specimens tested under a confining pressure of 0.2 psi, the net stress ($\sigma_c - u_a$) was essentially zero and the matric suction ($u_a - u_w$) depended primarily on the compaction water content. The variation of the initial matric suction with compaction

water content from the pressure plate tests reported in Chapter 7 is shown in Figure 10.38.

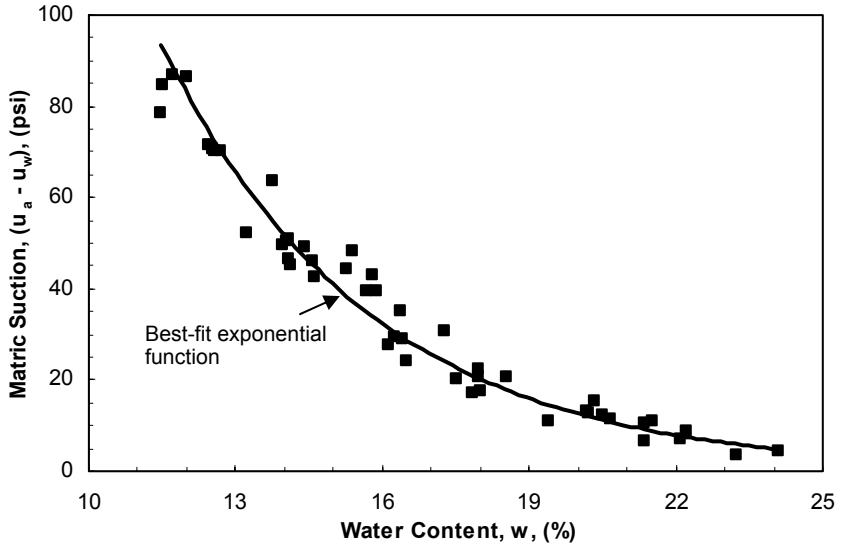

Figure 10.38. Compaction water content - matric suction relationship (from results of pressure plate tests).

The relationship between matric suction and water content could be expressed in the form of an exponential function expressed as follows:

$$(u_a - u_w) = 1395e^{-0.24w} \quad \text{..... (10.2)}$$

where w is the compaction water content (in percent) and $(u_a - u_w)$ is the matric suction. The initial matric suction of the specimens tested under undrained conditions was estimated based on their compaction water content using Equation 10.2. The variation of shear and constrained moduli with the estimated initial matric suction is discussed below.

10.5.1 SHEAR MODULUS

The variation of shear modulus with initial matric suction is illustrated in Figure 10.39 on both arithmetic and logarithmic scales. The shear modulus increased as the initial matric suction increased up to a matric suction of approximately 40 psi beyond which the shear modulus varied significantly for similar values of matric suction.

To investigate this variation at higher values of matric suction, the possible effect of compaction dry unit weight was examined. The variation of shear modulus with initial matric suction is illustrated in Figure 10.40 for specimens compacted at similar dry unit weights. For initial dry unit weights below about 105 pcf, the shear modulus increased as the initial matric suction increased, but at a decreasing rate, and then tended to approach a nearly constant value beyond which the shear modulus did not increase further for the range of matric suctions being tested. Similar observations were reported by Marinho et al. (1995) and Picornell and Nazarian (1998). Marinho et al. (1995) indicated that soil stiffness might even decrease at higher matric suctions. Mendoza et al. (2005) and Mendoza and Colmenares (2006) showed that the soil stiffness continuously increased as the initial matric suction increased without reaching a constant value. For initial dry unit weights, above about 105 pcf, the shear modulus increased as the initial matric suction increased with no evidence of reaching a limiting value for the range of matric suctions being tested.

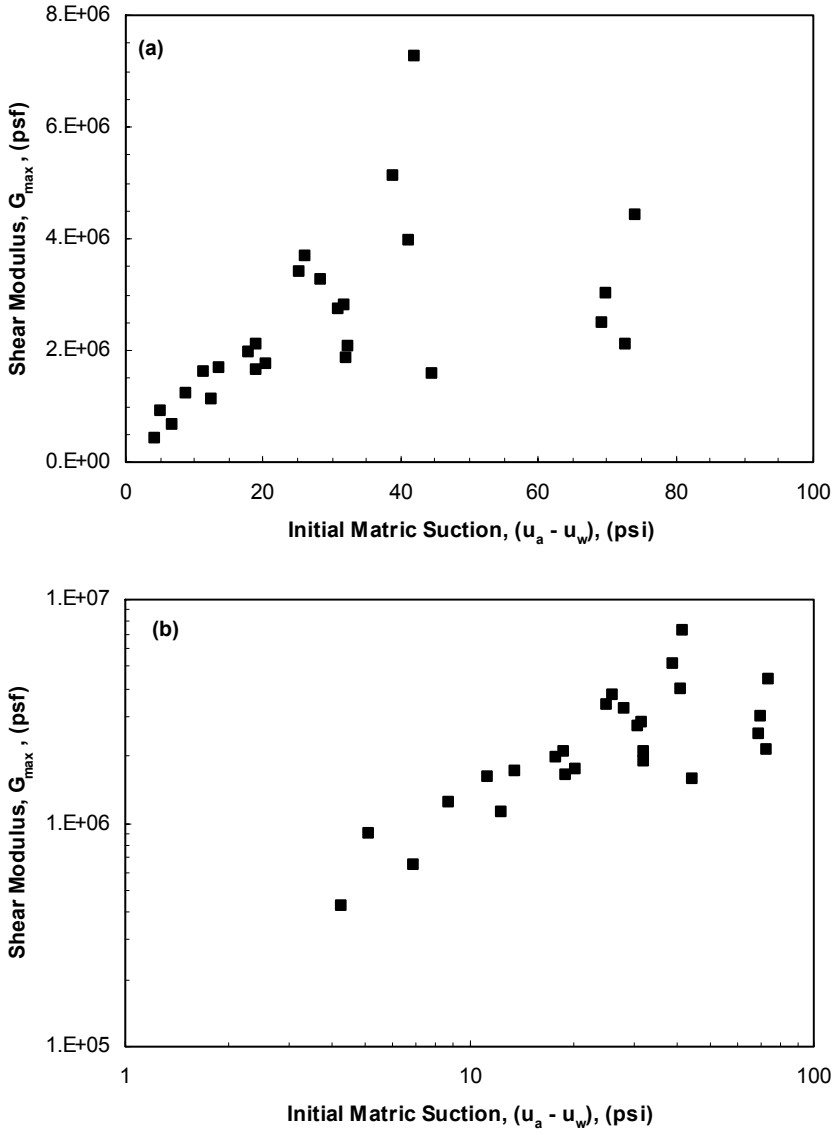

Figure 10.39. Effect of initial matric suction on shear modulus: (a) arithmetic scale and (b) logarithmic scale.

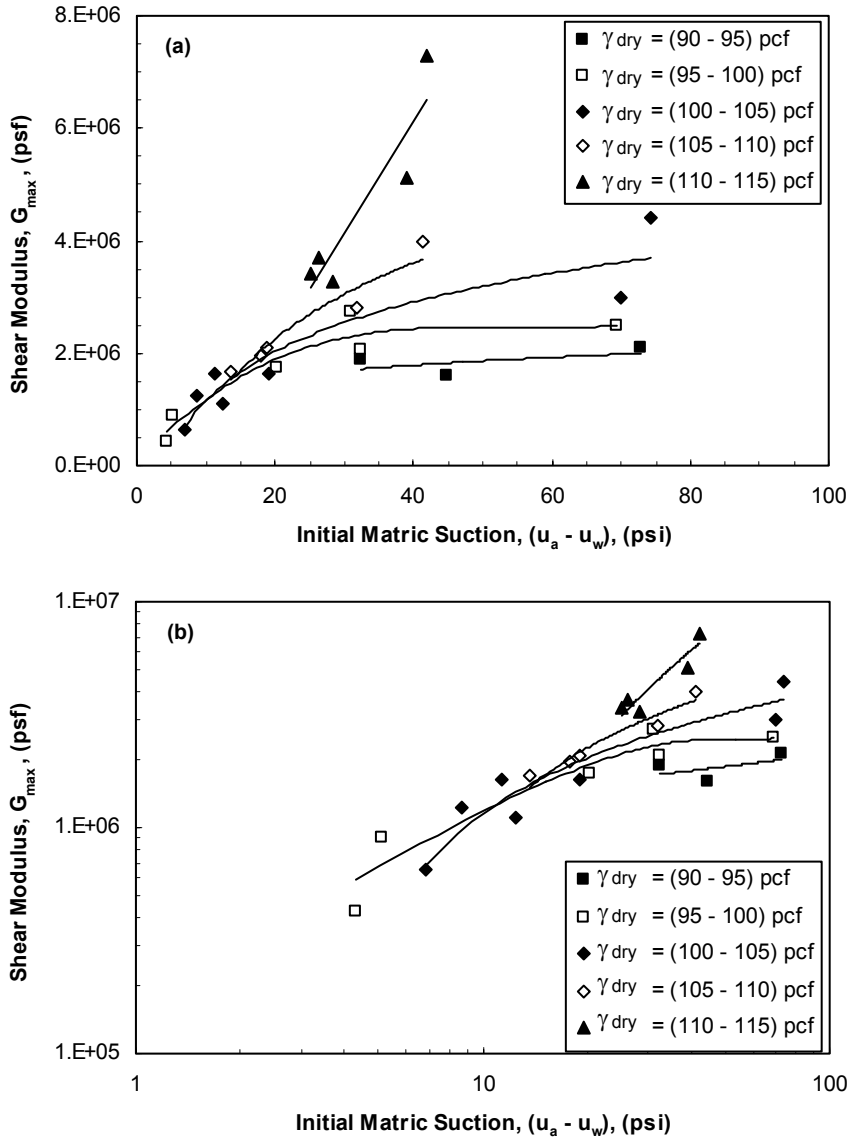

Figure 10.40. Effect of initial matric suction on shear modulus for specimens compacted at similar dry unit weights: (a) arithmetic scale and (b) logarithmic scale.

To reduce the effects of dry unit weight (void ratio) on the relationship between the shear modulus and matric suction, the shear modulus was normalized by the "F(e)" term defined by Hardin and Black (1968) for clays as follows:

$$F(e) = \frac{(2.97 - e)^2}{(1 + e)} \quad \text{.....} \quad (10.3)$$

where e is the void ratio. The relationship between the normalized shear modulus (G_{max}/F(e)) and the initial matric suction shown in Figure 10.41 shows less scatter than shown for the shear modulus (Figure 10.39), yet the normalized shear moduli were still different for a given value of matric suction.

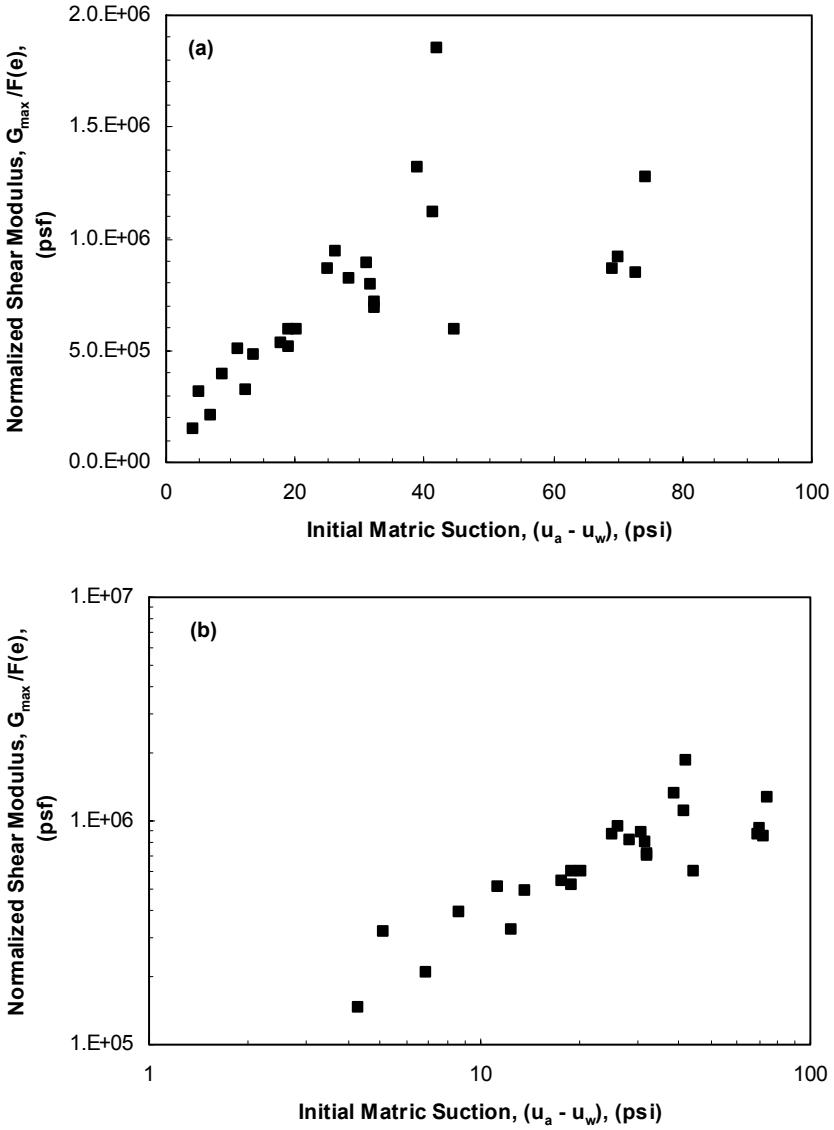

Figure 10.41. Effect of initial matric suction on normalized shear modulus: (a) arithmetic scale and (b) logarithmic scale.

The effect of degree of saturation on the relationship between shear modulus and matric suction was examined as illustrated in Figure 10.42. For similar initial degrees of saturation, the shear modulus increased as the matric suction increased for the range of matric suctions being tested.

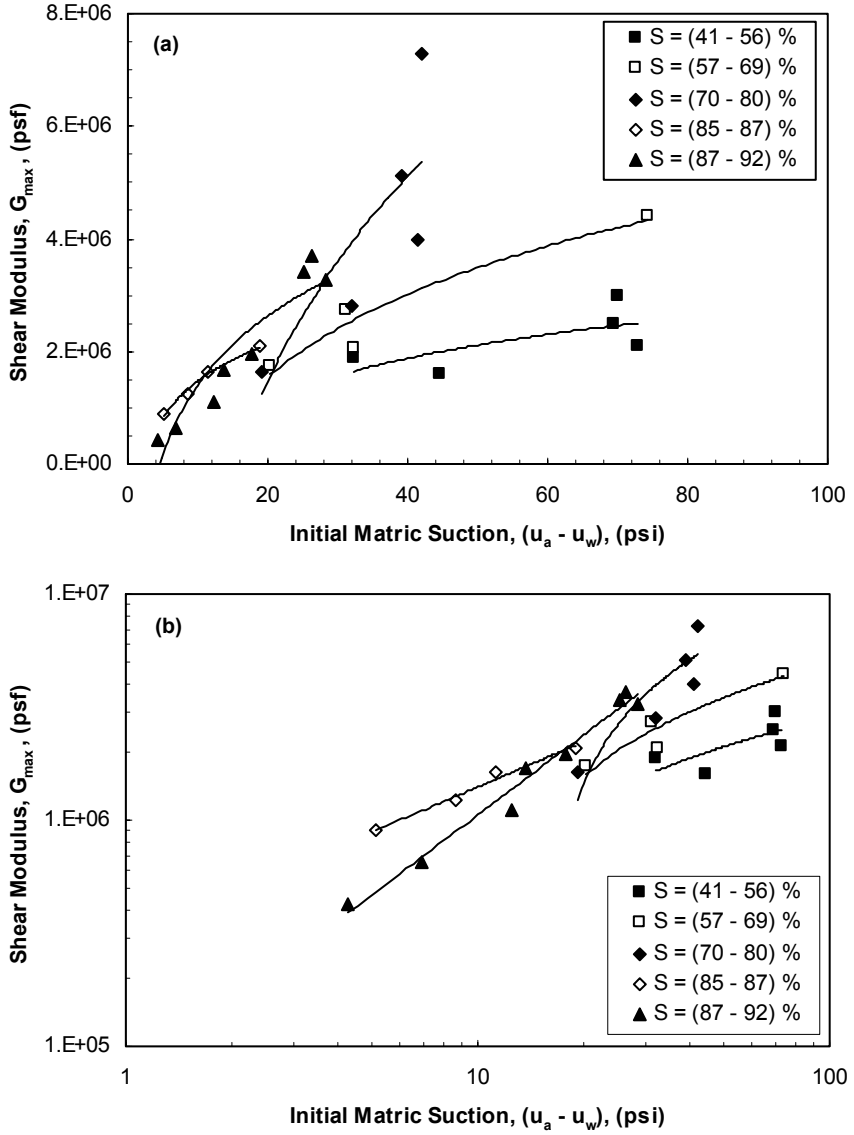

Figure 10.42. Effect of initial matric suction on shear modulus for specimens compacted at similar degrees of saturation: (a) arithmetic scale and (b) logarithmic scale.

The variation of shear modulus with initial matric suction is illustrated in Figure 10.43 for specimens compacted at similar compactive efforts. Interpolation was implemented to determine the shear wave velocity for specimens compacted dry of optimum as discussed in Section 10.2.1. The shear modulus increased as the initial matric

suction increased, but at a decreasing rate, and then approached a nearly constant value beyond which the shear modulus did not increase further for the range of matric suctions being tested. Sawangsuriya et al. (2006) reported that for specimens compacted at the same compactive effort, the soil stiffness continuously increased as the matric suction increased, which disagreed with the data reported in this study.

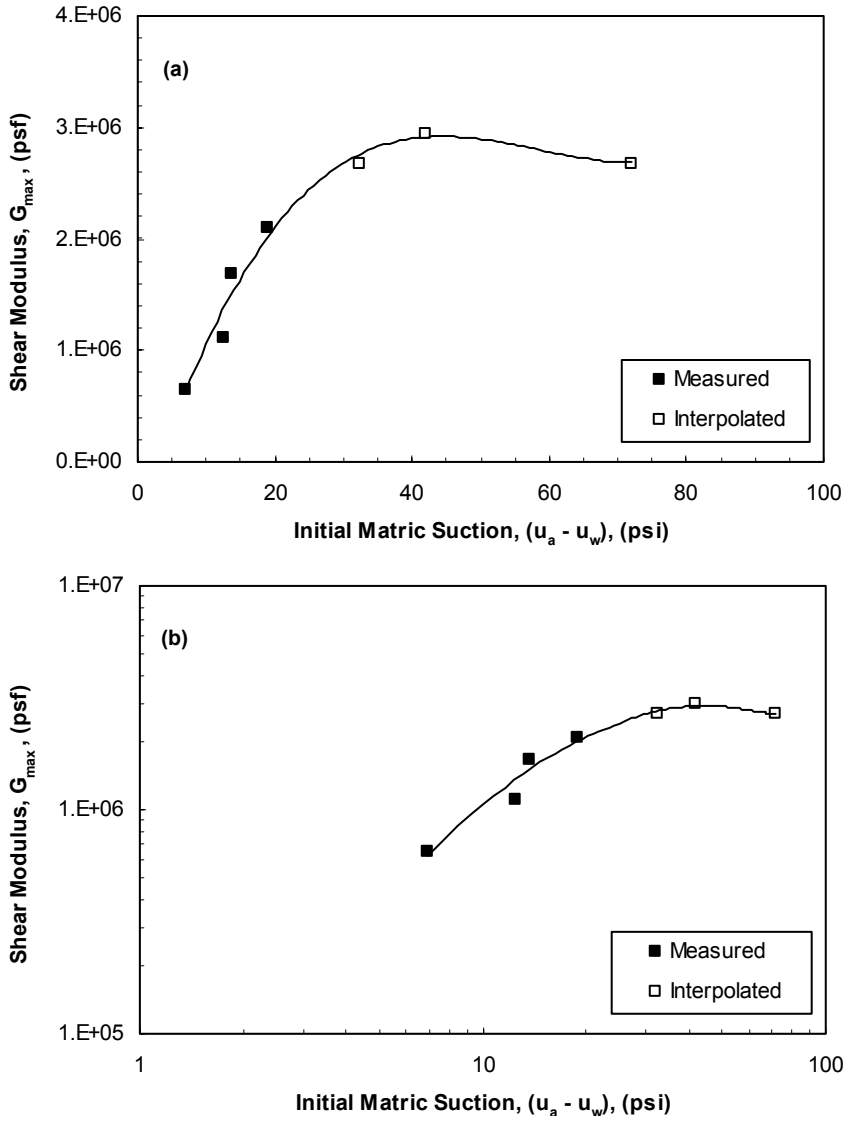

Figure 10.43. Effect of initial matric suction on shear modulus for specimens compacted at similar compactive efforts: (a) arithmetic scale and (b) logarithmic scale.

The observed trends for the variation of soil stiffness with matric suction can be explained by a model proposed by Fisher (1926). Fisher considered how the air-water meniscus affects the state of stress of two solid spheres. The air-water meniscus at the sphere contact introduces a force (ΔN) normal to the plane passing through the contact point between the two spheres as illustrated in Figure 10.44. The force ΔN equals:

$$\Delta N = \pi r_2^2 (u_a - u_w) + 2\pi r_2 T \quad \text{..... (10.4)}$$

where r_2 is the radius of the area of fluid connecting the two spheres, $(u_a - u_w)$ is the matric suction, and T is the surface tension. As the radius of the menisci (r_1) decreases, the matric suction increases, while the radius r_2 decreases. The variation of the force ΔN with matric suction is illustrated in Figure 10.44. The force ΔN increases as the matric suction increases, but at a decreasing rate, and approaches a nearly constant value beyond which the force ΔN does not increase further. The force ΔN reaches a nearly constant value at high matric suctions due to the progressive reduction in the radius of the menisci, which leads to the reduction of the radius of the area of fluid connecting the two spheres. Lu and Likos (2006) reported that the force between unsaturated soil particles might also decrease at high matric suctions.

As the force ΔN increases, the stress between soil particles increases. Because the stiffness increases as the stress between soil particles increases, an increase in the force ΔN will increase the stiffness. The increase in stiffness with matric suction is expected to follow pattern similar to the increase of the force ΔN with matric suction (Mancuso et al., 2002). Accordingly, the stiffness would increase as the matric suction increase, but at a decreasing rate and then tends towards a nearly constant value beyond which the stiffness does not increase further. The stiffness might even decrease at very high matric suctions.

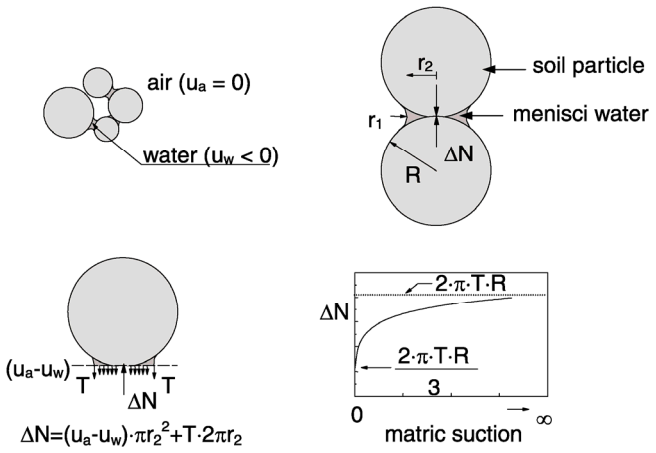

Figure 10.44. Effect of matric suction on the normal force between two solid spheres (from Mancuso et al, 2002).

For practical purposes, soils are typically compacted at degrees of saturation higher than 75%. The variation of shear modulus with matric suction for this range of degrees of saturation is shown in Figure 10.45. The shear modulus increased as the matric suction increased for the range of matric suctions being investigated.

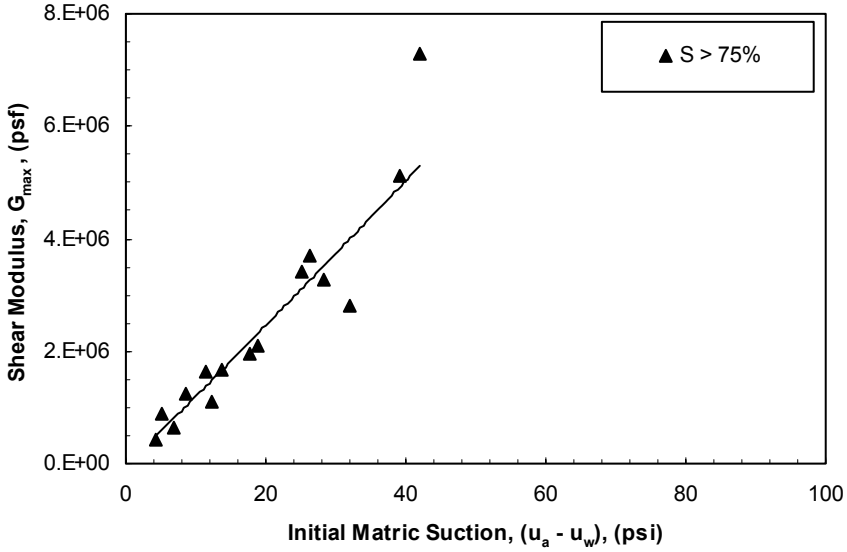

Figure 10.45. Effect of initial matric suction on shear modulus for specimens compacted at degrees of saturation higher than 75%.

10.5.2 CONSTRAINED MODULUS

The variation of constrained modulus with initial matric suction is illustrated in Figure 10.46. The constrained modulus increased as the initial matric suction increased up to a matric suction of approximately 40 psi beyond which the constrained modulus varied significantly for similar values of matric suction.

To investigate this variation at higher values of matric suction, possible effect of compaction dry unit weight was examined. The variation of constrained modulus with initial matric suction is illustrated in Figure 10.47 for specimens compacted at similar dry unit weights. For initial dry unit weights below about 95 pcf, the effect of the initial matric suction on constrained modulus was insignificant for the range of matric suctions investigated. For initial dry unit weights above about 95 pcf, the constrained modulus increased as the initial matric suction increased for the range of matric suctions investigated.

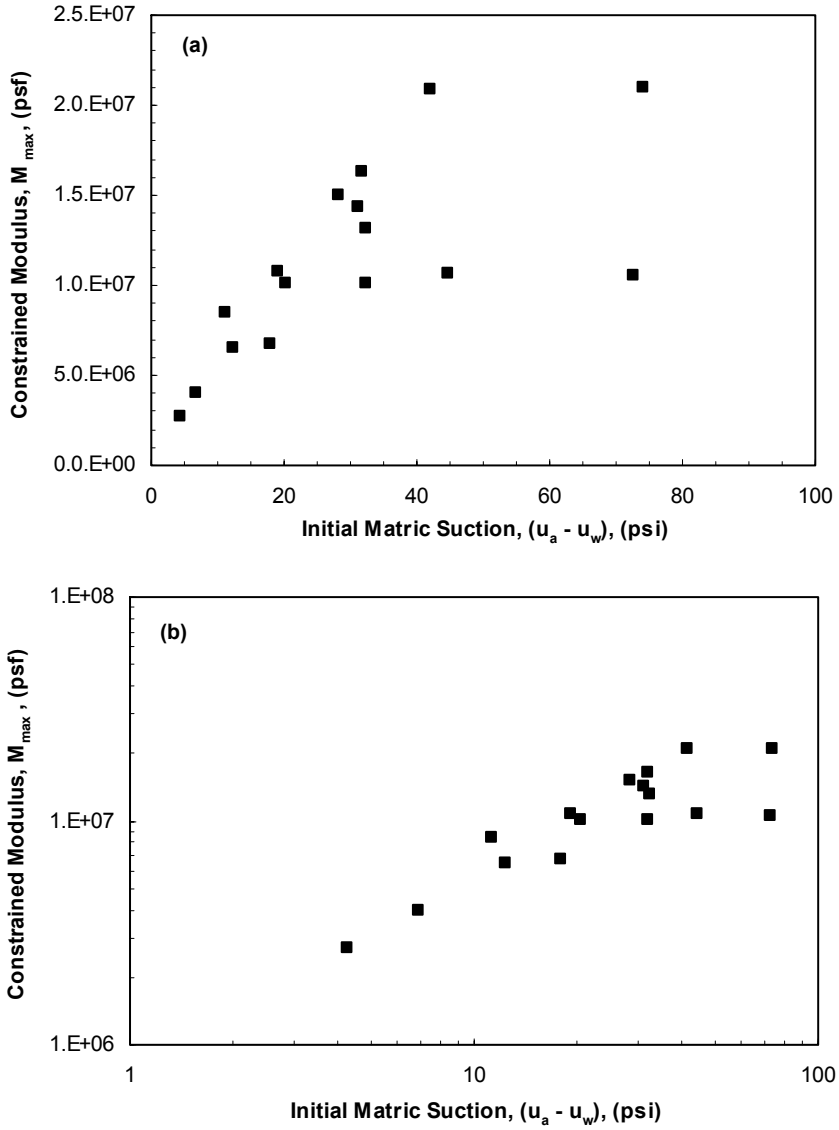

Figure 10.46. Effect of initial matric suction on constrained modulus: (a) arithmetic scale and (b) logarithmic scale.

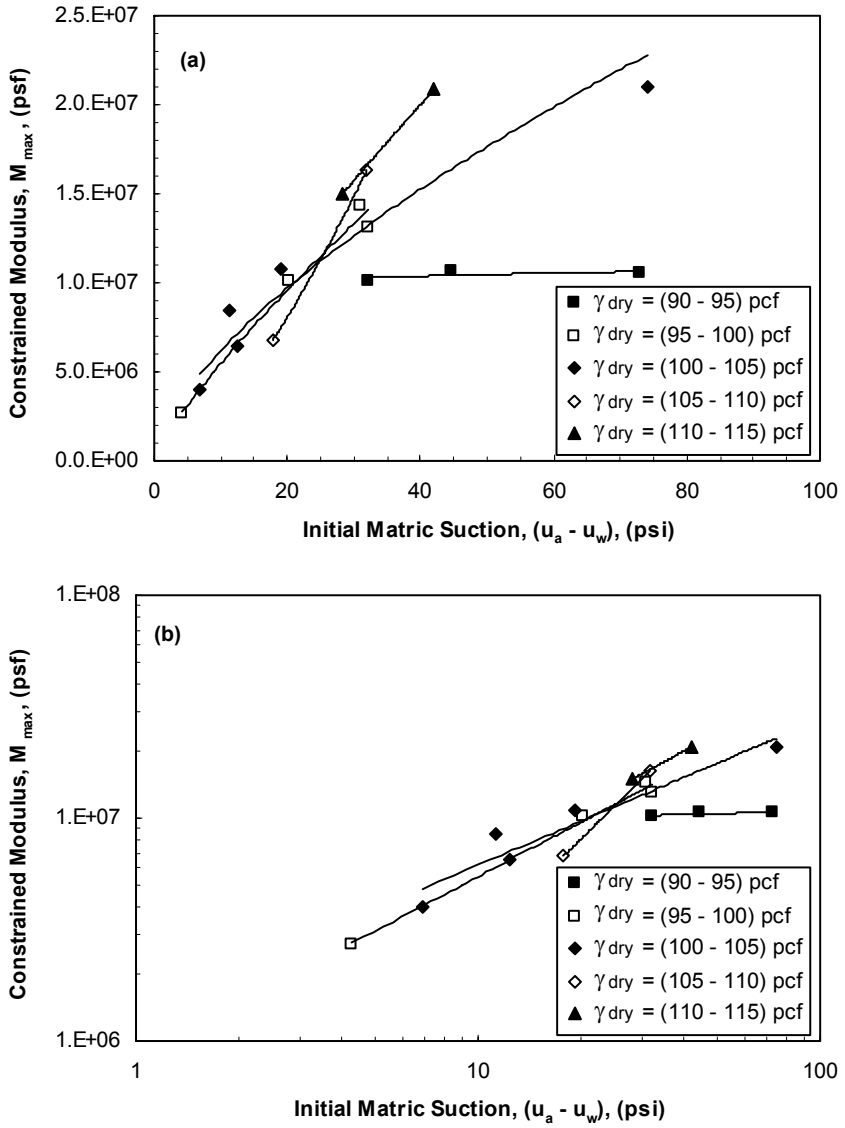

Figure 10.47. Effect of initial matric suction on constrained modulus for specimens compacted at similar dry unit weights: (a) arithmetic scale and (b) logarithmic scale.

To reduce the effects of dry unit weight (void ratio), the constrained modulus was normalized by the F(e) term defined in Equation 10.3. The relationship between the normalized constrained modulus (M_{max}/F(e)) and the initial matric suction shown in Figure 10.48 shows less scatter than shown for the constrained modulus (Figure 10.46),

yet the normalized constrained moduli were still different for a given value of matric suction.

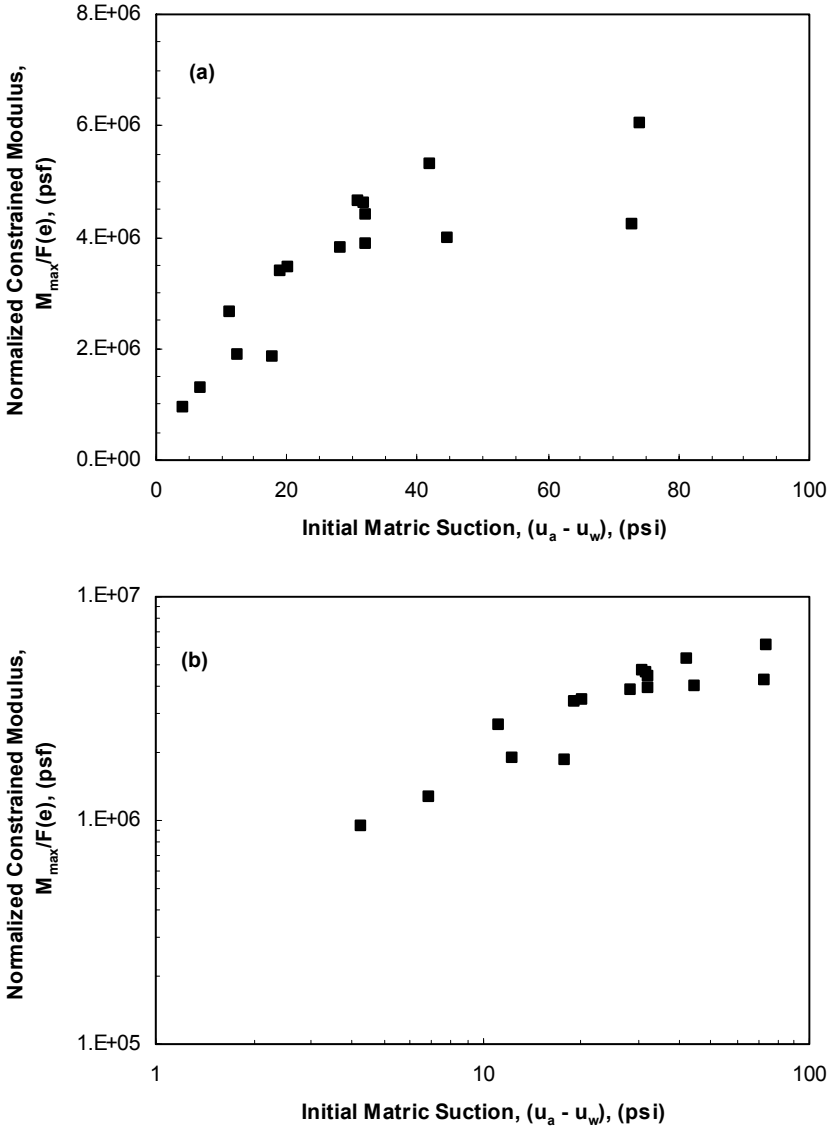

Figure 10.48. Effect of initial matric suction on normalized constrained modulus: (a) arithmetic scale and (b) logarithmic scale.

The effect of degree of saturation on the relationship between constrained modulus and matric suction is illustrated in Figure 10.49. For similar initial degrees of

saturation, the constrained modulus increased as the initial matric suction increased for the range of matric suctions being tested.

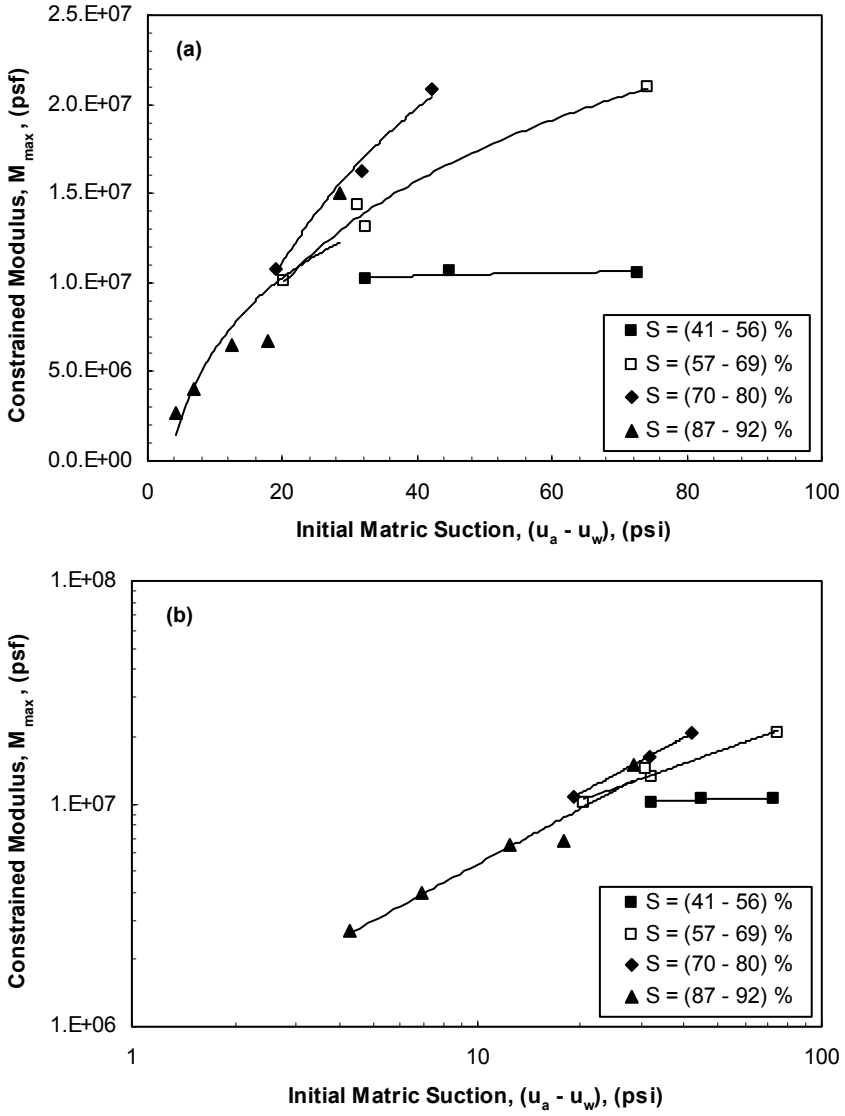

Figure 10.49. Effect of initial matric suction on constrained modulus for specimens compacted at similar degrees of saturation: (a) arithmetic scale and (b) logarithmic scale.

The variation of the constrained modulus with initial matric suction is illustrated in Figure 10.50 for specimens compacted at similar compactive efforts. Interpolation was

implemented to determine the compression wave velocity for specimens compacted dry of optimum as discussed in Section 10.2.2. The constrained modulus increased as the initial matric suction increased, but at a decreasing rate.

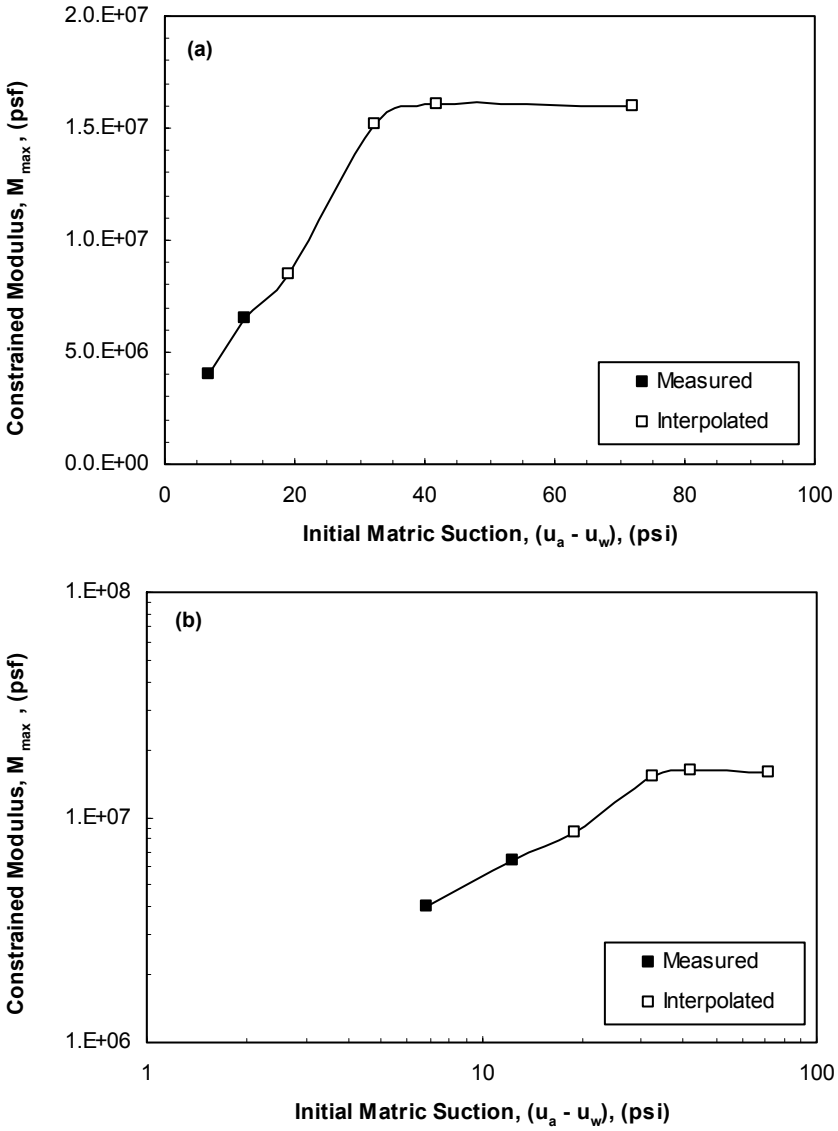

Figure 10.50. Effect of initial matric suction on constrained modulus for specimens compacted at similar compactive efforts: (a) arithmetic scale and (b) logarithmic scale.

For practical purposes, the variation of constrained modulus with matric suction for degrees of saturation higher than 75% was investigated as illustrated in Figure 10.51. The constrained modulus increased as the matric suction increased for the range of matric suctions being investigated.

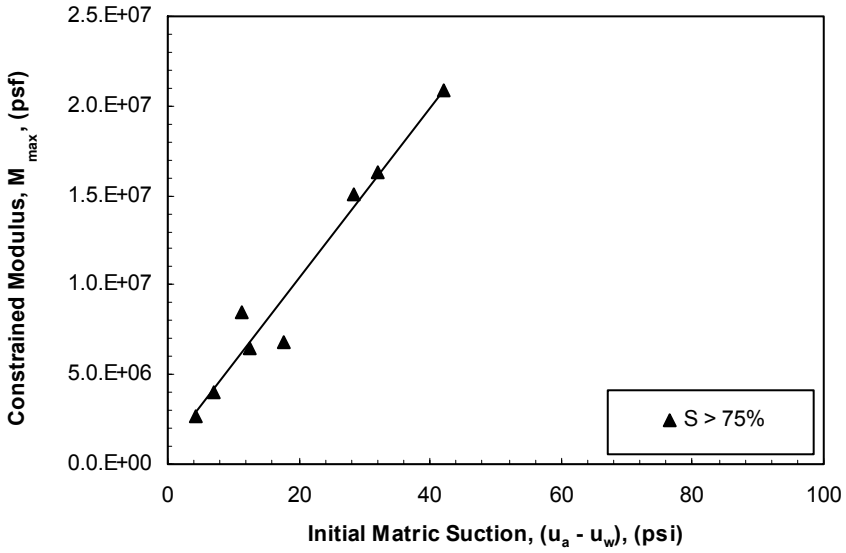

Figure 10.51. Effect of initial matric suction on constrained modulus for specimens compacted degrees of saturation higher than 75%.

10.5.3 DISCUSSION

The variation of shear and constrained moduli with matric suction are generally similar. This similarity is expected because both moduli represent the stiffness of the material skeleton for the range of degrees of saturation being tested (S < 99%) as discussed in Section 10.2.3.

Shear and constrained moduli measured under confining pressure of 0.2 psi represented the as-compacted values for soil stiffness. For specimens compacted at similar dry unit weights, the relationships between shear or constrained moduli and

matric suction (shown in Figures 10.40 and 10.47) were investigated to determine the applicability of using shear or constrained moduli complemented with matric suction measurements to determine dry unit weight for compaction control purposes. The variation observed in these relationships seemed to be beyond what can be used to determine dry unit weights for compaction control purposes.

10.6 Summary

A series of undrained triaxial tests was performed in which shear and compression wave velocities were measured to investigate the effects of compaction conditions on the soil stiffness. The effects of compaction conditions on shear wave velocities were investigated for specimens compacted at similar water contents, dry unit weights, degrees of saturation, and compactive efforts:

- For specimens compacted at similar initial dry unit weights or compactive efforts, the shear wave velocity generally decreased as the initial water content or degree of saturation increased. The decrease in shear wave velocity associated with increase in water content is partially due to decrease in matric suction.

- For similar initial degrees of saturation, the shear wave velocity decreased as the initial water content increased and increased as the initial dry unit weight increased. For similar water contents lower than 17% (w_{opt} = 19%), the shear wave velocity increased as the initial dry unit weight increased. For similar water contents higher than 17%, the effect of the initial dry unit weight on shear wave velocity was not pronounced. The difference between the trends

observed for specimens compacted at different water contents might be related to unexamined effects of soil fabric and overconsolidation ratio.

- For specimens compacted at similar compactive efforts and at water contents wet of optimum, the shear wave velocity increased as the dry unit weight increased, while for specimens compacted dry of optimum, the shear wave velocity decreased as the dry unit weight increased. Changes in shear wave velocity along the standard Proctor compaction curve could be partially attributed to changes in matric suctions and dry unit weights.

- For similar initial water contents lower than 17% (w_{opt} = 19%), the shear wave velocity increased as the initial degree of saturation increased. For specimens compacted at initial water contents ranging from 18 to 21%, the effect of the initial degree of saturation on shear wave velocity was not pronounced. At an initial water content of approximately 24%, the shear wave velocity decreased as the initial degree of saturation increased. The difference between the trends observed for specimens compacted at different water contents might be related to unexamined effects of soil fabric and overconsolidation ratio.

- For specimens compacted at degrees of saturation dry or wet of optimum, the product of the compaction water content and shear wave velocity varied linearly with the compaction dry unit weight.

The effects of compaction conditions on compression wave velocities were investigated for specimens compacted at similar water contents, dry unit weights, degrees of saturation, and compactive efforts. The effects of compaction conditions on shear and compression wave velocities were generally similar. This similarity was expected

because both velocities represented the velocity of waves through the material skeleton for the range of degrees of saturation being tested (S < 99%).

The velocities measured under confining pressure of 0.2 psi represented the as-compacted values for shear and compression wave velocities. The relationship between shear wave velocity and compaction dry unit weight depended on compaction water content. For specimens compacted at similar water contents, the initial dry unit weight did not seem to have a significant effect on the shear wave velocity. Similar trends were observed for compression wave velocities. Accordingly, shear and compression wave velocities were judged to be inapplicable to determine dry unit weights for compaction control purposes.

A series of tests was performed in which the specimens were compressed under undrained conditions and the variation of shear and compression wave velocities with confining pressure was investigated. Shear and compression wave velocities increased as the confining pressure increased. The compression wave velocities increased from approximately 1000 to 4500 fps upon increasing the confining pressure from 0.2 to 90 psi. The value of compression wave velocity of 4500 fps indicates that specimens were becoming saturated. In addition, a slight reduction in the rate of increase of shear wave velocity with increase in confining pressure was observed, as specimens approached saturation, which lead to the development of increasing positive pore-water pressures with increasing confining pressure.

Seven specimens were sheared to failure statically under undrained conditions at confining pressure of 90 psi up to an axial strain of approximately 20%. An average of eight measurements of shear and compression wave velocities could be made during shearing. For specimens compacted dry of optimum, shear and compression wave

velocities increased as the axial strain increased. This might be attributed to combined effects of decrease in void ratio and increase in normal stress. For specimens compacted wet of optimum, the shear wave velocity decreased as the axial strain increased, while the compression wave velocity remained either constant or increased slightly. The decrease in the shear wave velocity was probably due to a decrease in the effective normal stress caused by increase in pore-water pressures during shear.

Results from the previous pressure plate tests were used to estimate the initial matric suction for the specimens tested in the undrained triaxial apparatus. The variation of shear and constrained moduli with initial matric suction was investigated. The shear modulus increased as the initial matric suction increased up to a matric suction of approximately 40 psi beyond which the shear modulus varied significantly for similar values of matric suction. For specimens compacted at similar dry unit weights below about 105 pcf and for specimens compacted at similar compactive efforts, the shear modulus increased as the matric suction increased and then tended towards a nearly constant value beyond which the modulus did not increase further for the range of matric suctions being tested. For specimens compacted at similar degrees of saturation, the shear modulus increased as the initial matric suction increased for the range of matric suctions being tested. The relationship between constrained modulus and matric suction was generally similar to that for shear modulus. The relationships between soil stiffness and matric suction were not unique for the clay tested and depended on factors such as compaction dry unit weight and degree of saturation, which essentially relate to the soil fabric and overconsolidation ratio.

The relationship between soil stiffness and matric suction could be explained by the model proposed by Fisher (1926), in which the air-water meniscus was related to the

state of stress, and thus the stiffness of unsaturated soils. The air-water meniscus introduces a force (ΔN) normal to the contact point between two particles. This force (ΔN) increases as the matric suction increases, but at a decreasing rate, and approaches a nearly constant value beyond which the force ΔN does not increase further. The force Δ*N* reaches a nearly constant value at high matric suctions due to the progressive reduction in the radius of the menisci, which leads to the reduction of the area of water connecting two particles. As the force Δ*N* increases, the stress between the soil particles increases, and thus the soil stiffness increases. The variation of soil stiffness with matric suction is expected to follow pattern similar to the variation of the force Δ*N* with matric suction.

For specimens compacted at similar dry unit weights, the relationship between shear modulus and matric suction was investigated to determine the applicability of using shear modulus and matric suction to infer dry unit weight for compaction control purposes. The variation observed in these relationships seemed to be beyond what can be used to determine dry unit weights for compaction control purposes.

CHAPTER 11: TRIAXIAL APPARATUS AND PROCEDURES FOR MEASUREMENT OF STIFFNESS UNDER CONTROLLED STATES OF STRESS

11.1 Introduction

A suction-controlled triaxial cell equipped with piezoelectric transducers was designed and fabricated for this study to measure soil stiffness under controlled states of stress. Details of the apparatus and testing procedures followed to measure the soil stiffness under controlled states of stress are described in this chapter.

11.2 Apparatus

A new triaxial cell was designed and fabricated in collaboration with the Geotac Company (Houston, Texas) to evaluate the stiffness of unsaturated soils under controlled states of stress. The apparatus is a modified version of a standard triaxial cell. The cell allows independent measurements of the cell pressure, pore-water pressure, and pore-air pressure. In addition, volumetric strains and changes in water content can be measured independently. The apparatus used to perform shear and compression wave velocity measurements using piezoelectric transducers mounted in the platens of the triaxial cell are the same as those used in the undrained triaxial tests described in Chapter 8. A schematic diagram of the apparatus is shown in Figure 11.1. Individual components of the apparatus are described in detail below.

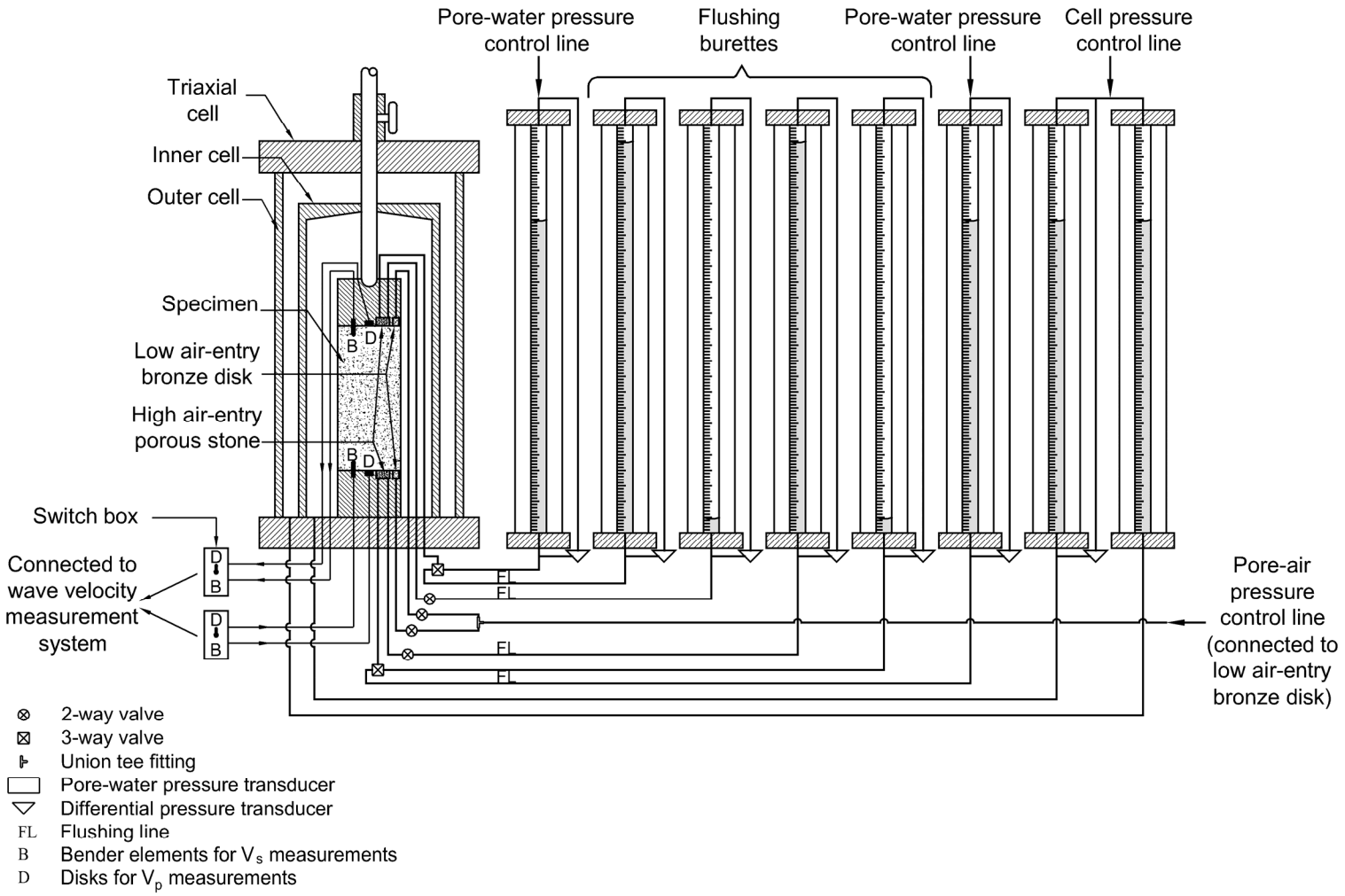

Figure 11.1. Schematic diagram of apparatus used to measure soil stiffness in suction-controlled triaxial apparatus.

11.2.1 END PLATENS

The end platens of the triaxial cell are made of acrylic with a diameter of 2 inches. Two different porous disks were mounted in each platen: a low air-entry bronze disk to control or measure the pore-air pressure, and a Soilmoisture Equipment Corp., model 0604D00.5-B15M1 15-bar high air-entry porous stone to control or measure the pore-water pressure. Each platen is equipped with a bender element and a disk to measure shear and compression wave velocities, respectively. Each piezoelectric transducer was mounted in a separate stainless steel block as discussed in Chapter 8, Section 8.2.1. A photograph and a schematic diagram of the platens are shown in Figures 11.2 and 11.3, respectively.

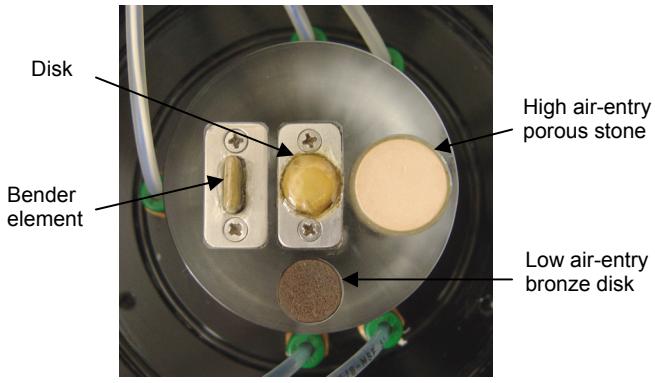

Figure 11.2. Triaxial platen designed to test specimens under controlled states of stress.

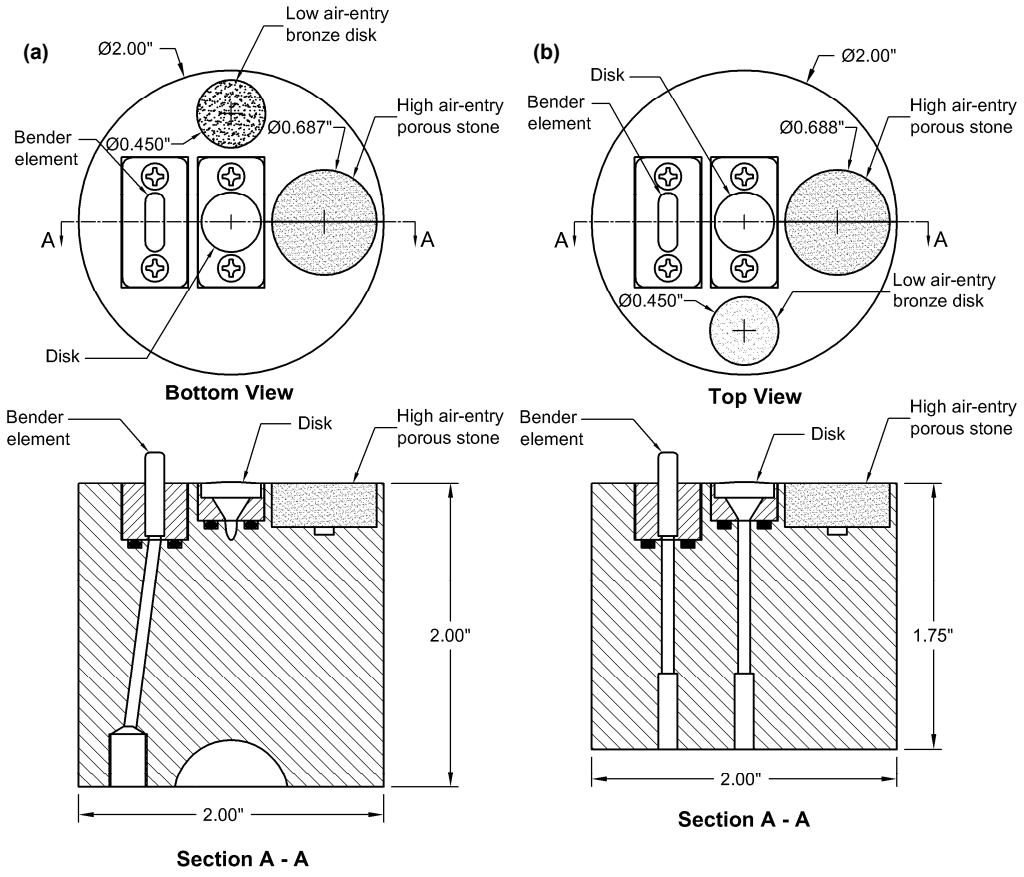

Figure 11.3. Schematic diagram of triaxial platens designed to test specimens under controlled states of stress: (a) top platen and (b) bottom platen.

The low air-entry bronze disk has a diameter of 0.44 inch. The 15-bar high air-entry porous stone has a diameter of 0.63 inch. Each platen has a cavity where the high air-entry porous stone was placed and sealed on the sides using a two-component epoxy resin. This epoxy resin was also used to seal the high air-entry porous stone in the pressure plate apparatus (Chapter 6, Section 6.2). A 0.125-inch wide by 0.05-inch deep groove was machined along the diameter of the cavity to allow flushing air that diffuses through the high air-entry porous stone during the test. The groove connects two 1/8-inch vertical holes drilled through the platen.

The inlet to the flushing groove was connected to a 3-way valve and the outlet was connected to a 2-way valve. One of the outlets of the 3-way valve was either connected to a pressure transducer used to measure the pore-water pressure in constant water content tests, or connected to a water pressure line used to control the water pressure in drained tests. The other outlet of the 3-way valve and the 2-way valve were connected to two double-walled burettes to flush de-aired water through the groove. Details of the design of suction-controlled triaxial platens are presented in Appendix J.

A single pressure line was split into two lines using a union tee fitting to apply air pressure to the top and bottom platens. The air pressure was applied using a Geotac Co. DigiFlow automated air pump. The flow pump was equipped with a Geotac Co., model PS150 pressure transducer with an operational pressure range of $\pm$ 150 psi. Water pressures were applied to the top and bottom platens through two pressure lines connected to the pressure panel. The pore-water pressures were measured from the top and bottom platens using two Geotac Co., model PS100 pressure transducers with an operational pressure range of $\pm$ 100 psi.

Plastic tubing was used for the water pressure lines that connected to the top platen of the triaxial cell. This tubing was selected to satisfy two requirements: 1. fast response of the measuring system of pore-water pressure, and 2. low air diffusivity. Both low-density polyethylene and nylon tubing were investigated. The nylon tubing is better than the low-density polyethylene tubing in providing faster response of the measuring system of pore-water pressure because the nylon tubing is stiffer than the low-density polyethylene tubing. To compare the susceptibility of both types of the low-density polyethylene and nylon tubing to air diffusivity, two equal lengths of each type of tubing were cut, saturated with de-aired water, and placed in a chamber filled with air under a

pressure of 100 psi. The pressure inside the two tubes was maintained at atmospheric. Air diffused through the low-density polyethylene tubing in about 90 minutes, while the nylon tubing resisted air diffusion for almost 24 hours. Therefore, the nylon tubing was selected for the water pressure lines connected to the top platen.

11.2.2 CELL CHAMBER

The triaxial cell consists of two chambers: an inner chamber and an outer chamber; both filled with water. Equal pressure was applied to both chambers. Since the pressure inside and outside the inner cell was equal, expansion of the inner cell was minimized. The inner cell was calibrated for its expansion under confining pressures ranging from 0 to 100 psi. The expansion of the inner cell was one tenth the expansion of the single-walled triaxial cell used to measure the soil stiffness under undrained conditions. Accordingly, the double-walled cell allowed specimen volume changes to be measured accurately by measuring the volume of water going into or out of the inner cell. The measured volume changes were corrected for the expansion of the inner cell. The water content changes were monitored by measuring the volume of water going into or out of the specimen through the high air-entry porous stones. A photograph and a schematic diagram of the triaxial apparatus are shown in Figures 11.4 and 11.5, respectively.

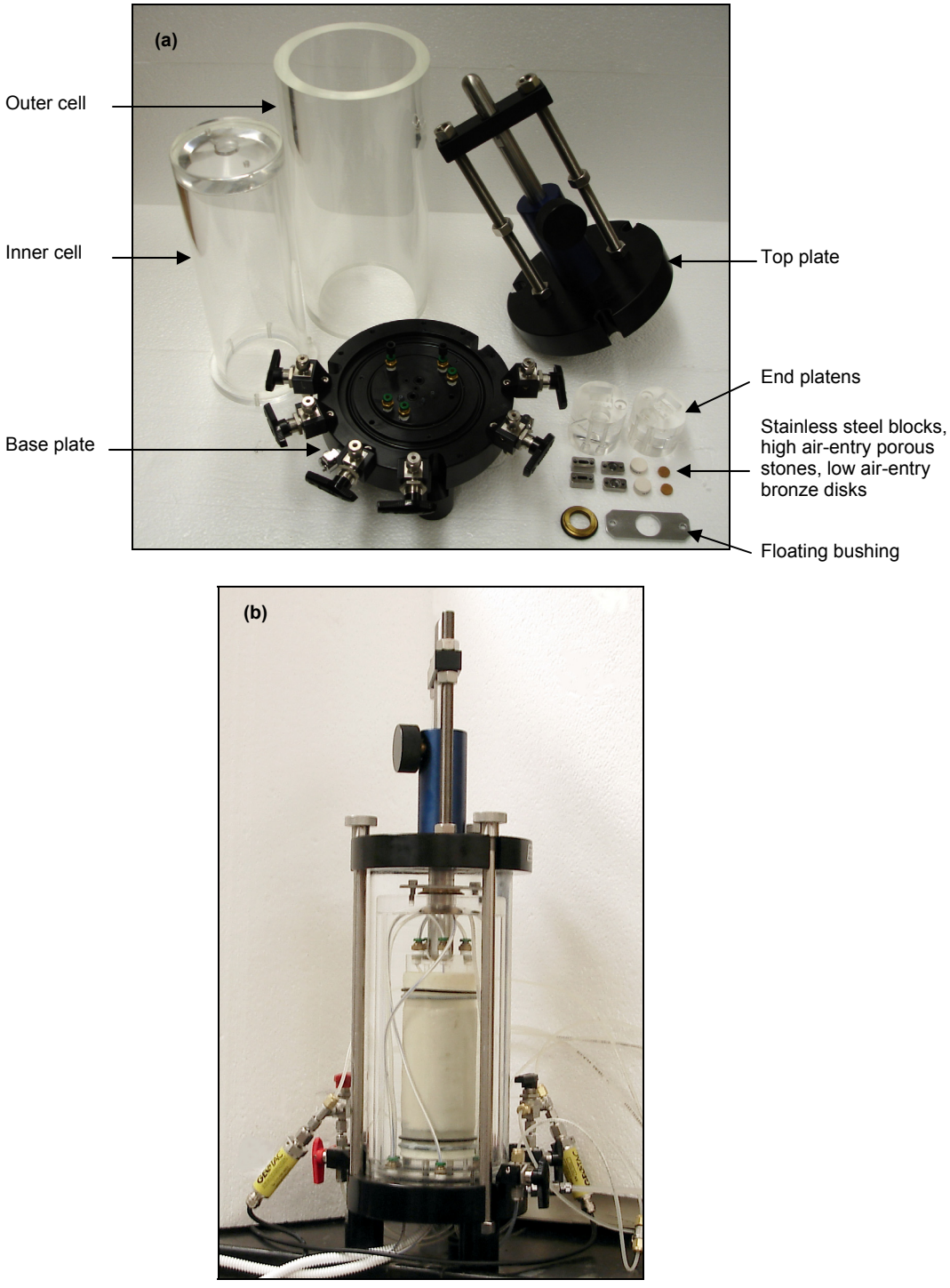

Figure 11.4. Suction-controlled triaxial apparatus: (a) disassembled and (b) assembled with a specimen in place.

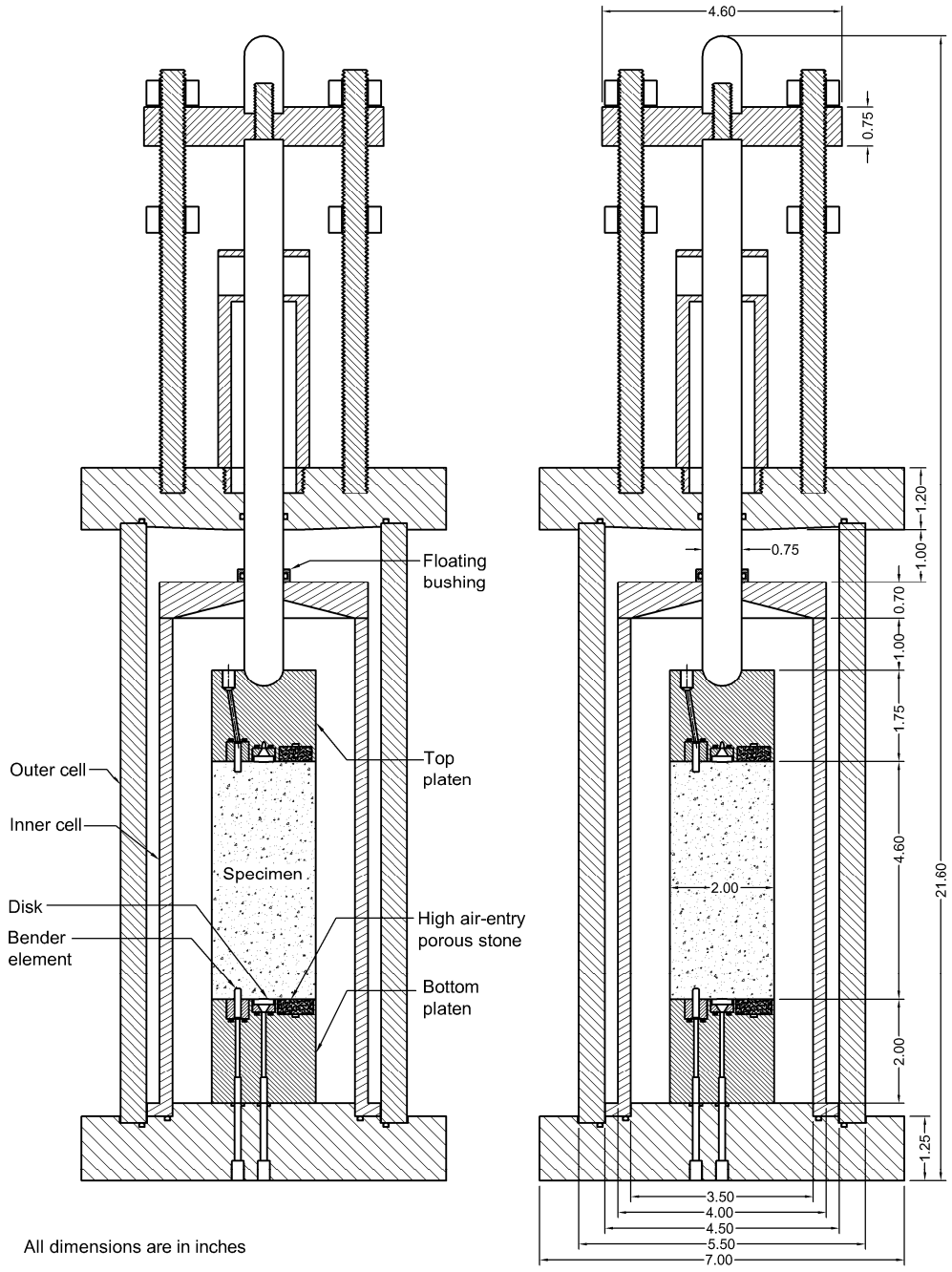

Figure 11.5. Schematic diagram of the suction-controlled triaxial apparatus: (a) labels of key parts and (b) dimensions.

The inner cell is made of acrylic tubing with an inner diameter of 3.5 inches and wall thickness of 0.25 inch. An acrylic plate is glued to the top of the cylinder using IPS Corp., Weldon #16 acrylic cement. In addition, a flange is glued to the bottom of the cylinder as shown in Figure 11.6. The flange has four holes. Three holes were used to attach the inner cell on the base plate using #8-32x3/4" socket head cap screws. The fourth hole was aligned with a hole drilled in the base plate to fill and drain the outer cell. The axial loading piston is 0.75 inch in diameter, and enters the inner cell through a floating bushing mounted on top of the inner cell. The floating bushing is held in place using a bracket and two #10-32x1/2" socket head cap screws as shown in Figure 11.7. The bracket was designed to withstand a pressure difference between the inner cell and outer cell of about 5 psi. The outer cell is made of acrylic with an inner diameter of 4.5 inches, wall thickness of 0.5 inch, and a design pressure of 300 psi.

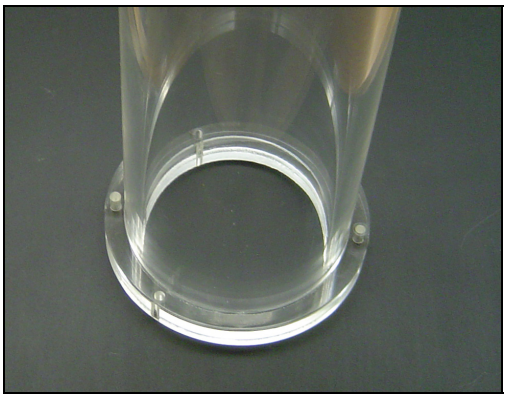

Figure 11.6. Flange glued to the bottom of the inner cell.

Figure 11.7. Floating bushing mounted on top of the inner cell using a bracket and two screws.

The bottom platen was fastened to the base plate with two #10-32x1-5/8" socket head cap screws. The base plate has ten 1/8-inch diameter holes. Four holes were used to exit the wires connected to the four piezoelectric transducers from the triaxial cell. The wires connected to the piezoelectric transducers mounted in the top platen were protected against moisture (from the cell fluid) in 1/8-inch polyethylene tubing. Four holes were used for the four water pressure lines connected to the high air-entry porous stones (two for each porous stone). Finally, two holes were used for the air pressure lines (one for each low air-entry bronze disk). The base plate was equipped with two valves to apply pressure to the inner and outer cells. A photograph of the base plate is shown in Figure 11.8.

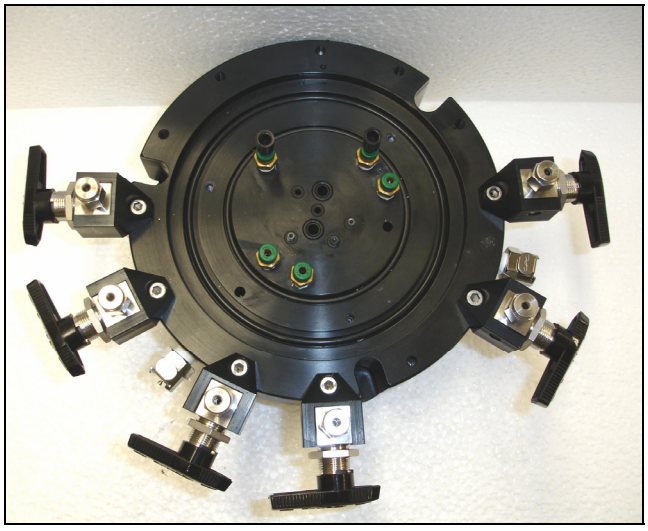

Figure 11.8. Base plate of suction-controlled triaxial cell.

A bracket was mounted on the top plate to prevent the piston from being ejected from the cell when the cell was pressurized as shown in Figure 11.9. The cell pressure was applied using a Geotac Co. DigiFlow automated air pump. The flow pump was equipped with a Geotac Co., model PS150 pressure transducer with an operational pressure range of $\pm$ 150 psi.

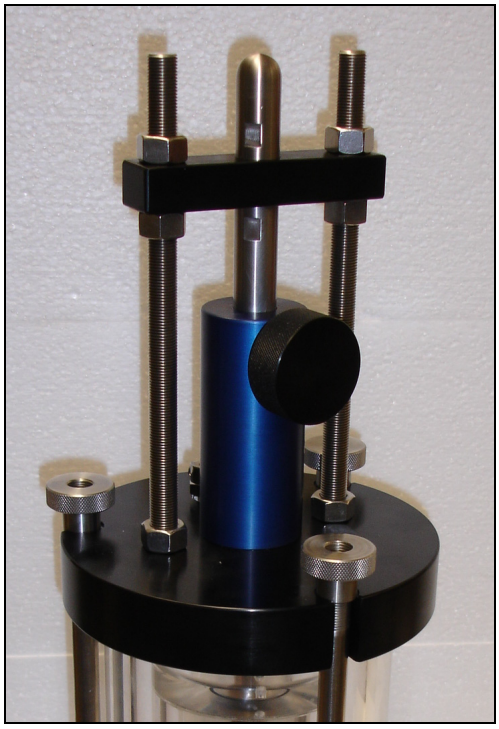

Figure 11.9. Bracket mounted on top plate of suction-controlled triaxial cell.

Volume changes of the specimen were monitored by measuring the volume of the cell fluid going into or out of the inner cell. Accordingly, corrections for inner cell expansion and penetration of the axial load piston into the inner cell were required. The overall volume changes of the specimen were measured using a Validyne Engineering Corp., model DP15-32 differential pressure transducer (DPT) connected from one side to the top and from the other side to the bottom of a 25-ml double-walled burette mounted on the pressure panel. The DPT had an operational pressure range of $\pm$ 2 psi, which provided a resolution of approximately 0.05 ml in volume change.

A Geotac Co. GeoJac automated load frame with a capacity of 2000 lb was used to measure the loads applied to the specimen. The axial load was measured using a Lebow Products Inc., model 3143-1K load cell with a capacity of 1000 lb. Axial

deformation of the specimen was measured using a Geotac Co., model LPT3 linear variable differential transformer (LVDT) with a range of 3 inches. A Geokon Inc., model 2100 Nold DeAerator water *deaerator* was used to supply de-aired water to the pressure panel.

11.2.3 DIFFUSED AIR FLUSHING SYSTEM

Any diffused air that accumulated in the water compartments behind both high air-entry porous stones and in the nylon tubing connected to the top platen was flushed periodically and an attempt was made to measure the volume of the diffused air. Each high air-entry porous stone was connected to two 25-ml double-walled burettes mounted on the pressure panel. The first burette was nearly full of de-aired water and the second burette was nearly empty. Water was flushed from the first burette, into the end platens and through the groove behind the high air-entry porous stone, then, into the second burette. The volume of the diffused air was assumed to be equal to the difference between the volume changes measured in both burettes before and after flushing. The volume change within each burette was measured using a Validyne Engineering Corp., model DP15-32 differential pressure transducer (DPT) connected from one side to the top and from the other side to the bottom of the burette. The DPT had an operational pressure range of $\pm$ 2 psi, which provided a resolution of approximately 0.05 ml in volume change. The volume of the diffused air could be measured in drained tests but could not be measured in constant water content tests as is discussed in Section 11.3.4.1.

The test set-up used for measuring soil stiffness under a controlled state of stress is shown in Figure 11.10. The system included the suction-controlled triaxial cell, a load frame, two pressure panels (only one is shown in picture), two automated flow pumps, a water *deaerator,* an oscilloscope, a function generator, an amplifier, and a personal

computer. Details of the data acquisition and control system involved in the suction-controlled triaxial tests are presented in Appendix C.

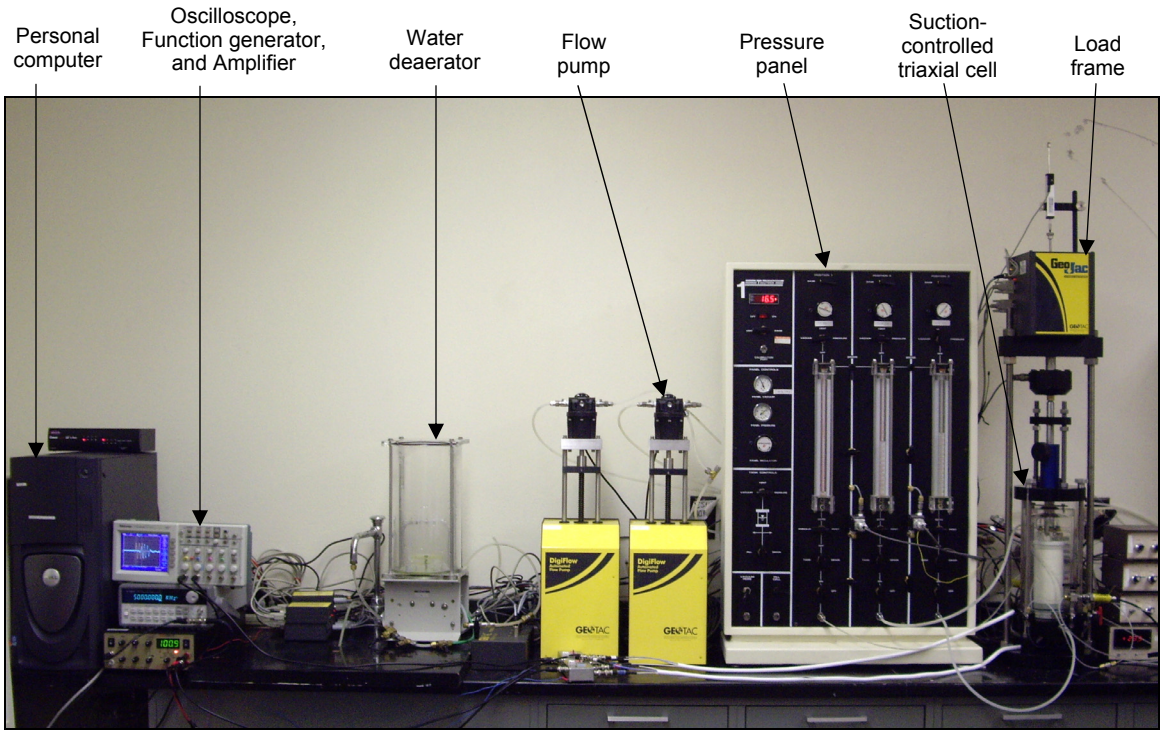

Figure 11.10. Apparatus used for measuring soil stiffness under controlled states of stress.

11.3 Test procedure

Two types of tests were conducted in the suction-controlled triaxial apparatus: a drained test and constant water content test. Details on the preparation of the apparatus prior to setting up the specimen, specimen set-up, and the test procedure followed in both types of tests are discussed in the following sections. The procedures for shear and compression wave velocity measurements are the same as those used in the undrained triaxial tests described in Chapter 8.

11.3.1 PREPARATION PRIOR TO SETTING UP SPECIMEN

The piezoelectric transducers were checked before each test to make sure that the transducers were functioning properly as discussed in Chapter 8. The system for measuring the pore-water pressure (high air-entry porous stones, water cavities beneath the porous stones, and pressure transducers) was saturated following the same procedures used for the pressure plate apparatus described in Chapter 6. The low air-entry bronze disks were removed from the end platens before starting the saturation process.

After completion of saturation of the system for measuring the pore-water pressure, the de-aired water used for this purpose was removed from the triaxial cell and the cell was disassembled. The next step was to purge the air pressure lines of water. The air pressure lines were dried by allowing air to flow from the pressure panel through the air pressure lines and out of the openings in the end platens. A pressure of 90 psi was used and airflow was continued until no water was observed in the air pressure lines. Excess water on the end platens was then removed and the low air-entry bronze disks were placed in the platens. All the differential pressure transducers mounted on the double-walled burettes for volume changes measurements were then saturated by flushing de-aired water through the transducers.

11.3.2 SPECIMEN SET-UP

The specimen was mounted between the platens of the triaxial cell such that the top and bottom piezoelectric transducers fit in the assigned intrusions that were carved in the ends of the specimen during compaction. A rubber membrane was placed around the specimen. The outside of the rubber membrane was then coated with a layer of silicon

grease and a layer of aluminum foil[1] was wrapped around the membrane and covered with a second rubber membrane. O-rings were used to seal the two membranes to the top and bottom platens. A thin coating of silicon grease was applied on the vertical sides of the top and bottom platens to aid in sealing the first membrane to the end platens. Double membranes with silicon grease and a layer of aluminum foil between the membranes were used to reduce the volume of air diffusing from the specimen to the surrounding cell fluid. Tap water was considered better than de-aired water as a cell fluid because the concentration of air in tap water is higher than that in de-aired water, which helped in reducing the volume of air diffusing from the specimen to the surrounding cell fluid.

The inner and outer cells were filled with tap water and the triaxial cell was placed on the load frame. A seating load of 2 lbs was applied using the axial load piston to insure good contact between the specimen and the piezoelectric transducers and high air-entry porous stones. The axial load piston was locked at fixed displacement before starting the test. The volume of water absorbed by the specimen through the high air-entry porous stones while mounting the specimen was insignificant.

11.3.3 DRAINED TEST PROCEDURE

The first test performed in the suction-controlled triaxial cell was a drained test. The specimen was compacted at a water content of 11% and a dry unit weight of 98 pcf. In this test, both pore air and pore water were allowed to flow freely into or out of the specimen when the confining pressure was applied. A schematic diagram of the apparatus used to perform drained tests in the suction-controlled triaxial cell is shown in Figure 11.1. The 2-way valves connected to the air pressure lines were opened. The 3-way

[1] Potato-chip bag – Lay's ®

valves, connected to the inlets of the water cavities beneath the high air-entry porous stones, were switched to connect the water pressure lines to the specimen while the 2-way valves, connected to the outlets of the water cavities, were closed. The cell, pore-air, and pore-water pressures were set to achieve the target values of matric suction ($u_a - u_w$) and net stress ($\sigma_c - u_a$). The pore-air pressure equalizes almost immediately after the application of the air pressure (Fredlund and Rahardjo, 1993). The specimen gradually absorbed or expelled water through the high air-entry porous stones depending on whether the initial matric suction was higher or lower than the target matric suction. The intent of this test was to measure the shear and compression wave velocities when the flow of water into or out of the specimen through the high air-entry porous stone essentially ceased, i.e. equilibrium was achieved.

The initial net stress ($\sigma_c - u_a$) of the specimen was zero. The initial matric suction ($u_a - u_w$) of the specimen was inferred from the pressure plate test results reported in Chapter 7 and estimated based on the data shown in Figure 11.11 to be about 105 psi. The target net stress and matric suction were 5 and 20 psi, respectively. The anticipated water content corresponding to the target matric suction was estimated from Figure 11.11 to be about 18%, neglecting the fact that the net stress in the pressure plate tests is zero, while the net stress for this test was 5 psi.

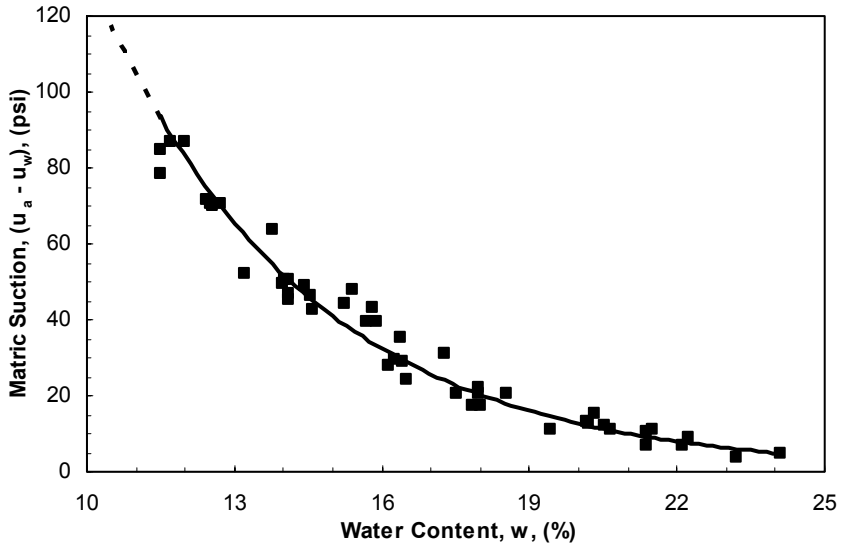

Figure 11.11. Compaction water content - matric suction relationship.

The variation of the water content of the specimen with time during equalization in this initial drained test is shown in Figure 11.12 on both arithmetic and logarithmic scales. The specimen absorbed water at a rate of 0.1 ml/day, which is equivalent to a rate of change of water content of about 0.025%/day. The specimen was expected to absorb eventually a total volume of water of about 28 ml at equilibrium under the imposed net stress and matric suction. Accordingly, it was estimated that about 280 days (approximately 3 months) would be required to reach equilibrium. This time required to reach equilibrium was judged to be excessive and the test was terminated after 60 days. An alternative test procedure was developed and is discussed in the following section.

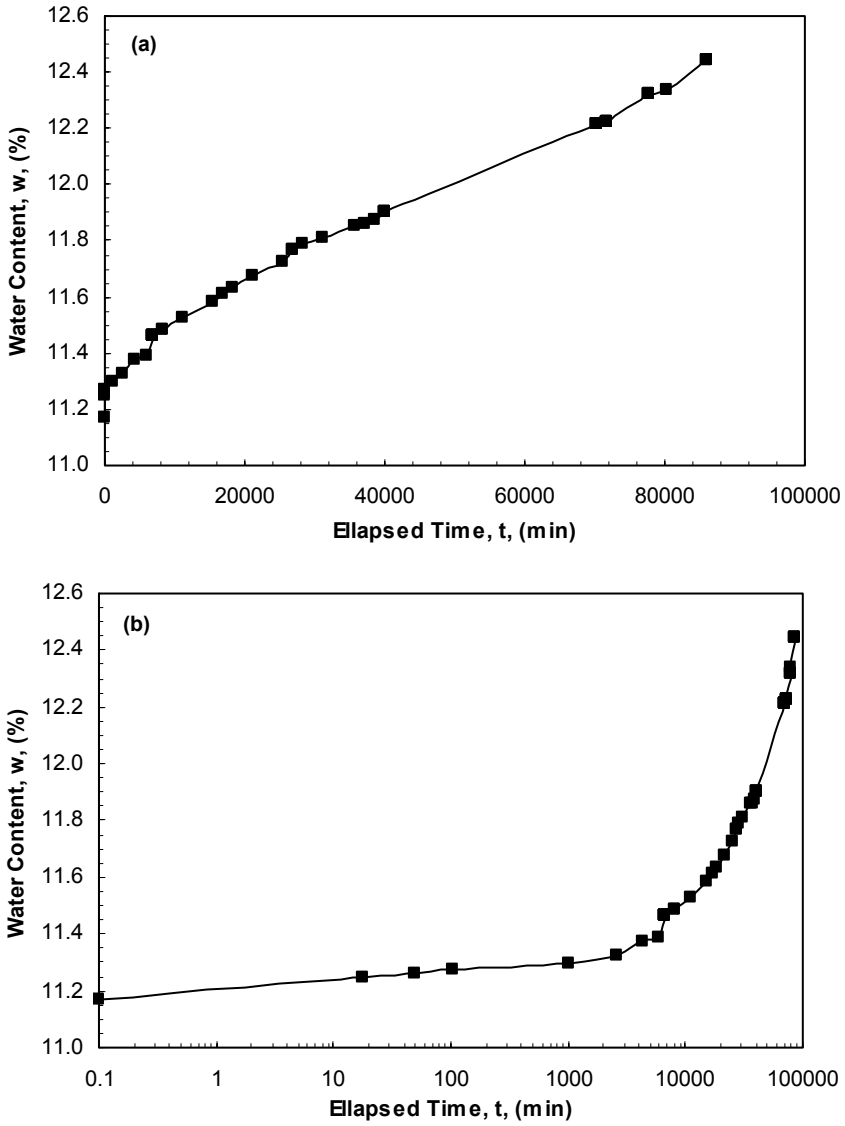

Figure 11.12. Water content changes during the equalization of specimen in drained test (a) arithmetic scale and (b) logarithmic scale.

The long equalization period experienced in this test was probably due to the low hydraulic conductivity of the tested clay. Even with higher hydraulic conductivities, relatively long periods have been reported in the literature to reach equilibrium. Rampino et al. (1999, 2000) performed drained tests on compacted *silty sand* under drained

conditions. The authors considered equilibrium was achieved when the rate of change of water content decreased to about 0.04%/day, which was lower than the initial rate of change of water content observed in the drained test performed in this study. The authors showed that their specimens equalized within 6 to 7 days (10000 minutes) irrespective of the target matric suction as shown in Figure 11.13. The soil being tested in this study had lower hydraulic conductivity, and thus the time required to reach equilibrium was much longer than that reported by Rampino et al. (1999, 2000).

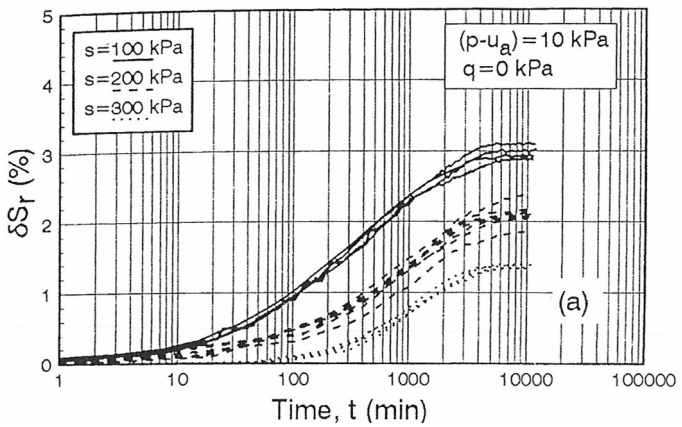

Figure 11.13. Degree of saturation changes during the equalization stage in drained tests (from Rampino et al., 2000).

The saturated hydraulic conductivity of the clay tested in this study was calculated from the coefficient of consolidation, c_v, and the coefficient of volume compressibility, m_v, measured during consolidation of another similar specimen under an effective stress of 15 psi ($k_{sat} = c_v.\gamma_w.m_v$). The saturated hydraulic conductivity was about $4x10^{-7}$ cm/sec. The unsaturated hydraulic conductivity of the clay was estimated using the hydraulic conductivity models developed by Brooks and Corey (1964) and van Genuchten (1980). In these models, the unsaturated hydraulic conductivity is related to the volumetric water content and parameters determined using the volumetric moisture content – matric

suction relationship (from pressure plate tests reported in Chapter 7) shown in Figure 11.14. The unsaturated hydraulic conductivity of the clay was estimated to range from $4x10^{-7}$ to $1x10^{-10}$ cm/sec for matric suctions ranging from 0 to 100 psi as shown in Figure 11.15. Because of this low hydraulic conductivity, which led to impractical long testing periods, no further drained tests were performed in this study.

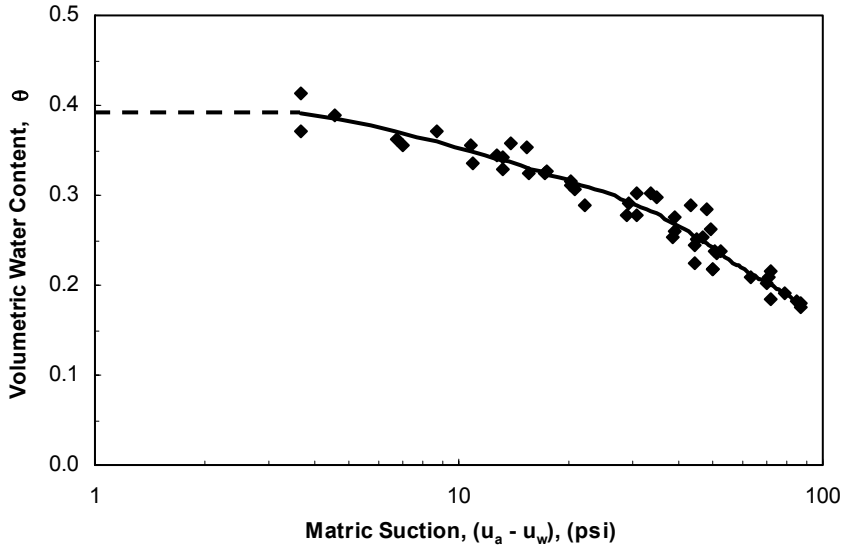

Figure 11.14. Volumetric water content – matric suction relationship.

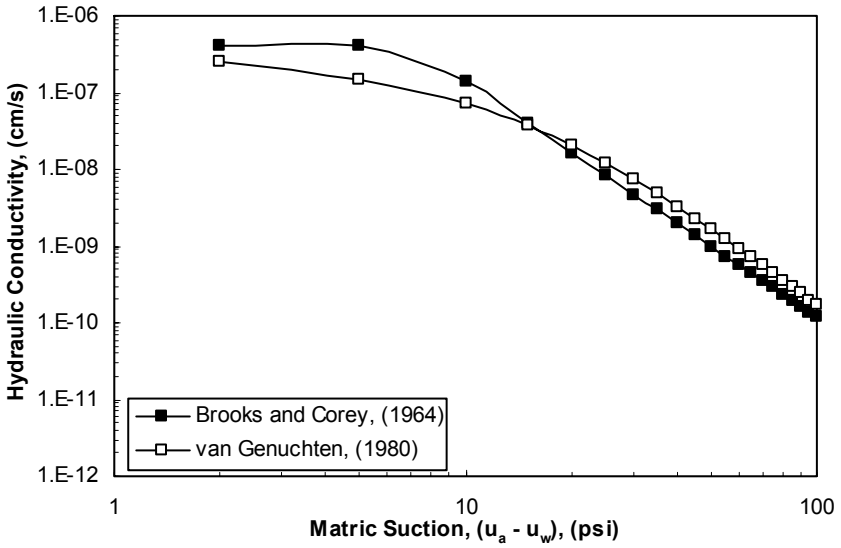

Figure 11.15. Hydraulic conductivity – matric suction relationship estimated using hydraulic conductivity models developed by Brooks and Corey (1964) and van Genuchten (1980).

During the drained test, air diffused through the high air-entry porous stones and the nylon tubing (connected to the top platen) into the system used to measure the pore-water pressure. The diffused air displaced the water in the water cavities introducing errors in the measurements of the volume of water flowing into or out of the specimen. The diffused air was flushed out of the water cavity, following the procedure outlined in Chapter 6, each time a considerable amount of air was observed in the cavity beneath the high air-entry porous stone and/or into the nylon tubing. The measurements for the volume of water flowing into or out of the specimen were then corrected for the amount of diffused air. At the end of the test, the pressure chamber was disassembled and the final water content of the specimen was determined.

11.3.4 CONSTANT WATER CONTENT TEST PROCEDURE

Because of the very long times experienced for water to flow into or out of the specimen in the drained test, an alternative test procedure was developed. In the alternative procedure, the water content was kept constant. Thus, no flow of water into or out of the specimen was required. In a constant water content test, the pore air was allowed to drain while the pore water was not when the confining pressure was applied. The test procedure was divided into two stages: an equalization stage and an isotropic compression stage. A schematic diagram of the test set-up for the constant water content tests is shown in Figure 11.16 and the procedure is described further below.

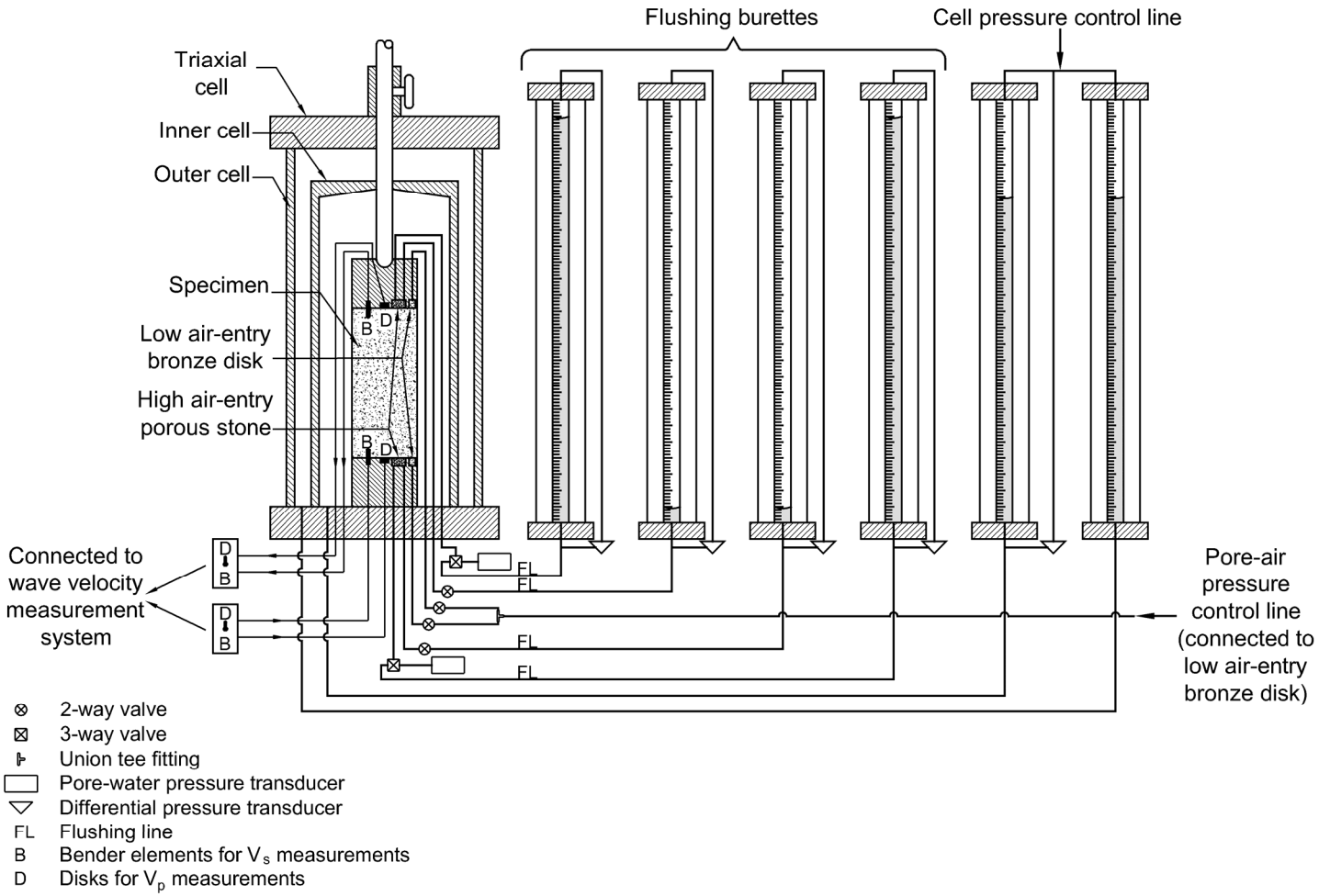

Figure 11.16. Schematic diagram of test set-up used to perform constant water content test in suction-controlled triaxial apparatus.

11.3.4.1Equalization stage

The aim of the equalization stage was to establish the initial values of matric suction ($u_a - u_w$) and net stress ($\sigma_c - u_a$) acting on the specimen after compaction without a change in the water content of the specimen. The net stress ($\sigma_c - u_a$) on the specimen after compaction was zero because the confining pressure and the pore-air pressure were atmospheric. Therefore, the cell and pore-air pressures were maintained equal throughout the equalization stage (to maintain a net stress of zero) by connecting the cell and pore-air pressure lines to a single flow pump. Before starting the equalization stage, the 3-way valves, connected to the inlets of the water cavities beneath the high air-entry porous stones, were switched to connect the pressure transducers to the water cavities, while the 2-way valves, connected to both the outlets of the water cavities and the air pressure lines, were opened.

The equalization stage started once the 2-way valves, connected to the outlets of the water cavities, were closed. The specimen immediately tended to draw water through the high air-entry porous stones, causing the transducers to start registering negative water pressures. One of the transducers for measuring the pore-water pressures was used to control the flow pump that controlled the cell and pore-air pressures (cell and pore-air pressures were maintained equal throughout the equalization stage). When the transducer controlling the flow pump registered a negative water pressure, the flow pump increased the cell and pore-air pressures (axis translation technique) automatically until the reading of the pressure transducer controlling the flow pump returned to zero. The other transducer for measuring pore-water pressure recorded the pore-water pressure developed on the other end of the specimen.

The readings of the pressure transducer controlling the flow pump were maintained at zero throughout the equalization stage. Equilibrium was inferred when the readings of the other pressure transducer stabilized. The differences between the pore-air and the pore-water pressures measured at equilibrium were equivalent to the matric suctions at the ends of the specimen. The average value of the matric suctions measured at the ends of the specimen was taken to represent the average matric suction of the specimen.

At equilibrium, inferred by the stabilization of pore-water pressures, shear and compression wave velocities were measured. To measure the exact distance between the piezoelectric transducers, the axial load piston was unlocked and a deformation rate of 0.005 inch/min (using the load frame) was used to apply 2 lbs to the specimen. The displacement of the axial load piston was measured using the linear variable differential transformer (LVDT) mounted on the load frame. The axial deformation of the specimen during equalization was equal to the displacement of the axial load piston. Accordingly, the distance between the piezoelectric transducers at the end of the equalization stage could be determined.

During the equalization stage, air diffused through the high air-entry porous stones and the nylon tubing (connected to the top platen) into the system for measuring the pore-water pressure. The diffused air was flushed out of the water cavities following the procedure outlined in Chapter 6. The diffused air was flushed out once air was observed in the water cavities because it affected the pore-water pressure measurements. The volume of diffused air could not be determined because it was smaller than the minimum volume the measuring system could accurately measure ($\pm$ 0.05 ml).

11.3.4.2Compression stage

For the compression stage, the specimens were isotropically compressed by increasing the cell pressure. Tests were performed at increasing net stresses ($\sigma_c - u_a$) ranging from 10 to 40 psi. The pore-air pressure was maintained constant at the value it had at the end of the equalization stage. A flow pump was used to maintain the air pressure at the target value. The cell pressure was increased using a second flow pump. For each target cell pressure (depending on the target net stress), the pressure was increased at a rate of 10 kPa/hr, which was reported by Macari and Hoyos (2001) to be appropriate for avoiding breaking the menisci and destroying the suction within the specimen. Pore-water pressures were recorded at the two ends of the specimen. Equilibrium was inferred when the readings of the pressure transducers for measuring pore-water pressures stabilized. The differences between the pore-air and the pore-water pressures measured at equilibrium were equivalent to the matric suctions at the ends of the specimen. The average value of the matric suctions measured at the ends of the specimen was taken to represent the average matric suction of the specimen. At equilibrium, inferred by the stabilization of pore-water pressures, shear and compression wave velocities were measured. The exact distance between the piezoelectric transducers was measured using the same procedure explained in Section 11.3.4.1.

At the end of the test, the pressure chamber was disassembled and the final water content of the specimen was determined. During the compression stage, air diffused through the high air-entry porous stones and the nylon tubing (connected to the top platen) into the system for measuring the pore-water pressure. The diffused air was flushed out of the water cavities following the procedure outlined in Chapter 6.

11.4 Summary

A suction-controlled triaxial cell equipped with piezoelectric transducers was developed to measure soil stiffness under controlled states of stress. The cell allows independent measurements of cell pressure, pore-water pressure, and pore-air pressure. In addition, volumetric strains and changes in water content can be measured independently. The triaxial cell consists of two chambers: an inner chamber and an outer chamber; both filled with water. Equal pressure was applied to both chambers. Since the pressure inside and outside the inner cell was equal, expansion of the inner cell was minimized. The double-walled cell allowed specimen volume changes to be measured accurately by measuring the volume of water going into or out of the inner cell. The water content changes were monitored by measuring the volume of water going into or out of the specimen through the high air-entry porous stones.

Two types of tests were performed in the suction-controlled triaxial apparatus: drained and constant water content tests. In the drained test, both pore air and pore water were allowed to flow freely into or out of the specimen when the confining pressure was applied. The drained test procedure required very long equalization periods due to the low hydraulic conductivity of the tested clay. An alternative test procedure was developed in which the water content of the specimen was kept constant. The constant water content test procedure was divided into two stages: an equalization stage and an isotropic compression stage. In drained and constant water content tests, air diffused through the high air-entry porous stones and the nylon tubing (connected to the top platen) into the system for measuring pore-water pressure. The diffused air was periodically flushed. The volume of diffused air could be determined in drained tests, but could not be determined in constant water content tests.

CHAPTER 12: MEASUREMENTS OF SOIL STIFFNESS UNDER CONTROLLED STATES OF STRESS

12.1 Introduction

A series of tests at constant water content was performed in the suction-controlled triaxial apparatus (described in Chapter 11) to investigate the effect of state of stress on soil stiffness at small strains. The procedure used to interpret shear and compression waveforms is discussed in Chapter 9. The variation of the state of stress in the soil during the equalization and isotropic compression stages is discussed in this chapter. The effects of matric suction and net stress on shear and compression wave velocities are also presented and discussed. Finally, stiffness measurements recorded at zero net stress are compared to the stiffness measurements that were made at a confining pressure of 0.2 psi in the undrained triaxial apparatus (described in Chapter 8).

12.2 Soil state of stress in constant water content tests

Eight specimens were tested in the suction-controlled triaxial apparatus under constant water content conditions. The specimens were compacted at water contents ranging from 12 to 19% and dry unit weights ranging from 98 to 111 pcf (Figure 12.1). The compaction water contents, dry unit weights, and degrees of saturation for all specimens are summarized in Table 12.1 and presented in Appendix K.

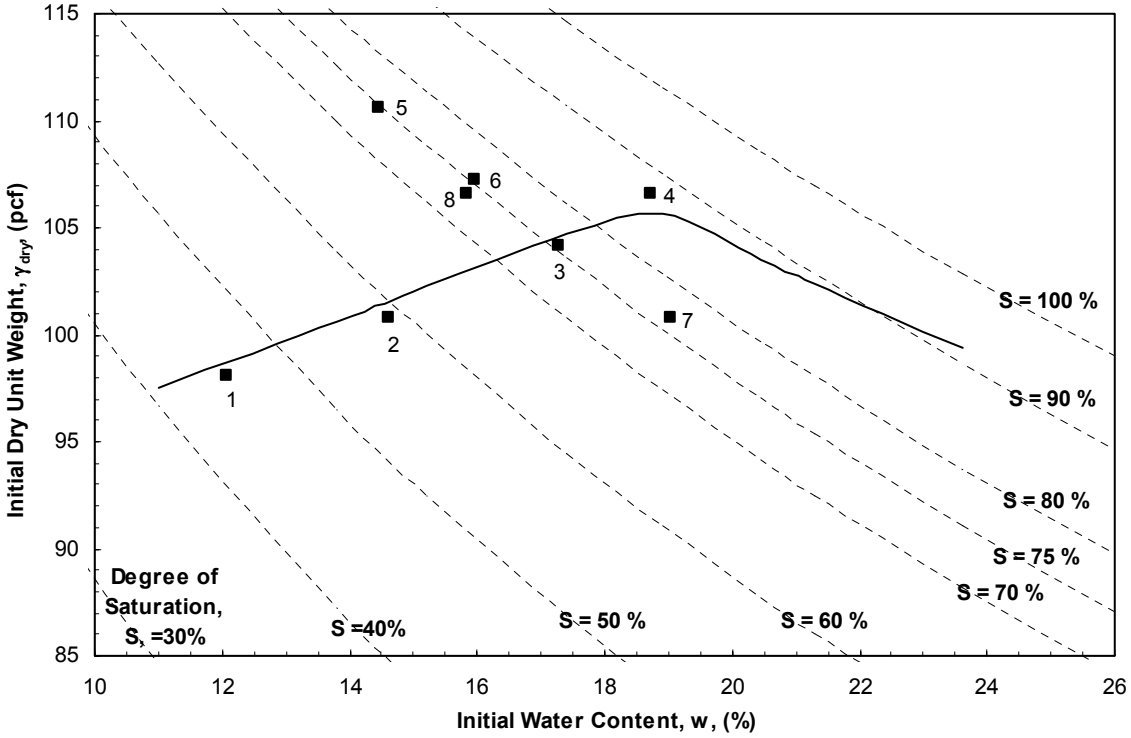

Figure 12.1. Standard Proctor compaction curve with specimens tested in suction-controlled triaxial apparatus.

Table 12.1. Compaction conditions for specimens tested in the suction-controlled triaxial apparatus.

Test #	w, (%)	γ_{dry}, (pcf)	S, (%)
1	12.1	98.1	45.4
2	14.6	100.8	58.7
3	17.3	104.1	75.4
4	18.7	106.6	87.0
5	14.4	110.6	74.5
6	16.0	107.3	75.6
7	19.0	100.8	76.4
8	15.8	106.6	73.7

The test procedure for tests at constant water content is outlined in Chapter 11 and consisted of 2 stages: (1) an equalization stage and (2) an isotropic compression stage. The variation of the state of stress in the soil during the equalization and compression stages is discussed below.

12.2.1 EQUALIZATION STAGE

The aim of the equalization stage was to establish the initial values of matric suction ($u_a - u_w$) and net stress ($\sigma_c - u_a$) acting on the specimen after compaction without changing the water content of the specimen. During the equalization stage, the cell and pore-air pressures were maintained equal (resulting in zero net stress) and were adjusted automatically to maintain zero pore-water pressure within the specimen. Typical suction-time response curves, the effect of air diffusion on the matric suction measurements, and the volume changes observed during the equalization stage are presented and discussed below.

12.2.1.1Typical suction-time response curves

A typical suction-time response curve for the equalization stage is shown in Figure 12.2. The matric suction was measured at both ends of the specimen. The variation of matric suction with time during the equalization stage is very similar to that reported for the pressure plate tests in Chapter 7. The matric suction increased with time at a decreasing rate until it reached an asymptotic value, i.e. equilibrium was achieved. At equilibrium, the average value of the matric suctions measured at the two ends of the specimen was taken to represent the average matric suction in the specimen. The difference in matric suctions between the ends of all eight specimens ranged from 0 to

10% of the average matric suction in the specimen, which was considered a small difference.

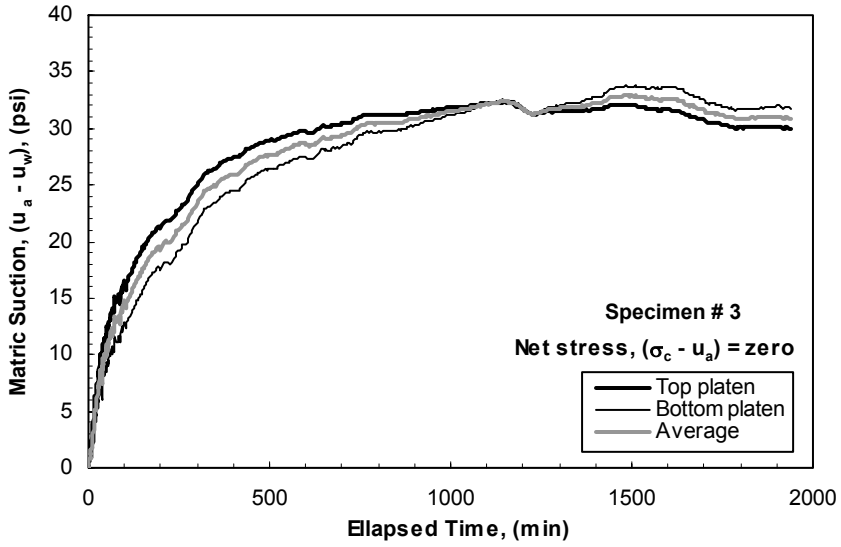

Figure 12.2. Typical suction-time response curve recorded in equalization stage.

During the equalization stage, the cell and pore-air pressures were adjusted automatically at short adjustment intervals using the flow pump as discussed in Chapter 11. Short adjustment intervals sometimes caused "overshooting" in the measured matric suctions as illustrated in Figure 12.3. Similar observations were reported by Bocking and Fredlund (1980). Overshooting in the suction-time response curve was observed to occur more often at lower compaction water contents. The irregularities observed in the suction-time response curve shown in Figure 12.3 are due to air diffusion and are discussed later in Section 12.2.1.2. The suction-time response curves recorded in the equalization stage for all tests are presented in Appendix K.

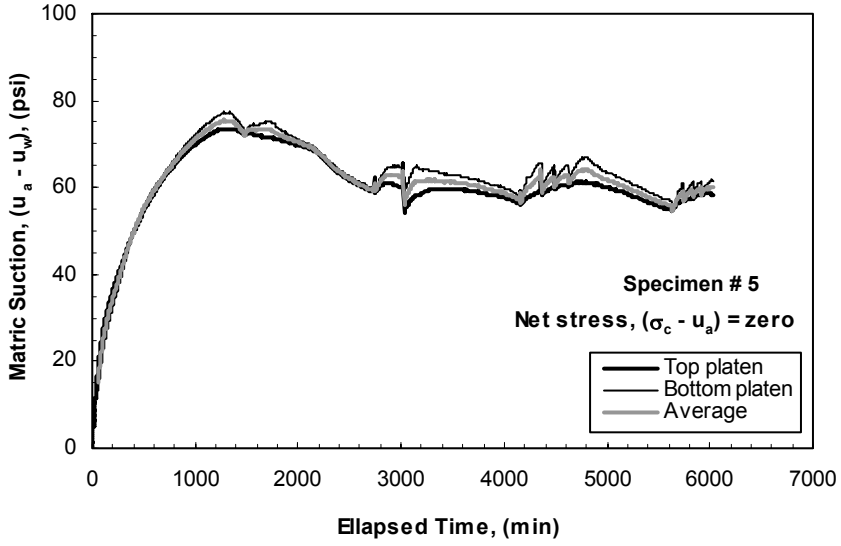

Figure 12.3. Suction-time response curve for equalization stage in which overshooting was observed in the measured matric suctions.

Matric suctions measured during the equalization stage are compared to the suctions measured in the pressure plate tests (reported in Chapter 7) in Figure 12.4. The matric suctions measured during the equalization stage for five specimens (out of eight specimens) were on the upper bound of the range of matric suctions measured in the pressure plate tests. For the other three specimens (circled in Figure 12.5), the matric suctions appeared to be even larger and are believed to be unreasonably high. Thixotropy is not believed to be the reason for these larger matric suctions because the specimens tested in the suction controlled triaxial apparatus and the pressure plate apparatus were stored after compaction and before testing for comparable periods. However, no explanation could be found for the larger matric suctions measured in the equalization stage.

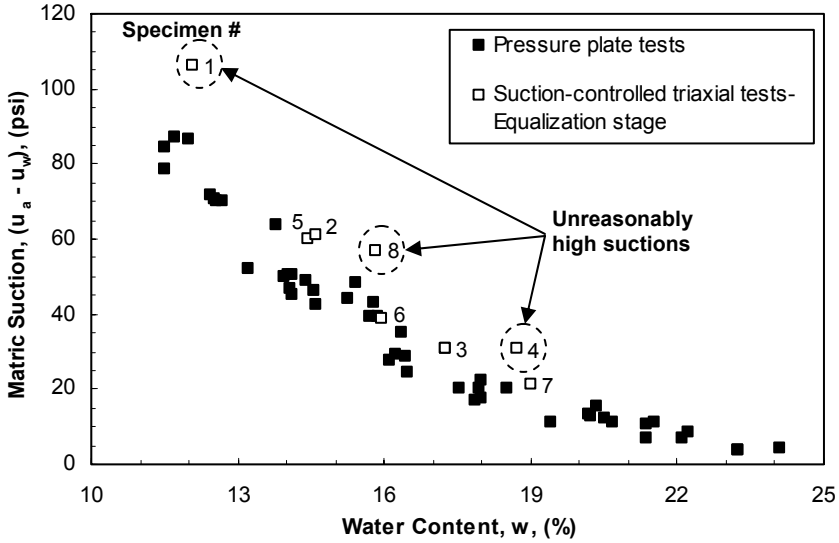

Figure 12.4. Comparison of matric suctions measured in the pressure plate tests and in the equalization stage of the suction-controlled triaxial tests.

12.2.1.2Effect of air diffusion on matric suction measurements

The effect of air diffusion on matric suctions measured during the equalization stage was similar to that discussed for the pressure plate tests in Chapter 7. The matric suction decreased when air diffused into the measuring system. The effect of air diffusion on matric suction measurements was minimized by periodically flushing de-aired water through the water cavities behind the high air-entry porous stones. After flushing the diffused air, the matric suction increased and then started to drop again as air re-diffused into the water cavities. Periodic flushing of the diffused air caused some irregularities in the suction-time response curve as shown in Figure 12.5. A significant drop in the matric suction occurred at each time water was flushed through the water cavities behind the high air-entry porous stones. The amount of air diffusion was larger for specimens compacted at lower water contents and as the test duration increased.

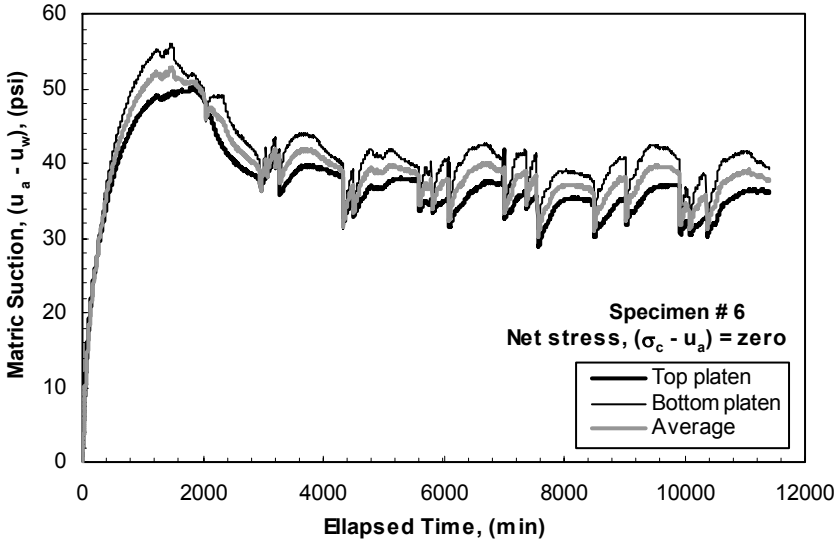

Figure 12.5. Effect of air diffusion followed by water flushing on the suction-time response curve recorded in equalization stage.

12.2.1.3Volume changes during equalization stage

Insignificant volume changes were anticipated during the equalization stage because the states of stress in the specimens were the same before and after this stage. However, the specimens experienced about 1 to 4% compression during the equalization stage, which was close to the amount of volume changes experienced upon increasing the net stresses from 0 to 40 psi. Volume changes occurred during the equalization stage as the pore-water pressure equalized within the specimen. By the end of the equalization stage, the volume changes of the specimen ceased. A typical volumetric strain - time response curve for a test is shown in Figure 12.6. The volumetric strain - time response curves for all tests are presented in Appendix K.

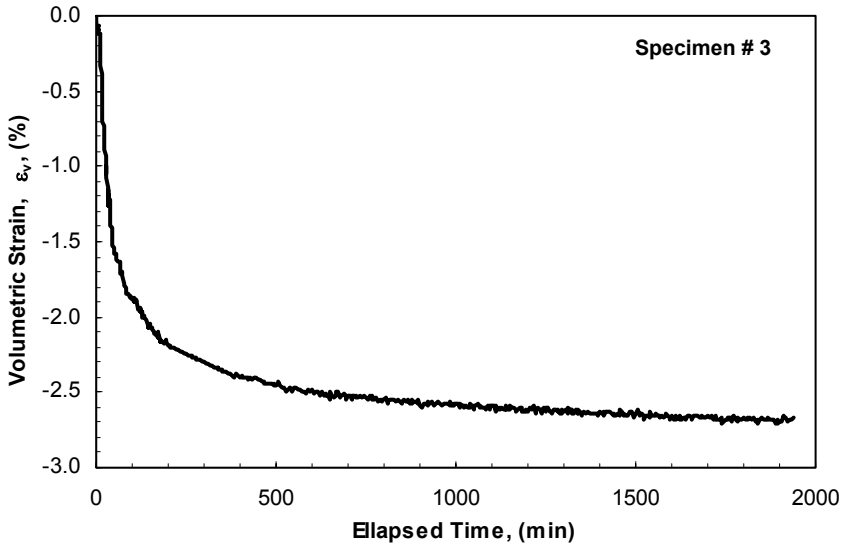

Figure 12.6. Typical volume change - time response curve recorded in equalization stage.

12.2.2 COMPRESSION STAGE

During the compression stage, the specimens were isotropically compressed by increasing the cell pressure while maintaining the pore-air pressure constant at the value it had at the end of the equalization stage. Tests were performed at net stresses ($\sigma_c - u_a$) ranging from 0 to 40 psi. For the eight specimens tested in the suction-controlled triaxial apparatus, six specimens were compressed at a rate of 10 kPa/hr, and one specimen (specimen # 8) was compressed at a rate of 400 kPa/hr. One specimen (specimen # 1, which was compacted at a water content of 12%) was not compressed because the cell and pore-air pressures at the end of the equalization stage reached the maximum pressures the apparatus could provide. Typical suction-time response curves, the effect of air diffusion on the matric suction measurements, and the effect of rate of loading during compression are presented and discussed below.

12.2.2.1Typical suction-time response curves

A typical suction-time response curve for a specimen in which the net stress was increased from 0 to 40 psi in four 10-psi increments is shown in Figure 12.7. The specimen was isotropically compressed during each increment at a loading rate of 10 kPa/hr. The matric suction was measured at both ends of the specimen. For each increment of net stress, the matric suction decreased with time at a decreasing rate until it reached an asymptotic value, i.e. equilibrium was achieved. At equilibrium, the average value of the matric suctions measured at the ends of the specimen was taken to represent the average matric suction of the specimen. The variation of matric suctions and volumetric strains during the compression stage is presented in Appendix K for all tests.

The difference in matric suctions between the two ends of the specimens generally ranged from about 0 to as much as 45% of the average matric suction of the specimen. One specimen (specimen # 7, which was compacted at water content of 19% and dry unit weight of 100.8 pcf) showed a larger difference of 88% at a net stress of 40 psi. For this specimen, the average matric suction measured at a net stress of 40 psi was 0.1 psi. For such a low matric suction, a difference of 0.06 psi between the matric suctions measured at the two ends of the specimen resulted in a percentage difference of 88% of the average matric suction of the specimen. This large percentage difference is misleading because a difference of 0.06 psi between matric suctions at the two ends of the specimens is considered insignificant.

The difference in matric suctions measured at the two ends of the specimen in the compression stage (0 to 45%) was higher than that measured in the equalization stage (0 to 10%). This behavior might be attributed to non-homogeneity in the structure of the

compacted specimens. The initial matric suction measured in the equalization stage was primarily dependent on the compaction water content as discussed in Chapter 7. However, non-homogeneity in the structure of the compacted specimen might have resulted different pore-water pressures being developed at the two ends of the specimen during the compression stage.

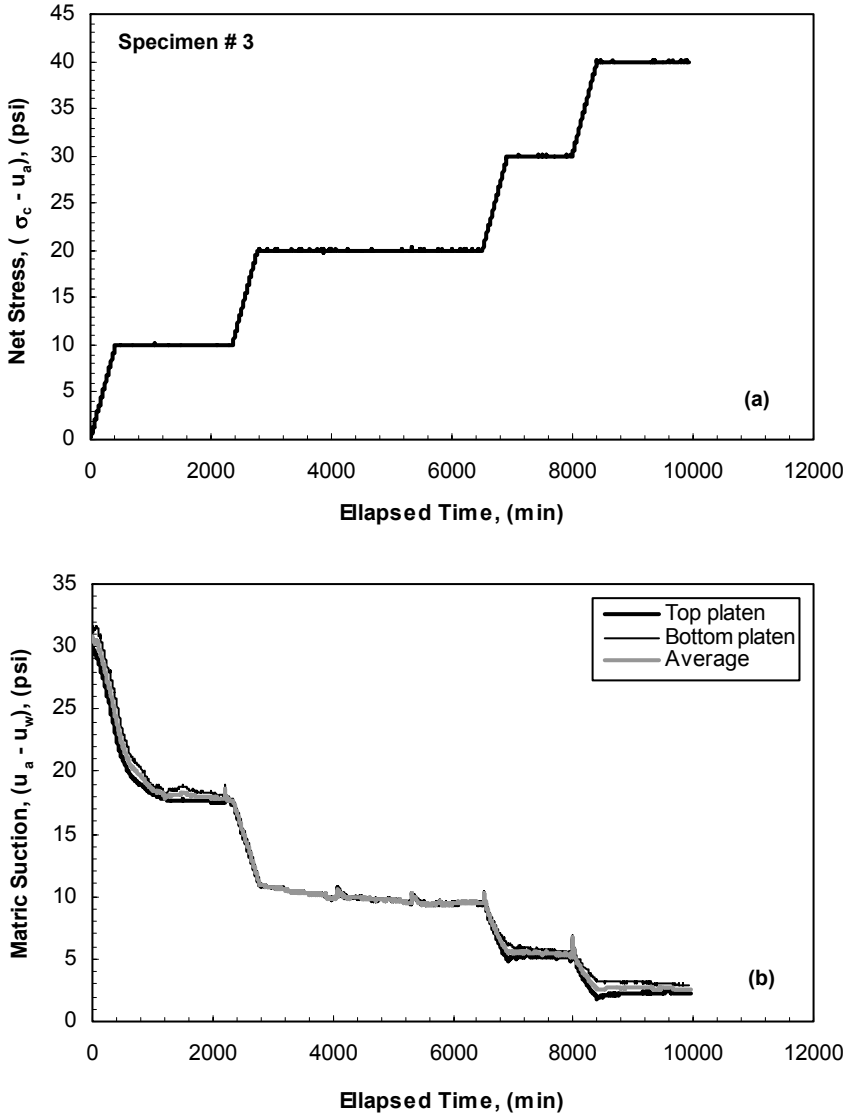

Figure 12.7. Typical variation of: (a) net stress and (b) matric suction with time recorded during the isotropic compression stage.

The variation of matric suction with net stress for the specimens compressed at the rate of 10 kPa/hr is shown in Figure 12.8. For specimens compacted at water contents less than 17% (2% dry of optimum), the matric suction decreased almost linearly as the net stress increased for the range of net stress being applied. While, for specimens compacted at water contents higher than 17%, the matric suction decreased at a

decreasing rate as the net stress increased. The specimen compacted at a water content of 19% and dry unit weight of 107 pcf is one of the three specimens that had unreasonably high initial matric suctions discussed in Section 12.2.1.1.

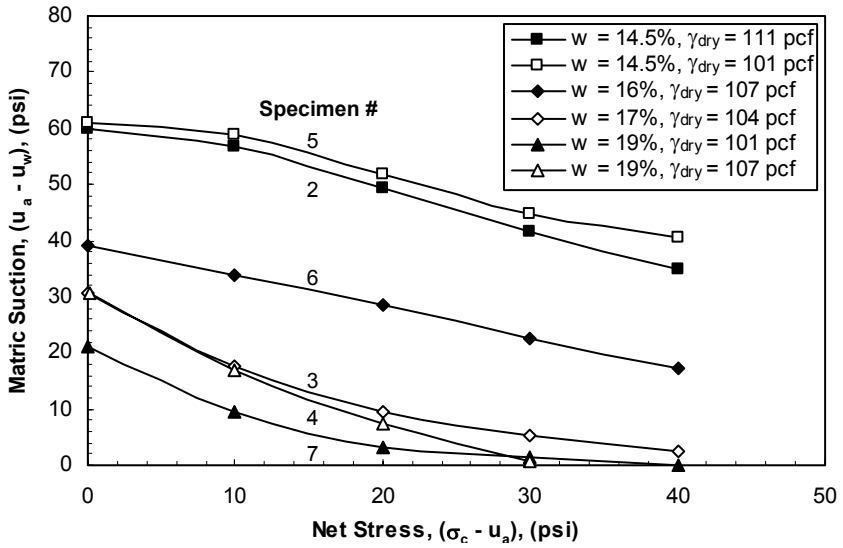

Figure 12.8. Variation of matric suction with net stress in compresion stage for specimens compressed at a loading rate of 10 kPa/hr.

12.2.2.2 Effect of air diffusion on matric suction measurements

The effect of air diffusion on matric suction measurements during the isotropic compression stage is similar to that discussed for pressure plate tests (in Chapter 7) and for the equalization stage in Section 12.2.1.2. Periodic flushing of the diffused air caused some irregularities in the suction-time response curve as shown in Figure 12.9. A significant drop in the matric suction occurred at each time water was flushed through the water cavities behind the high air-entry porous stones. The amount of air diffusion was larger for specimens compacted at lower water contents and as the test duration

increased. In addition, the amount of air diffusion decreased as the net stress increased during compression.

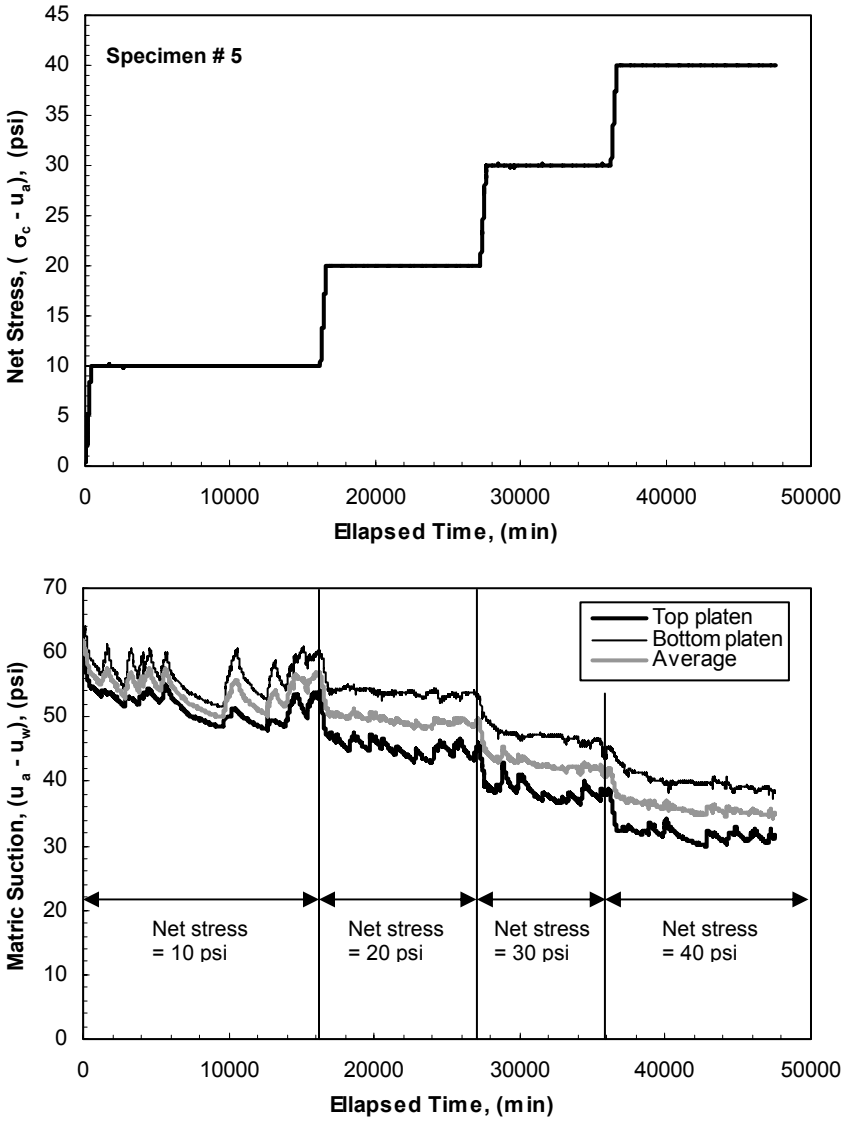

Figure 12.9. Effect of air diffusion followed by water flushing on the suction-time response curve recorded in compression stage.

12.2.2.3Effect of rate of loading during compression on measured suction

Two tests were performed on nearly identical specimens compacted at water content of approximately 16% and dry unit weight of approximately 107 pcf to investigate the effect of rate of loading on the measured matric suction during the isotropic compression stage. One specimen was compressed at a rate of 10 kPa/hr, while the other specimen was compressed at a rate of 400 kPa/hr. The two specimens should have had similar initial matric suctions as they were compacted at similar water contents, however, the specimen compressed at a rate of 400 kPa/hr was one of the three specimens that had unreasonably high initial matric suctions (measured during the equalization stage) discussed in Section 12.2.1.1. The variation of matric suction with net stress for the two tests is compared in Figure 12.10. For net stresses ranging from 10 to 40 psi, the rate of reduction in matric suction with increase in net stress increased by approximately 40% as the loading rate increased from 10 to 400 kPa/hr. Accordingly, it was concluded that an inappropriate rate of loading might cause the menisci to break apart, and the effect of the matric suction to be lost. Similar observations were reported by Macari and Hoyos (2001). For the current research, a consistent rate of loading of 10 kPa/hr was applied in the compression stage.

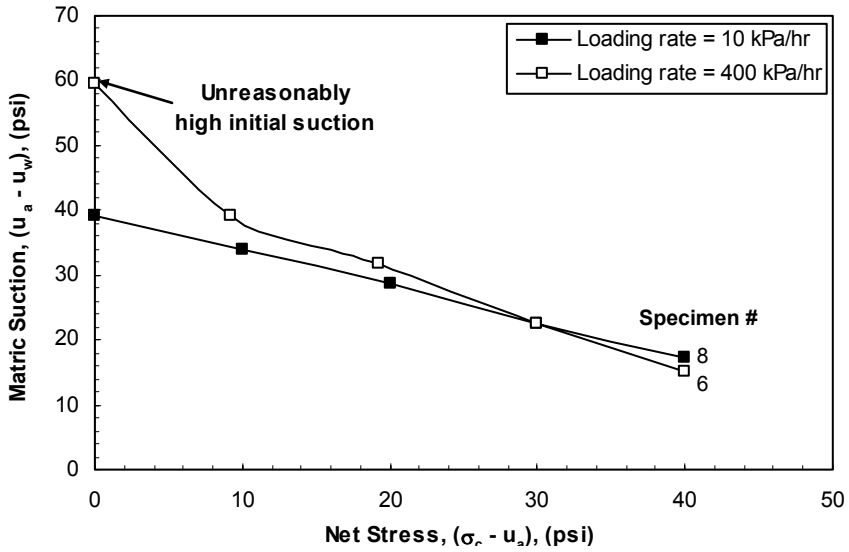

Figure 12.10. Effect of rate of loading on variation of matric suction with net stress in compression stage.

12.3 Shear and compression wave velocities measured under controlled state of stress

The results of the tests performed on the seven specimens that were compressed isotropically using a consistent rate of loading of 10 kPa/hr were investigated to study the effects of the state of stress on the soil stiffness. Shear and compression wave velocities were measured at the end of the equalization stage and at the end of each increment of loading during the compression stage. A summary table with the water contents, dry unit weights, degrees of saturation, states of stress, and shear and compression wave velocities measured for all specimens is presented in Appendix K.

Ideally, the effects of state of stress on soil stiffness should be investigated for specimens compacted at the same compaction conditions (compactive effort, degree of saturation, water content, and dry unit weight) and tested at different states of stress. The

effect of state of stress on soil stiffness could be investigated for specimens compacted at the same compaction conditions by performing drained tests, in which matric suction and net stress are controlled. However, in tests at constant water content performed in this study, only the net stress was controlled while the matric suction was measured. Accordingly, for the current research, the effects of state of stress on soil stiffness were investigated for specimens compacted at different compaction conditions, with one common characteristic. Two series of tests were performed. In the first series, specimens were compacted at similar degrees of saturation (Figure 12.11); and in the second series, specimens were compacted to coincide with the standard Proctor compaction curve, i.e. presumably at similar compactive efforts (Figure 12.24). The results of the two series of tests and the effects of compaction conditions on the relationship between the soil stiffness and state of stress are presented and discussed below.

12.3.1 SPECIMENS COMPACTED AT SIMILAR DEGREES OF SATURATION

The first series of tests was performed on four specimens compacted at similar degrees of saturation that ranged from 74 to 77%. These degrees of saturation corresponded to compaction water contents ranging from 14 to 19%, and dry unit weights ranging from 101 to 111 pcf (Figure 12.11). Shear and compression wave velocities were measured for each specimen at net stresses of 0, 10, 20, 30, and 40 psi. The effects of matric suction and net stress on shear and compression wave velocities are presented and discussed below.

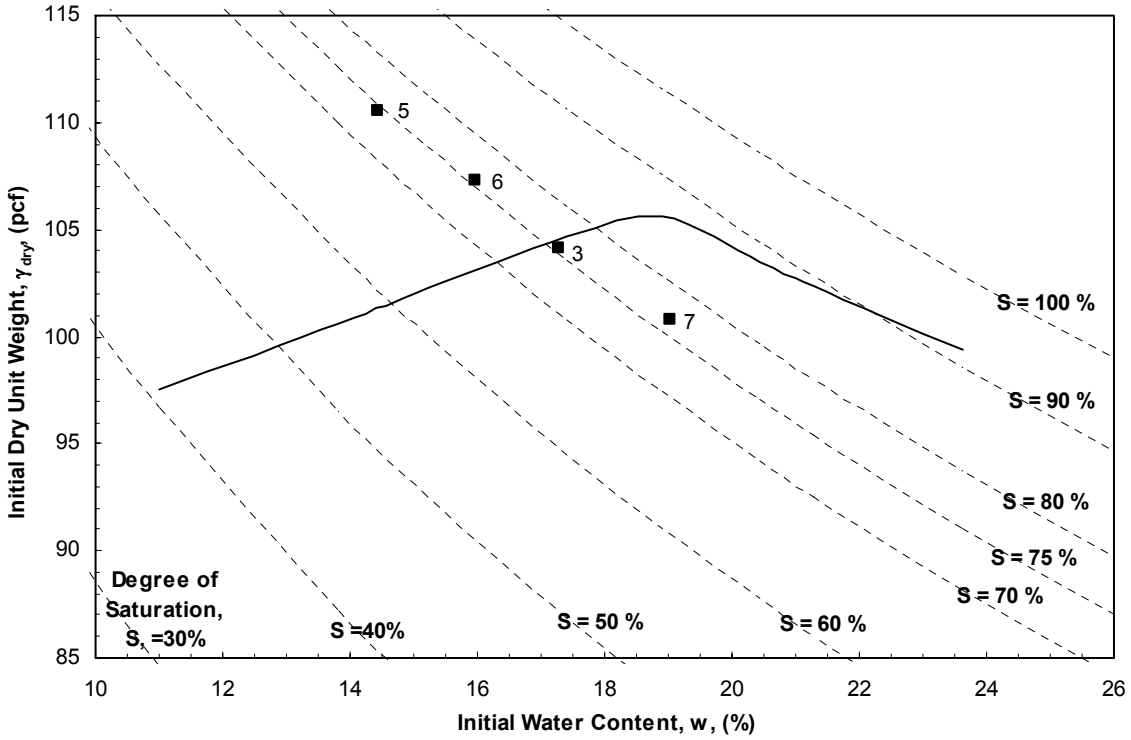

Figure 12.11. Standard Proctor compaction curve with specimens compacted at similar degrees of saturation.

12.3.1.1Shear wave velocities

The variation of shear wave velocity with matric suction is illustrated in Figure 12.12 (arithmetic and logarithmic scales) for net stresses of 0, 10, 20, 30, and 40 psi. For a given net stress, the shear wave velocity increased as the matric suction increased but at a decreasing rate. Also, for a given matric suction, the shear wave velocity increased as the net stress increased for the range of matric suctions being tested.

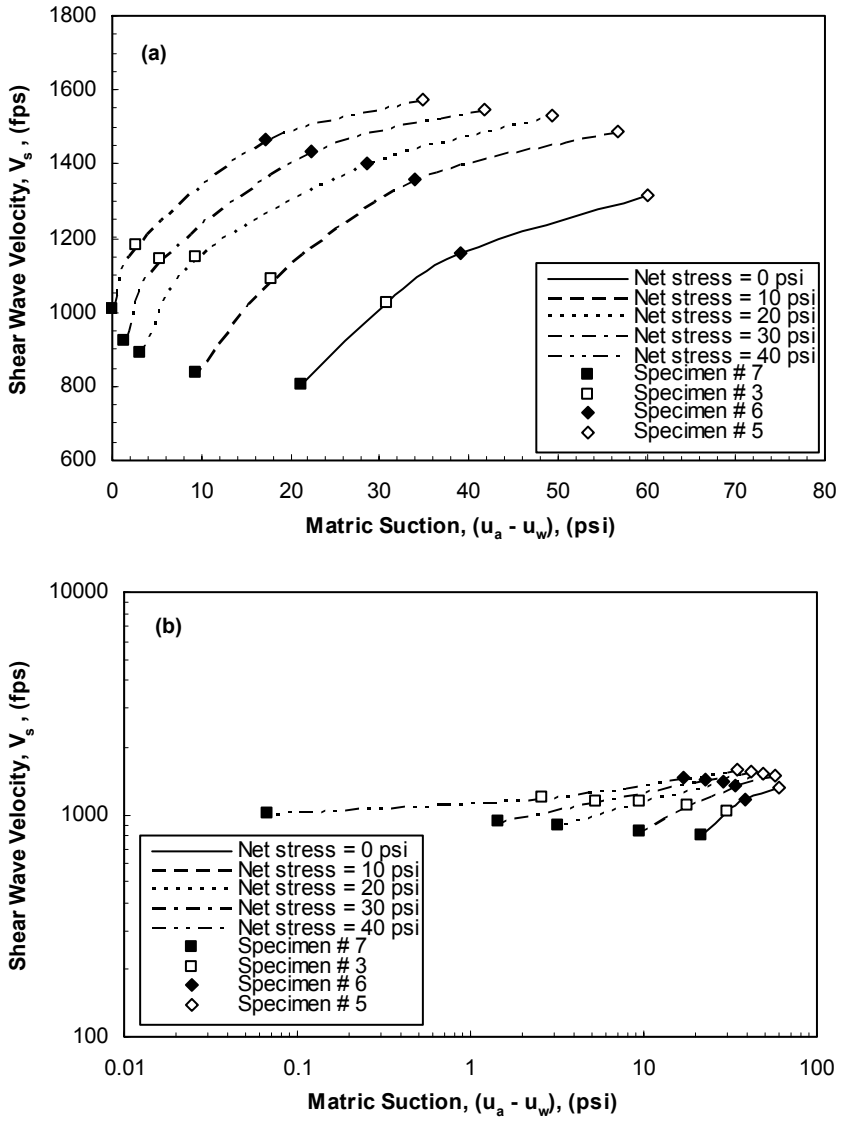

Figure 12.12. Variation of shear wave velocity with matric suction and net stress for specimens compacted at similar degrees of saturation: (a) arithmetic scale and (b) logarithmic scale.

The variation of the shear modulus with matric suction is shown for net stresses of 0, 10, 20, 30, and 40 psi in Figure 12.13. The variations are similar to those presented in Figure 12.12 for the shear wave velocity. Similar observations regarding the relationship between shear modulus, matric suction, and net stress were reported by Vinale et al.

(1999), Vassalo and Mancuso (2000), and Mancuso et al. (2002) for silty sand specimens compacted at the same compaction conditions and tested under drained conditions. Cabarkapa et al. (1999) reported almost linear increase in the soil stiffness with increasing the matric suction at constant net stress for quartz silt specimens compacted at the same compaction conditions and tested under drained conditions.

To reduce the effects of dry unit weight (void ratio), the shear modulus was normalized by the F(e) term defined by Hardin and Black (1968) for clays as follows (same as used in Chapter 10):

$$F(e) = \frac{(2.97 - e)^2}{(1 + e)} \quad \text{.....} \quad (12.1)$$

where e is the void ratio. The variation of normalized shear modulus ($G_{max}/F(e)$) with matric suction is shown for the five net stresses in Figure 12.14. The variations are similar to those presented for the shear wave velocity and shear modulus. Three-dimensional diagrams illustrating the variation of shear wave velocity, shear modulus, and normalized shear modulus with matric suction and net stress are shown in Figures 12.15, 12.16, and 12.17, respectively. Further discussion on the results is presented in Section 12.3.3.

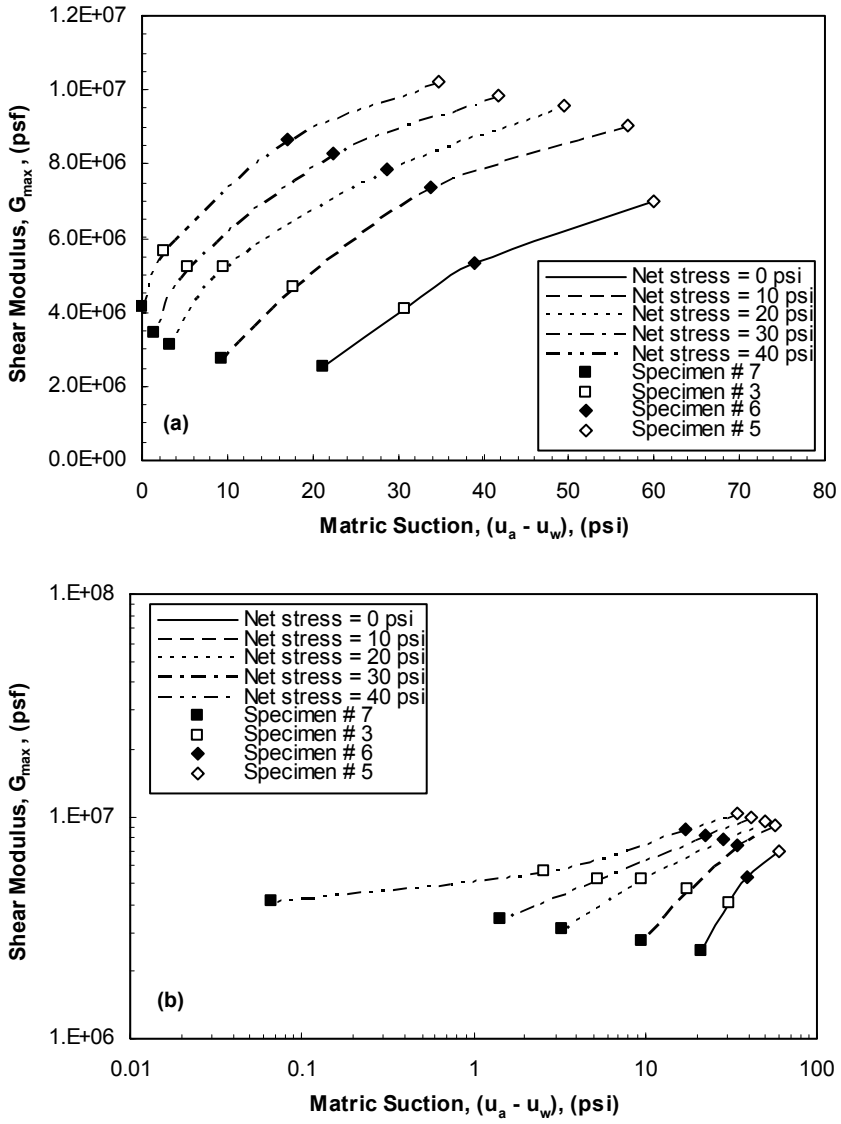

Figure 12.13. Variation of shear modulus with matric suction and net stress for specimens compacted at similar degrees of saturation: (a) arithmetic scale and (b) logarithmic scale.

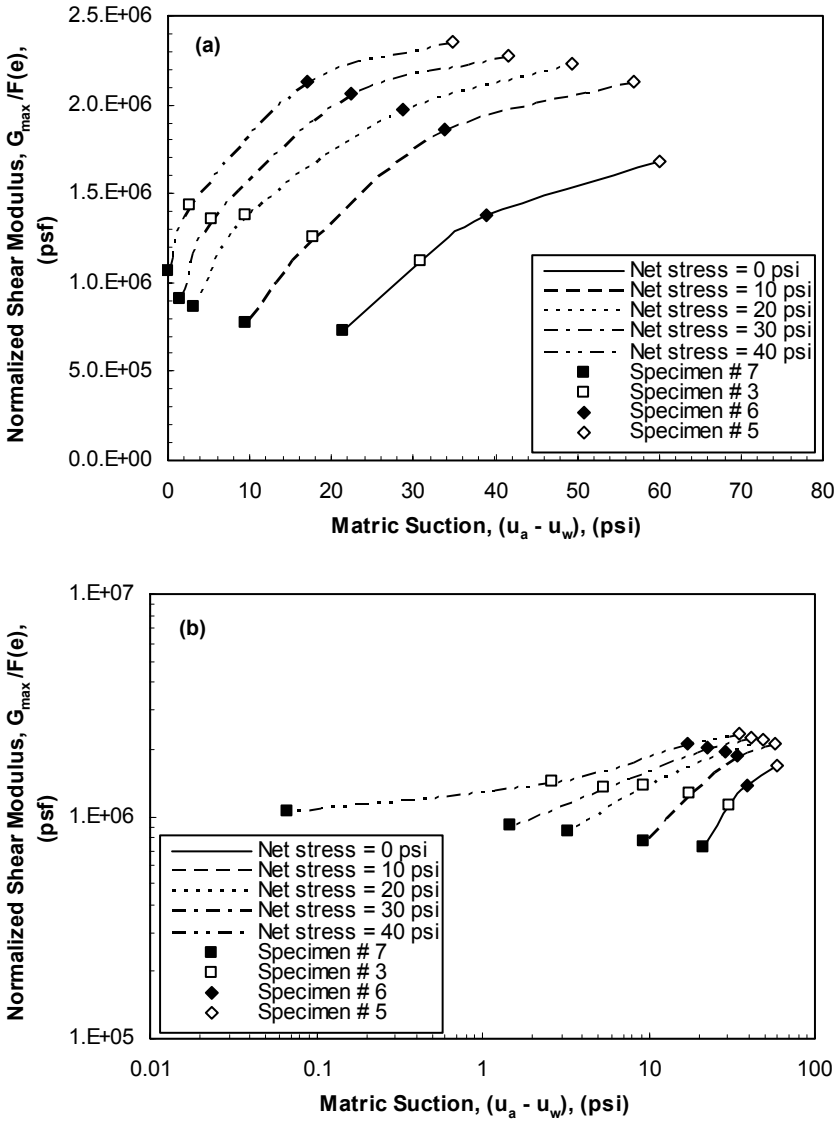

Figure 12.14. Variation of normalized shear modulus with matric suction and net stress for specimens compacted at similar degrees of saturation: (a) arithmetic scale and (b) logarithmic scale.

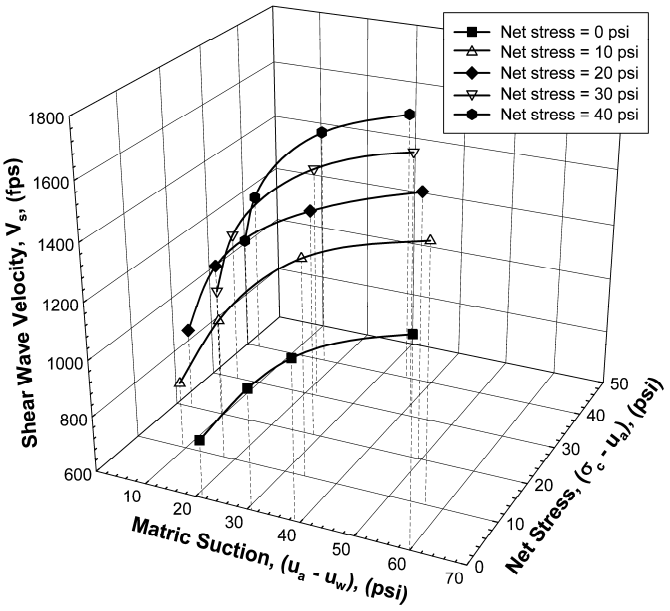

Figure 12.15. Three-dimensional diagram for shear wave velocity, matric suction, and net stress for specimens compacted at similar degrees of saturation.

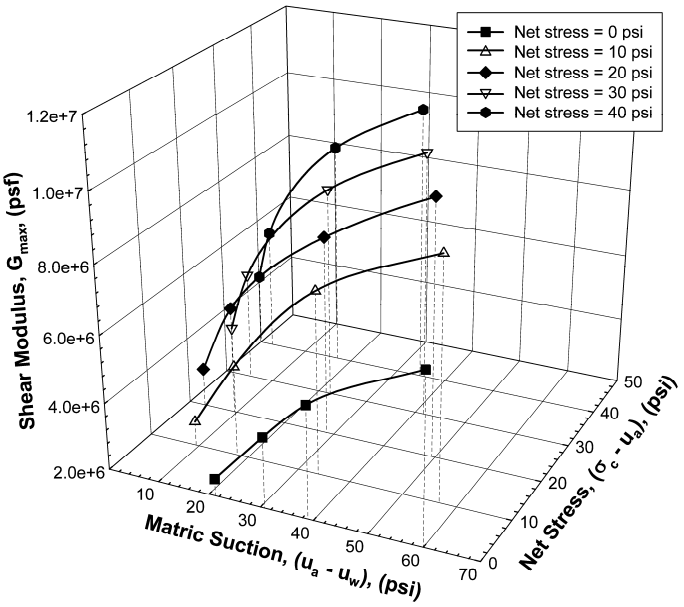

Figure 12.16. Three-dimensional diagram for shear modulus, matric suction, and net stress for specimens compacted at similar degrees of saturation.

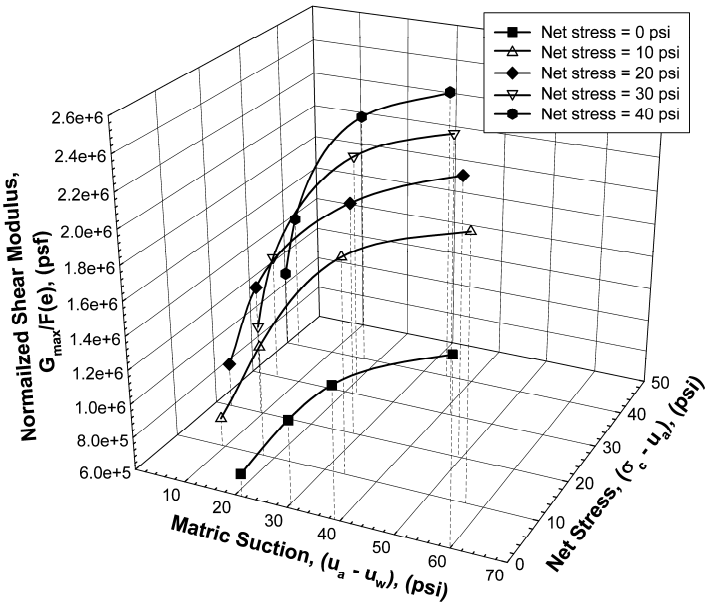

Figure 12.17. Three-dimensional diagram for normalized shear modulus, matric suction, and net stress for specimens compacted at similar degrees of saturation.

12.3.1.2Compression wave velocities

The variation of compression wave velocity with matric suction is illustrated in Figure 12.18 for net stresses of 0, 10, 20, 30, and 40 psi. At a net stress of zero, the compression wave velocity increased as the matric suction increased but at a decreasing rate. For net stresses of 10, 20, 30, and 40 psi, the compression wave velocity increased as the matric suction increased and then tended towards a threshold beyond which the compression wave velocity did not increase further for the range of matric suctions being tested. The matric suction where the compression wave velocity stopped increasing was highest at a net stress of 0 psi and decreased to the lowest value at a net stress of 40 psi. For a given matric suction, the compression wave velocity increased as the net stress increased. For the specimen compacted at a water content of approximately 19% and dry unit weight of 101 pcf, the matric suction decreased to approximately 0.1 psi at a net stress of 40 psi.

The degree of saturation of the specimen was calculated based on the volume changes measurements to be 97.9%. This specimen was not fully saturated at this matric suction, and accordingly, the compression wave velocity did not increase to 5000 fps.

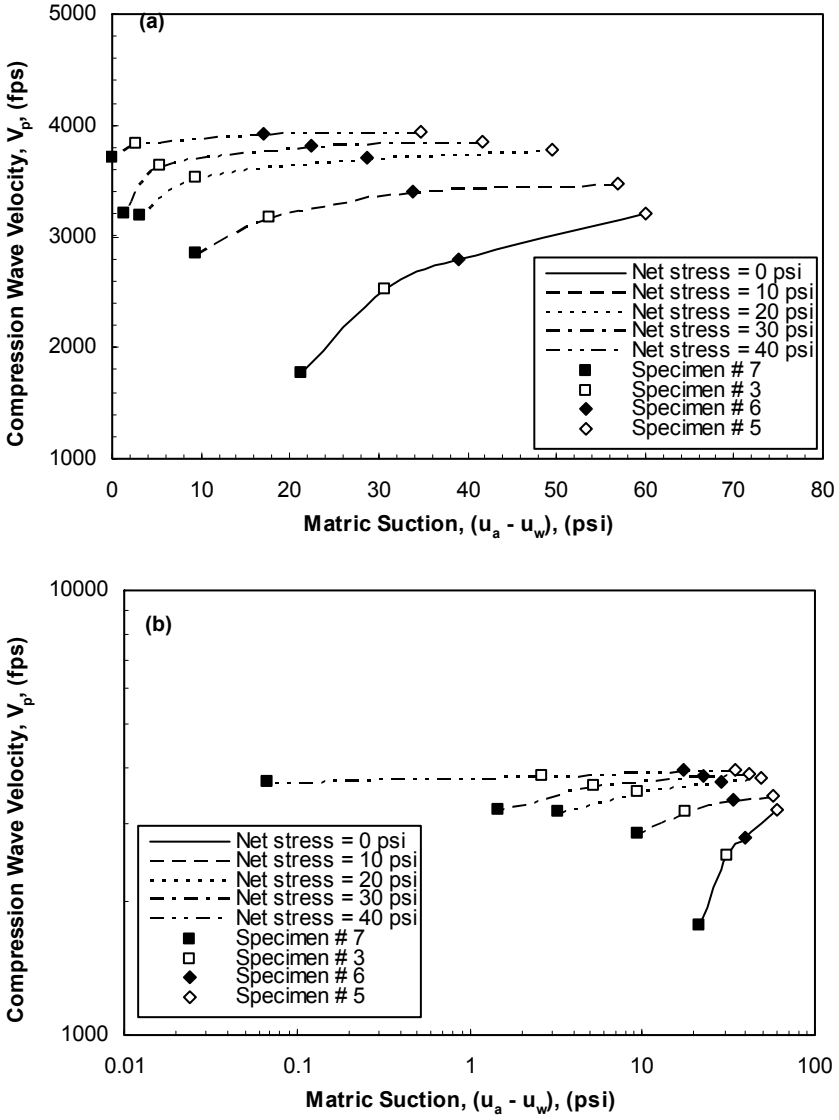

Figure 12.18. Variation of compression wave velocity with matric suction and net stress for specimens compacted at similar degrees of saturation: (a) arithmetic scale and (b) logarithmic scale.

The variations of the constrained modulus with matric suction are shown for net stresses of 0, 10, 20, 30, and 40 psi in Figure 12.19. The variations are similar to those presented in Figure 12.18 for the compression wave velocity. To reduce the effects of dry unit weight (void ratio), the constrained modulus was normalized by the F(e) term defined by Equation 12.1. The variations of normalized constrained modulus ($M_{max}/F(e)$) with matric suction are shown for the five net stresses in Figure 12.20. The variations are similar to those presented for the compression wave velocity and constrained modulus. Three-dimensional diagrams illustrating the variation of the compression wave velocity, constrained modulus, and normalized constrained modulus with matric suction and net stress are shown in Figures 12.21, 12.22, and 12.23, respectively. Further discussion on the results is presented in Section 12.3.3.

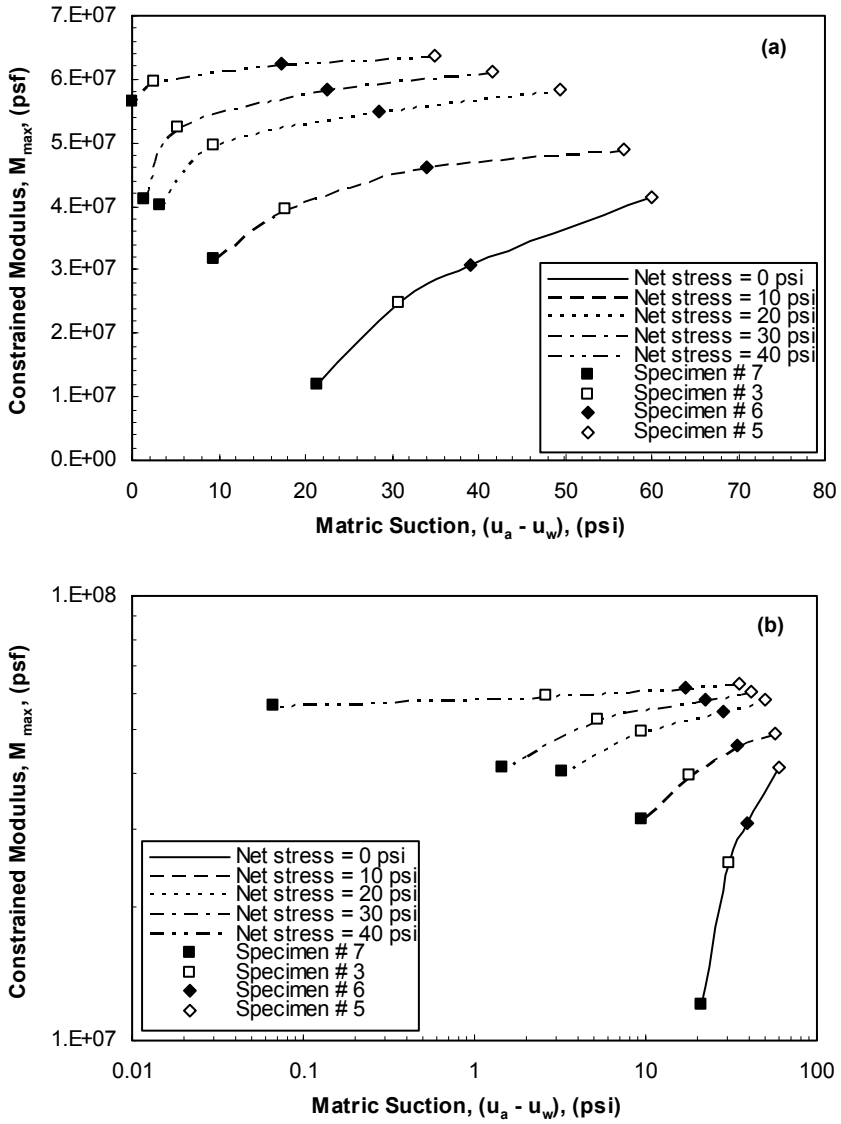

Figure 12.19. Variation of constrained modulus with matric suction and net stress for specimens compacted at similar degrees of saturation: (a) arithmetic scale and (b) logarithmic scale.

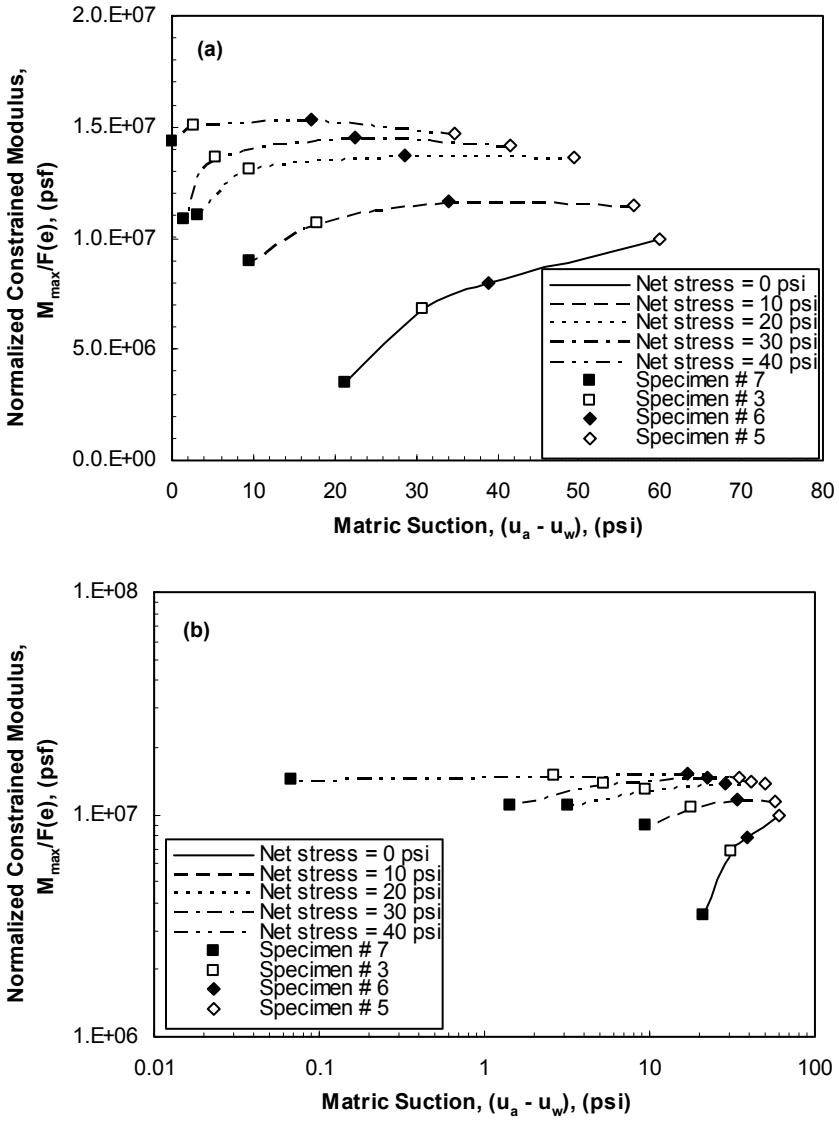

Figure 12.20. Variation of normalized constrained modulus with matric suction and net stress for specimens compacted at similar degrees of saturation: (a) arithmetic scale and (b) logarithmic scale.

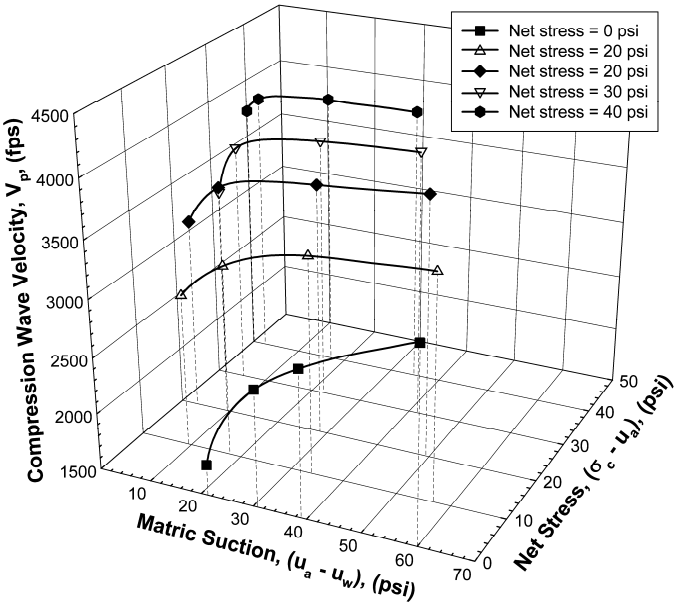

Figure 12.21. Three-dimensional diagram for compression wave velocity, matric suction, and net stress for specimens compacted at similar degrees of saturation.

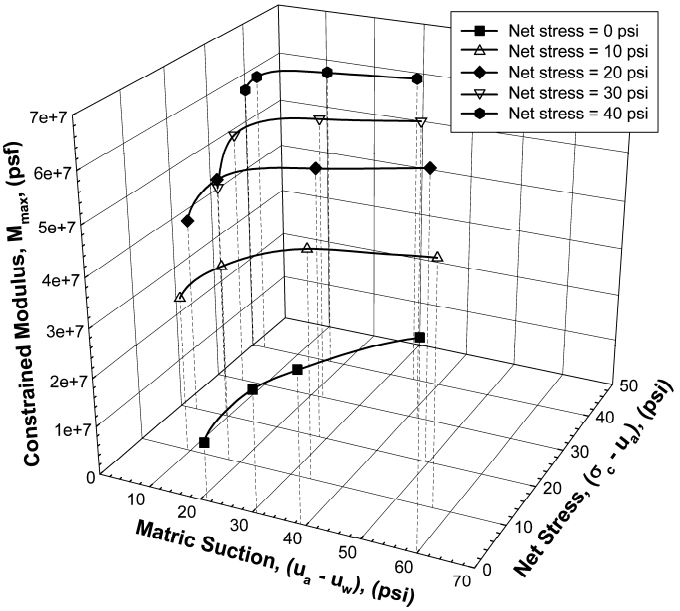

Figure 12.22. Three-dimensional diagram for constrained modulus, matric suction, and net stress for specimens compacted at similar degrees of saturation.

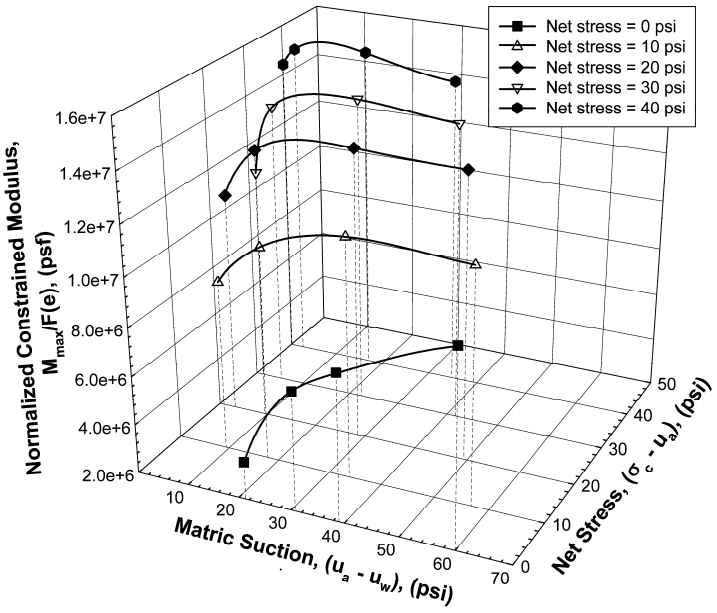

Figure 12.23. Three-dimensional diagram for normalized constrained modulus, matric suction, and net stress for specimens compacted at similar degrees of saturation.

12.3.2 SPECIMENS COMPACTED AT SIMILAR COMPACTIVE EFFORTS

The second series of tests was performed on four specimens compacted to water contents and dry unit weights that coincide approximately with the standard Proctor compaction curve (Figure 12.24). The specimens were compacted at water contents ranging from 12 to 19% and dry unit weights ranging from 98 to 107 pcf.

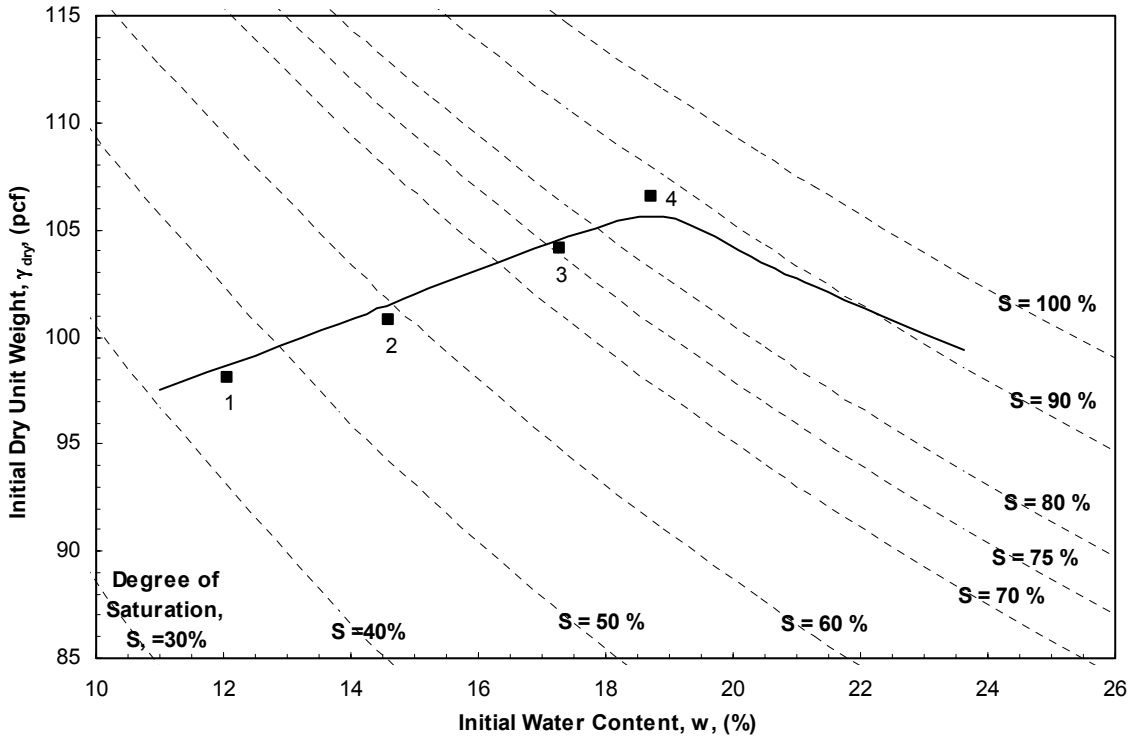

Figure 12.24. Standard Proctor compaction curve with specimens compacted at similar compactive efforts.

Two of the four specimens could not be tested for the full range of net stresses (0 to 40 psi) used in the previous section. Specimen # 1, which was compacted at a water content of 12%, was not compressed as discussed in Section 12.2.2, and, therefore, shear and compression wave velocities were only measured at a net stress of zero. Specimen # 4, which was compacted at a water content of 19%, became nearly saturated during compression at a net stress of 30 psi and the matric suction dropped to 0.7 psi. Therefore, shear and compression wave velocities were measured at net stresses of only 0, 10, 20, and 30 psi for this specimen. Accordingly, the effect of matric suction on shear and compression wave velocities was studied for four specimens at zero net stress, three specimens at net stresses of 10, 20, and 30 psi, and two specimens at a net stress of 40

psi. The effects of matric suction and net stress on shear and compression wave velocities are presented and discussed below.

12.3.2.1Shear wave velocities

The variation of shear wave velocity with matric suction is illustrated in Figure 12.25 for net stresses of 0, 10, 20, 30, and 40 psi. At zero net stress, the shear wave velocity increased as the matric suction increased and then decreased as matric suction increased to about 105 psi. The test performed on specimen number 1 was repeated and similar matric suction and shear wave velocity were measured, which confirmed the trend observed in Figure 12.25 at zero net stress. Similar observations were reported by Marinho et al. (1995). At higher net stresses than zero, the shear wave velocity increased at a decreasing rate as the matric suction increased over the range of matric suctions being measured (up to about 60 psi). For a given matric suction, the shear wave velocity increased as the net stress increased for the range of matric suctions being tested.

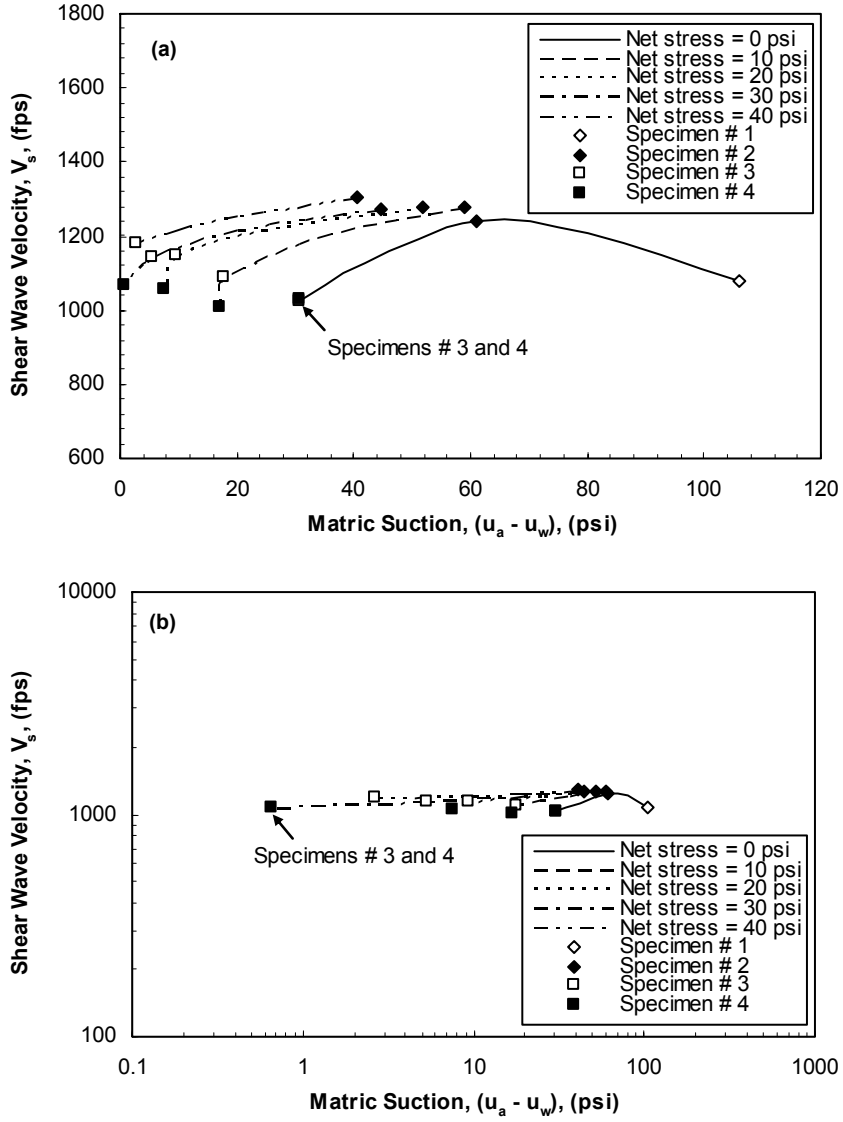

Figure 12.25. Variation of shear wave velocity with matric suction and net stress for specimens compacted at similar compactive efforts: (a) arithmetic scale and (b) logarithmic scale.

The variations of the shear modulus and normalized shear modulus with matric suction are shown for net stresses of 0, 10, 20, 30, and 40 psi in Figures 12.26 and 12.27, respectively. These variations are similar to those presented in Figure 12.25 for the shear wave velocity. Three-dimensional diagrams illustrating the variation of the shear wave

velocity, shear modulus, and normalized shear modulus with matric suction and net stress are shown in Figures 12.28, 12.29, and 12.30, respectively. Further discussion on the results is presented in Section 12.3.3.

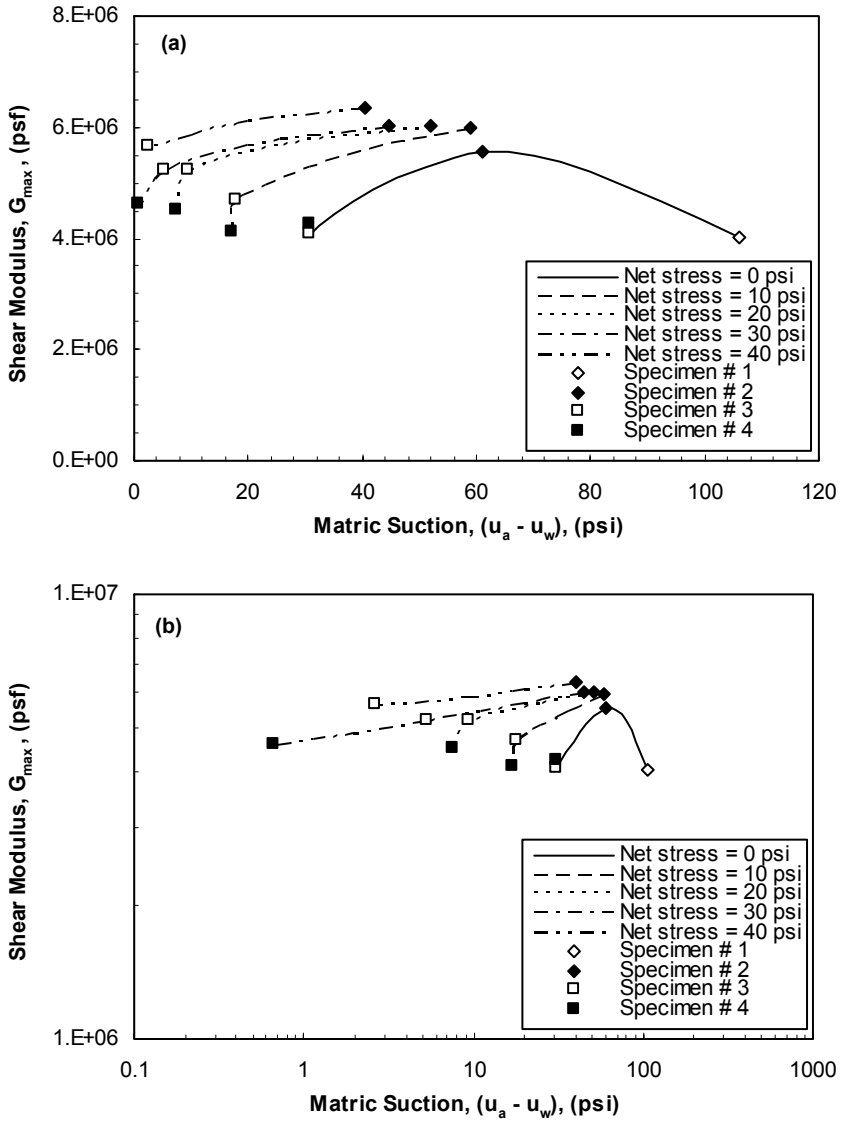

Figure 12.26. Variation of shear modulus with matric suction and net stress for specimens compacted at similar compactive efforts: (a) arithmetic scale and (b) logarithmic scale.

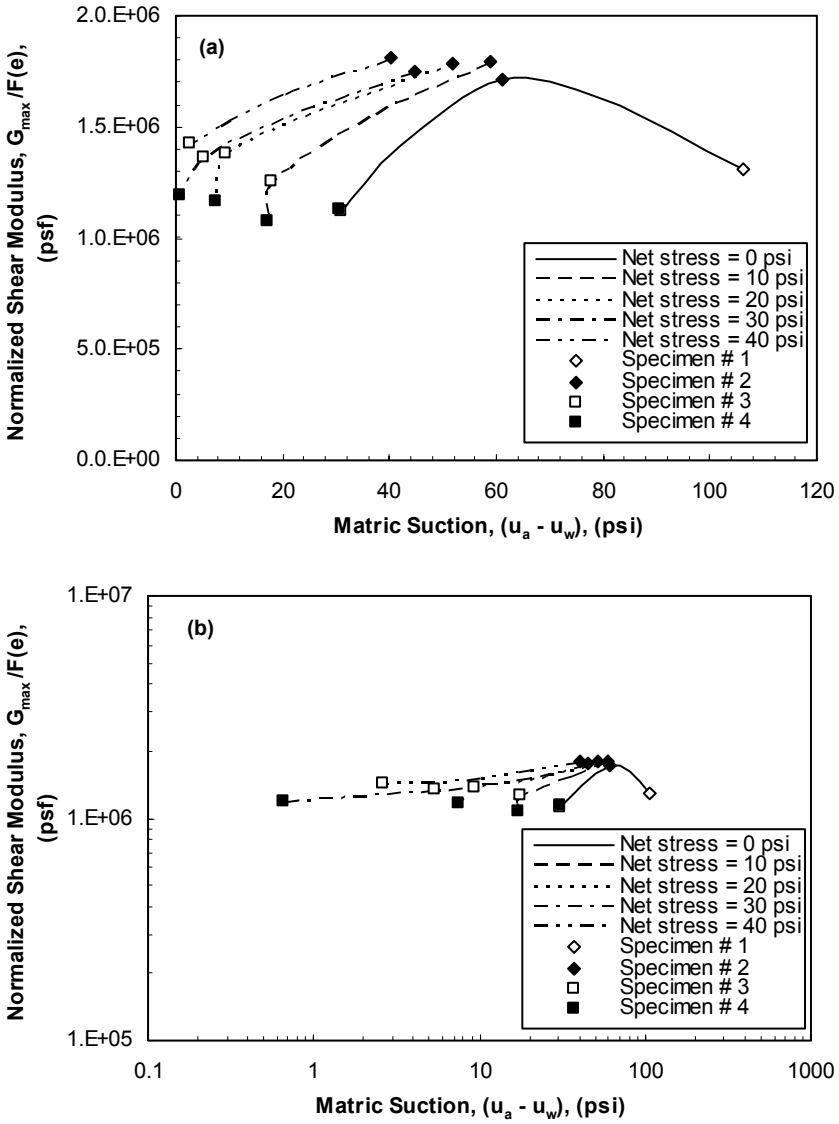

Figure 12.27. Variation of normalized shear modulus with matric suction and net stress for specimens compacted at similar compactive efforts: (a) arithmetic scale and (b) logarithmic scale.

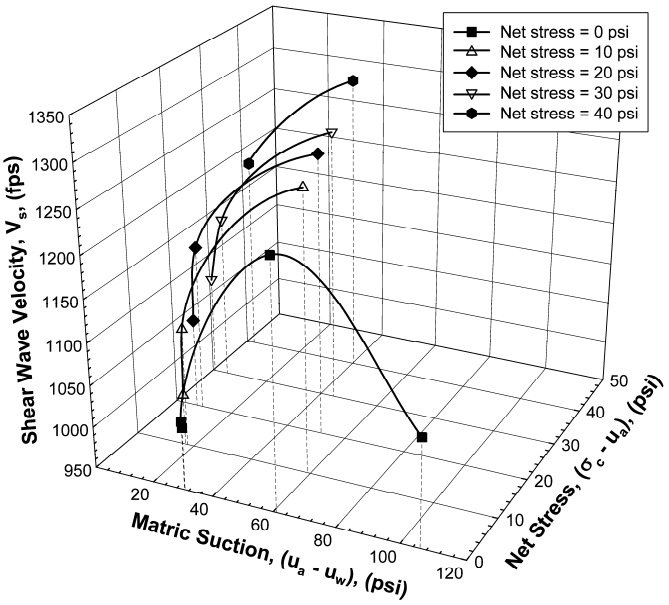

Figure 12.28. Three-dimensional diagram for shear wave velocity, matric suction, and net stress for specimens compacted at similar compactive efforts.

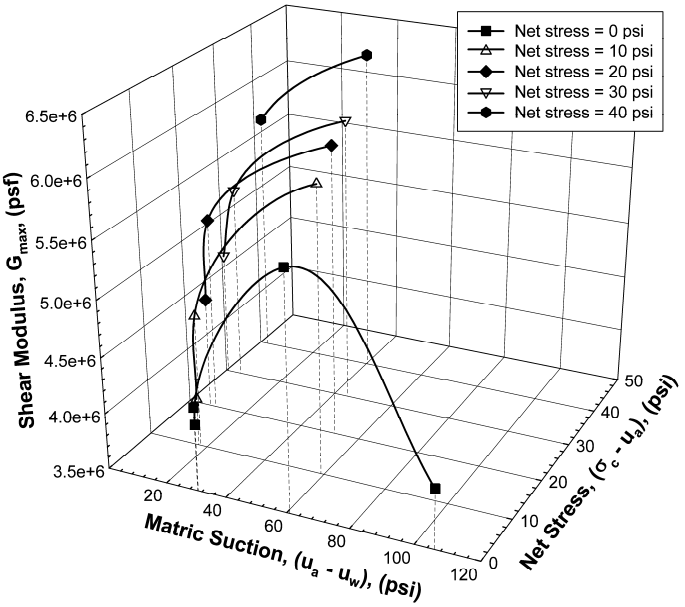

Figure 12.29. Three-dimensional diagram for shear modulus, matric suction, and net stress for specimens compacted at similar compactive efforts.

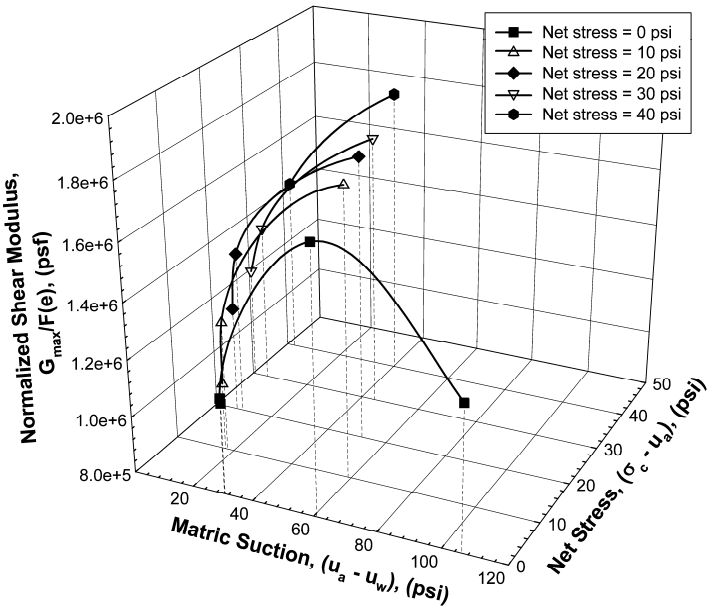

Figure 12.30. Three-dimensional diagram for normalized shear modulus, matric suction, and net stress for specimens compacted at similar compactive efforts.

12.3.2.2Compression wave velocities

The variation of compression wave velocity with matric suction is illustrated in Figure 12.31 for net stresses of 0, 10, 20, 30, and 40 psi. At zero net stress, the compression wave velocity increased as the matric suction increased and then decreased as matric suction increased to about 105 psi. The test performed on specimen number 1 was repeated and similar matric suction and compression wave velocity were measured, which confirmed the trend observed in Figure 12.31 at zero net stress. At net stresses higher than zero, the compression wave velocity decreased as the matric suction increased at a decreasing rate. No clear explanation could be found for the trend observed in the relationship between compression wave velocity and matric suction at net stresses higher than zero. For a given matric suction, the compression wave velocity increased as

the net stress increased from zero to 10 psi, but then the compression wave velocity appeared not to be affected for further increase in the net stress.

For specimen # 4, which was compacted at a water content of approximately 19% and dry unit weight of 106.6 pcf, the matric suction decreased to approximately 0.7 psi at a net stress of 30 psi. The degree of saturation of the specimen was calculated based on the volume changes measurements to be 95.5%. However, the compression wave velocity increased to approximately 5000 fps, which indicated that the specimen probably had a degree of saturation higher than 99% (Allen et al., 1980 and Valle, 2006). The volume changes measurements using this apparatus were believed to be accurate and should track the changes in degrees of saturation precisely. An error in the specific gravity of this specimen was suspected to be the reason for the underestimated value of the degree of saturation. A change in the specific gravity from 2.70 to 2.64 would cause the degree of saturation to change from 95.5 to 99.7%. The compression wave velocities measured for specimen # 4 at net stresses of 30 and 40 psi were affected by the pore-water; and did not represent the velocity through the material skeleton.

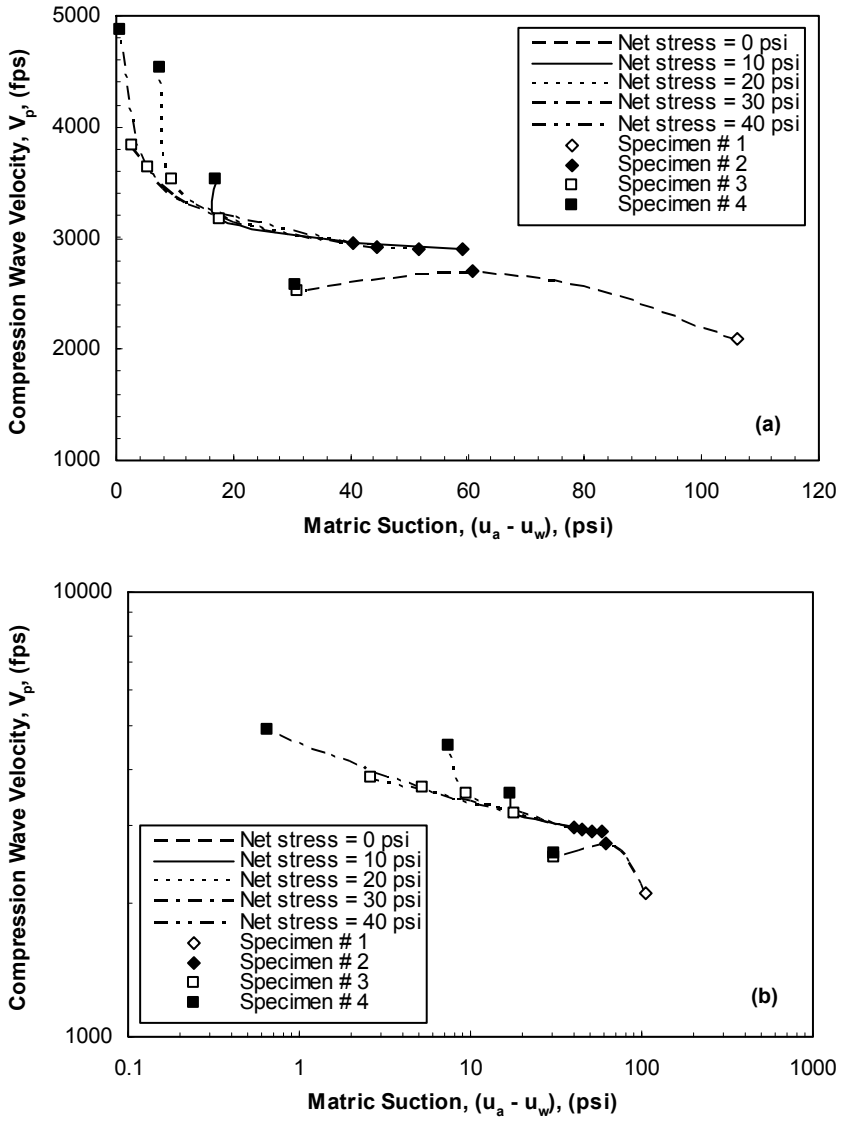

Figure 12.31. Variation of compression wave velocity with matric suction and net stress for specimens compacted at similar compactive efforts: (a) arithmetic scale and (b) logarithmic scale.

The variations of the constrained modulus and normalized constrained modulus with matric suction are shown for net stresses of 0, 10, 20, 30, and 40 psi in Figures 12.32 and 12.33, respectively. These variations are similar to those presented in Figure 12.31 for the compression wave velocity. Three-dimensional diagrams illustrating the variation

of the compression wave velocity, constrained modulus, and normalized constrained modulus with matric suction and net stress are shown in Figures 12.34, 12.35, and 12.36, respectively. Further discussion on the results is presented in the following section.

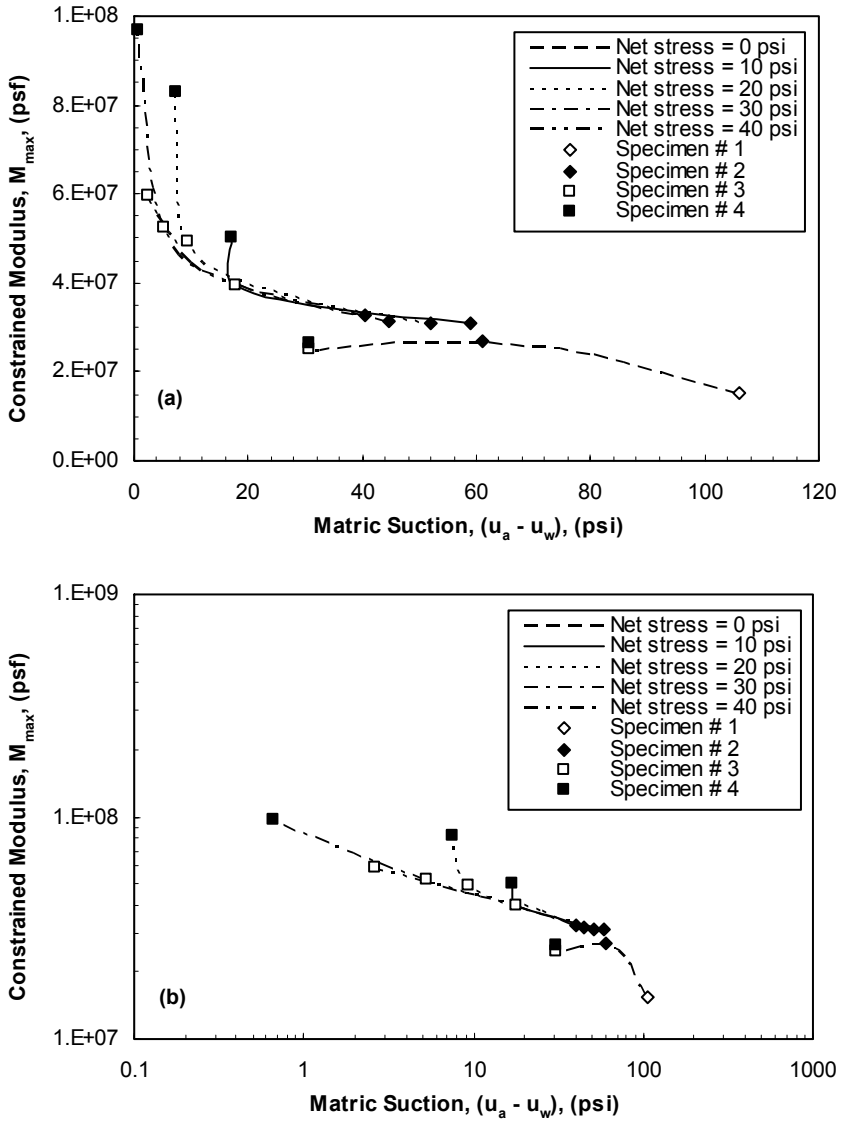

Figure 12.32. Variation of constrained modulus with matric suction and net stress for specimens compacted at similar compactive efforts: (a) arithmetic scale and (b) logarithmic scale.

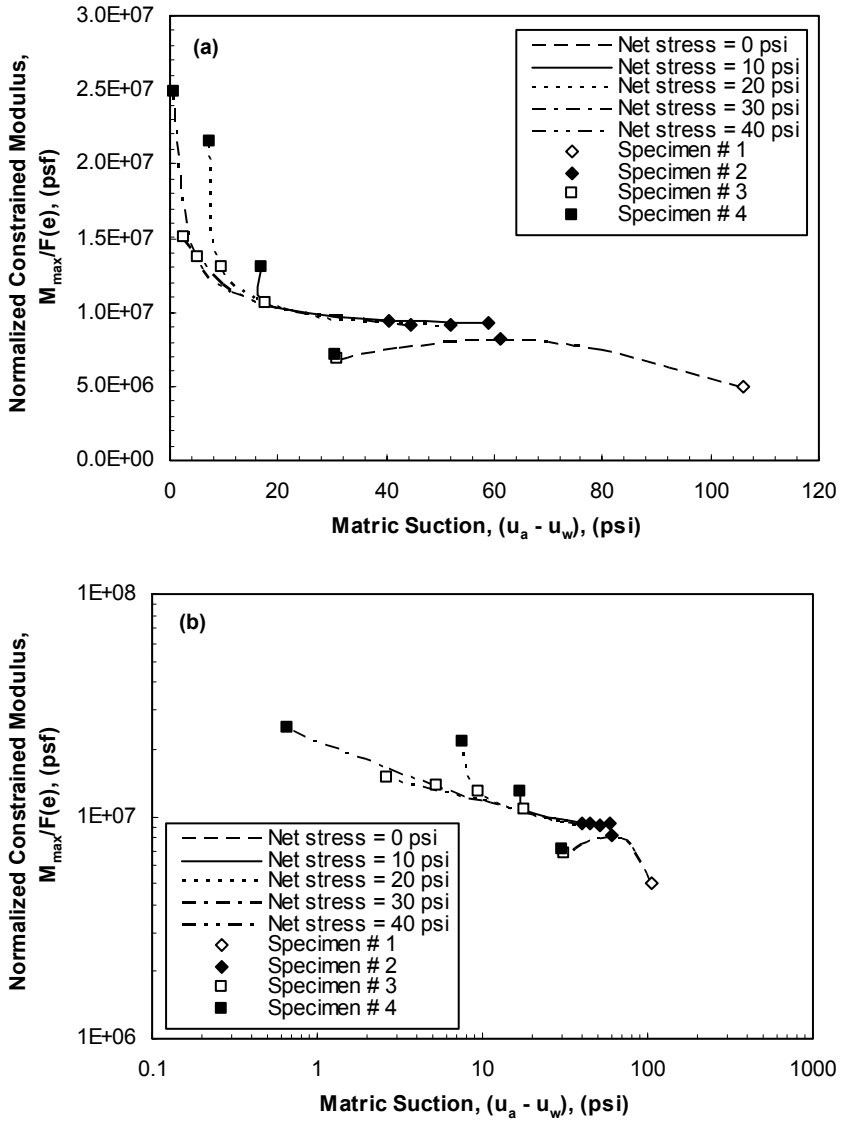

Figure 12.33. Variation of normalized constrained modulus with matric suction and net stress for specimens compacted at similar compactive efforts: (a) arithmetic scale and (b) logarithmic scale.

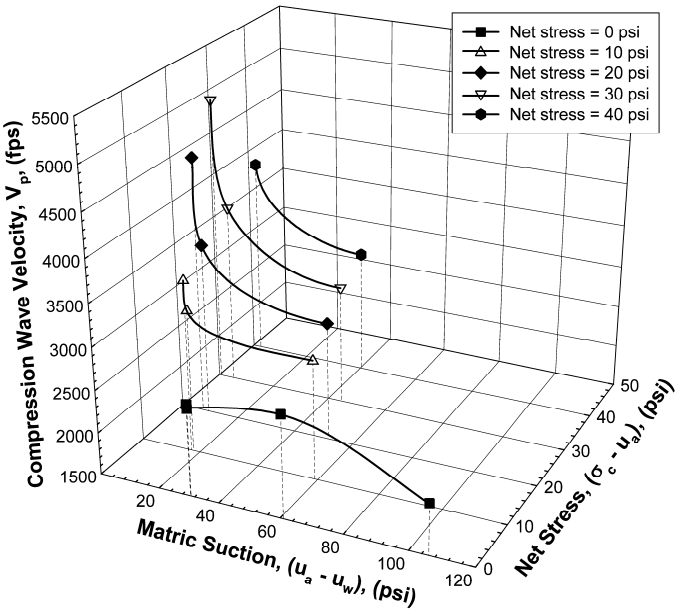

Figure 12.34. Three-dimensional diagram for compression wave velocity, matric suction, and net stress for specimens compacted at similar compactive efforts.

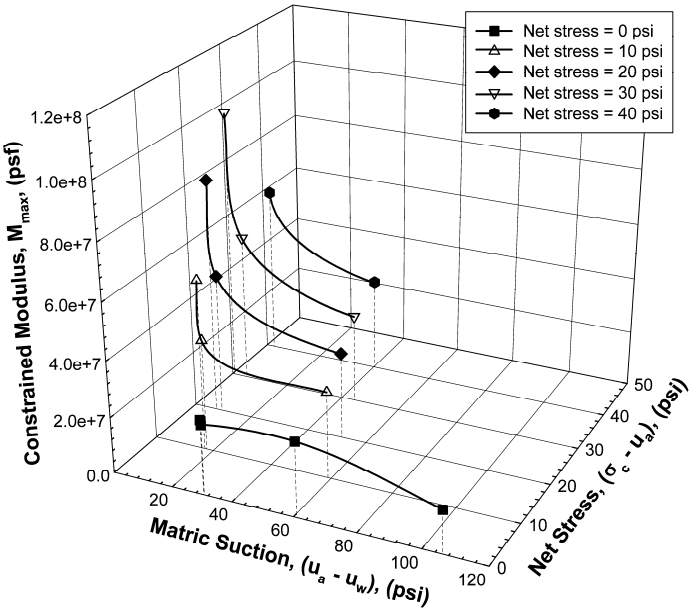

Figure 12.35. Three-dimensional diagram for constrained modulus, matric suction, and net stress for specimens compacted at similar compactive efforts.

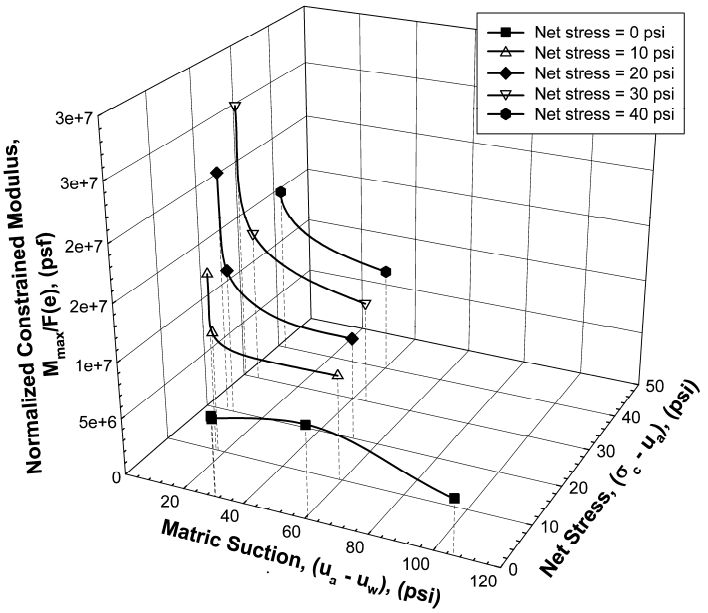

Figure 12.36. Three-dimensional diagram for normalized constrained modulus, matric suction, and net stress for specimens compacted at similar compactive efforts.

12.3.3 DISCUSSION

Effects of compaction conditions on the relationships between normalized shear and constrained moduli, matric suction, and net stress were investigated by comparing the results of tests performed on specimens compacted at similar degrees of saturation and compactive efforts. The variations of normalized shear and constrained moduli with matric suction at net stresses of 0, 10, 20, 30, and 40 psi were compared for the two series of tests and illustrated in Figures 12.37 and 12.38. The variations of normalized shear and constrained moduli with matric suction and net stress for the two series of tests were different. Accordingly, it was concluded that the relationships between normalized shear and constrained moduli, matric suction, and net stress are not unique for the soil tested and depend on factors such as compaction degree of saturation and compactive effort, which essentially relate to the soil fabric and overconsolidation ratio. Similar

observations were reported by Mancuso et al. (2002) and Sawangsuriya et al. (2006) for specimens compacted at different compaction water contents as shown in Figure 12.39.

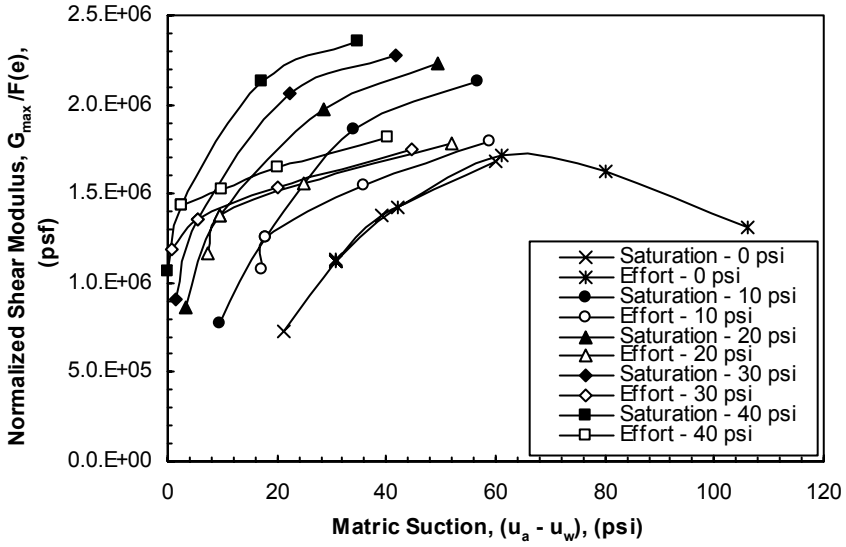

Figure 12.37. Variation of normalized shear modulus with matric suction at net stresses of 0, 10, 20, 30, and 40 psi for specimens compacted at similar degrees of saturation and compactive efforts.

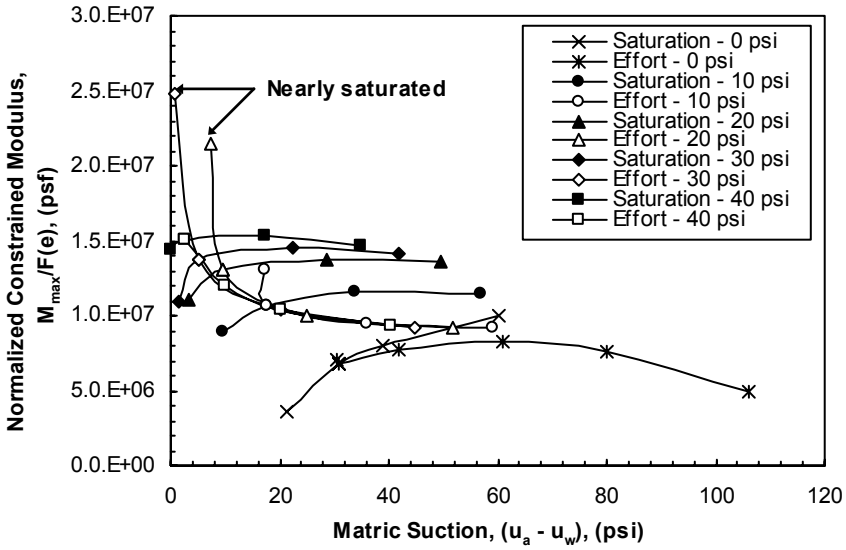

Figure 12.38. Variation of normalized constrained moduli with matric suction at net stresses of 0, 10, 20, 30, and 40 psi for specimens compacted at similar degrees of saturation and compactive efforts.

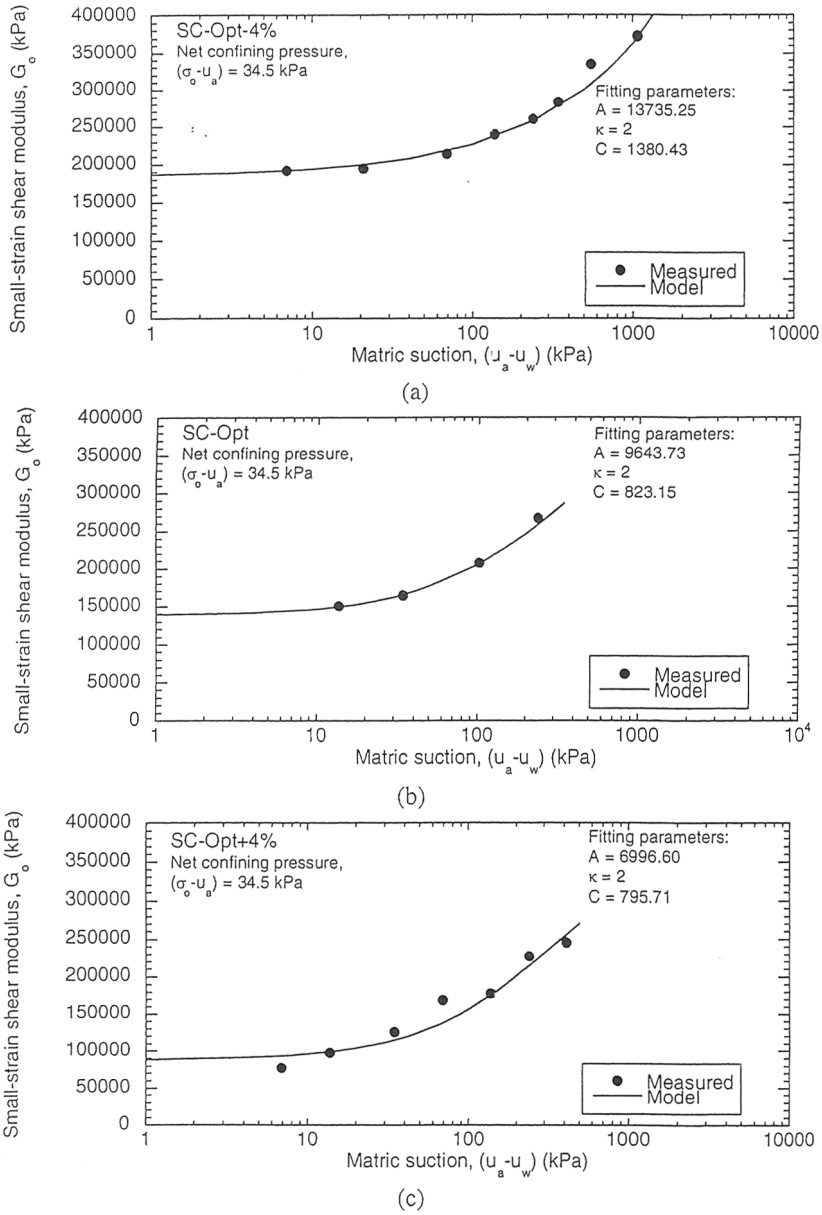

Figure 12.39. Variation of shear modulus with matric suction for a given net stress for specimens compacted at different compaction water contents (from Sawangsuriya et al., 2006).

The variation of soil stiffness with state of stress has been investigated in the previous sections in terms of two stress state variables ($u_a - u_w$) and ($\sigma_c - u_a$). The variation of stiffness with ($\sigma_c - u_w$) and ($\sigma_c - u_a$) was also investigated as illustrated in

Figure 12.40. The shear modulus generally increased as the ($\sigma_c - u_w$) increased, with appreciable scatter. There was no clear trend for the effect of the net stress ($\sigma_c - u_a$) on the relationship between the shear modulus and ($\sigma_c - u_w$). The data seemed to be grouped into two groups as illustrated in Figure 12.41; one group corresponded to tests performed on specimens compacted at similar degrees of saturation and the other group corresponded to tests conducted on specimens compacted at similar compactive efforts. For each series of tests, the variation of the shear modulus could be reasonably expressed in terms of one stress state variable ($\sigma_c - u_w$) instead of two variables, ($u_a - u_w$) and ($\sigma_c - u_a$), which simplifies the problem from a three dimensional to two dimensional problem. For the constrained modulus, the scatter observed in the relationships presented in Figures 12.42 and 12.43 suggests that the two stress state variables ($u_a - u_w$) and ($\sigma_c - u_a$) are more suitable in representing the variation constrained modulus with the soil state of stress.

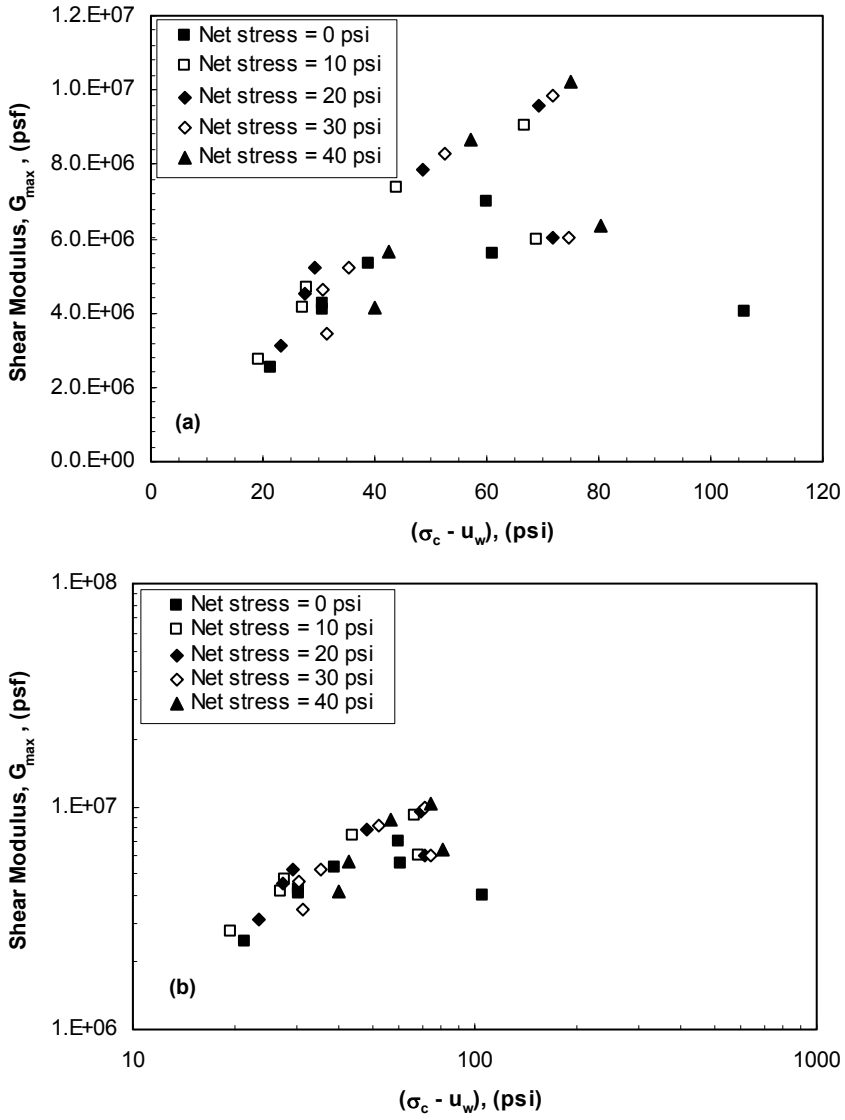

Figure 12.40. Variation of shear modulus with (σ_c – u_w) at net stresses of 0, 10, 20, 30, and 40 psi: (a) arithmetic scale and (b) logarithmic scale.

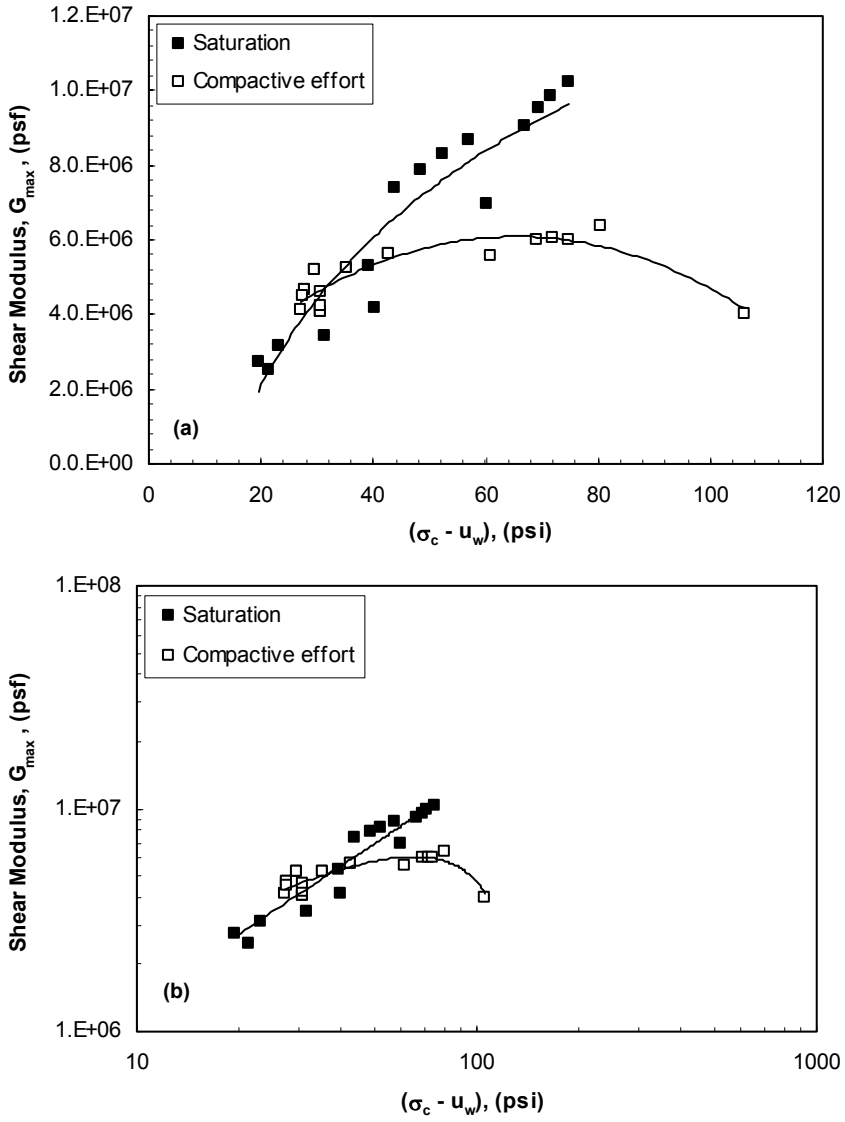

Figure 12.41. Variation of shear modulus with (σ_c – u_w) for specimens compacted at similar degrees of saturation and compactive efforts: (a) arithmetic scale and (b) logarithmic scale.

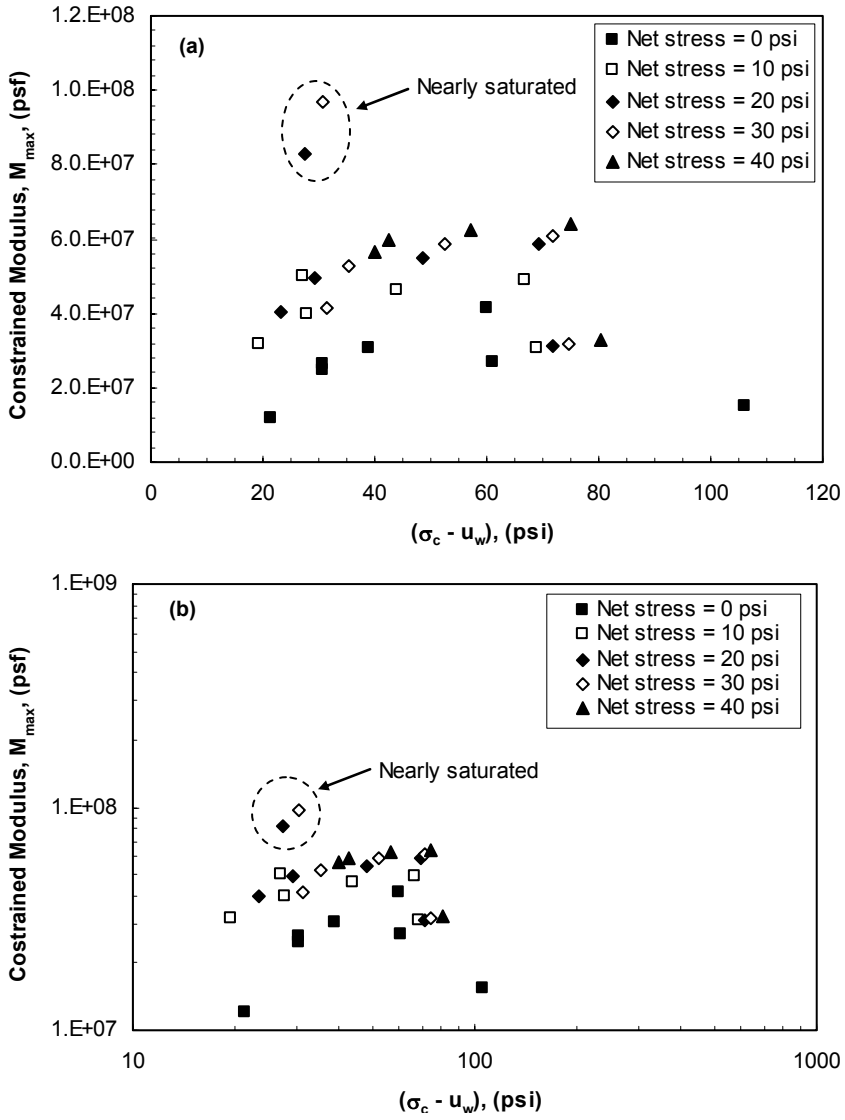

Figure 12.42. Variation of constrained modulus with ($\sigma_c - u_w$) at net stresses of 0, 10, 20, 30, and 40 psi: (a) arithmetic scale and (b) logarithmic scale.

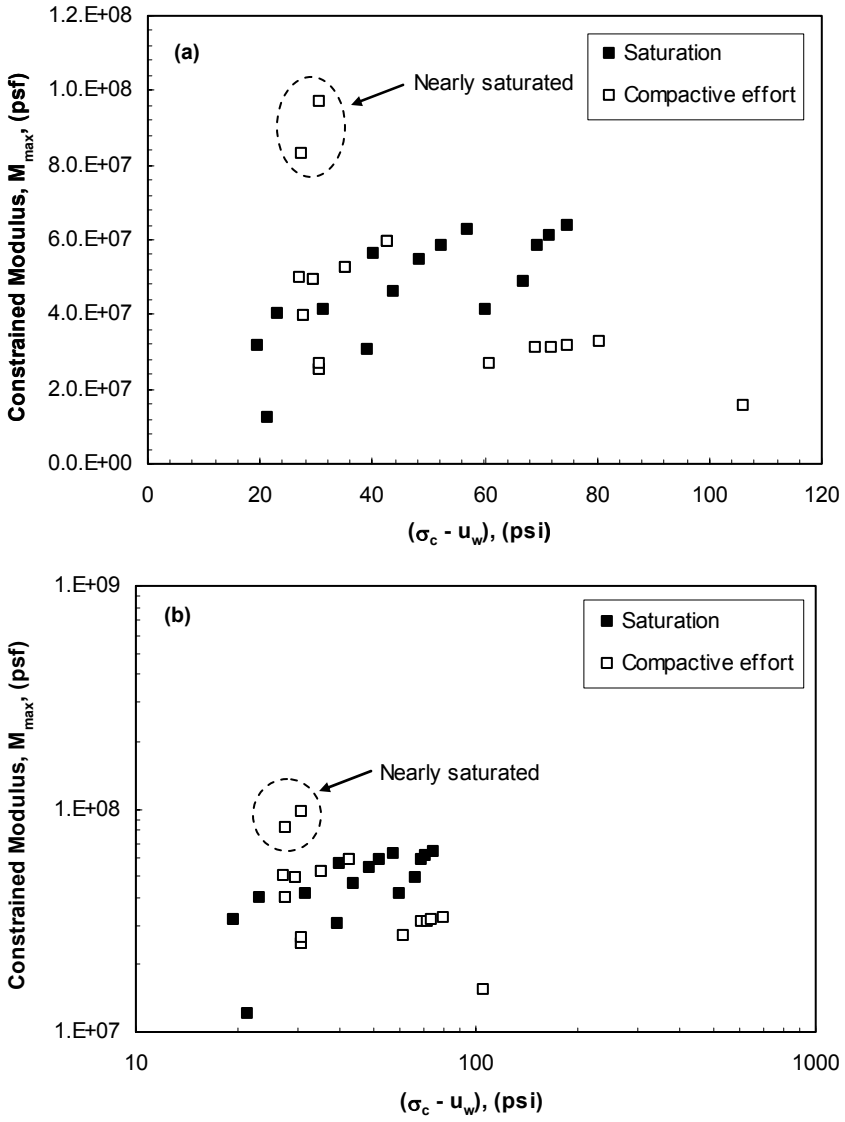

Figure 12.43. Variation of constrained modulus with $(\sigma_c - u_w)$ for specimens compacted at similar degrees of saturation and compactive efforts: (a) arithmetic scale and (b) logarithmic scale.

12.4 Comparison with results from undrained triaxial tests

Shear and compression wave velocities measured in the undrained triaxial apparatus under a confining pressure of 0.2 psi and in the suction-controlled triaxial

apparatus under zero net stress are compared below. In both series of tests, the net stress was zero and the matric suctions were equivalent to the initial matric suctions in the specimens after compaction.

12.4.1 SHEAR WAVE VELOCITIES

The standard Proctor compaction curve and measured shear wave velocities for both series of tests are presented in Figure 12.44. For similar water contents and dry unit weights, shear wave velocities measured in the suction-controlled triaxial apparatus were higher than those measured in the undrained triaxial apparatus. The initial matric suctions of the specimens tested in the suction-controlled triaxial apparatus were also higher than those inferred for the specimens tested in the undrained triaxial apparatus (using pressure plate tests) as discussed in Section 12.2.1.1. To determine if the higher velocities measured for the specimens tested in the suction-controlled triaxial apparatus were related to higher matric suctions, the relationship between shear wave velocity and initial matric suction was plotted for the two series of tests as shown in Figure 12.45. The variation of shear wave velocity with matric suction for the specimens tested in the undrained and suction-controlled triaxial apparatus agreed to a great extent. The higher velocities measured for the specimens tested in the suction-controlled triaxial apparatus were attributed to their higher matric suctions.

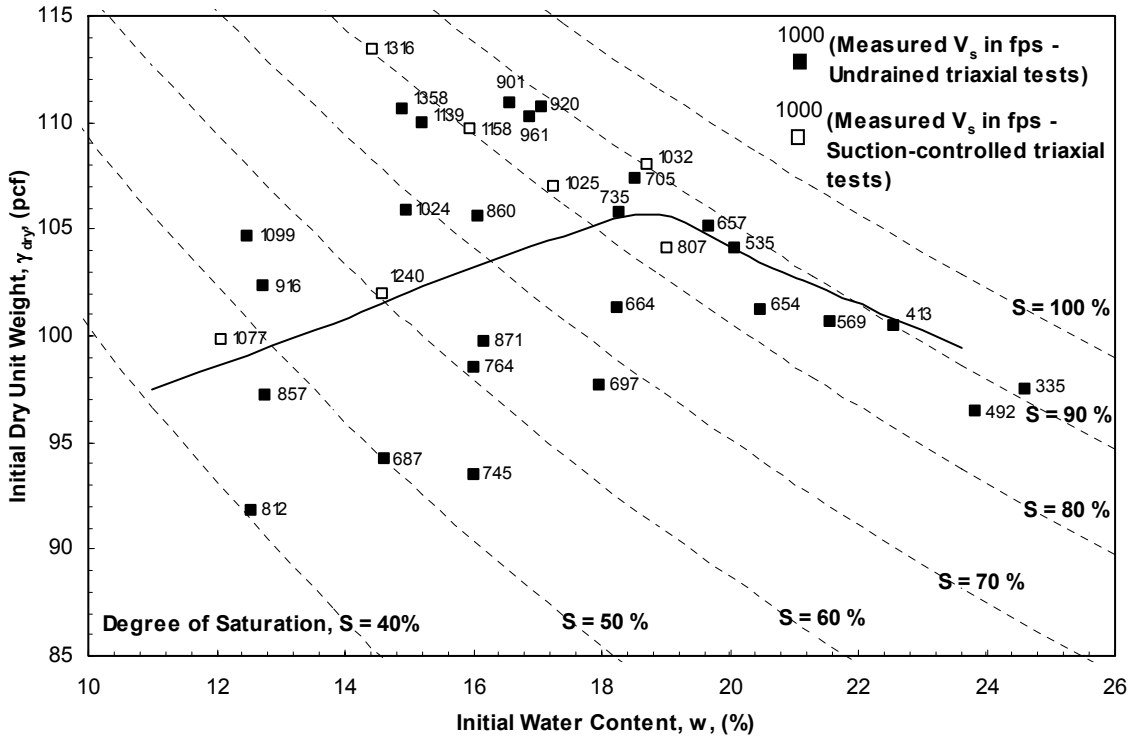

Figure 12.44. Shear wave velocity for specimens tested in undrained traxial apparatus under confining pressure of 0.2 psi and suction-controlled triaxial apparatus under zero net stress.

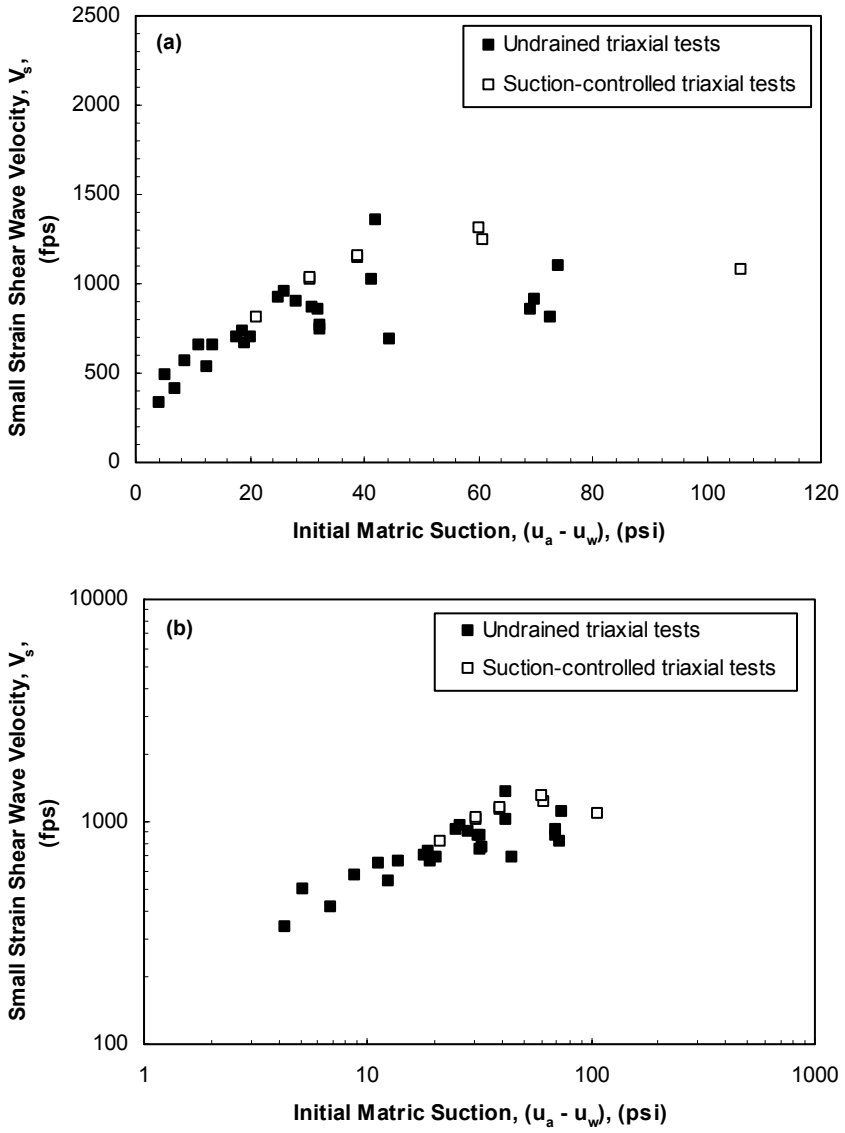

Figure 12.45. Variation of shear wave velocity with initial matric suction for specimens tested in undrained and suction-controlled triaxial apparatus: (a) arithmetic scale and (b) logarithmic scale.

12.4.2 COMPRESSION WAVE VELOCITIES

The standard Proctor compaction curve and measured compression wave velocities for specimens tested in the two apparatus are presented in Figure 12.46. For similar water contents and dry unit weights, compression wave velocities measured in the

suction-controlled triaxial apparatus were higher than those measured in the undrained triaxial apparatus. To determine if the higher velocities measured for the specimens tested in the suction-controlled triaxial apparatus were related to their higher matric suctions; the relationship between compression wave velocity and initial matric suction was plotted for the two series of tests as shown in Figure 12.47. The variation of compression wave velocity with matric suction seemed to follow trends similar to those observed for shear wave velocity. The higher velocities measured for specimens tested in the suction-controlled triaxial apparatus were attributed to their higher matric suctions.

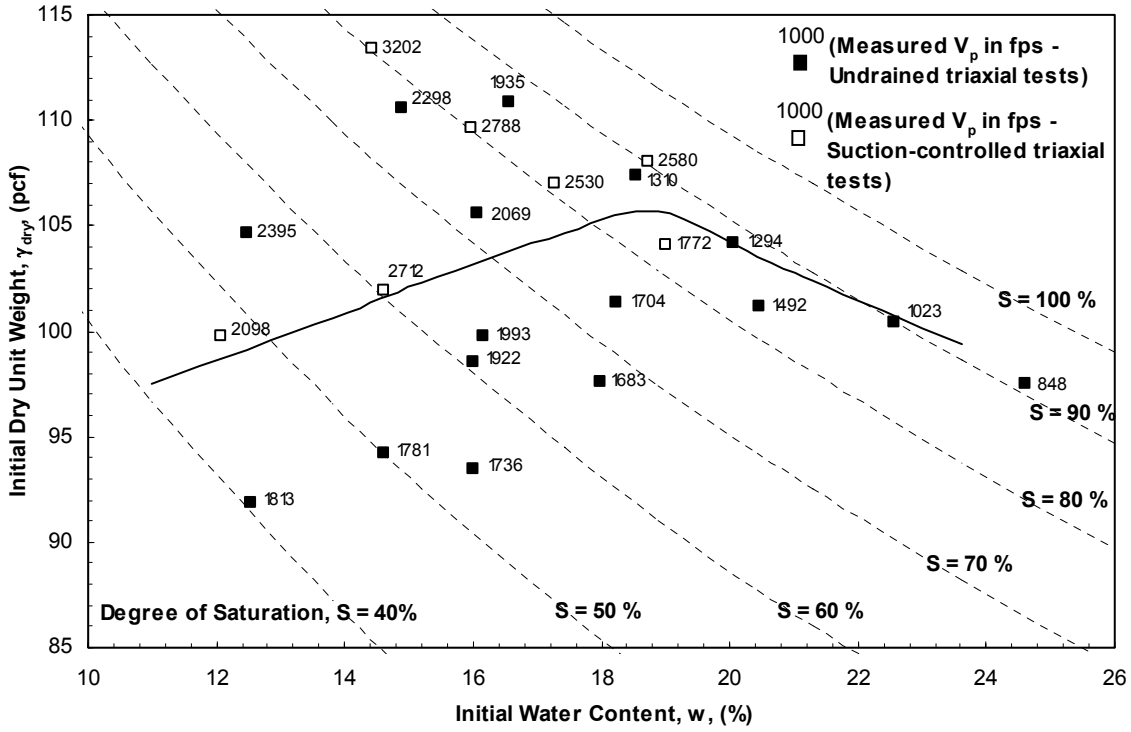

Figure 12.46. Compression wave velocity for specimens tested in undrained traxial apparatus under confining pressure of 0.2 psi and suction-controlled triaxial apparatus under zero net stress.

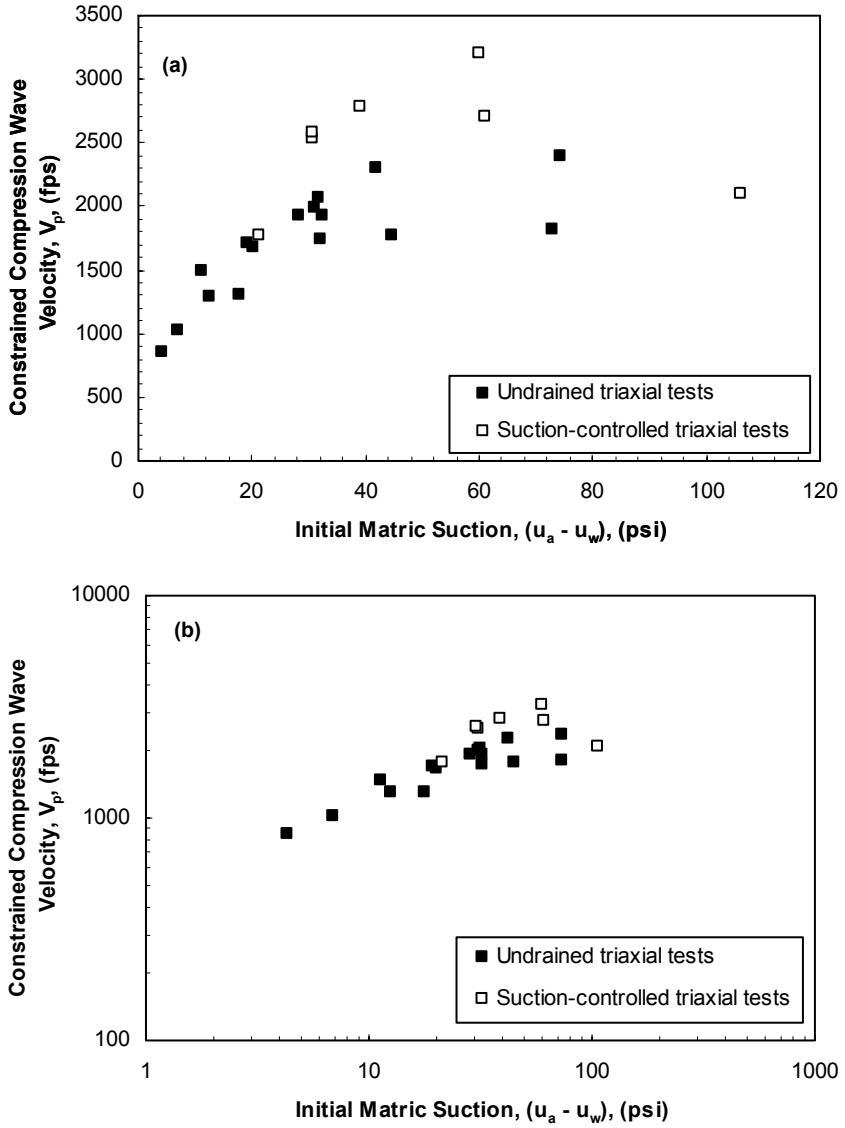

Figure 12.47. Variation of compression wave velocity with initial matric suction for specimens tested in undrained and suction-controlled triaxial apparatus: (a) arithmetic scale and (b) logarithmic scale.

12.5 Summary

A series of constant water content tests was performed in a suction-controlled triaxial apparatus equipped with piezoelectric transducers to investigate the effect of the

state of stress on soil stiffness at small strains. A constant water content test procedure was used, consisting of an equalization and an isotropic compression stage. Matric suctions measured in the equalization stage were either at the upper bound of the range of matric suctions measured in the pressure plate tests or higher. No explanation could be found for the higher matric suctions measured in the constant water content tests versus the pressure plate tests. The specimens experienced about 1 to 4% compression during the equalization stage as the pore-water pressure equalized within the specimen.

During the compression stage, the matric suction decreased as the net stress increased. The rate of reduction in matric suction with the increase in net stress increased as the loading rate increased during compression. Accordingly, it was concluded that an inappropriate rate of loading might cause the menisci to break apart, and the effect of the matric suction to be lost. For the current research, a consistent rate of loading of 10 kPa/hr was applied in the compression stage. The amount of air diffusion was larger for specimens compacted at lower water contents and as the test duration increased. In addition, the amount of air diffusion decreased as the net stress increased during the compression stage. The effect of air diffusion on matric suction measurements was minimized by periodically flushing de-aired water through the water cavities behind the high air-entry porous stones.

Variations of shear and compression wave velocities with the soil state of stress were investigated for specimens compacted at similar degrees of saturation:

- For a given net stress, the shear wave velocity increased as the matric suction increased but at a decreasing rate. For a given matric suction, the shear wave velocity increased as the net stress increased.

- At a net stress of zero, the compression wave velocity increased as the matric suction increased but at a decreasing rate. For net stresses of 10, 20, 30, and 40 psi, the compression wave velocity increased as the matric suction increased and then tended towards a threshold beyond which the compression wave velocity did not increase further. For a given matric suction, the compression wave velocity increased as the net stress increased.

- Three-dimensional diagrams illustrating the variation of the shear and compression wave velocities with the matric suction and net stress were developed.

Variations of shear and compression wave velocities with the soil state of stress were investigated for specimens compacted using similar compactive efforts:

- At a net stress of zero, the shear wave velocity increased as the matric suction increased and then decreased as matric suction increased to about 105 psi. At net stresses of 10, 20, 30, and 40 psi, the shear wave velocity increased but at a decreasing rate as the matric suction increased for the range of matric suctions being tested (up to about 60 psi). For a given matric suction, the shear wave velocity increased as the net stress increased.

- At zero net stress, the compression wave velocity increased as the matric suction increased and then decreased as matric suction increased to about 105 psi. At higher net stresses than zero, the compression wave velocity decreased as the matric suction increased, but at a decreasing rate. For a given matric suction, the compression wave velocity increased as the net stress increased

from zero to 10 psi but then the compression wave velocity appeared not to be affected as the net stress increased further.

- Three-dimensional diagrams illustrating the variation of the shear and compression wave velocities with the matric suction and net stress were developed.

The variations of shear and compression wave velocities with matric suction at constant net stress for specimens compacted at similar degrees of saturation was different from that observed for specimens compacted using similar compactive efforts. Accordingly, it was concluded that the relationships between shear or compression wave velocities, matric suction, and net stress are not unique for the soil tested and depended on factors such as compaction degree of saturation and compactive effort, which essentially relate to the soil fabric and overconsolidation ratio.

Shear and compression wave velocities measured in the undrained triaxial apparatus and in the suction-controlled triaxial apparatus under essentially zero net stress were compared. For similar compaction water contents and dry unit weights, shear and compression wave velocities measured in the suction-controlled triaxial apparatus were higher than those measured in the undrained triaxial apparatus. The variation of the velocities with matric suction for the specimens tested in the two series of tests agreed. The higher velocities measured for the specimens tested in the suction-controlled triaxial apparatus were attributed to their higher matric suctions.

CHAPTER 13: EMPERICAL EQUATIONS RELATING SMALL-STRAIN STIFFNESS TO STATE OF STRESS

13.1 Introduction

Several empirical equations have been proposed in the literature to describe the variation of the small-strain shear modulus of soils with the state of stress. Equations developed by Hardin and Black (1968), Picornell and Nazarian (1998), Mendoza et al. (2005), Sawangsuriya et al. (2006), and Vassallo et al. (2006) are evaluated in this chapter with respect to their validity for modeling the variation of shear modulus with stress for the soil tested in this study. The equations are classified into three groups: (1) equations developed for saturated soils, based on effective stress; (2) equations developed for unsaturated soils, based on matric suction (at zero net stress); and (3) equations developed for unsaturated soils, based on matric suction and net stress.

13.2 Equations for saturated soils - Hardin and Black (1968)

Hardin and Black (1968) reported that small-strain soil stiffness for saturated soils could be calculated as follows:

$$G_{\max} = AF(e)(OCR)^{k}(\sigma')^{n} \quad \text{..... (13.1)}$$

where A is a parameter that depends on soil fabric, OCR is the overconsolidation ratio, k is a parameter that depends on the plasticity index (PI) of the soil, σ' is the mean effective stress, and n is a stress exponent (typically equals 0.5 for normally consolidated saturated soils). The $F(e)$ term is a void ratio function defined by Hardin and Black (1968) for clays as follows:

$$F(e) = \frac{(2.97 - e)^2}{1 + e} \quad \text{.....} \quad (13.2)$$

where *e* is the void ratio. This expression for F(e) is the same used in Chapters 10 and 12 to reduce the effect of dry unit weight (void ratio) on shear modulus.

For the current research, the equation proposed by Hardin and Black (1968) was modified to relate shear modulus to matric suction rather than effective stress. Thus, Equation 13.1 is expressed as:

$$\frac{G_{\max}}{F(e)} = A(OCR)^k (u_a - u_w)^n \quad \text{.....} \quad (13.3)$$

The overconsolidation ratio of the clay tested was not determined. Accordingly, the effect of *OCR* on the relationship between the shear modulus and matric suction is not known. The parameter *n* and the product of the parameter *A* and the term $(OCR)^k$ were evaluated by fitting a power function to the measured shear moduli using Microsoft Excel Trendlines. The variations of measured and predicted normalized shear moduli (G_{max}/F(e)) with matric suction at zero net stress are shown in Figure 13.1 (arithmetic and logarithmic scales). In Figure 13.1, the predicted normalized shear modulus continuously increased as the matric suction increased. Equation 13.3 could not predict the limiting value beyond which the measured normalized shear moduli did not increase further for the range of matric suctions being investigated.

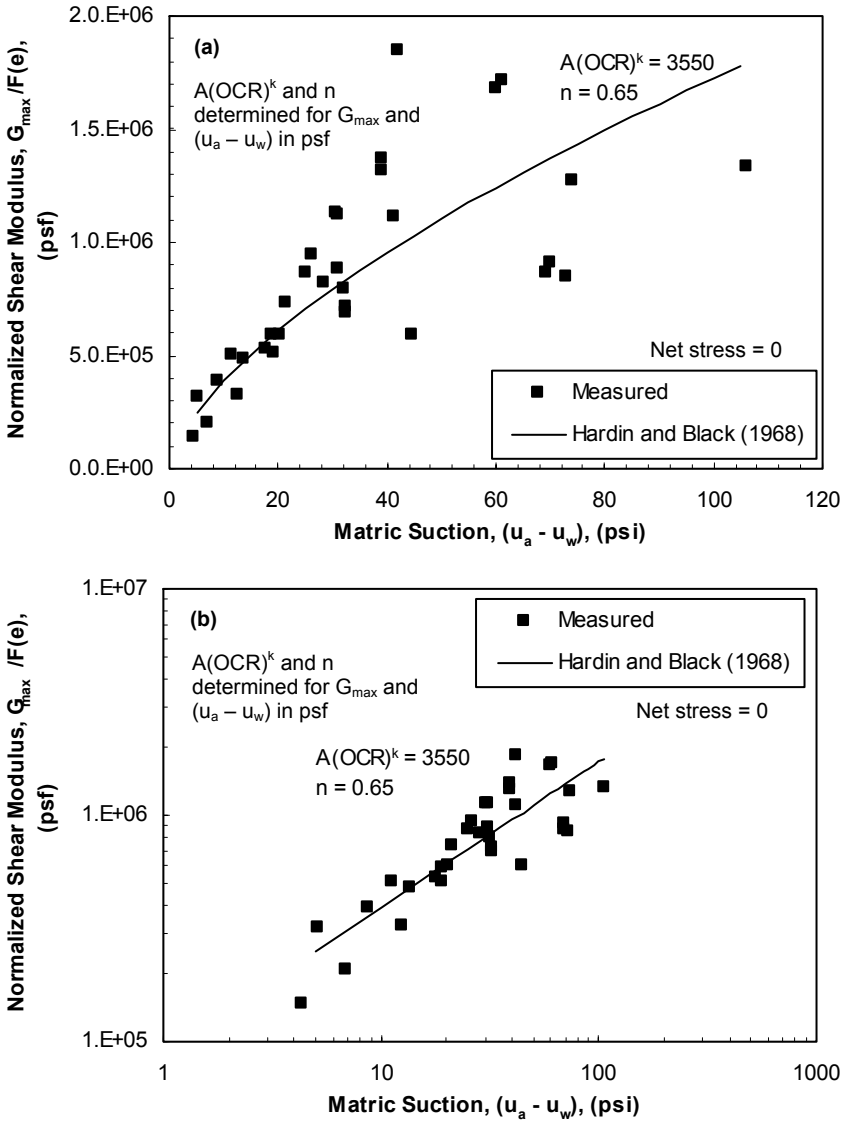

Figure 13.1. Variation of predicted (Hardin and Black, 1968) and measured normalized shear moduli with matric suction: (a) arithmetic and (b) logarithmic scales.

For practical purposes, soils are typically compacted at degrees of saturation higher than 75%. The variations of measured and predicted normalized shear moduli ($G_{max}/F(e)$) with matric suction for this range of degrees of saturation are shown in Figure 13.2. Soil stiffness increased as the matric suction increased for the range of matric suctions being investigated. Equation 13.3 fit the data shown in Figure 13.2 relatively

well up to matric suction of about 40 psi. The values of the stress exponent (n) evaluated for the two sets of data shown in Figures 13.1 and 13.2 are high compared to those typically evaluated for saturated soils (less than 0.5). No clear explanation could be found for these higher n values.

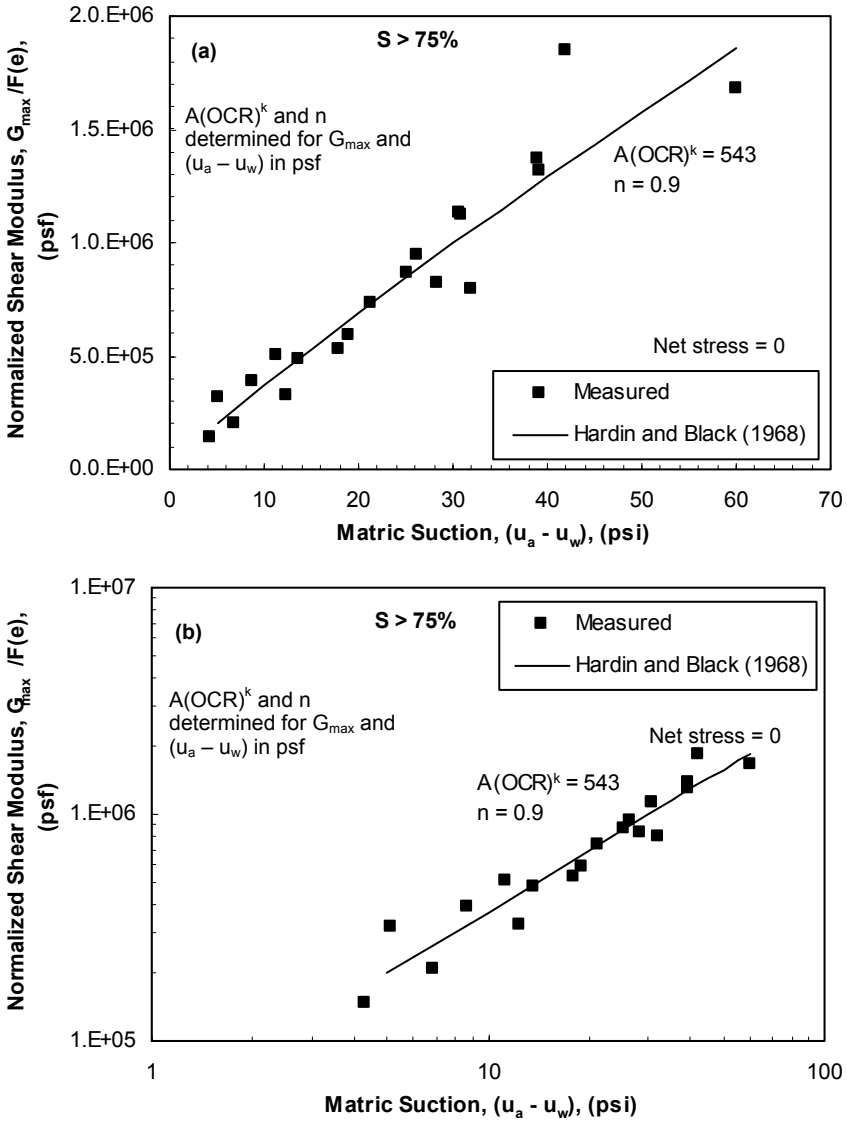

Figure 13.2. Variation of predicted (Hardin and Black, 1968) and measured normalized shear moduli with matric suction for specimens compacted at degrees of saturation higher than 75%: (a) arithmetic and (b) logarithmic scales.

Soil stiffness generally increases as net stress increases as discussed in Chapter 12 and shown in Figure 13.3 for specimens compacted at degrees of saturation ranging from 74 to 77%. The variation of shear modulus with matric suction and net stress cannot be modeled using the equation proposed by Hardin and Black (1968) because this equation

does not consider the net stress. In summary, the correlation proposed by Hardin and Black (1968) cannot predict the limiting value beyond which the stiffness does not increase for further increase in matric suction and cannot predict the variation of soil stiffness with net stress. However, for practical purposes, this correlation can be used to predict soil stiffness for specimens compacted at degrees of saturation higher than 75%.

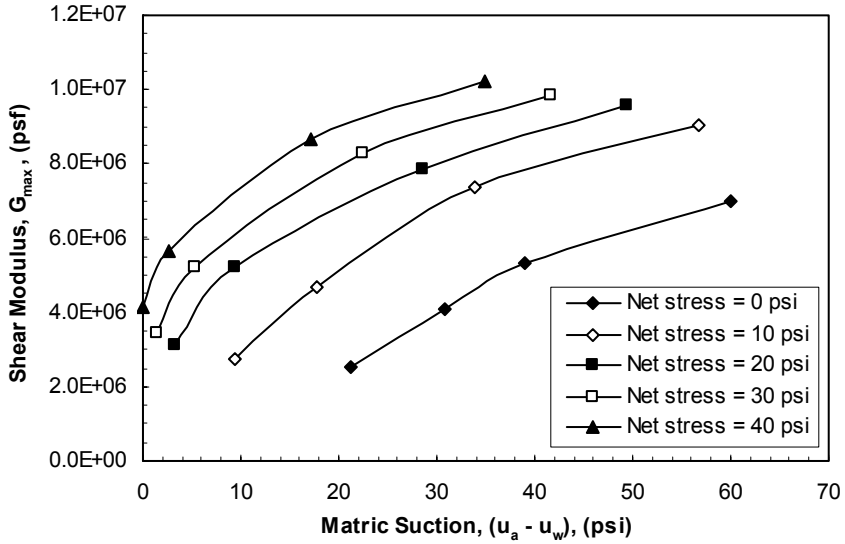

Figure 13.3. Variation of shear modulus with matric suction and net stress for specimens compacted at degrees of saturation ranging from 74 to 77%.

13.3 Equations for unsaturated soils based on matric suction

Picornell and Nazarian (1998) and Mendoza et al. (2005) related the small-strain shear modulus to matric suction ($u_a - u_w$) at zero net stress ($\sigma_c - u_a$). Their equations are discussed below.

13.3.1 PICORNELL AND NAZARIAN (1998)

Picornell and Nazarian (1998) studied both silts and clays. They related the shear modulus to matric suction using second-degree polynomials as shown in Figure 13.4.

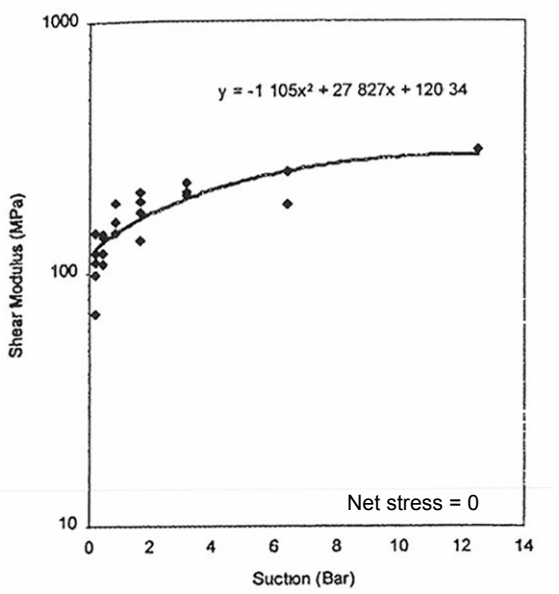

Figure 13.4. Variation of shear modulus with matric suction (from Picornell and Nazarian, 1998).

Second-degree polynomials were fit to the shear moduli measured in this study using Microsoft Excel Trendlines. The relationship between shear modulus and matric suction is expressed as follows:

$$G_{\max} = A(u_a - u_w)^2 + B(u_a - u_w) + C \quad \text{..... (13.4)}$$

where A, B, and C are the best-fit coefficients of the polynomial. The variations of measured and predicted shear moduli with matric suction at zero net stress are shown in Figure 13.5. Second-degree polynomials could predict the general trend for the variation of measured shear modulus with matric suction, though the data are still significantly scattered around the predicted values. For practical purposes, the variations of measured and predicted shear moduli with matric suction for specimens compacted at degrees of saturation higher than 75% were investigated and are shown in Figure 13.6. Second-degree polynomials fit the data relatively well.

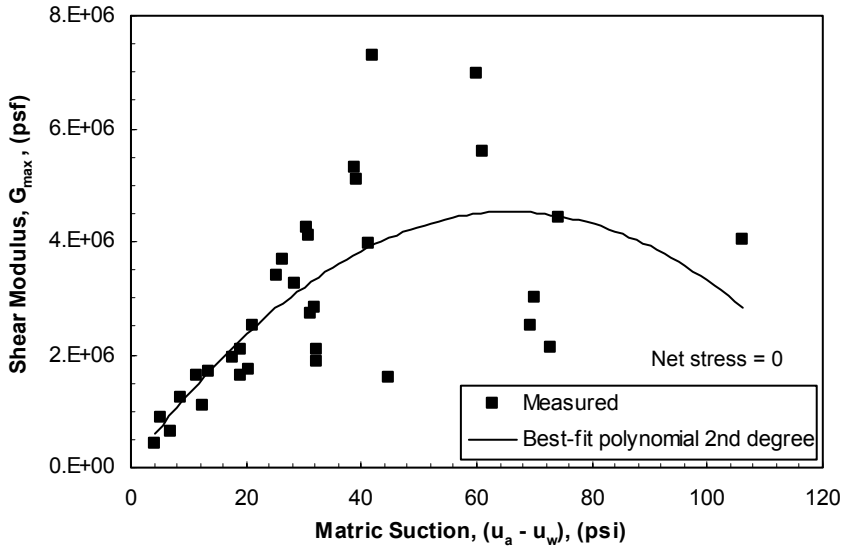

Figure 13.5. Variation of predicted (Picornell and Nazarian, 1998) and measured shear moduli with matric suction.

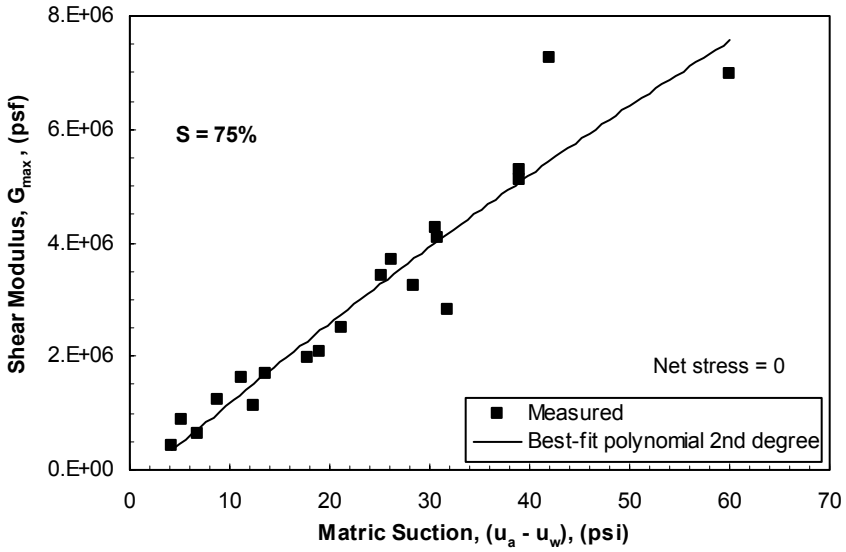

Figure 13.6. Variation of predicted (Picornell and Nazarian, 1998) and measured shear moduli with matric suction for specimens compacted at degrees of saturation higher than 75%.

The equation proposed by Picornell and Nazarian (1998) did not consider the net stress, and thus could not be used to model the variation of shear modulus with matric suction and net stress. In summary, the equation proposed by Picornell and Nazarian (1998) could predict the general trend for the variation of shear modulus with matric suction at zero net stress. However, further investigation is required to understand the effect of factors such as the compaction dry unit weight, degree of saturation, overconsolidation ratio, soil fabric, and plasticity index on the fitting coefficients A, B, and C.

13.3.2 MENDOZA ET AL. (2005)

Mendoza et al. (2005) studied the variation of small-strain shear modulus with matric suction at zero net stress for compacted kaolin. The authors proposed the following equation relating shear modulus to matric suction:

$$G_{\max} = 13300F(e)\left[\ln(u_a - u_w)\right]^{1.35} \quad \text{(13.5)}$$

where *F(e)* is a void ratio function. The authors defined the void ratio function as:

$$F(e) = \left(\frac{(2.3-e)^2}{1+e}\right) \quad \text{(13.6)}$$

The units for the shear modulus were consistent with units of matric suction (international system). For the current research, Equation 13.5 is expressed as follows:

$$\frac{G_{\max}}{F(e)} = A\left[\ln(u_a - u_w)\right]^n \quad \text{(13.7)}$$

The void ratio function *F(e)* has been consistently defined in this study for the clay tested using Equation 13.2. *A* and *n* are parameters evaluated by fitting a power function to the measured shear moduli – matric suction data. Fitting was done using Microsoft Excel Trendlines.

The variations of measured and predicted normalized shear moduli with matric suction at zero net stress are shown in Figure 13.7. The predicted normalized shear modulus continuously increased as the matric suction increased. Equation 13.7 could not predict the limiting value beyond which the measured normalized shear moduli did not increase further for the range of matric suctions being investigated. The variation of the predicted normalized shear modulus with matric suction was generally similar to that predicted using Equation 13.3 (modified Hardin and Black, 1968). For practical purposes, the variations of measured and predicted shear moduli with matric suction for specimens compacted at degrees of saturation higher than 75% were investigated and are shown in Figure 13.8. Equation 13.7 fit the data shown in Figure 13.8 relatively well up to matric suction of about 40 psi.

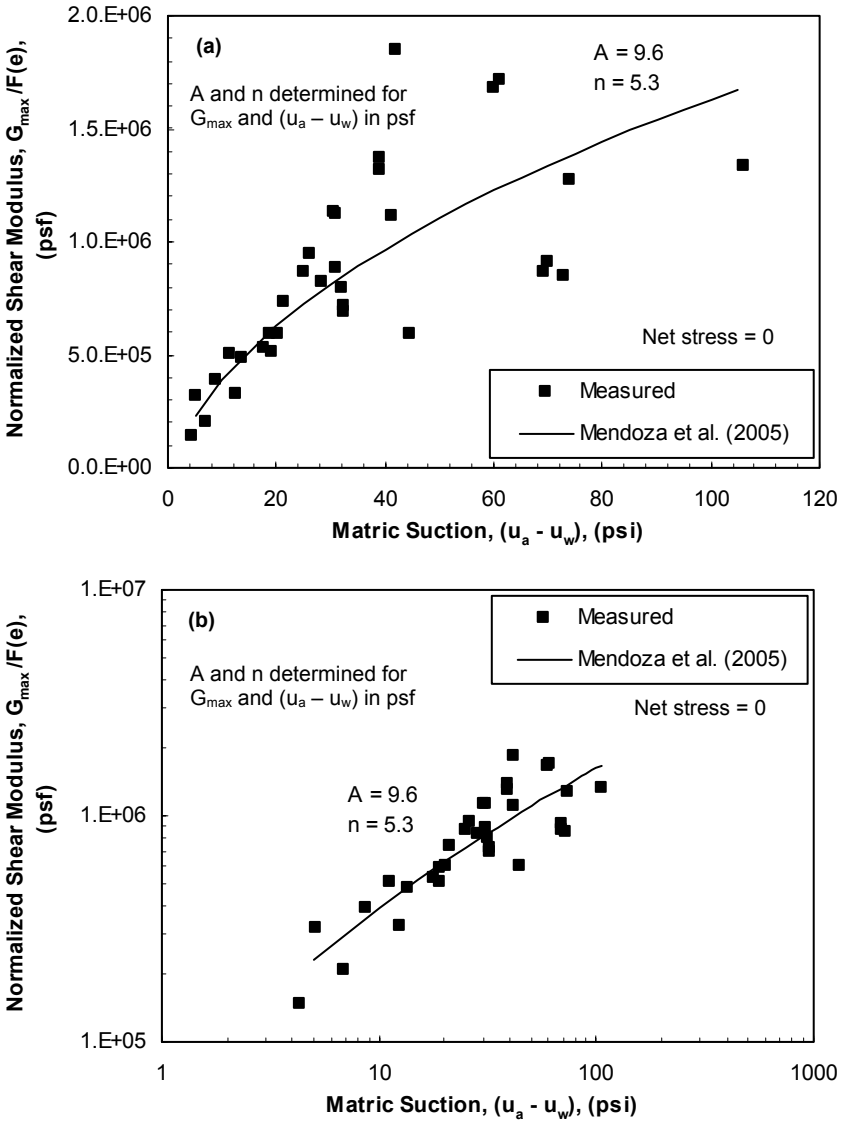

Figure 13.7. Variation of predicted (Mendoza et al., 2005) and measured normalized shear moduli with matric suction: (a) arithmetic and (b) logarithmic scales.

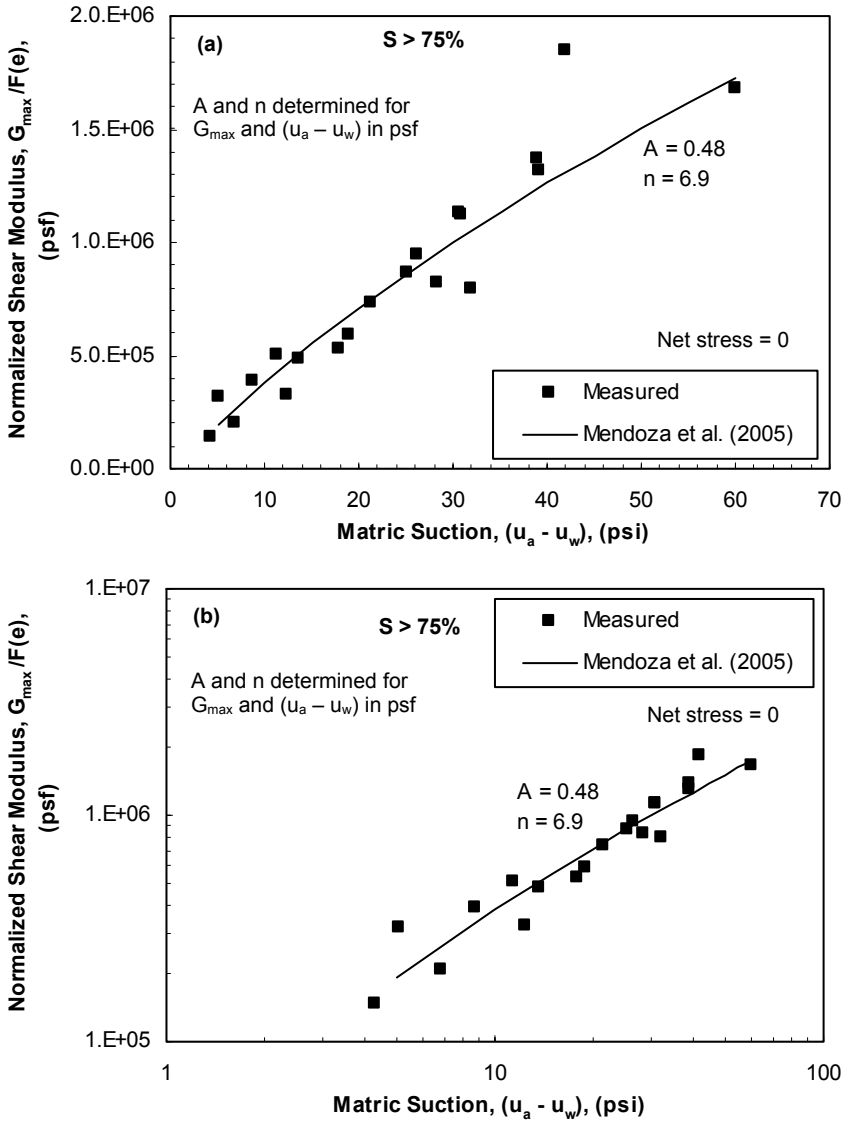

Figure 13.8. Variation of predicted (Mendoza et al., 2005) and measured normalized shear moduli with matric suction for specimens compacted at degrees of saturation higher than 75%: (a) arithmetic and (b) logarithmic scales.

The equation proposed by Mendoza et al. (2005) does not consider the net stress, and thus could not be used to predict the variation of shear modulus with matric suction and net stress. In summary, the equation proposed by Mendoza et al. (2005) cannot predict the limiting value beyond which the stiffness does not increase for further

increase in matric suction and cannot predict the variation of soil stiffness with net stress. However, for practical purposes, this equation can be used to predict soil stiffness for specimens compacted at degrees of saturation higher than 75%.

13.4 Equations for unsaturated soils based on matric suction and net stress

Sawangsuriya et al. (2006) and Vassallo et al. (2006) performed studies where they related the small-strain shear modulus to both matric suction ($u_a - u_w$) and net stress ($\sigma_c - u_a$). For the current research, the relationship between soil stiffness, matric suction, and net stress was found to be different for specimens compacted at similar degrees of saturation and compactive efforts as discussed in Chapter 12 and shown in Figure 13.9. Therefore, the equations proposed by Sawangsuriya et al. (2006) and Vassallo et al. (2006) were to be examined for each set of data separately. The relationship between stiffness and matric suction for specimens compacted at similar compactive efforts was defined by two or three data points for each net stress, which were judged to be insufficient to fit into empirical equations. Accordingly, the equations proposed by Sawangsuriya et al. (2006) and Vassallo et al. (2006) were examined only for the set of data obtained for specimens compacted at similar degrees of saturation (ranging from 74 to 77%).

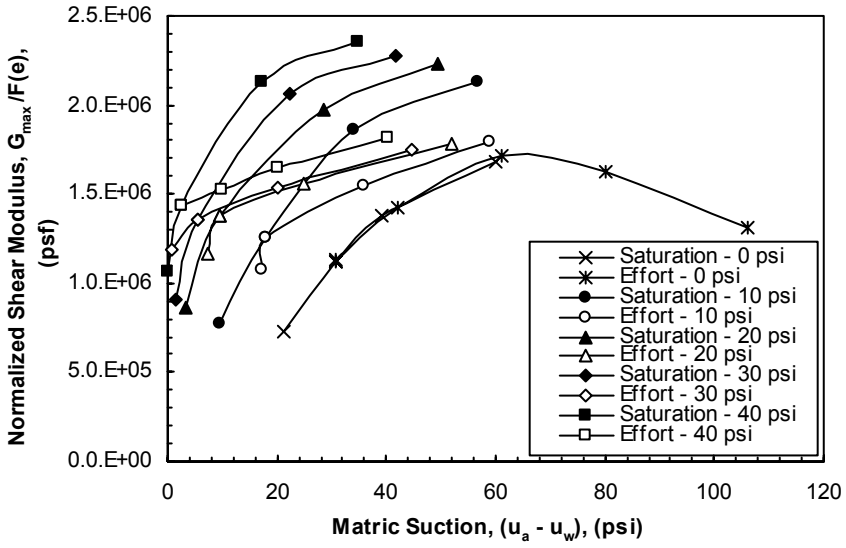

Figure 13.9. Variation of normalized shear modulus with matric suction at net stresses of 0, 10, 20, 30, and 40 psi for specimens compacted at similar degrees of saturation and compactive efforts

13.4.1 SAWANGSURIYA ET AL. (2006)

Sawangsuriya et al. (2006) tested a compacted clayey sand at a constant net stress of 34.5 kPa. They proposed the following equation relating the shear modulus to matric suction and net stress:

$$G_{\max} = AF(e)(\sigma_c - u_a)^n + C\left(\frac{\theta - \theta_r}{\theta_s - \theta_r}\right)^k (u_a - u_w) \quad \text{..... (13.8)}$$

where n is an exponent, assumed to be 0.5, θ_r is the residual volumetric water content, θ_s is the saturated volumetric water content, and θ is the volumetric water content. The authors used the void ratio function $F(e)$ defined by Hardin (1978) as:

$$F(e) = \frac{1}{(0.3 + 0.7e^2)} \quad \text{..... (13.9)}$$

The parameters *A*, *C*, and *k* were determined by fitting to measured shear moduli data. An example of the variation of measured and predicted shear moduli with matric suction reported by Sawangsuriya et al. (2006) is shown in Figure 13.10. The authors referred to the net stress as "net confining pressure" in their study.

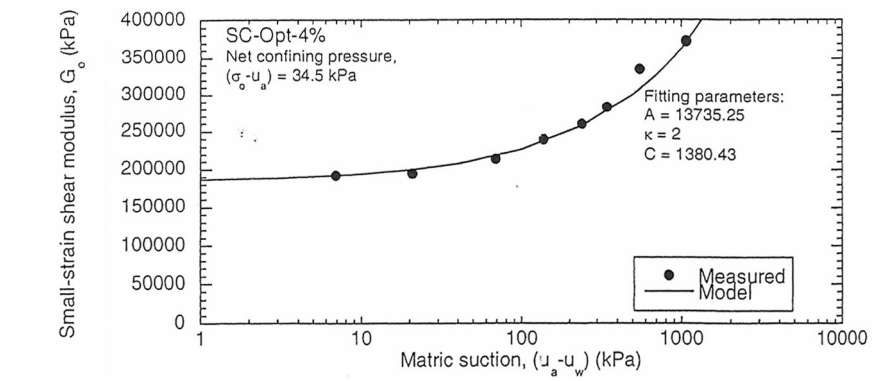

Figure 13.10. Variation of predicted and measured shear moduli with matric suction at constant net stress (from Sawangsuriya et al., 2006).

For the current research, the void ratio function *F(e)* has been consistently defined for the clay tested using Equation 13.2. The exponent *n* was assumed to be 0.5. For dry unit weights ranging from 90 to 115 pcf, the saturated volumetric water content, θ_s, for the soil tested ranged from 0.33 to 0.46. An average value of 0.4 was assumed for the saturated volumetric water content, θ_s. The residual volumetric water content, θ_r, was calculated from the equation:

$$\theta_r = n' S_r \quad \text{..... (13.10)}$$

where n' is the porosity and S_r is the residual degree of saturation. The porosity, n', is equal to the saturated volumetric water content (0.4). Typical values for residual degrees of saturation for clays range from 0.1 to 0.2 (Ning Lu and Griffiths, 2004). A value of

0.15 was assumed for the residual degree of saturation, S_r. Accordingly, the residual volumetric water content was 0.06.

The parameters A, C, and k were determined by fitting to the shear moduli data measured at net stresses of 0, 10, 20, 30, and 40 psi using a least-squares optimization procedure, applied using Microsoft Excel Solver. The variation of the shear modulus with matric suction is illustrated in Figure 13.11 for net stresses of 0, 10, 20, 30, and 40 psi. At constant net stress, the shear modulus from Equation 13.8 increased almost linearly as the matric suction increased, however, the measured shear modulus increased as matric suction increased, but at a decreasing rate. Accordingly, the equation proposed by Sawangsuriya et al. (2006) was judged to be inapplicable to describe the variation of shear modulus with matric suction and net stress.

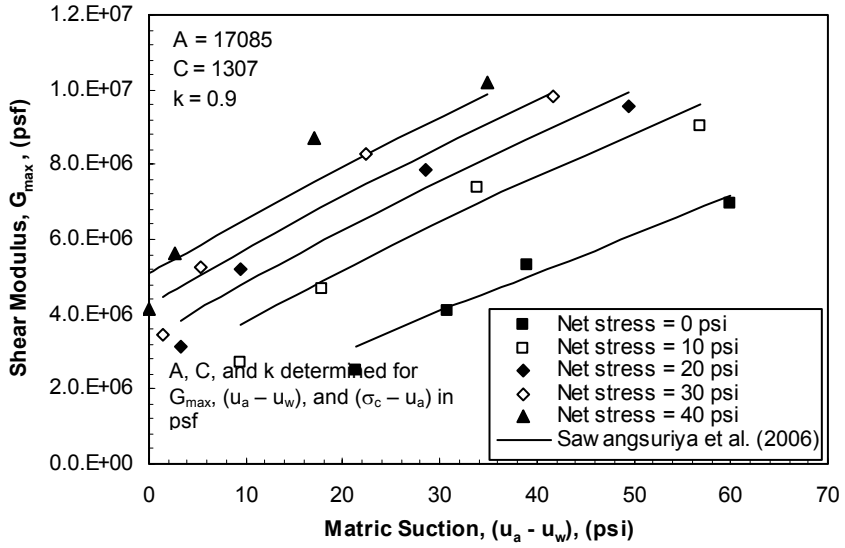

Figure 13.11. Variation of predicted (Sawangsuriya et al., 2006) and measured shear moduli with matric suction and net stress.

13.4.2 VASSALLO ET AL. (2006)

Vassallo et al. (2006) tested a compacted silt. They proposed the following equation relating the shear modulus to matric suction and net stress:

$$G_{\max} = SF(e)P_a\left(\frac{\sigma_c - u_a}{P_a}\right)^n (OCR)^m + F(u_a - u_w) \quad \text{(13.11)}$$

where $F(e)$ is the void ratio function defined by Hardin and Black (1968) and expressed in Equation 13.2, P_a is atmospheric pressure, and S, n, and m are fitting parameters. $F(u_a - u_w)$ is a function that expresses the variation of soil stiffness with matric suction. For the current research, a second-degree polynomial was chosen to express the function $F(u_a - u_w)$ and is expressed as follows:

$$F(u_a - u_w) = A(u_a - u_w)^2 + B(u_a - u_w) + C \quad \text{(13.12)}$$

where A, B, and C are the coefficients of the second-degree polynomial.

The overconsolidation ratio of the clay tested was not determined. Accordingly, the effect of OCR on the relationship between the shear modulus, matric suction, and net stress is not known. The parameters A, B, C, and n and the term $S(OCR)^m$ were evaluated by fitting to the shear moduli data measured at net stresses of 0, 10, 20, 30, and 40 psi using a least-squares optimization procedure, applied using Microsoft Excel Solver. The variation of measured and predicted shear moduli with matric suction at net stresses of 0, 10, 20, 30, and 40 psi is illustrated in Figure 13.12. The shear moduli calculated using Equation 13.11 fit the measured shear moduli well for net stresses greater than zero. The predicted shear moduli had negative values at a net stress of zero. Accordingly, the equation proposed by Vassallo et al. (2006) was judged to be applicable to model the variation of shear modulus with matric suction for net stresses greater than zero.

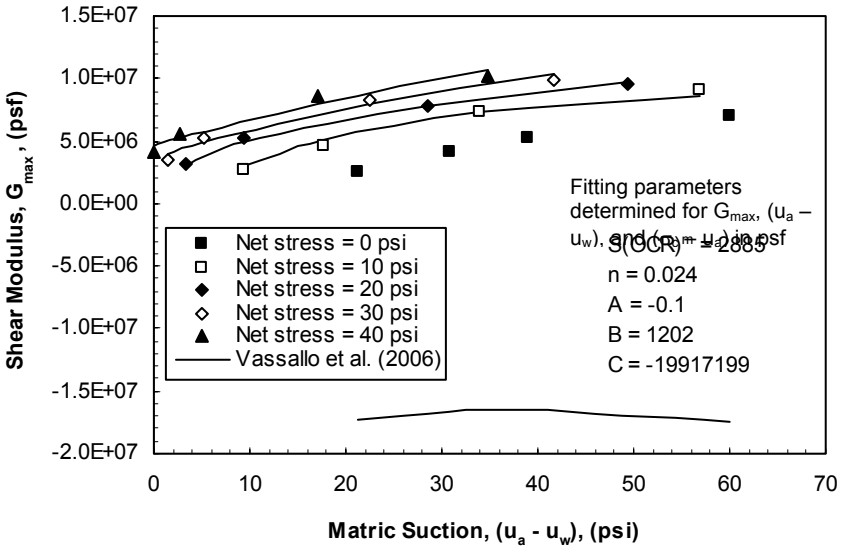

Figure 13.12. Variation of predicted (Vassallo et al., 2006) and measured shear moduli with matric suction and net stress.

13.5 Summary

Empirical equations proposed by Hardin and Black (1968), Picornell and Nazarian (1998), Mendoza et al. (2005), Sawangsuriya et al. (2006), and Vassallo et al. (2006) were evaluated with respect to their validity for modeling the variation of shear modulus with stress for the soil tested in this study. The equation proposed by Hardin and Black (1968) was modified to relate shear modulus to matric suction rather than effective stress. The equation proposed by Hardin and Black (1968) (after modification) and the equations proposed by Picornell and Nazarian (1998) and Mendoza et al. (2005) related the shear modulus to matric suction. The equations proposed by Sawangsuriya et al. (2006) and Vassallo et al. (2006) related the shear modulus to matric suction and net stress.

For the variation of shear modulus with matric suction at zero net stress, the equations proposed by Hardin and Black (1968), after modification, and Mendoza et al. (2005) could not predict the limiting value beyond which the stiffness does not increase for further increase in matric suction. The equation proposed by Picornell and Nazarian (1998) could predict the general trend for the variation of shear modulus with matric suction at zero net stress. For practical purposes, the three correlations could be used to predict soil stiffness for specimens compacted at degrees of saturation higher than 75% and at matric suctions less than about 40 psi. For the variation of shear modulus with matric suction and net stress, the equation proposed by Sawangsuriya et al. (2006) did not fit the measured data well, while the equation proposed by Vassallo et al. (2006) fit the measured data relatively well for net stresses greater than zero.

CHAPTER 14: SUMMARY, CONCLUSIONS, AND RECOMMENDATIONS

14.1 Summary

The objective of the research presented in this dissertation was to investigate the effects of compaction conditions and the state of stress on the small-strain stiffness of unsaturated specimens of a low plasticity clay. An experimental study was conducted to address this objective. A pressure plate apparatus was developed to study the effects of compaction conditions on the soil matric suction ($u_a - u_w$). Matric suctions were measured for specimens prepared at initial water contents ranging from 10 to 25%, and initial dry unit weights ranging from 90 to 115 pcf.

A triaxial cell equipped with piezoelectric transducers was developed to investigate the effects of compaction conditions on soil stiffness under undrained test conditions. Piezoelectric transducers consisted of bender elements and disks to measure shear and compression wave velocities, respectively. Bender elements and disks are generally fragile, and could be easily damaged during the test. A special technique was implemented to incorporate the bender elements and disks in the end platens of the triaxial cell to facilitate replacing the transducer if it was damaged. Each piezoelectric transducer was mounted in a separate stainless steel block, which was fastened into the triaxial platen. If one of the transducers was damaged, the block and the transducer were replaced without damaging the other transducer mounted in the same platen.

Piezoelectric transducers were excited using sinusoidal waves with peak excitation voltages of 100 and 200 for bender elements and disks, respectively. Waves with frequencies ranging from 3 to 8 kHz were used to excite the bender elements. Waves

with frequencies ranging from 5 to 55 kHz were used to excite the disks. For these frequency ranges, the velocities were independent of the excitation frequency. Signal-processing procedures of stacking and filtering were applied to the received signals to increase the signal to noise ratio.

The time required for shear and compression waves to travel through the specimen was measured to determine soil stiffness. Three approaches were investigated to determine the total travel times using: (1) the first arrival of the received signal; (2) characteristic points corresponding to the first peaks, first troughs, and zero-crossings of input and output signals; and (3) the computed cross-correlation between input and output signals. Total travel times determined using the three approaches were different because the shapes of the transmitted and received waveforms were not identical for several reasons, among which are wave dispersion, wave reflections, and near-field effects (for shear waves). For this study, total travel times based on the first arrival of the received signal were judged to correspond to the correct and most reliable travel times because the first arrival is less affected by wave dispersion and reflections. For shear wave velocities, near-field effects were minimized by exciting the transducers with excitation frequencies that produced a minimum number of waves traveling within the length of the specimen of approximately 1.5. Measured total travel times were corrected for the time delay introduced by the electronics, the transducers, and the coating materials used to ground and waterproof the transducers.

Shear and compression wave velocities were measured under confining pressure of 0.2 psi for specimens compacted at water contents ranging from 12 to 25% and dry unit weights ranging from 92 to 112 pcf. The effects of compaction water content, dry unit weight, and degree of saturation on soil stiffness were investigated. Results from the

pressure plate tests were used to estimate the initial matric suction for the specimens tested in the undrained triaxial cell to investigate also the effects of matric suction on soil stiffness.

A suction-controlled triaxial cell equipped with piezoelectric transducers was developed also to investigate the effects of matric suction ($u_a - u_w$) and net stress ($\sigma_c - u_a$) on soil stiffness. The apparatus allows for independent measurements of cell, pore-air, and pore-water pressures. Volumetric strains and changes in water content were also measured independently. The volume changes were monitored by measuring the volume of water flowing into or out of the triaxial cell. To minimize the effects of cell expansion on volume changes measurements, a double-walled triaxial cell was used and volume changes were monitored by measuring the volume of water flowing into or out of the inner cell. Changes in water content were monitored by measuring the volume of water flowing into or out of the specimen through the high air-entry porous stones.

A potential problem with testing low-permeability unsaturated soils is the long period required for specimens to equalize under certain states of stress. In this study, two high air-entry porous stones were mounted in the top and bottom platens to reduce equalization durations. In contrast, the majority of suction-controlled triaxial cells reported in the literature are equipped with a single high air-entry porous stone mounted in the bottom platen to control pore-water pressure.

Another problem encountered with testing unsaturated soils is air diffusion. Air diffused from the specimen into the system for measuring pore-water pressure through the high air-entry porous stones. The effect of air diffusion on matric suction measurements was minimized by periodically flushing de-aired water through the water cavities behind the high air-entry porous stones. Air also diffused from the specimen to

the surrounding cell fluid. This problem was minimized by using double membranes with silicon grease and a layer of aluminum foil (potato-chip bag) between the two membranes.

Two types of tests were performed in the suction-controlled triaxial apparatus: drained tests and constant water content tests. In drained tests, both pore air and pore water were allowed to flow freely into or out of the specimen when the confining pressure was applied. The intent of the drained test was to have the specimen equilibrate under certain matric suction and net stress and then measure the shear and compression wave velocities. Equilibrium was inferred when the flow of water into or out of the specimen essentially ceased. Only one drained test was performed in this study. The drained test showed that very long times were required due to the low hydraulic conductivity of the clay being tested. Accordingly, an alternative, "constant water content", test procedure was developed that allowed for shorter testing periods.

In constant water content tests, when the confining pressure was applied, the pore air was allowed to drain but the pore water was not. The test procedure was divided into two stages: an equalization stage and an isotropic compression stage. The aim of the equalization stage was to establish the initial values of matric suction ($u_a - u_w$) and net stress ($\sigma_c - u_a$) acting on the specimen after compaction without a change in the water content. In this stage, the cell and pore-air pressures were adjusted to maintain approximately zero pore-water pressure in the specimen with no drainage. For the compression stage, the specimen was compressed by increasing the cell pressure. The pore-air pressure was maintained constant at the initial value and the pore-water pressure was measured. Equilibrium was inferred during the equalization and compression stages when pore-water pressures stabilized. Once equilibrium was reached, shear and

compression wave velocities were measured. Two series of constant water content tests were performed. The first series was conducted on specimens compacted at similar degrees of saturation, and the second series was conducted on specimens compacted at similar compactive efforts.

During pressure plate tests and suction-controlled triaxial tests, air diffused through the high air-entry porous stones. For the drained test performed in the suction-controlled triaxial apparatus, the diffused air was flushed out of the water cavity each time a considerable amount of air was observed into the cavities behind the high air-entry porous stones. The measurements for the volume of water flowing into or out of the specimen were then corrected for the amount of diffused air. For pressure plate tests and constant water content tests performed in the suction-controlled triaxial apparatus, the diffused air was flushed out once air was observed in the water cavities because it affected the pore-water pressure measurements. However, the actual volume of the diffused air could not be determined, because it was smaller than the volume the measuring system could accurately measure in the pressure plate tests and constant water content tests. The amount of air diffusion was larger for specimens compacted at lower water contents and as the test duration increased. In addition, the amount of air diffusion decreased as the net stress increased during the compression stage in the suction-controlled triaxial tests.

Empirical equations proposed by Hardin and Black (1968), Picornell and Nazarian (1998), Mendoza et al. (2005), Sawangsuriya et al. (2006), and Vassallo et al. (2006) were evaluated with respect to their validity for modeling the variation of shear modulus with stress for the soil tested in this study. The equation proposed by Hardin and Black (1968) was originally developed to relate shear modulus to effective stress for

saturated soils. For the current research, this equation was modified to relate shear modulus to matric suction instead of effective stress.

14.2 Conclusions

In order for the axis translation technique to be applicable for measuring matric suction, the air phase within the specimen should be continuous. Data reported in the literature suggested that the air phase in the soil becomes occluded near and above the optimum water content. However, in this study, matric suctions measured directly and using the axis translation technique, for specimens compacted on the wet side of the line of optimums, matched well.

In the suction-controlled triaxial tests, it was found that different rates of loading during the isotropic compression stage results in different values of matric suctions. One reason is that faster rates of loading can cause the menisci to break, and the matric suction to be lost. Accordingly, for this study, a consistent slow rate of loading of 10 kPa/hr was applied during the compression stage.

One of the objectives of this study was to determine the applicability of using soil stiffness to infer dry unit weight for compaction control purposes. The results of this study show that shear and compression wave velocities are primarily governed by the compaction water content and to a much lesser extent by the dry unit weight. The velocities generally decrease as the compaction water content increases. The variation of shear and compression wave velocities with dry unit weight depends on the compaction water content. For specimens compacted at similar water contents, the initial dry unit weight does not seem to have a significant effect on shear and compression wave

velocities. Accordingly, soil stiffness was judged to be inapplicable to determine dry unit weights for compaction control purposes.

Soil stiffness primarily depends on the soil state of stress. For all tested specimens, matric suction decreased as the compaction water content increased regardless of the dry unit weight and degree of saturation, which explains why shear and compression wave velocities were primarily governed by the compaction water content more than the dry unit weight.

At zero net stress, the soil stiffness of specimens compacted at either similar dry unit weights or similar compactive efforts generally increased as the matric suction increased, but at a decreasing rate and then tended towards a nearly constant value beyond which the stiffness did not appear to increase further. For specimens compacted at similar degrees of saturation, the soil stiffness increased as the matric suction increased for the range of matric suctions being investigated. The relationship between soil stiffness and matric suction is in accordance with the model proposed by Fisher (1926), in which the air-water meniscus is related to the state of stress, and thus to the stiffness of unsaturated soils. The air-water meniscus introduces a force (ΔN) normal to the contact points between soil particles. This force (ΔN) increases as the matric suction increases, but at a decreasing rate, and approaches a nearly constant value beyond which the force ΔN does not increase further. The force ΔN reaches a nearly constant value at high matric suctions due to the progressive reduction in the radius of the menisci, which leads to the reduction of the area of water between soil particles. The variation of soil stiffness with matric suction measured in this study followed pattern similar to that proposed by Fisher (1926) for the variation of the force ΔN with matric suction. Overall, the relationships between soil stiffness and matric suction are not unique and depend on factors such as

compaction dry unit weight, degree of saturation, compactive effort, soil fabric, and overconsolidation ratio.

For specimens compacted at similar dry unit weights, the relationship between soil stiffness and matric suction was investigated to determine the applicability of using soil stiffness complemented with matric suction measurements to determine dry unit weight for compaction control purposes. The variation observed in this relationship seems to be beyond what can be used to determine dry unit weights for compaction control purposes.

Three-dimensional diagrams were plotted to illustrate and examine the variation of soil stiffness with matric suction and net stress. Generally, the soil stiffness increased as the matric suction increased, at a decreasing rate. Stiffness also increased as the net stress increased. The variations of soil stiffness with matric suction and net stress for specimens compacted at similar degrees of saturation were different from that observed for specimens compacted at similar compactive efforts. Accordingly, the relationships between soil stiffness, matric suction, and net stress are not unique and depend on factors such as compaction dry unit weight, degree of saturation, compactive effort, soil fabric, and overconsolidation ratio. Similar observations were reported in the literature for coarser silts and sands, and were confirmed in this study for the clay tested.

Empirical equations proposed by Hardin and Black (1968), after modification, Picornell and Nazarian (1998), and Mendoza et al. (2005) related the shear modulus to matric suction at zero net stress. The equations proposed by Hardin and Black (1968) and Mendoza et al. (2005) could not predict the limiting value beyond which the stiffness does not increase for further increase in matric suction. The equation proposed by Picornell and Nazarian (1998) could predict the general trend for the variation of shear

modulus with matric suction at zero net stress. For practical purposes, all three equations could be used to predict soil stiffness for specimens compacted at degrees of saturation higher than 75% relatively well, up to matric suctions of about 40 psi. Empirical equations proposed by Sawangsuriya et al. (2006) and Vassallo et al. (2006) related the shear modulus to matric suction and net stress. The equation proposed by Sawangsuriya et al. (2006) did not fit the measured data well, while the equation proposed by Vassallo et al. (2006) fit the measured data relatively well for net stresses greater than zero.

14.3 Recommendations for further research

The following recommendations are suggested for further research:

- Air that diffuses through high air-entry porous stones mounted in pressure plate and suction-controlled triaxial apparatus is believed to lead to longer periods to reach equilibrium conditions. Automating the flushing procedure would allow flushing the diffused air over shorter periods, which might reduce the time required to reach equilibrium conditions.

- Compacting specimens manually did not allow higher dry unit weights to be achieved. Automating the kneading compaction procedure would allow higher compaction pressures to be applied, which would permit higher dry unit weights.

- Three-dimensional diagrams illustrating the variation of soil stiffness with matric suction and net stress for clay specimens compacted *at the same compaction water content and dry unit weight* would provide better understanding of how soil stiffness varies exclusively with matric suction and

net stress. Testing identical specimens will require use of the drained test procedure described in this dissertation. In order to use this procedure, however, some technique for reducing long equalization times will be needed. Exploration of possible alternative techniques is recommended.

- The effects of dry unit weight, water content, degree of saturation, overconsolidation ratio, and soil fabric on the relationship between soil stiffness, matric suction, and net stress are unknown and still need further investigation.

APPENDICES

Appendix A: Compaction mold

An aluminum split mold was designed and fabricated at The University of Texas at Austin. The mold consisted of four quadrants, a base, and a collar. The four quadrants were assembled using #5-40x3/4" socket head cap screws. Details of the design of the compaction mold are presented in Figures A.1 and A.2.

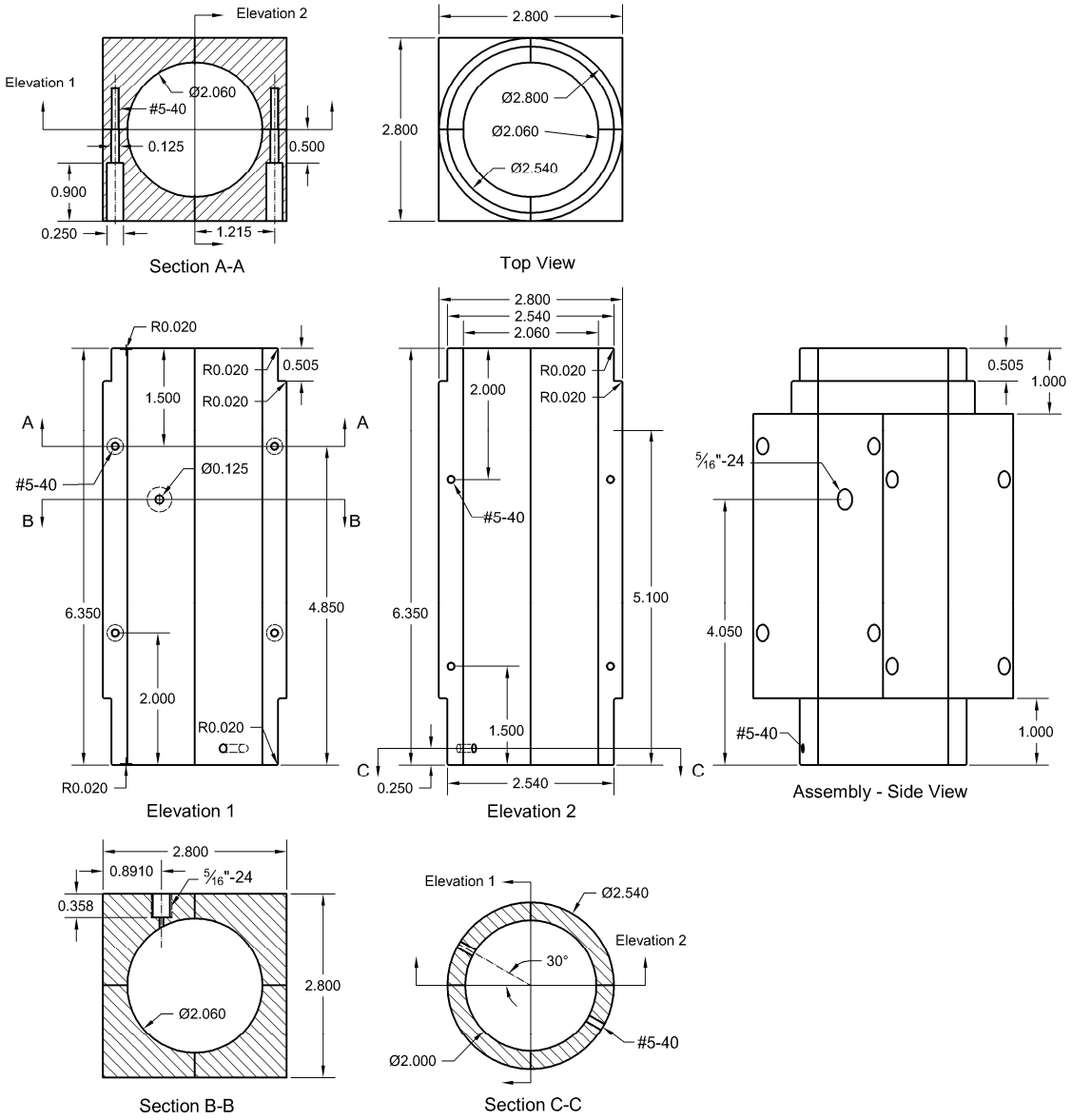

Figure A.1. Details of compaction split mold.

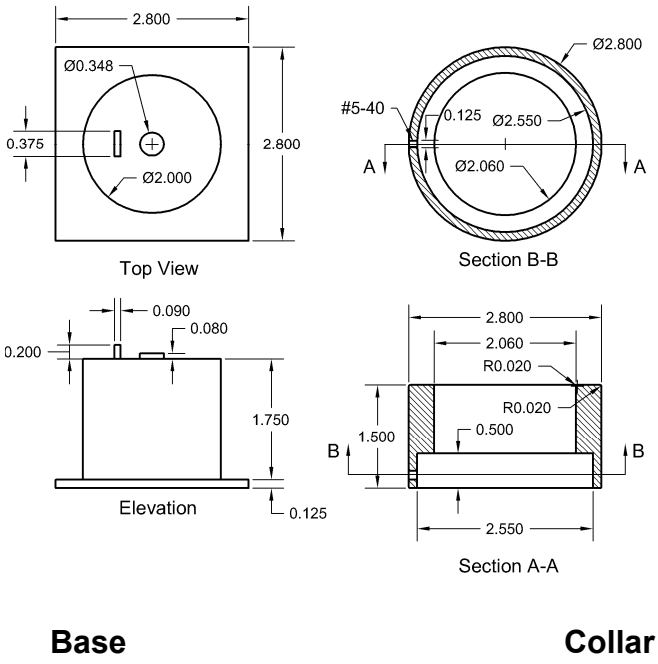

Figure A.2. Details of compaction split mold (cont'd).

Appendix B: Pressure plate platen

Two pressure plate acrylic platens were designed and fabricated at The University of Texas at Austin to measure the soil matric suction. The platens are 2 inches in diameter. Each platen has a cavity to house a high air-entry porous stone. One platen is equipped with a 5-bar high air-entry porous stone; and the other platen is equipped with a 15-bar high air-entry porous stone. Each platen was fastened to the base plate of the pressure chamber of the pressure plate apparatus with a single 1/4-20x1-1/4" socket head cap screw. Details of the design of the pressure plate platen are presented in Figure B.1.

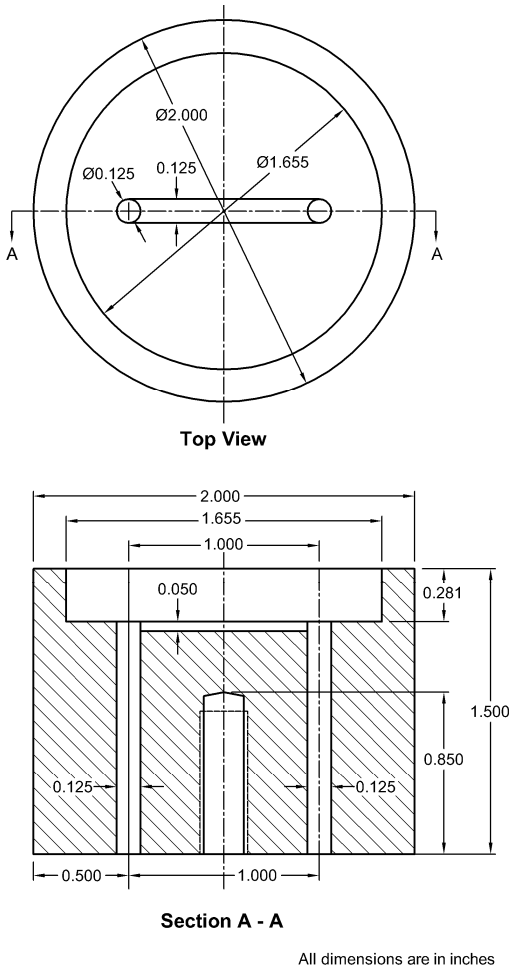

Figure B.1. Details of pressure plate platen.

Appendix C: Data acquisition and control system

A data acquisition and control system was used for all of triaxial and pressure plate tests. The system consisted of various transducers, a series of interconnected modules for data logging and controlling, and a personal computer.

C.1 INSTRUMENTATION

Instrumentation included pressure transducers, load cells, displacement transducers, and a temperature sensor. A brief description of the accuracy and calibration of the various devices is presented in the following sections.

C.1.1 Pressure transducers

A total of twelve Validyne Engineering Corp. and four Geotac Co. pressure transducers was used to measure pressures in the various tests. All pressure transducers were calibrated periodically. The pressure transducers used for measuring air and/or water pressures were calibrated using a precision test gage with pressure range of 0 to 100 psi divided into 0.1-psi subdivisions. The differential pressure transducers used for measuring volume changes were calibrated using a 25-ml double walled burette. Table C.1 summarizes the different types of pressure transducers including the manufacturer, model, range, accuracy specified by the manufacturer, and the maximum error measured during calibration. The maximum errors measured during calibration were within the limits specified by the manufacturer except for the Validyne pressure transducer model DP15-46, where the errors were still in an acceptable range.

Table C.1. Manufacturers, models, ranges, and accuracies of pressure transducers.

Manufacturer	Model	Range	Accuracy (from specifications)	Maximum error during calibration
Validyne Engineering Corp.	DP15-32	± 2 psi	± 0.018 in^3	0.012 in^3
Validyne Engineering Corp.	DP15-40	± 12.5	± 0.03 psi	0.031 psi
Validyne Engineering Corp.	DP15-46	± 50 psi	± 0.125 psi	0.283 psi
Validyne Engineering Corp.	DP15-50	± 100 psi	± 0.31 psi	0.32 psi
Geotac Co.	PS150	± 150 psi	± 0.375 psi	0.311 psi
Geotac Co.	PS100	± 100 psi	± 0.3 psi	0.25 psi

C.1.2 Load cells

Two Lebow Products Inc. load cells were used to measure load in the triaxial tests. The load cells were calibrated in compression periodically using known weights. Table C.2 summarizes data for the two load cells with the manufacturer, model, range, accuracy specified by the manufacturer, and the maximum error measured during calibration. The maximum errors measured during calibration were within the limits specified by the manufacturer.

Table C.2. Manufacturers, models, ranges, and accuracies of load cells.

Manufacturer	Model	Range	Accuracy (from specifications)	Maximum error during calibration
Lebow Products Inc.	3167	± 300 lb	± 0.15 lb	0.15 lb
Lebow Products Inc.	3143-1K	± 1000 lb	± 0.6 lb	0.4 lb

C.1.3 Displacement transducers

One Trans-Tek Inc. and one Geotac Co. linear variable differential transformers (LVDTs) were used to measure the axial deformation of specimens in triaxial tests. The LVDTs were calibrated periodically using a micrometer with a full displacement range of

50 mm (2 inches) and 0.0001 mm subdivisions. Table C.3 summarizes data for the two LVDTs with the manufacturer, model, range, accuracy specified by the manufacturer, and the maximum error measured during calibration. The maximum errors measured during calibration were within the limits specified by the manufacturer.

Table C.3. Manufacturers, models, ranges, and accuracies of LVDTs.

Manufacturer	Model	Range	Accuracy (from specifications)	Maximum error during calibration
Trans-Tek Inc.	0243-	± 0.75 in	± 0.00375 in	0.001 in
Geotac Co.	LPT3	± 3 in	± 0.003 in	0.0007 in

C.1.4 Temperature sensor

A Geotac Co., model TEMP-022 temperature sensor was used to measure temperature changes in the lab during all tests. The sensor had a working range from 0 to 100 degrees Celsius. The accuracy of the temperature sensor as specified by the manufacturer was $\pm$ 0.25 degree Celsius.

C.2 DATA ACQUISITION MODULES AND SOFTWARE

A series of Geotac Co. interconnected modules was used to control the load frame and the two flow pumps and for data collection. The modules were connected to the computer via a serial (COM) port. Each module was automatically assigned a unique address by the computer at power-up. The load frame and the two flow pumps were controlled via three modules. An additional four modules provided twenty channels of analog data acquisition. The data were collected at a sample rate of 80 readings per second per channel at a resolution of 22 bits. Input signal ranges could be independently set for individual channels at $\pm$ 10V, $\pm$ 1V, $\pm$ 0.1V, and $\pm$ 0.01V. The modules provided

either 5 or 10 VDC for sensor excitation. A linear regulated DC power supply was used to provide power to all modules and for sensors excitation.

Geotac Co. *TruePath* software was used to operate the load frame and the two flow pumps and to acquire and record data from all sensors. *TruePath* software is a *Microsoft Windows* based 32-bit program. Data acquired during the tests were presented live on the computer screen and recorded in tab-limited ASCII text files for further analyses.

Appendix D: Measurements of matric suction in pressure plate tests

Matric suctions measured in the pressure plate tests using the axis translation technique are summarized in Table D.1. In addition, the compaction water content, dry unit weight, and degree of saturation for each test are included. Each test is defined by a Test ID, which is expressed as: pressure plate (PP) – compaction water content in % - pressure applied to the air piston during compaction in psi, followed by (#) if 2 specimens had similar compaction water contents and pressures. The time response curves for matric suction measurements of all tests are presented in this appendix.

Table D.1. Test ID, compaction conditions, and matric suction measurements in pressure plate tests.

Test ID	Water content, w, (%)	Dry unit weight, γ_{dry}, (pcf)	Degree of saturation, S, (%)	Matric suction, (psi)
PP-12%-15psi#1	11.7	91.7	37.8	87.0
PP-12%-15psi#2	12.0	91.4	38.5	86.6
PP-12%-25psi	11.5	96.4	41.6	84.5
PP-12%-35psi	11.5	101.5	47.0	78.4
PP-13%-15psi	12.5	91.1	39.6	71.6
PP-13%-25psi	12.6	97.8	46.9	70.0
PP-13%-35psi	12.5	101.4	51.2	70.6
PP-13%-40psi#1	12.7	102.7	53.6	70.3
PP-13%-40psi#2	13.2	108.0	63.7	52.3
PP-14%-15psi#1	13.8	92.9	45.7	63.8
PP-14%-15psi#2	14.0	94.6	48.3	49.7
PP-14%-25psi#1	14.0	101.6	57.6	50.4
PP-14%-25psi#2	14.1	101.7	58.0	50.7
PP-14%-35psi#1	14.1	107.5	67.1	45.1
PP-14%-35psi#2	14.4	110.0	73.2	49.0
PP-14%-40psi	14.1	109.1	70.0	46.6
PP-15%-10psi	14.6	95.5	51.6	42.5
PP-15%-15psi#1	14.6	91.8	47.1	46.2
PP-15%-15psi#2	15.3	97.3	56.4	44.2
PP-15%-40psi	15.4	112.4	83.4	48.1
PP-16%-10psi	16.4	94.5	56.5	35.1
PP-16%-15psi#1	15.9	100.2	62.9	39.3
PP-16%-15psi#2	16.4	102.5	69.0	28.9

Test ID	Water content, w, (%)	Dry unit weight, γ_{dry}, (pcf)	Degree of saturation, S, (%)	Matric suction, (psi)
PP-16%-25psi#1	15.7	105.7	71.4	39.4
PP-16%-25psi#2	16.2	107.9	78.1	29.3
PP-16%-35psi	15.8	109.7	79.6	43.0
PP-16%-40psi	16.1	112.4	87.3	27.7
PP-17%-10psi	17.3	96.9	63.2	63.2
PP-17%-35psi	16.5	112.2	88.7	24.3
PP-18%-10psi	18.0	98.3	68.1	22.2
PP-18%-15psi	18.0	104.9	80.0	20.4
PP-18%-25psi	17.5	108.3	85.3	20.3
PP-18%-35psi	18.0	109.4	90.1	17.5
PP-18%-40psi	17.9	110.0	90.8	17.2
PP-19%-15psi	18.5	101.8	76.3	20.4
PP-19%-25psi	19.4	105.7	91.2	10.9
PP-20%-10psi	20.2	98.9	77.4	13.2
PP-20%-15psi	20.2	103.6	87.2	12.6
PP-20%-25psi	20.3	104.5	89.6	15.3
PP-21%-10psi	21.4	100.7	85.7	10.7
PP-21%-15psi#1	20.5	103.4	87.9	12.3
PP-21%-15psi#2	20.7	103.2	88.3	11.2
PP-21%-15psi#3	21.4	101.5	87.4	6.6
PP-22%-7psi	22.1	98.0	83.1	7.0
PP-22%-15psi	22.2	100.8	89.3	8.7
PP-22%-20psi	21.5	102.7	90.6	11.0
PP-23%-15psi	23.2	98.5	88.3	3.7
PP-24%-7psi	24.1	91.7	90.8	4.5

Test ID: PP-12%-15psi#1
Water content: 11.7%
Dry unit weight: 91.7 pcf
Degree of saturation: 37.8%
Matric suction: 87.0 psi
Notes: 1. Specimen compacted on the dry side of the line of optimums. 2. Air diffused through the high-air entry porous stone near the end of the test. Periodical flushing of the diffused air caused irregularities in the curve.

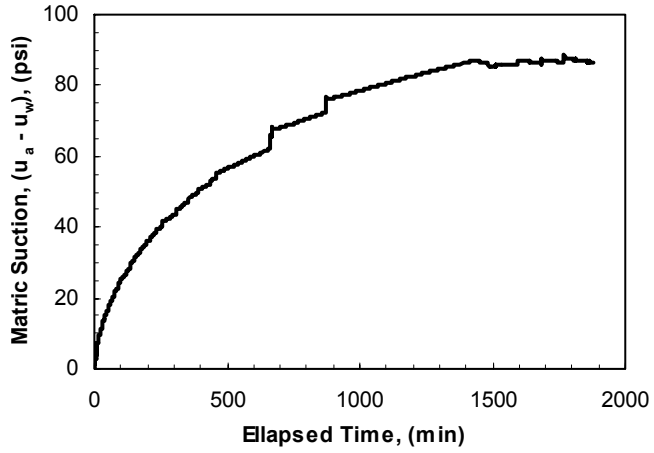

Test ID: PP-12%-15psi#2
Water content: 12%
Dry unit weight: 91.4 pcf
Degree of saturation: 38.5%
Matric suction: 86.6 psi
Notes: 1. Specimen compacted on the dry side of the line of optimums. 2. The pore-water pressure transducer stopped responding when the output voltage reached a value corresponding to a pore-water pressure of -0.6 psi. Two flat segments were observed in the curve before reaching equilibrium.

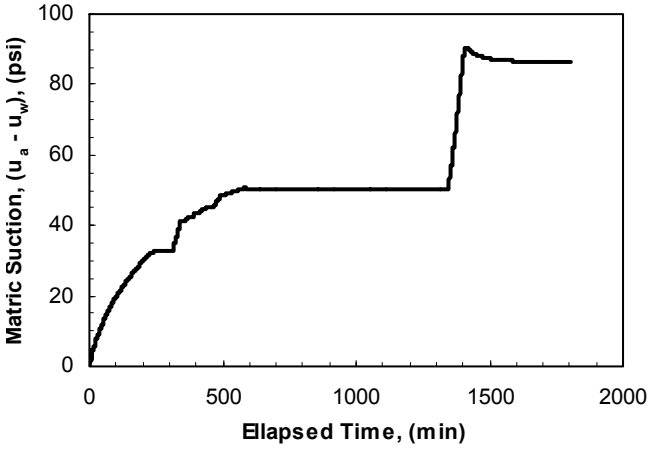

Test ID: PP-12%-25psi
Water content: 11.5%
Dry unit weight: 96.4 pcf
Degree of saturation: 41.6%
Matric suction: 84.5 psi
Notes: 1. Specimen compacted on the dry side of the line of optimums.

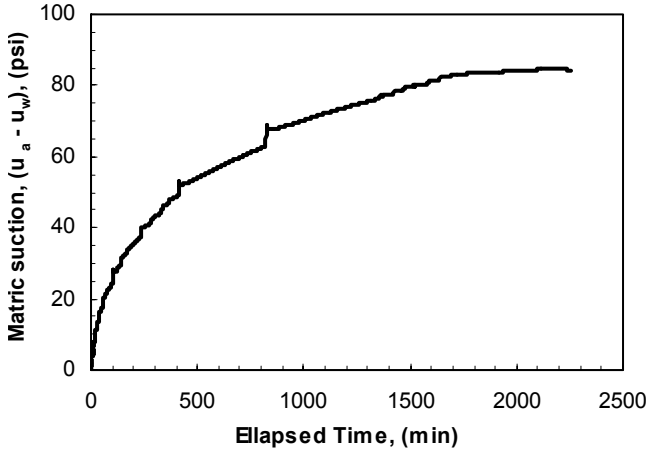

Test ID: PP-12%-35psi
Water content: 11.5%
Dry unit weight: 101.5 pcf
Degree of saturation: 47.0%
Matric suction: 78.4 psi
Notes: 1. Specimen compacted on the dry side of the line of optimums.

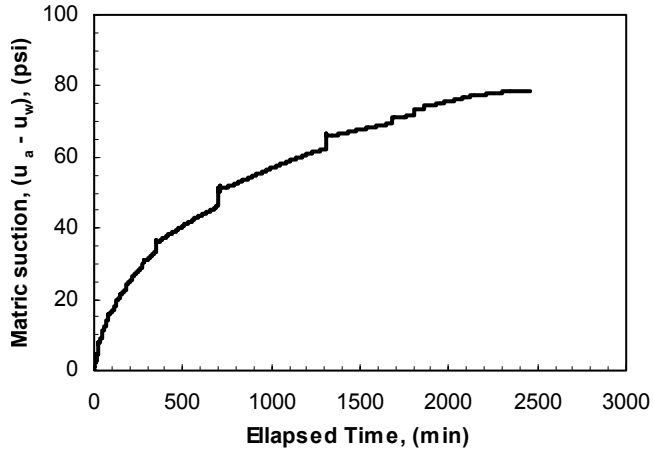

Test ID: PP-13%-15psi
Water content: 12.5%
Dry unit weight: 91.1 pcf
Degree of saturation: 39.6%
Matric suction: 71.6 psi
Notes: 1. Specimen compacted on the dry side of the line of optimums.

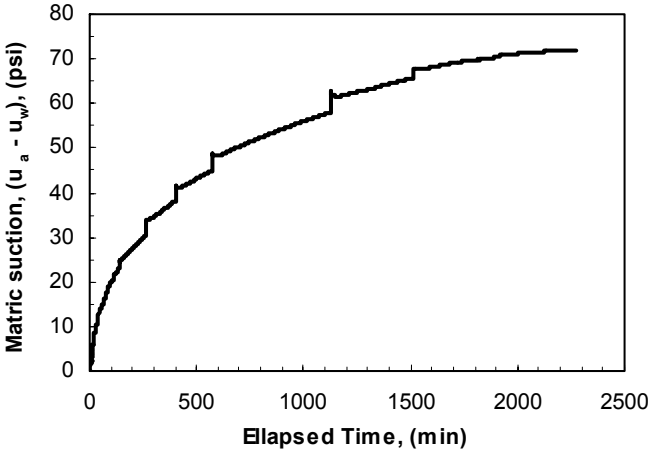

Test ID: PP-13%-25psi
Water content: 12.6%
Dry unit weight: 97.8 pcf
Degree of saturation: 46.9%
Matric suction: 70.0 psi
Notes: 1. Specimen compacted on the dry side of the line of optimums.

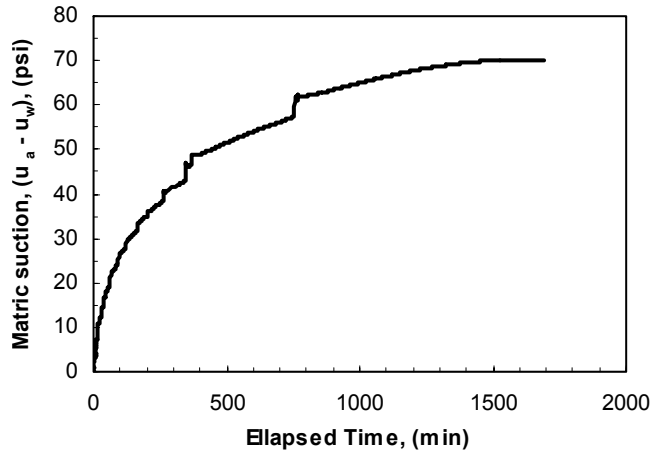

Test ID: PP-13%-35psi
Water content: 12.5%
Dry unit weight: 101.4 pcf
Degree of saturation: 51.2%
Matric suction: 70.6 psi
Notes: 1. Specimen compacted on the dry side of the line of optimums.

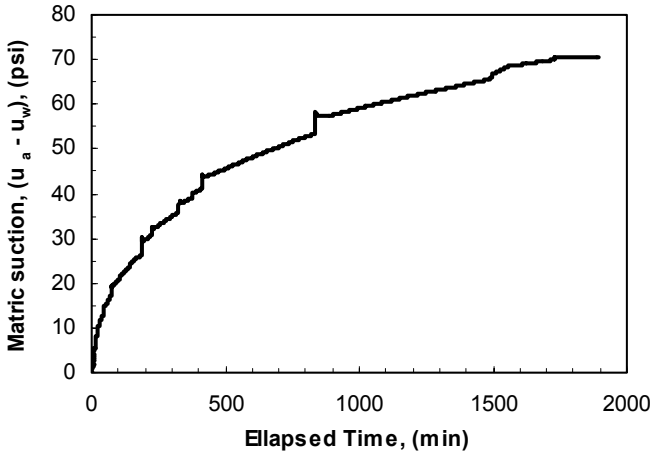

Test ID: PP-13%-40psi#1
Water content: 12.7%
Dry unit weight: 102.7 pcf
Degree of saturation: 53.6%
Matric suction: 70.3 psi
Notes: 1. Specimen compacted on the dry side of the line of optimums.

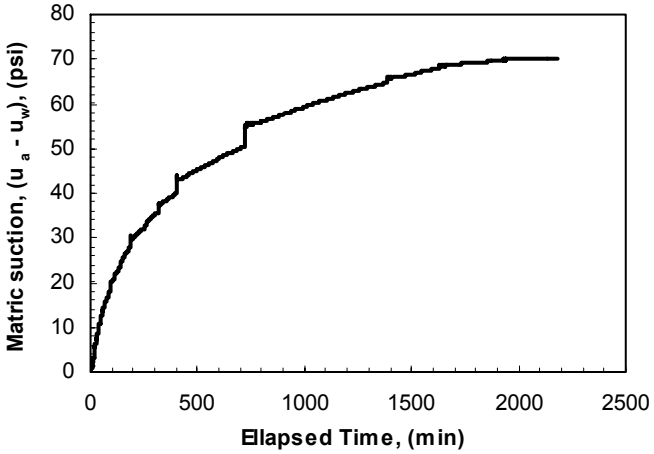

Test ID: PP-13%-40psi#2
Water content: 13.2%
Dry unit weight: 108.0 pcf
Degree of saturation: 63.7%
Matric suction: 52.3 psi
Notes: 1. Specimen compacted on the dry side of the line of optimums.

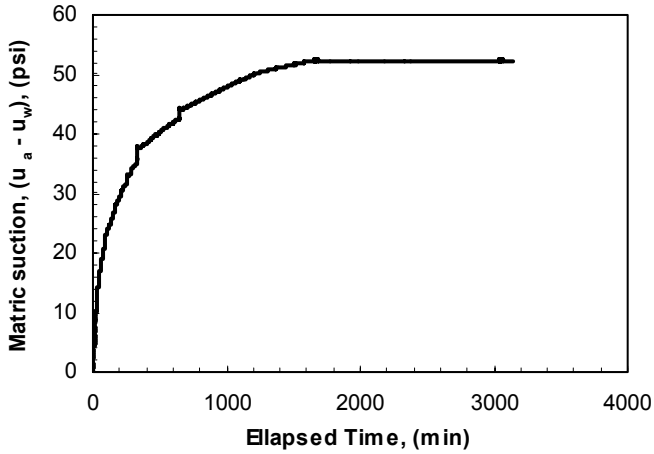

Test ID: PP-14%-15psi#1
Water content: 13.8%
Dry unit weight: 92.9 pcf
Degree of saturation: 45.7%
Matric suction: 63.8 psi
Notes: 1. Specimen compacted on the dry side of the line of optimums. 2. Air diffused through the high-air entry porous stone near the end of the test. Periodical flushing of the diffused air caused irregularities in the curve.

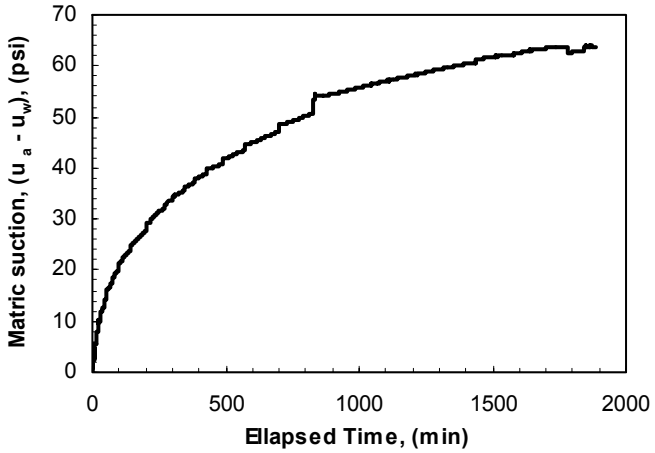

Test ID: PP-14%-15psi#2
Water content: 14.0%
Dry unit weight: 94.6 pcf
Degree of saturation: 48.3%
Matric suction: 49.7 psi
Notes: 1. Specimen compacted on the dry side of the line of optimums.

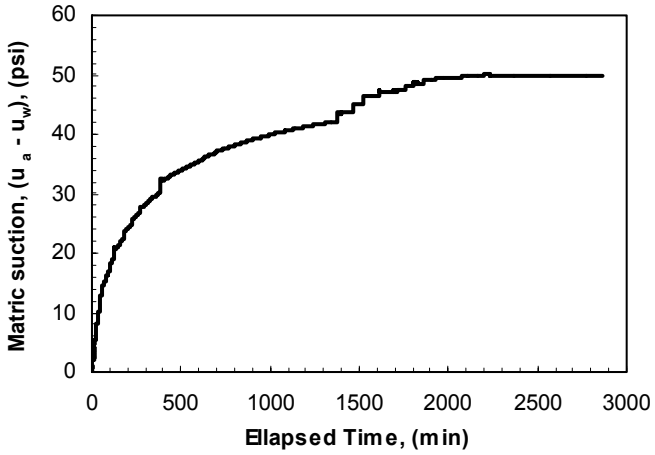

Test ID: PP-14%-25psi#1
Water content: 14.0%
Dry unit weight: 101.6 pcf
Degree of saturation: 57.6%
Matric suction: 50.4 psi
Notes: 1. Specimen compacted on the dry side of the line of optimums.

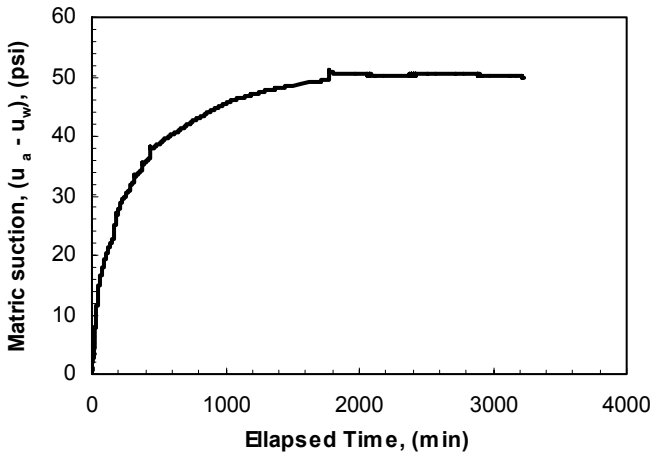

Test ID: PP-14%-25psi#2
Water content: 14.1%
Dry unit weight: 101.7 pcf
Degree of saturation: 58.0%
Matric suction: 50.7 psi
Notes: 1. Specimen compacted on the dry side of the line of optimums.

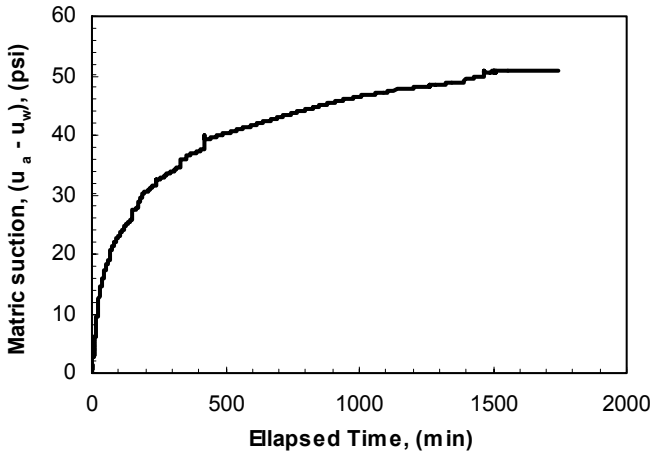

Test ID: PP-14%-35psi#1
Water content: 14.1%
Dry unit weight: 107.5 pcf
Degree of saturation: 67.1%
Matric suction: 45.1 psi
Notes: 1. Specimen compacted on the dry side of the line of optimums.

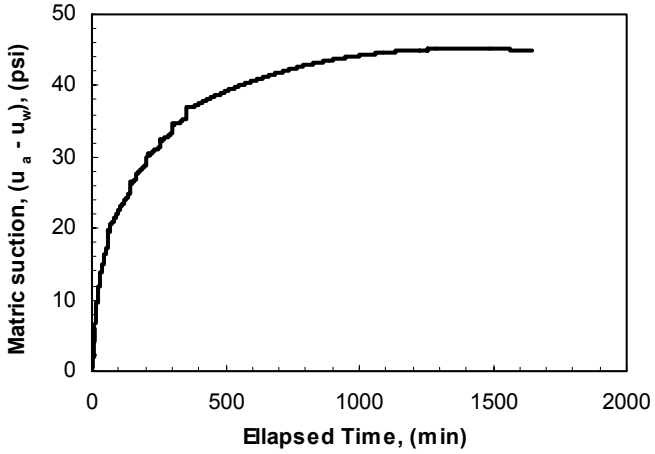

Test ID: PP-14%-35psi#2
Water content: 14.4%
Dry unit weight: 110.0 pcf
Degree of saturation: 73.2%
Matric suction: 49.0 psi
Notes: 1. Specimen compacted on the dry side of the line of optimums.

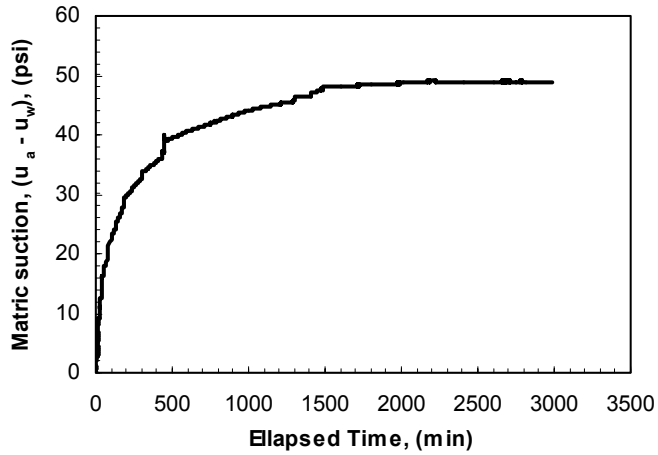

Test ID: PP-14%-40psi
Water content: 14.1%
Dry unit weight: 109.1 pcf
Degree of saturation: 70.0%
Matric suction: 46.6 psi
Notes: 1. Specimen compacted on the dry side of the line of optimums.

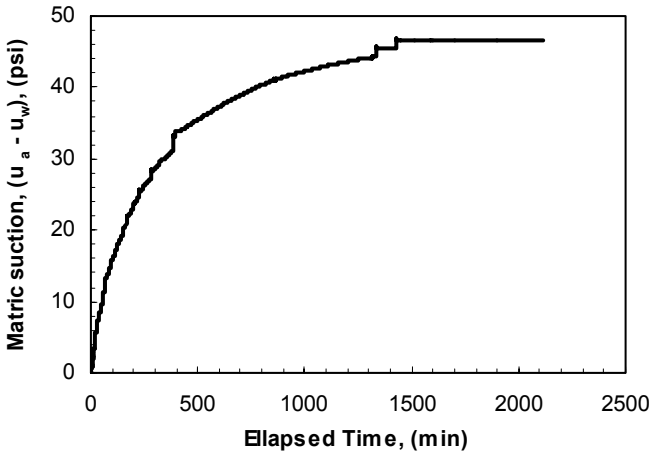

Test ID: PP-15%-10psi
Water content: 14.6%
Dry unit weight: 95.5 pcf
Degree of saturation: 51.6%
Matric suction: 42.5 psi
Notes: 1. Specimen compacted on the dry side of the line of optimums.

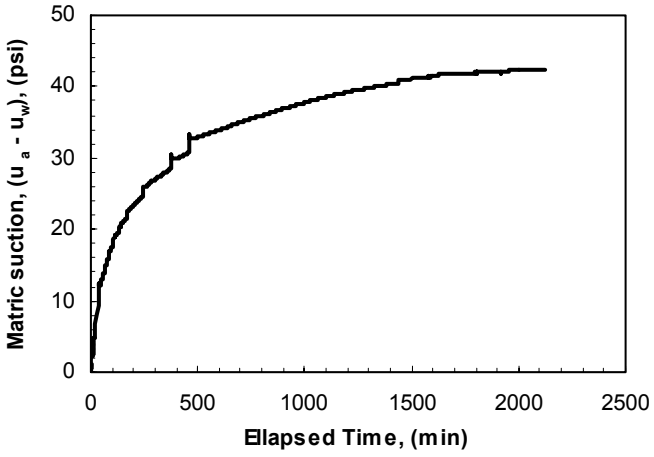

Test ID: PP-15%-15psi#1
Water content: 14.6%
Dry unit weight: 91.8 pcf
Degree of saturation: 47.1%
Matric suction: 46.2 psi
Notes: 1. Specimen compacted on the dry side of the line of optimums.

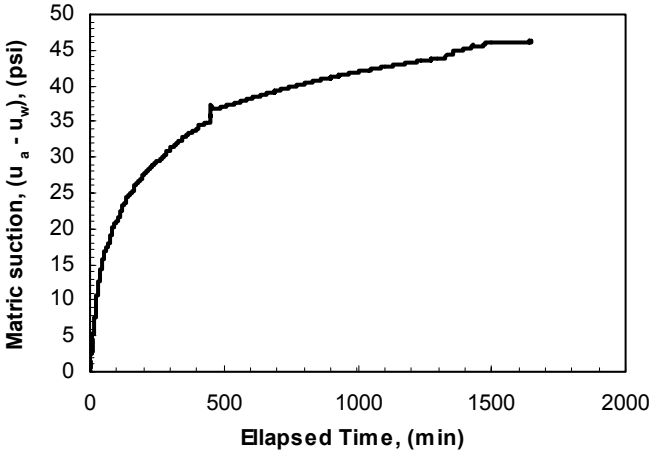

Test ID: PP-15%-15psi#2
Water content: 15.3%
Dry unit weight: 97.3 pcf
Degree of saturation: 56.4%
Matric suction: 44.2 psi
Notes: 1. Specimen compacted on the dry side of the line of optimums.

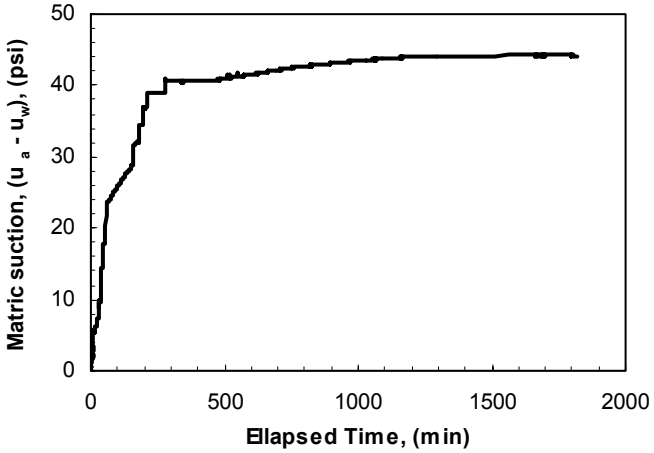

Test ID: PP-15%-40psi
Water content: 15.4%
Dry unit weight: 112.4 pcf
Degree of saturation: 83.4%
Matric suction: 48.1 psi
Notes: 1. Specimen compacted on the dry side of the line of optimums. 2. Sudden drop in matric suction due to a procedural error during the test.

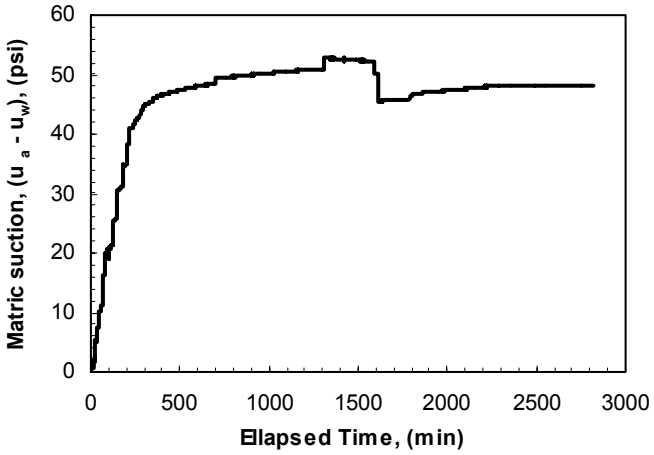

Test ID: PP-16%-10psi
Water content: 16.4%
Dry unit weight: 94.5 pcf
Degree of saturation: 56.5%
Matric suction: 35.1 psi
Notes: 1. Specimen compacted on the dry side of the line of optimums.

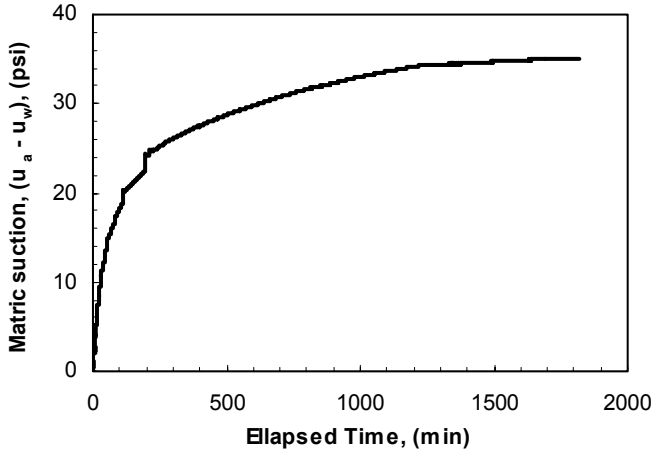

Test ID: PP-16%-15psi#1
Water content: 15.9%
Dry unit weight: 100.2 pcf
Degree of saturation: 62.9%
Matric suction: 39.3 psi
Notes: 1. Specimen compacted on the dry side of the line of optimums.

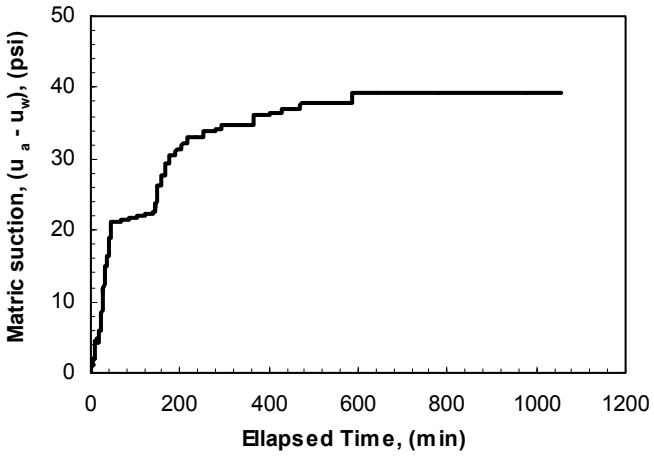

Test ID: PP-16%-15psi#2
Water content: 16.4%
Dry unit weight: 102.5 pcf
Degree of saturation: 69.0%
Matric suction: 28.9 psi
Notes: 1. Specimen compacted on the dry side of the line of optimums.

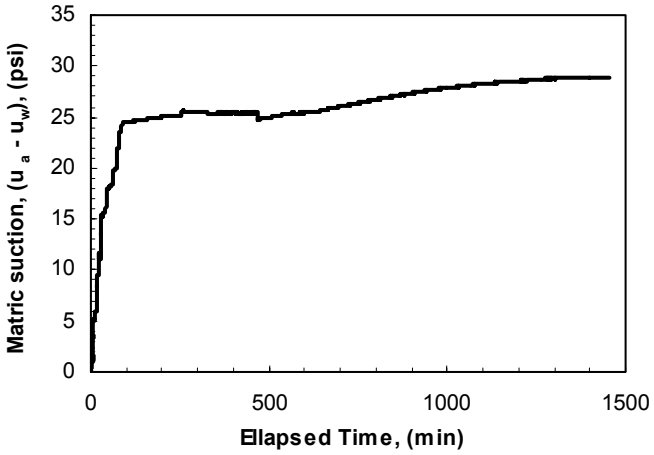

Test ID: PP-16%-25psi#1
Water content: 15.7%
Dry unit weight: 105.7 pcf
Degree of saturation: 71.4%
Matric suction: 39.4 psi
Notes: 1. Specimen compacted on the dry side of the line of optimums.

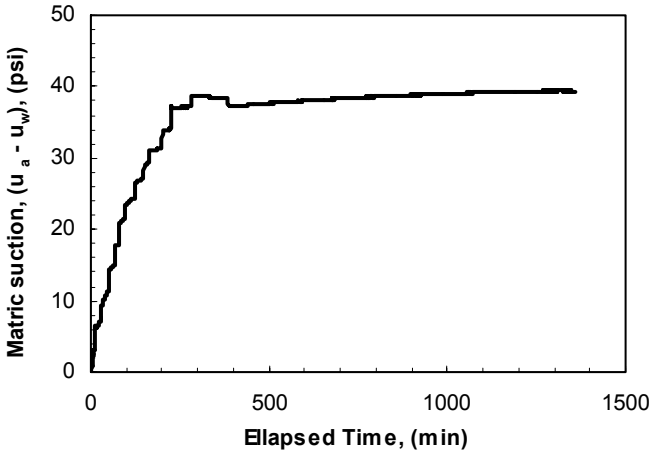

Test ID: PP-16%-25psi#2
Water content: 16.3%
Dry unit weight: 107.9 pcf
Degree of saturation: 78.1%
Matric suction: 29.3 psi
Notes: 1. Specimen compacted on the dry side of the line of optimums.

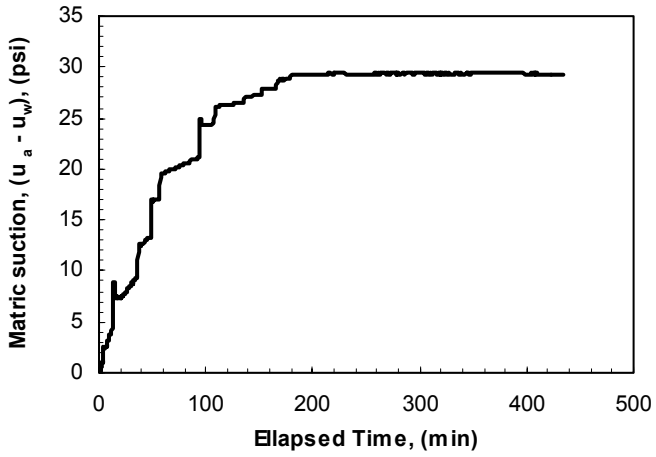

Test ID: PP-16%-35psi
Water content: 15.8%
Dry unit weight: 109.7 pcf
Degree of saturation: 79.6%
Matric suction: 43.0 psi
Notes: 1. Specimen compacted on the dry side of the line of optimums.

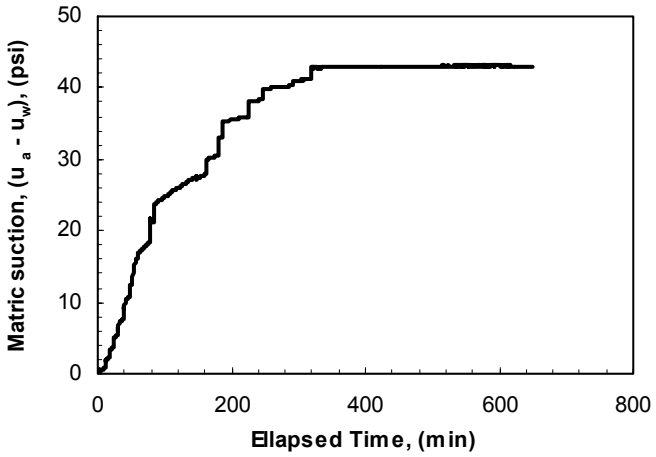

Test ID: PP-16%-40psi
Water content: 16.1%
Dry unit weight: 112.4 pcf
Degree of saturation: 87.3%
Matric suction: 27.7 psi
Notes: 1. Specimen compacted on the wet side of the line of optimums. 2. Matric suction slightly peaked before reaching equilibrium. Pore-air pressure, controlled manually, exceeded the pressure required to prevent the specimen from sucking water from the porous stone. Pore-water pressure increased gradually until equilibrium was achieved.

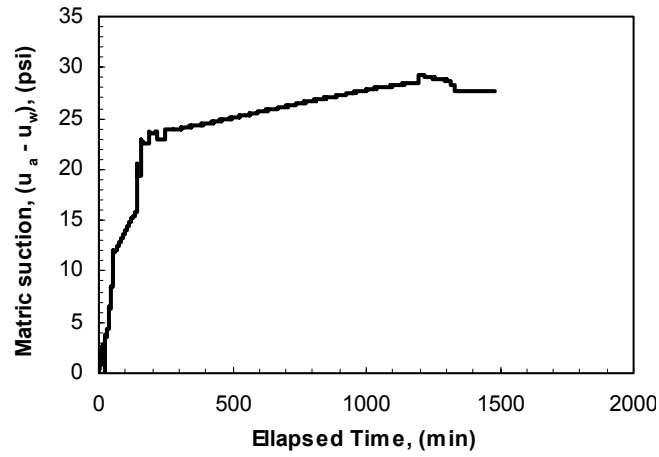

Test ID: PP-17%-10psi
Water content: 17.3%
Dry unit weight: 96.9 pcf
Degree of saturation: 63.2%
Matric suction: 30.8 psi
Notes: 1. Specimen compacted on the dry side of the line of optimums.

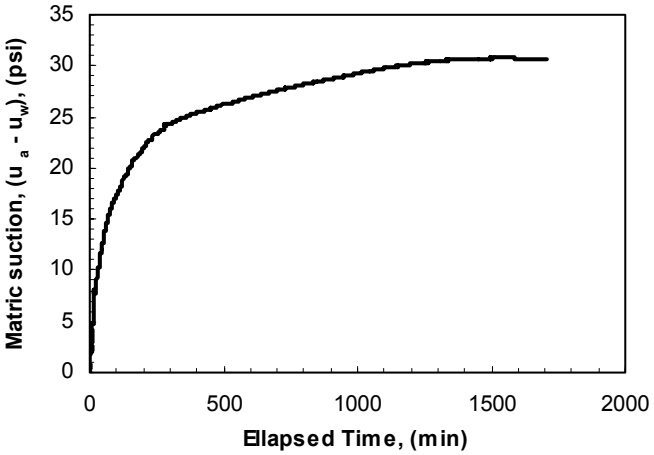

Test ID: PP-17%-35psi
Water content: 16.5%
Dry unit weight: 112.2 pcf
Degree of saturation: 88.7%
Matric suction: 24.3 psi
Notes: 1. Specimen compacted on the wet side of the line of optimums. 2. Matric suction slightly peaked before reaching equilibrium. Pore-air pressure, controlled manually, exceeded the pressure required to prevent the specimen from sucking water from the porous stone. Pore-water pressure increased gradually until equilibrium was achieved.

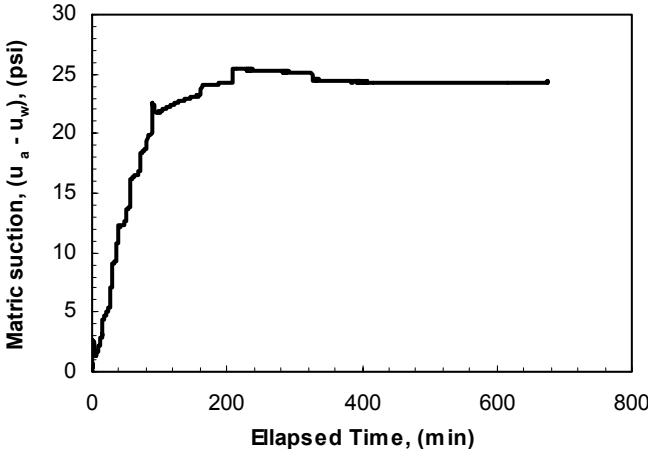

Test ID: PP-18%-10psi
Water content: 18.0%
Dry unit weight: 98.3 pcf
Degree of saturation: 68.1%
Matric suction: 22.2 psi
Notes: 1. Specimen compacted on the dry side of the line of optimums. 2. Sudden drop in matric suction due to a procedural error during the test.

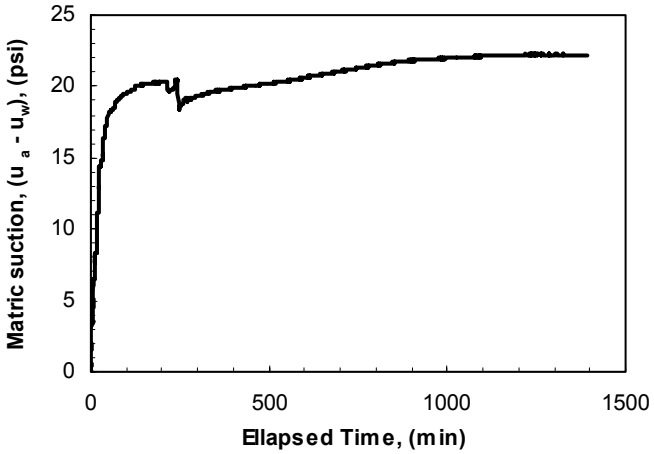

Test ID: PP-18%-15psi
Water content: 18.0%
Dry unit weight: 104.9 pcf
Degree of saturation: 80.0%
Matric suction: 20.4 psi
Notes: 1. Specimen compacted on the dry side of the line of optimums. 2. Matric suction slightly peaked before reaching equilibrium. Pore-air pressure, controlled manually, exceeded the pressure required to prevent the specimen from sucking water from the porous stone. Pore-water pressure increased gradually until equilibrium was achieved.

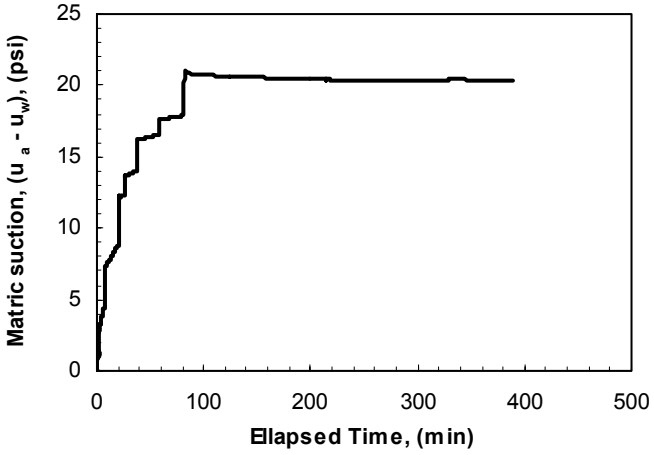

Test ID: PP-18%-25psi
Water content: 17.5%
Dry unit weight: 108.3 pcf
Degree of saturation: 85.3%
Matric suction: 20.3 psi
Notes: 1. Specimen compacted on the dry side of the line of optimums.

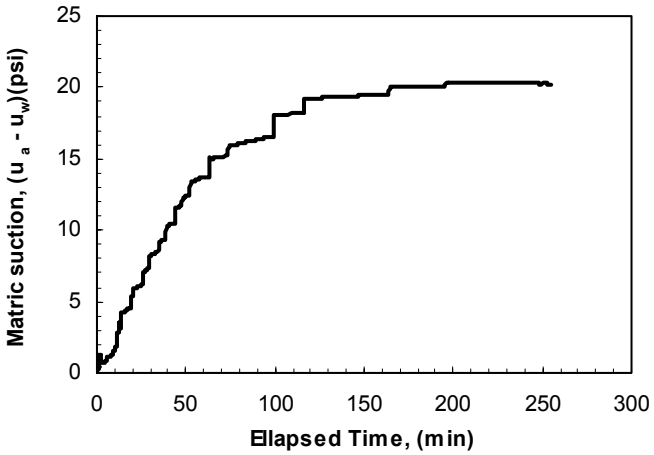

Test ID: PP-18%-35psi
Water content: 18.0%
Dry unit weight: 109.4 pcf
Degree of saturation: 90.1%
Matric suction: 17.5 psi
Notes: 1. Specimen compacted on the wet side of the line of optimums.

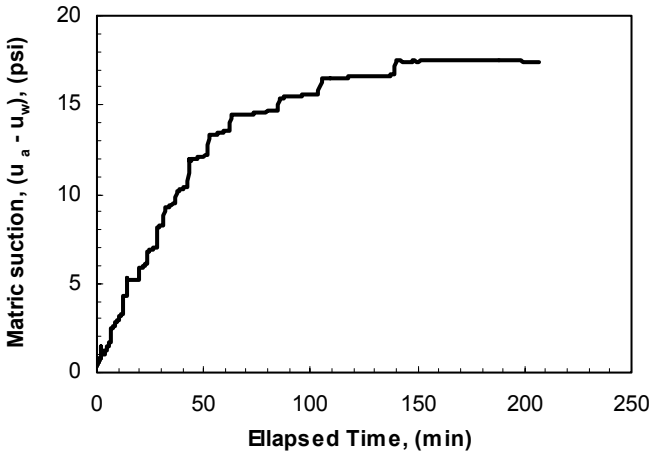

Test ID: PP-18%-40psi
Water content: 17.9%
Dry unit weight: 110.0 pcf
Degree of saturation: 90.8%
Matric suction: 17.2 psi
Notes: 1. Specimen compacted on the wet side of the line of optimums.

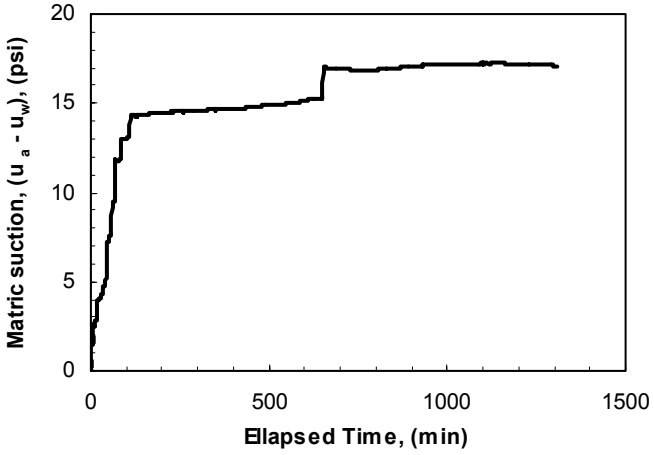

Test ID: PP-19%-15psi
Water content: 18.5%
Dry unit weight: 101.8 pcf
Degree of saturation: 76.3%
Matric suction: 20.4 psi
Notes: 1. Specimen compacted on the dry side of the line of optimums.

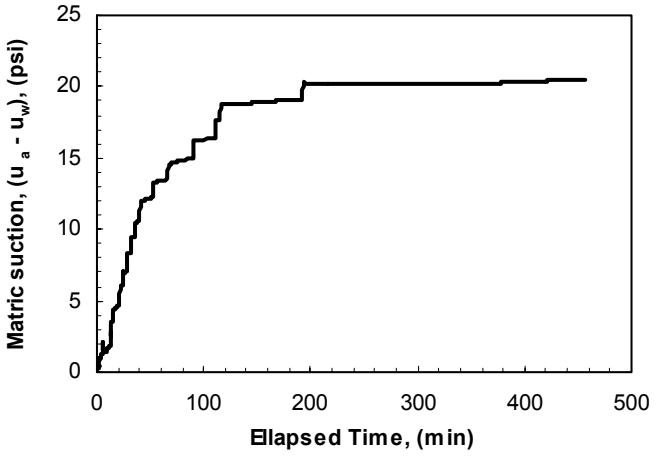

Test ID: PP-19%-25psi
Water content: 19.4%
Dry unit weight: 105.7 pcf
Degree of saturation: 91.2%
Matric suction: 10.9 psi
Notes: 1. Specimen compacted on the wet side of the line of optimums. 2. Matric suction peaked before reaching equilibrium. Pore-air pressure, controlled manually, exceeded the pressure required to prevent the specimen from sucking water from the porous stone. Pore-water pressure increased gradually until equilibrium was achieved.

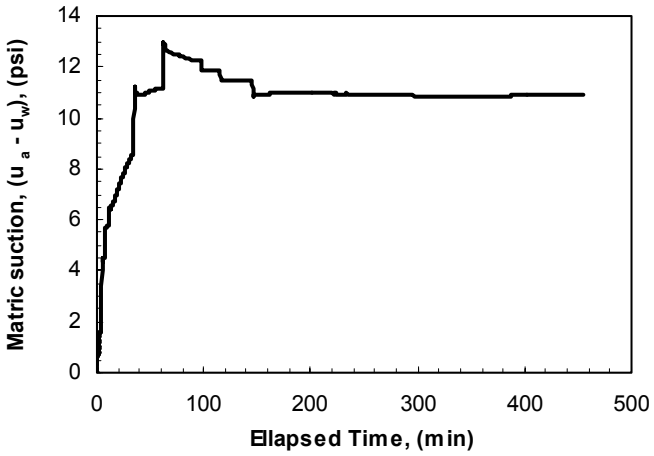

Test ID: PP-20%-10psi
Water content: 20.2%
Dry unit weight: 98.9 pcf
Degree of saturation: 77.4%
Matric suction: 13.2 psi
Notes: 1. Specimen compacted on the dry side of the line of optimums.

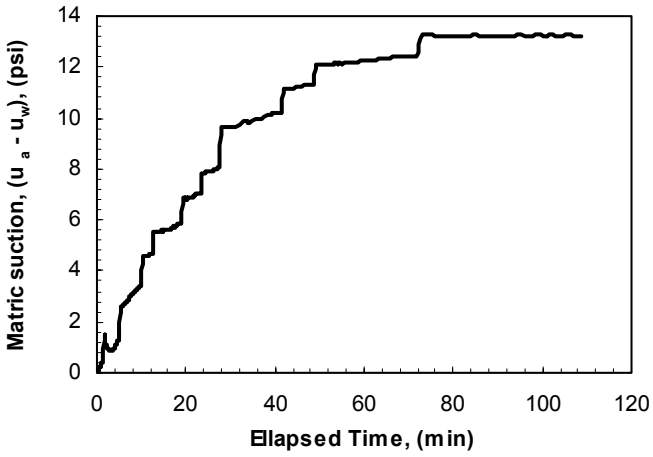

Test ID: PP-20%-15psi
Water content: 20.2%
Dry unit weight: 103.6 pcf
Degree of saturation: 87.2%
Matric suction: 12.6 psi
Notes: 1. Specimen compacted on the wet side of the line of optimums.

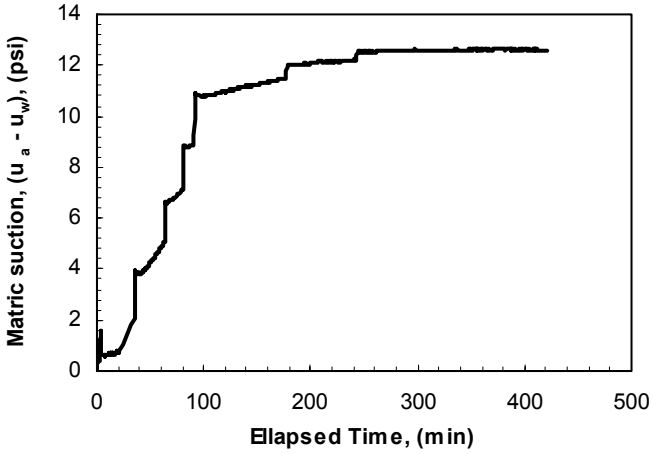

Test ID: PP-20%-25psi
Water content: 20.3%
Dry unit weight: 104.5 pcf
Degree of saturation: 89.6%
Matric suction: 15.3 psi
Notes: 1. Specimen compacted on the wet side of the line of optimums.

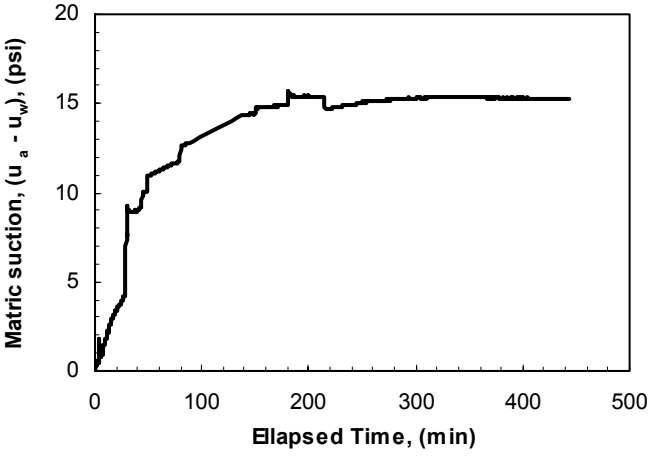

Test ID: PP-21%-10psi
Water content: 21.4%
Dry unit weight: 100.7 pcf
Degree of saturation: 85.7%
Matric suction: 10.7 psi
Notes: 1. Specimen compacted on the dry side of the line of optimums.

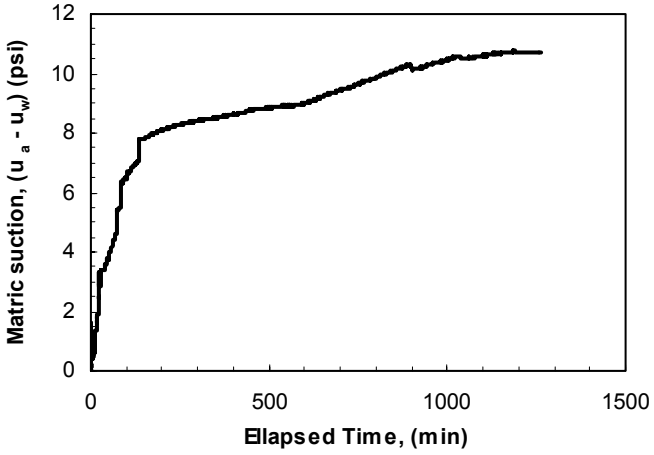

Test ID: PP-21%-15psi#1
Water content: 20.5%
Dry unit weight: 103.4 pcf
Degree of saturation: 87.9%
Matric suction: 12.3 psi
Notes: 1. Specimen compacted on the wet side of the line of optimums.

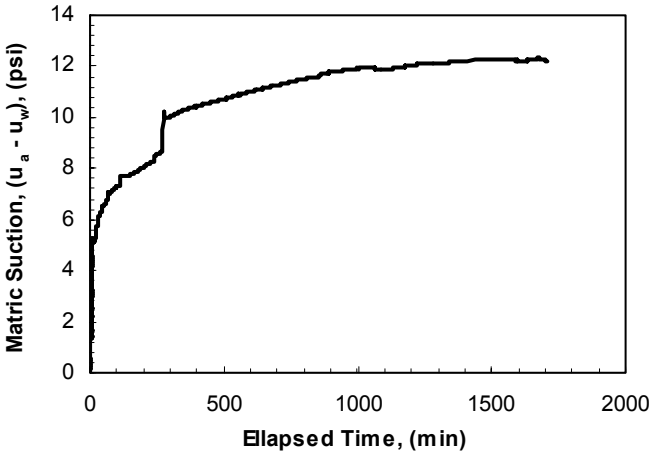

Test ID: PP-21%-15psi#2
Water content: 20.7%
Dry unit weight: 103.2 pcf
Degree of saturation: 88.3%
Matric suction: 11.2 psi
Notes: 1. Specimen compacted on the wet side of the line of optimums. 2. Matric suction peaked before reaching equilibrium. Pore-air pressure, controlled manually, exceeded the pressure required to prevent the specimen from sucking water from the porous stone. Pore-water pressure increased gradually until equilibrium was achieved.

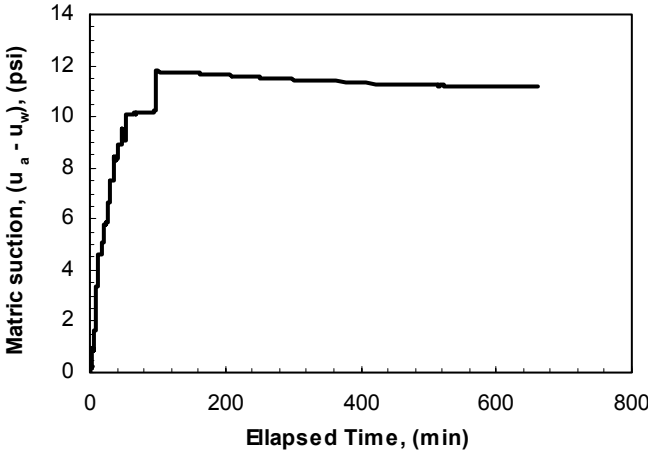

Test ID: PP-21%-15psi#3
Water content: 21.4%
Dry unit weight: 101.5 pcf
Degree of saturation: 87.4%
Matric suction: 6.6 psi
Notes: 1. Specimen compacted on the wet side of the line of optimums.

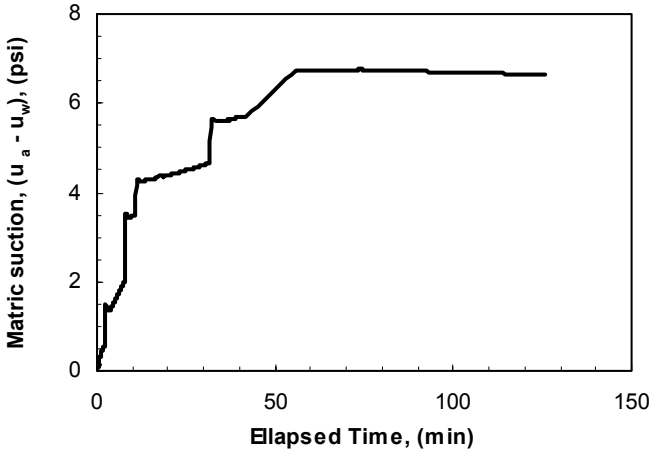

Test ID: PP-22%-7psi
Water content: 22.1%
Dry unit weight: 98.0 pcf
Degree of saturation: 83.1%
Matric suction: 7.0 psi
Notes: 1. Specimen compacted on the dry side of the line of optimums.

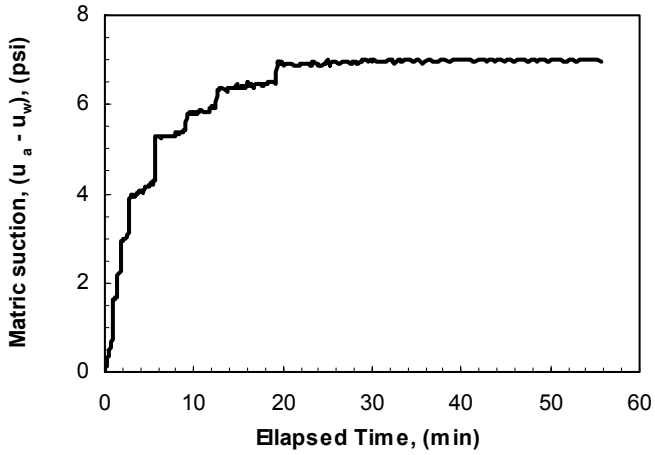

Test ID: PP-22%-15psi
Water content: 22.2%
Dry unit weight: 100.8 pcf
Degree of saturation: 89.3%
Matric suction: 8.7 psi
Notes: 1. Specimen compacted on the wet side of the line of optimums.

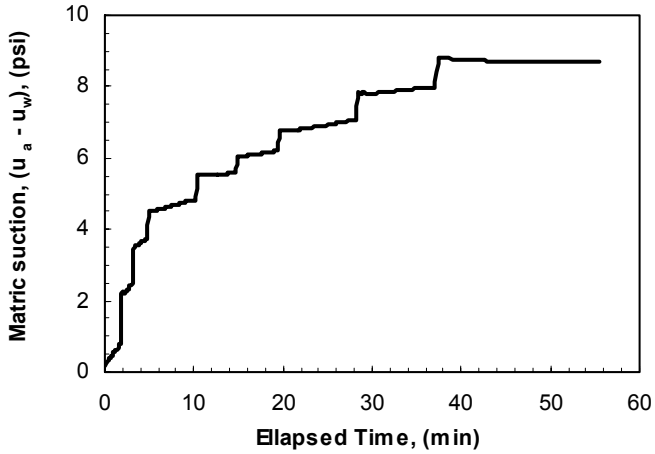

Test ID: PP-22%-20psi
Water content: 21.5%
Dry unit weight: 102.7 pcf
Degree of saturation: 90.6%
Matric suction: 11.0 psi
Notes: 1. Specimen compacted on the wet side of the line of optimums.

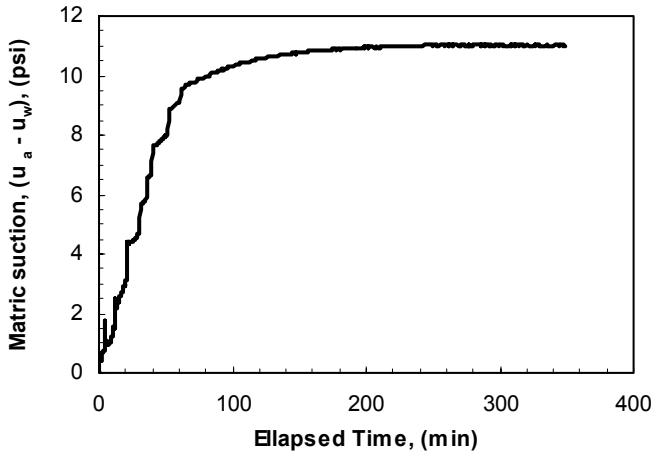

Test ID: PP-23%-15psi
Water content: 23.2%
Dry unit weight: 98.5 pcf
Degree of saturation: 88.3%
Matric suction: 3.7 psi
Notes: 1. Specimen compacted on the wet side of the line of optimums.

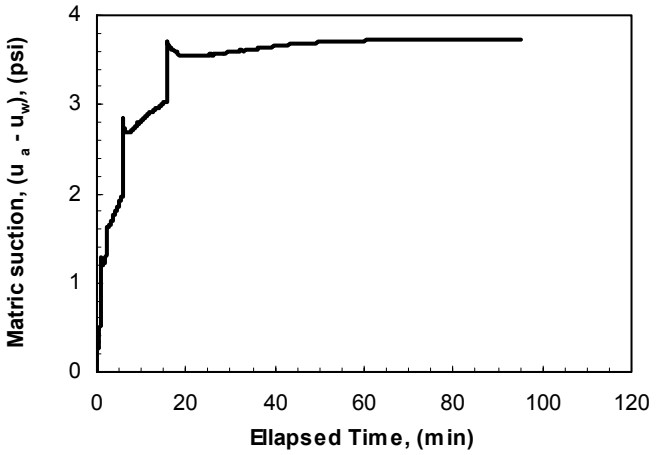

Test ID: PP-24%-7psi
Water content: 24.1%
Dry unit weight: 98.1 pcf
Degree of saturation: 90.8%
Matric suction: 4.5 psi
Notes: 1. Specimen compacted on the wet side of the line of optimums.

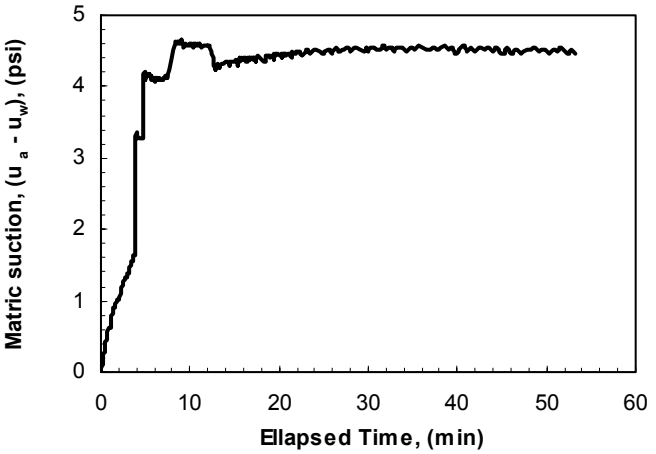

Appendix E: Preparation of piezoelectric transducers prior testing

Shear and compression wave velocities were measured using piezoelectric transducers. Details on the physical properties of the piezoelectric transducers used in this study and the required stages of preparation of the transducers prior to assembly in the apparatus and use are presented in this appendix.

E.1 PHYSICAL PROPERTIES OF PIEZOELECTRIC TRANSDUCERS

Morgan Electro Ceramics Corp., model PZT-5H bender elements were used to measure shear wave velocity while Morgan Electro Ceramics Corp., model PZT-5A disks were used to measure compression wave velocity. The transducers were made of lead zirconate titanate. The bender element had a height of 0.5 inch (12.7 mm), width of 0.315 inch (8 mm), and thickness of 0.025 inch (0.635 mm). The maximum voltage and temperature that the bender element could withstand as specified by the manufacturer were 125 volts and 100 degrees Celsius, respectively. The disk had a diameter of 0.315 inch (8 mm) and a thickness of 0.1 inch (2.54) mm. The maximum voltage and temperature that the disk could withstand as specified by the manufacturer were 500 volts and 150 degrees Celsius, respectively. A photograph of the piezoelectric transducers is shown in Figure E.1.

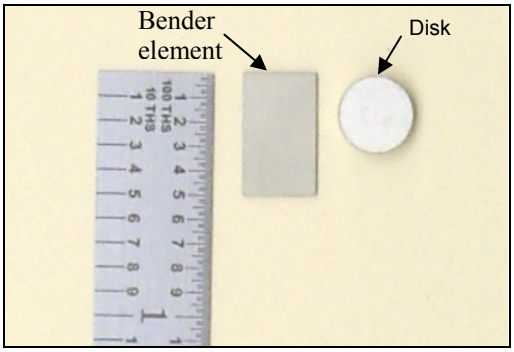

Figure E.1. Piezoelectric transducers used in this study.

E.2 PREPARATION OF PIEZOELECTRIC TRANSDUCERS PRIOR TO ASSEMBLY IN APPARATUS

Each piezoelectric transducer had to go through several stages of preparation prior to assembly in the apparatus and use. The transducer was cleaned with a general duty defluxer (Ecoline Flux Remover, Tech Spray L.P.) to avoid short-circuiting upon applying the voltage. The main lead of a Cooner Wire Inc., model CW2040-3650F teflon-coated coaxial cable was soldered to one side (electrode) of the transducer and the shielding of the coaxial cable (ground) was soldered to the other side (electrode). The transducer was cleaned again with the defluxer after soldering the coaxial cable.

Electrical insulation and water proofing of the transducer were achieved by coating the transducer with two layers of two-component epoxy resin (Kyowa Electronic Instruments Co., EP-34B). Each layer was left to cure for 24 hours at room temperature. This epoxy provided high moisture resistance under high pressures. Then, the transducer was coated with two layers of polyurethane coating (Measurement Group Inc., M-coat A), which was less viscous than the two-component epoxy. Each polyurethane coating layer was allowed to cure for 24 hours at room temperature.

Electrical shielding of the piezoelectric transducer was performed by coating the transducer with a conductive paint (GC/Waldom Electronics Inc., Silver Print II) and connecting the transducer to a grounding wire. The conductive paint consisted of an acrylic resin with silver particles in suspension for conductivity. The transducer was coated with a layer of the conductive paint, which was allowed to cure for 24 hours at room temperature. A Cooner Wire Inc., model CW6325 teflon-coated grounding wire was connected to the electric shielding paint. Finally, two layers of the polyurethane coating were applied to protect the shielding of the transducer; each layer was allowed to cure for 24 hours at room temperature. Photographs of the piezoelectric transducers at the different stages of preparation prior testing are shown in Figure E.2.

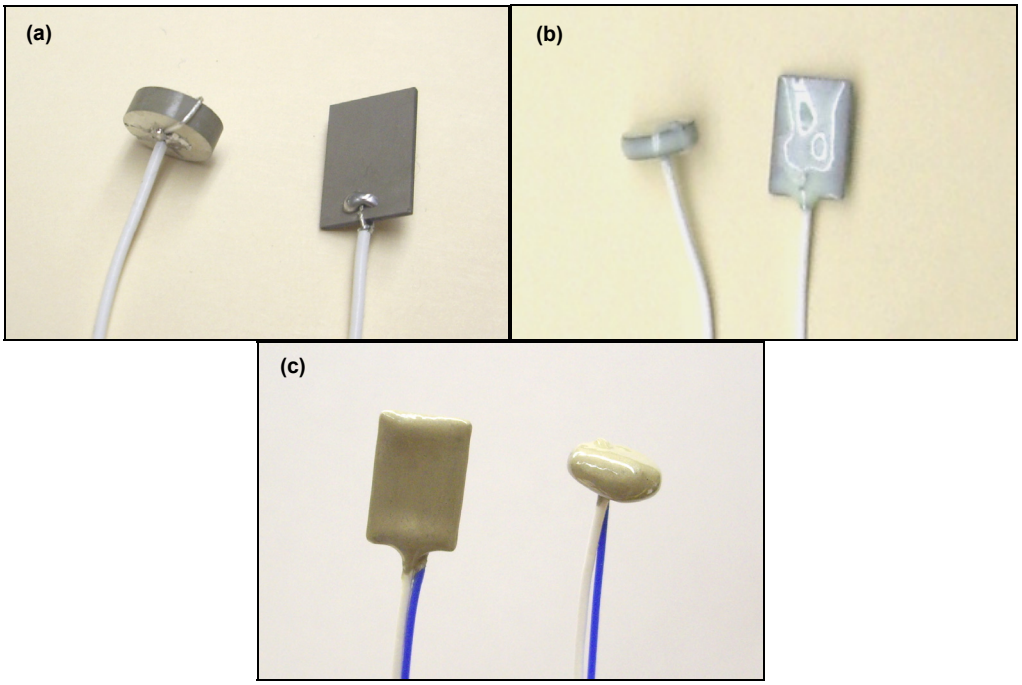

Figure E.2. Piezoelectric transducers at different stages of preparation prior to assembly: (a) soldering coaxial cable, (b) insulating and waterproofing, (c) and electrical shielding.

The piezoelectric transducers were mounted in stainless steel blocks, shown in Figure E.3, using two-component epoxy resin (5 Minute Epoxy, ITW Devcon Co.) and were allowed to cure for 24 hours at room temperature. Details of the design of the stainless steel blocks are presented in Appendix G. The stainless steel blocks were screwed in top and bottom platens of a triaxial cell. The bender elements and the disks protruded into the specimens about 0.16 to 0.24 inch (4 to 6 mm) and 0.02 to 0.08 inch (0.5 to 2 mm), respectively. The coaxial and grounding wires were soldered from the other end to female BNC connectors.

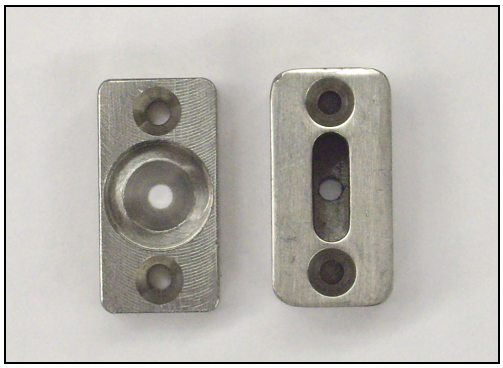

Figure E.3. Stainless steel blocks used to house piezoelectric transducers.

Appendix F: Triaxial platens for stiffness measurements under undrained conditions

Top and bottom triaxial acrylic platens were designed and fabricated at The University of Texas at Austin to measure soil stiffness under undrained test conditions. The platens were mounted in a standard triaxial cell. The end platens are 2 inches in diameter with cavities to accommodate the housing of bender elements and disks used to measure shear and compression wave velocities, respectively. The bottom platen was fastened to the base plate of the triaxial cell using a single 1/4-20x1-1/4" socket head cap screw. The top platen has a cavity for the seating of the loading piston. Details of the design of the bottom and top triaxial platens are presented in Figures F.1 and F.2, respectively.

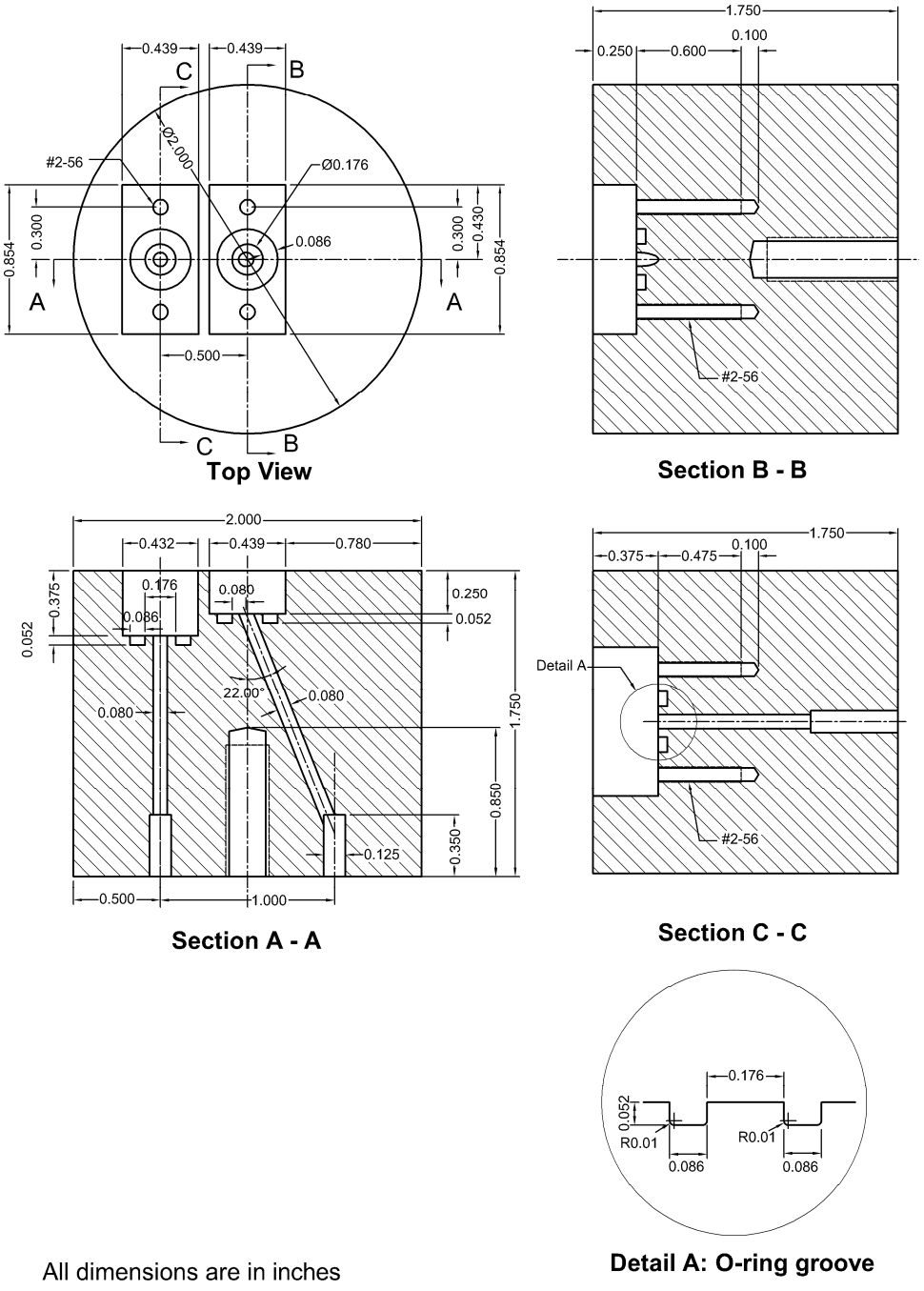

Figure F.1. Details of bottom platen designed to measure soil stiffness under undrained conditions.

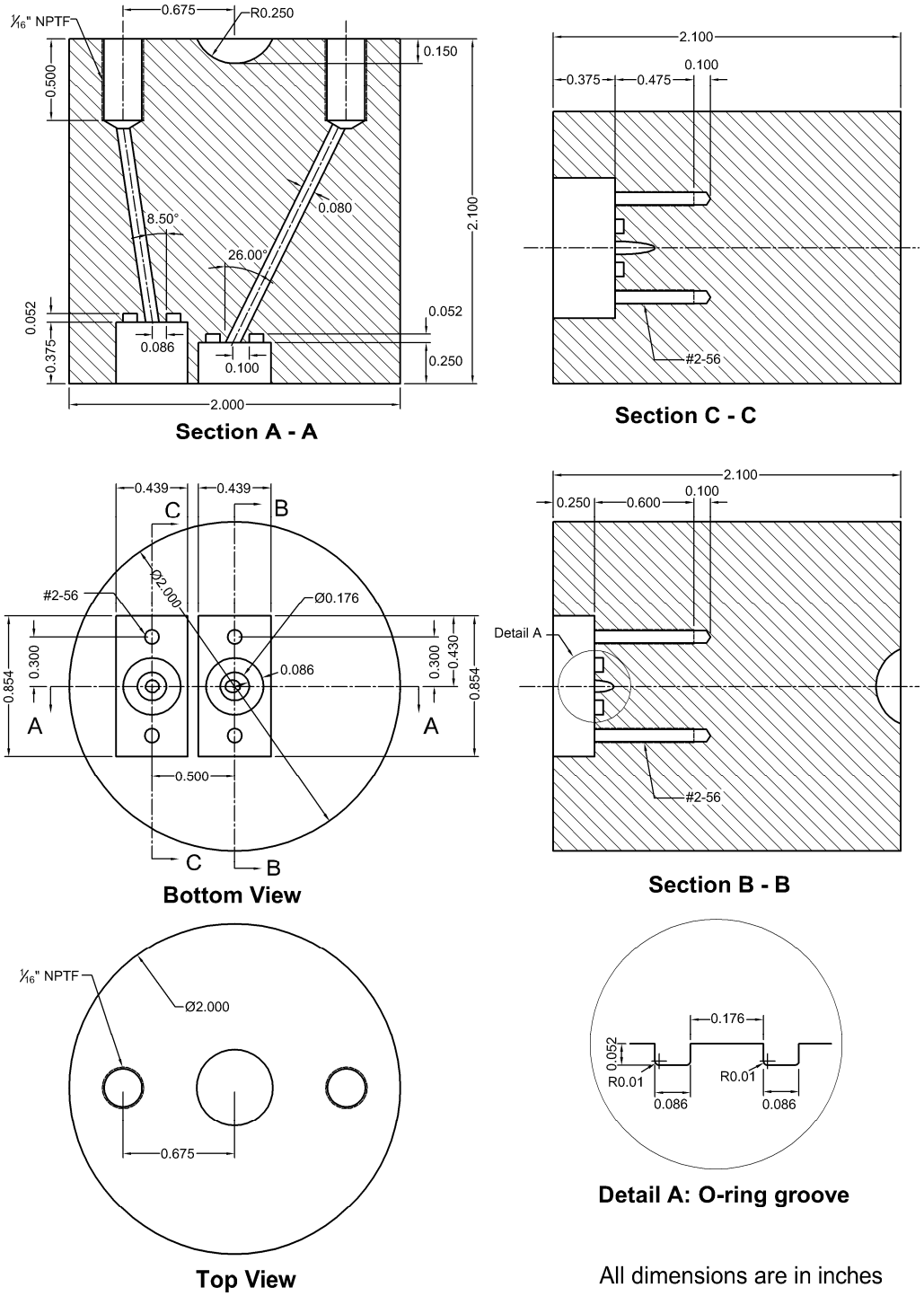

Figure F.2. Details of top platen designed to measure soil stiffness under undrained conditions.

Appendix G: Stainless steel blocks for housing piezoelectric transducers

A special technique was implemented to incorporate the bender elements and disks in the end platens of the triaxial cell. Each piezoelectric transducer was mounted in a separate stainless steel block, which was fastened into the triaxial platen using #2-56x1/2" flat head machine screws. If one of the transducers was damaged, the block and the transducer could be exchanged without damaging the other transducer mounted in the same platen. Details of the design of the stainless steel blocks used to house bender elements and disks are presented in Figures G.1 and G.2, respectively.

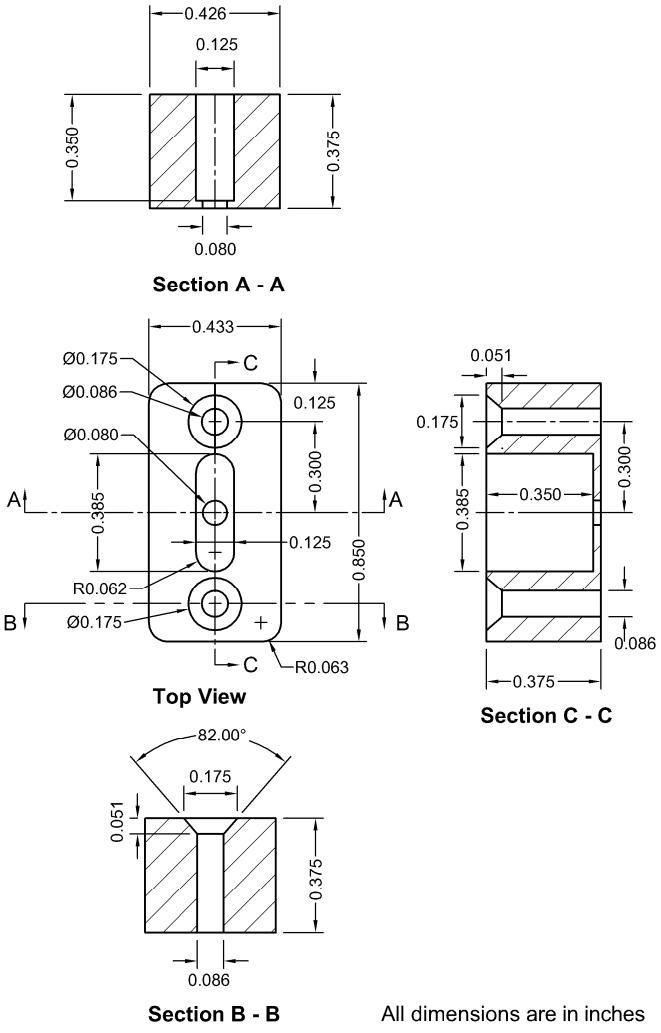

Figure G.1. Details of stainless steel block used to house bender elements.

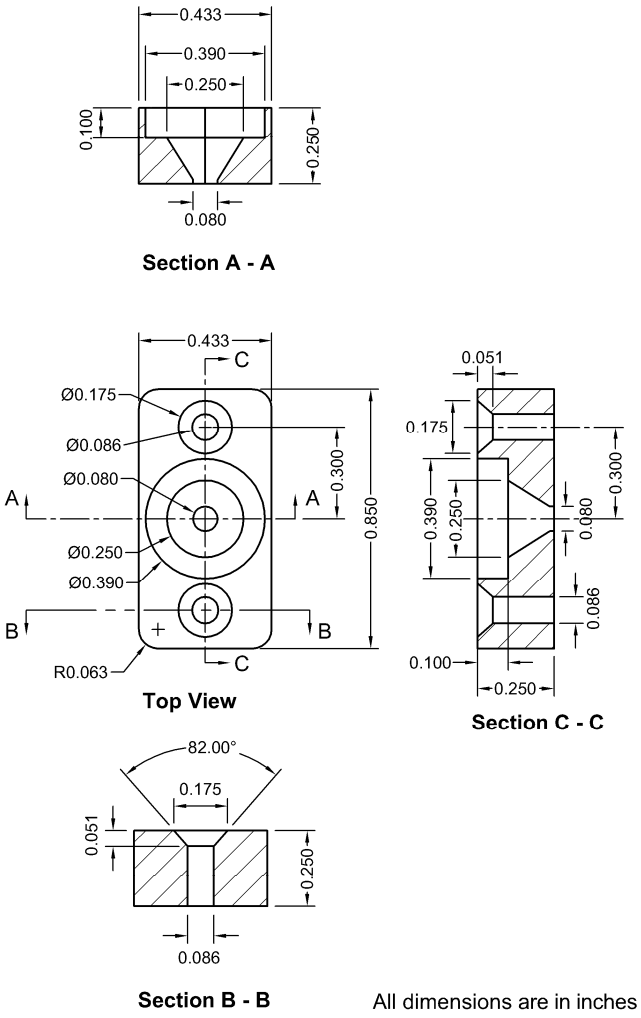

Figure G.2. Details of stainless steel block used to house disks.

Appendix H: MATLAB functions

A moving average (MA) digital filter was designed to reduce the amplitude of the high-frequency noise observed in the recorded signals. The MATLAB function (m-file) written to compute and implement the filter is presented in Figure H.1. The cross-correlation technique was investigated to determine the total travel time of transmitted shear and compression waves. The MATLAB function (m-file) written to compute the cross-correlation sequence between input and output signals is presented in Figure H.2.

```
function wfilt(j)
[IF inpath]= uigetfile('*.csv');
FL=dir([inpath,'*.csv'])
for i = 1:size(FL)
        A(i,:)={FL(i).name}
end
for k =1:size(A)
        inputfile=[inpath,char(A(k))]
        fid = fopen(inputfile);
        C = textscan(fid, '%s%s%s%s%s$s$s',1,'delimiter',',');
        data=dlmread(inputfile,',',1,0);
        a=1;
        for i=1:j
                b(i)=1/j;
        end
        data(:,4)=filtfilt(b,a,data(:,4));
        outputfile=[inputfile(1:(size(inputfile,2)-4)),'-f','.csv']
        fid2=fopen(outputfile,'w');
        fprintf(fid2,'%s','CH1-dt,CH1-Volts,CH2-dt,CH1-Volts');
        fclose(fid2);
        dlmwrite(outputfile, data,'-append','delimiter',',','roffset',1);
end
```

Figure H.1. MATLAB function to compute and implement moving average filter.

```
function [F data T D]=TT3()
[F DIR]=uigetfile('*.csv');
cd(DIR);
%Data Read
data = csvread(F,2,0);
%Adjust amplitude zero reference
data(:,2)=data(:,2)-data(1,2);
data(:,4)=data(:,4)-data(1,4);
figure
plot(data(:,1),data(:,4)*1000,data(:,1),data(:,2))
dt=(data(2,1)-data(1,1));
%Cross correlation of original signal
D(:,1)=xcorr(data(:,2),data(:,4)*100);
[d i]=max(D(:,1)); % D is the max xcorr value and i is the position
T(1,1)=(length(data)-i)*dt;
figure
plot(D(:,1))
```

Figure H.2. MATLAB function to compute cross-correlation sequence.

Appendix I: Measurements of soil stiffness under undrained conditions

Shear and compression wave velocities measured in a triaxial apparatus under undrained conditions at confining pressures of 0.2 and 15 psi are summarized in Tables I.1 and I.2, respectively. In addition, the compaction water content, dry unit weight, and degree of saturation for each test are included. Each test is defined by a Test ID which is expressed as: stiffness/undrained conditions (S/U) – compaction water content in % - pressure applied to the air piston during compaction in psi.

Table I.1. Test ID, compaction conditions, and stiffness measurements for specimens tested under a confining pressure of 0.2 psi.

Test ID	w, (%)	γ_{dry}, (pcf)	S, (%)	V_s, (fps)	V_p, (fps)	υ
S/U-13%-15psi	12.6	91.8	40.6	812	1813	0.37
S/U-13%-25psi	12.8	97.2	48.2	857	NA	NA
S/U-13%-35psi	12.7	102.4	54.8	916	NA	NA
S/U-13%-40psi	12.5	104.7	57.0	1099	2395	0.37
S/U-15%-15psi	14.6	94.2	50.1	687	1781	0.41
S/U-15%-25psi	15.0	105.9	70.6	1024	NA	NA
S/U-15%-35psi	15.2	110.0	80.1	1139	NA	NA
S/U-15%-40psi	14.9	110.6	79.6	1358	2298	0.23
S/U-16%-10psi	16.0	93.5	55.2	745	1736	0.39
S/U-16%-15psi	16.0	98.5	60.8	764	1922	0.41
S/U-16%-15psi	16.2	99.7	65.1	871	1993	0.38
S/U-16%-20psi	16.1	105.6	75.1	860	2069	0.40
S/U-17%-25psi	16.9	110.3	89.5	961	NA	NA
S/U-17%-35psi	17.1	110.7	91.6	920	NA	NA
S/U-17%-40psi	16.6	110.9	89.3	901	1935	0.36
S/U-18%-10psi	18.0	97.6	68.7	697	1683	0.40
S/U-18%-15psi	18.2	101.3	74.3	664	1704	0.41
S/U-18%-25psi	18.3	105.8	86.0	735	NA	NA
S/U-19%-35psi	18.5	107.4	90.9	705	1310	0.30
S/U-20%-15psi	20.1	104.1	87.7	535	1294	0.40
S/U-20%-25psi	19.7	105.1	90.9	657	NA	NA
S/U-21%-10psi	20.5	101.2	85.5	654	1492	0.38
S/U-22%-10psi	21.6	100.7	86.5	569	NA	NA
S/U-23%-15psi	22.6	100.5	90.0	413	1023	0.40
S/U-24%-7psi	23.8	96.5	86.2	492	NA	NA
S/U-25%-15psi	24.6	97.5	91.2	335	848	0.41

NA: Not available

Table I.2. Test ID, compaction conditions, and stiffness measurements for specimens tested under a confining pressure of 15 psi.

Test ID	w, (%)	γ_{dry}, (pcf)	S, (%)	V_s, (fps)	V_p, (fps)	υ
S/U-13%-15psi	12.6	91.8	40.6	1101	2310	0.35
S/U-13%-25psi	12.8	97.2	48.2	1151	2544	0.37
S/U-13%-35psi	12.7	102.4	54.8	1120	NA	NA
S/U-13%-40psi	12.5	104.7	57.0	1113	2979	0.42
S/U-15%-15psi	14.6	94.2	50.1	962	2218	0.38
S/U-15%-25psi	15.0	105.9	70.6	1162	2870	0.40
S/U-15%-35psi	15.2	110.0	80.1	1302	NA	NA
S/U-15%-40psi	14.9	110.6	79.6	1401	2462	0.26
S/U-16%-10psi	16.0	93.5	55.2	842	1941	0.38
S/U-16%-15psi	16.0	98.5	60.8	942	2240	0.39
S/U-16%-15psi	16.2	99.7	65.1	938	2215	0.39
S/U-16%-20psi	16.1	105.6	75.1	1001	2891	0.43
S/U-17%-25psi	16.9	110.3	89.5	1104	2828	0.41
S/U-17%-35psi	17.1	110.7	91.6	1011	3511	0.45
S/U-17%-40psi	16.6	110.9	89.3	1183	3270	0.42
S/U-18%-10psi	18.0	97.6	68.7	786	1804	0.38
S/U-18%-15psi	18.2	101.3	74.3	803	2425	0.44
S/U-18%-25psi	18.3	105.8	86.0	857	2725	0.45
S/U-19%-35psi	18.5	107.4	90.9	823	3139	0.46
S/U-20%-15psi	20.1	104.1	87.7	702	2544	0.46
S/U-20%-25psi	19.7	105.1	90.9	756	2543	0.45
S/U-21%-10psi	20.5	101.2	85.5	724	2117	0.43
S/U-22%-10psi	21.6	100.7	86.5	644	2429	0.46
S/U-23%-15psi	22.6	100.5	90.0	563	2395	0.47
S/U-24%-7psi	23.8	96.5	86.2	556	2237	0.47
S/U-25%-15psi	24.6	97.5	91.2	418	2225	0.48

NA: Not available

Appendix J: Triaxial platens for stiffness measurements under controlled state of stress

Top and bottom triaxial acrylic platens were designed and fabricated in collaboration with the Geotac Company (Houston, Texas) to evaluate the stiffness of unsaturated soils under controlled states of stress. The platens were mounted in a modified version of a standard triaxial cell. The end platens are 2 inches in diameter with cavities to accommodate the housing of bender elements and disks used to measure shear and compression wave velocities, respectively. Two different porous disks were mounted in each platen: a low air-entry bronze disk to control or measure the pore-air pressure, and a 15-bar high air-entry porous stone to control or measure the pore-water pressure. The bottom platen was fastened to the base plate with two #10-32x1-5/8" socket head cap screws. The top platen has a cavity for the seating of the loading piston. Details of the design of the bottom and top triaxial platens are presented in Figures J.1, J.2, J.3, and J.4.

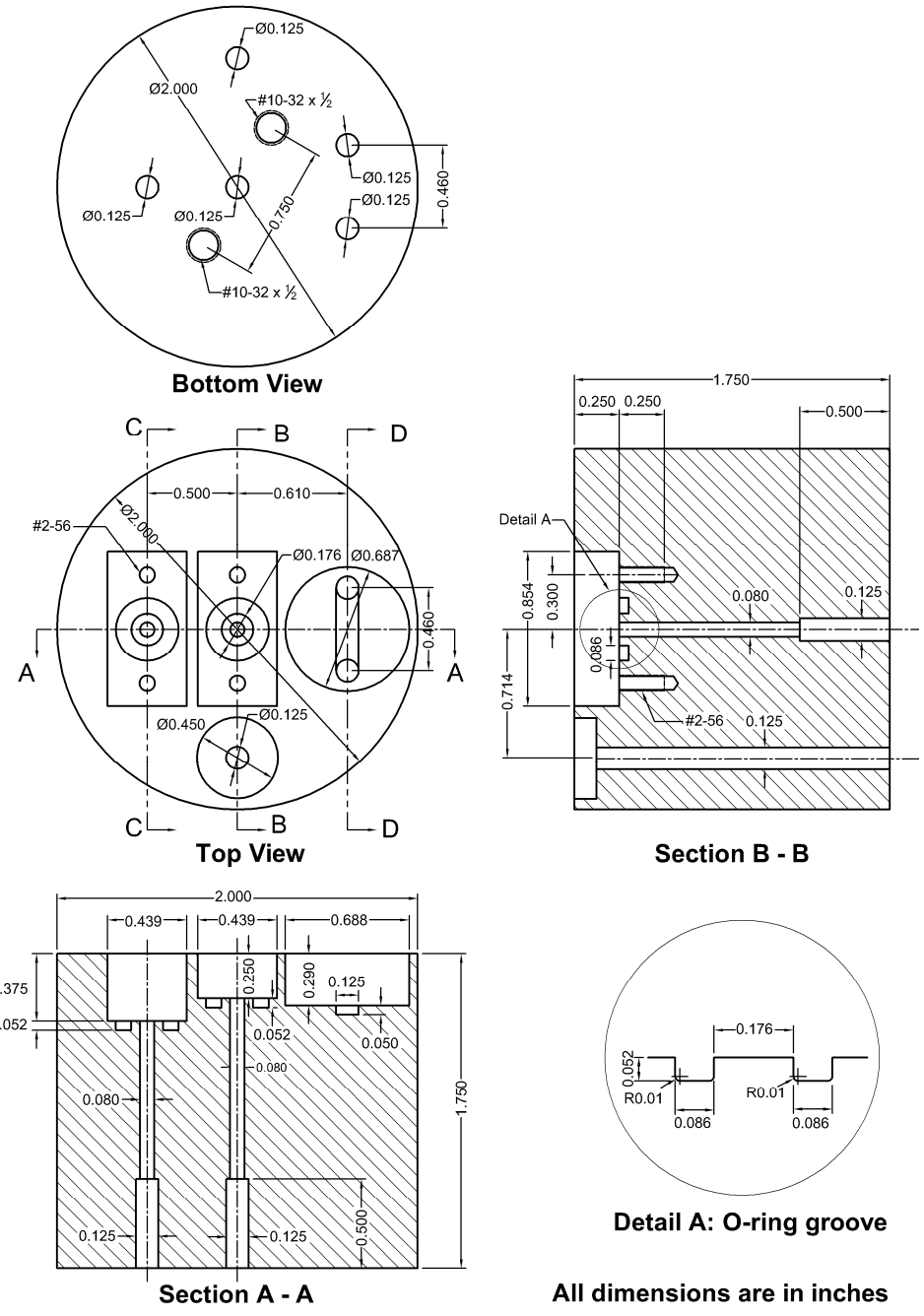

Figure J.1. Details of bottom platen designed to measure soil stiffness under controlled state of stress.

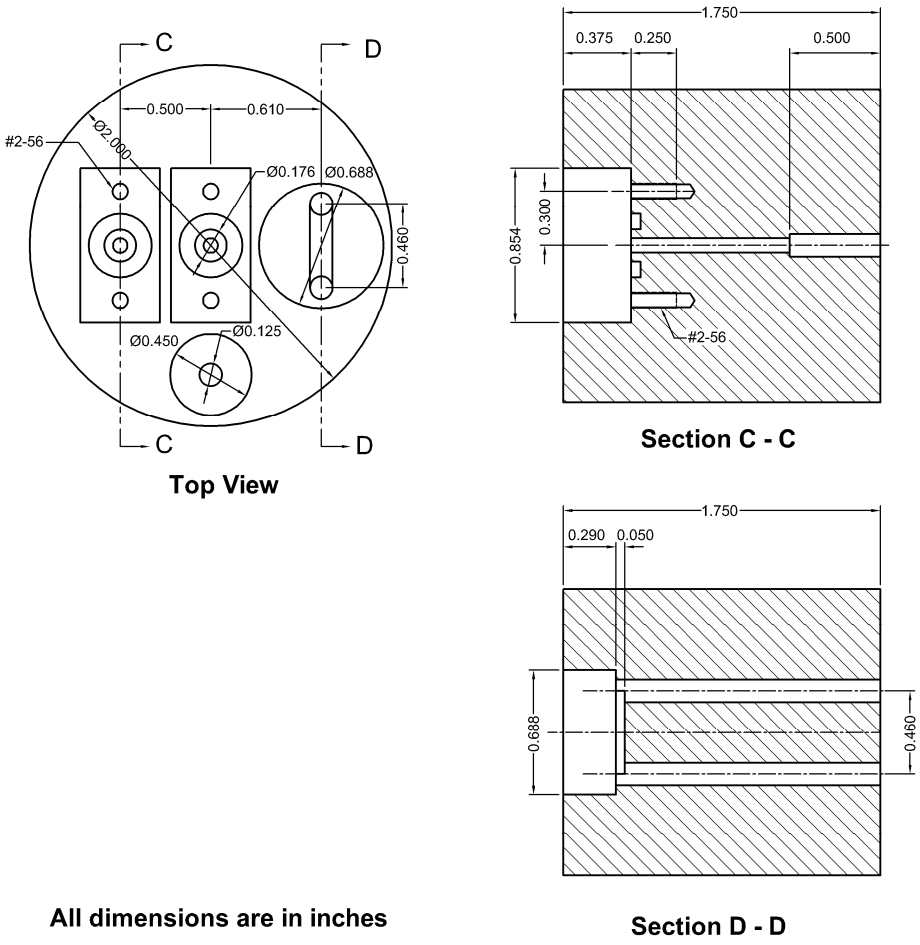

Figure J.2. Details of bottom platen designed to measure soil stiffness under controlled state of stress (cont'd).

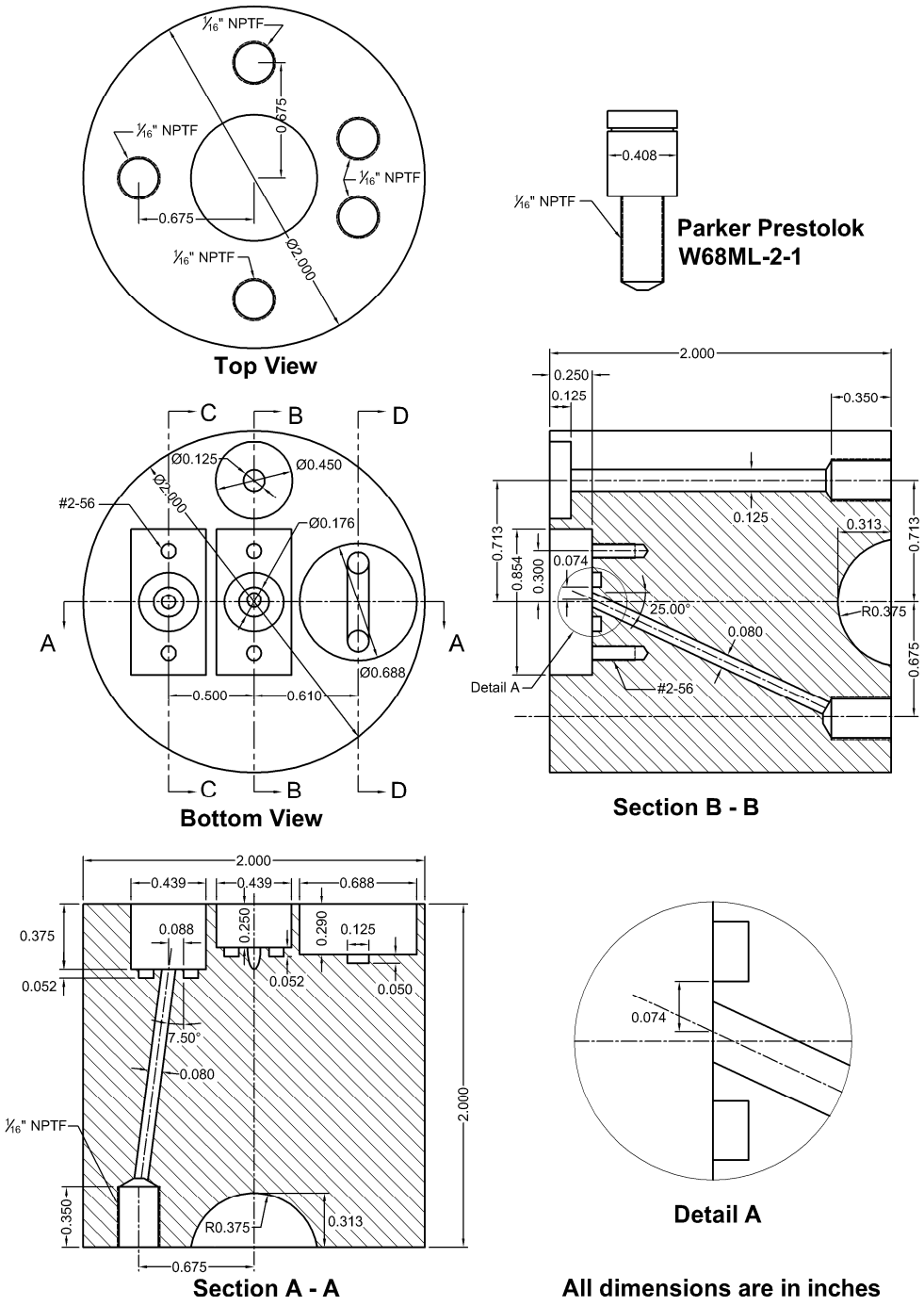

Figure J.3. Details of top platen designed to measure soil stiffness under controlled state of stress.

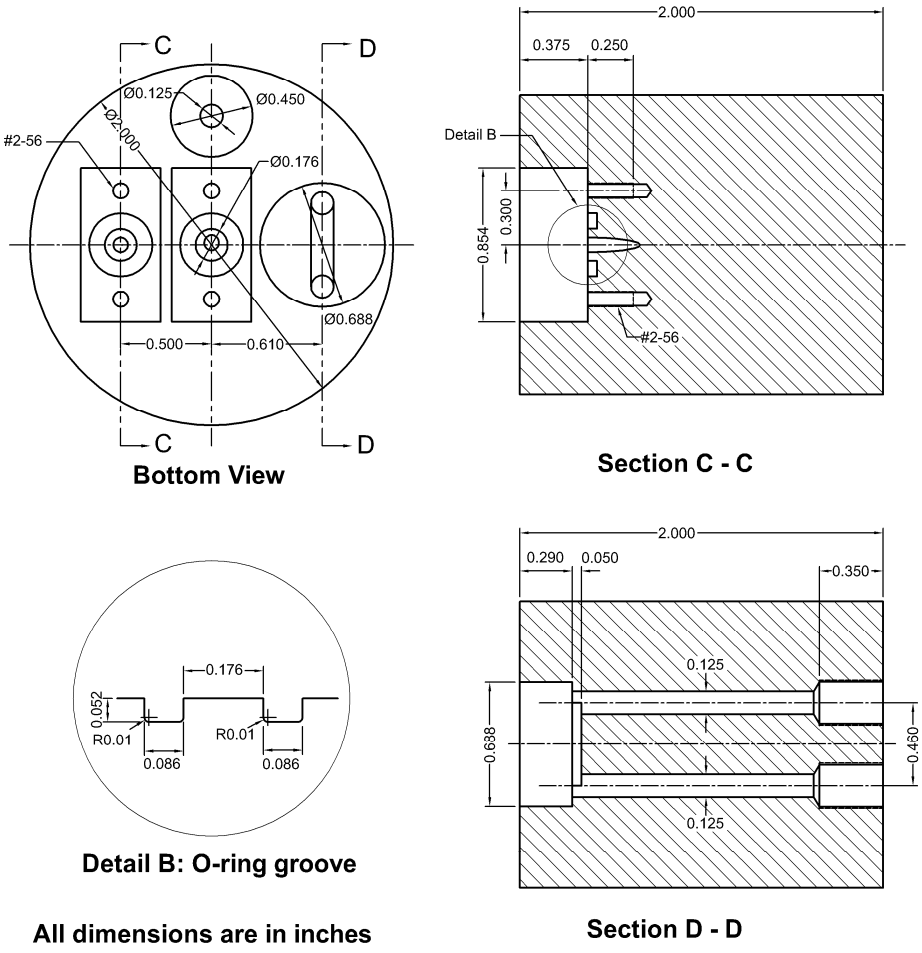

Figure J.4. Details of top platen designed to measure soil stiffness under controlled state of stress (cont'd).

Appendix K: Measurements of soil stiffness under controlled states of stress

The compaction water contents, dry unit weights, and degrees of saturation of specimens tested in the suction-controlled triaxial apparatus are summarized in Table K.1. Shear and compression wave velocities, water content, dry unit weight, void ratio, degree of saturation, net stress, matric suction, and volumetric strains measured for each test are summarized in Table K.2. Each test is defined by a Test ID, which is expressed as: stiffness/suction-controlled conditions (S/SC) – compaction water content in % - pressure applied to the air piston during compaction in psi. The time response curves for net stresses, matric suctions, and volumetric strains of all tests are presented in this appendix.

Table K.1. Test ID and compaction conditions for specimens tested under controlled states of stress.

Specimen ID	w, (%)	γ_{dry}, (pcf)	S, (%)
S/SC-12%-20psi	12.1	98.1	45.4
S/SC-14%-35psi	14.4	110.6	74.5
S/SC-15%-21psi	14.6	100.8	58.7
S/SC-16%25psi	15.8	106.6	73.7
S/SC-16%-31psi	16.0	107.3	75.6
S/SC-17%-12psi	17.3	104.1	75.4
S/SC-19%-7psi	19.0	100.8	76.4
S/SC-19%-25psi	18.7	106.6	87.0

Table K.2. Stiffness measurements under controlled states of stress.

Specimen ID	w, (%)	γ_{dry}, (pcf)	e	S, (%)	Net stress, (psi)	Matric suction, (psi)	$\Delta\varepsilon_v$, (%)	V_s, (fps)	V_p, (fps)	υ
S/SC-12%-20psi	12.1	99.8	0.688	47.3	0	106.1	-1.69	1077	2098	0.32
S/SC-14%-35psi	14.4	113.4	0.485	80.4	0	60.0	-2.24	1316	3202	0.40
		114.6	0.470	83.0	10	56.8	-0.99	1490	3467	0.39
		115.0	0.465	83.9	20	49.4	-0.35	1529	3783	0.40
		115.4	0.460	84.7	30	41.7	-0.30	1549	3859	0.40
		115.8	0.455	85.7	40	34.8	-0.33	1576	3938	0.40
S/SC-15%-21psi	14.6	102.0	0.652	60.4	0	61.0	-1.23	1240	2712	0.37
		103.0	0.635	62.0	10	59.0	-1.01	1277	2900	0.38
		103.6	0.626	63.0	20	51.8	-0.58	1280	2897	0.38
		104.3	0.615	64.1	30	44.6	-0.63	1272	2918	0.38
		105.2	0.601	65.6	40	40.4	-0.82	1303	2958	0.38
S/SC-16%-31psi	16.0	109.7	0.536	80.4	0	39.0	-1.89	1158	2788	0.40
		110.9	0.519	83.0	10	33.9	-1.08	1358	3398	0.40
		111.3	0.514	83.9	20	28.6	-0.38	1401	3700	0.42
		111.9	0.506	85.1	30	22.4	-0.47	1435	3811	0.42
		112.4	0.498	86.5	40	17.1	-0.50	1464	3929	0.42
S/SC-17%-12psi	17.3	107.0	0.575	81.1	0	30.8	-2.67	1025	2530	0.40
		108.0	0.560	83.3	10	17.8	-0.93	1091	3175	0.43
		108.8	0.548	85.1	20	9.5	-0.75	1148	3533	0.44
		109.5	0.538	86.6	30	5.3	-0.60	1145	3630	0.44
		110.9	0.520	89.7	40	2.6	-1.14	1183	3839	0.45
S/SC-19%-7psi	19.0	104.1	0.618	83.1	0	21.3	-3.24	807	1772	0.37
		105.6	0.596	86.2	10	9.4	-1.32	835	2846	0.45
		106.9	0.576	89.2	20	3.2	-1.22	891	3186	0.46
		108.9	0.547	93.9	30	1.5	-1.69	923	3201	0.45
		110.9	0.525	97.9	40	0.1	-1.35	1010	3716	0.46
S/SC-19%-25psi	18.7	108.5	0.553	91.3	0	30.6	-1.40	1032	2580	0.40
		109.5	0.539	93.7	10	17.1	-0.86	1011	3522	0.46
		109.8	0.535	94.5	20	7.5	-0.28	1057	4529	0.47
		110.1	0.530	95.4	30	0.7	-0.33	1068	4880	0.47

Test ID: S/SC-12%-20psi
Compaction water content: 12.1%
Compaction dry unit weight: 98.1 pcf
Compaction degree of saturation: 45.4%
Stage: Equalization
Notes: 1. Air diffused through high-air entry porous stones. Periodical flushing of diffused air caused irregularities in suction-time response curve. 2. Matric suction at equilibrium was unreasonably high for this water content for unknown reasons.

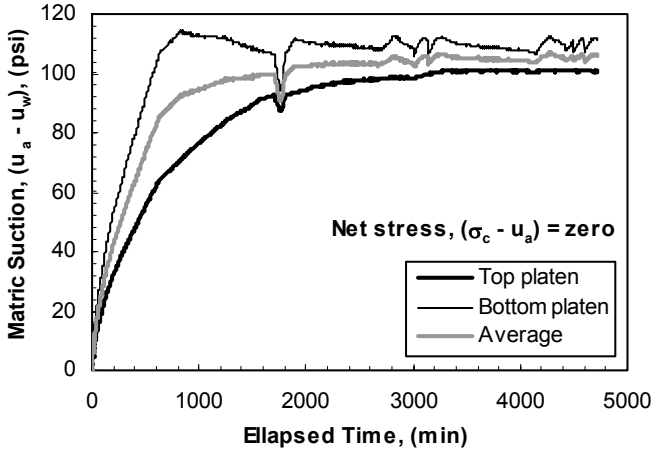

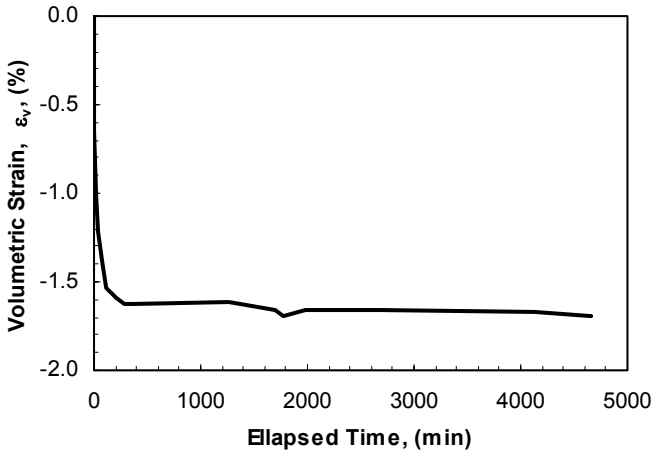

Test ID: S/SC-14%-35psi
Compaction water content: 14.4%
Compaction dry unit weight: 110.6 pcf
Compaction degree of saturation: 74.5%
Stage: Equalization
Notes: 1. Air diffused through high-air entry porous stones. Periodical flushing of diffused air caused irregularities in suction-time response curve. 2. Overshooting in suction-time response curve due to short adjustment intervals of cell and pore-air pressures.

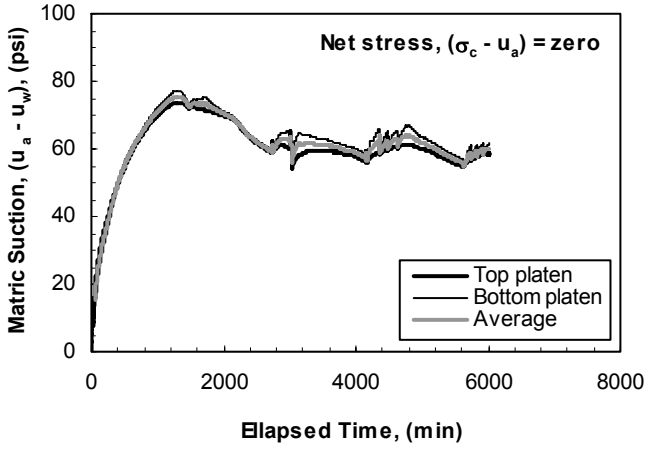

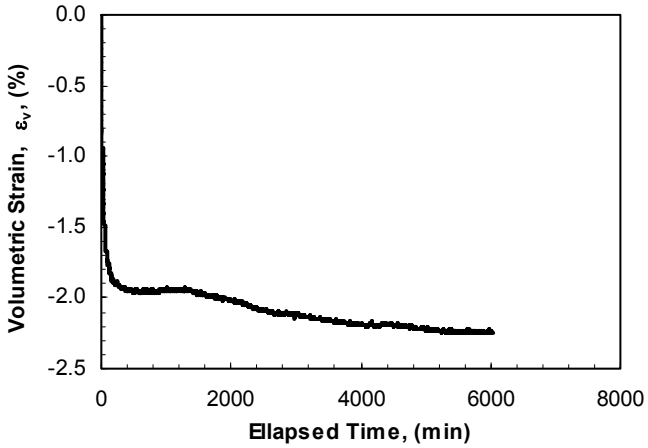

Test ID: S/SC-14%-35psi
Compaction water content: 14.4%
Compaction dry unit weight: 110.6 pcf
Compaction degree of saturation: 74.5%
Stage: Compression
Notes: 1. Specimen was compressed at a rate of 10 kPa/hr. 2. Air diffused through high-air entry porous stones. Periodical flushing of diffused air caused irregularities in suction-time response curve.

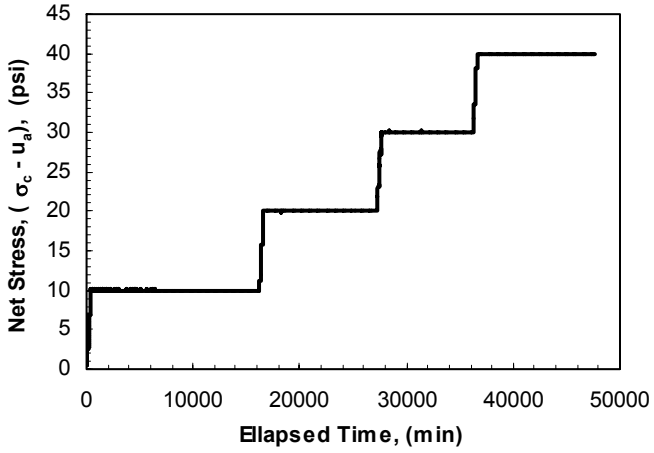

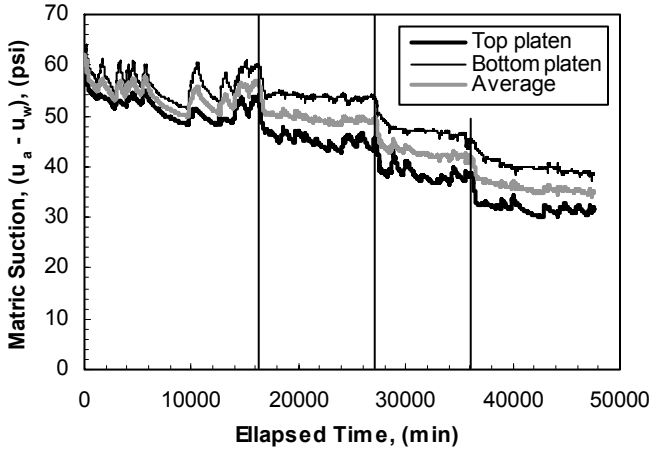

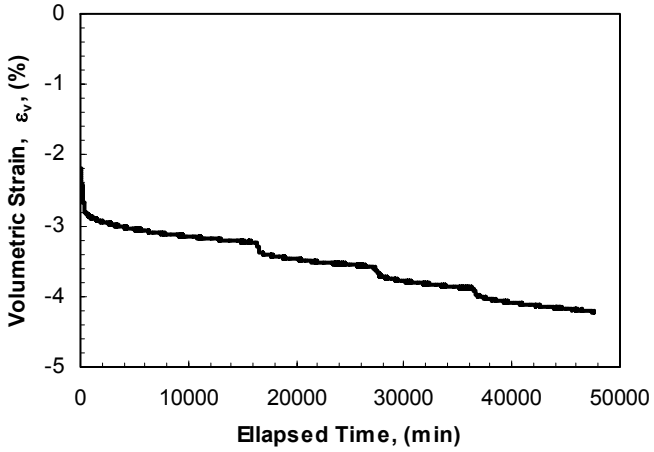

Test ID: S/SC-15%-21psi
Compaction water content: 14.6%
Compaction dry unit weight: 100.8 pcf
Compaction degree of saturation: 58.7%
Stage: Equalization
Notes: 1. Air diffused through high-air entry porous stones. Periodical flushing of diffused air caused irregularities in suction-time response curve. 2. Overshooting in suction-time response curve due to short adjustment intervals of cell and pore-air pressures. 3. Several peaks due to problems encountered with flow pump controlling cell and pore-air pressures. Pump was stopped before end of equalization stage.

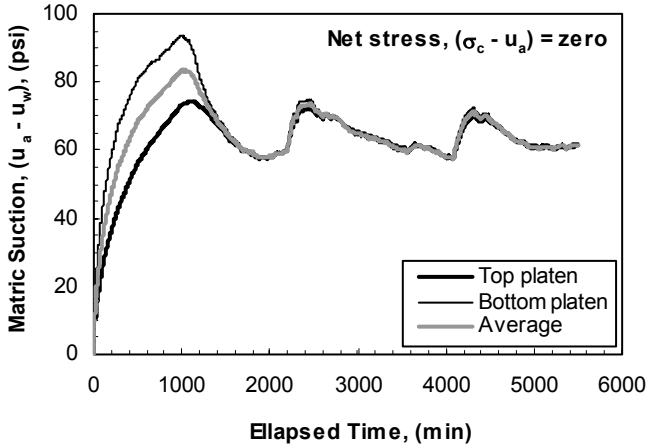

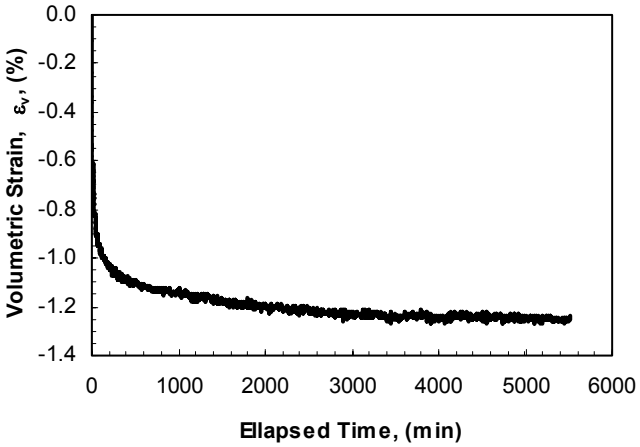

Test ID: S/SC-15%-21psi
Compaction water content: 14.6%
Compaction dry unit weight: 100.8 pcf
Compaction degree of saturation: 58.7%
Stage: Compression
Notes: 1. Specimen was compressed at a rate of 10 kPa/hr. 2. Air diffused through high-air entry porous stones. Periodical flushing of diffused air caused irregularities in suction-time response curve.

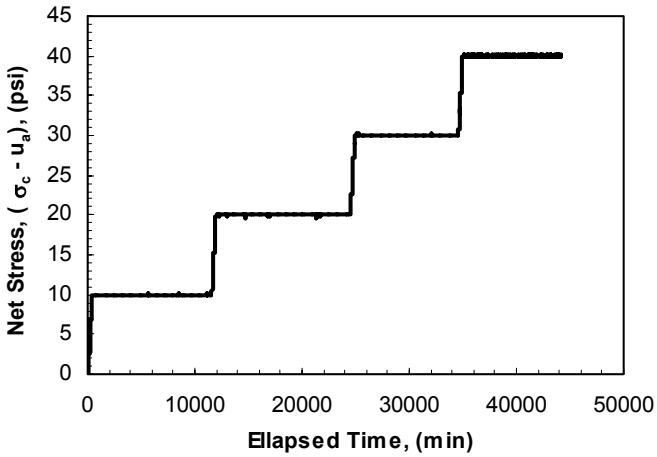

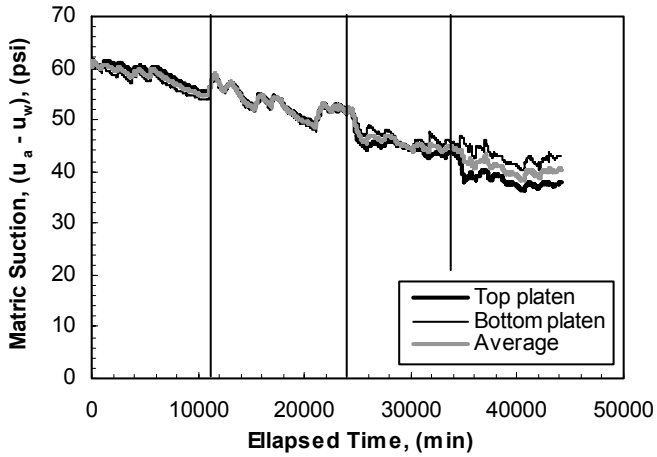

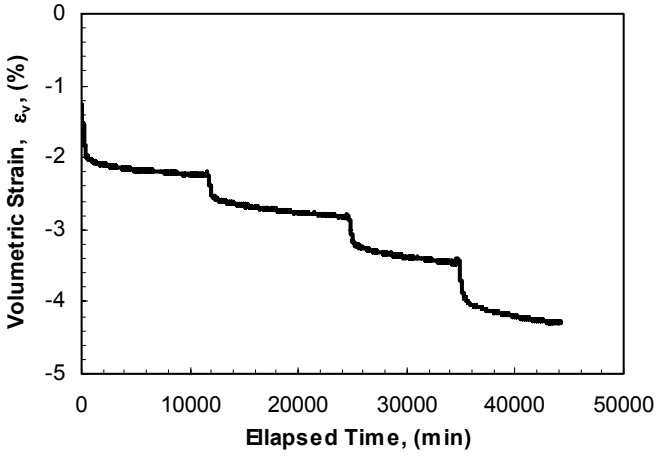

Test ID: S/SC-16%-25psi
Compaction water content: 15.8%
Compaction dry unit weight: 106.6 pcf
Compaction degree of saturation: 73.7%
Stage: Equalization
Notes: 1. Air diffused through high-air entry porous stones. Sudden drop in matric suction due to procedural error during flushing diffused air. 2. Matric suction at equilibrium was unreasonably high for this water content for unknown reasons.

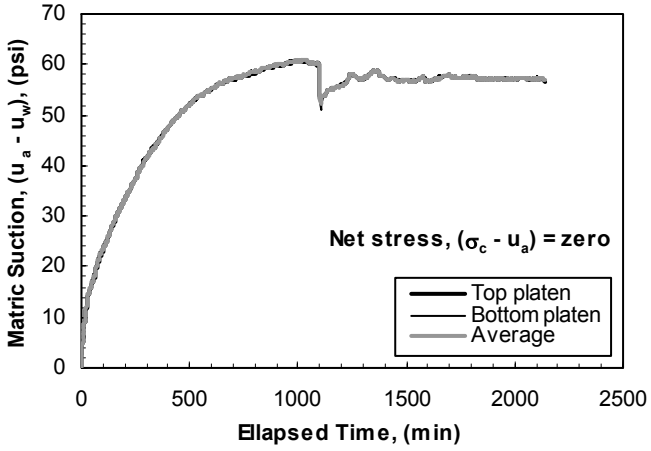

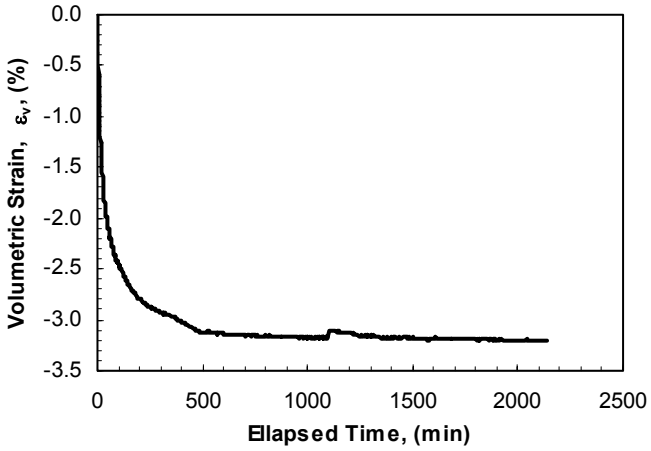

Test ID: S/SC-16%-25psi
Compaction water content: 15.8%
Compaction dry unit weight: 106.6 pcf
Compaction degree of saturation: 73.7%
Stage: Compression
Notes: 1. Specimen was compressed at a rate of 400 kPa/hr. 2. Air diffused through t high-air entry porous stones. Periodical flushing of diffused air caused irregularities in suction-time response curve.

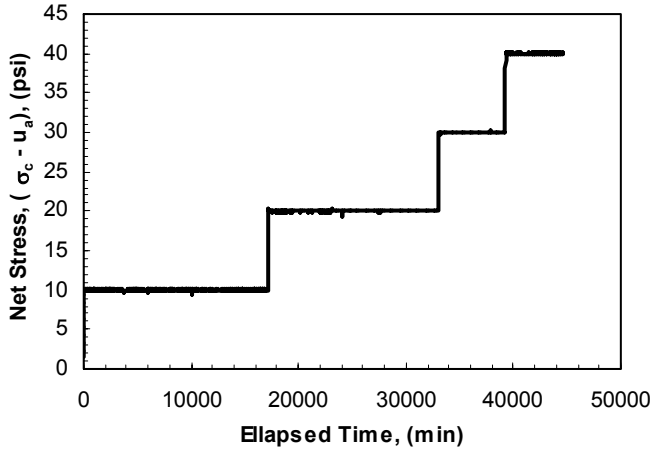

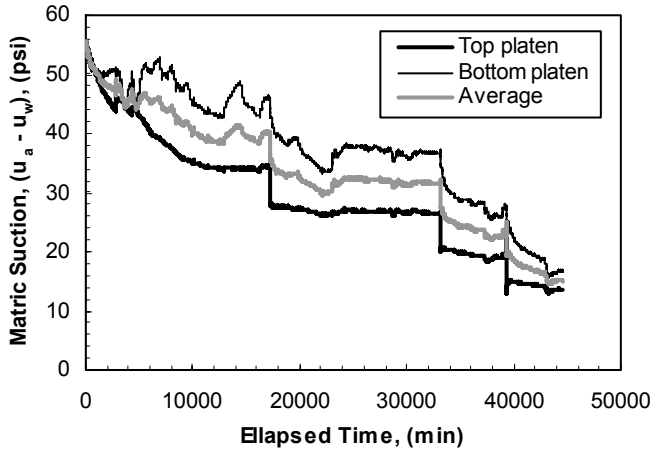

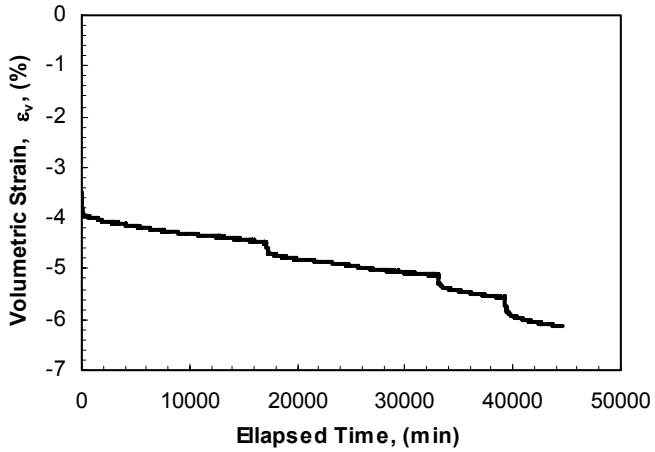

Test ID: S/SC-16%-31psi
Compaction water content: 16.0%
Compaction dry unit weight: 107.3 pcf
Compaction degree of saturation: 75.6%
Stage: Equalization
Notes: 1. Air diffused through high-air entry porous stones. Periodical flushing of diffused air caused irregularities in suction-time response curve. 2. Overshooting in suction-time response curve due to short adjustment intervals of cell and pore-air pressures.

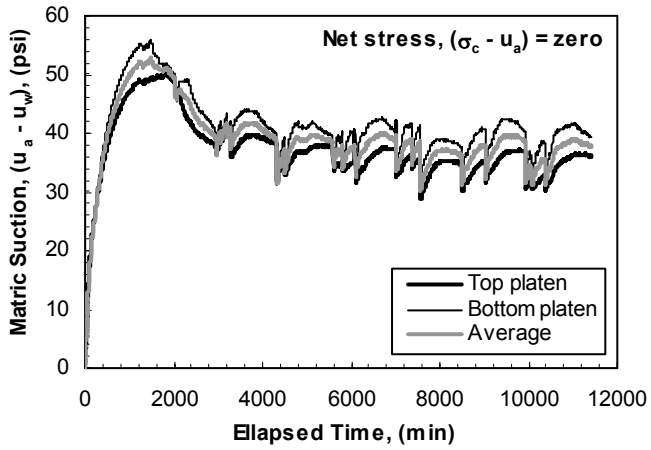

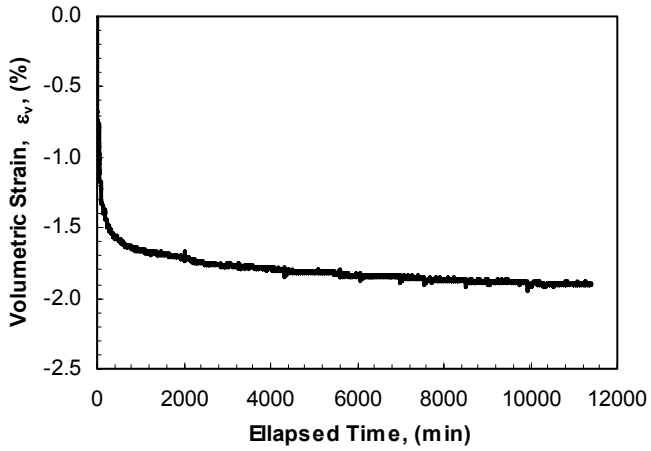

Test ID: S/SC-16%-31psi
Compaction water content: 16.0%
Compaction dry unit weight: 107.3 pcf
Compaction degree of saturation: 75.6%
Stage: Compression
Notes: 1. Specimen was compressed at a rate of 10 kPa/hr. 2. Air diffused through high-air entry porous stones. Periodical flushing of diffused air caused irregularities in suction-time response curve.

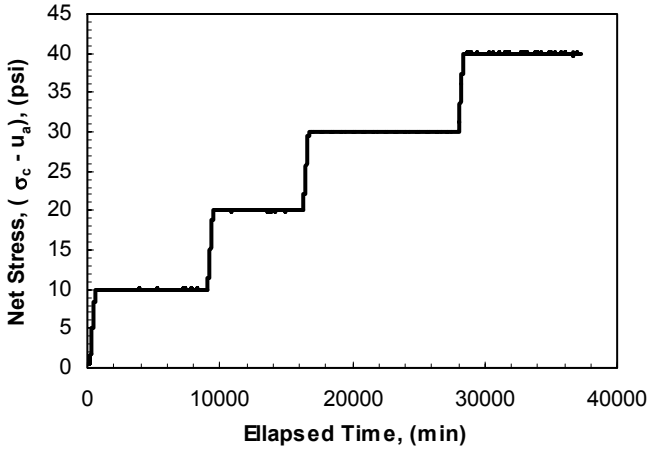

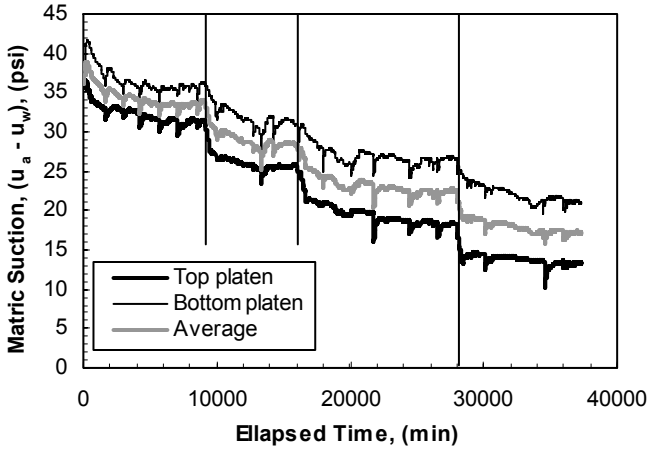

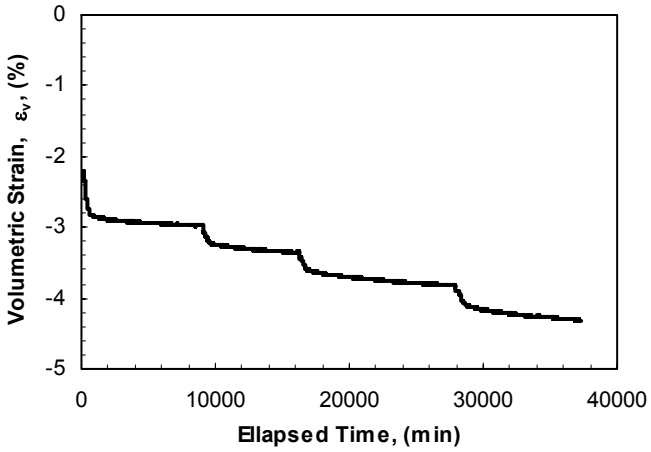

Test ID: S/SC-17%-12psi
Compaction water content: 17.3%
Compaction dry unit weight: 104.1 pcf
Compaction degree of saturation: 75.4%
Stage: Equalization
Notes: 1. Air diffusion had small effect on shape of suction-time response curve.

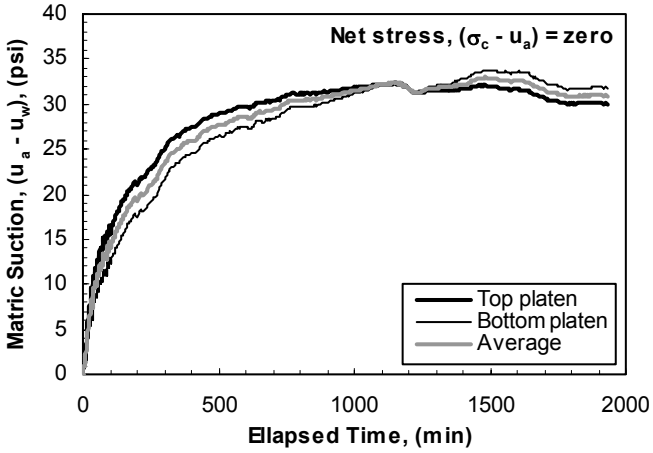

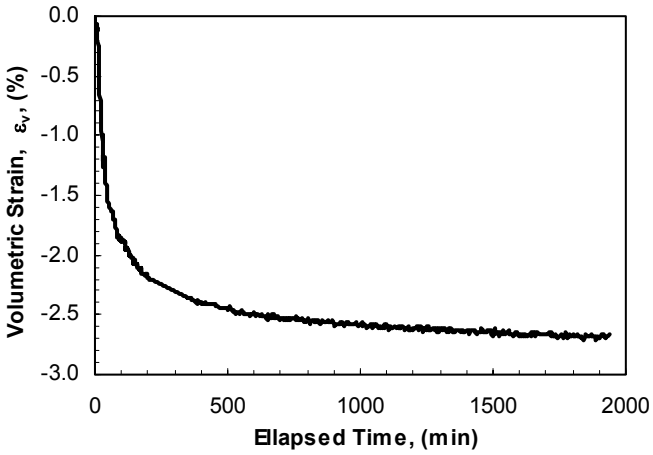

Test ID: S/SC-17%-12psi
Compaction water content: 17.3%
Compaction dry unit weight: 104.1 pcf
Compaction degree of saturation: 75.4%
Stage: Compression
Notes: 1. Specimen was compressed at a rate of 10 kPa/hr. 2. Air diffusion had small effect on shape of suction-time response curve.

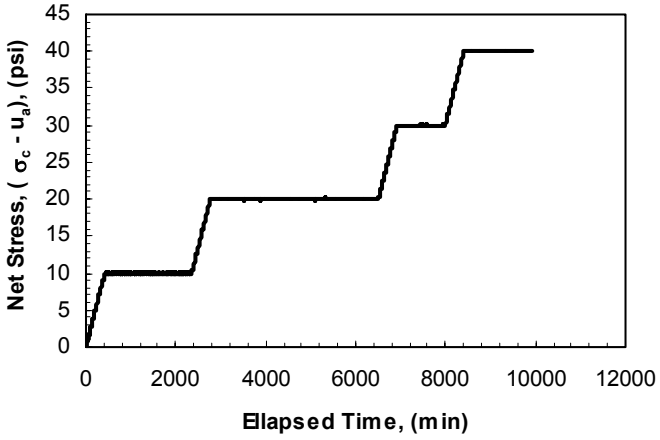

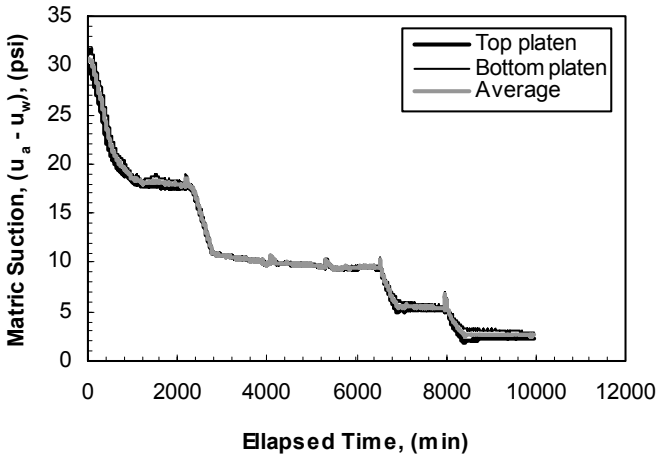

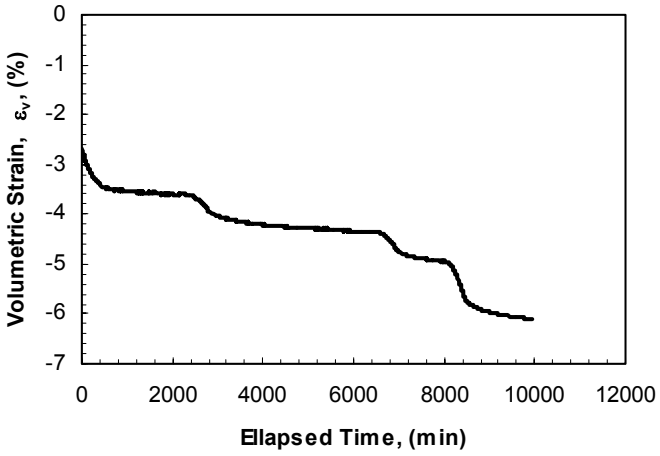

Test ID: S/SC-19%-7psi
Compaction water content: 19%
Compaction dry unit weight: 100.8 pcf
Compaction degree of saturation: 76.4%
Stage: Equalization
Notes: 1. Air diffusion had small effect on shape of suction-time response curve recorded at top platen. 2. Irregularities in shape of suction-time response curve recorded at bottom platen due to procedural error during flushing diffused air.

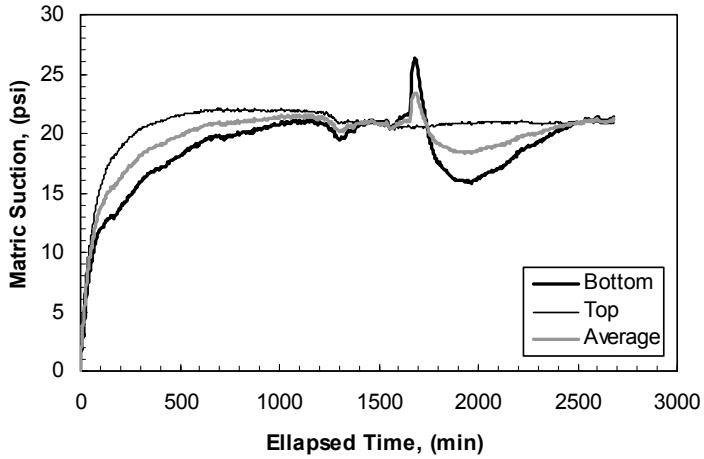

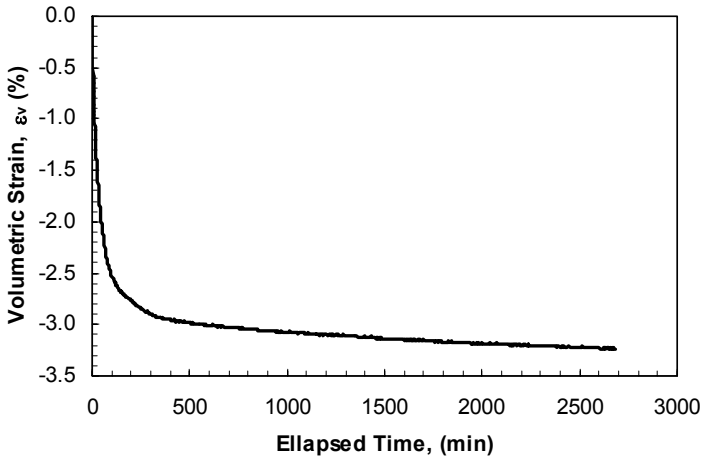

Test ID: S/SC-19%-7psi
Compaction water content: 19%
Compaction dry unit weight: 100.8 pcf
Compaction degree of saturation: 76.4%
Stage: Compression
Notes: 1. Specimen was compressed at a rate of 10 kPa/hr. 2. Air diffusion had small effect on shape of suction-time response curve.

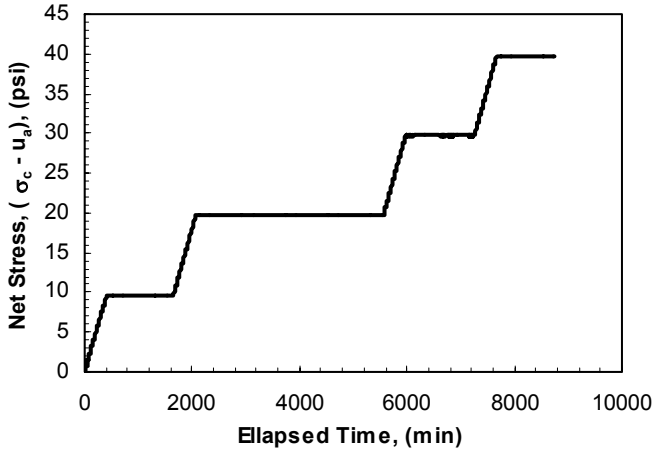

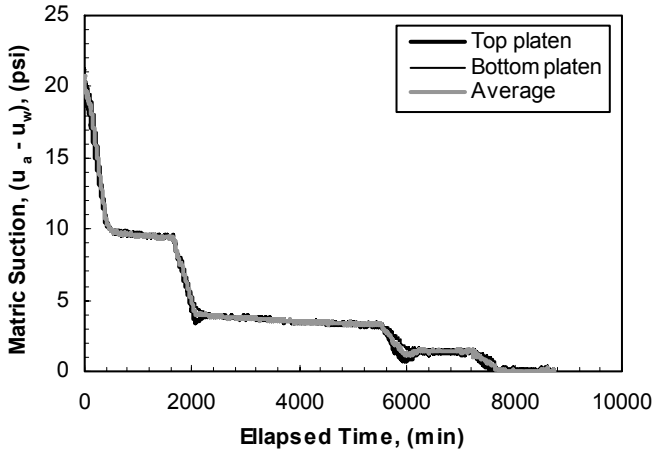

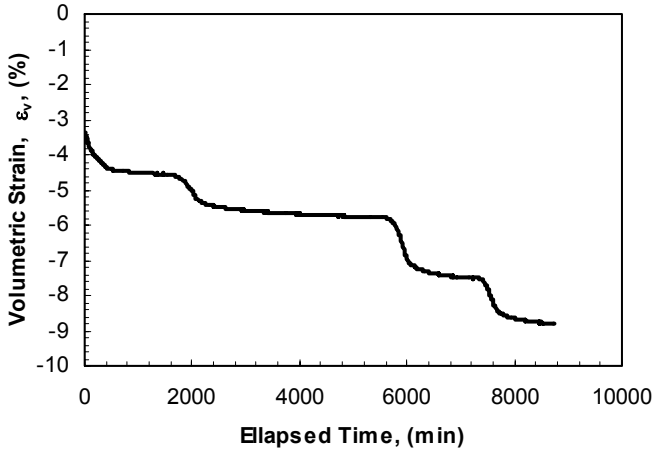

Test ID: S/SC-19%-25psi
Compaction water content: 18.7%
Compaction dry unit weight: 106.6 pcf
Compaction degree of saturation: 87.0%
Stage: Equalization
Notes: 1. Air diffused through high-air entry porous stones. Periodical flushing of diffused air caused irregularities in suction-time response curve. 2. Overshooting in suction-time response curve due to short adjustment intervals of cell and pore-air pressures. 2. Matric suction at equilibrium was unreasonably high for this water content for unknown reasons.

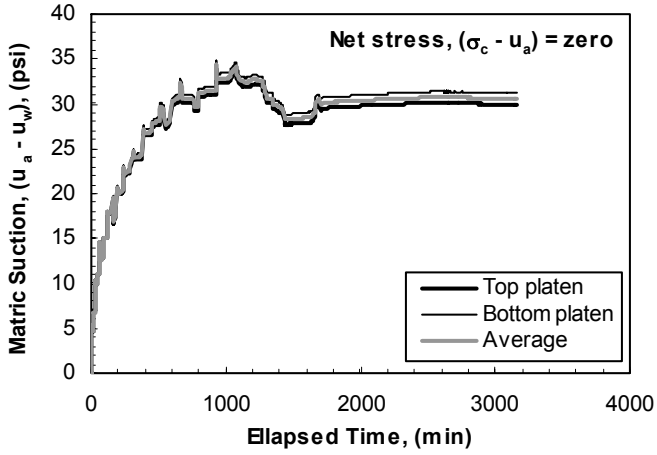

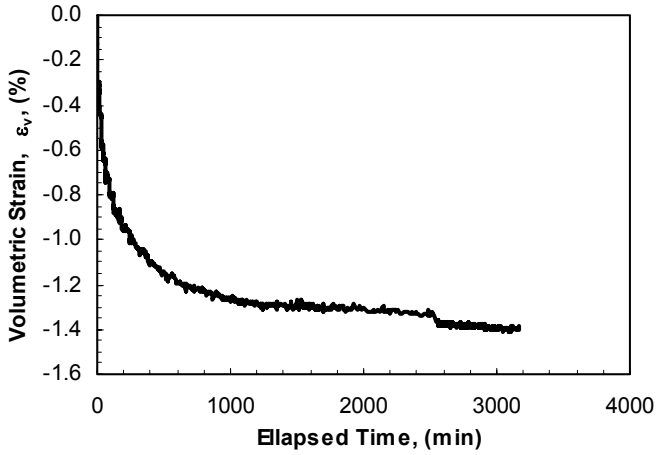

Test ID: S/SC-19%-25psi
Compaction water content: 18.7%
Compaction dry unit weight: 106.6 pcf
Compaction degree of saturation: 87.0%
Stage: Compression
Notes: 1. Specimen was compressed at a rate of 10 kPa/hr. 2. Air diffusion had small effect on shape of suction-time response curve.

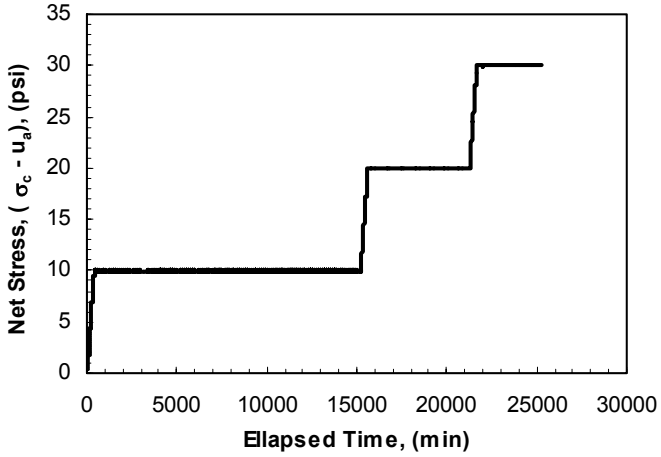

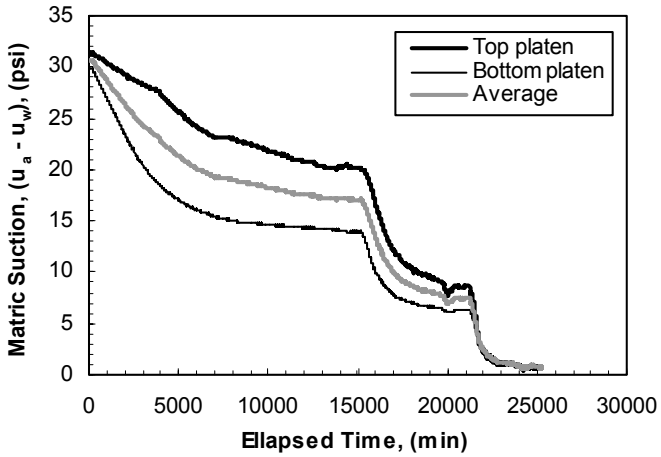

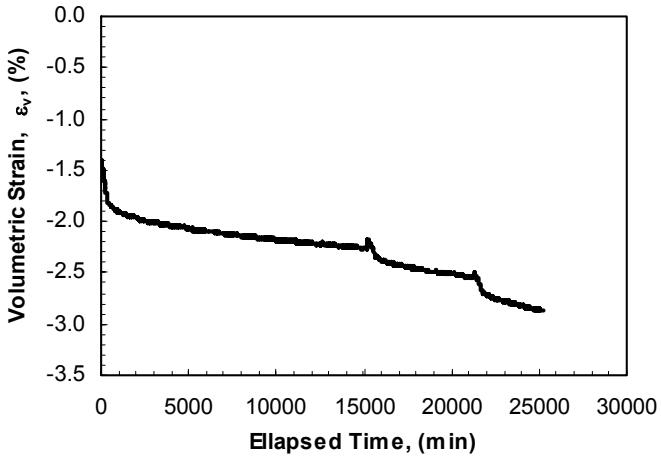

REFERENCES

Agarwal, T.K., and Ishibashi, I. (1991). "Multi-directional wave velocity by piezoelectric crystals," Geotechnical Special Publication, No. 29, pp. 102-117.

Agus, S.S., and Schanz, T. (2006). "Drying, wetting, and suction characteristic curves of a bentonite-sand mixture," Geotechnical Special Publication, No. 147, Vol. 2, pp. 1405-1414.

Aitchison, G.D. (1961). "Relationship of moisture and effective stress functions in unsaturated soils," Pore Pressure and Suction in Soils, conference organized by the British National Society of the International Society of Soil Mechanics and Foundation Engineering, at the Institution of Civil Engineers, London, England: Butterworths, pp. 47-52.

Aitchison, G.D. (1965). "Soil properties, shear strength, and consolidation," Proceedings of the 6th International Conference on Soil Mechanics and Foundation Engineering, Montereal, Vol.3, pp. 318-321.

Aitchison, G.D. (1973). "The quantitative description of the stress-deformation behavior of expansive soils – Preface to set of papers," Proceedings of the 3rd International Conference on Expansive Soils, Vol. 2, pp. 79-82.

Aitchison, G.D., and Richards, B.G. (1965). "A broad-scale study of moisture conditions in pavement subgrades throughout Australia. 2: Techniques adopted for the measurement of moisture variables," Moisture Equilibria and Moisture Changes in the Soils Beneath Covered Areas, Australia, Butterworths, pp. 191-204.

Allen, N.F., Richart, F.E., and Woods, R.D. (1980). "Fluid wave propagation in saturated and nearly saturated sands," Journal of the Geotechnical Engineering Division, Vol. 106, No. 3, pp. 235-254.

Arulnathan, R., Boulanger, R.W., and Riemer, M.F. (1998). "Analysis of bender element tests," Geotechnical Testing Journal, Vol. 21, No. 2, pp. 120-131.

ASTM C 117, "Standard test method for materials finer than 75-μm (No. 200) sieve in mineral aggregates by washing," Annual Book of ASTM Standards, 2003.

ASTM D 1557, "Standard test methods for laboratory compaction characteristics of soil using modified effort," Annual Book of ASTM Standards, 2002.

ASTM D 2487, "Standard practice for classification of soils for engineering purposes (Unified Soil Classification System)," Annual Book of ASTM Standards, 2000.

ASTM D 2850, "Standard test method for unconsolidated-undrained triaxial compression test on cohesive soils," Annual Book of ASTM Standards, 2003.

ASTM D 422, "Standard test method for particle-size analysis of soils," Annual Book of ASTM Standards, 1998.

ASTM D 4318, "Standard test methods for liquid limit, plastic limit, and plasticity index of soils," Annual Book of ASTM Standards, 2000.

ASTM D 698, "Standard test methods for laboratory compaction characteristics of soil using standard effort," Annual Book of ASTM Standards, 2000.

ASTM D 854, "Standard test methods for specific gravity of soil solids by water pycnometer," Annual Book of ASTM Standards, 2002.

Aversa, S., and Nicotera, M.V. (2002). "A triaxial and oedometer apparatus for testing unsaturated soils," Geotechnical Testing Journal, Vol. 25, No. 1, pp. 3-15.

Barden, L., and Pavlakis, G. (1971). "Air and water permeabilities of compacted unsaturated cohesive soil," Journal of Soil Science, Vol. 22, No. 3, pp. 302-318.

Bates, C.R. (1989). "Dynamic soil property measurements during triaxial testing," Geotechnique, Vol. 39, No. 4, pp. 721-726.

Bennell, J.D., Smith, D.T., and Davis, A.M. (1984). "Resonant-Column testing of marine sediments," Oceanology International, Brighton, pp1.9.1-1.9.24.

Bernier, F., Volckaert, G., Alonso, E., and Villar, M. (1997). "Suction-controlled experiments on Boom clay," Engineering Geology, Vol. 47, No. 4, pp. 325-338.

Bishop, A.W. (1959). "The principle of effective stress," Teknisk Ukeblad, Vol. 106, No. 39, pp. 859-863.

Bishop, A.W., Alpan, I., Blight, G.E., and Donald, I.B. (1960). "Factors controlling the strength of partly saturated cohesive soils," Research Conference on Shear Strength of Cohesive Soils, Boulder, Colorado, pp. 503-531.

Bishop, A.W., and Blight, G.E. (1963). "Some aspects of effective stress in saturated and unsaturated soils," Geotechnique, Vol. 13, No. 3, pp. 177-197.

Bishop, A.W., and Donald, I.B. (1961). "Experimental study of partly saturated soil in the triaxial apparatus," Proceedings of the 5th International Conference on Soil Mechanics and Foundation Engineering, Paris, Vol. 1, pp. 13-21.

Blewett, J., Blewett, I.J., and Woodward, P.K. (2000). "Phase and amplitude responses associated with the measurements of shear wave velocity in sand by bender element," Canadian Geotechnical Journal, Vol. 37, pp. 1348-1357.

Blight, G.E. (1965). "A study of effective stresses for volume change," Moisture Equilibria and Moisture Changes in the Soils Beneath Covered Areas, Australia, Butterworths, pp. 259-269.

Bocking, K.A., and Fredlund, D.G. (1980). "Limitations of the axis translation technique," Proceedings of the 4th International Conference on Expansive Soils, Denver, CO, pp. 117-135.

Brignoli, E.G.M., Gotti, M., and Stokoe, K.H. (1996). "Measurement of shear waves in laboratory specimens by means of piezoelectric transducers," Geotechnical Testing Journal, Vol. 19, No. 4, pp. 384-397.

Brocanelli, D., and Rinaldi, V. (1998). "Measurement of low-strain material damping and wave velocity with bender elements in the frequency domain," Canadian Geotechnical Journal, Vol. 35, No. 6, pp. 1032-1040.

Brooks, R.H., and Corey, A.T. (1964). "Hydraulic properties of porous media," Hydrology Paper No. 3, Civil Engineering Department, Colorado State University, Fort Collins, Colorado.

Burland, J.B. (1964). "Effective stress in partly saturated soils," Geotechnique, Vol. 14, pp. 65-68.

Burland, J.B. (1965). "Some aspects of the mechanical behavior of partly saturated soils," Moisture Equilibria and Moisture Changes in the Soils Beneath Covered Areas, Australia, Butterworths, pp. 270-278.

Cabarkapa, Z., Cuccovillo, T., and Gunn, M. (1999). "Some aspects of the pre-failure behavior of unsaturated soil," Proceedings of the 2nd International Conference on Pre-failure Behavior of Geomaterials, Turin, Vol. 1, pp. 159-165.

Callisto, L., and Rampello, S. (2002). "Shear strength and small-strain stiffness of a natural clay under general stress conditions," Geotechnique, Vol. 52, No. 8, pp. 547-560.

Chavez, C., Romero, E., and Alonso, E.E. (2005). "Volume change measurement of partially saturated rockfill in triaxial tests," Advanced Experimental Unsaturated Soil Mechanics – Trento, Italy, 27-29 June, pp. 93-98.

Cherry, J. (1962). "The azimuthal and polar radiation pattern from a horizontal stress applied at the surface of an elastic half space," Bulletin of the Seismological Society of America, Vol. 52, pp. 27-36.

Chiu, C.F. (2001). "Behaviour of unsaturated loosely compacted weathered materials," Ph.D. Dissertation, The Hong Kong University of Science and Technology, Hong Kong.

Cho, G.C., and Santamarina, J.C. (2001). "Unsaturated particulate materials – Particle-level studies," Journal of Geotechnical and Geoenviromental Engineering, Vol. 127, No. 1, pp. 84-96.

Coleman, J.D. (1962). "Stress/strain relations for partly saturated soils," Geotechnique, Vol. 12, No. 4, pp. 348-350.

Corey, A.T. (1957). "Measurement of water and air permeability in unsaturated soil," Proceedings of the Soil Science Society of America, Vol. 21, No. 1, pp. 7-10.

Croney, D., and Coleman, J.D. (1948). "Soil thermodynamics applied to the movement of moisture in road foundations," Proceedings of the 7th International Congress Applied Mechanics, Vol. 3, pp. 163-177.

Croney, D., and Coleman, J.D. (1954). "Soil structure in relation to soil suction (pF)," Journal of Soil Science, Vol. 5, No., 1, pp. 75-84.

Croney, D., Coleman, J.D., and Black, W.P.M. (1958). "Movement and distribution of water in soil in relation to highway design and performance," Water and Its Conduction in Soils, Highway Research Board, Special Report, No. 40, pp. 226-252.

Croney, D., Coleman, J.D., and Bridge, P.M. (1952). "The suction of moisture held in soil and other porous materials," Road Research Technical Paper No. 24.

Cui, Y.J., and Delage, P. (1996). "Yielding and plastic behaviour of an unsaturated compacted silt," Geotechnique, Vol. 46, No. 2, pp. 291-311.

D'Onforio, A., and Penna, A. (2003). "Influence of compaction variables on the small strain behaviour of a clayey silt," Deformation Characteristics of Geomaterials: Proceedings of the 3rd International Symposium on Deformation Characteristics of Geomaterials, Lyon, France, pp. 337-344.

Day, P.R. (1955). "Effect of shear on water tension in saturated clay," Annual Reports I and II, Western Regional Research Project W-30, 1954-1955, University of California, Berkeley.

de Alba, P., and Baldwin, K.C. (1991). "Use of bender elements in soil dynamics experiments," Geotechnical Special Publication, No. 29, pp. 86-101.

Diaz-Rodriguez, J.A., Moreno-Carrizales, P., and Lopez-Flores, L. (2001). "A study of Soil Microstructure using bender element tests," Proceedings of the 4th International Conference on Recent Advances in Geotechnical Earthquake Engineering and Soil Dynamics, San Diego, CA, Paper No. 1.39.

Dyvik, R. (1984). "The use of piezoceramic bender elements to measure G_{max} in the laboratory," Norwegian Geotechnical Institute, Internal Report, No. 40014-3.

Dyvik, R., and Madshus, C. (1985). "Laboratory measurements of G_{max} using bender elements," Advances in the Art of Testing Soils Under Cyclic Conditions, ASCE, pp. 186-196.

Dyvik, R., and Olsen, T.S. (1989). "G_{max} measured in oedometer and DSS tests using bender elements," Proceedings of the 12th International Conference on Soil Mechanics and Foundation Engineering, Rio de Janeiro , Vol. 1, pp. 39-42.

Egeli, I. (1992). "Some tests for studying volume change and pore water pressure behaviour of unsaturated clays on the wet side of optimum water content," Canadian Geotechnical Conference, Innovation Conservation & Rehabilitation, pp. 6/1-6/10.

Fam, M., and Santamarina, C. (1995). "Study of geoprocesses with complementary mechanical and electromagnetic wave measurements in an oedometer," Geotechnical Testing Journal, Vol. 18, No. 3, pp. 307-314.

Filson, H.L. (1980). "A study of heave analysis using the oedometer test," M.Sc. Thesis, University of Saskatchewan, Saskatoon, Canada.

Fisher, R.A. (1926). "On the capillary forces in an ideal soil," Journal of Agricultural Science, Vol. 16, pp. 492-505.

Fredlund, D.G., and Morgenstern, N.R. (1977). "Stress state variables for unsaturated soils," Journal of the Geotechnical Engineering Division, ASCE, Vol. 103, No. 5, pp. 447-466.

Fredlund, D.G., and Rahardjo H. (1993). "Soil mechanics for unsaturated soils," John Wiley & Sons, New York, 560 p.

Fredlund, D.G., Morgenstern, N.R., and Widger, R.A. (1978). "The shear strength of unsaturated soils," Canadian Geotechnical Journal, Vol. 15, No. 3, pp. 313-321.

Fung, Y.C. (1977). "A first course in continuum mechanics," Prentice-Hall, Inc., New Jersey, 340 p.

Gajo, A., Fedel, A., and Mongiovi, L. (1997). "Experimental analysis of the effects of fluid-solid coupling on the velocity of elastic waves in saturated porous media," Geotechnique, Vol. 47, No. 5, pp. 993-1008.

Gallage, C.P.K., and Uchimura, T. (2006). "Effects of wetting and drying on the unsaturated shear strength of a silty sand under low suction," Geotechnical Special Publication, No. 147, Vol. 1, pp. 1247-1258.

Geiser, F., Laloui, L., and Vulliet, L. (2000). "On the volume measurement in unsaturated triaxial test," Unsaturated Soils for Asia: Proceedings of the Asian Conference on Unsaturated Soils, UNAT-ASIA, pp. 669-674.

Gohl, W.B., and Finn, W.D.L. (1991). "Use of piezoceramic bender elements in soil dynamics testing," Geotechnical Special Publication, No. 29, pp. 118-133.

Gonzalez, N.A., and Colmenares, J.E. (2006). "Influence of matric suction on the volume change behaviour of a compacted clayey soil," Geotechnical Special Publication, No. 147, Vol. 1, pp. 825-836.

Hamdi, F., and Taylor-Smith, D. (1981) "Soil consolidation behavior assessed by seismic velocity measurements," Geophysics Prospecting, Vol. 29, pp. 715-729.

Hardin, B.O. (1978). "The nature of stress-strain behavior of soils," Proceedings of the ASCE Geotechnical Engineering Division Specialty Conference on Earthquake Engineering and Soil Dynamics, Pasadena, CA, pp. 3-90.

Hardin, B.O., and Black, W.L. (1968). "Vibration modulus of normally consolidated clay," Journal of Soil Mechanics and Foundations Division, ASCE, Vol. 94, No. SM2, pp. 353-369.

Hilf, J.W. (1956). "An investigation of pore-water pressure in compacted cohesive soils," Ph.D. Dissertation, Technical Memorandum No. 654, U.S. Department of the Interior, Bureau of Reclamation, Design and Construction Division, Denver, Colorado.

Hoar, R.J., and Stokoe, K.H.II. (1978). "Generation and measurement of shear waves in situ," ASTM Special Technical Publication, No. 654, pp. 3-29.

Hoyos Jr., L.R., and Macari, E.J. (2001). "Development of a stress/suction-controlled true triaxial testing device for unsaturated soils," Geotechnical Testing Journal, Vol. 24, No. 1, pp. 5-13.

Inci, G., Yesiller, N., and Kagawa, T. (2003). "Experimental investigation of dynamic response of compacted clayey soils," Geotechnical Testing Journal, Vol. 26, No. 2, pp. 125-141.

Jamiolkowski, M., Lancellotta, R., and Lo Presti, D.C.F. (1995). "Remarks on the stiffness at small strains of six Italian clays," Developments in Deep Foundations and Ground Improvement Schemes, Balasubramaniam et al., Eds., Balkema, Rotterdam, pp. 197-216.

Jennings, J.E. (1961). "A revised effective stress law for use in the prediction of the behavior of unsaturated soils," Pore Pressure and Suction in Soils, conference organized by the British National Society of the International Society of Soil Mechanics and Foundation Engineering, at the Institution of Civil Engineers, London, England: Butterworths, pp. 26-30.

Jennings, J.E., and Burland, J.B. (1962). "Limitations to the use of effective stresses in partly saturated soils," Geotechnique, Vol. 12, No. 2, pp. 125-144.

Josa, A., Alonso, E.E., Lloret, A., and Gens, A. (1987). "Stress-strain behaviour of partially saturated soils," Proceedings of the 9th European Conference on Soil Mechanics and Foundation Engineering, Dublin, pp. 561-564.

Jovicic, V., and Coop, M.R. (1997a). "Discussion on Interpretation of bender element tests," Geotechnique, Vol. 47, No. 4, pp. 873-877.

Jovicic, V., and Coop, M.R. (1997b). "Stiffness of coarse-grained soils at small strains," Geotechnique, Vol. 47, No. 3, pp. 545-561.

Jovicic, V., and Coop, M.R. (1998). "The measurement of stiffness anisotropy in clays with bender element tests in the triaxial apparatus," Geotechnical Testing Journal, Vol. 21, No. 1, pp. 3-10.

Jovicic, V., Coop, M.R., and Simic, M. (1996). "Objective criteria for determining G_{max} from bender element tests," Geotechnique, Vol. 46, No. 2, pp. 357-362.

Juca, J.F.T. (1993). "Flow properties of unsaturated soils under controlled suction," Unsaturated Soils, pp. 151-162.

Jung, M.J. (2005). "Shear wave velocity measurements of normally consolidated Kaolinite using bender elements," M.Sc. Thesis, The University of Texas at Austin.

Kawaguchi, T., Mitachi, T., and Shibuya, S. (2001). "Evaluation of shear wave travel time in laboratory bender element test," Proceedings of the 15th International Conference on Soil Mechanics and Geotechanics Engineering, pp. 155-158.

Krahn, J., and Fredlund, D.G. (1972). "On total, matric, and osmotic suction," Journal of Soil Science, Vol. 114, No. 5, pp. 339-348.

Kung, T.C., Ou, C.Y., and Hsieh, P.G. (2004). "Measurement of shear modulus of soil using bender elements," Journal of the Southeast Asian Geotechnical Society, Vol. 35, No. 1, pp. 1-7.

Kuwano, R., and Jardine, R.J. (1998). "Stiffness measurements in a stress-path cell," Pre-failure Deformation Behavior of Geomaterials, pp. 391-394.

Ladd, C.C. (1960). "Mechanics of swelling of compacted clays," Highway Research Board Bulletin No. 245, National Research Council, pp. 10-26.

Ladd, R.S., and Dutko, P. (1985). "Small strain measurements using triaxial apparatus," Advances in the Art of Testing Soils Under Cyclic Conditions, ASCE, pp. 148-165.

Lambe, T.W., and Whitman, R.V. (1969). "Soil Mechanics," John Wiley & Sons, New York, 553 p.

Langfelder, L.J., Chen, C.F., and Justice, J.A. (1968). "Air permeability of compacted cohesive soils," Journal of Soil Mechanics and Foundations Division, ASCE, Vol. 94, No. SM4, pp. 981-1001.

Lauer, C., and Engel, J. (2004). "A triaxial device for unsaturated sand – new developments," Unsaturated Soils: Proceedings of the International Conference 'From Experimental Evidence Towards Numerical Modeling of Unsaturated Soils', Weimar, Germany, 18-19 September, 2003, Vol. I, pp. 301-314.

Lauer, C., and Engel, J. (2005). "Investigations on the unsaturated stress-strain behaviour and on the SWCC of Hostun Sand in a double-walled triaxial cell," Advanced

Experimental Unsaturated Soil Mechanics – Trento, Italy, 27-29 June, pp. 185-191.

Lawrence, C.A., Houston, W.N., Houston, S.L., and Harraz, A.M. (2005). "Pressure pulse technique for measuring diffused air volume," Advanced Experimental Unsaturated Soil Mechanics – Trento, Italy, 27-29 June, pp. 9-13.

Lawrence, F.V. (1963). "Propagation velocity of ultrasonic waves through sand," Research Report R63-08, Boston, Massachusetts Institute of Technology.

Lawrence, F.V. (1965). "Ultrasonic shear wave velocities in sand and clay," Research Report R65-05, Boston, Massachusetts Institute of Technology.

Lee, J.S., and Santamarina, J.C. (2005). "Bender elements: performance and signal interpretation," Journal of Geotechnical and Geoenviromental Engineering, Vol. 131, No. 9, pp. 1063-1070.

Leong, E.C., Agus, S.S., and Rahardjo, H. (2004). "Volume change measurement of soil specimen in triaxial test," Geotechnical Testing Journal, Vol. 27, No. 1, pp. 1-10.

Leong, E.C., Cahyadi, J., and Rahardjo, H. (2006). "Stiffness of a compacted residual soil," Geotechnical Special Publication, No. 147, Vol. 1, pp. 1169-1180.

Leong, E.C., Yeo, S.H., and Rahardjo, H. (2005). "Measuring shear wave velocity using bender elements," Geotechnical Testing Journal, Vol. 28, No. 5, pp. 488-498.

Leslie, J.R. (1950). "Pulse techniques applied to dynamic testing," Proceedings - American Society for Testing Materials, Vol. 50, pp.1314-1323.

Lohani, T.N., Imai, G., and Shibuya, S. (1999). "Determination of shear wave velocity in bender element test," Proceedings of the 2nd International Conference on Earthquake Geotechnical Engineering, Rotterdam, Vol. 1, pp. 101-106.

Lu, N., and Likos, W.J. (2006). "Suction stress characteristic curve for unsaturated soil," Journal of Geotechnical and Geoenviromental Engineering, Vol. 132, No. 2, pp. 131-142.

Macari, E.J., and Hoyos Jr., L.R. (2001). "Mechanical behavior of an unsaturated soil under multi-axial stress states," Geotechnical Testing Journal, Vol. 24, No. 1, pp. 14-22.

Mancuso, C., Vassallo, R., and d'Onforio, A. (2002). "Small strain behavior of a silty sand in controlled-suction resonant column – torsional shear tests," Canadian Geotechnical Journal, Vol. 39, No. 1, pp. 22-31.

Manke, P.G., and Gallaway, B.M. (1966). "Pulse velocities in flexible pavement construction materials," Highway Research Record, No. 131, pp. 128-153.

Marinho, E.A.M., Chandler, R.J., and Crilly, M.S. (1995). "Stiffness measurements on an unsaturated high plasticity clay using bender elements," Proceedings of the 1st International Conference on Unsaturated Soils, Paris, Vol. 1, pp. 535-539.

Matyas, E.L. (1967). "Air and water permeability of compacted soils," Permeability and Capillarity of Soils, ASTM STP 417, American Society for Testing and Materials, pp. 160-175.

Matyas, E.L., and Radhakrishna, H.S. (1968). "Volume change characteristics of partially saturated soils," Geotechnique, Vol. 18, pp. 432-448.

Mendoza, C.E., and Colmenares, J.E. (2006). "Influence of the suction on the stiffness at very small strains," Geotechnical Special Publication, No. 147, Vol. 1, pp. 529-540.

Mendoza, C.E., Colmenares, J.E., and Merchan, V.E. (2005). "Stiffness of an unsaturated compacted clayey soil at very small strains," Advanced Experimental Unsaturated Soil Mechanics – Trento, Italy, 27-29 June, pp. 199-204.

Mitchell J.K. (1976). "Fundamentals of soil behavior," John Wiley & Sons, New York, 422 p.

Modoni G., Flora, A., Mancuso, C., Viggiani, C., and Tatsuoka, F. (2000). "Evaluation of gravel stiffness by pulse wave transmission tests," Geotechnical Testing Journal, Vol. 23, No. 4, pp. 506-521.

Mohsin, A.K.M., and Airey, D.W. (2003). "Automating G_{max} measurement in triaxial tests," Deformation Characteristics of Geomaterials, Proceedings of the 3rd International Symposium on Deformation Characteristics of Geomaterials, Lyon, France, 22-24 September, pp. 73-80.

Mou, C.H., and Chu, T.Y. (1981). "Soil suction approach for swelling potential evaluation," Transportation Research Record No. 790, pp. 54-60.

Mun, B., Aubeny, C.P., and Lytton, R.L. (2006). "Calculation of pseudo strain and dissipated pseudo strain energy in unsaturated soil," Geotechnical Special Publication, No. 147, Vol. 2, pp. 1956-1967.

Nakagawa, K., Soga, K., and Mitchell, J.K. (1996). "Pulse transmission system for measuring wave propagation in soils," Journal of Geotechnical Engineering, Vol. 122, No. 4, pp. 302-308.

Ng, C.W.W., and Chiu, C.F. (2001). "Behaviour of a loosely compacted unsaturated volcanic soil," Journal of Geotechnical and Geoenviromental Engineering, Vol. 127, No. 12, pp. 1027-1036.

Ng, C.W.W., Zhan, L.T., and Cui, Y.J. (2002). "A new simple system for measuring volume changes in unsaturated soils," Canadian Geotechnical Journal, Vol. 39, No. 3, pp. 757-764.

Ning Lu, and Griffiths, D.V. (2004). "Profiles of steady-state suction stress in unsaturated soils," Journal of Geotechnical and Geoenviromental Engineering, Vol. 130, No. 10, pp. 1063-1076.

Oloo, S.Y., and Fredlund, D.G. (1996). "A method for determination of Φ^b for statically compacted soils," Canadian Geotechnical Journal, Vol. 33, No. 2, pp. 272-280.

Olson, R.E. (1963). "Effective stress theory of soil compaction," Journal of Soil Mechanics and Foundations Division, ASCE, Vol. 89, No. SM2, pp. 27-45.

Olson, R.E., and Langfelder, L.J. (1965). "Pore water pressures in unsaturated soils," Journal of Soil Mechanics and Foundations Division, ASCE, Vol. 91, No. SM4, pp. 127-150.

Ooi, P.S.K., and Pu, J. (2002). "Evaluating compaction of tropical soils using soil stiffness," Bearing capacity of roads, railways and airfields: Proceedings of the 6th International Conference on the Bearing Capacity of Roads and Airfields, Lisbon, Portugal, pp. 1143-1149.

Ooi, P.S.K., and Pu, J. (2003). "Use of stiffness for evaluating compactness of cohesive pavement geomaterials," Transportation Research, No. 1849, 03-4052, pp. 11-19.

Padilla, J.M., Houston, W.N., Lawrence, C.A., Fredlund, D.G., Houston, S.L., and Perez, N.P. (2006). "An automated triaxial testing device for unsaturated soils," Geotechnical Special Publication, No. 147, Vol. 2, pp. 1775-1786.

Pennington, D.S., Nash, D.F.T., and Lings, M.L. (2001). "Horizontally mounted bender elements for measuring anisotropic shear moduli in triaxial clay specimens," Geotechnical Testing Journal, Vol. 24, No. 2, pp. 133-144.

Picornell, M., and Nazarian, S. (1998). "Effect of soil suction on the low-strain shear modulus of soils," Proceedings of the 2nd International Conference on Unsaturated Soils, Beijing, China, Vol. 2, pp. 102-107.

Puppala, A.J., Kadam, R., Madhyannapu, R.S., and Hoyos, L.R. (2006). "Small-strain shear moduli of chemically stabilized sulfate-bearing cohesive soils," Journal of Geotechnical and Geoenvironmental Engineering, Vol. 132, No. 3, pp. 322-336.

Qian, X., Gray, D.H., and Woods, R.D. (1991). "Resonant column tests on partially saturated sands," Geotechnical Testing Journal, Vol. 14, No. 3, pp. 266-275.

Rampello, S., Viggiani, G.M.B., and Amorosi, A. (1997). "Small- strain stiffness of reconstituted clay compressed along constant triaxial effective stress ratio paths," Geotechnique, Vol. 47, No. 3, pp. 475-489.

Rampino, C., Mancuso, C., and Vinale, F. (1999). "Laboratory testing on an unsaturated soil: equipment, procedure, and first experimental results," Canadian Geotechnical Journal, Vol. 36, No. 1, pp. 1-12.

Rampino, C., Mancuso, C., and Vinale, F. (2000). "Experimental behaviour and modeling of an unsaturated compacted soil," Canadian Geotechnical Journal, Vol. 37, No. 4, pp. 748-763.

Richards, B.G. (1967). "Moisture flow and equilibria in unsaturated soils for shallow foundations," Permeability and Capillarity of Soils, ASTM STP 417, American Society for Testing and Materials, pp. 4-34.

Romero, E., Facio, J.A., Lloret, A., Gens, A., and Alonso, E.E. (1997). "A new suction and temperature controlled triaxial apparatus," Proceedings of the 14th International Conference on Soil Mechanics and Foundation Engineering, Hamburg, Vol. 1, pp. 185-188.

Sanchez-Salinero, I., Roesset, J.M., and Stokoe, K.H.II. (1986). "Analytical studies of body wave propagation and attenuation," Geotechnical Engineering Report GR86-15, The University of Texas at Austin.

Santamarina, J.C., and Fam, M.A. (1997). "Discussion on Interpretation of bender element tests," Geotechnique, Vol. 47, No. 4, pp. 873-877.

Santamarina, J.C., Klein, K.A., and Fam, M.A. (2001). "Soils and Waves: particulate materials behavior, characterization and process monitoring," John Wiley & Sons, New York, 488 p.

Sawangsuriya, A., Edil, T.B., Bosscher, P.J., and Wang, X. (2006). "Small-strain stiffness behavior of unsaturated compacted subgrade," Geotechnical Special Publication, No. 147, Vol. 1, pp. 1121-1132.

Schultheiss, P.J. (1981). "Simultaneous measurement of P & S wave velocities during conventional laboratory soil testing," Marine Geotechnology, Vol. 4, No. 4, pp. 343-367.

Schwarz, V., Becker, A., and Vrettos, C. (2006). "An initial study on the viscous behaviour of a partially saturated kaolinite clay based on triaxial tests," Geotechnical Special Publication, No. 147, Vol. 2, pp. 1811-1820.

Shackel, B. (1973). "Changes in soil suction in a sand-clay subjected to repeated triaxial loading," Highway Research Record, No. 429, pp. 29-39.

Sheeran, D.E., Baker, W.H., and Krizek, R.J. (1967). "Experimental study of pulse velocities in compacted soils," Highway Research Record, No. 177, Highway Research Board, pp. 226-238.

Shibuya, S., Hwang, S.C., and Mitachi, T. (1997). "Elastic shear modulus of soft clays from shear wave velocity measurement," Geotechnique, Vol. 47, No. 3, pp. 593-601.

Shirly, D.J., and Anderson, A.L. (1975). "Acoustic and engineering properties of sediments," Applied Research Laboratory, The University of Texas at Austin, Report No. ARL-TR-75-58.

Silva, C.H.C., Porras Ortiz, F.O., Fratta, D., and Macari, E.J. (2002). "Mechanical response of unsaturated particulate materials – a stiffness assessment study under controlled matric suction," Proceedings of IMEC2002, ASME International Mechanical Engineering Congress & Exposition, New Orleans, Louisiana, 17-22 November, pp. 269-274.

Sivakumar, V. (1993). "A critical state framework for unsaturated soils," Ph.D. Dissertation, University of Sheffield, Sheffield, U.K.

Sivakumar, V., and Wheeler, S.J. (2000). "Influence of compaction on the mechanical behaviour of an unsaturated compacted clay. Part 1: wetting and isotropic compression," Geotechnique, Vol. 50, No. 4, pp. 359-368.

Stephenson, R.W. (1978). "Ultrasonic testing for determining dynamic soil moduli," Dynamic Geotechnical Testing, ASTM STP 654, ASTM International, West Conshohocken, PA, pp. 179-195.

Strassburger, E. (1982). "Use of piezoelectric transducers for stiffness and density measurements of soils," M.Sc. Thesis, The University of Texas at Austin.

Sudhakar, M.R., and Revanasiddappa, K. (2000). "Role of matric suction in collapse of compacted clay soil," Journal of Geotechnical and Geoenviromental Engineering, Vol. 126, No. 1, pp. 85-90.

Sudhakar, M.R., and Revanasiddappa, K. (2003). "Role of soil structure and matric suction in collapse of a compacted clay soil," Geotechnical Testing Journal, Vol. 26, No. 1, pp. 102-110.

Sun D.A., Sheng, D.C., Cui, H.B., and Li, J. (2006). "Effect of density on the soil-water-retention behaviour of compacted soil," Geotechnical Special Publication, No. 147, Vol. 2, pp. 1338-1347.

Sun, D.A., Matsuoka, H., and Xu, Y.F. (2004). "Collapse behavior of compacted clays in suction-controlled triaxial tests," Geotechnical Testing Journal, Vol. 27, No. 4, pp. 1-9.

Sun, D.A., Matsuoka, H., Cui, H.B., and Xu, Y.F. (2003). "Three-dimensional elasto-plastic model for unsaturated compacted soils with different initial densities," Journal for Numerical and Analytical Methods in Geomechanics, Vol. 27, No. 12, pp. 1079-1098.

Taha, M.R., Hossain, M.K., and Abdul Mofiz, S. (2000). "Effect of suction on the strength of unsaturated soil" Geotechnical Special Publication, No. 99, pp. 210-221.

Terzaghi, K. (1936). "The shear resistance of saturated soils," Proceedings of the 1st International Conference on Soil Mechanics and Foundation Engineering, Cambridge, Vol. 1, pp. 54-56.

Theron, M., Clayton, C.R.I., and Best, A.I. (2003). "Interpretation of side-mounted bender element results using phase shift and group velocity," Deformation Characteristics of Geomaterials: Proceedings of the 3rd International Symposium on Deformation Characteristics of Geomaterials, Lyon, France, pp. 127-132.

Thomann, T.G., and Hryciw, R.D. (1990). "Laboratory measurement of small strain shear modulus under K_o conditions," Geotechnical Testing Journal, Vol. 13, No. 2, pp. 97-105.

Toyota, H., Sakai, N., and Nishimura, T. (2001). "Effects of stress history due to unsaturation and drainage condition on shear properties of unsaturated cohesive soil," Soils and Foundations, Vol. 41, No. 1, pp. 13-24.

Tsai, C., and Petry, T.M. (1995). "Suction study on compacted clay using three measurement methods," Transportation Research Record, No. 1481, pp. 28-34.

Vaghela, J.G., and Stokoe, K.H.II. (1995). "Small strain dynamic properties of soils from free-free Resonant Column testing," Geotechnical Engineering Report GT95-1, The University of Texas at Austin.

Valle, C. (2006). "Measurements of V_p and V_s in dry, unsaturated, and saturated sand specimens with piezoelectric transducers," Ph.D. Dissertation, The University of Texas at Austin, Texas, USA.

van Genuchten, M.T. (1980). "A closed-form equation for predicting the hydraulic conductivity of unsaturated soils," Soil Science Society of America Journal, Vol. 44, pp. 892-898.

Vassallo, R., and Mancuso, C. (2000). "Soil behavior in the small and the large strain range under controlled suction conditions," Experimental Evidence and Theoretical Approaches in Unsaturated Soils, Proceedings of an International Workshop on Unsaturated Soils, Trento, Italy, pp. 75-90.

Vassalo, R., Mancuso, C., and Vinale, F. (2006). "Effects of stress-strain history on the initial shear stiffness of an unsaturated compacted silt," Geotechnical Special Publication, No. 147, Vol. 1, pp. 1145-1156.

Viggiaini, G., and Atkinson, J.H. (1995a). "Interpretation of bender element tests," Geotechnique, Vol. 45, No. 1, pp. 149-154.

Viggiaini, G., and Atkinson, J.H. (1995b). "Stiffness of fine-grained soil at very small strains," Geotechnique, Vol. 45, No. 2, pp. 249-265.

Viggiaini, G., and Atkinson, J.H. (1997). "Discussion on Interpretation of bender element tests," Geotechnique, Vol. 47, No. 4, pp. 873-877.

Vinale, F., D'Onofrio, A., Mancuso, C., Santucci de Magistris, F., and Tatsuoka, F. (1999). "The pre-failure behaviour of soils as construction materials," Pre-Failure Deformation Characteristics of Geomaterials, pp. 955-1007.

Walker, S.C., Gallipoli, D., and Toll, D.G. (2005). "The effect of structure on the water retention of soil tested using different methods of suction measurement," Advanced Experimental Unsaturated Soil Mechanics, Proceedings of the International Symposium on Advanced Experimental Unsaturated Soil Mechanics, Trento, Italy, pp. 33-39.

Wan, A.W.L., Gray, M.N., and Graham, J. (1995). "On the relations of suction, moisture content, and soil structure in compacted clays," Proceedings of the 1st International Conference on Unsaturated Soils, Vol. 1, pp. 215-222.

Wheeler, S.J., and Sivakumar, V. (1992). "Critical state concepts for unsaturated soil," Proceedings of the 7th International Conference on Expansive Soils, Vol. 1, pp. 167-172.

Widger, R.A. (1976). "Slope stability in unsaturated soils," M.Sc. Thesis, University of Saskatchewan, Saskatoon, Canada.

Woods, R. D. (1978). "Measurement of dynamic soil properties," Proceedings of the ASCE geotechnical engineering division specialty conference on earthquake engineering and soil dynamics, Pasadena,, Vol. 1, pp. 91-178.

Wu, S., Gray, D.H., and Richart, F.E. (1984). "Capillary effects on dynamic modulus of sands and silts," Journal of Geotechnical Engineering, Vol. 110, No. 9, pp. 1188-1203.

Yesiller, N., Inci, G., and Miller, C.J. (2000). "Ultrasonic Testing for Compacted Clayey Soils," Geotechnical Special Publication, No. 99, pp. 54-68.

Yong, R. N. (1980). "Some aspects of soil suction, shear strength and soil stability," Geotechnical Engineering, Vol. 11, No. 1, pp. 55-76.

Zeng, X., Figueroa, J.L., and Fu, L. (2004). "Measurement of base and subgrade layer stiffness using bender element technique," Geotechnical Special Publication, No. 123, pp. 35-45.

VITA

Manal Abdelsalam Salem was born in Giza, Egypt, on April 8, 1979, the daughter of Abdelsalam M. Salem and Laila A. El-Alfy. After graduating from high school, she enrolled in the Faculty of Engineering at Cairo University in September 1996. She earned her Bachelor of Science in Civil Engineering with highest honors in July 2001. Manal started her graduate studies at Cairo University in September 2001 specializing in geotechnical engineering. In October 2003, she received her Master of Science in Civil Engineering with distinction under the supervision of Professors Magda Abdel-Rahman and Omar Ezzeldin. Manal started her doctoral studies at the University of Texas at Austin in August 2003. Throughout her studies, Manal received several awards for her academic achievements from Cairo University, Egyptian Engineering Syndicate, and American Association of University Women (AAUW).

Permanent address:42 Lebanon street, Giza, Egypt.

This dissertation was typed by the author.